NITRIDING OF AUSTENITIC STAINLESS STEEL

BY

AJIT RAMCHANDANI

A thesis submitted for the degree of Master of Philosophy
of Aston University

October 1985

The University of Aston in Birmingham

Title : NITRIDING OF AUSTENITIC STAINLESS STEEL

Author : AJIT RAMCHANDANI

Degree : M.Phil.

Date : October 1985

SUMMARY

Stainless steel is a difficult material to nitride because a passive oxide film is present on its surface. Hence it is essential to remove this film by chemical or mechanical means before any surface treatment can be carried out. This increases the cost of the treatment substantially.

The commonly used processes for the surface treatment of stainless steel have been gas nitriding, salt bath nitrocarburising and lately plasma nitriding. Plasma nitriding due to its operating conditions, does not require any prior treatments for removal of the passive oxide film. Plasma nitriding also provides the possibility of treatment at low temperature, which is important to retain corrosion resistance of stainless steel.

The fact that nitriding of stainless steel improves the wear characteristics but impairs the corrosion resistance has been reported by many researchers. However, very little work has been carried out to study and analyse this problem. This research work has studied the corrosion and wear properties of austenitic stainless steels using the three different nitriding techniques mentioned above. It was also the objective to study the optimum plasma nitriding conditions required to achieve optimum wear and corrosion properties.

Corrosion has been studied by using an electro-chemical technique. A microprocessor based Princeton Applied Research Model-350 Corrosion Measurement System was used. Linear polarisation curves have been plotted so that the comparison could be made between different processes, different grades of untreated austenitic stainless steel and nitrided stainless steel. The evaluation of wear properties was carried out by using the Falex testing technique.

It was concluded that the plasma nitriding of austenitic stainless steel at 460^{o}C followed by a post-oxidation treatment resulted in better wear and corrosion properties than the other treatments and would be suitable where wear requirements are more rigid than the corrosion resistance. Plasma nitriding of the 321 grade stainless steel at 380^{o}C would be suitable where the corrosion resistance was a primary requirement. Salt bath nitrocarburising of austenitic stainless steel also resulted in better corrosion and wear properties than gas nitriding. The results showed that the wear rates obtained by using the above different techniques of nitriding, were different. However, the corrosion rate was observed to be the same over long periods.

KEYWORDS : Plasma Nitriding, Gas Nitriding, Salt Bath Nitrocarburising, Corrosion, Wear.

List of Contents

		Page
1.0	INTRODUCTION	1
1.1	Plasma Nitriding	2
1.1.1	Principles of the Process	2
1.1.2	Glow Discharge	3
1.1.3	Regions of Glow Discharge	6
1.1.4	Reaction Kinetics	10
1.2	Gas Nitriding	13
1.3	Salt Bath Nitrocarburising	16
1.4	Post-Oxidation Treatment	19
2.0	METALLURGICAL ASPECTS of NITRIDING	21
2.1	Diffusion Mechanism of Nitrogen	21
2.2	Compound Zone	26
2.3	Diffusion Zone	30
3.0	WEAR	34
3.1	Wear Mechanism	34
4.0	CORROSION	40
4.1	Theory of Corrosion	40
4.2	Electro-Chemical Theory of Corrosion	42
4.2.1	Tafel Plot Technique	48
4.2.2	Linear Polarisation Technique	49

		Page
5.0	EXPERIMENTAL PROCEDURE	50
5.1	Material Preparation	50
5.2	Plasma Nitriding	52
5.2.1	Equipment	52
5.2.2	Treatment	55
5.3	Gas Nitriding	60
5.3.1	Equipment	60
5.3.2	Treatment	60
5.4	Salt Bath Nitrocarburising	61
5.4.1	Equipment	61
5.4.2	Treatment	62
5.5	Corrosion Measurement	62
5.5.1	Equipment	62
5.5.2	Testing Procedure	65
5.6	Wear Measurement	66
5.6.1	Equipment	66
5.6.2	Testing Procedure	69
5.7	Metallography	70
5.8	Case Hardness	70
6.0	RESULTS	72
6.1	Visual Appearance	72
6.1.1	Plasma Nitriding	72
6.1.2	Gas Nitriding	72
6.1.3	Tufftriding	72
6.2	Metallography	73

		Page
6.3	Microhardness	83
6.4	Corrosion Measurement	83
6.4.1	Linear Polarisation Curves	83
6.5	Wear Measurement	102
7.0	DISCUSSION	127
7.1	Metallography	127
7.1.1	Untreated Specimens	127
7.1.2	Plasma Nitrided Specimens	127
7.1.3	Tufftrided Specimens	129
7.1.4	Gas Nitrided Specimens	130
7.2	Microhardness	130
7.3	Corrosion	133
7.4	Wear	137
8.0	CONCLUSIONS	140
9.0	SUGGESTIONS for FURTHER WORK	143
10.0	ACKNOWLEDGEMENTS	144
11.0	APPENDIX-1	145
12.0	APPENDIX-2	148
13.0	LIST of REFERENCES	149

LIST OF FIGURES

		Page
Fig.1	Voltage-Current characteristics of different types of discharge.	4
Fig.2	Zones involved in ionisation.	7
Fig.3	Equilibrium diagram of ammonia with pure iron.	15
Fig.4	Iron-nitrogen phase diagram.	27
Fig.5	Iron-Carbon-Nitrogen phase diagram.	27
Fig.6	Potential-Current relationship for a mixed electrode system.	45
Fig.7	Pin and Block for Falex test.	51
Fig.8	Falex machine.	68
Fig.9	Hardness profile for plasma nitrided specimens at 380°C.	84
Fig.10	Hardness profile for plasma nitrided specimens at 420°C.	85
Fig.11	Hardness profile for plasma nitrided specimens at 460°C.	86
Fig.12	Hardness profile for plasma nitrided specimens at 500°C.	87
Fig.13	Hardness profile for plasma nitrided specimens at 540°C.	88
Fig.14	Hardness profile for plasma nitrided specimens at 570°C.	89
Fig.15	Hardness profile for plasma nitrided specimens at 460°C with post-oxidation.	90

		Page
Fig.16	Hardness profile for plasma nitrided specimens at 500°C with post-oxidation.	91
Fig.17	Hardness profile for plasma nitrided specimens at 540°C with post-oxidation.	92
Fig.18	Hardness profile for plasma nitrided specimens at 570° with post-oxidation.	93
Fig.19	Hardness profile for Tufftrided specimens.	94
Fig.20	Hardness profile for gas nitrided specimens.	95
Fig.21	Hardness profile for gas nitrided specimens under different conditions	96
Fig.22	Hardness profile for AISI 304 grade steel after various treatments.	97
Fig.23	Hardness profile for AISI 316 grade steel after various treatments.	98
Fig.24	Hardness profile for AISI 321 grade steel after various treatments.	99
Fig.25	Hardness profile for plasma nitrided specimens at 460°C under incorrect furnace conditions.	100
Fig.26	Hardness profile for plasma nitrided specimens at 570°C under incorrect furnace conditions.	101
Fig.27	Corrosion plot for Tufftride Treatment.	104
Fig.28	Corrosion plot for gas nitriding	105
Fig.29	Corrosion plot for plasma nitriding at 380°C.	106
Fig.30	Corrosion plot for plasma nitriding at 420°C.	107
Fig.31	Corrosion plot for plasma nitriding at 460°C.	108
Fig.32	Corrosion plot for plasma nitriding at 500°C.	109
Fig.33	Corrosion plot for plasma nitriding at 540°C.	110

Page

Fig.34 Corrosion plot for plasma nitriding at 570°C. 111

Fig.35 Corrosion plot for plasma nitriding at 460°C. 112
with post-oxidation.

Fig.36 Corrosion plot for plasma nitriding at 500°C. 113
with post-oxidation.

Fig.37 Corrosion plot for plasma nitriding at 540°C. 114
with post-oxidation.

Fig.38 Corrosion plot for plasma nitriding at 570°C. 115
with post-oxidation.

Fig.39 Corrosion plot for untreated stainless steel. 116

Fig.40 Corrosion plot for AISI 304 grade steel after 117
various treatments.

Fig.41 Corrosion plot for AISI 316 grade steel after 118
various treatments.

Fig.42 Corrosion plot for AISI 321 grade steel after 119
various treatments.

LIST OF PLATES

		Page
Plate-1	Plasma nitriding unit at Aston University.	53
Plate-2	Microprocessor based corrosion measurement equipment.	63
Plate-3	Microstructure of untreated AISI 304 grade steel.	74
Plate-4	Microstructure of untreated AISI 316 grade steel.	74
Plate-5	Microstructure of untreated AISI 321 grade steel.	75
Plate-6	Microstructure of plasma nitrided AISI 304 grade steel.	75
Plate-7	Microstructure of plasma nitrided AISI 316 grade steel.	76
Plate-8	Microstructure of plasma nitrided AISI 321 grade steel.	76
Plate-9	Microstructure of plasma nitrided AISI 304 with post-oxidation.	77
Plate-10	Microstructure of plasma nitrided AISI 316 with post-oxidation.	77
Plate-11	Microstructure of plasma nitrided AISI 321 with post-oxidation.	78
Plate-12	Microstructure of plasma nitrided AISI 304 grade steel at 380^{o}C.	78
Plate-13	Microstructure of plasma nitrided AISI 316 grade steel at 380^{o}C.	79
Plate-14	Microstructure of plasma nitrided AISI 321 grade steel at 380^{o}C.	79
Plate-15	Microstructure of Tufftrided AISI 304 grade steel.	80

		Page
Plate-16	Microstructure of Tufftrided AISI 316 grade steel.	80
Plate-17	Microstructure of Tufftrided AISI 321 grade steel.	81
Plate-18	Microstructure of gas nitrided AISI 304 grade steel.	81
Plate-19	Microstructure of gas nitrided AISI 316 grade steel.	82
Plate-20	Microstructure of gas nitrided AISI 321 grade steel.	82
Plate-21	Untreated specimens after corrosion tests.	120
Plate-22	Plasma nitrided specimens after corrosion test.	120
Plate-23	Plasma nitrided specimens with post-oxidation after corrosion test.	121
Plate-24	Plasma nitrided specimens at 380^{o}C after corrosion test.	121
Plate-25	Tufftrided specimens after corrosion test.	122
Plate-26	Gas nitrided specimens after corrosion test.	122
Plate-27	Slightly scuffed specimen after Falex test.	125
Plate-28	Scuffed specimen after Falex test.	125
Plate-29	Badly scuffed specimen after Falex test.	126
Plate-30	Totally seized and sheared specimen after Falex test.	126

LIST OF TABLES

		Page
Table-1	Chemical composition of material for test programme.	56
Table-2	Chemical composition of material for Falex test.	56
Table-3	Experimental test programme for plasma nitriding.	56-57
Table-4	Results of test runs on Falex machine.	123-124

1.0. INTRODUCTION.

There are several methods of surface hardening materials depending on the type of material, its application, its geometry and the end properties desired. Some of these conventional techniques are:

1) Salt Bath Cyaniding.
2) Salt Bath Nitriding or Liquid Nitriding.
3) Salt Bath Nitrocarburising.
4) Gas Carburising.
5) Gas Nitriding.

The above techniques have been in use over several decades. However recent developments have involved commercial exploitation of plasma nitriding.

The process of plasma carburising holds equally good promise but is at the development stage though in the USA equipment is commercially available (2) and in use.

The process of nitriding is basically used when it is required to heat-treat components below AC1 temperatures thereby not causing any metallurgical changes in the material structure and hence providing high dimensional stability as compared to the carburising process which normally requires the components to be heat-treated in the austinitic range. Among the most popular techniques of nitriding are:

1) Gas Nitriding.
2) Liquid Nitrocarburising.
3) Plasma Nitriding.

1.1. Plasma Nitriding.

The process was originally established in Germany by Bernard Berghans (1) in the early 1930's, following which there was much fundamental research concerned with establishment and control of glow discharges from high currents. The research work was then shifted to metallurgical aspects of the process (3), such as the properties of the nitrided layers produced and how various types of materials responded to this treatment.

The basic research led to rapid growth in the commercial development of this process, when it became evident that this process promised several advantages over the other conventional processes.

As mentioned earlier, many types of media are used in the nitriding process such as: liquid nitriding, gas nitriding or even solid nitriding (pack nitriding). In addition to these three states there is a fourth, more active one, known as the plasma or ionic state. Nitriding under this state is termed plasma or ionitriding.

1.1.1. Principles of the Process.

When a D.C. Voltage is applied between an anode and a cathode in a low pressure atmosphere containing nitrogen, a glow discharge is produced and the nitrogen is ionised and impinges on the cathode surface. The minimum voltage required to initiate and maintain the glow is a function of the treatment gas pressure, the nature of the gas, the distance between the electrode and their size, shape and material (4). With the minimum potential difference between the electrodes, the molecules and atoms of the treatment gas are excited and are ionised to form a conducting medium. The current flow consists of two species (5),

negatively charged electrons moving towards the anode, and positively charged ions moving towards the cathode. The ions bombard the cathode surface with considerable kinetic energy, a part of which is converted to heat, sufficient to raise the components to the required nitriding temperatures. Thus, in principle the system does not require any external heating source.

1.1.2. Glow Discharge.

The phenomenon of the low pressure glow discharge is well established in physics. Understanding of this principle is important for its successful application to plasma nitriding.

The dependence of potential on currents for various kinds of discharge between the electrodes is shown in Figure 1. When the potential difference is applied between the electrodes, the electrons which are randomly drifting between the electrodes will be attracted towards anode. By virtue of their motion, they produce ions and also excite molecules and hence photons. This ionisation occurs in random bursts and is unstable. As the current is further increased, photons striking the cathode will release electrons which by further collisions will travel to the anode and at this stage the current becomes self sustaining. A discharge of this type is called Townsend or dark discharge and the voltage at which this can occur is called the break down voltage V_B.

In this region the current can be considerably increased with no change in the potential between the electrodes. If the current is allowed to increase further (upto 10^{-4}amps.) two striking effects are observed. Firstly the glow becomes faintly visible with light and dark spaces arranged between the electrodes. Secondly potential across the electrodes drops considerably. This is the region of glow discharge and is of major

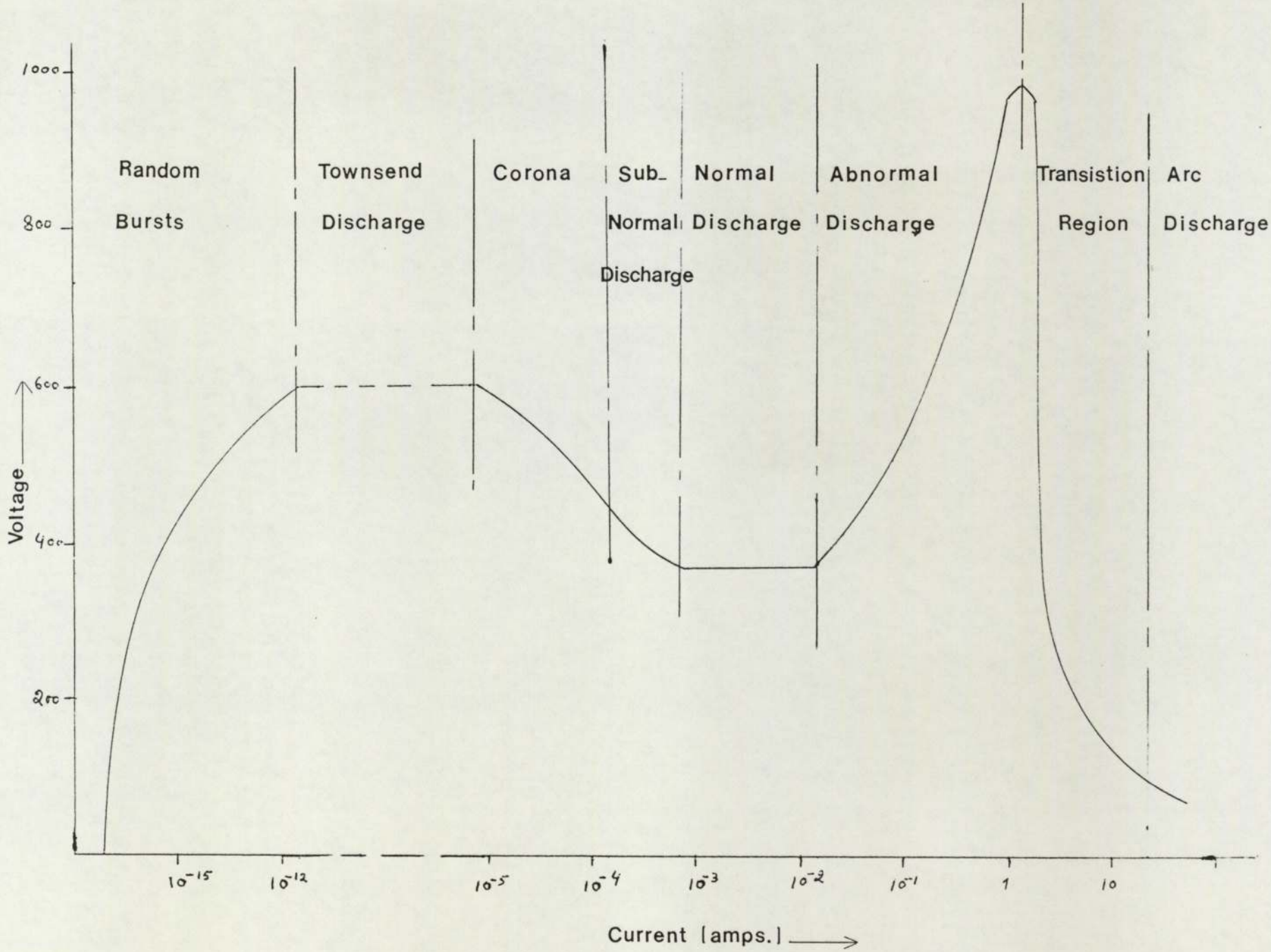

FIGURE-1 Voltage-Current Characteristics of Different Types of Discharge

importance to the nitriding process.

In the NORMAL discharge region it can be seen that the discharge only covers part of the cathode, the area covered being propotional to the current density. Most of the research on the phenomenon of the glow discharge appears to have been carried out in this region. For example, the industrial uses of this glow discharge include glow lamps and fluorescent tubes.

As the current is increased the glow envelops a larger area of cathode while the current density remains constant. When the cathode is completely covered, a further increase in current results in an increase in the potential across the discharge. This is called the region of ABNORMAL DISCHARGE and this is the region used for ionitriding. Any further increase in current causes the voltage to rise to a maximum and at large currents to break down to an ARC DISCHARGE.

In plasma nitriding in the ABNORMAL DISCHARGE region, the glow discharge tends to degenerate into an ARC DISCHARGE fairly easily. This can occur as a result of entrapped gases in work pieces, moisture, oxides and other contaminants on the surface. The heat of the process is sufficient to release such impurities resulting in the whole glow being concentrated into an intense arc. This could lead to overheating or localised melting, causing damage to work pieces. Consequently current density rather than total current governs the glow in this region of ABNORMAL DISCHARGE. This difficulty is normally controlled by using high speed switching circuitry (6) which extinguishes the current for a fraction of a second whenever an arc is formed. The recent developments in this field have given rise to usage of high frequency impulse current generators (2). It is claimed that these generators allow very high plasma energy levels with high voltage and low currents which thus effectively eliminate arc formation.

1.1.3. Regions of Glow Discharge.

Glow discharge for an abnormal discharge has various parts. Starting at the cathode the following parts exist (Figure 2) (6,7,8).

1) Aston or Primary Dark Space.

Aston or primary dark space is a very thin totally dark layer and is surrounded by the first cathode layer.

2) First Cathode Layer.

The first cathode layer is a thin layer of feeble light and may be followed by another dark space bounded by further cathode layers.

3) Cathode Dark Space.

The cathode dark space (also called CROOKES or HITTORF dark space) is usually taken as the whole region between the cathode and the negative glow and thus includes the cathode layers and dark spaces. This region is also reffered to as the "Cathode fall" since most of the potential drops in this region.

Staines and Bell (8) attribute this to the different rates of movements of the charged particles within the vacuum chamber, with heavier positive ions moving to the cathode more slowly than the electrons moving to the anode. Consequently virtually the whole voltage drop occurs in this zone, only a few millimeters from the cathode surface. Consequently, the positive charge density is a maximum in this zone. Since this is the most important region, it will be discussed in more detail later.

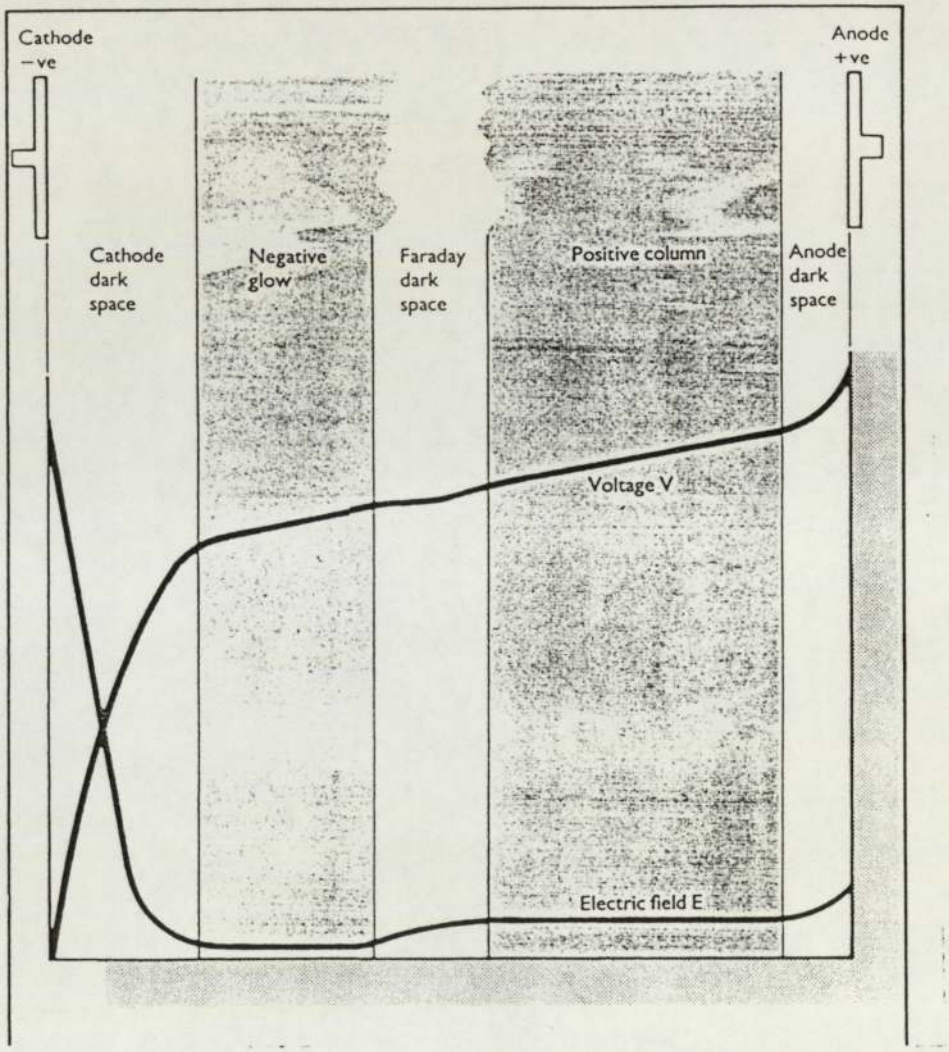

FIGURE-2 Zones Involved in Ionisation

4) The Negative Glow.

This is the most luminous zone. The colour of discharge is characteristic of the treatment gas. This also has a distinct boundary with the cathode dark space but is diffused on its anode side where it merges into the FARADAY dark space.

5) Faraday Dark Space.

This zone is relatively dark and depends on the gas used. it's size also depends on the size of the chamber being wider in large furnaces.

6) Bright Column.

The positive long bright column fills the rest of the furnace with its colour which is characteristic of the gas used but is neither the same colour as the negative glow nor is it so bright.

7) Anode Dark Space and Glow.

A thin dark space at the end of the positive column and a glow on the surface of the anode may be observed. At high current densities this glow may break up into a series of bright rings or spots. These spots are very sensitive to the presence of impurities. Their arrangement is explained by the minimum principle (9). In this particular arrangement the necessary current is conveyed to the anode by the least applied potential, hence these are the function of the cathode/anode shape and are the points where the potential is likely to breakdown to an arc discharge.

In summary, the plasma state of the treatment gas is only produced within the cathode fall region. This is where all the collision and ionisation occurs.

1.1.3.1. Cathode Dark Space.

As explained above, this zone has high electric field strength, positive charge and current density. Under favourable conditions most of the applied potential can be developed here. This potential is called Cathode fall.

An increase in the treatment gas pressure causes all the negative regions to be compressed towards the cathode, whereas a decrease in pressure has a reverse effect. The development of a relationship between abnormal cathode fall, treatment gas pressure and current density is attributed mainly to Guthersultze (10) and his associates. The abnormal cathode fall has been measured for various current densities greater than NORMAL. From this an empirical relationship has been developed (11) as shown below:

$$J/P^2 = A V_c^B \text{ ----------(1)}$$

J = Current Density

P = Treatment Gas Pressure

V_c = Abnormal Cathode Fall

A&B = Constants

The cathode geometry also plays an important role. Very early experimental work by Little and Von Engel (12) has shown that electrons in the cathode dark space behave very much like a beam directed normally away from the surface. For example, when two cathodes are placed facing each other, the beam from each other would be directed in opposite directions and the negative glow would coalesce. A cathode which has a hole behaves in a similar fashion, with both the diameter and the length of the hole

affecting the discharge, which is called "Hollow Cathode" or "Schuler Discharge". The current density increases for a given gas condition (i.e. pressure P) with decreasing cathode separation "a".

With their electron beam technique, Little and Von Engel (12) developed an empirical relationship for small cathode separation, as given below:

$$J/P^2 \propto (1/aP)^{5/2} \text{ ----------(2)}$$

The "Hollow Cathode" effect can be easily interpreted physically, by reducing the separation between cathodes, the cathode dark space is compressed, and since the cathode fall voltage V_c is maintained, the field gradient becomes steeper and ion density rises. As a result, ion velocity and kinetic energy are increased. In the region of a hollow cathode, increased cathode sputtering and high localised temperatures can be expected (13).

The experimental work carried out by Dixon (14) shows that in order to avoid hollow cathode effects, the work pieces must be arranged in such a way in the furnace so that the product of treatment gas pressure and spacing of the work piece is greater than 20mm-torr.

1.1.4. Reaction Kinetics.

As has been mentioned earlier, the plasma state is induced by ionisation of gas. The energies of the ions and electrons in the cathode fall region are extremely high and have kinetic energies ranging from a few to several hundred electron volts, depending on the voltage applied and the number of particles available (6). Reaction kinetics are explained by the following equation:

$$E_{ion} = A + E_{kin} + Q$$

The ion energy is converted into work(A) to detatch atoms and electrons from the metal surface and into kinetic energy of the detatched particles (E_{kin}). The remaining energy is converted into heat(Q). This gives rise to what is called "Sputtering Action".

Spectrographic analysis (15) has shown that the sputtered material has the same composition as the cathode material. The rate of ejection increases with the energy of impact of the bombarding ions. The sputtering rate also depends on the cathode material. Thus with sputtering, metal particals are displaced from the surface of the work pieces by these high velocity ions. Non-metallic elements such as carbon, oxygen and nitrogen may also be sputtered off.

The surface conditions of the cathode also has a marked effect on the sputtering rate. The stable oxides on the cathode surface reduce the rate of sputtering but once these have been removed, sputtering increases greatly. Surface impurities always reduce the sputtering rate.

Gunter Schluze (10) developed an empirical relationship between the material sputtered per second (M), cathode fall voltage (V_c), pressure (P) and the distance between the parallel plates (d).

$$M \times P \times d = \text{Costant} \times V_c$$

The constant is a function of cathode material, cathode temperature and mass of bombarding ions.

Theoretically sputtering is due to evaporation from the small local regions on the cathode surface where the impact of ions produce for a short time a very high temperature (several thousand degrees). It may be noted here that only the atoms with high velocity actually escape and

the majority of these are recondensed back on the surface.

Hanau (15) observed a different type of sputtering in abnormal discharge and suggested that an increase in alloy content in the material can result in an increase in sputtering rate.

Sputtering results in cleaning of the surface of the material and removal of any oxide layer. This is very important for the treatment of steels of the stainless type which have passive oxide layers on the surface which need to be removed by mechanical or chemical treatments before any nitriding can take place in most other conventional processes. Whereas when plasma nitriding stainless steel such expensive treatments could be eliminated.

As this research work will show even under the conditions of plasma nitriding, there are certain rigid requirements on the furnace parameters such as purging and gas conditions which can result in only partial depassivation of the stainless steel surface causing lower than expected hardness of the surface.

1.2. Gas Nitriding.

Gas nitriding is a well established process. Present day gas nitriding is carried out in a vertical pit type furnace or in a bell type furnace. The treatment is carried out in this gas tight retort or inner chamber in an ammonia gas atmosphere. The ammonia is either cracked outside with a special unit or fed into the furnace directly from gas bottles and is allowed to crack in the hot inner chamber. Normally nitriding is carried out in the temperature range of 500°C to 575°C (16).

At nitriding temperatures ammonia catalytically dissociates on contact with the hot steel chamber, allowing nascent nitrogen to be liberated during dissociation. The reaction kinetic (17) is shown below.

$$NH_3 \rightleftharpoons 3/2\ H_2 + [N]$$

$$\text{Hence} \quad [\%N] = K \times P_{NH_3} / (P_{H_2})^{3/2}$$

Where,

K is the equilibrium constant at a given temperature and P_{NH_3} and P_{H_2} are the partial pressures of ammonia and hydrogen, respectively in the gas. When pure ammonia is introduced into the furnace it decomposes to some extent at the surfaces and if a fraction (X) has been dissociated then,

$$P_{NH_3}/P_{H_2}{}^{3/2} = [(1-X)/(1+X)] \times [(1+X)/3X/2]^{3/2}$$

Normally the composition of the furnace atmosphere is expressed as a fraction (1-Y) of ammonia plus a fraction (Y) of fully dissociated

ammonia as determined by the exit gas composition.

$$P_{NH_3} / (P_{H_2})^{3/2} = (1-Y)/(3Y/4)^{3/2}$$

When the nitriding potential of gas mixtures is such that the concentration (strictly the activity) of nitrogen in iron exceeds that in equilibrium with iron nitrides $\gamma' Fe_4N$ or epsilon $Fe_2N_{(1-x)}$ (17) then these phases can form at the specimen surface. Figure 3 shows the equilibria for the reaction of ammonia with pure iron and the concentration of dissolved nitrogen in equilibrium with gas mixtures.

For alloy bearing steels, if the alloying elements such as Al, Cr, Mo, V, Ti, W, which interact with the nitrogen (18), are present then the rate of nitriding of the alloy depends on the strength of that interaction, ease with which precipitates can nucleate and grow, the concentration of alloying elements,the nitriding potential of gas mixtures and the temperature of the treatment. This is discussed further under "Diffusion Mechanism of Nitrogen" in section 2.1.

The nitriding of steels can be carried out in two ways (19).

1) Single Stage.
2) Double Stage or Floe Process.

In single stage process, a temperature in the range of about 495°C to 525°C is used, and the dissociation rates range from 15% to 30%. This process produces a brittle nitrogen rich layer known as "White Layer" at the surface of the nitrided steel.

The double stage process, also known as the Floe process (U.S.A. Patent 2437249) has the advantage of reducing the thickness of white nitrided layer. The first stage of the double stage process is, except

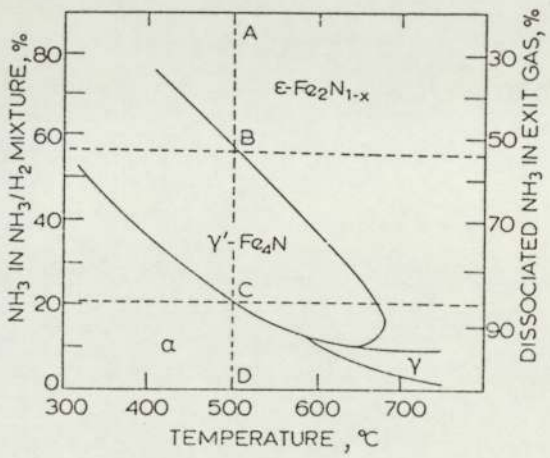

FIGURE-3 Equilibrium Diagram of Ammonia with Pure Iron

for time, a duplication of the single stage process. The second stage may proceed at the nitriding temperature employed for the first stage, or it may be increased to 550°C to 565°C. However, at either temperature, the rate of dissociation in the second stage is increased from 65% to 85%. Generally an external ammonia dissociator is necessary for obtaining the second stage dissociation.

There is no advantage in using the double stage process unless the amount of white layer produced on the surface in single stage nitriding cannot be tolerated on the finished parts.

As regards stainless steels (19), these are nitrided in single stage cycles at temperatures from 500°C to 575°C for periods ranging from 20 to 45 hours, depending on the depth of case required.

Gas nitriding of stainless steel (19) also requires prior surface treatment. The film of chromium oxide that protects stainless alloy from oxidation and corrosion must be removed. This may be accomplished by sand blasting, pickling, chemical reduction in a reducing atmosphere, or submersion in molten salts. If there is any doubt about the complete and uniform depassivation of the surfaces, further reduction of oxide may be done in the furnace by the means of a reducing hydrogen atmosphere. Hydrogen must be dry and free of oxygen.

To test the rigidity of the above conditions some trials were carried out during this research Project. The results are presented and discussed in sections 6.0 and 7.0.

1.3. Salt Bath Nitrocarburising.

Salt bath nitrocarburising is a liquid nitrocarburising process. The basic process involves the treatment of components in a cyanide and cyanate bath containing the salts of sodium and potassium. There are

a number of cyanide nitocarburising treatments in use. Though there are only two main treatments, of which all other processes appear to be minor variants. These patented processes have the trade names Tufftride, also called Tenifer and Sulfinuz. For the purpose of this research, the Tufftride process was used.

The Tufftride processs is also known by several other alternative names such as mild nitriding (21), activated nitriding (22) and aerated bath nitriding (23). The basic equipment for Tufftriding consists of a pit type pot furnace with resistance heating. The pot is made from solid Titanium and surrounded by top exhaust hood for fume extraction. The aeration is carried out by an aeration tube also made from titanium. The salts used for the treatment are patented as TF2, TF1,TF1A and REG1. Originally TF1 salts were used which have a high percentage of cyanide and presently these have been replaced by TF1 and TF1A which carry low cyanide and presumably cyanate is the main constituent. The REG salt is normally used for replenishing the bath. The basic purpose behind aeration of the bath is to supply sufficient oxygen in the bath for the conversion of cyanide into cyanate.

The components are preheated to about 350^{o}C to 400^{o}C and then transferred to the nitrocarburising baths at 570^{o}C to 580^{o}C. At the treatment temperature, the Tufftride process is controlled by two reactions (22), the oxidation reaction and the catalytic reaction:

a) The oxidation of cyanide takes place at the salt/air interface, at the treatment temperature to give cyanate. In sodium bearing salts this can be expressed as:

$$2NaCN + O_2 \longrightarrow 2NaCNO$$

b) The break down of this cyanate takes place at the treatment temperature, producing carbon mono-oxide and nitrogen, which are the actual products which react with the steel surface to form a compound layer. For sodium bearing salts this can be expressed as:

$$4NaCNO \longrightarrow Na_2CO_3 + CO + 2N + 2NaCN$$

As a result of this treatment, a wear resistant, nitogen and carbon rich compound layer is formed on the surface of the component. The thickness of this layer (24) is typically in the range of 8-20 microns, depending on the material being treated and the process time, which usually is less than three hours.

Taylor (26) suggests that in alloy steels, the lower the content of the alloying elements, the greater the increase in fatigue resistance produced. This is because the alloying elements oppose the penetration of nitrogen resulting in more sluggish reaction. However, this does not preclude Tufftriding alloy materials but suggests longer cycles to achieve desired results.

The diffusion characteristics however are independent of the type of nitrocarburising media, whether salt bath or gaseous. This is disscused separately later.

For the Tufftriding of stainless steel, the normal cycle carried out is to treat the components at 580^{o}C for 90 minutes to 2 hours in TF1 bath folllowed by quenching in AB1 bath for 20 minutes at 370^{o}C and then water washed. AB1 (Patented) quenching salts are claimed to be designed for use with the Tufftride process as these baths destroy the low cyanide and cyanate content of the adhering salts during cooling in this bath (27) and hence render the effluent from washing non-toxic.

1.4. Post Oxidation Treatment.

The NITROTEC process has been developed by Lucas industries plc. (61). It is essentially a derivative of earlier gaseous nitrocarburising techniques, with the important addition of pre-quench oxidation treatment. Dawes et al (64,65) have shown that mixtures of ammonia and variety of carrier gases may be used to develop similar surface characteristics.

The initial nitrocarburising treatment is carried in an atmosphere of ammonia and a carrier gas at a temperature between 550^{o}C and 750^{o}C. On completion of this cycle, components are transferred to an oxidising atmosphere and held in it momentarily prior to quenching. As a result of this processing sequence a thin non-metallic oxygen rich iron nitride compound layer is formed on the component's surface beneath which is the nitrogen rich diffusion layer. This oxide rich iron nitride layer is claimed to be responsible for improvement in corrosion properties.

A recent further development of the NITROTEC process is a newly developed process called NITROTEC-S (62). It has been found that the ability to vary oxidation conditions, nitriding temperatures and potentials, are the key factors in increasing the scope of this process. It is very important to control precisely the length of the oxidising treatment. The depth of the oxide layer should not exceed 1.0 micron otherwise the surface may exfoliate during quenching. The optimum arrest time has been found to be between 2 and 20 seconds.

The protective nature of the oxide layer depends on two main factors (62). Firstly, how impervious the oxide is to the passage of metal ions and secondly, how well the oxide adheres to the treated component's surface. It has been suggested recently (63) that oxide/nitride misfit is less than the metal/oxide volume misfit i.e. an oxide film on treated components will be more stable and less likely

to spall or exfoliate than the same oxide on metal.

As is known, corrosion resistance of plasma nitrided stainless steel drops considerably and is a major disadvantage. Though conditions prevailing under ionitriding are different from those under normal nitrocarburising treatments, this research work carried out the post oxidation treatment to develop an oxide layer during quenching and studied the effects of this treatment on the corrosion properties.

2.0. METALLURGICAL ASPECTS OF NITRIDING.

Extensive research work has been done in the past on metallurgical aspects including diffusion mechanism, compound layer, phase and structures and diffusion layer formation.

2.1.0 Diffusion Mechanism of Nitrogen.

Earlier it was believed that (28) ionitriding was solely due the occlusion of ions into the iron lattice by ion bombardment. However Kolbel (3) and Tibbetts (30) showed, and it is now generally believed, that the nitride case is formed by a nitrogen rich phase on the surface of the cathode, formed at the onset of ionitriding.

Attempts have been made to reduce the extremely long treatment times associated with conventional gas nitriding by accelarating the process of nitrogen occlusion. It has now been established that ionitriding considerably reduces the time of nitrogen occlusion as compared to gas nitriding (6). However with increasing treatment time the difference becomes small as the process becomes diffusion controlled. It is important from the metallurgical point of view to know which factors contribute to the accelarated diffusion of nitrogen. The explanation remained inconclusive till Kolbe (3) published his findings. Thus, at the very onset of ionitriding process, the nitrogen rich phase (FeN) is condensed on the surface of the work piece. Its immediate disintegration liberates nitrogen which diffuses in the work piece.

In gas nitriding, the surface concentration of nitrogen is established gradually. Jindal (4) suggests that for a given temperature, conventional gas nitriding requires an incubation time for the formation of a surface layer of iron nitride whereas with plasma nitriding a

constant level of nitrogen is reached immediately due to the most important factor of sputtering and recondensation under plasma conditions. For precisely these reasons the classical nitriding processes as pack, gas and salt bath nitriding can not be used below 500°C due to their strong dependence on temperature for the amount of nitrogen being supplied by various nitrogen carrying media (31). Thus making low temperature nitriding difficult and therefore a higher temperature of 570°C is necessary which causes problems in practice because not all types of steels are suitable for heat-treatment at this temperature. Whereas in the ionitriding process the nitrogen potential, being independent of temperature of the charge, can be carried out even at temperatures as low as 350°C.

As explained above, the FeN iron nitride which is condensed on the surface of the cathode (work piece) and resulting in high concentration of nitrogen yields a concentration gradient which is very steep at the begining. Experimental results (6) show that it is only after treatment times of 10 hours and more that the nitrogen penetration in ionitriding no longer progresses at a faster rate than in gas nitriding. From this it is obvious that the increased concentration gradient alone cannot be responsible for the accelarated diffusion rate.

Experimental work carried by Noren and Kindbrom (66) on gas nitriding and on ionitrided specimens showed that the diffusion of nitrogen in the first stage of the gas nitriding process mainly occurs on the grain boundries. This is understandable, considering that the catalytic dissociation of ammonia gas on the surface of the steel would occur preferably in the areas of high energy. In intercrystalline diffusion, the nitrogen contacts the carbide phases in the grain boundries. Due to occlusion of nitrogen in carbides these tend to grow considerably and are, at the same time converted into carbonitrides. For

this reason the intercrystalline diffusion of nitrogen in gas nitriding (characterised by the formation of finely dispersed nitrides) is retarded.

However in ionitriding the nitrogen is found to undergo transcrysalline diffusion from the start. This effect is due to the even condensation of iron nitrides from the plasma on the entire surface of the material, allowing a plane diffusion front to enter the whole material (6). Furthermore, controllable partial sputtering of the carbon from the surface and the after diffusion of carbon, mainly along the grain boundries, cause something like decarburisation of grain boundries in the area close to the surface, so that those nitrogen atoms which diffuse along the grain boundries cannot form any carbonitride phases which could inhibit further diffusion.

As seen, two essential factors of the accelarated diffusion of nitrogen in ionitriding are the high surface concentration of nitrogen which is of particular significance at the begining of the process, and the increased rate of nitrogen penetration due to a different diffusion mechanism.

The nitriding of steels containing alloying elements is much more complex. The effect of substitutional alloying elements on the behaviour of nitrogen in iron is also different at different temperatures (33).

At temperatures where the substituent atoms move readily through an iron matrix, they will combine with nitrogen to precipitate metal nitrides. In many binary metal-nitrogen systems, there are several nitrides, for example CPH Cr_2N and FCC CrN in the Cr-N system and FCC Mn_4N, CPH Mn_5N_2 and FCT Mn_3N_2 in the Mn-N system. These have different relative stability, so that the equilibrium precipitate will depend on the variables of the system i.e. the temperature, the activities of two solutes and other thermodynamic factors.

At very low temperatures (350^{o} C or below) at which the alloying elements are virtually unable to move at all through the matrix, only the iron nitrides can be precipitated from the nitrogen super saturated solid solution. Despite this the substitutional solutes have a marked effect because they either increase (Si, C) or decrease (Ti, V, Nb, Ta, Cr, Mo, W, Mn) the activity coefficient of nitrogen in iron and also the size and distribution of iron nitrides.

Free energy plots of chromium nitrides Cr_2N and CrN show that below 575^{o}C CrN is always more stable than Cr_2N and is hence precipitated and also that only above 14% wt-%Cr, even at high temperatures, is Cr_2N obtained. In Fe-Cr alloys the nitride produced depends not only on the chromium ion concentration and temperature but also on the nitrogen potential (33). Using NH_3/H_2 mixtures the precipitates is always CrN but under similar conditions with N_2/H_2 both nitrides may be precipitated, lower Cr_2N being observed at higher temperatures and in the higher chromium alloys.

For austenitic grade, the phase has FCC structure. This provides a suitable matrix which with even small additions of (strong) nitride formers like Ti, V, Nb and Mo can be constant activity nitrided at 400^{o}C-800^{o}C, to give homogeneous precipitation. It may also be noted that diffusion in FCC is slower than in BCC (ferrite) metals, as research done by Fast & Verrij (34) show. They show that at 540^{o}C diffusion coefficient of nitrogen in iron has already surpassed that of nitrogen in γ iron at 950^{o}C. At 950^{o}C extrapolated value in α iron is 50 times more than γ iron. They also found analogous phenomenon for interstitial diffusion of carbon.

When there is strong interaction between nitrogen and substitutional solutes, nitriding proceeds by the formation of a hard subscale, thickness of which increases progressively. The depth (d) of the

sub-scale varies with time according to (17):

$$d^2 = 2.D.t.[N] / r.[X]$$

where,

[N] is the surface nitrogen concentration (at. %).

[X] is the original alloy element concentration (at. %).

r is the ratio of nirogen to alloying element in the nitriding phase.

D is the diffusivity of nitrogen.

Implication of this is that the higher nitriding rates can be achieved by increasing the surface nitrogen concentration.

The formula also shows that the square of subscale thickness is inversly proportional to the alloy concentration. The increase in hardness is roughly proportional to the square root of the alloy content. Therefore in a given nitriding time, the material with high alloy content compared to low alloy content would give lower case depths but higher hardness. This relationship is true for titanium, molybedenum and high chromium bearing materials.

It has been observed (17) that depending on chromium concentration, iron chromium alloys can show nitriding responses characterstic of strong or weak interactions. The critical solubility product for nucleation of homogeneous precipitation, K_s = [%Cr][%N], is higher than TiN but not as high as the nitride phase in Fe-Mo alloys, where [%Cr] is chromium concentration and [%N] is the concentration of nitrogen for the homogeneous precipitation of alloy nitrides.

It has also been shown (17) that the diffusiveness of the interface, is proportional to Ks/[%Cr][%N], where [%Cr] is the original chromium concentration and [%N] is the surface nitrogen concentration. Thus as the temperature of nitriding is increased, the value of Ks will increase and with it the diffuseness of the interface. With increasing nitrogen surface concentration and increasing alloy content, the boundary will become sharper. This in turn will affect the mechanical properties of nitrided components due to sharp case/core interface.

In summary, nitriding of ferrous alloys involves the interaction of one or more substitutional solutes with interstitial nitrogen. This interaction is different for different treatment temperatures. At temperatures as low as 350^{o}C substitutional atoms are almost immobile, but because they change the activity coefficient of nitrogen in iron, their effects on the amount, the particle size and the rate of precipitation of iron nitrides from the supersaturated solutions are marked.

For the reasons explained above this present research work on plasma nitriding was carried out at low temperature and effects on corrosion and wear properties of stainless steel were studied. The corrosion behaviour was of particular interest since high corrosion resistance of austentic stainless steels is normally associated with the presence of chromium in the iron matrix.

2.2 Compound Zone.

With nitrogen or nitrogen-hydrogen mixtures, treatment is carried out essentially according to binary Fe-N system (35). However with hydrocarbons added to the gas mixtures, the layers develop according to the ternary Fe-C-N system (36) (Refer Figures 4 and 5).

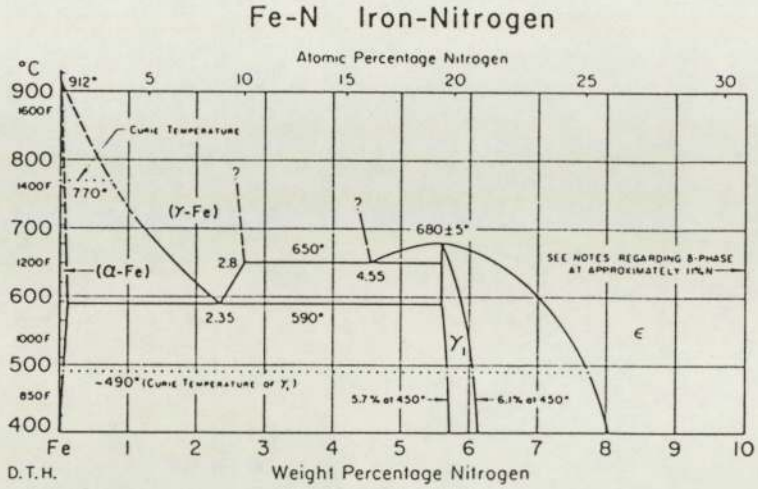

FIGURE-4 Iron-Nitrogen Phase Diagram

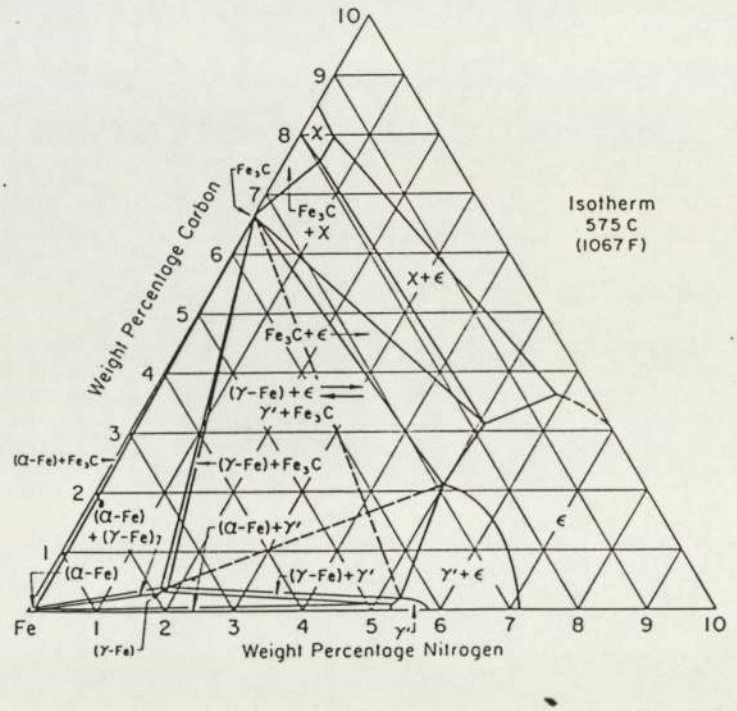

FIGURE-5 Iron-Carbon-Nitrogen Phase Diagram

Comprehensive investigations with regard to ductility, wear resistance to rolling friction etc., have shown that the usefulness of the compound layer depends mainly on two factors (6): Homogeneity of the nitrided structure and the thickness of the layer. With regard to homogeneity of the nitride structure, mechanical properties have been found to be considerably better if the compound layer consisted of one nitride phase only i.e. either γ' or epsilon nitride. In polyphased compound layers consisting of a homogeneous mixtures of γ' & epsilon phases, there are high inherent stresses in the transitional regions between the different lattice structures(γ' is FCC and epsilon is hexagonal) which may give rise to microcracks under even slight external stress. The brittleness of the compound layer produced by gas nitriding (always polyphased γ' plus epsilon) and the less brittle compound layer of Tufftrided components (exclusively epsilon nitride) confirm the influence of layer homogeneity.

As far as the thickness of the nitride layer is concerned, it is known that the ductility of the layer decreases with increasing layer thickness.

Based on these two factors, the optimum properties would be produced when the compound layer is monophased and of the minimum thickness necessary to meet specific property requirements, such as wear and corrosion. Plasma nitriding with careful control of the process parameters could meet this requirement.

The structure of the compound layer in ionitriding is mainly determined by the carbon content of the plasma (6). In carbon free plasma only the γ' phase can be obtained in accordance with Fe-N system. The epsilon nitride or epsilon carbonitride will prevail however, when the plasma is enriched with carbon. The exclusive build up of the epsilon

phase is due to the restriction of the γ' phase field in Fe-C-N system, with increasing carbon content.

The compound layer formed under Tufftriding treatment shows the presence of a variety of carbon and nitrogen based phases (22). A systematic study of cyanide nitrocarburising treatment by Mitchel and Dawes (22) indicated that the best anti-scuffing properties were obtained for Tufftride treatments when the compound layer consisted mainly of a close packed hexagonal phase of variable carbon and nitrogen concentration. The study of ternary Fe-C-N shows that the phase in question is epsilon carbonitride phase. They also claimed that the epsilon phase was predominant, within the compounded layer. The presence of small amounts of other phases, particularly Fe_4N and Fe_3C had no adverse effects on anti-scuffing behaviour.

These findings were confirmed by Neustroer and Bogdanov in 1970 (37). Their work showed that after a 3 hour treatment, a conglomerate of phases of epsilon carbonitride $Fe_3(NC)$, Fe_4N and Fe_3C was observed and with increasing processing time the intensity of Fe_4N lines become weaker. Also, with over 2% carbon and 6% nitrogen, the layer had a two phase structure-$Fe_3(NC)$ and Fe_3C. However, in alloy steels the formation of carbonitrides is slowed down and hence the greater the alloying elements, the wider the range of permissible cyaniding conditions.

A high level of oxygen within the compound layer of Tufftrided components has been reported by Prenosil (38). However the role that oxygen plays is that of promoting the cyanide to cyanate reaction and whether this reaction is essential for improved mechanical properties has not been established. Work carried out on ionitriding by Edenhofer (6) shows that sputtering plays an important role in controlling the thickness of the compound layer. Depending on the intensity of sputtering, other

factors, such as temperature and time, may also be more or less important for the growth of a compound layer. In the extreme case intensive sputtering (i.e. high voltage) no compound layer at all will be produced even with the long treatment times.

The growth of a monophase γ' compound layer, reaches 6-8 microns after about two hours, then remains constant. This phenomenon of the limited thickness of γ' layer could be due to the narrow composition range of this phase, only about 0.4% nitrogen, resulting in a concentration gradient which is too flat to induce further growth of the layer beyond 8 microns.

In a similar way, the thickness of a compound layer of epsilon phase can be varied between 6 microns to a maximum of 50 microns by variation of sputtering rate. Edenhofer also claimed that a thickness of less than 6 microns can also be obtained by ionitriding in a plasma containing addditional carbon which gives rise to to a compound layer containing Fe_3C and epsilon nitride.

For the same layer thickness it has been found that the γ' phase appears to be somewhat softer than epsilon phase. It is apparent that the high ductility of the γ' phase may be explained by the fact that the face centered cubic lattice of this type of phase offers better gliding plane conditions than the hexagonal lattice of the epsilon phase.

2.3. Diffusion Zone.

Parameters for the formation of a diffusion layer can be considered in the same way as the compound layer. The extent of surface hardening and embrittlement are of main importance for mechanical properties. Hence the main requirements that should be fulfilled by a nitriding process would be optimum hardening of the diffusion zone by the

precipitation of the alloy nitrides (or iron nitrides) during nitriding and the possibility of a small loss of ductility by the prevention of embrittlement phenomenon.

Good hardening of the surface of the alloy steel is obtained by means of finely dispersed precipitates of alloy nitrides. If the iron lattice contains sufficient dissolved alloying elements capable of giving rise to formatin of nitrides such as Al, Cr, Mo, Ti, V etc., their precipitation is governed by the type of alloying element, supply of nitrogen and the nitriding temperatures. As explained earlier, due to condensation of FeN on the surface of the material, the nitrogen contents of the iron lattice near the surface is very high in ionitriding and hence the high intercrystalline nitrogen diffusion (6). The process also provides the flexibility to change the nitrogen content by varying the composition of treatment gases.

The treatment temperature influences the solubility of nitrogen in the iron lattice as explained earlier. According to Edenhofer (6), optimum nitriding temperature for carbon steel is beween 550^{o}C to 580^{o}C.

Regarding alloy steels, the kinetics of precipitation of alloy nitrides is also dependent on treatment temperature. According to Edenhofer (31) for tool steels and medium carbon alloy steel, the maximum hardness is obtained at 450^{o}C treatment temperature and suggests that the temperature range of 400^{o}C to 500^{o}C for ionitriding. He also claims that after treatment at 550^{o}C and above, there is a considerable drop in the hardness of the diffusion zone due to the precipitation of coarse nitrides at high temperature. Furthermore for nitriding grade steels, there is additional loss in ductility caused partly by the precipitation of carbonitrides along former austenitic grain boundries besides the normal decrease in ductility of the material due to its

elevated yield point due to nitriding. The brittleness of carbonitrides could give rise to micro cracks and thus initiate fatigue failure.

Such carbonitride precipitates are typical of gas nitrided steels and to almost the same extent after bath nitriding claims Edenhofer (6). His work shows that in ionitriding in carbon free gas and at a high rate of sputtering these characterstic grain boundry precipitates could be supressed in the outer regions of the diffusion zone to a distance of about 80-150 microns. The reason for the supression is the partial sputtering of carbon which gives rise to decarburisation at the surface of the material and prevents the formation of carbonitrides, and nitrogen which is occluded simultaneously with the removal of carbon, will stabilise the stucture to a great extent. Hence the total effect cannot be compared with decarburisation followed by conventional nitriding which results in unfavourable mechanical properties.

During any ferritic nitrocarburising treatments (24) such as Tufftriding, only the nitrogen diffuses inwards from the carbonitrided compound layer. This is because nitrogen is more soluble than carbon in ferrous materials and diffuses into the work while carbon forms carbonitrides near the surface (26). There is more nitrogen available in the bath than can be absorbed and held at the surface in a compound zone, it begins to diffuse further into the matrix of the material being treated.

In alloy steels, the depth of diffusion zone decreases as the level of nitride forming elements in the material increases due to the fact that the alloying elements oppose the penetration of nitrogen, resulting in a more sluggish reaction. Astley (39) found that the layers formed, on salt bath nitriding of stainless steel, however have totally different appearance and characteristics from that produced on other materials.

In summary, together with the treatment time, the alloy content and the nitriding temperatures, are responsible for the depth and hardness of the diffusion zone.

3.0. WEAR.

3.1. Wear Mechanism.

Wear may be defined as unintentional removal of material from rubbing surfaces. Whilst this definition appears quite simple, the actual causes of wear and the mechanisms involved are far from simple. Wear includes such diverse phenomena as abrasion, adhesion, surface fatigue and corrosion. In any particular instance of wear there may be any of these mechanisms either operating singly or in combination.

The present research work however is restriced to the study of abrasive and adhesive wear or scuffing and gouging effects after performing three different surface treatments on stainless steel i.e. plasma nitriding, gas nitriding and salt bath nitrocarburising.

Adhesive wear is the form of wear which always occurs when two surfaces are in sliding contact. It is often called frictional wear since it arises from the same basic mechanism as friction that is from welding and subsequent shearing of minute surface asperities.

The adhesion (welding) arises in the following manner (40). When two nominally flat surfaces, no matter how smooth are brought in contact, they will touch at a relatively few isolated points. This is because even the most finely machined, or even polished surfaces are very rough on a molecular scale. These small areas carry all the load between the two surfaces. Hence because of the very small size of the true area of contact, even under small loads, the local pressures are very high and usually exceed the yield point of the material in contact. The high local pressures and plastic deformation cause minute welds to form at each of the local contact areas. When relative movement occurs, these welds are sheared. Whilst they may shear at their original contact,in general,

welds are stronger due to work hardening, than the softer of the two base materials with the result that the shear occurs not at the original surface but in the softer of the two materials. The net result is that the softer material is transferred to the other (harder) surface. From this it would appear that all the wear transfer will be from the softer material. In practice most of the wear does come from it but by no means all. This suggests that in hard materials there are some regions of low strength balanced by regions of high strength in the softer materials.

The amount of adhesive transfer is profoundly affected by the nature of surfaces and the ambient conditions (40). Cleanliness of the surface greatly facilitates adhesive wear. For example, in vacuum, especially if the surfaces have been heated to drive off any adsorbed films and oxides, they will adhere strongly under very low pressures. Any oxide or adsorbed films, such as water vapour, oxygen, etc. reduces this tendency.

In general high temperatures increase adhesive wear because welding on an atomic scale is invariably increased at high temperatures. As the melting point of the material is approached, then the adhesive welding becomes more and more severe until the point of gross transfer - scuffing or seizure is reached; hence low melting point materials in general show greater tendencies towards scuffing and seizure than high melting points ones.

In many instances, the temperature in question may be generated by the frictional heat. This is often a self-regenerating process in which the initial adhesive transfer of material produces a "high spot" on the surface which increases friction and thus the rate of heating and temperature rise. This leads to greater transfer which in turn raises the temperature. If this process continues, it can lead to large scale welding so that severe damage to the surface is caused, this is the state

of scuffing and ultimately seizure.

So far it has been assumed that all the material removed from one surface is transferred and adheres to the other surface. In fact it may become detatched from the other surface as a result of further motion or because the particles may have sufficient stored elastic energy to overcome the energy of adhesion.

The adhesive force between a particle and the body to which it adheres is proportional to the area of contact (40). On the other hand the strain energy within a particle is proportional to its volume. There is a critical size for particles below which they remain bonded to the surface and above which the strain energy of deformation within the fragments is sufficient to ensure their detatchment.

Eyre (42) states that the area of contact is inversely proportional to hardness and thus wear decreases with increasing asperity hardness. He also suggests that the transferred particles and wear debris may be work hardened and, in some cases, phase hardened and thus cause abrasive wear.

The delamination theory of wear (44) relates wear to dislocations near a surface. During a sliding process, many dislocations are generated in the contacting metals due to the general plastic and microplastic deformation of asperities, with a greater number of dislocations being generated in the softer metal. Among the dislocations generated, some of those which are closely parallel to the surface and located within a finite distance from the surface may disappear as soon as the free surface is exposed. This will be the case unless dislocations are constrained by the strong nodal points within the lattice. Therefore the dislocation density near the surface is always less than the dislocation density away from the surface. This means that the very surface layer cold works less than the sub-surface and thus is able to

undergo relatively large plastic deformation.

The thickness of the low dislocation density zone of the surface layer depends on the energy of the metal and the magnitude of the drag stress (frictional force) acting on the dislocations. Suh (44) suggests that this layer will be thicker for F.C.C. metals than B.C.C. metals.

de Gee (46) has also discussed the influence of crystal structure on wear. According to him close packed hexagonal lattice structures, for example, tend to become oriented with the (hexagonal) basal planes parallel to the direction of movement thus eliminating interlocking phenomenon. On plastic deformation of most crystal lattices (in particular cubic ones), extensive micro-roughing of the surfaces occur giving rise to saw tooth patterns which cause interlocking and block tangential motion quite effectively. With hexagonal lattice orientation parallel to the sliding surface, such saw tooth patterns do not occur. By addition of various alloying elements the crystal structure itself can be modified or the transition of the original metal from its hexagonal lattice structure to cubic crystal lattice can be delayed until higher temperatures are reached, thus producing anti-wear material. An example of this is the use of CoMo, CoW or CoCr compounds in the anti-wear materials, since the presence of these alloying elements shifts the transition point of cobalt (hexagonal to cubic), from a lower temperature to a higher temperature.

As the dislocation density builds up at the sub surface layers, cracks and voids can form. The rate of void formation may be increased when there are hard particles present in the metal, since the motion of mobile dislocations generated by the applied load may be blocked by these particles. When these hard particles are stronger than the cohesive strength of the matrix, cracks and voids can be nucleated under the stress of the dislocation pile ups. Crack formation around hard particles is

likely to be one of the most important mechanisms of void formation, since in most commercial grade metals, there are many hard particles such as oxides, borides, carbides and nitrides.

de Gee (46) suggests that lubricants are used to reduce adhesive wear by acting as a boundry lubricant. The term boundry lubricant implies that the conditions of load, speed and lubricant supply are such that the lubricant can exert its action only through its physical and chemical interactions with the contacting surfaces and not by the virtue of its viscosity (i.e. no hydrodyanamic lubrication effect). The lubricants on reaction with the metal form metal soaps. Such metal soaps function as low friction solid lubricants.

In summary, adhesive wear occurs by the removal of oxide debris from an oxidised surface supported on a work hardened substrate (42). Transition to severe wear is initiated by the break down of the protective surface oxide produced at low loads. Plastic deformation of the substrate occurs due to a higher bulk temperature and the wear rate increases considerably with the production of metallic debris. As the surface temperatures rise, this can give rise to phase hardening to produce a hard layer which prevents deformation and helps to establish an oxide layer once more. At this point wear rate is reduced considerably but is not as low as observed at the start. Thus the wear under adhesive conditions is subject to sharp transitions in behaviour unlike abrasive wear.

In the abrasive type of wear, the removal of solid material from a surface is accomplished not by its adhesion to the other surface and being pulled off, but by being ploughed or gouged out by a much harder surface or body.

The prime requirement for abrasive wear is that there must be a significant diffference in hardness between the sliding surfaces. Generally the rule follows that the abrasion resistance is proportional to

hardness. Elasticity is also important and ductile materials are more abrasion resistant than brittle ones.

Whilst lubrication (40) has been stated to be the most effective method of reducing adhesive wear, this is not so with abrasive wear. There are instances where abrasion is increased by the use of lubricant, for instance it may actually assist the cutting process by reducing adhesion on the hard materials. Further, the lubricant may induce loose particles between sliding surfaces or it may hold debris in that region, grease has this effect.

The only effective way of controlling abrasive wear is to use hard, tough materials and to exclude all foreign matter from between the sliding surfaces.

4.0. CORROSION.

4.1.0. Theory of Corrosion.

Corrosion processes are chemical reactions that takes place at the surface of a metal and obey well established chemical laws. The fact that corrosion is a surface reaction means that its progress may be controlled by the properties of corrosion products. The metal compound formed may act as a barrier between the environment and the metal, and the rate of corrosion of metal may be slowed down if the effectiveness of the barrier layer increases with the time. This is frequently observed in the reaction of metals with gaseous environment. If however the corrosion products can be removed from the site of reaction, the corrosion rate cannot be expected to diminish with time. This is the case when soluble corrosion products are formed by corrosion of certain metals in aqueous solutions. All metals are prone to corrosion attack if the environment is sufficiently aggresive.

Most corrosion phenomena are related to the break down of an oxide film on the metal surface. Metal surfaces exposed to clean, dry air are usually covered with a transparent oxide film that acts as a barrier against further reaction with dry air. When iron and steel are placed in an aggresive environment such as on aqeous solution of sodium chloride, corrosion is accompanied by a loss of air formed film, dissolution of substrate and deposition of precipitated corrosion products (58).

The passivity of the surface film depends on the metal and alloy composition (59). Stainless steel is a good example of this. This material builds up a highly protective film (mainly Cr_2O_3) on the surface of the metal and such materials resist attack by extremely corrosive environments provided small amounts of oxygen (or other

oxidising agents) are present in the solution to keep the film in good repair.

Evans (59) suggests that in an aggresive environment, in the case of thin invisible oxide film present on iron , the metal ions can probably pass through such films and cause reductive dissolution. If ferrous material is to resist a liquid , two conditions must be fulfilled:

1). Reductive dissolution must be avoided.

2). Fresh film must be formed at any weak place, which may arise.

According to Evans, the oxide film present on the surface of stainless steel contains both chromium and iron. When placed in acid the outer iron rich part of the film suffers reductive dissolution, leaving an inner chromium rich part undissolved. This is because, the reduction of Cr_2O_3 to Cr^{2+} would require very much lower potential than possible on simple immersion in acid. However this only shows that chromium in the film makes complete reductive dissolution difficult but if such a steel is to resist acid solution, some oxygen or oxidising agent must be present to ensure that at any discontinuity which may arise, the reaction will heal the discontinuity.

Townsend et al (57) studied the effect of various types of oxide films on steel surfaces exposed to chloride solution. According to them, the tendency of break down of air formed oxide film on ordinary steel is very high. Stainless steel undergoes localised break down, whereas titanium is resistant to break down.

In their experiment, they broke down air formed oxide films on steel surfaces by sputter etching follwed by deposition of other types of oxide films (Cr_2O_3, Al_2O_3 and TiO_2) by a sputter deposition

method. When exposed to chloride solution, these films showed initially more noble potentials than air formed films but the rusting of the type observed on steel with air formed film occured with all the oxide films. Thus sputter deposited films offer only short lived additional protection to the steel

Austenitic stainless steels are considered to be the steel most resistant to corrosion in industrial atmospheres and acid media (60). Besides chromium, addition of Mo (over 2%) promotes resistance to pitting.

The major disadvantage of nitriding austenitic stainless steel is the precipitation of chromium nitrides, thereby depleting the matrix of chromium and reducing its corrosion resistance.

4.2. Electro-chemical Theory of Corrosion.

According to mixed potential theory, any electrochemical reaction can be divided into two or more oxidation and reduction reactions and there can be no accumulation of electrical charge during the reaction. In a corroding system then, oxidation of metal (corrosion) and reduction of some species in solution is taking place at the same rate and the net measurable current is zero.

$$I_{MEAS} = I_{RED} - I_{OX} = 0$$

When a metal or alloy is placed in contact with a solution, the metal will assume a potential that is dependent on the metal and nature of solution. This open circuit potential i.e. no external potential is applied to the cell, is called the corrosion potential E_{corr}.

Mechanism of corrosion is more complex than a homogeneous chemical system as described above. The reason being, that in a corroding

system, not only may several different elements be present but several different compounds may also be present or formed.

In a simple corroding system containing Z and Z^+ at equilibrium,

$$Z^+ + e^- \rightleftharpoons Z$$

and $$I_{R,Z} = I_{O,Z} = I_{EX}$$

where,

$I_{R,Z}$ = current for reduction of Z^+.

$I_{O,Z}$ = current for oxidation of Z.

I_{EX} = Exchange current (analogues to I_{corr} in corroding system).

When a potential is imposed on the metal from an external source and the reaction rate is controlled by a slow chemical step that requires activation energy (54) then,

$$I_{R,Z} = I_{EX}e^{-n/B'}$$

$$I_{O,Z} = I_{EX}e^{n/B''}$$

where,

n = over voltage, the difference between the potential imposed on the specimen and the corrosion potential ($E_{APP} - E_{corr}$).

B',B" = constants.

Taking log of the above equations and solving for n, yields:

$$n = -B_c \log(I_{R,Z}/I_{EX})$$

$$n = B_a \log(I_{O,Z}/I_{EX})$$

where,

$$B_c = 2.3\ B' \text{ and}$$
$$B_a = 2.3\ B''$$

These are called Tafel equations and B_a and B_c are Tafel constants.

In a corroding system however, the situation is more complicated. Wagner and Trand (52) showed theoretically in 1938, that the polarisation curves for a corroding electrode, obtained by plotting the applied current against potential change, are linear at low values of potential change.

Stern and Geary (51) have provided a firm theoritical background for linear polarisation measurements and established the occurance of linear corrosion kinetics, experimentally.

$$M^+ + e^- \rightleftharpoons M$$

$$Z^+ + e^- \rightleftharpoons Z$$

where M is the corroding metal and Z is a specie in solution. The current potential relationship of such a mixed couple system is shown in Figure 6. The equalibrium potential of the couples in the above equations are

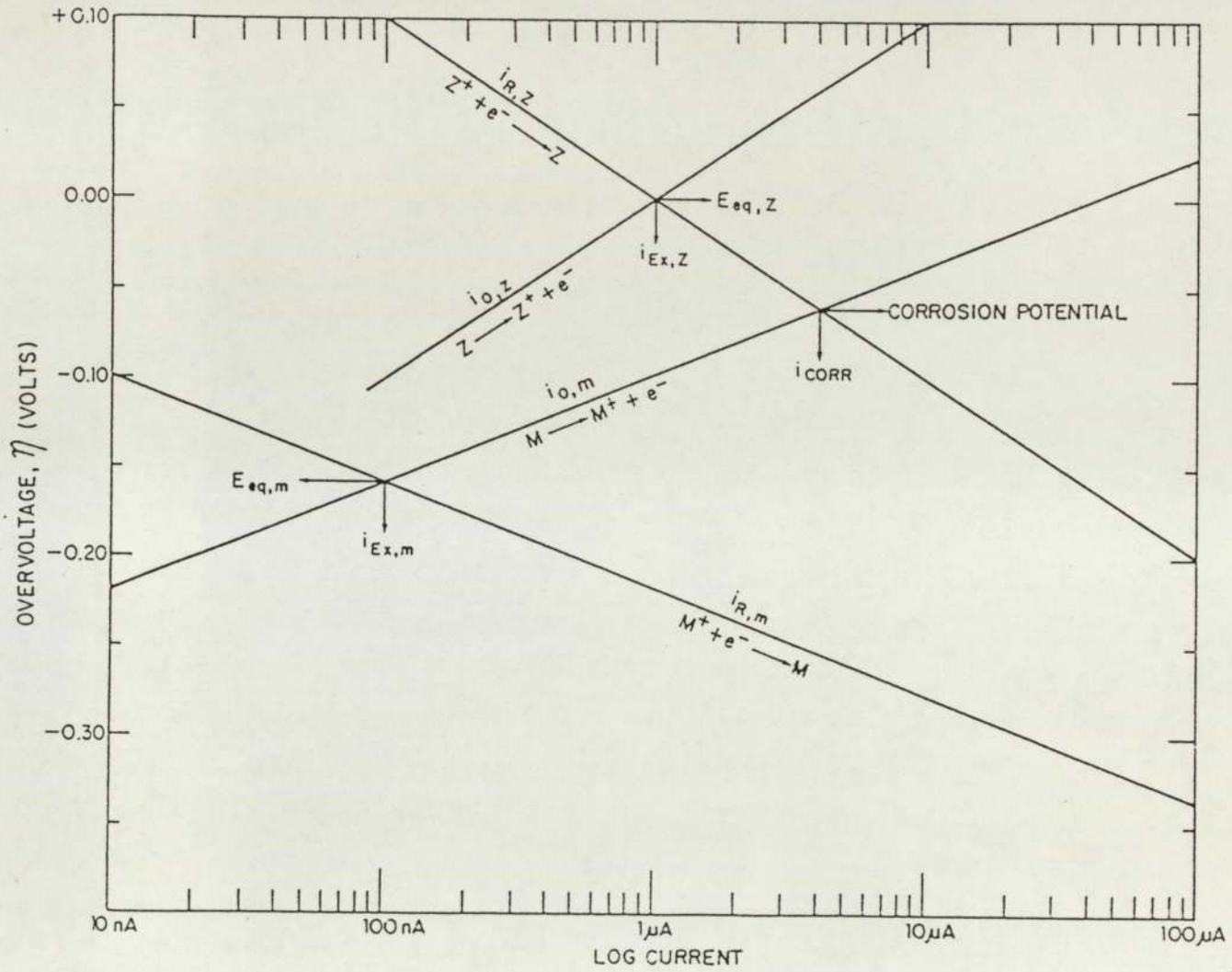

FIGURE-6 Potential-Current Relationship of a Mixed Electrode System

labeled $E_{EQ,M}$ and $E_{EQ,Z}$ respectively.

When the corrosion potential is sufficiently removed from $E_{EQ,M}$ and $E_{EQ,Z}$, the rate of reduction of M^+ becomes insignificant compared to rate of oxidation of M, and the rate of oxidation of Z becomes insignificant with respect to the rate of reduction of Z^+. The corrosion potential is the potential at which the rate of oxidation of M (defined by current $I_{O,M}$) is equal to the rate of reduction of Z^+ (defined by current $I_{R,Z}$). Since the net current is the difference between the oxidation and reduction currents, the current measured by external device would be zero.

$$I_{MEAS} = I_{O,M} - I_{R,Z} = 0 \quad \text{at } E = E_{corr}$$

$$I_{corr} = I_{O,M} = I_{R,Z}$$

When a potential is imposed on the metal specimen from an external source, a current will pass accordingly to the following equation.

$$I_{MEAS} = I_{O,M} - I_{R,Z}$$

The anodic and cathodic currents obey the Tafel equations,

$$n = B_a \log(I_{O,M}/I_{corr}) \text{ and}$$

$$n = -B_c \log(I_{R,Z}/I_{corr})$$

The Tafel equations can be arranged to give:

$$\log(I_{O,M}/I_{corr}) = n/B_a$$

$$\log(I_{R,Z}/I_{corr}) = -n/B_c$$

or $$10^{n/Ba} = (I_{O,M})/(I_{corr})$$

$$10^{-n/Bc} = (I_{R,Z})/(I_{corr})$$

substitution of these equations give:

$$I_{MEAS} = I_{corr}\,(10^{n/Ba} - 10^{-n/Bc})$$

10^x can be approximated by the following power series.

$$10^x = 1 + 2.3x + (2.3x)^2/2! + \ldots\ldots\ldots\ldots (2.3x)^n/n!$$

If x in this series is small, then it can be approximated to

$$10^{n/B_a} = 1 + 2.3n/B_a$$

$$10^{-n/B_c} = 1 - 2.3n/B_c$$

substituting these equations, we get,

$$I_{MEAS} = 2.3\, I_{corr}.n.[(B_a+B_c)/(B_a.B_c)]$$

Hence rearranging for polarisation resistance,

$$n/I_{MEAS} = B_a.B_c/[2.3I_{corr}.(B_a+B_c)]$$

Taking derivatives of both sides with current with respect to potential evaluated at $E = E_{corr}$,

$$[dI/dE]_{E_{corr}} = 2.3I_{corr}[1/B_a+1/B_c=1/R_p]$$

simplifying,

$$I_{corr} = [(B_a.B_c)/2.3(B_a+B_c)] \times 1/R_p = K/R_p$$

where $R_p = (dE/dI)_{corr}$, the polarisation resistance and slope of potential Vs. Current plot at $E = E_{corr}$. The factor K is the explicit function of Tafel slopes.

It is important to realise that these equations are valid only if n/8 is very small. Therefore it is important to keep over voltage in the range of 10-20mv, as suggested by Stern and Roth (53). However, Barnarrt (55) suggests that in some cases linear relationship is obeyed over a potential range of 60mv or more depending on anodic to cathodic Tafel slopes.

Mansfield (56) has also suggested that for large differences in the Tafel slopes(B_a,B_c) the calculations of I_{corr} by the above formula would give error upto 10% due to non-linearity of the curves.

4.2.1. Tafel Plot Technique.

By a technique of Tafel plotting, a controlled potential scan is typically applied to a sample, by starting at E_{corr} and extending in either anodic or cathodic direction for a hundred millivolts. When the resultant potential-current function is plotted on a semi-log scale, it characterstically exhibits a linear region. This is true for both anodic

and cathodic regions. The plot itself is known as Tafel plot and slopes of the linear regions are known as Tafel constants.

The Tafel plot technique can be used as a mean of determining corrosion rates. However, a polarisation technique, as described later, has an advantage over this technique in the sense that the Tafel plot extends over a large enough range and the former is scanned over much smaller range. The wide range of Tafel plot engenders changes in the surface characterstics of the specimen. As a result a Tafel plot that begins at a slightly cathodic potential, and scans through E_{corr} to some anodic potential is subject to error due to specimen surface changes. The polarisation resistance technique, by comparision uses a scan so small as to reduce possible error from this source to a negligible level.

Under this research work, Tafel plot was used only to determine Tafel constants. The values of these constants were used to determine I_{corr} by using the technique of polarisation resistance.

4.2.2. Polarisation Resistance or Linear Polarisation Technique.

This technique is performed by applying a controlled potential scan over a small range, typically 25mv with respect to E_{corr}. The resultant current is plotted linearly against potential. The slope of this potential current function at E_{corr} is identically the polarisation resistance, which together with the Tafel constants can be used to determine I_{corr}.

The linear polarisation has an additional advantage of being a rapid procedure, thus making it more useful. Additionally, since applied potential is never far removed from the corrosion potential, the surface of the specimen is not materially affected by the experiment, thus can often be used for other studies.

5.0. EXPERIMENTAL PROCEDURE.

5.1. Material Preparation.

The stainless steel used for the trials was received in bars of 10mm diameter, with a ground finish. The chemical composition of the material received is shown in Table-1.

The bars were polished by using 200 and 450 grit wet and dry papers on a lathe. Specimens of length 20mm were cut from these bars, using a mechanised hack-saw. They were then turned on a lathe. All the sharp edges were smoothened and the burrs removed. Two specimens of each steel, prepared as described, were used for each trial. One of these was used for corrosion testing and the other for metallographic testing.

An additional specimen of the same size was also prepared to act as a "dummy" for the purpose of accurate measurement of the temparature in the treatment chamber of the plasma nitrider. A hole of approximately 1.2mm diameter and 10mm deep was drilled in it to facilitate the insertion of a thermocouple tip.

The specimens for wear testing on the Faville-Levally or Falex machine were prepared in accordance with the manufacturer's specifications (47). The material required for each test is a set of two V-blocks and a pin .

For the preparation of pins (Figure 7) of size 32mm length and 6.4mm diameter, the bars of different grades of austenitic stainless steel were used. Their chemical compositions are shown in Table-2.

The pins were polished before nitriding. The surface finish of the pins was measured on a Rank-Taylor-Hobson Talysurf machine and found to be in the range of 0.85-1.0 microns.

For the preparation of V-blocks (figure 7) of length 10mm and

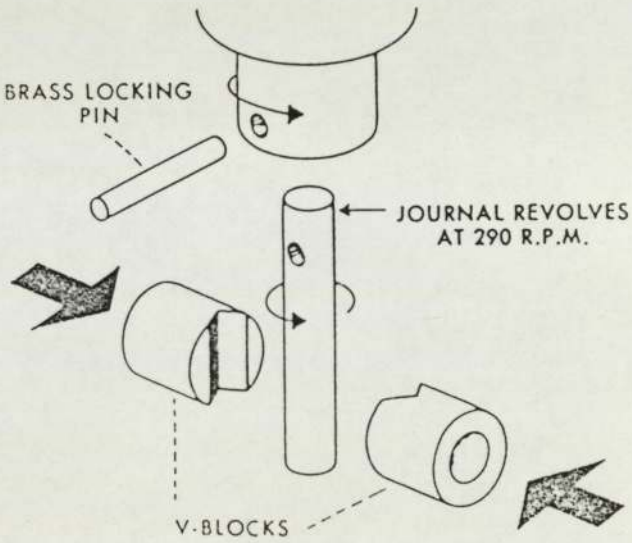

FIGURE-7 Pin and Block for Falex Test

12.7mm diameter, the bars of different grades of austenitic steel were used. The chemical composition is shown in Table-2.

The surface finish of the blocks was measured on a Rank-Taylor-Hobson Talysurf machine and found to be in the range of 1.2-1.5 microns inside the "V" angle.

5.2. Plasma Nitriding.

5.2.1. Equipment.

Plasma nitriding equipment is commercially available with various attachments as may be required, depending on the process parameters, size of components etc.

The plasma nitriding unit at The Aston University is shown in Plate-1 and described below.

There are three basic units in the equipment.

1) Vacuum Equipment.

This consists of a vacuum bell in two sections joined by flanges and vacuum seals. The flanges are bolted together. The outer shell of the bell is water cooled.

The inside space contains heating elements (optional) next to the bell inner shell, radiation shields and a central loading table. The latter is a metallic tray mounted on the central screw which is shielded to prevent any arcing. The bell wall serves as the anode and the charge table as the cathode. All the connections are brought out from the bottom of the bell.

The bottom of the bell has facilities for placing two

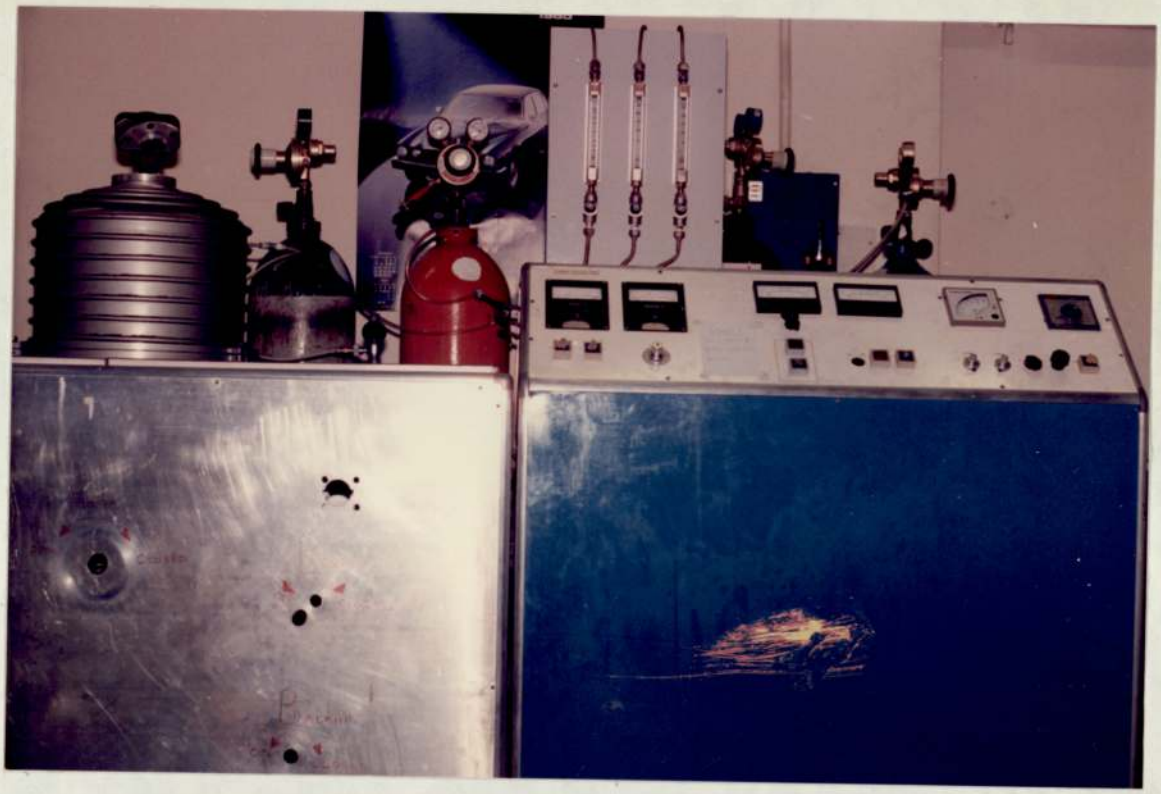

Plate-1 Plasma Nitriding Unit at Aston University

thermocouples. Two thermocouple probes are used, one for inserting directly in to a dummy specimen, to measure accurately the charge temperature, this is connected to the main indicator, the other is connected to a solid state blind controller which controls the furnace temperature.

The side of the bell has connections for a vacuum pump, pressure gauges through pressure switches and also an air entry pipe.

The vacuum pump is of the two-stage rotary type and sustains the vacuum inside the chamber at less than 10^{-1}mbar. The vacuum pump has a manual monitoring valve on the front of the panel.

2) Gas Distribution System.

This consists of a battery of gas bottles connected through flexible tubing and copper tubes, to the flow meters mounted on a panel. The gases flow through a common pipe line to the vacuum bell with a main needle valve provided for the regulation and control of the flow.

3) Electric Unit.

The power supply is connected to a three phase thyristor unit feeding the primary winding of a three phase power transformer, capable of output of 10 KVA.

The temperature of the furnace is controlled by a modified standard temparature comparator and regulator to give wide band proportional control with error signal feeding in to the thyristor unit. Thus power to the work load is proportional to the offset of temperature.

Arcing is reduced by a control system which monitors discharge voltage and fluctuations in current. This is fully automated system in that once the desired temperature has been reached, any fluctuations in current is detected and reduced or the current is cut-off momentarily (micro-seconds) to restore normal conditions. This is also provided with a current limiter and an under voltage circuit and a Ramp generator to

bring the work load to the temperature at preselected controlled rate.

Some of the commercially available units may carry additional provision for diffusion pumps to give a vacuum down to 10^{-3}mbar. Provision can also be made for a circulating fan to accelarate cooling.

Recent developments in the electrical circuitary include provision for a high frequency impulse generator which allows very high plasma energy levels with high voltages and low currents. This is claimed to eliminate arc formation effectively (2).

The equipments can also be provided with microprcessors which regulate automatically the set point variables including time, temperature, pressure and gas composition.

5.2.2. Treatment.

Table-3a shows the treatments that were carried out to study the effect of furnace parameters on nitriding of stainless steel. The different types of treatment that were carried out under correct conditions are shown in Table-3b. The treatment cycles chosen were those which facilitate nitriding at low temperatures as well as post oxidation treatment on the components nitrided at high temperatures. Although the temperature and time periods vary from treatment to treatment, the operating method for the plasma nitriding equipment remains the same. The hydrogen to nitrogen gas ratio was maintained at 75:25 for all the treatments.

Prior to the treatment, all the specimens were cleaned ultrasonically to remove any metallic debris, oil, grease etc. following the turning operation on the lathe. The specimens were then rinsed in running tap water, followed by acetone cleaning to remove any grease or finger print and dried. Care was taken to avoid any further finger

Material AISI	%C	%Si	%Mn	%P	%S	%Cr	%Mo	%Ni	%Ti
304	0.024	0.40	1.48	0.027	<0.003	18.42	-	10.12	-
316	0.05	0.58	1.58	0.040	0.012	16.60	2.09	10.55	-
321	0.055	0.52	1.70	0.015	0.015	17.32	00.03	9.17	00.45

Table-1 Chemical Composition of Material for Test Programme

Material AISI	%C	%Si	>Mn	%P	%S	%Cr	%Mo	%Ni	%Ti
304	0.024	0.51	1.08	0.029	00.002	18.10	00.26	10.08	-
316	0.05	0.31	1.68	0.027	0.004	17.10	2.30	11.05	-
321	0.055	0.52	1.70	0.015	0.015	17.32	0.03	9.17	0.45

Table-2 Chemical Composition of Material for Falex Test

Trial No.	Treatment	Temp. (^{o}C)	Time	Initial vaccum (m.bar)	No. of purging cycles
A	Hydrogen sputter	460	45 minutes	$<2\times10^{-1}$	2
	Plasma nitride	460	20 hours		
B	Hydrogen sputter	540	45 minutes	$<2\times10^{-1}$	2
	Plasma nitride	540	7 hours		

Table-3a Experimental Test Programme for Plasma Nitriding

Trial No.	Treatment	Temp. (°C)	Time	Initial vacuum (m.bar)	No. of purging cycles
1	Hydrogen sputter	380	2 hours	$>10^{-1}$	5
	Plasma nitride	380	48 hours		
2	Hydrogen sputter	420	2 hours	$>10^{-1}$	5
	Plasma nitride	420	24 hours		
3	Hydrogen sputter	460	2 hours	$>10^{-1}$	5
	plasma nitride	460	20 hours		
4	Hydrogen sputter	500	2 hours	$>10^{-1}$	5
	plasma nitride	500	12 hours		
5	Hydrogen sputter	540	2 hours	$>10^{-1}$	5
	Plasma nitride	540	7 hours		
6	Hydrogen sputter	570	2 hours	$>10^{-1}$	5
	Plasma nitride	570	4 hours		
7	Hydrogen sputter	460	2 hours	$>10^{-1}$	5
	Plasma nitride	460	20 hours		
	post-oxidation	460	20 seconds		
8	Hydrogen sputter	500	2 hours	$>10^{-1}$	5
	Plasma nitride	500	12 hours		
	post-oxidation	500	20 seconds		
9	Hydrogen sputter	540	2 hours	$>10^{-1}$	5
	Plasma nitride	540	7 hours		
	post-oxidation	540	20 seconds		
10	Hydrogen sputter	570	2 hours	$>10^{-1}$	5
	Plasma nitride	570	4 hours		
	post-oxidation	570	20 seconds		

Table-3b Experimental Test Programme for Plasma Nitriding

contact with the specimens. For each cycle, six cylindrical specimens, one of each grade of austenitic stainless steel and one Falex pin of each of the steel were used.

Prior to loading of specimens in the vacuum chamber of the plasma nitriding furnace, the loading table and its accessories including nuts, washers etc. were cleaned by sand blasting, washed, acetone cleaned, rinsed in water and thoroughly dried. This procedure was followed for all the cycles.

The specimens along with the "dummy" specimen for the thermocouple probe were placed on the loading table with spacing between them. These were arranged in such a manner to ensure that the product of the distance between specimens and the pressure, at all the working pressures of the treatment gases in the chamber, is greater than 20mm-torr (14).

After loading, the top half of the bell is placed on the lower half and bolted on with neoprene seal inbetween. The air inlet valve is closed and the manual vacuum valve is opened and the air is evacuated from the chamber to a pressure of 10^{-1}mbar or lower.

After reaching the desired vacuum, the purging of the vacuum chamber is carried out with oxygen free hydrogen and nitrogen gases. The chamber pressure is raised to one atmosphere during purging and then the gas entry valves are closed to allow for the build up of vacuum to the same order of 10^{-1}mbar or lower. The whole chamber is purged in this manner for five times. The purging is carried out to remove air pockets prior to the start of the treatment cycle.

After the purging, the hydrogen entry valve is opened slowly to allow the chamber pressure to rise to 1 torr before the E.H.T. (Electrical High Tension) is switched on and the current is increased till the voltage of approximately 300 volts is reached, this is the voltage required to

obtain the plasma.

After the initial start, the control is switched over to the Ramp control and the current is slowly increased to facilitate the temperature rise. Ramp control is maintained till the furnace temperature of about 200^{o}C is reached. Ramp control is used to obtain a slow and controlled rate of heating and later the control is changed over to NORMAL to raise the temperature of the charge to the treatment temperature.

The specimens are heated up to the treatment temperature in the hydrogen plasma at pressures between 5-8 torr and sputtered for two hours to remove the surface oxide film present on the stainless steel. After the sputtering, nitrogen is allowed to enter the chamber and the ratio of 75% hydrogen and 25% nitrogen is maintained at the working pressure of 4-5 torr.

On completion of the treatment cycle the E.H.T. is switched off. The nitrogen and hydrogen gas flow is increased and the pressure in the chamber is allowed to rise to atmospheric. Thus gas quenching is achieved. On reaching room temperature, the gas supply is shut-off and vacuum is allowed to build upto 10^{-1}mbar. Then the air inlet valve is opened to facilitate the air entry into the chamber before opening the chamber to remove the specimens.

For the treatment cycles with the post oxidation treatment after the completion of the nitriding cycle, the hydrogen and nitrogen supply was shut-off, just prior to the oxygen ingress, while retaining the plasma. Oxygen was then introduced for 20 Seconds, after which the plasma and oxygen supply was switched off and the nitrogen and hydrogen reintroduced to aid cooling.

5.3. Gas Nitriding.

The present day gas nitriding is mostly carried out in a vertical sealed retort type pit furnace or a bell furnace. The treatment for this research was carried out in a bell type of a furnace.

5.3.1. Equipment.

The furnace used for the treatment has useful working dimensions of 1.2 meter diameter and 4.5 meter depth. The outer casing is fabricated from mild steel which is duly reinforced, followed by thermal insulation. The design of the furnace is a bell type with a fixed base, a recirculating fan, a removable inner hood or a retort and an outer heating hood or a furnace.

The heating of the furnace is carried out by electrical resistance heating elements built into the lining of the furnace. The temperature control is achieved by an electrical controller in conjunction with a thermo couple, by controlling the heating current via a contactor. This arrangement allows to maintain a constant temperature at a present value. The uncracked ammonia is fed into the furnace and is allowed to crack inside the charge space which is surrounded by a gas tight inner hood or a retort.

5.3.2. Treatment.

Prior to the treatment, specimens were sand blasted. The specimens were then thoroughly cleaned in running tap water followed by ultrasonic cleaning in a micro-clean solution. The specimens were then acetone cleaned and dried. Just prior to the gas nitriding, specimens

were acid pickled in a 15% sulphuric acid bath for 1/2 an hour.

An additional batch of the specimens was also prepared as above but without any of the prior treatments of sand blasting and acid pickling. This batch was used to study the importance of these prior treatments on the gas nitriding of stainless steel.

All the specimens were gas nitrided at 540^{o}C for 45 hours.

5.4.0. Salt Bath Nitrocarburising.

The salt bath nitrocarburising treatment, carried out for the purpose of this research is known by the patented name Tufftride and will be so called here after.

5.4.1.Equipment.

The furnace used for the treatment has useful working dimensions of 800 mm diameter and 1000 mm depth. The outer casing is fabricated from mild steel backed by thermal insulation. The salt bath pot is made from solid titanium. The salt vapours are removed through a vent-hood which is provided with an exhauster.

The heating of the furnace is carried out by electrical resistance radiation heating elements built into the lining of the furnace.

The aeration of the bath is carried out by means of a compressor and an aeration tube together with suction filters, a needle valve and a set of distributer pipes.

A thermocouple together with an electronic controller automatically controls the heating current via a contactor, thus maintaining a constant temperature at a present level.

5.4.2. Treatment.

The specimens were preheated to about 350°C before being transferred to the Tufftriding bath at 580°C and held in the bath for 90 minutes. This was followed by quenching in a salt bath; also known as AB1 bath by its patented name. The temperature of the quenching bath was maintained at 370°C and specimens were held in this bath for 20 minutes. The specimens were then cleaned in running tap water.

Prior to the treatment, all the specimens were cleaned ultrasonically in a micro-clean solution to remove any metallic debris, oil, grease, etc. following the turning operation on the lathe. The specimens were then rinsed in running tap water, followed by acetone cleaning and then dried.

5.5. Corrosion Measurement.

5.5.1. Equipment.

The equipment used for measuring the corrosion of specimens was a Princeton Applied Research Model-350-Corrosion Measurement System (Plate-2).

The equipment can be divided into two parts (49).

1). Cell

2). Console

The cell consists of following components.

Plate-2 Microprocessor based Corrosion Measurement Equipment

A). Counter Electrode.

The counter electrode to be used must be of noble metal. The electrode is immersed into a test solution and connected to the console.

B). Specimen.

The specimen, with electrical contact point emerging from it, is also immersed into the same solution as the counter electrode above and connected to the console.

C). Reference Electrode.

The reference electrode is a saturated calomel electrode. It is dipped into the solution containing super saturated potassium chloride and connected to the test solution via a reference electrode bridge tube. The reference electrode can also be dipped in the test solution directly, provided the test solution has a composition such that it does not contaminate it.

2). Console Unit.

The console unit of the system is a microprocessor that controls the excitation programme to be applied to the specimen as well as the nature and frequency of measurements. It addionally makes possible interaction between the operater, the control and display panel. The interaction aids and directs the operater in setting up the instruments for an analysis or play back.

The indivdual parameters entered are stored in the memory and they are available for an automatic recall. The analysis run is initiated by pressing 'RUN' push button and the procedure is automatically controlled. The real time results are plotted on play back. Also the data collected in a single run can be played back in any of the several different formats.

5.5.2. Testing Procedure.

To carry out the corrosion measurements on the equipment as described above, It is necessary to have an electrical contact with the specimen. For this, a nichrome wire was spot welded on one of the end faces of the cylindrical specimens.

To avoid an attack by the testing solution on the wire, the end face and the length of the nichrome wire projecting outward were carefully laquered. Specimens were thorougly cleaned after this to ensure that the exposed surface of the specimens are free from any contamination including finger prints.

The test solution was prepared by dissolving 5 parts by weight of sodium chloride in 95 parts of distilled water. The sodium chloride had a chemical purity of 99.9%. The pH of this solution was adjusted to the range of 3.1 to 3.3 as measured on a pH meter, by addition of acetic acid.

The specimens were dipped into this solution and a regular check carried out to ensure that the pH of the solution remained constant.

The tests were carried out on each specimen over a period of three weeks, with one weekly test on each specimen. The same solution in which the specimens remained dipped was used for all the corrosion tests. Platinum was used as the counter electrode. The reference electrode was

connected to the testing solution via a salt bridge. The cell was connected to the microprocessor cosole unit in the manner as described earlier.

Prior to the testing, the area of the exposed part of the specimen was calculated, since this is required to be fed into the microprocessor for the purpose of calculating corrosion current.

Each specimen was given a working code for the purpose of identification. The specimen number was decided on the basis of the type of material, type of treatment, type of treatment cycle and the time period after which it was tested. The key to this four digit number is given in Appendix-1.

After each test, the results were printed out by the microprocessor including the sample number. Thus with the help of the key to the sample number, one immediately knows, on examining the print outs, the history of the treatment, the type of the material and the testing conditions.

The Tafel plot technique was used to determine the Tafel constants and these values were used for the linear polarisation technique. The cell arrangement as described above is the same for both the techniques.

5.6. Wear Measurement.

5.6.1. Equipment.

There are several techniques for the measurement of wear. Two of the most popular techniques commonly used are:

1). Faville- Levally or Falex Technique.

2). Pin on Disc Technique.

For the purpose of this research, Falex technique on Faville-Levally equipment was used for wear measurements.

The Faville- Levally or Falex machine is shown in Figure 8. The test pin of 6.4 mm diameter and 32mm length is attached to the main drive shaft by means of a shear pin, and two blocks or jaws, having 90^{o} notch, fit into holes in the lever arm. The jaws are clamped around the rotating test pin and a load exerted by them which can be gradually increased. The test pin rotates at 290 rpm and gauges are provided to indicate torque and jaw loads.

The machine is a commonly used instrument in the industry, to check efficiency of nitrided components. The tests are carried out by using treated pins against untreated blocks. The more usual procedure is to treat both test pins and blocks (48).

Several techniques are used for testing. In one method the test is carried out by gradually increasing the jaw load until scuffing occurs or until the limit of the machine is reached. In other methods, the test is carried out for a predetermined fixed time period, at a constant load. The wear rate is calculated by determining the weight loss or if the specimen seizes, the time taken to seizure is recorded.

Both test pins and blocks can be totally immersed in a small tank containing lubricant or any other fluid or test can be done under dry conditions.

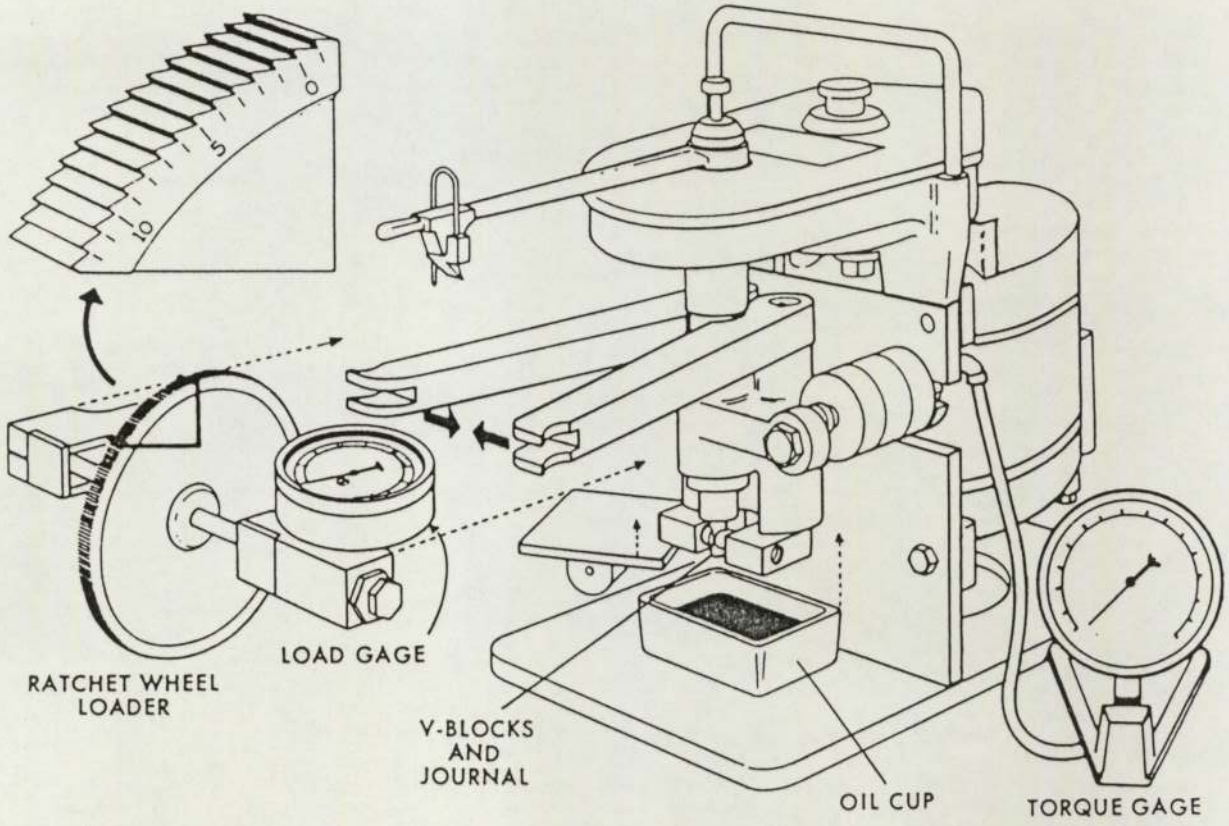

FIGURE-8 Falex Machine

5.6.2. Testing Procedure.

A set of V-blocks and pins were cleaned in a ultrasonic cleaner using micro-clean solution and then acetone. Every pin was weighed prior to testing. For each set one pin and two blocks are required. The technique of the fixed time and fixed load as described earlier was used under dry testing conditions. The test time of 7 minutes at the constant load of 250lbs. (actual load) was chosen.

Prior to the start of the test, load and torque readings were caliberated and recorded on the chart recorder. The Falex machine was turned on and the load was slowly increased to 330lbs gauge load; this gauge load corresponds to the actual load of 250lbs.

As the run proceeds, material is worn away. The radius of the pin is reduced and a wear scar develops. These changes cause the pin/block sqeezed dimensions to decrease. This dimensional decrease reduces the load because the load is applied by the spring-type tension in the load cell assembly. Hence during the experimentation, it was found necessary to make minor manual adjustments to hold the load at the steady value. The test was terminated either after 7 minutes or on seizure of the material. For the latter, the time was recorded for seizure.

After the tests, pins were once again cleaned ultrasonically in micro-clean solution and then acetone. The pins were weighed and weight loss was recorded.

All the nitrided pins, except the ones that were nitrocarburised in Tufftride bath, were tested against the blocks which were nitrocarburised in Tufftride bath, to provide a common and uniform base. Those pins which were nitrocarburised in Tufftride bath were tested against the blocks which were plasma nitrided at 570^{o}C for 4 hours.

5.7. Metallography.

For metallography, a thin disc was removed from the end face of the specimen. A Buchler cut-off machine with ceramic bonded cutting wheel was used for this.

The disc was ultrasonically cleaned in a micro-clean solution and then acetone, to remove any metal debris, oil or grease. The disc was mounted using bakelite with edgemount. The latter is used for retaining the hard edges of the treated specimens. The mounting was carried out in such a way that the viewing would be in transverse direction.

The mounted specimens were polished on polishing wheel using several grades of wet and dry papers, starting with 120 grit size to 1200 grit size, followed by diamond wheel polishing on 6 microns and 1 micron pads to obtain smooth and scratch free surface.

The specimens were then electrolytically etched using 10% oxalic acid, at 6 volts, for 1 minute. For eletrolytic etching, the specimen is made the anode and a sheet of stainless steel the cathode. After the etching, the specimens were water rinsed, followed by methanol and then dried.

The microstructures were observed under Poly- Var-Met optical microscope and photographs were taken using 35 mm camera.

5.8. Case Hardness.

Microhardness indentations were carried out on a Vicker's micro-hardness tester using a 50 gram load with an indentation time of 30 seconds.

A series of hardness profiles for each of the nitrided specimen was obtained. The first indentation on each specimen was made at 13.3

microns from the specimen surface. The second was made at 26.6 microns, and successive readings were taken at 26.6 micron intervals to a maximum of 215 microns.

6.0 RESULTS

6.1 Visual Appearance

6.1.1 Plasma Nitriding

The specimens that were plasma nitrided at lower temperatures (380^{o}C or 420^{o}C) showed a light grey appearance.

The specimens treated at higher temperatures (500^{o}C and above) showed a dark grey appearance, the higher the temperature darker was the shade observed.

All the specimens that were given post-oxidation treatment showed a marked blue hue on all exposed surfaces, indicating that a thin oxide film exists on the nitride case.

Edges near the bottom face appeared darker or had white rings around them. The specimens treated at higher temperatures, particularly those with longer cycle times showed white rings and those treated at lower temperatures irrespective of the cycle time showed a darker shade. This is due to the 'Hollow-Cathode' effect between workpiece and supporting ring (or loading table).

6.1.2 Gas Nitriding

All the gas nitrided specimens showed a deep grey appearance.

6.1.3 Tufftriding

All the Tufftrided specimens showed a dark or black appearance. This is due to the presence of an oxide film on the surface which presumably is due to the aeration of the bath carried out during the

treatment.

6.2.0 Metallography

The untreated specimens (Plates 3, 4 and 5) show that the bar surface had previously undergone some cold working, with the grains at the surface being distorted and elongated. The stabilised grade 321 stainless steel had a finer grain size.

The plasma nitrided specimens (Plates 6, 7 and 8) show a distinct presence of a compound zone and of a diffusion zone.

The specimens that were given post-oxidation treatment after plasma nitriding (Plates 9, 10 and 11) also show the presence of a compound zone and of a diffusion zone. However there is no distinct evidence of an oxide layer.

The specimens that were plasma nitrided at a lower temperature ($380^{o}C$) show a very thin compound zone. This is followed by a diffusion zone which can clearly be defined (Plates 12, 13 and 14).

The Tufftrided specimens show a clear presence of a compound zone followed by a diffusion zone (Plates 15, 16 and 17). The compound zone appears to be of a lesser thickness for the 321 grade stainless steel compared to the other two grades.

The gas nitrided specimens (Plates 18, 19 and 20) show a non uniform compound layer on the 304 and the 316 grade stainless steels, followed by a diffusion zone. The 321 grade stainless steel does not show any distinct presence of a compound zone. However, the diffusion zone is clearly seen.

Plate-3 Microstructure of Untreated AISI 304 Stainless Steel X178

Plate-4 Microstructure of Untreated AISI 316 Stainless Steel X178

Plate-5 Microstructure of Untreated AISI 321 Stainless Steel X178

Plate-6 Microstructure of Plasma Nitrided AISI 304 Stainless Steel X178

Plate-7 Microstructure of Plasma Nitrided AISI 316 Stainless Steel X178

Plate-8 Microstructure of Plasma Nitrided AISI 321 Stainless steel X178

Plate-9 Microstructure of Plasma Nitrided AISI 304 Stainless Steel With Post-Oxidation X178

Plate-10 Microstructure of Plasma Nitrided AISI 316 Stainless Steel With Post-Oxidation X178

Plate-11 Microstructure of Plasma Nitrided AISI 321 Stainless Steel With Post-Oxidation X178

Plate-12 Microstructure of Plasma Nitrided AISI 304 Stainless Steel at $380^{o}C$ X178

Plate-13 Microstructure of Plasma Nitrided AISI 316 Stainless Steel at 380^{o}C X178

Plate-14 Microstructure of Plasma Nitrided AISI 321 Stainless Steel at 380^{o}C X178

Plate-15 Microstructure of Tufftrided AISI 304 Stainless Steel X178

Plate-16 Microstructure of Tufftrided AISI 316 Stainless Steel X178

Plate-17 Microstucture of Tufftrided AISI 321 Stainless Steel X178

Plate-18 Microstructure of Gas Nitrided AISI 304 Stainless Steel X178

Plate-19 Microstructure of Gas Nitrided AISI 316 Stainless Steel X178

Plate-20 Microstructure of Gas Nitrided AISI 321 Stainless Steel X178

6.3.0 Microhardness

Microhardness profiles obtained after plasma nitriding under different conditions (refer Table-3b) are shown in Figures 9 to 18. As can be seen the post-oxidation treatment does not result in any significant change in hardness values.

Figure 19 shows the microhardness profiles for the Tufftrided specimens.

Figure 20 shows the microhardness profiles for the gas nitrided specimens which were given prior surface treatments. The microhardness profiles for those without any prior treatments (refer Section 5.3.2) are shown in Figure 21.

The microhardness profiles for the comparison of the different treatments on the same steel are shown in Figures 22, 23 and 24 respectively, for different grades of stainless steels.

Figures 25 and 26 show the microhardness profiles for the plasma nitrided specimens under incorrect furnace conditions (refer Table-3a and Section 5.2.2).

6.4.0 Corrosion Measurement

6.4.1 Linear Polarisation Curves

Linear polarisation curves obtained on corrosion testing of the specimens in sodium chloride salt solution with acetic acid added to adjust the pH to 3.1, are shown in Appendix-1. These curves were used to calculate I_{corr} values. In some instances it was found necessary to correct these values; this is due to the inherent error in measuring with the microprocessor based corrosion measurement equipment. The method

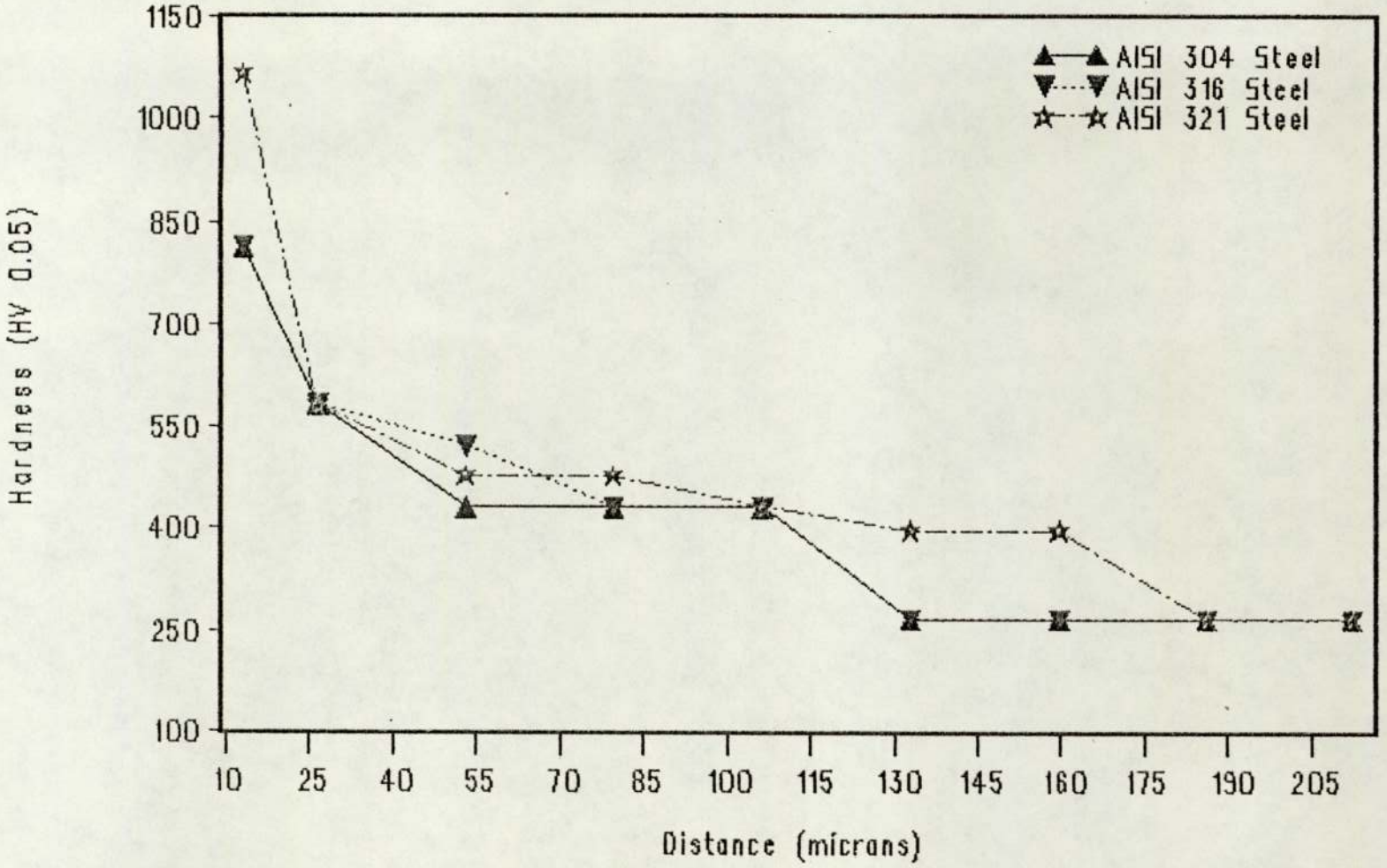

Hardness Vs Distance Plot for Plasma Nitriding at 380C

FIGURE-9

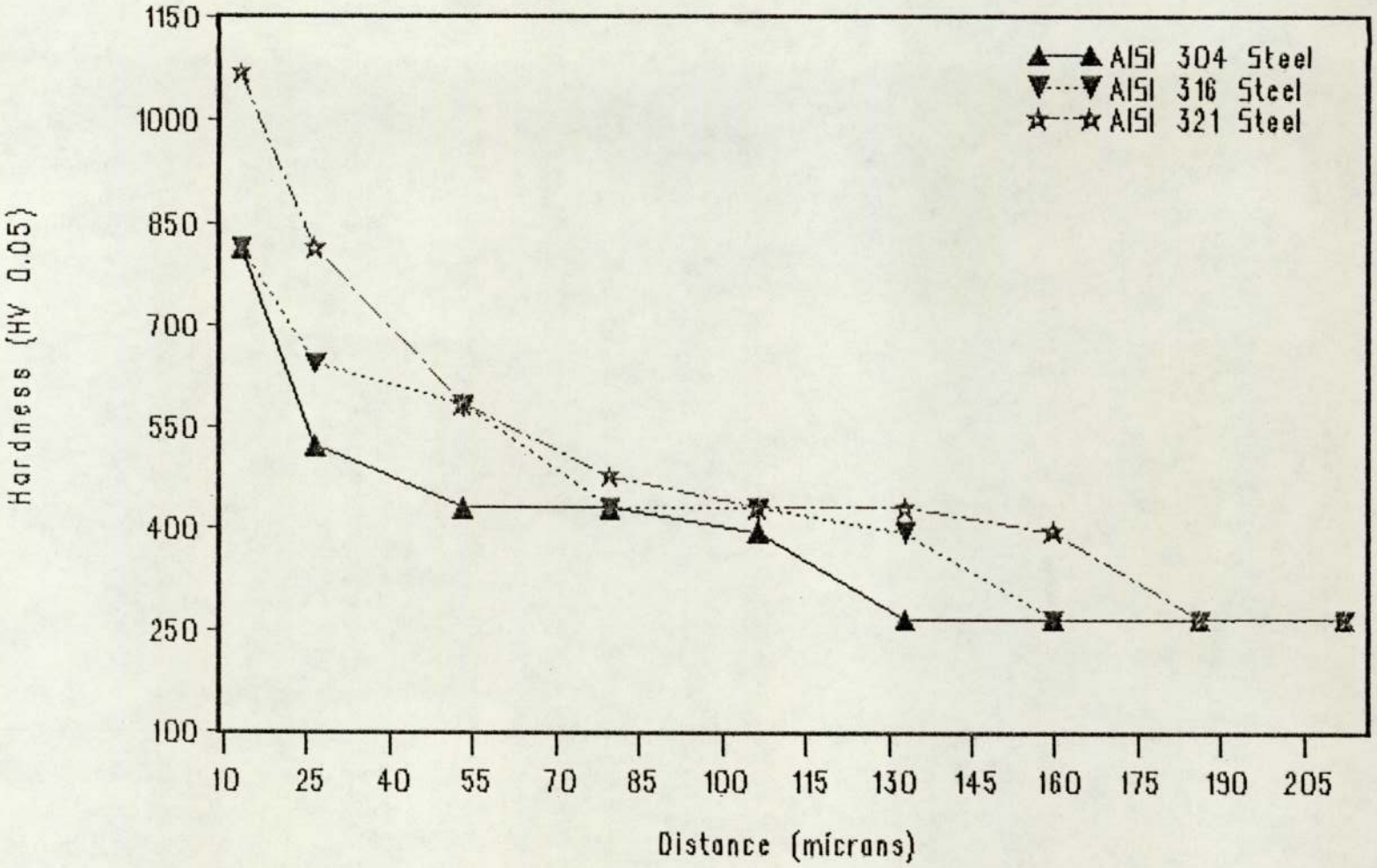

Hardness Vs Distance Plot for Plasma Nitriding at 420C

FIGURE-10

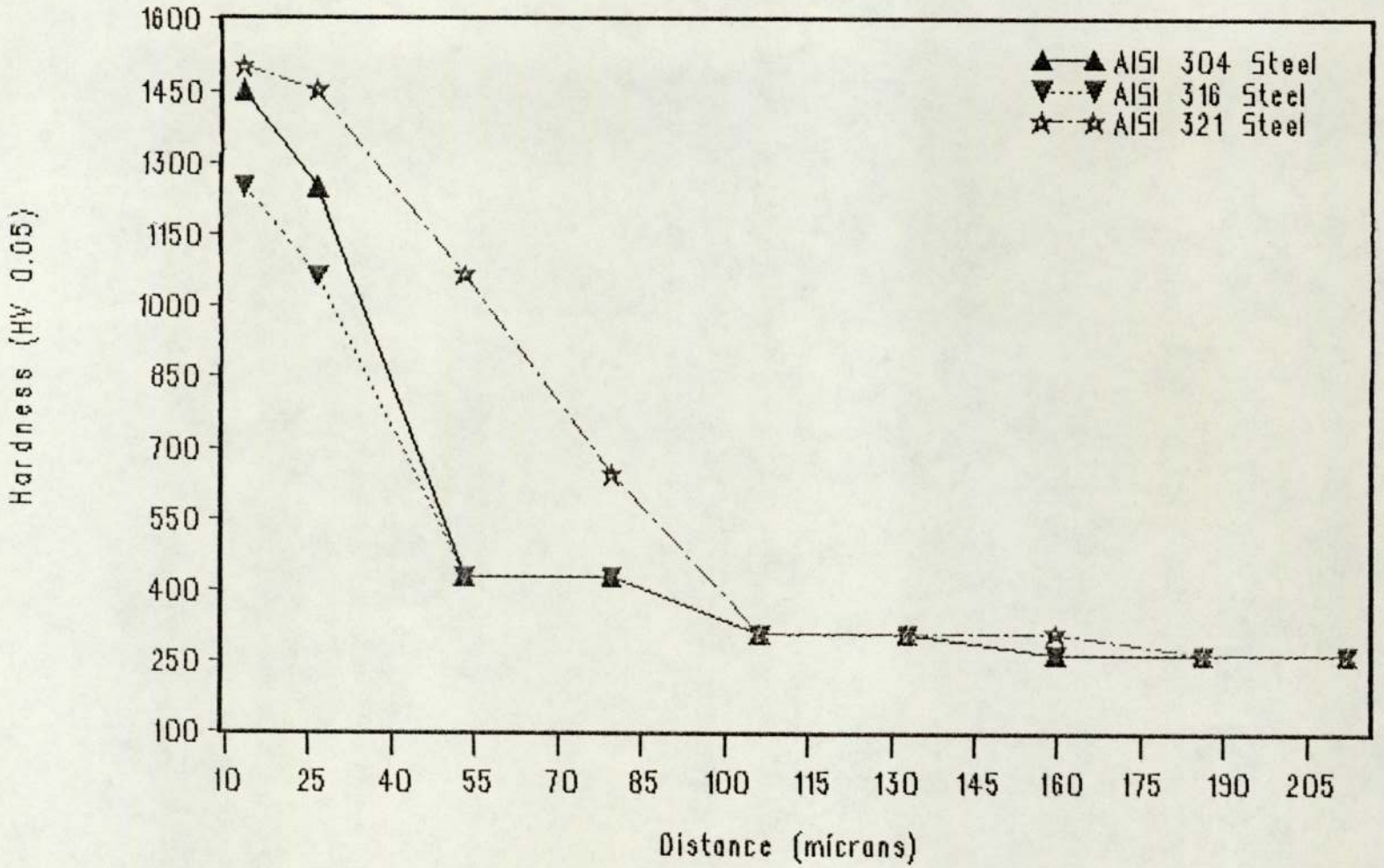

Hardness Vs Distance Plot for Plasma Nitriding at 460C

FIGURE-11

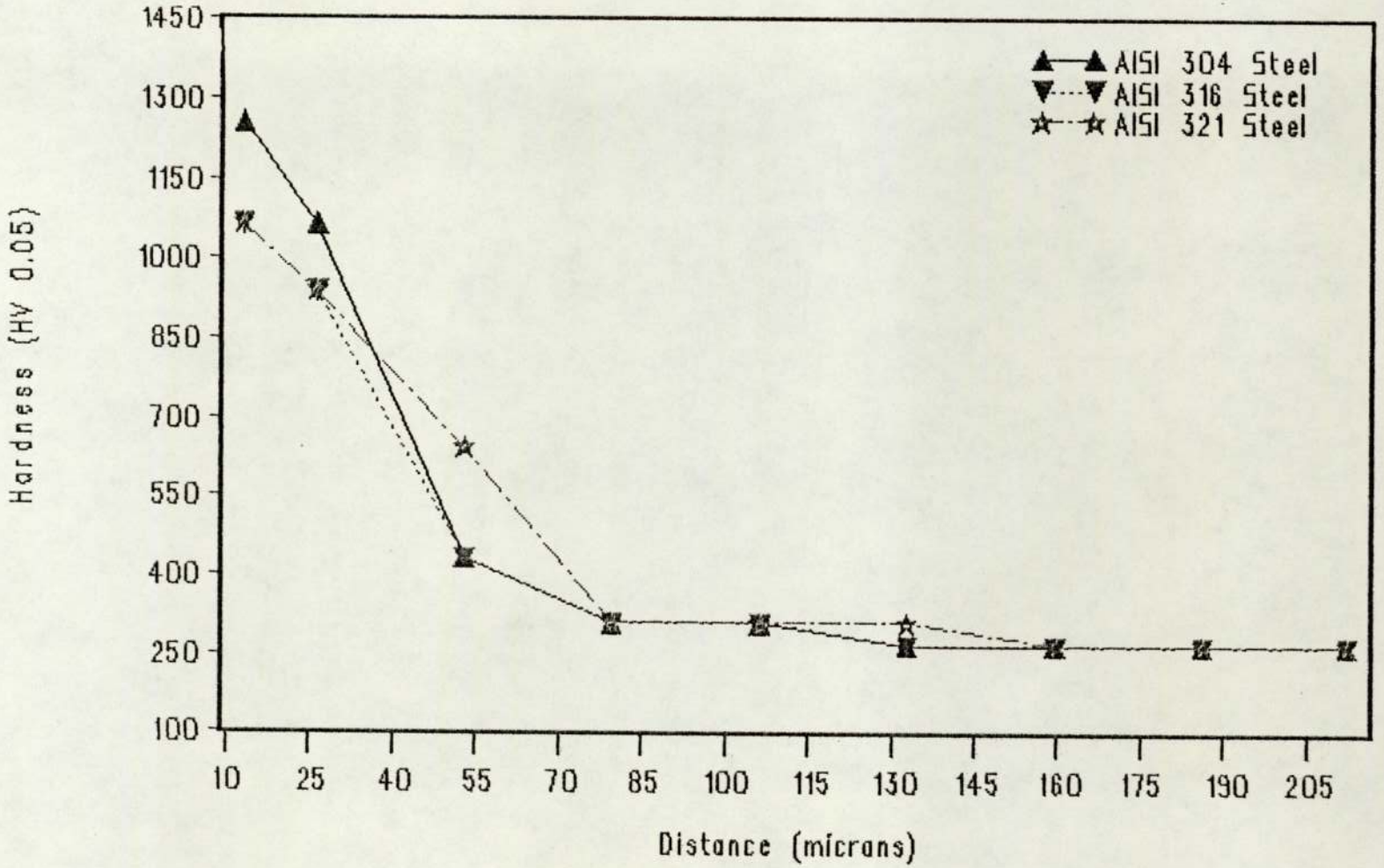

Hardness Vs Distance Plot for Plasma Nitriding at 500C

FIGURE-12

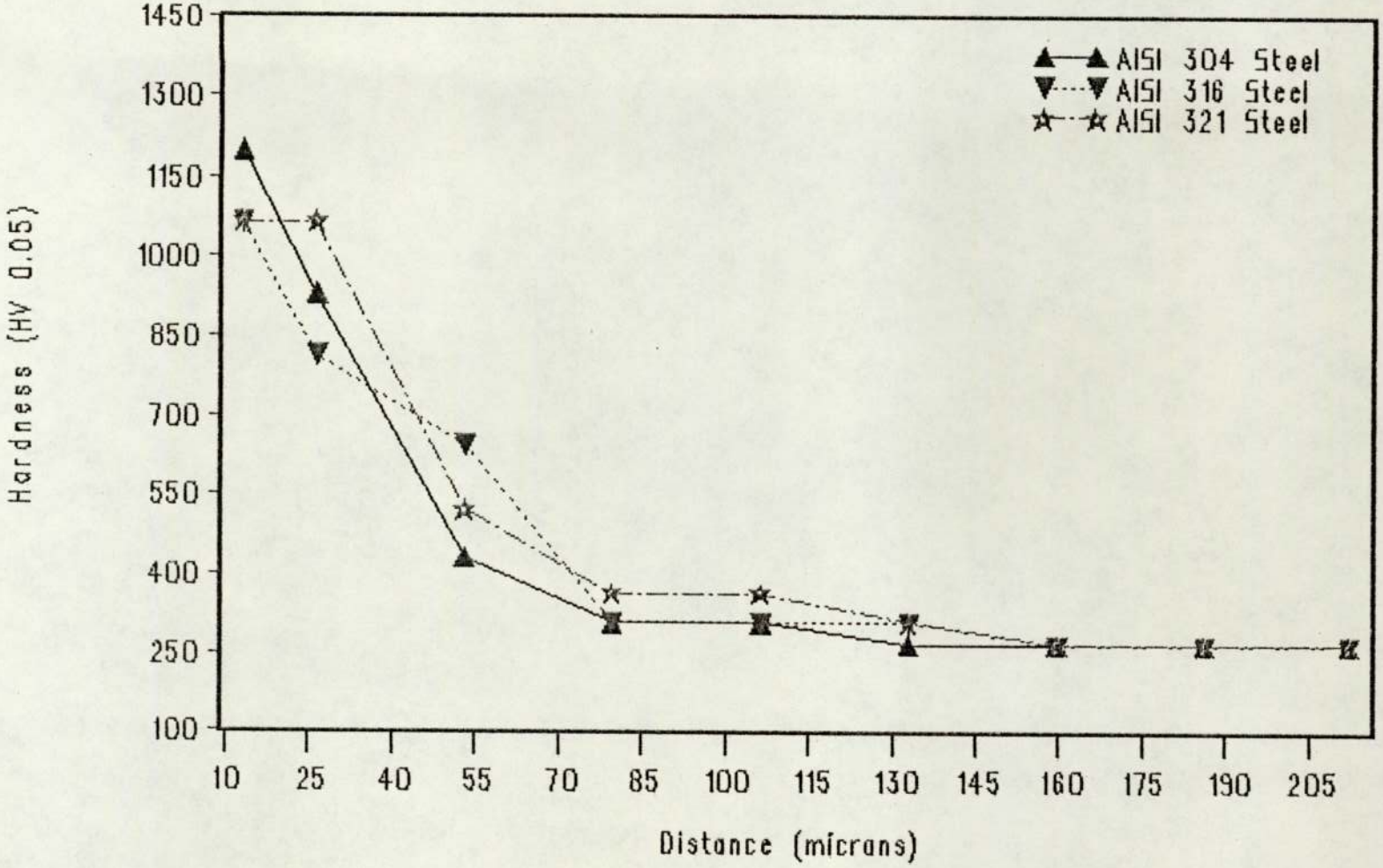

Hardness Vs Distance Plot for Plasma Nitriding at 540C

FIGURE-13

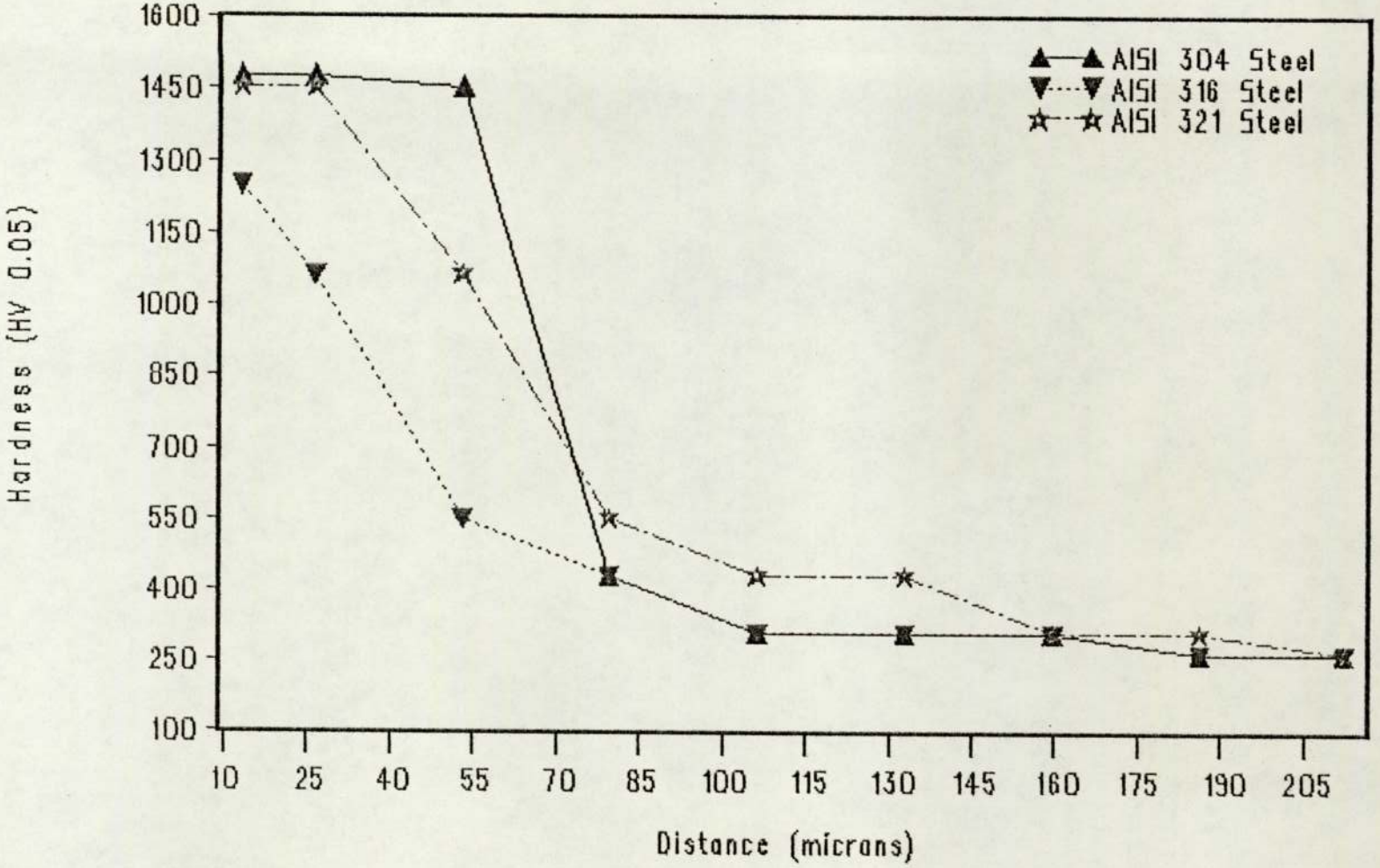

Hardness Vs Distance Plot for Plasma Nitriding at 570C

FIGURE-14

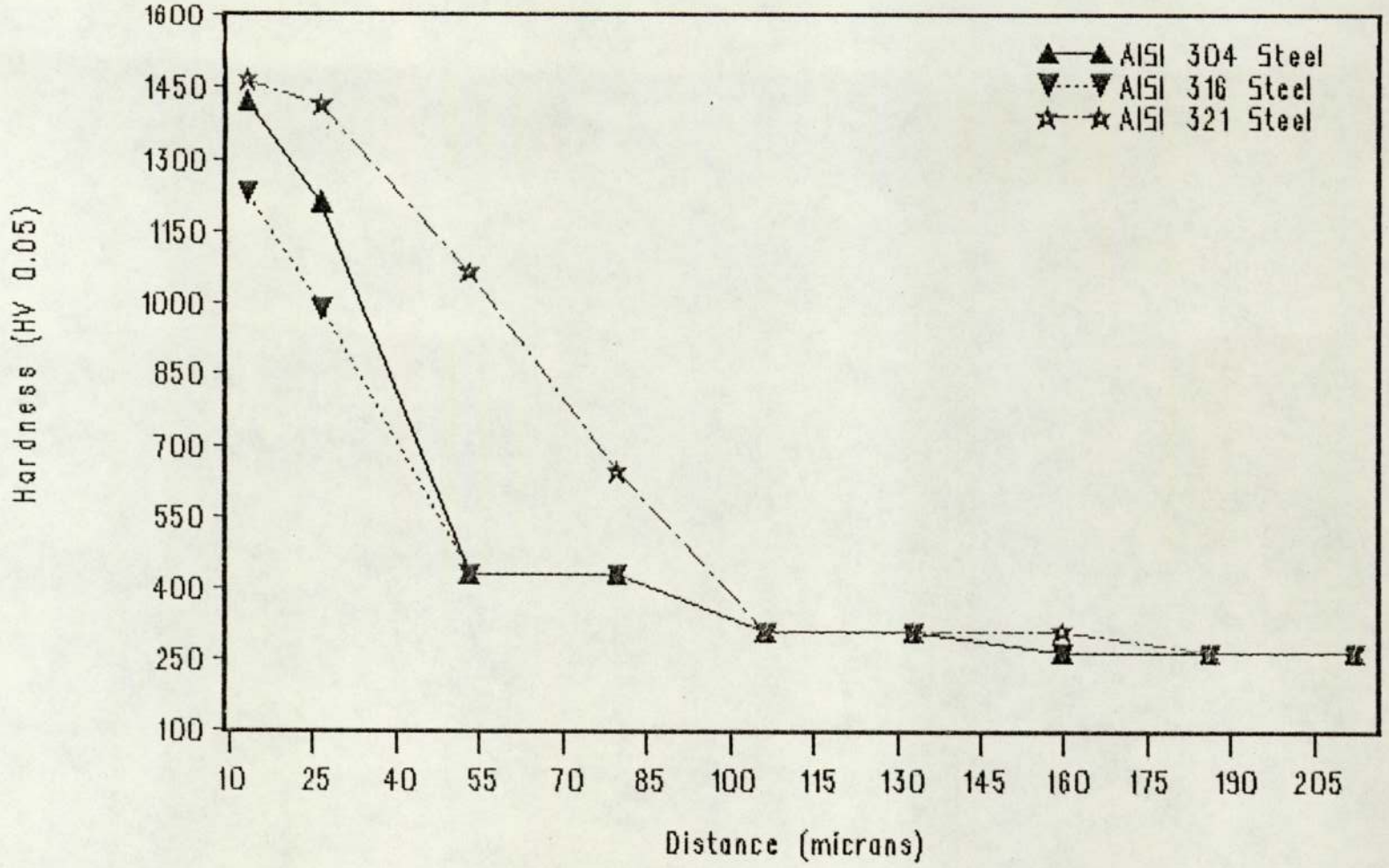

Plasma Nitriding at 460C with Post Oxidation

Hardness Vs Distance Plot

FIGURE-15

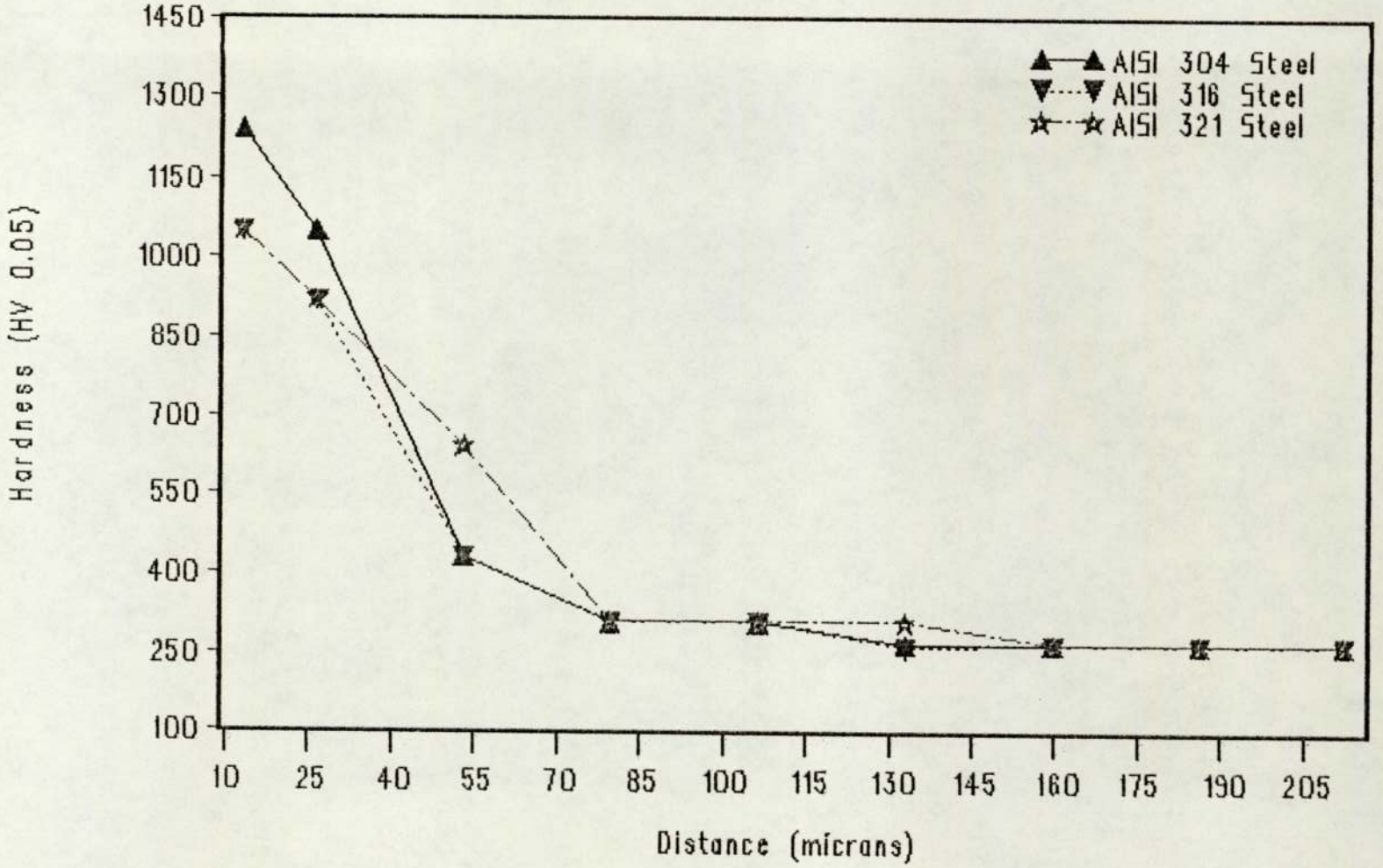

Plasma Nitriding at 500C with Post Oxidation

Hardness Vs Distance Plot

FIGURE-16

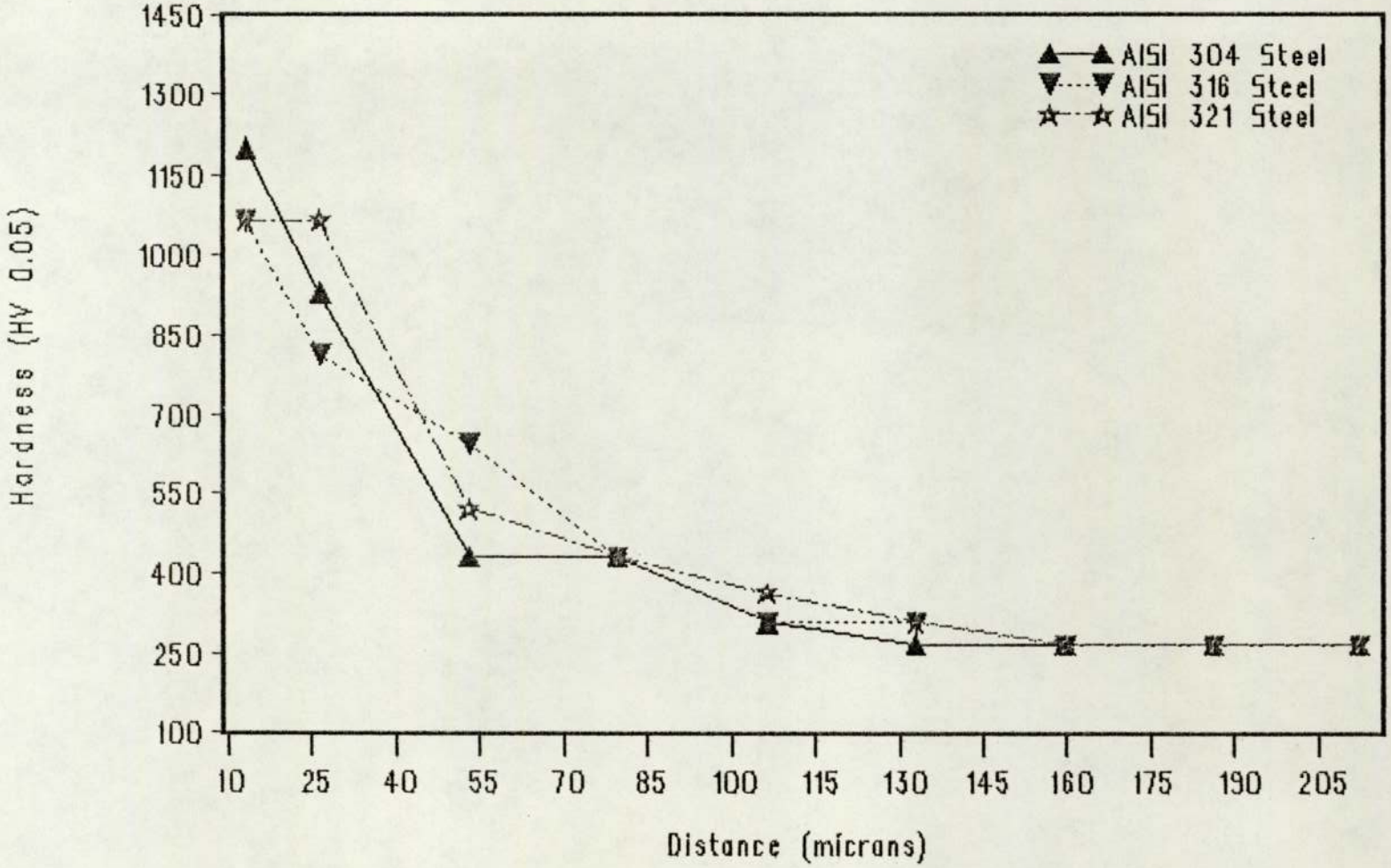

Plasma Nitriding at 540C with Post Oxidation

Hardness Vs Distance Plot

FIGURE-17

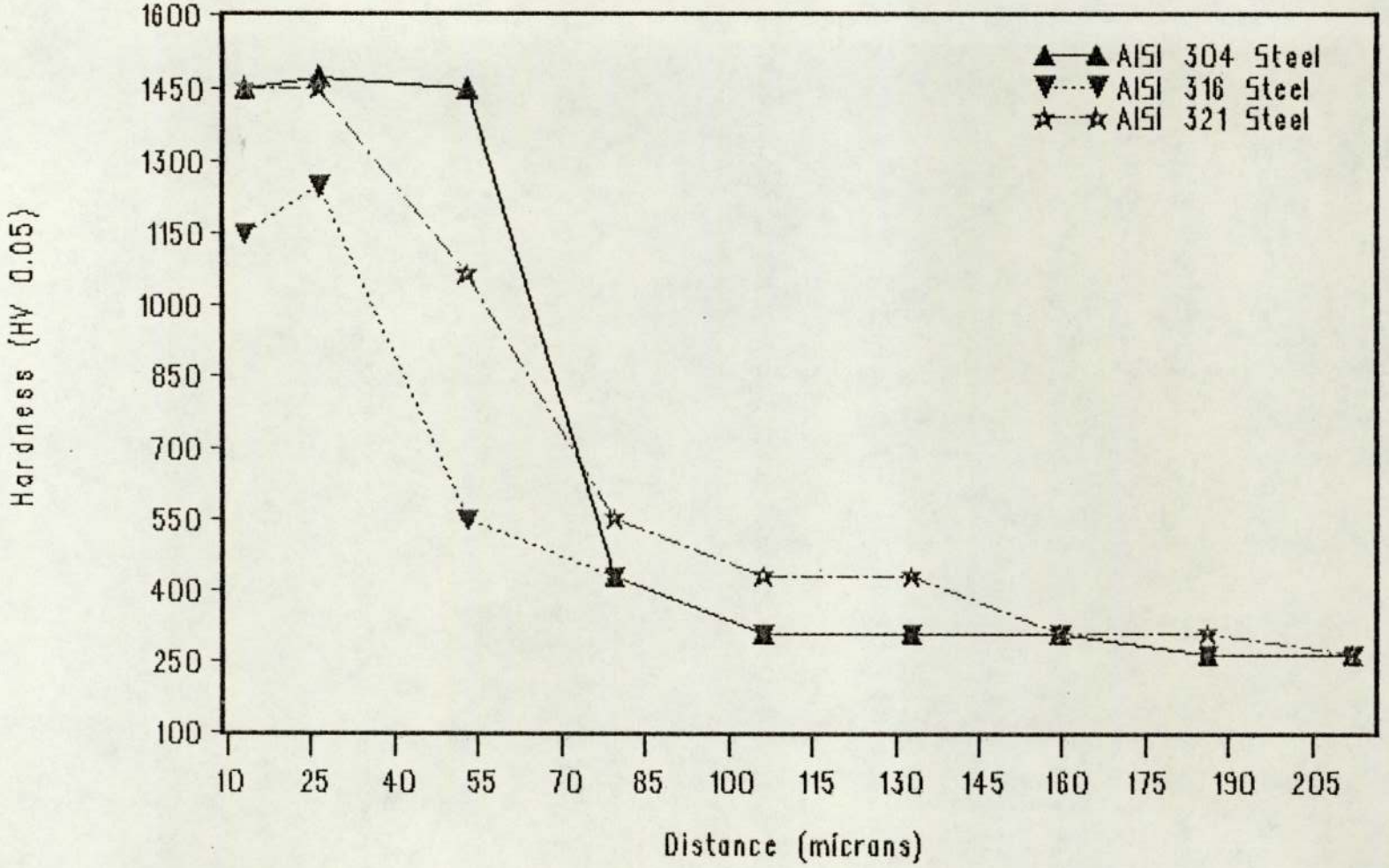

Plasma Nitriding at 570C with Post Oxidation

Hardness Vs Distance Plot

FIGURE–18

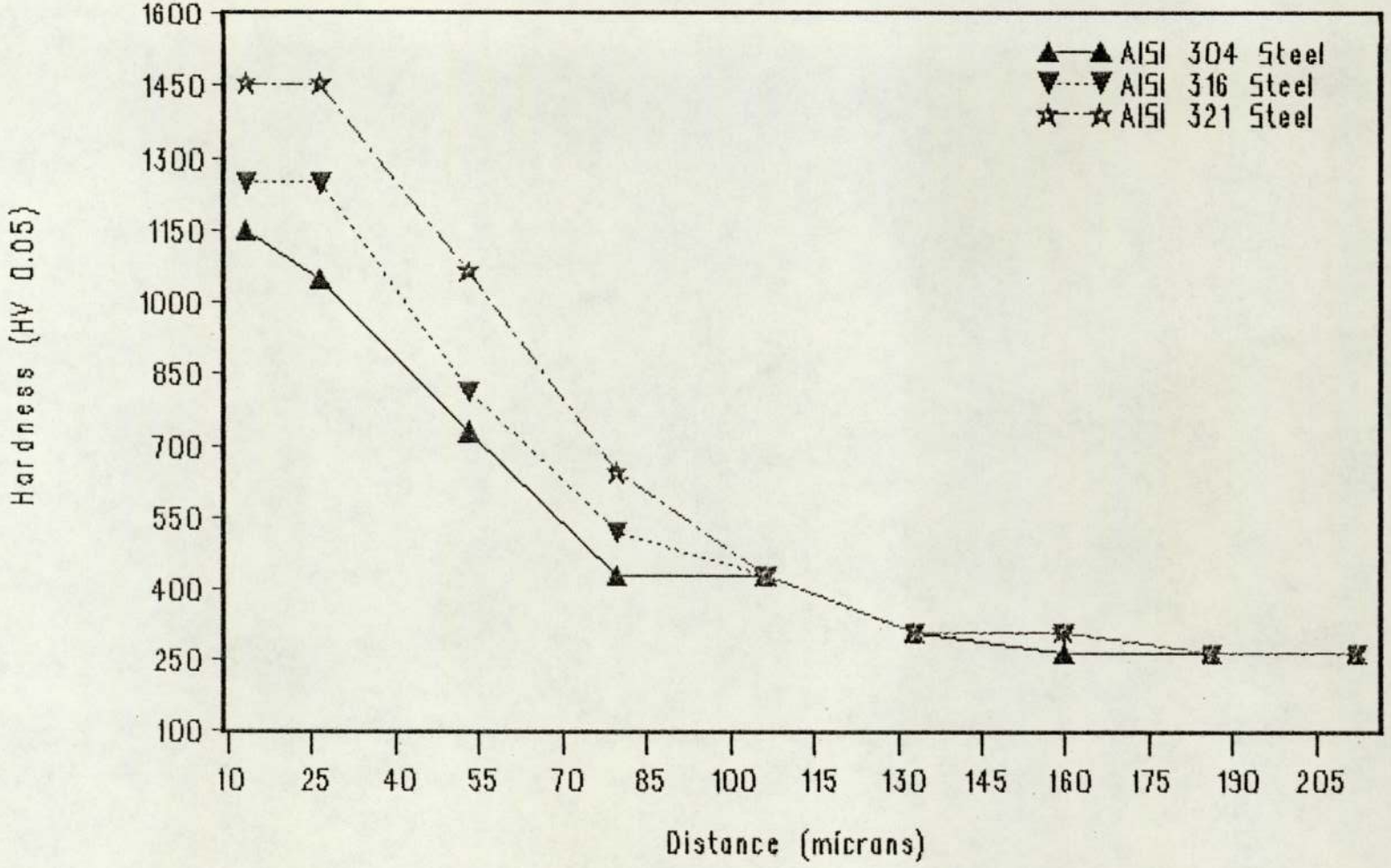

Hardness Vs Distance Plot for Tufftride Treatment

FIGURE-19

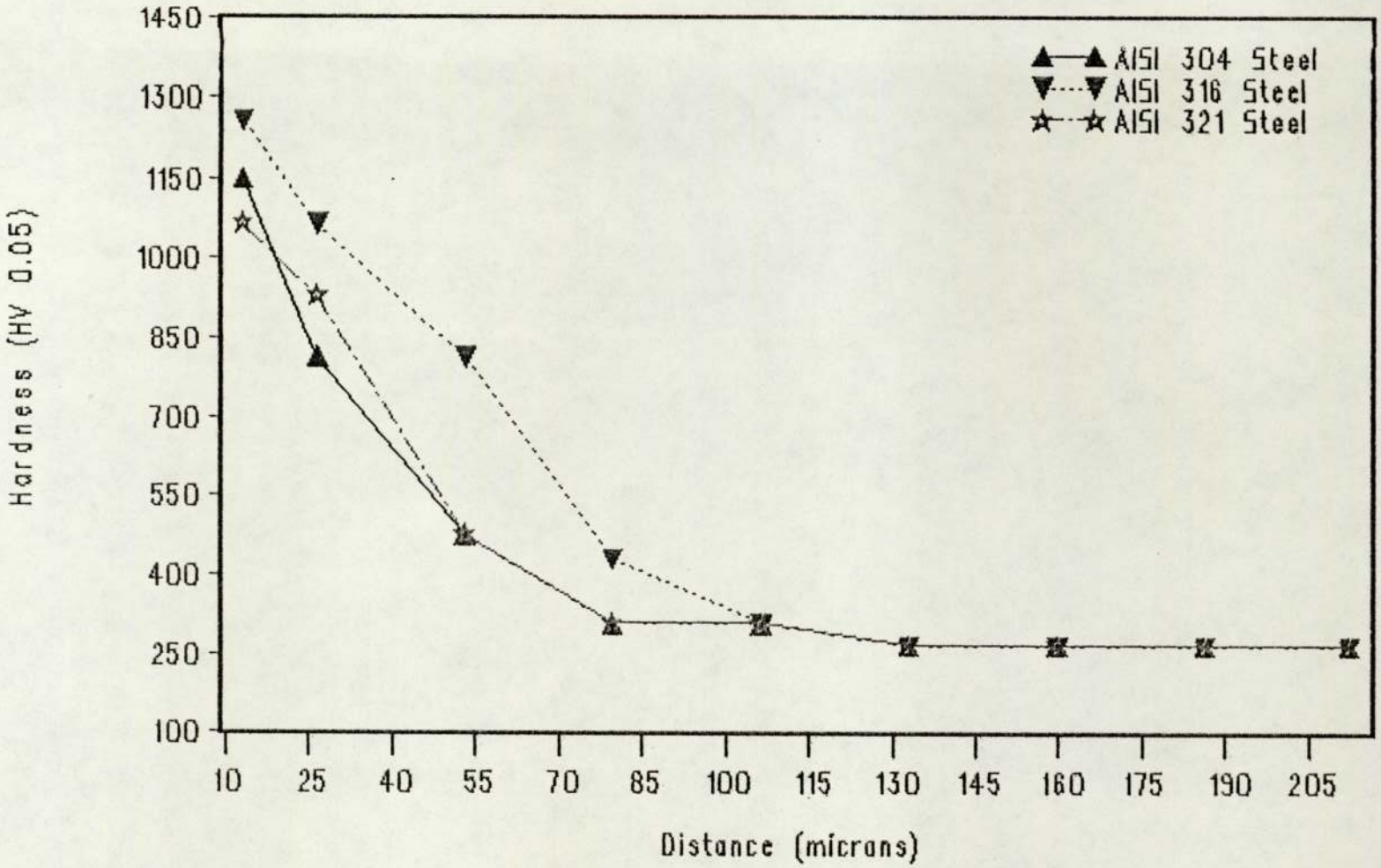

Hardness Vs Distance Plot for Gas Nitriding

FIGURE-20

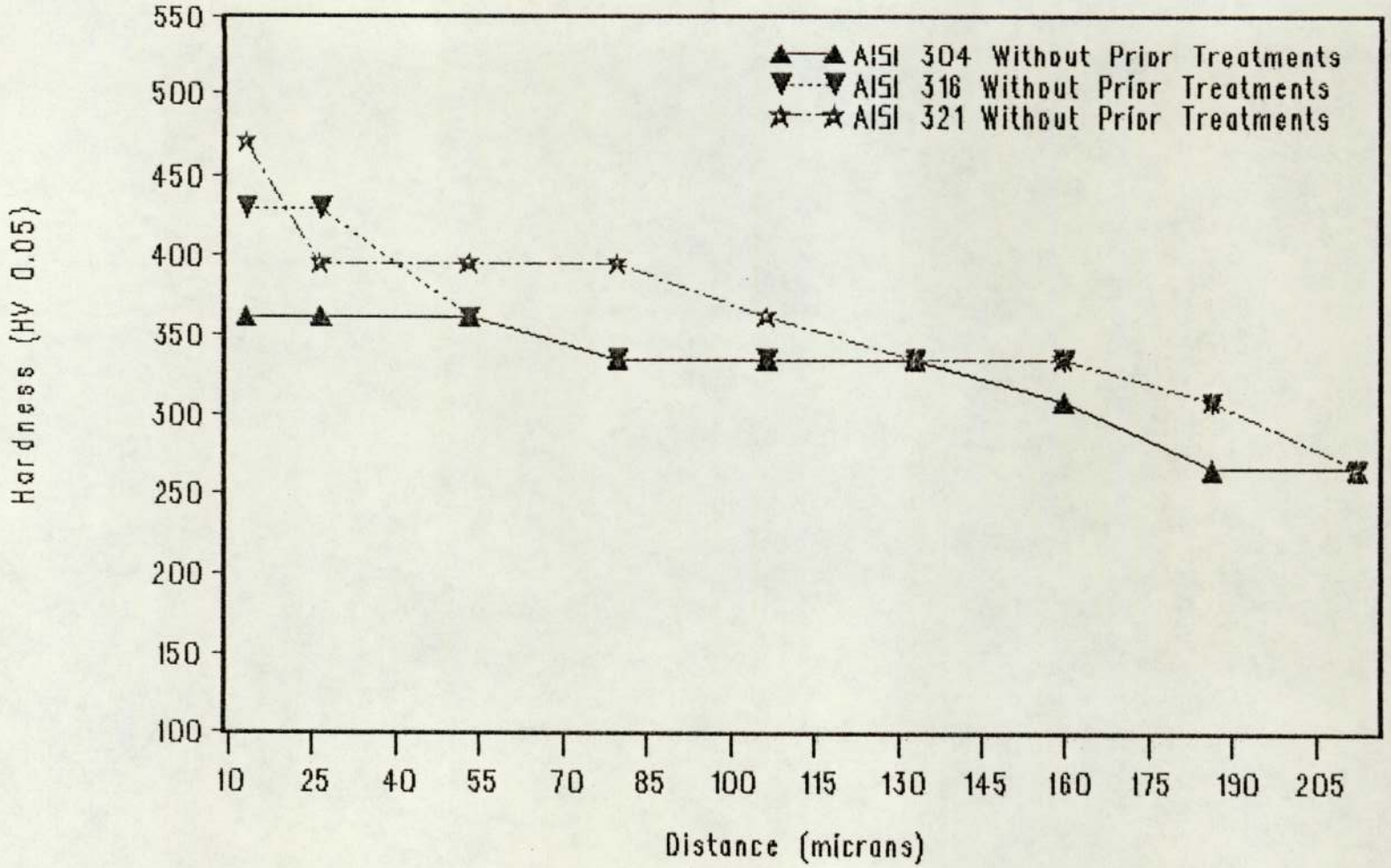

Hardness Vs Distance Plot for Gas Nitriding

FIGURE-21

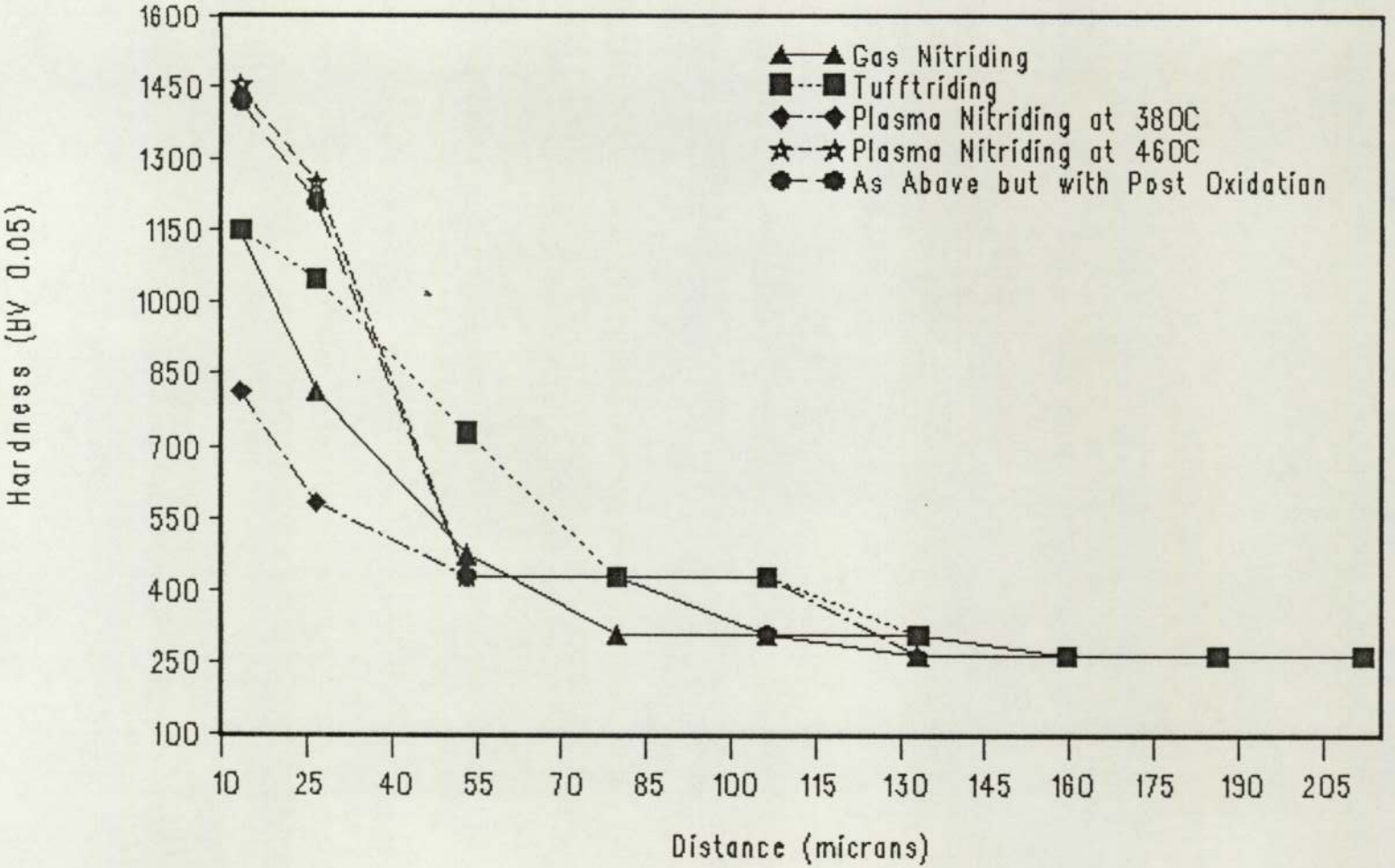

Hardness Vs Distance Plot for AISI 304 after various Treatments

FIGURE-22

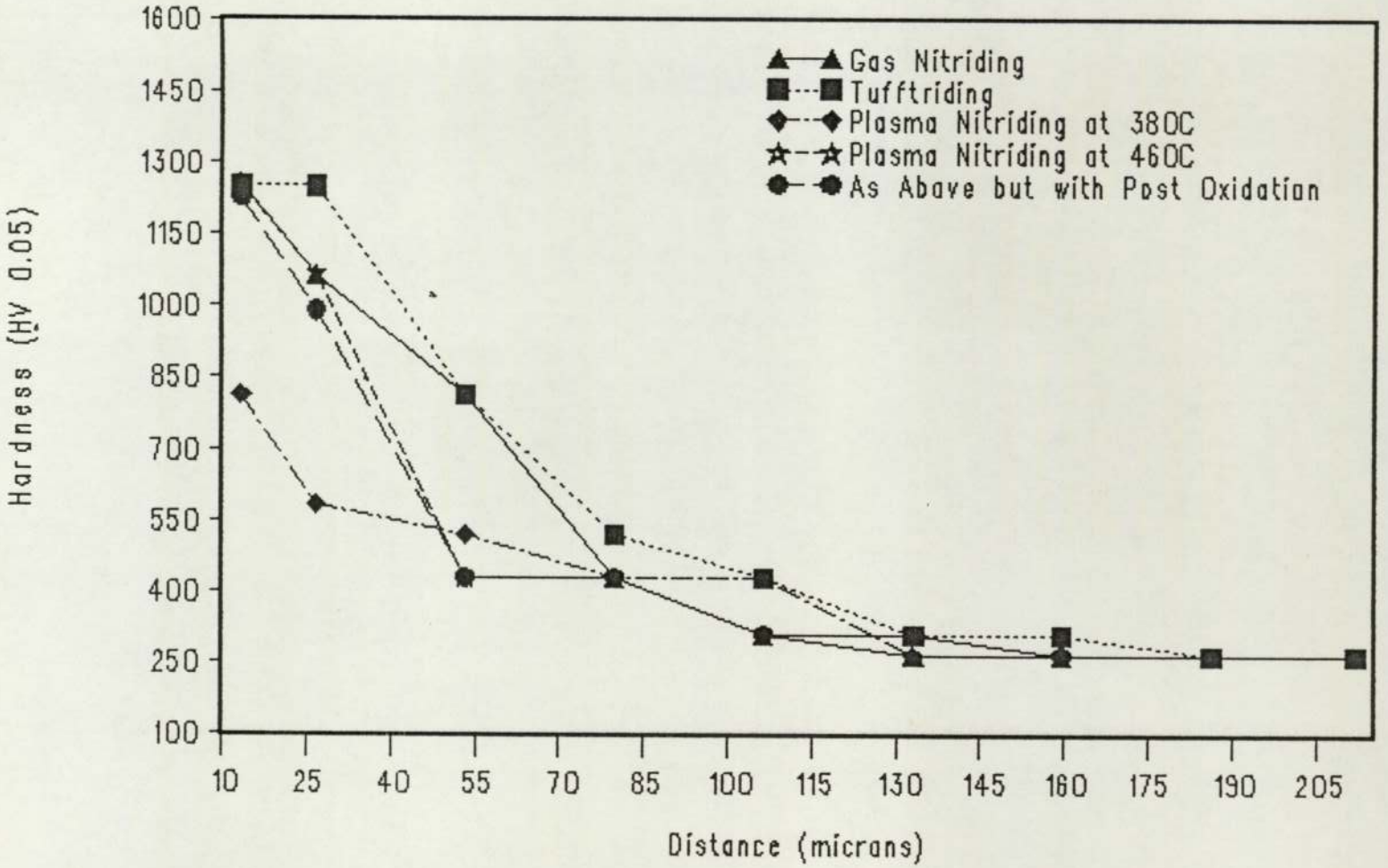

Hardness Vs Distance Plot for AISI 316 after various Treatments

FIGURE-23

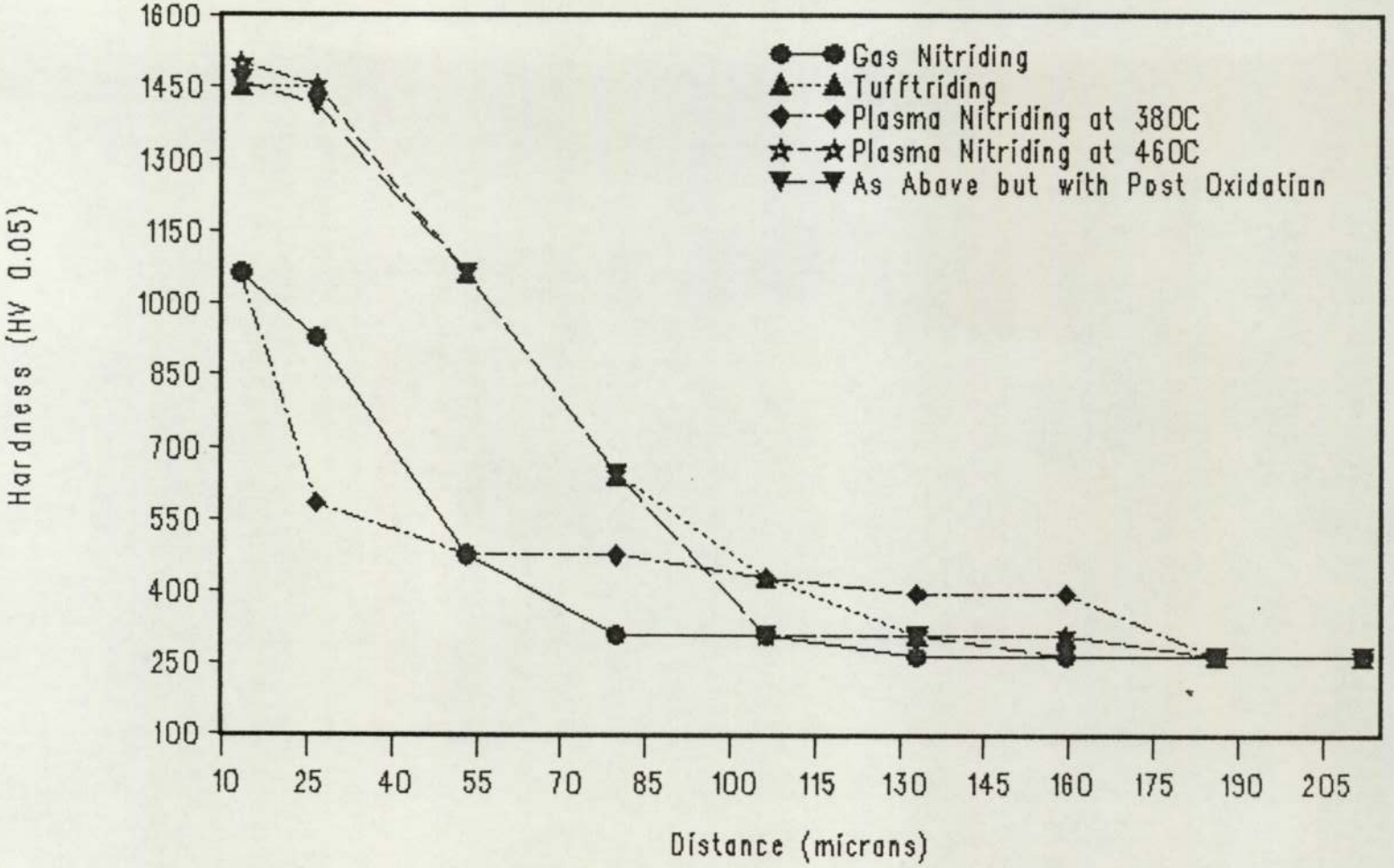

Hardness Vs Distance Plot for AISI 321 after various Treatments

FIGURE-24

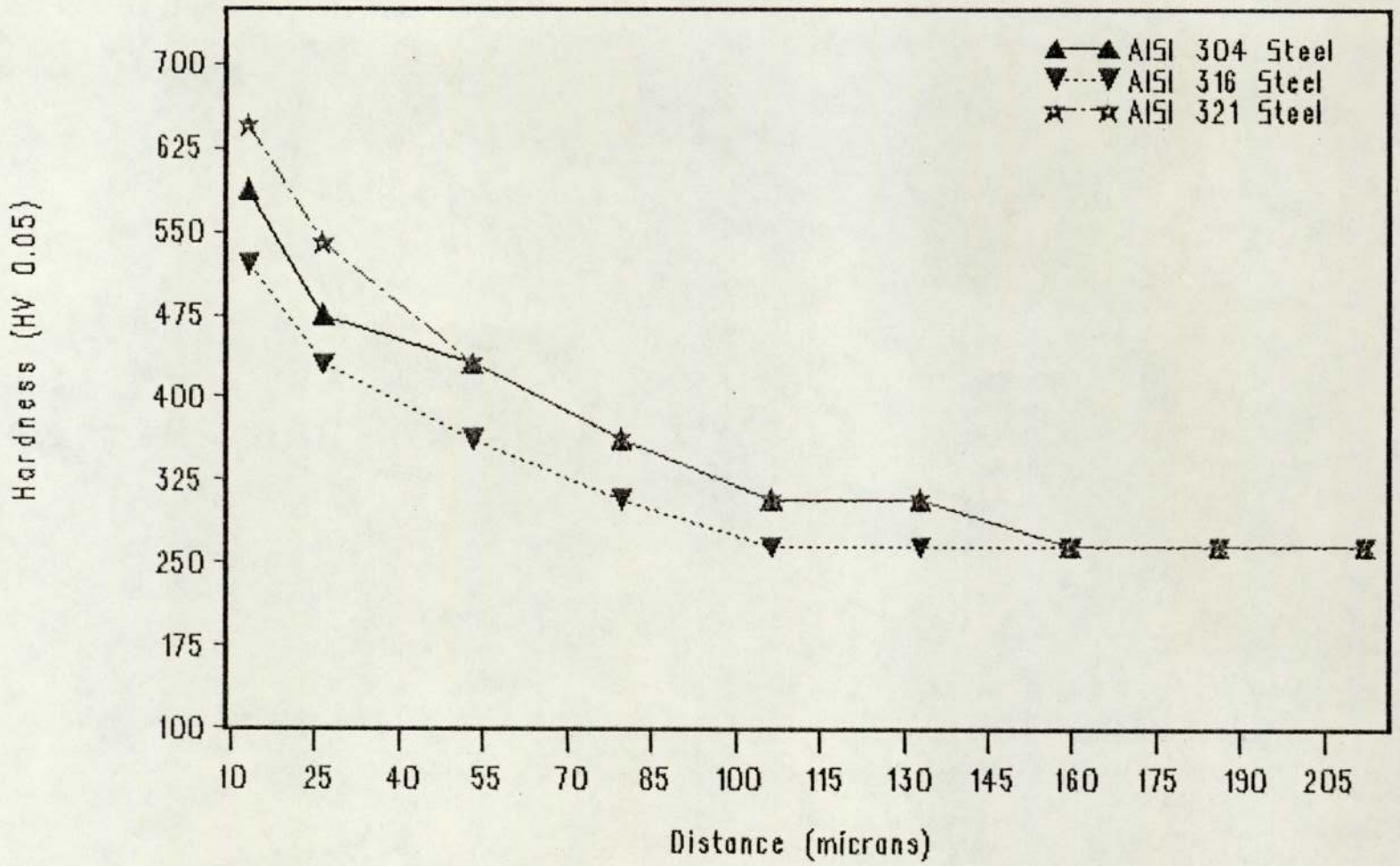

Plasma Nitriding at 460C under Improper Furnace Conditions
Hardness Vs Distance Plot
FIGURE-25

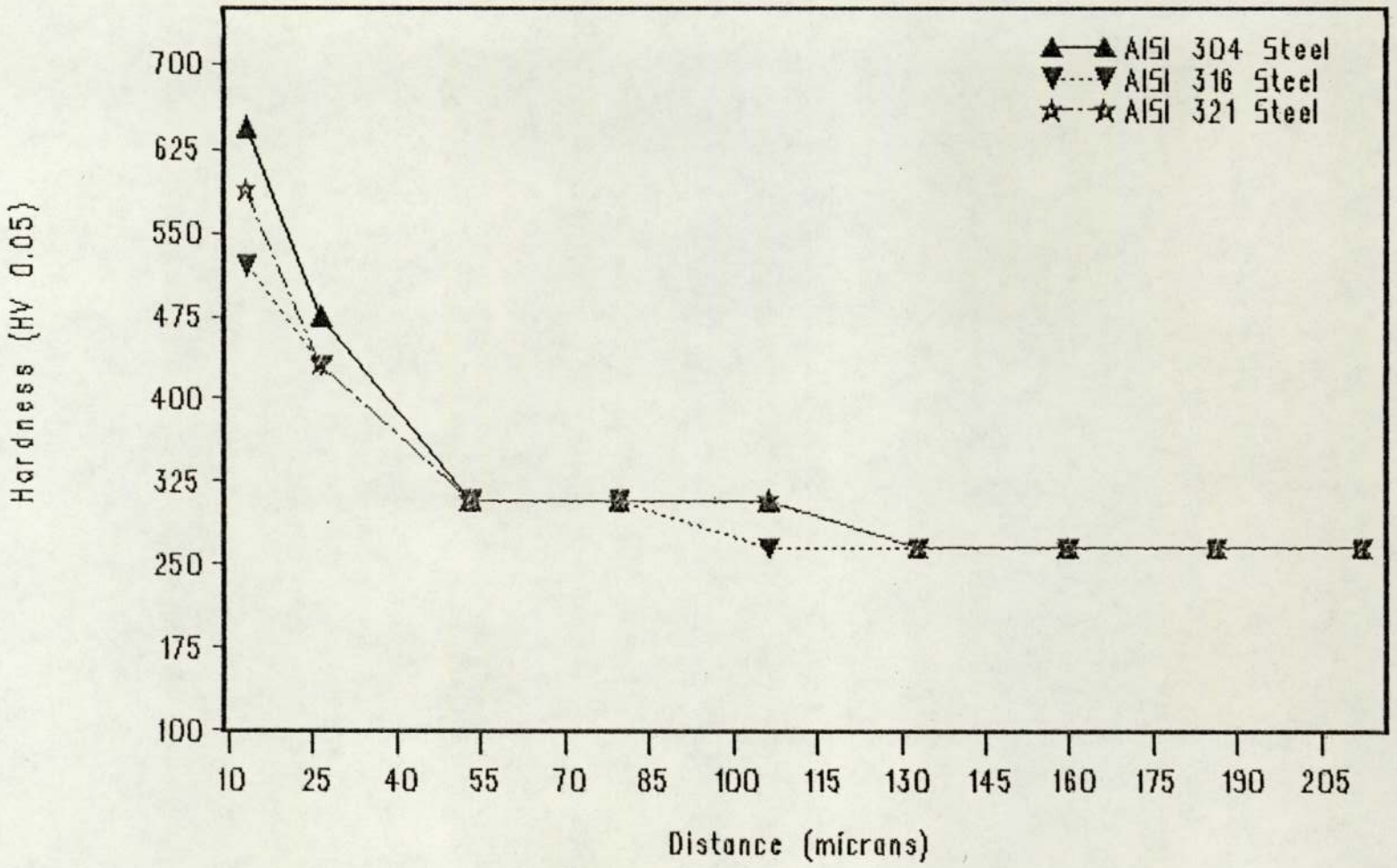

Plasma Nitriding at 540C under Improper Furnace Conditions
Hardness Vs Distance Plot

FIGURE-26

adopted for carrying out the corrections is explained in Appendix-1. The corrosion plots were obtained by plotting I_{corr} (log 10) against time.

Figures 27 and 28 show the corrosion plots of the Tufftrided specimens and the gas nitrided specimens respectively.

The corrosion plots of the specimens that were plasma nitrided under various conditions (refer Table-3b) are shown in Figures 29 to 38.

Figure 39 shows the corrosion plot of the different grades of untreated stainless steel.

The corrosion plots for the comparison of the different treatments on the same steel are shown in Figure 40, 41 and 42 respectively, for different grades of stainless steel.

The visual appearance of the untreated specimens after the corrosion test (Plate 21) shows very little corrosion compared to the ones subjected to various treatments (Plates 22 to 26) and the luster of the material is clearly visible underneath the thin layer of corrosion products on the surface.

6.5 Wear Measurement

Table-4 shows the results from a series of tests on pins of different grades of stainless steel which were treated under different conditions.

For those pins which seized in less than 7 minutes the time to seizure has been shown, otherwise the pin mass loss has been shown along with the wear rate. The wear rate is defined as the mass lost by a pin divided by the run time, hence

$$W = \delta mp/T$$

Where,

W = Wear rate

δmp = mass lost in milligrams

T = Time in seconds

The visual appearance of the pins after the Falex test could be classified into the following categories (Plates 27, 28, 29 and 30):

a) Slightly scuffed

b) Scuffed

c) Badly scuffed

d) Totally seized and sheared

The typical behaviour of the load and the torque during the wear testing under the above described conditions of wear are shown in Graphs Appendix-2.

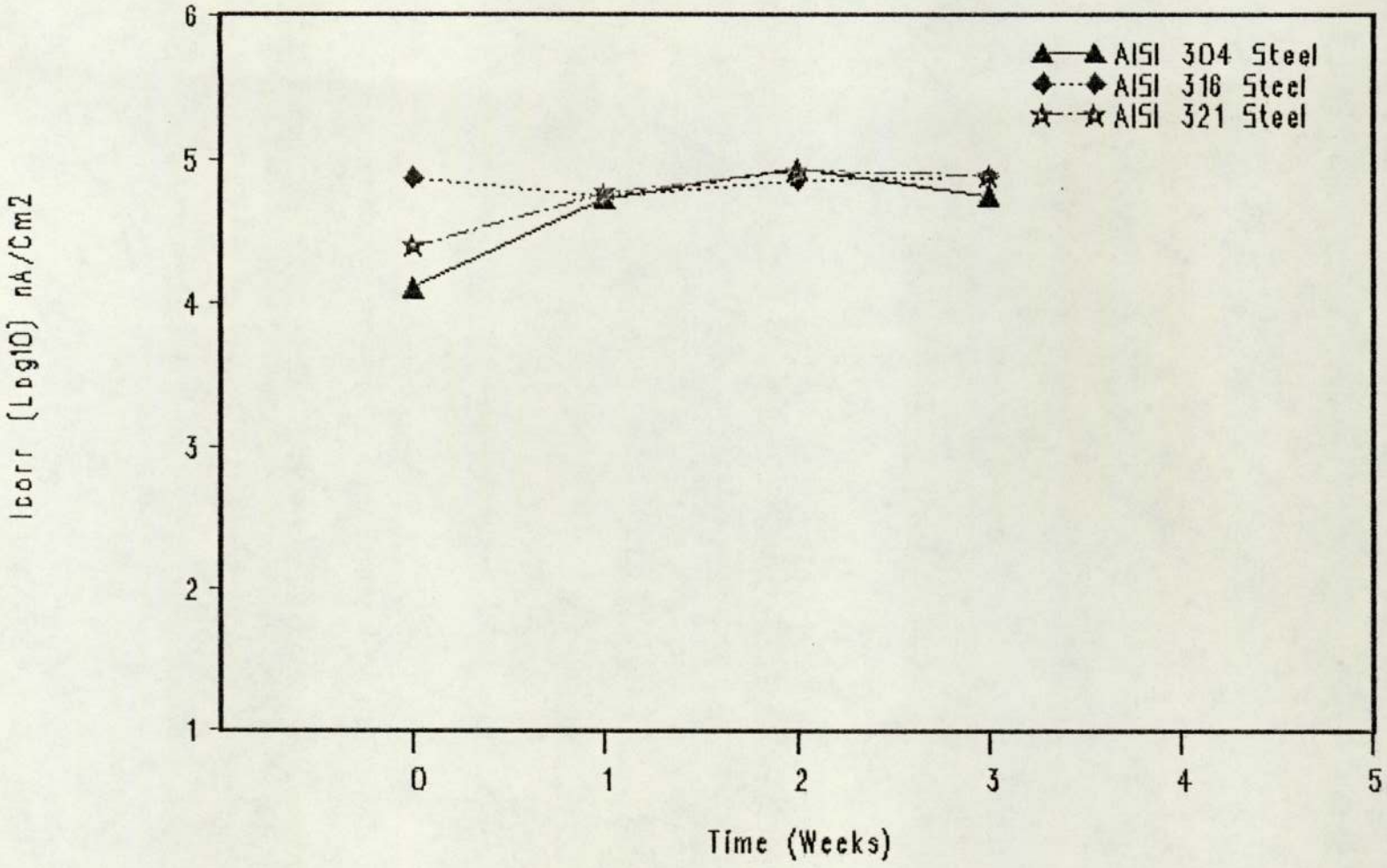

Corrosion Plot for Tufftride Treatment

FIGURE-27

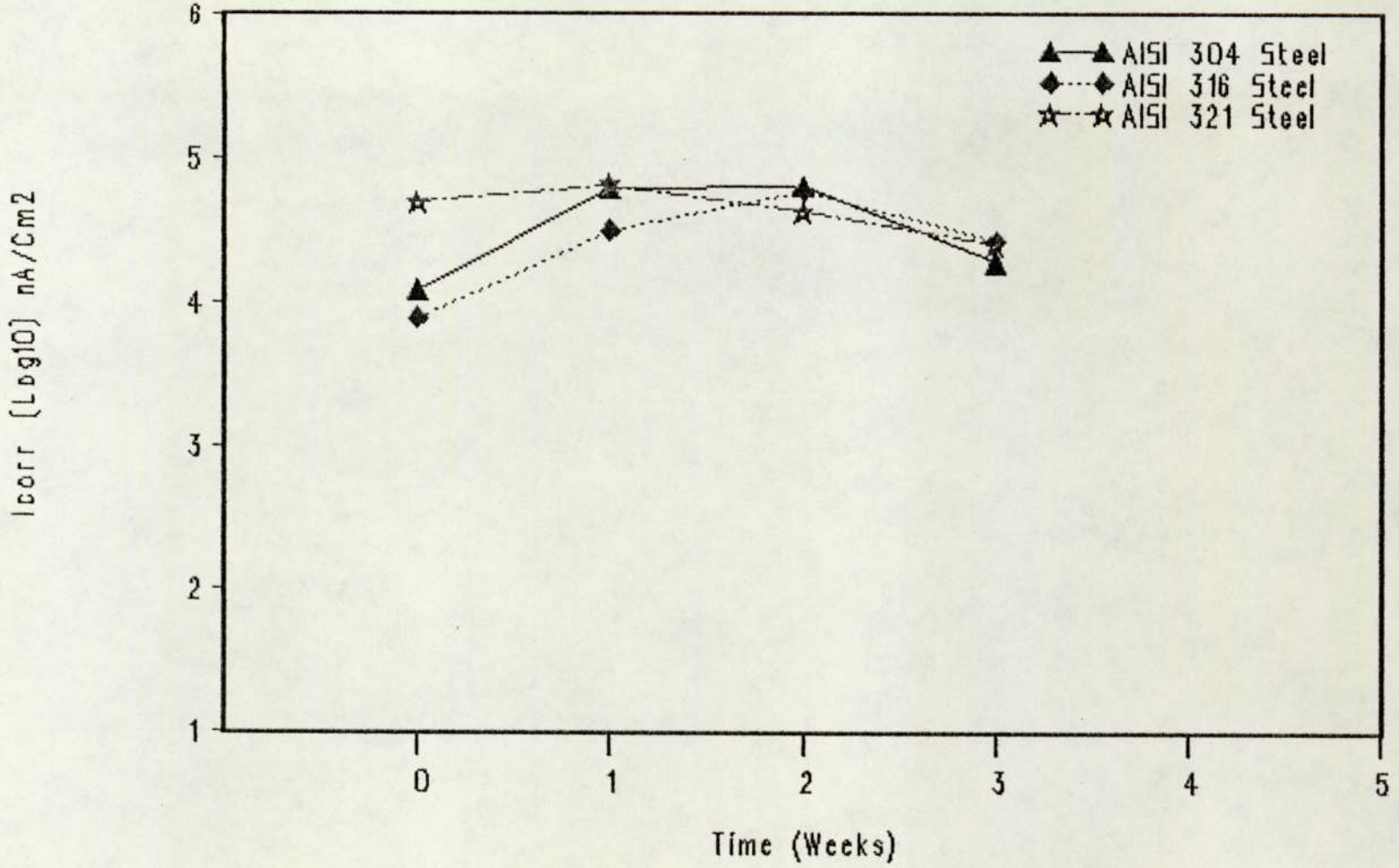

Corrosion Plot for Gas Nitriding Treatment

FIGURE-28

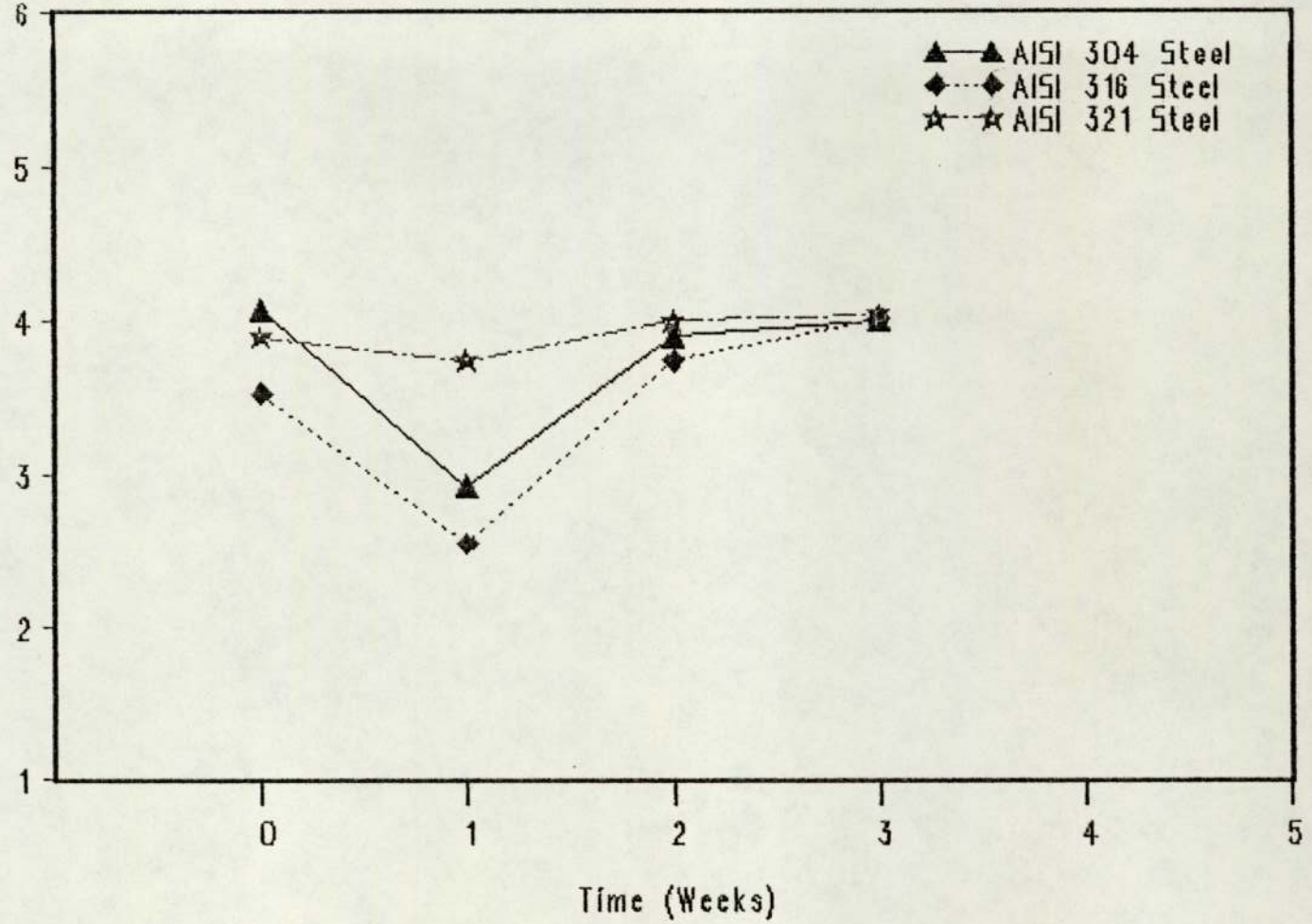

Corrosion Plot for Plasma Nitriding Treatment at 380C

FIGURE-29

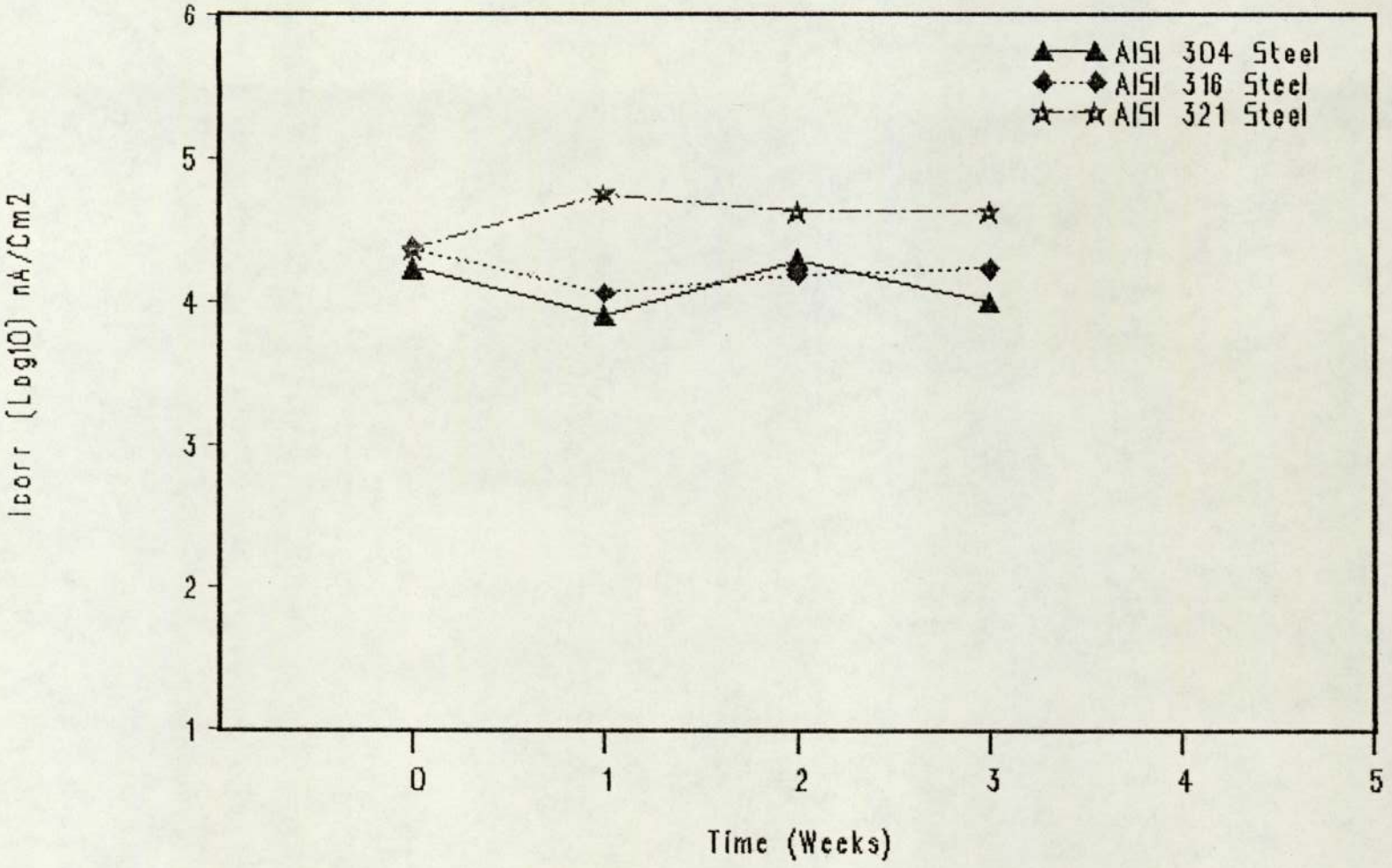

Corrosion Plot for Plasma Nitriding Treatment at 420C

FIGURE-30

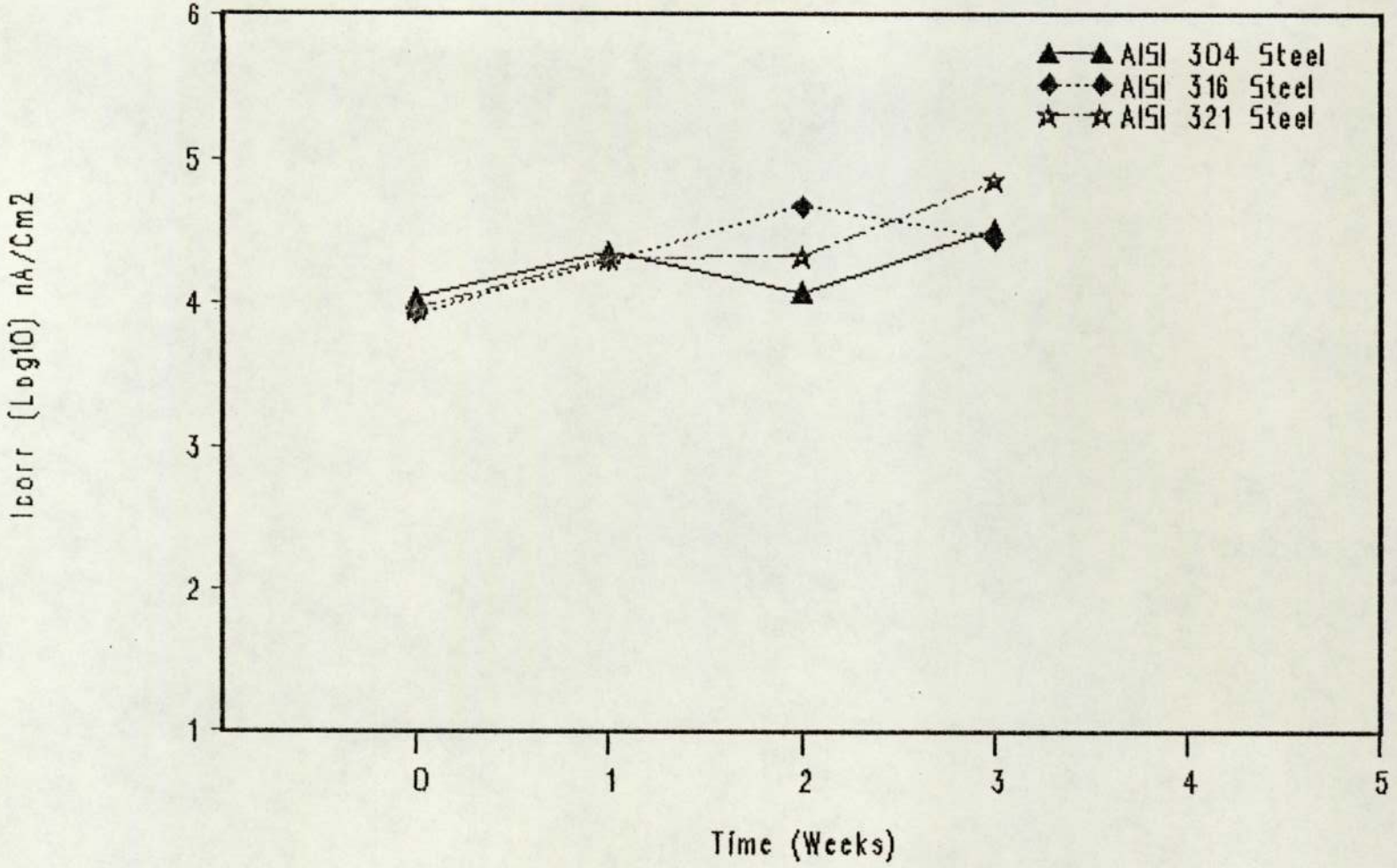

Corrosion Plot for Plasma Nitriding Treatment at 460C

FIGURE-31

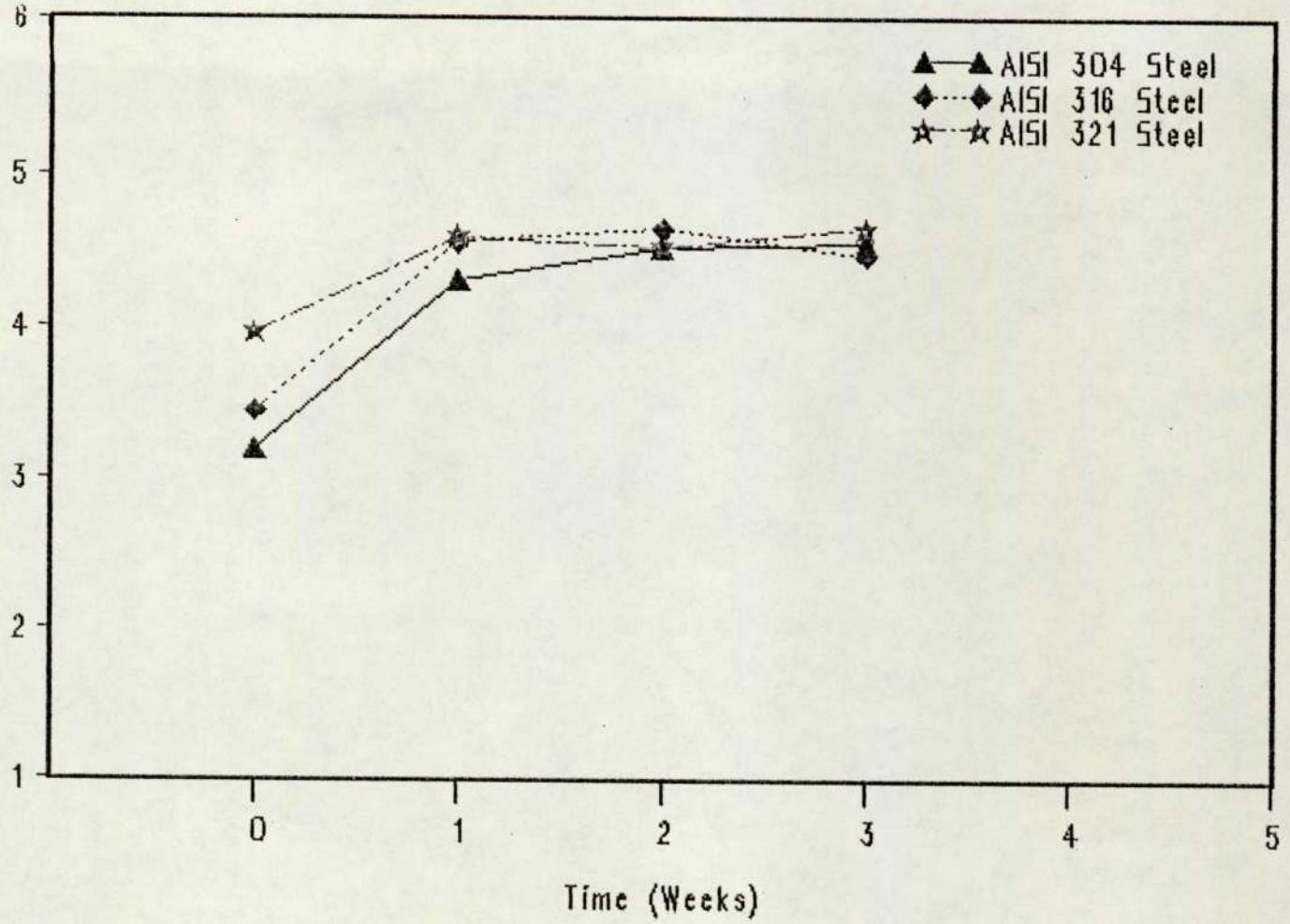

Corrosion Plot for Plasma Nitriding Treatment at 500C

FIGURE-32

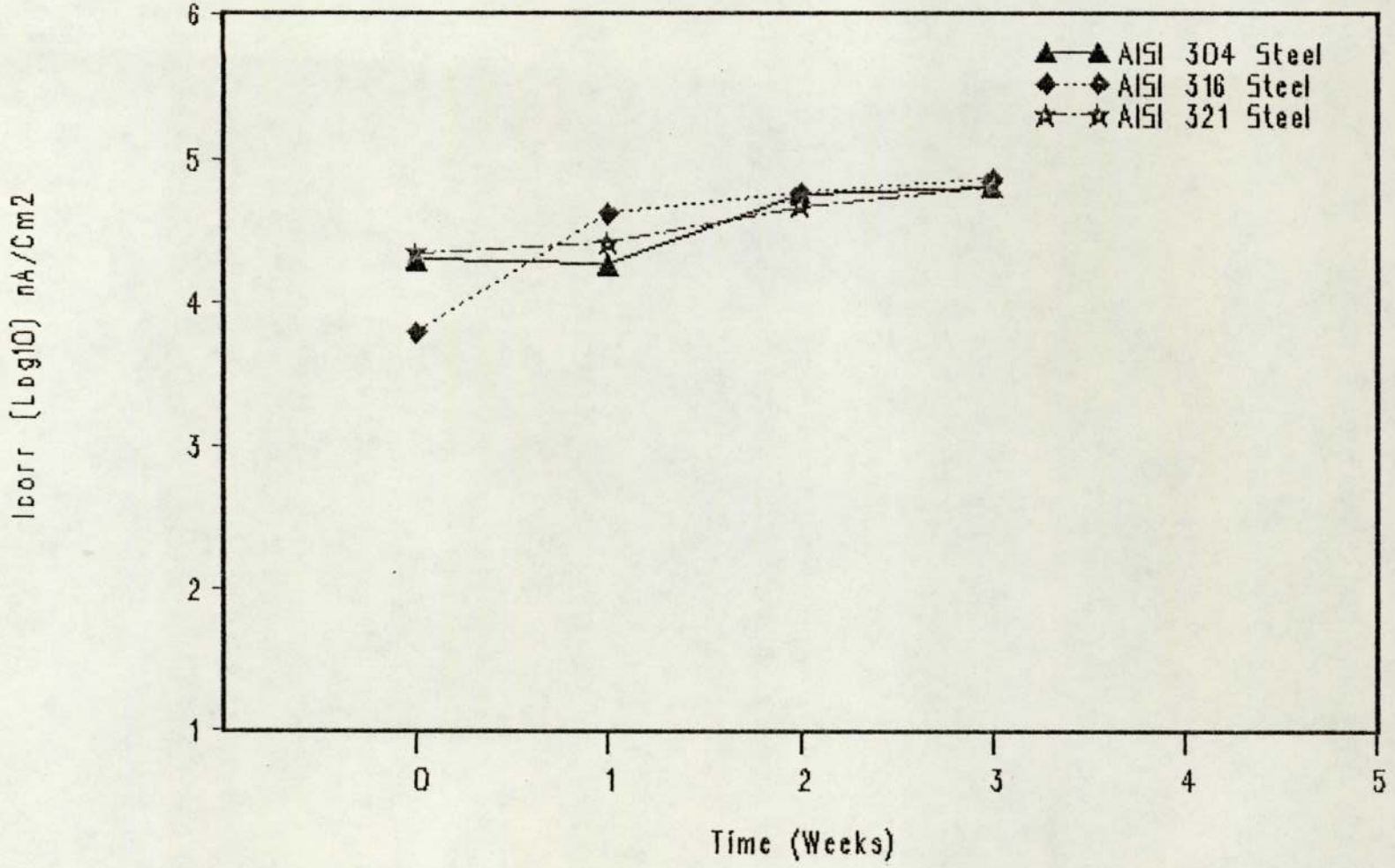

Corrosion Plot for Plasma Nitriding Treatment at 540C

FIGURE-33

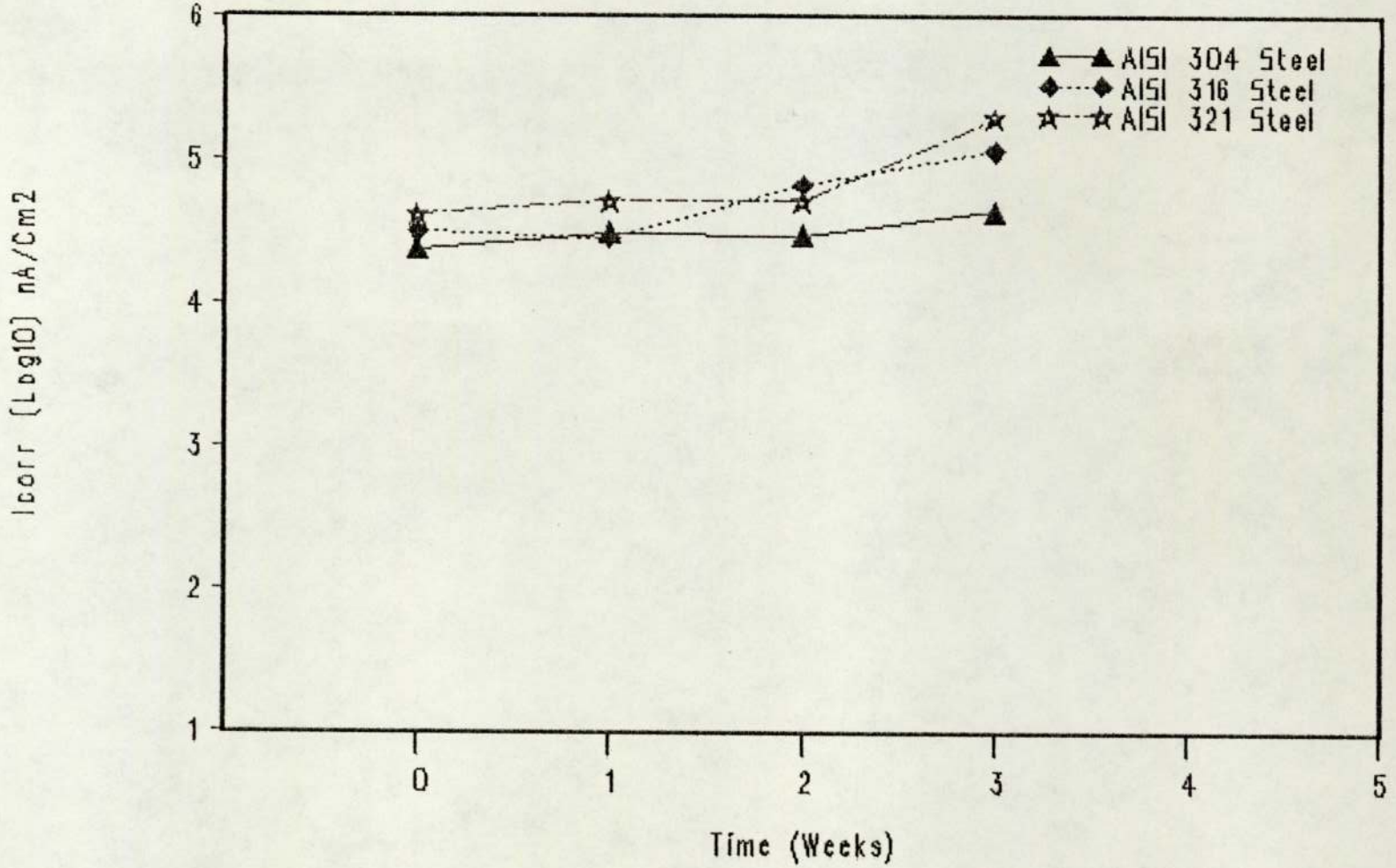

Corrosion Plot for Plasma Nitriding Treatment at 570C

FIGURE-34

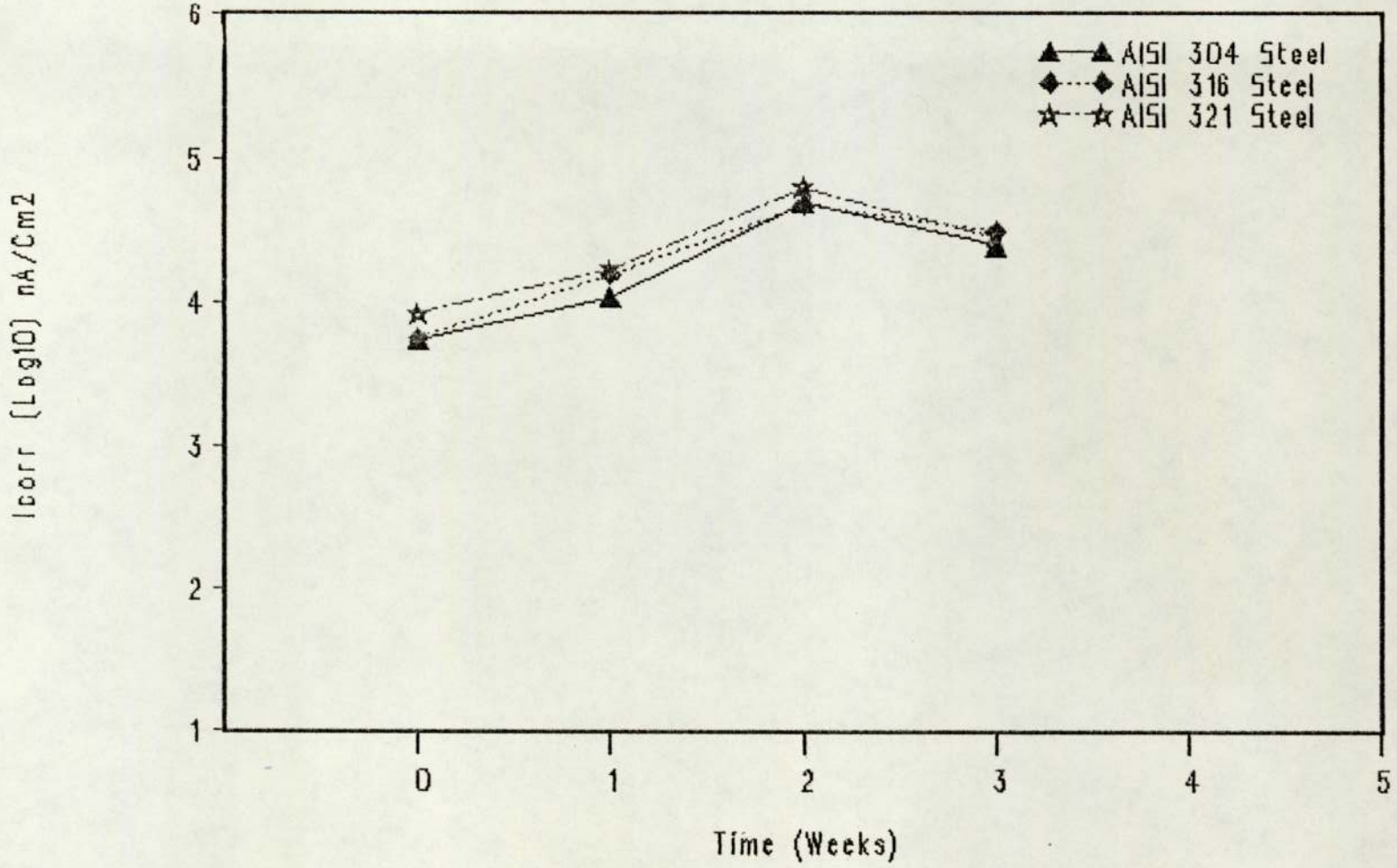

Corrosion Plot for Plasma Nitriding at 460C with Post Oxidation

FIGURE-35

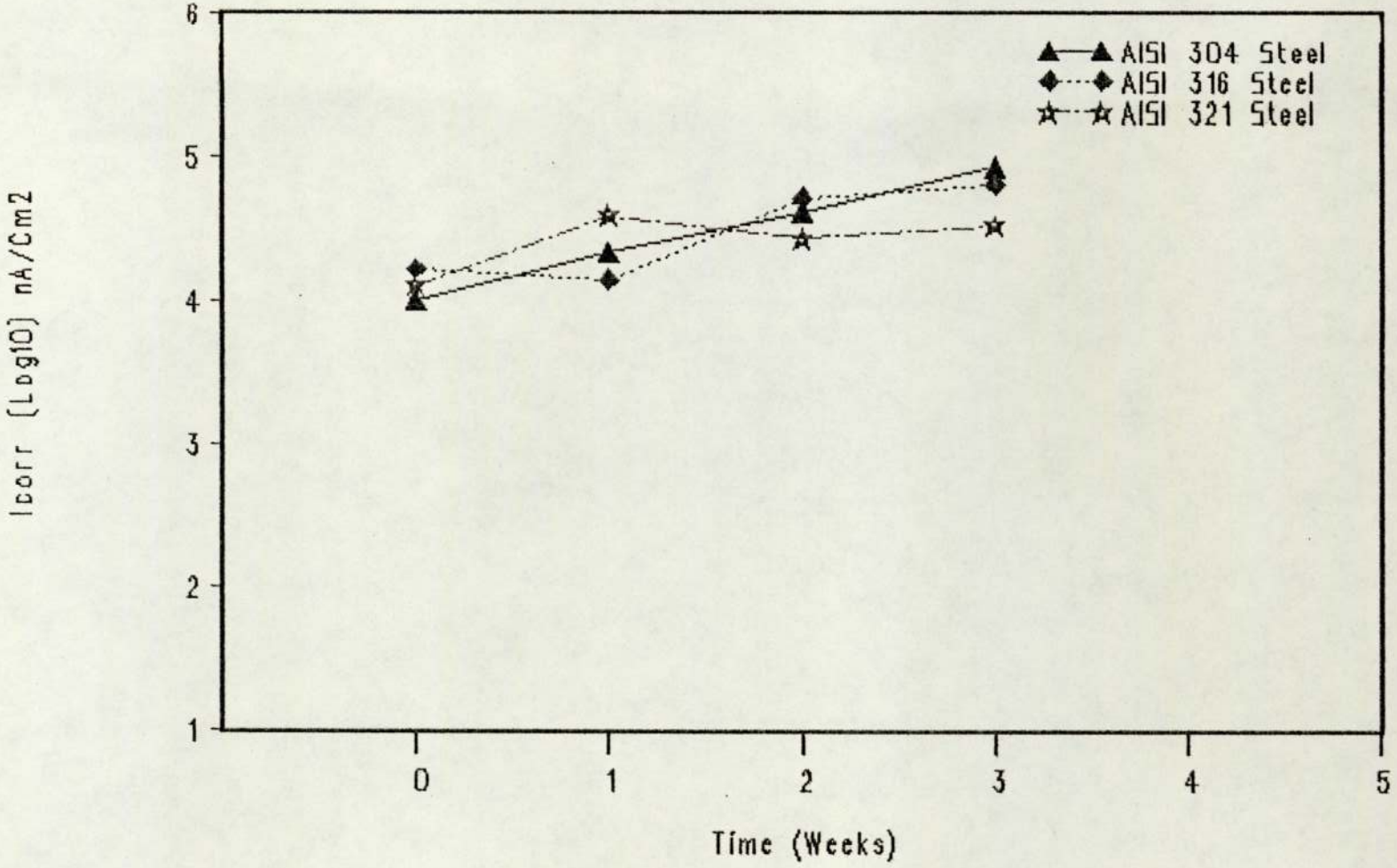

Corrosion Plot for Plasma Nitriding at 500C with Post Oxidation

FIGURE-36

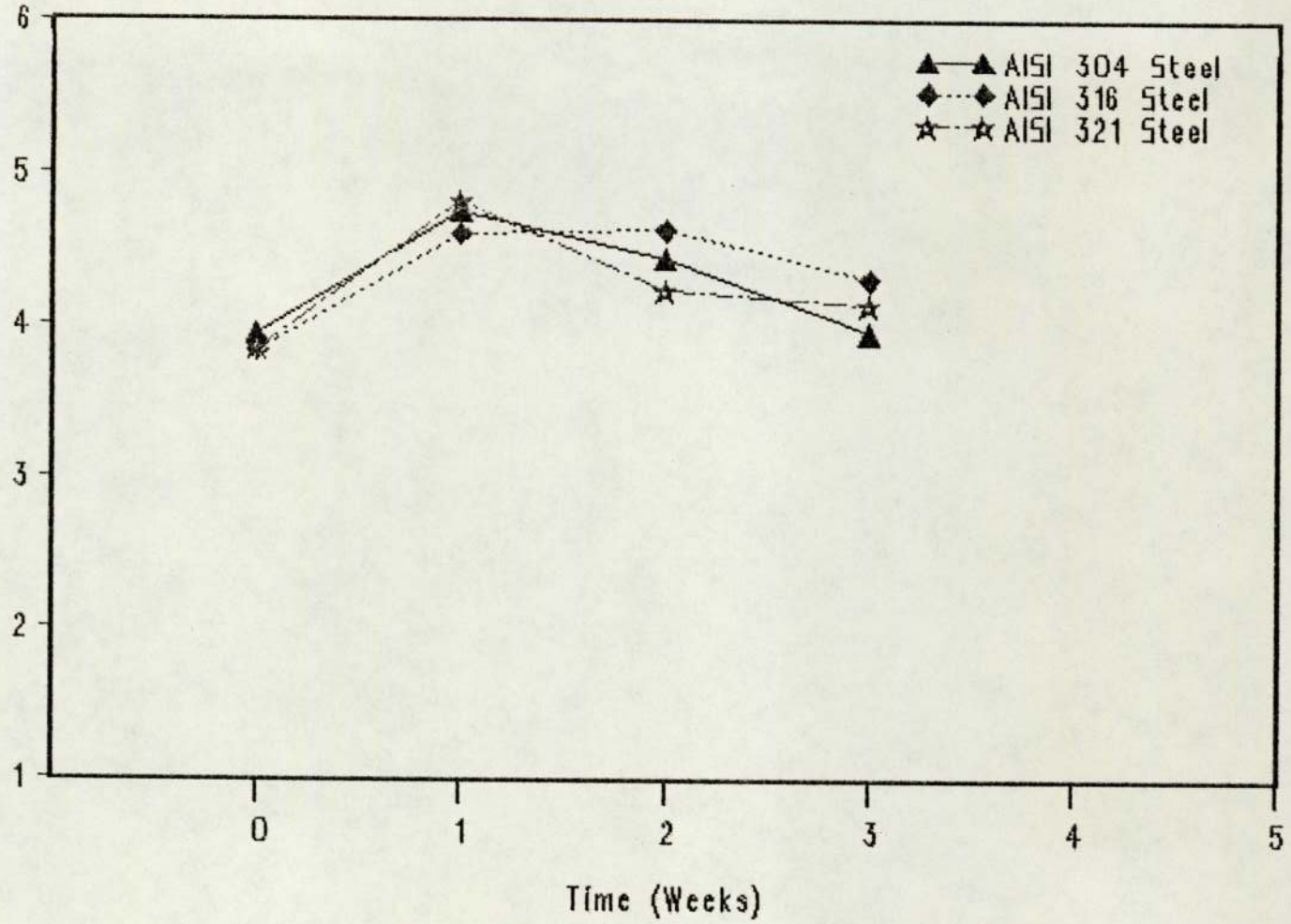

Corrosion Plot for Plasma Nitriding at 540C with Post Oxidation

FIGURE-37

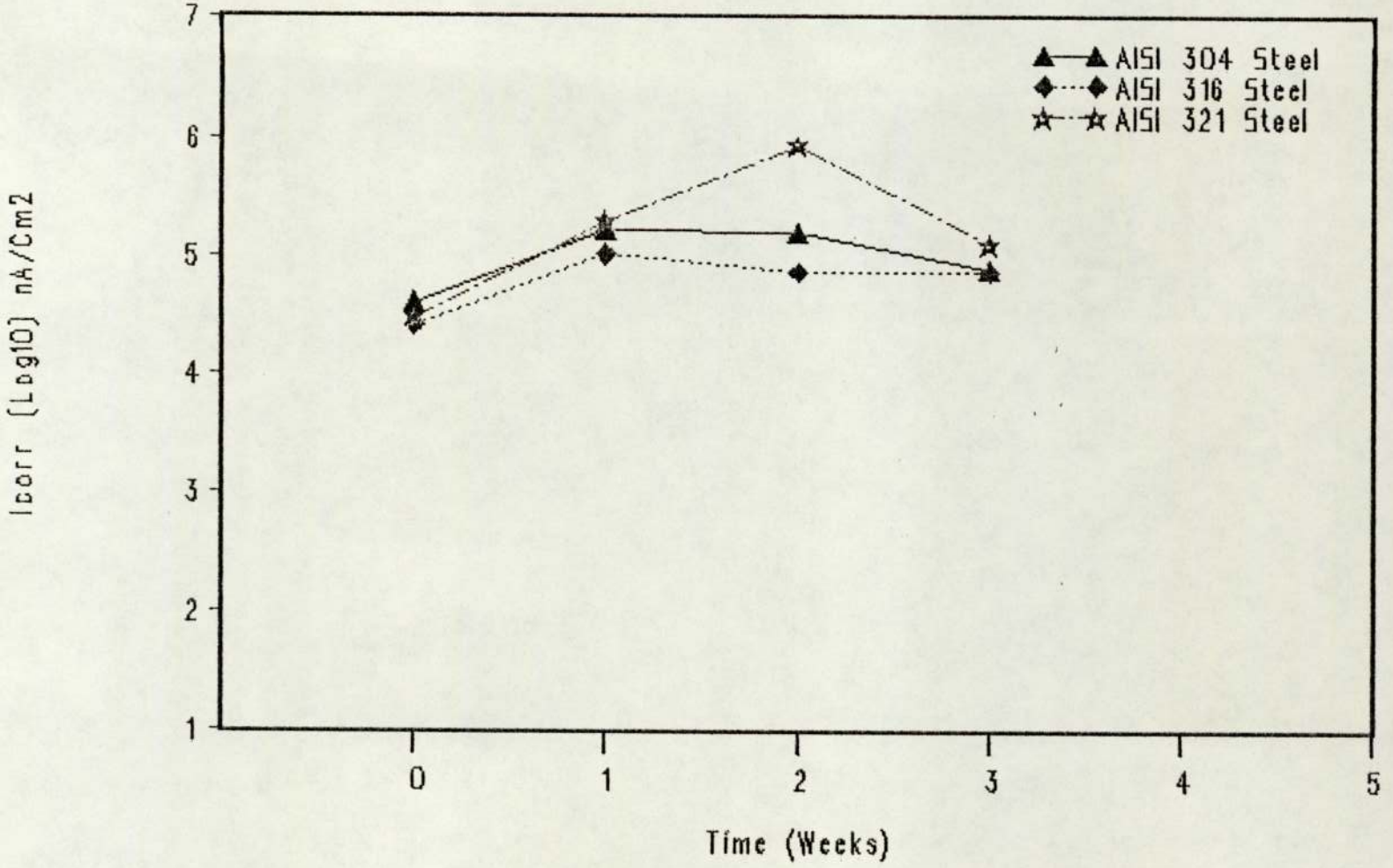

Corrosion Plot for Plasma Nitriding at 570C with Post Oxidation

FIGURE-38

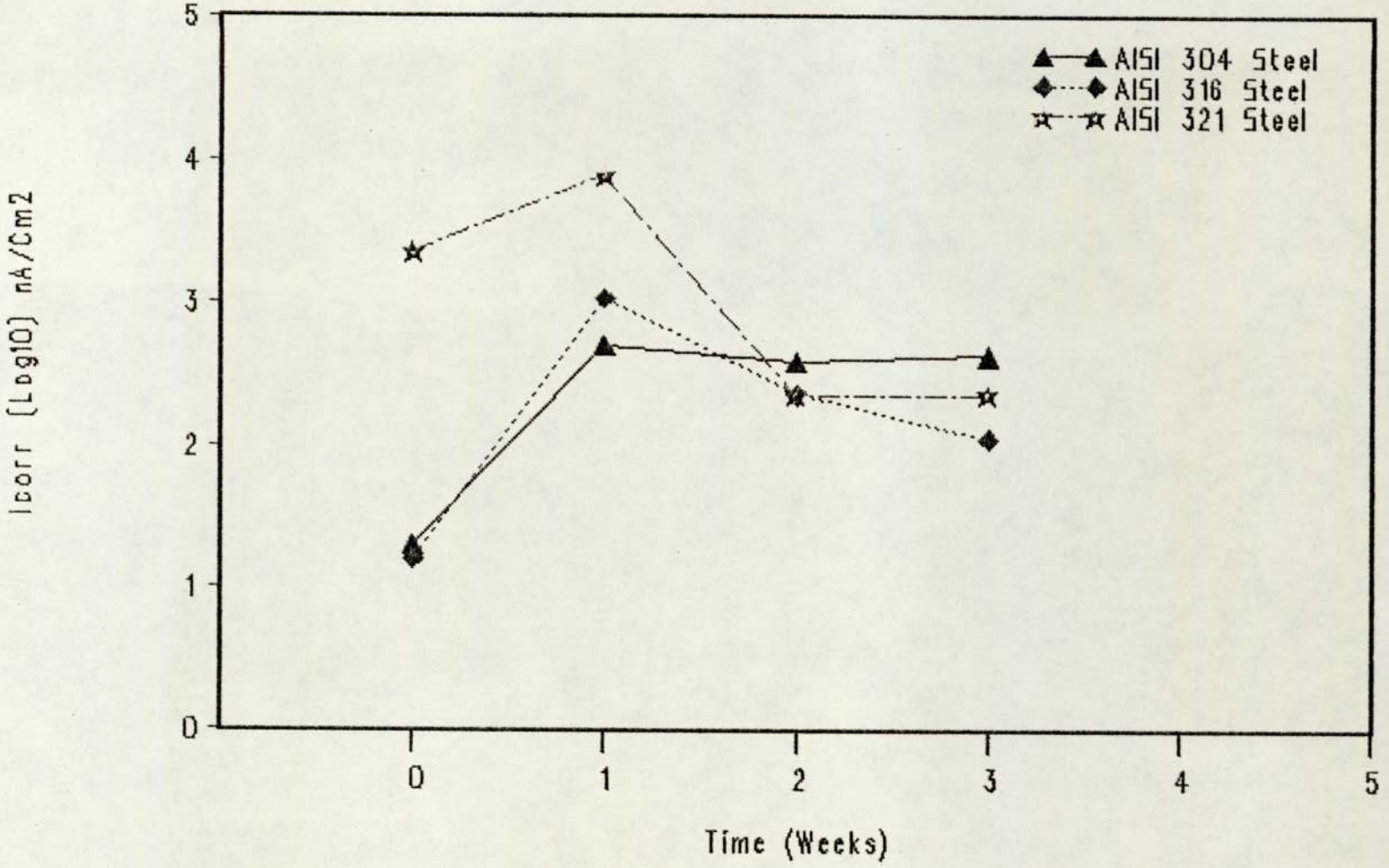

Corrosion Plot for Untreated Stainless Steels

FIGURE-39

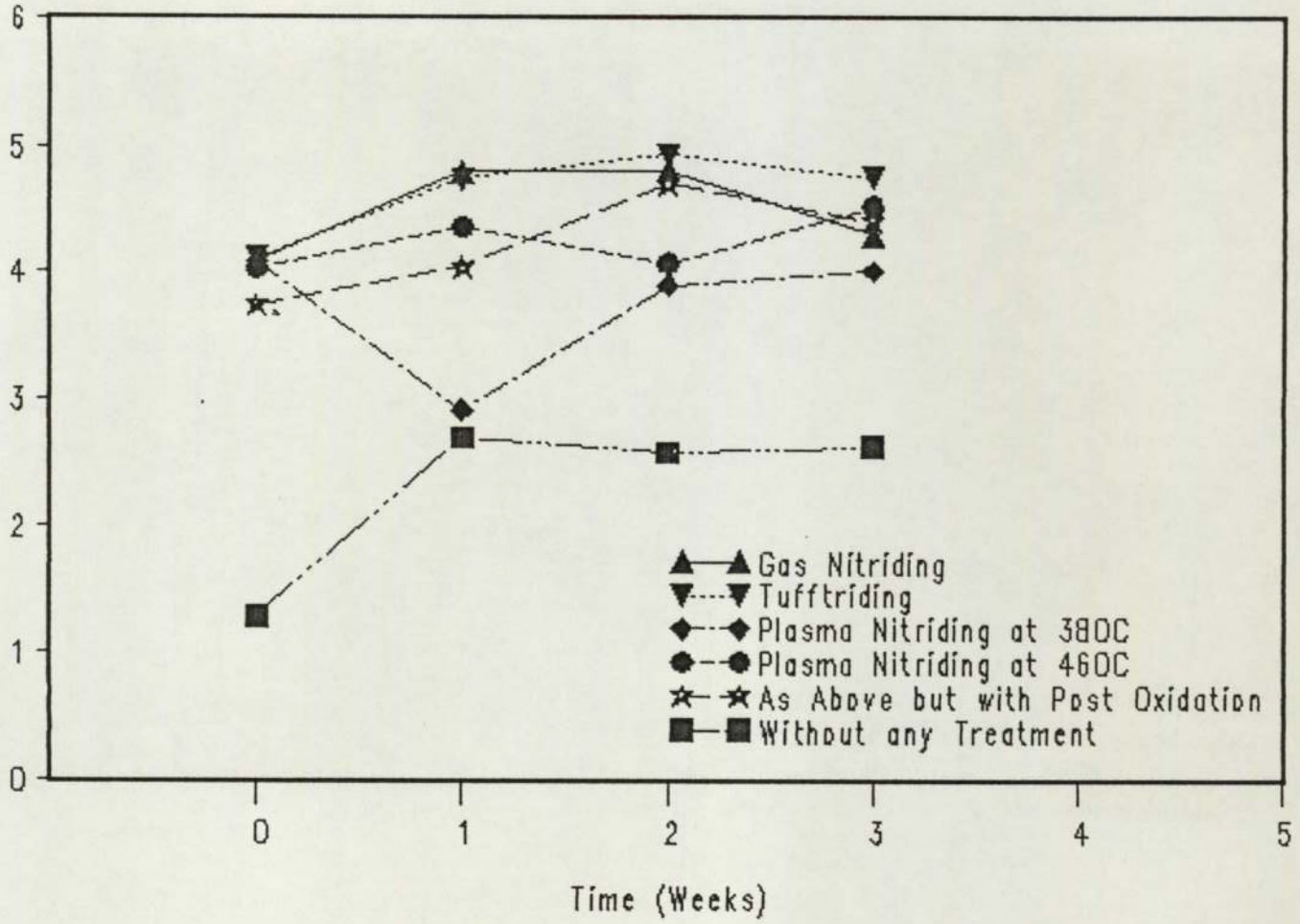

Corrosion Plot for AISI 304 Steel after various Treatments

FIGURE-40

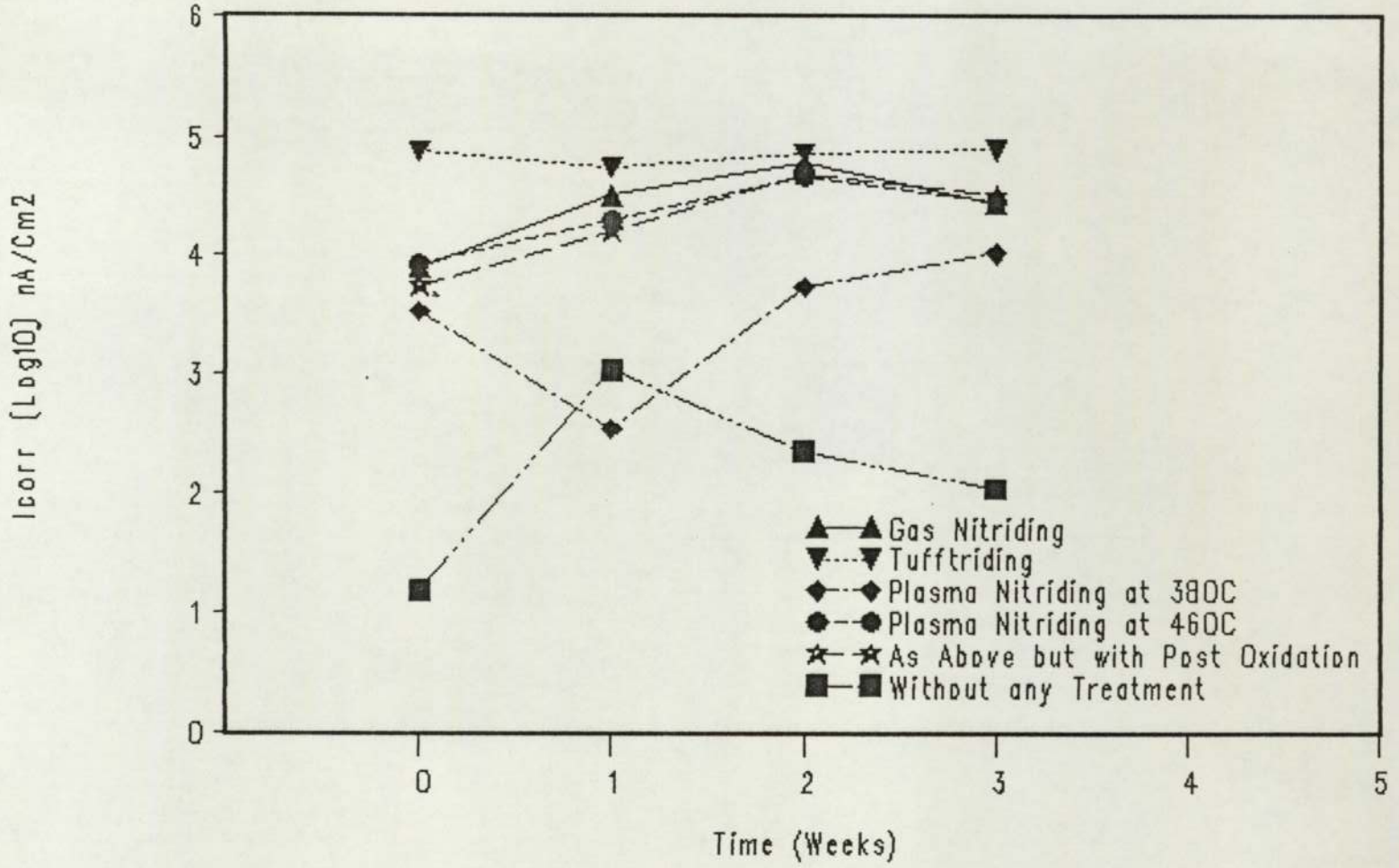

Corrosion Plot for AISI 316 Steel after various Treatments

FIGURE-41

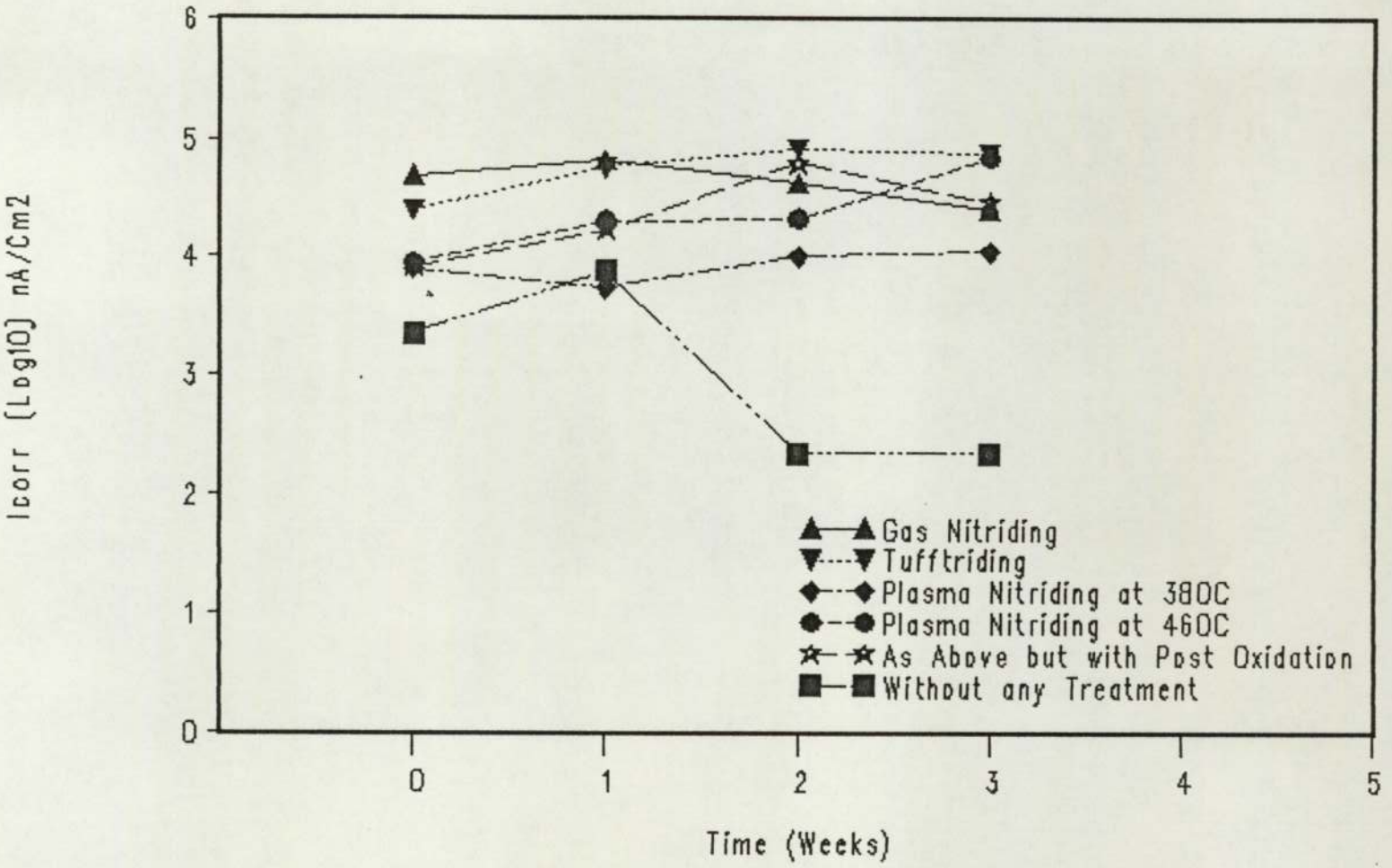

Corrosion Plot for AISI 321 Steel after various Treatments

FIGURE-42

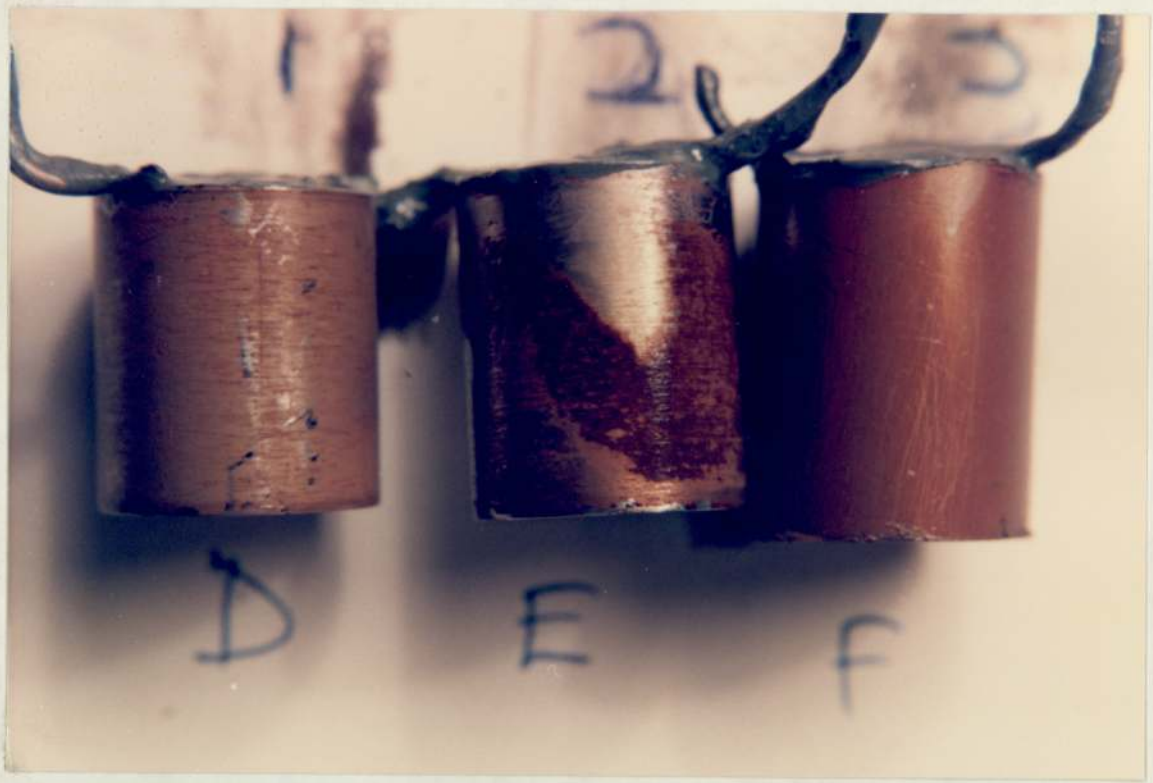

D-AISI 304 Grade E-AISI 316 Grade F-AISI 321 Grade

Plate-21 Untreated Stainless Steel Specimens after Corrosion Test

Plate-22 Plasma Nitrided Stainless Steel Specimens after Corrosion Test

Plate-23 Plasma Nitrided Stainless Steel Specimens With Post-Oxidation

4-AISI 304 Grade 5-AISI 316 Grade 6-AISI 321 Grade

Plate-24 Plasma Nitrided Stainless Steel Specimens at 380^{o}C after Corrosion Test

1-AISI 304 Grade 2-AISI 316 Grade 3-AISI 321 Grade

Plate-25 Tufftrided Stainless Steel Specimens after Corrosion Test

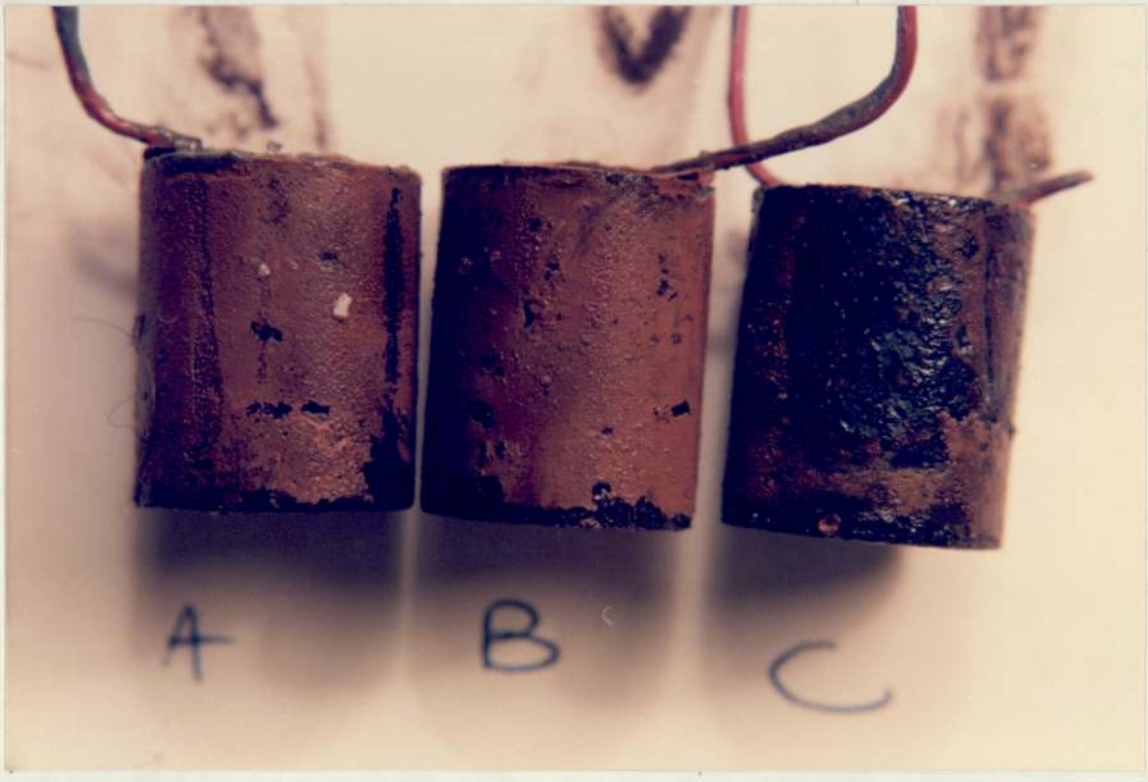

A-AISI 304 Grade B-AISI 316 Grade C-AISI 321 Grade

Plate-26 Gas Nitrided Stainless Steel Specimens after Corrosion Test

Treatment	Pin mass loss (mg)			Average wear rate (mg/s)×10^{-2}			Time to seizure (minutes)			Surface condition		
	A	B	C	A	B	C	A	B	C	A	B	C
Tufftriding	24.7	30.0	46.0	5.80	7.15	10.95	-	-	-	SS	SS	SS
Gas nitriding	43.8	-	76.8	10.43	-	18.30	-	3.92	-	S	SH	S
Plasma nitriding at 380°C	-	-	51.31	-	-	12.20	3.52	3.42	-	SH	SH	BS
Plasma nitriding at 420°C	-	85.38	42.57	-	20.33	10.13	4.00	-	-	SH	BS	BS
Plasma nitriding at 460°C	41.90	27.35	19.87	9.98	6.51	4.73	-	-	-	S	S	S
Plasma nitriding at 500°C	18.56	69.79	65.38	4.42	16.60	15.60	-	-	-	SS	S	S

Continued on next page

Table-4 Results of Test Runs on Falex Machine.

Table-4 continued

Treatment	Pin mass loss (mg)			Average wear rate (mg/s)×10^{-2}			Time to seizure (minutes)			Surface condition		
	A	B	C	A	B	C	A	B	C	A	B	C
Plasma nitriding at 540^{o}C	29.40	54.02	65.77	4.42	16.60	15.66	-	-	-	S	S	S
Plasma nitriding at 570^{o}C	7.02	23.15	16.55	1.67	5.51	3.94	-	-	-	SS	S	SS
Plasma nitriding at 460^{o}C with post-oxidation	18.3	15.98	8.47	9.12	3.80	2.02	-	-	-	SS	SS	SS
Plasma nitriding at 500^{o}C with post-oxidation	10.55	11.90	28.49	2.51	2.83	6.78	-	-	-	SS	SS	S
Plasma nitriding at 540^{o}C with post-oxidation	9.87	10.50	14.44	2.35	2.50	3.44	-	-	-	SS	SS	SS
Untreated	-	-	-	-	-	-	1.0	1.53	2.16	SH	SH	SH

A - AISI 304 stainless steel, B - AISI 316 stainless steel, C - AISI 321 stainless steel,
SS - slightly scuffed, S - scuffed, BS - badly scuffed, SH - totally seized and sheared.

All the specimens were tested at a constant load of 250lbs for 7 minutes unless otherwise indicated.

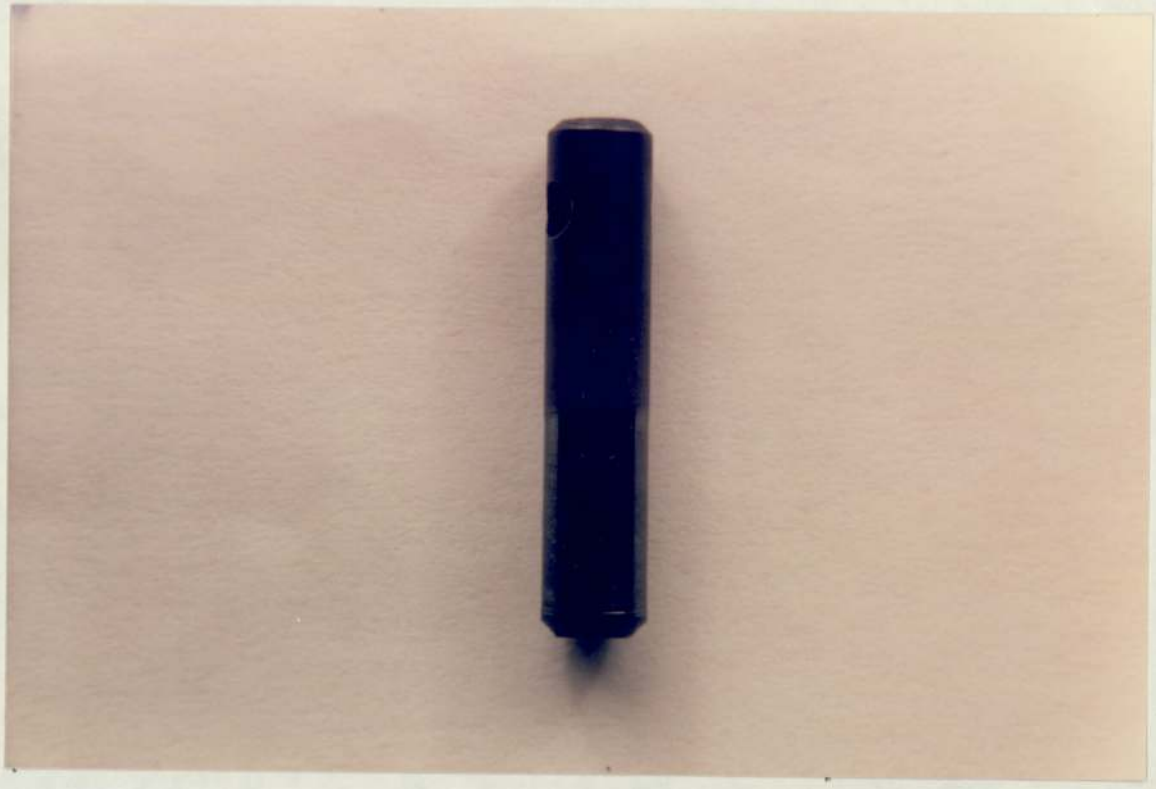

Plate-27 Slightly Scuffed Specimen after Falex Test

Plate-28 Scuffed Specimen after Falex Test

Plate-29 Badly Scuffed Specimen after Falex Test

Plate-30 Totally Seized and Sheared Specimen after Falex Test

7.0 DISCUSSION

7.1 Metallography

7.1.1 Untreated Specimens

All the untreated specimens show an austenitic matrix, the major differences appear in the grain size and alloying elements (Plates 3, 4 and 5). The unstablized 304 grade stainless steel shows a larger grain size than the 316 and the 321 grades of stainless steels. The 321 grade stainless steel shows very fine grains compared to the other two grades. Differences in grain size will lead to variation in case depth even though the different stainless steels will have received the same surface treatment. Nitrogen is preferentially absorbed at regions of high energy such as grain boundaries, therefore the smaller the grain size the greater the nucleation sites for the nitrogen. The free nitrogen also diffuses inwards preferentially along the grain boundaries.

The surface layers of all the specimens show some distortion, therefore the stainless steel bars have undergone some cold working, this is particularly distinct in the 304 grade stainless steel. This cold work will lead to high energy regions where the nitride can nucleate.

7.1.2 Plasma Nitrided Specimens

All the plasma nitrided specimens show the classical nitrided structure, i.e. a) a compound zone and b) a diffusion zone.

The specimens that were plasma nitrided at 460^{o}C and above show a thicker compound zone and a diffusion zone (Plates 6, 7 and 8) compared to those nitrided at temperatures of 380^{o}C and 420^{o}C (Plates

12, 13 and 14). This is because at low temperatures the alloying elements are not mobile enough to combine with the nitrogen and therefore cannot be easily precipitated from the nitrogen supersaturated solid solution. The alloying elements (Ti, Cr, Mo) present in stainless steel decrease the activity coefficient of nitrogen in iron and also affect the rate of precipitation of iron nitrides from supersaturated solid solution thereby, reducing the depth of subscale formed. Under the conditions of plasma nitriding, due to the sputtering phenomenon, some of these alloying elements are sputtered out of the metal matrix even at a low temperature and combine with the nitrogen to form alloy nitrides. The microstructure of the 321 grade stainless steel, that was plasma nitrided at a low temperature of 380^{o}C, shows a clear presence of yellowish pink cuboids of titanium nitrides in the compound zone as well as in the diffusion zone.

All the specimens that were plasma nitrided at 400^{o}C and above also show the precipitated nitrides and all the specimens of the 321 grade stainless steel show a clear presence of the titanium nitrides in the form of yellowish pink cuboids.

The work hardening of steels leads to regions of high energy where the nitrides would preferentially nucleate. This was discussed in Section 7.1.1. The 304 grade stainless steel in particular shows this effect very clearly. The precipitated nitrides can be seen along the flow pattern on the distorted grains (Plates 6 and 9).

The specimens that were plasma nitrided with post-oxidation treatment show almost the same structure as those without any post-oxidation treatment (Plates 9, 10 and 11). However, with these specimens there is no distinct presence of any oxide layer, but there are chain links of grey oxides found along the grain boundaries. These oxides do not show any continuity and are spread out with certain areas totally

devoid of any oxides. The absence of any continuous oxide layer is presumably due to the sputtering effect observed under the conditions of plasma nitriding. This is unlike the Nitrotec process which allows a successful build up of an oxide layer after post-oxidation treatment (refer Section 1.4); Nitrotec is a chemical process and has no sputtering phenomenon.

7.1.3 Tufftrided Specimens

The Tufftrided specimens show the classical structure of a compound zone near the surface, followed by a diffusion zone (Plates 15, 16 and 17).

The structure of the specimens show the precipitates of carbo-nitrides and nitrides. The 321 grade stainless steel shows a clear presence of yellowish pink cuboids of titanium nitrides. The structure also shows the presence of grey oxides in almost the same pattern as observed for the specimens which were plasma nitrided with a post-oxidaton treatment. During Tufftriding aeration of the bath is carried out (refer Section 1.3), which gives rise to the formaton of oxides. The presence of oxides in the Tufftrided structure was also observed by Prenosil (38).

The structure of the 304 grade and the 316 grade stainless steels show a thicker compound zone compared to the 321 grade stainless steel. As discussed in Section 7.1.1, the 321 grade stainless steel shows a fine grained structure compared to the other two grades. The nitrogen diffuses preferentially at regions of high energy, that is along grain bounaries. The diffusion of nitrogen during Tufftriding is only through the grain boundaries unlike plasma nitriding, in which the nitrigen is found to undergo transcrystalline diffusion from the start (6).

Therefore in the Tufftrided 321 grade stainless steel, the nitrogen has preferentially diffused inwards which explains the comparatively thin compound zone. This did not occur in the specimens that were plasma nitrided. However, similar results were obtained for the specimens that were gas nitrided as in Tufftriding. In gas nitriding the diffusion of the nitrogen is also through the grain boundaries (refer Section 2.1).

7.1.4 Gas Nitrided Specimens

The gas nitrided specimens of 304 and 316 grade stainless steels show a clear presence of a compound zone followed by a diffusion zone (Plates 18 and 19). However, 321 grade stainless steel does not show any clear presence of a compound zone (Plate 20). This has been explained under Section 7.1.3. It can be seen that the compound zone of the 304 and 316 grade stainless steels is non-uniform and the top layer seems susceptable to cracking and spalling.

The structures of the specimens show the precipitates of nitrides and carbo-nitrides along the grain boundaries. The 321 grade stainless steel shows a clear presence of titanium nitrides. The structure also shows the scattered presence of oxides, particularly along the grain boundaries. The gas nitriding was carried out in a gas tight retort which inspite of purging with the treatment gas, still retained a large number of oxygen molecules in the chamber which caused the oxidation of grain boundaries.

7.2 Microhardness

The results of the gas nitriding trials, that were carried out without any prior surface treatments to remove the passive oxide film from

the surface of stainless steels, show that the surface hardness obtained is very low (Figure 21). The stainless steels which were given prior surface treatments have developed good surface hardness (Figure 20). These results therefore confirm that it is absolutely essential to remove the passive oxide film from the surface of stainless steels before they can be successfully gas nitrided.

It has been shown by many researchers that such prior surface treatments as described above are not essential for plasma nitriding of stainless steels. However no mention has been made of the initial furnace conditions. As the results of this research show, under incorrect conditions of the furance (refer Table-3a), the hardness values obtainable are comparatively low (Figures 25 and 26). Due to the low initial vacuum in the treatment chamber and insufficient purging, a large number of oxygen molecules are still present in the chamber which does not allow the surface of stainless steels to be totally depassivated inspite of the sputtering. Thus nitriding does not take place successfully and a low surface hardness is produced.

Figures 9 to 18 show that under correct furnace conditions (refer Table-3b) high surface hardness values are obtainable after plasma nitriding without any prior surface treatments which were found essential for gas nitriding. This indicates that sputtering plays an important role in plasma nitriding and enables it to be a cost effective treatment for stainless steel. The salt bath nitrocarburising treatment also does not require any prior surface treatments due to the chemical reaction of salts with the stainless steel surface which results in a breakdown of the passive oxide film.

The comparison of different grades of austenitic stainless steel shows that plasma nitriding at low temperatures of 380^{o}C and 420^{o}C results in higher hardness values for the 321 grade compared with the

other two grades (Figures 9 and 10). This is due to the fact that at low temperatures substitutional solutes are not active enough to form nitrides. However, the critical solubility product for nulceation of homogeneous precipitation of titanium nitride is lower than chromium nitride and molybedenum nitride(17). Thus titanium nitride has precipitated in the 321 grade even at low temperatures, this fact is also corroborated by the microstructure of the 321 grade stainless steel which shows the presence of yellowish pink cuboids of titanium nitrides. This then can explain the higher hardness values obtained.

The plasma nitriding treatment at 460^{o}C and the Tufftride treatment have also resulted in a slightly higher surface hardness for the 321 grade stainless steel (Figures 11 and 19), whereas the plasma nitriding treatments at 500^{o}C and above have resulted in a higher surface hardness for the 304 grade stainless steel (Figures 12, 13 and 14). The gas nitriding has resulted in higher hardness values for the 316 grade stainless steel (Figure 20). At higher temperatures (460^{o}C and above) substitutional solutes are sufficiently mobile to react with the free nitrogen to form nitrides. The nitrides formed have different relative stability, so that the equilibrium precipitates will depend on the variables of the system, i.e. the temperature, the relative activities of the solutes and other thermodynamic factors (33). Hence, the results above indicate that different treatments have resulted in different hardness values for different grades of stainless steel.

The stainless steels which have been plasma nitrided with a post-oxidation treatment have not shown any significant change in hardness values compared to those without a post-oxidation treatment (Figures 15 to 18). The presence of a soft oxide layer will result in lowering of the surface hardness. Hence the above results indicate that apparently there is no continuous oxide layer present; this fact is also corroborated by

microstructure observations as discussed in Section 7.1.

The comparison of different treatments on the 304 grade stainless steel shows that the plasma nitriding at 460^{o}C with or without a post-oxidation treatment has resulted in superior surface hardness values (Figure 22).

Figure 23 shows that Tufftriding, plasma nitriding (at 460^{o}C with or without post-oxidation) and gas nitriding have resulted in almost the same surface hardness on 316 grade stainless steel. However, the Tufftride treatment gave a better hardness gradient.

The comparison of different treatments on the 321 grade stainless steel shows that the plasma nitriding at 460^{o}C with or without any post-oxidation treatment and the Tufftride treatment have resulted in not only higher and almost the same hardness but also have a similar hardness gradient. The gas nitriding however, was shown to be inferior. The surface hardness obtained at a distance of 13.3 microns from the surface after gas nitriding is the same as that for the plasma nitriding at a low temperature of 380^{o}C though the hardness profile for the gas nitriding treatment, shows a better gradient than the other (Figure 24).

7.3 Corrosion

The results of corrosion measurements indicate a marked drop in corrosion resistance of stainless steel after nitriding. The test solution of sodium chloride with acetic acid added to adjust the pH to 3.1, provides a strong corroding environment. The microprocessor based corrosion measurement equipment indicates even minor variatons in I_{corr} values. However, in real terms, as long as the I_{corr} value indicated has the same power of 10, the drop in corrosion resistance will be almost the same. This fact is also corroborated by the visual appearance of the

specimens after the corrosion test. To analyse the data provided by the linear polarisation curves (Appendix-1), I_{corr} ($\log_{10}$) values are plotted against time.

The results indicate that the corrosion rate in almost all the cases seems to drop over a period but then increase again. This drop in corrosion rate is significant for the plasma nitriding treatment at 380°C (Figure 29). The passivity of the stainless steel surface is due to the protective film (mainly Cr_2O_3) on its surface. To resist the attack by the corrosive environment, reductive dissolution must be avoided and a fresh film must be formed immediately at any weak place, which may arise. The above results show that the fresh film at weak spots seems to have formed in almost all the cases except the plasma nitriding treatment at 570°C (Figure 34). Nitriding at such a high temperature has probably resulted in a high loss of chromium from the metal matrix and thus not enough chromium is available to form a new protective film on the surface. The results also indicate that the drop in corrosion rate followed by a rise again, occurs after different time periods for different treatments. This is because the corrosion measurements by the technique of resistance polarisation relate themselves to the equilibrium potential of a couple i.e. rate of oxidation of metal in the corrosive environment and the rate of reduction of corrosive species in the solution. The time period required for achieving the equilibrium, where the rate of oxidation of a metal is in equilibrium with the rate of reduction of corrosive species in solution, will be different for different corroding systems; stainless steels nitrided under different conditions will form different corroding systems.

The corrosion rate for the plasma nitriding treatment at 460°C with or without post-oxidation, is almost the same for all the grades of stainless steel (Figures 31 and 35). The same trend is indicated by the

results of all the other treatments (Figures 32, 33, 34, 36, 37 and 38) including the gas nitriding and the Tufftriding (Figures 27 and 28). The results therefore indicate that the passivity of the stainless steel surface is chiefly due to the presence of Cr_2O_3 film on the surface and that the loss of chromium from the metal matrix has been responsible for the corrosion. The loss of any other alloying element (Mo or Ti) does not seem to reflect any change in the rate of corrosion which is the same for all the three grades of stainless steel. The corrosion rates indicated by the results for the plasma nitriding treatments at low temperatures of 380°C and 420°C however, do not seem to conform to the above trend (Figures 29 and 30). These results indicate that the initial corrosion rate is almost the same and lower for the 304 and the 316 grades of stainless steels compared to the 321 grade stainless steels though, over longer periods, the corrosion rates are almost the same for all the grades. The microhardness profiles for the above treatment indicate higher hardness for 321 grade stainless steel compared to the other two grades (Figures 9 and 10). Also the microstructures of the 321 grade stainless steel after the above low temperature treatments show the presence of titanium nitrides. Hence this indicates that the loss of titanium from the metal matrix may cause higher initial corrosion rates.

The corrosion resistance of the untreated stainless steel shows that the corrosion rate for the 304 grade and the 316 grade stainless steels is almost the same (Figure 39). The 321 grade shows higher initial corrosion which drops significantly after one week in the test solution and remains steady over the longer periods and also is of the same order as the other two grades. It appears that the initial high corrosion rate shown by the 321 grade is due to the error in measurement by the microprocessor based equipment. The problem arose because of breaking of the spot welded wire on the specimen and this had to be

rewelded.

The results do not show any significant difference in the corrosion rate between the stainless steels which were plasma nitrided without any post-oxidation (Figures 31, 32, 33 and 34) and those that were given post-oxidation treatment (Figures 35, 36, 37 and 38). The microstructure of the stainless steels which were given post-oxidation treatment do not show any presence of a uniform oxide layer (refer Section 7.1). The presence of the chain links of oxides in these stainless steels do not seem to have any effect on the corrosion rate. A uniform surface oxide layer is claimed to improve corrosion resistance (62).

Examination of the results of various treatments on the stainless steel show that the plasma nitriding treatment at a low temperature of 380^{o}C has resulted in very low corrosion rate (Figures 40, 41 and 42). This is due to the fact that at low temperatures the chromium does not form any nitrides and thereby is retained in the matrix, resulting in improved corrosion resistance. This is in agreement with the work of Zhang et al (67), who concluded that the surface layer after plasma nitriding at low temperatures (below 400^{o}C) is completely free of chromium nitrides.

Comparison of different nitriding techniques show that the initial corrosion rate for the plasma nitriding treatments is lower than that for the gas nitriding and the Tufftriding (Figures 40, 41 and 42), the gas nitriding and the Tufftriding have shown almost the same initial rate of corrosion. Over a longer perid, the rate of corrosion is almost the same for all the nitriding treatments except for the plasma nitriding treatments at a low temperature of 380^{o}C, which remains significantly lower.

7.4 Wear

The wear measurements on the Falex machine has certain limitations which can bring about uncertainties in the measured results. The force on the specimen is proportional to the tension applied at the ends of the 'nutcracker' lever arm. This tension is applied by a spring mechanism contained in the dial load gauge (Figure 8). This mechanism has a tendency to stick and then jump rather than decrease smoothly as a run proceeds. Such behaviour causes large load fluctuations during the run as well as non-reproducibility of initial loading conditions. The accuracy of reading the gauge load at lower loads is very poor. Further, the Falex machine has been provided with a trip switch which cuts out the motor prematurely before a trial is completed. The early trials indicated that this depends on the heat generated in the system which is fairly high under dry run conditions and thereby causes fairly quick cut-off of the dry runs before they can be completed.

The above problems have been reduced by some researchers by replacing the spring/dial assembly with an electronic load cell (Amtec Model CT-50) in conjunction with AIM65 microcomputer (68). The load cell provides readings which are claimed to be stable and the microcomputer electronically monitors the load applied at the pin. The computer also stores these time dependent load readings which can be periodically printed out.

Considering the limitations of the equipment available for this research work and also the limitation on the availability of a large number of specimens that would be necessary to reduce the probability of error in measurements, it was decided to use the Falex machine for checking the efficiency of the treatments and for measuring the wear rates by mass loss method only. No calculations were carried to

determine the dynamic coefficients of friction and volume wear rates. Initial trials indicated that the actual load of 250lbs and the time period of 7 minutes under dry run conditions would be suitable for the wear measurements. Since the load applied in the Falex test is very high and the pin rotates at a high rate of 290rpm, wear measurements on the Falex machine should be used as indicative of the efficiency of the treatment only.

The results indicate that a marked improvement in scuffing resistance may be brought about by nitriding of the stainless steel (Table-4). Tests on the untreated stainless steels resulted in a total seizure and shearing of the test pins. Among the three grades of the untreated stainless steel, the 321 grade took a longer time to seizure than the other two grades.

The results indicate that though the surface hardness has shown a marked effect on the wear properties higher hardness has not, in all the instances, resulted in better wear rates.

The plasma nitriding treatments at low temperatures (380^{o}C and 420^{o}C) have not resulted in good wear properties. The 304 grade and the 316 grade stainless steels that were plasma nitrided at 380^{o}C have badly scuffed and sheared, whereas the 321 grade has badly scuffed. The pins that were plasma nitrided at slightly higher temperature of 420^{o}C have shown similar results (Table-4).

The results of the plasma nitriding treatments at different temperatures under different conditions of the treatment indicate that the plasma nitriding at 460^{o}C and at 540^{o}C, both with the post-oxidation treatments, have resulted in better wear rates and have shown better resistance to scuffing. The microstructures of the stainless steels after the above treatments have shown the presence of oxides. It is known that any surface oxides will reduce adhesive wear (40).

Comparison of the different techniques of nitriding show that the gas nitriding has resulted in a poor wear performance. The Tufftriding has shown good resistance to scuffing though its wear rates are higher than those for the plasma nitriding treatments at 460^{o}C and 540^{o}C (with post-oxidation). However, the Tufftride treatment has performed better than those plasma nitriding treatments which were not given any post-oxidation treatment. The structure of the top compound layer obtained after plasma nitriding is γ' which has FCC lattice structure. The compound layer obtained after Tufftriding is mainly of epsilon nitride and epsilon carbonitride which has a hexagonal lattice structure. The above results of the wear performance are in an agreement with the work carried out by deGee (46) on the effect of crystal lattice structure on wear. He found that the hexagonal lattice structure tends to become oriented with the (hexagoal) basal planes parallel to the direction of the movement and thus eliminates interlocking phenomena which cause adhesive wear. The cubic lattice structure on plastic deformation causes extensive microroughning of the surface giving rise to sawtooth patterns which cause interlocking and hence high adhesive wear. However, this is at variance with the work of Edenhofer (6) who concluded that the γ' phase provides better gliding planes than the hexagonal lattice of the epsilon phase.

8.0 CONCLUSIONS

1. Nitriding has the effect of decreasing markedly the corrosion resistance of austenitic stainless steel. However, the wear properties are improved substantially.

2. Nitriding at high temperatures (400^{o}C and above) resulted in similar rates of corrosion for all the grades of austenitic stainless steel. This establishes that the loss of chromium from the metal matrix is chiefly responsible for the increase in rate of corrosion. The loss of any other alloying element (Ti, Mo) does not seem to have any effect on the corrosion behaviour in the salt/acetic acid solution after nitriding at high temperatures.
   Nitriding at low temperatures (380^{o}C and 420^{o}C) resulted in a slightly higher initial rate of corrosion for the titanium bearing grade 321 stainless steel than for the other grades. The microstucture of this stainless steel also showed the presense of yellowish pink cuboids of titanium nitrides. Consequently nitriding at low temperatures results in a loss of some titanium from the metal matrix which may have an effect on the initial corrosion rate of the stainless steel.

3. A high temperature (460^{o}C and above) plasma nitriding treatment followed by oxidation has not resulted in any significant improvement in the corrosion resistance of the austenitic stainless steel. However, it was observed that the post-oxidation treatment improved the resistance to scuffing and resulted in improved wear rate.
   Plasma nitriding at low temperatures (380^{o}C and

420°C) provided a marked improvement in the corrosion rate of the austenitic stainless steel but resulted in very high wear rates.

4. The different plasma nitriding treatments resulted in different corrosion and wear properties. The plasma nitriding at 460°C with a post-oxidation treatment gave better properties than the other treatments. Though the above treatment showed a higher corrosion rate than the plasma nitriding at a low temperature of 380°C, the wear properties obtained were far superior. In an environment where the corrosion resistance is more important than the wear properties, plasma nitriding at 380°C will result in a better performance, this is particularly so for the 321 grade stainless steel.

5. Comparison of the different techniques of nitriding show that the plasma nitriding at 460°C (with or without a post-oxidation treatment) resulted in a lower initial corrosion rate than the other two treatments namely, the salt bath nitrocarburising and the gas nitriding. The corrosion rates for all the above treatments were found to be almost the same over longer periods.
The wear properties obtained after plasma nitriding at 460°C (with a post-oxidation treatment) were better than the salt bath nitrocarburising and the gas nitriding. The gas nitrided specimens in particular performed very poorly. The salt bath nitrocarburising resulted in better wear properties than the plasma nitriding treatment without a post-oxidation cycle. This indicates that the epsilon phase with its hexagonal lattice structure provides

better gliding planes than the γ' phase with its FCC structure.

9.00 SUGGESTIONS FOR FURTHER WORK

Chromium nitride seems to be responsible for the loss in corrosion resistance of austenitic stainless steel. To establish the processing conditions whereby some degree of control over the loss in corrosion resistance of nitrided stainless steel could be predicted, it is necessary to quantify the amount of chromium precipitated as chromium nitride. The electron probe technique will be necessary to establish this.

The different techniques of nitriding result in different wear properties. It is suggested here to carry out TEM studies to analyse the effect of the crystal structure on wear. TEM studies are also required to analyse the behaviour of dislocations in a monophased and a polyphase compound layer, to establish with a high degree of certainty the role played by these structures in the wear mechanism.

10.0. ACKNOWLEDGEMENTS.

The author wishes to thank his supervisor Dr.J K Dennis for his guidance throughout the work and Mr. H C Child for his suggestions and guidance at almost every stage of the project.

The author also wishes to thank the staff of the Wolfson heat-treatment centre. In particular, thanks must go to Mr.A.Hick without whose assistance some of the trials could not have been carried out.

Finally, thanks must go to the academic and technical staff for their support and co-operation.

11.0 APPENDIX-1

11.1.0 Coding System for Linear Polarisation Curves.

Each specimen has been given a four digit number on the basis of the type of material, type of treatment, type of treatment cycle and the time period after which it was tested. The key to this four digit number is given below.

1. First digit shows the type of material.

   4 = 304 grade stainless steel.

   6 = 316 grade stainless steel.

   1 = 321 grade stainless steel.

2. Second digit shows the treatment given.

   0 = Untreated.

   1 = Salt Bath Nitrocarburising.

   2 = Gas Nitriding.

   3 = Plasma Nitriding.

3. Third digit shows the treatment cycle (Refer Table-3b).

   1 = Plasma nitriding at 460^{o}C.

   2 = Plasma nitriding at 380^{o}C.

   3 = Plasma nitriding at 500^{o}C.

   4 = Plasma nitriding at 540^{o}C.

   5 = Plasma nitriding at 570^{o}C.

   6 = Plasma nitriding at 420^{o}C.

   7 = Plasma nitriding at 460^{o}C. with Post-Oxidation.

   8 = Plasma nitriding at 500^{o}C. with Post-Oxidation.

9 = Plasma nitriding at 540°C. with Post-Oxidation.

0 = Plasma nitriding at 570°C. with Post-Oxidation.

The salt bath nitrocarburising and the gas nitriding have one treatment cycle (refer sections 5.3.2 and 5.4.2). Hence, the third digit for both these treatments is "1".

4. Fourth digit shows the time period for which the specimen was kept immersed in the testing solution before carring out the corrosion test.

0 = 2 hours.

1 = One week.

2 = Two weeks.

3 = Three weeks.

The code number 4322 for example, signifies that the grade 304 stainless steel (first digit-4) has been plasma nitrided (second digit-3) at 380°C (third digit-2) and the corrosion test has been carried out after two weeks (fourth digit-2).

11.2.0 Correction of Icorr Values.

It has been explained in sections 4.2 and 4.2.2 that the polarisation resistance (R_p) is the slope of the linear region of potential Vs. current plot at $E = E_{corr}$. The microprocessor has been programmed to calculate the slope (polarisation resistance) and use this value to determine the I_{corr} of the corroding system.

For some unknown reason, in certain cases the slope of the plot is incorrectly drawn by the microprocessor which gives rise to an error in determining R_p and therefore I_{corr}. It was necessary to carry out manual corrections in these cases which was done by determining the slope of the polarisation curve in the linear region and using this value in the

following formula to calculate I_{corr} values (refer section 4.2).

$$I_{corr} = (B_a \cdot B_c)/ 2.3(B_a + B_c) \times 1/R_p$$

Where,

B_a and B_c are Tafel constants. The values of B_a and B_c given by the Tafel plot were used.

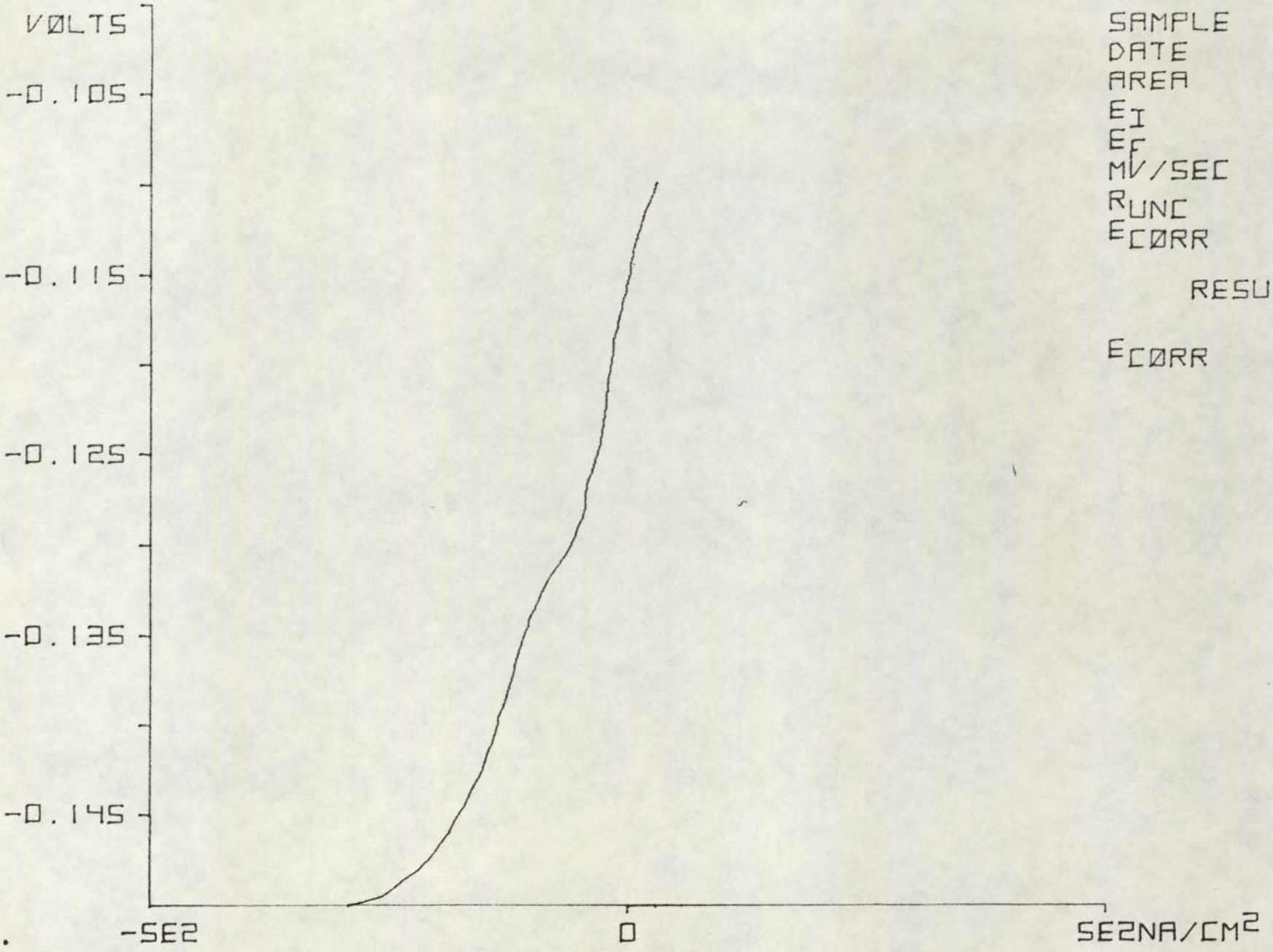

SAMPLE	4000
DATE	23.05
AREA	1.083E1
E_I	-0.150
E_f	-0.110
MV/SEC	0.166
R_{UNC}	2.111
$E_{CØRR}$	-0.130

RESULTS

$E_{CØRR}$ -0.115

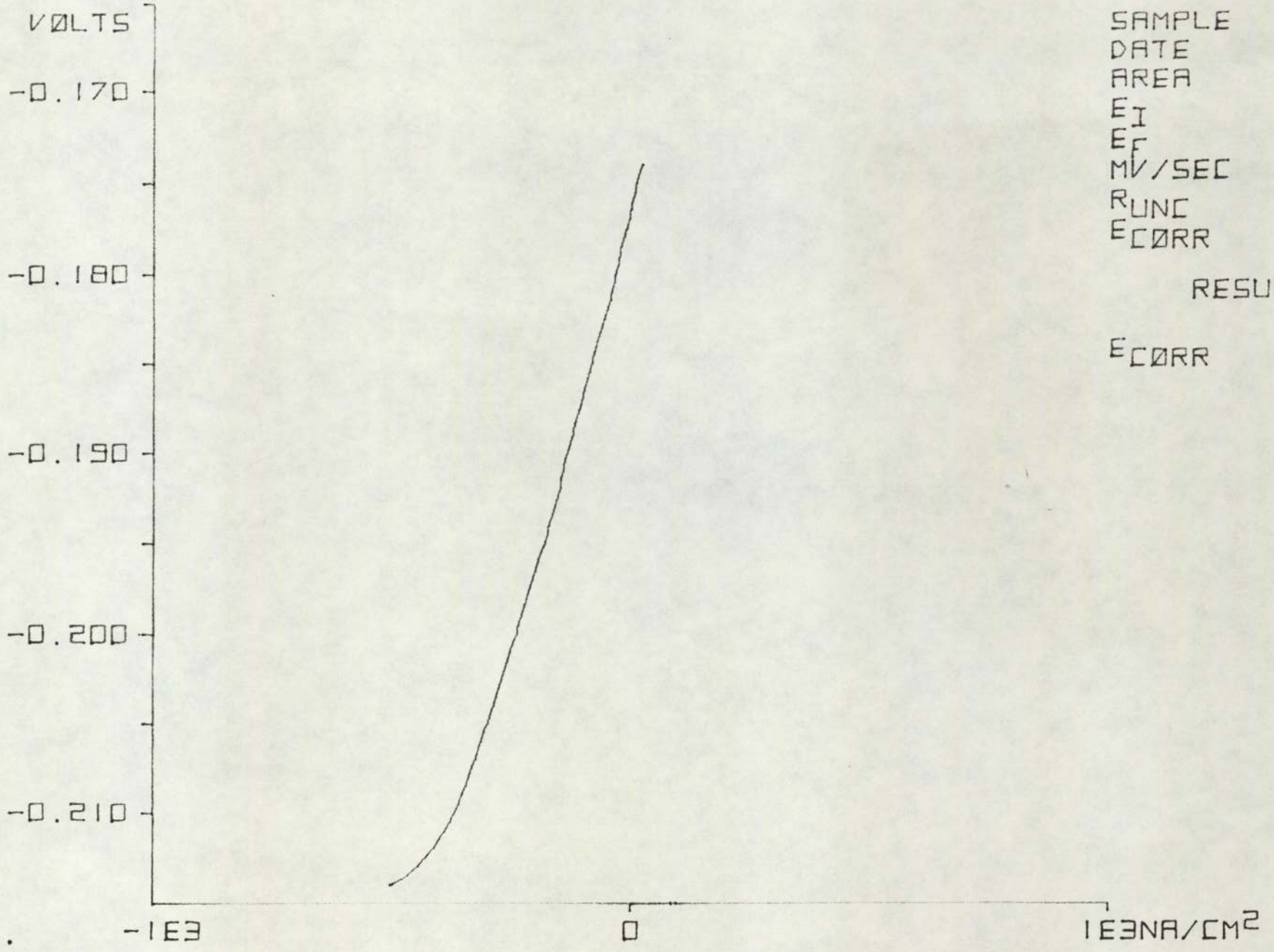

SAMPLE	6000
DATE	23.05
AREA	1.181E1
E_I	-0.214
E_F	-0.174
MV/SEC	0.166
R_{UNC}	2.306
$E_{CØRR}$	-0.194

RESULTS

$E_{CØRR}$ -0.177

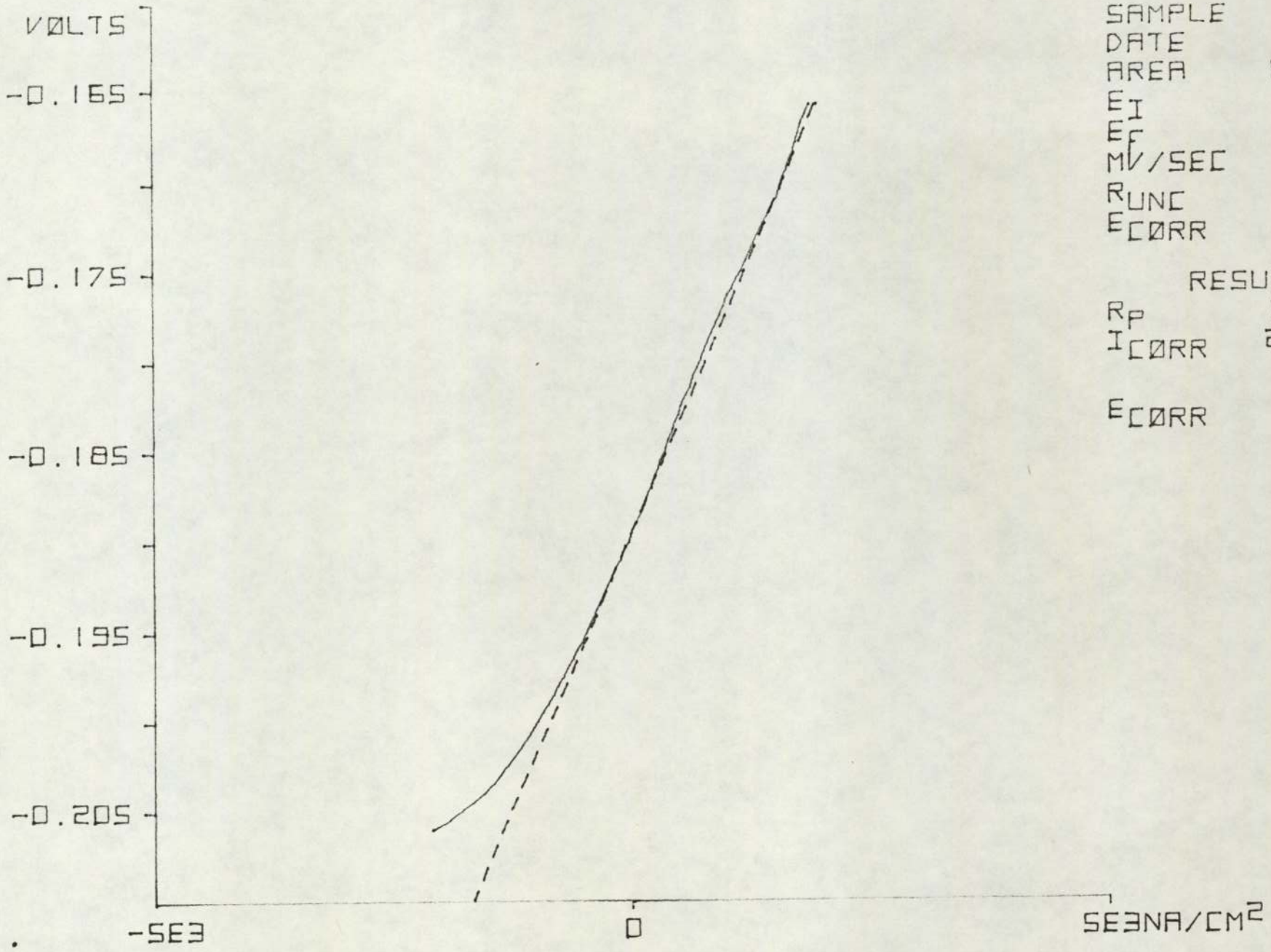

SAMPLE	1000
DATE	23.05
AREA	1.235E1
E_I	-0.206
E_F	-0.166
MV/SEC	0.166
R_{UNC}	1.925
$E_{CØRR}$	-0.186

RESULTS

R_P	1.219E4
$I_{CØRR}$	2.262E3
$E_{CØRR}$	-0.190

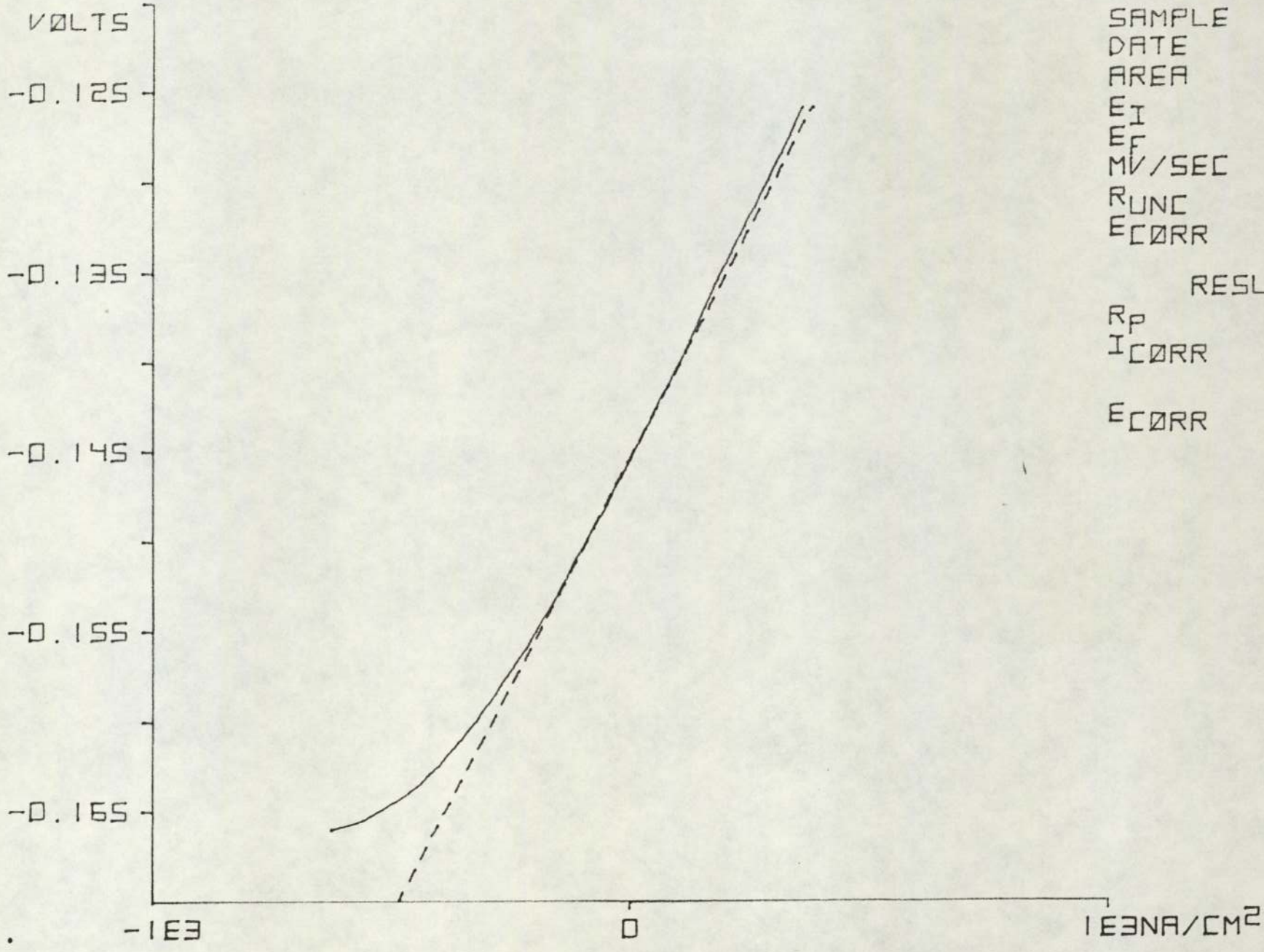

SAMPLE	4001
DATE	30.05
AREA	1.083E1
E_I	-0.166
E_F	-0.126
MV/SEC	0.166
R_{UNC}	1.778
$E_{CØRR}$	-0.146

RESULTS

R_P	5.110E4
$I_{CØRR}$	5.014E2
$E_{CØRR}$	-0.146

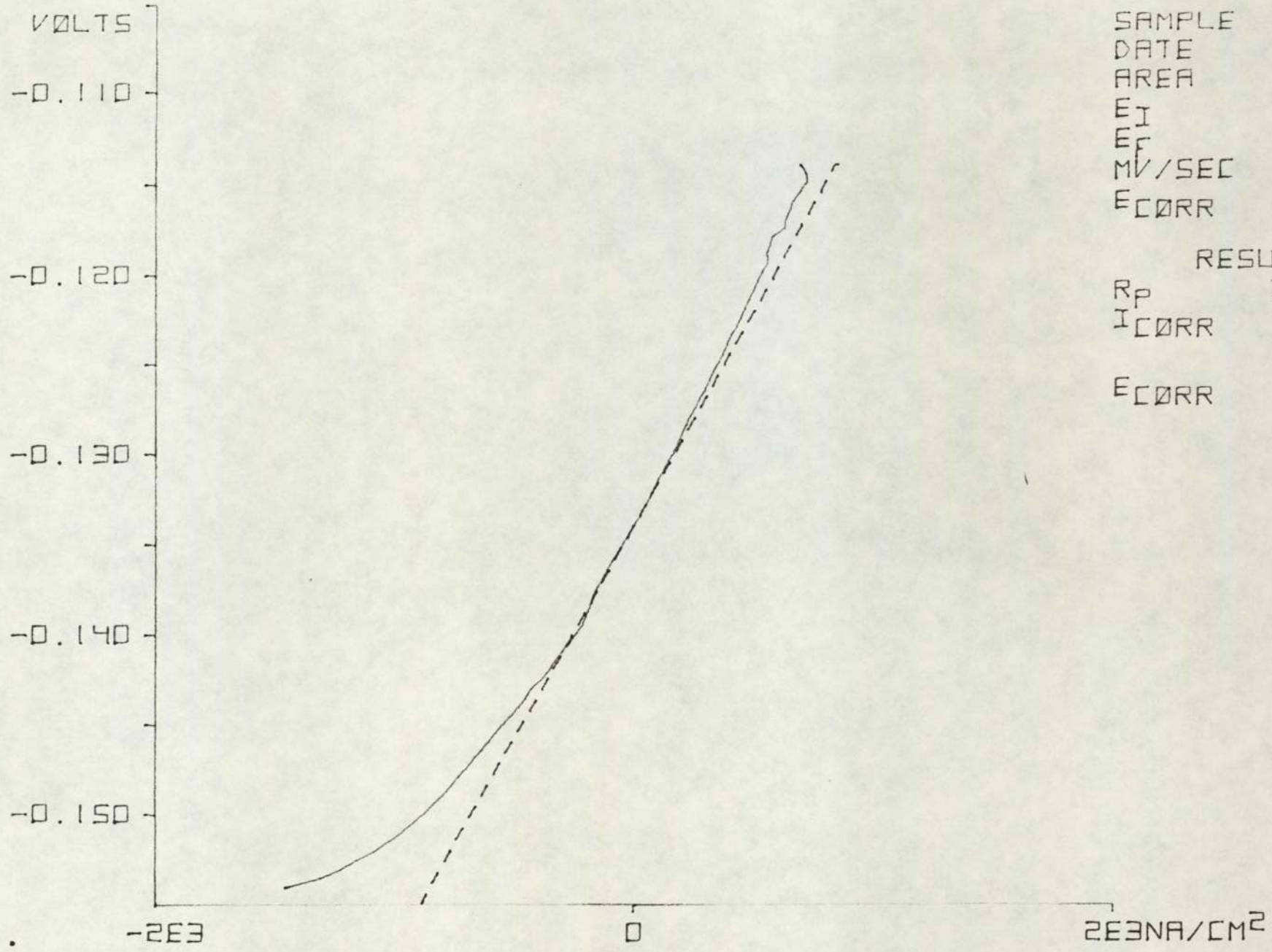

SAMPLE	6001
DATE	30.05
AREA	1.181E1
E_I	-0.154
E_F	-0.114
MV/SEC	0.166
$E_{CØRR}$	-0.134

RESULTS

R_P	2.387E4
$I_{CØRR}$	1.092E3
$E_{CØRR}$	-0.134

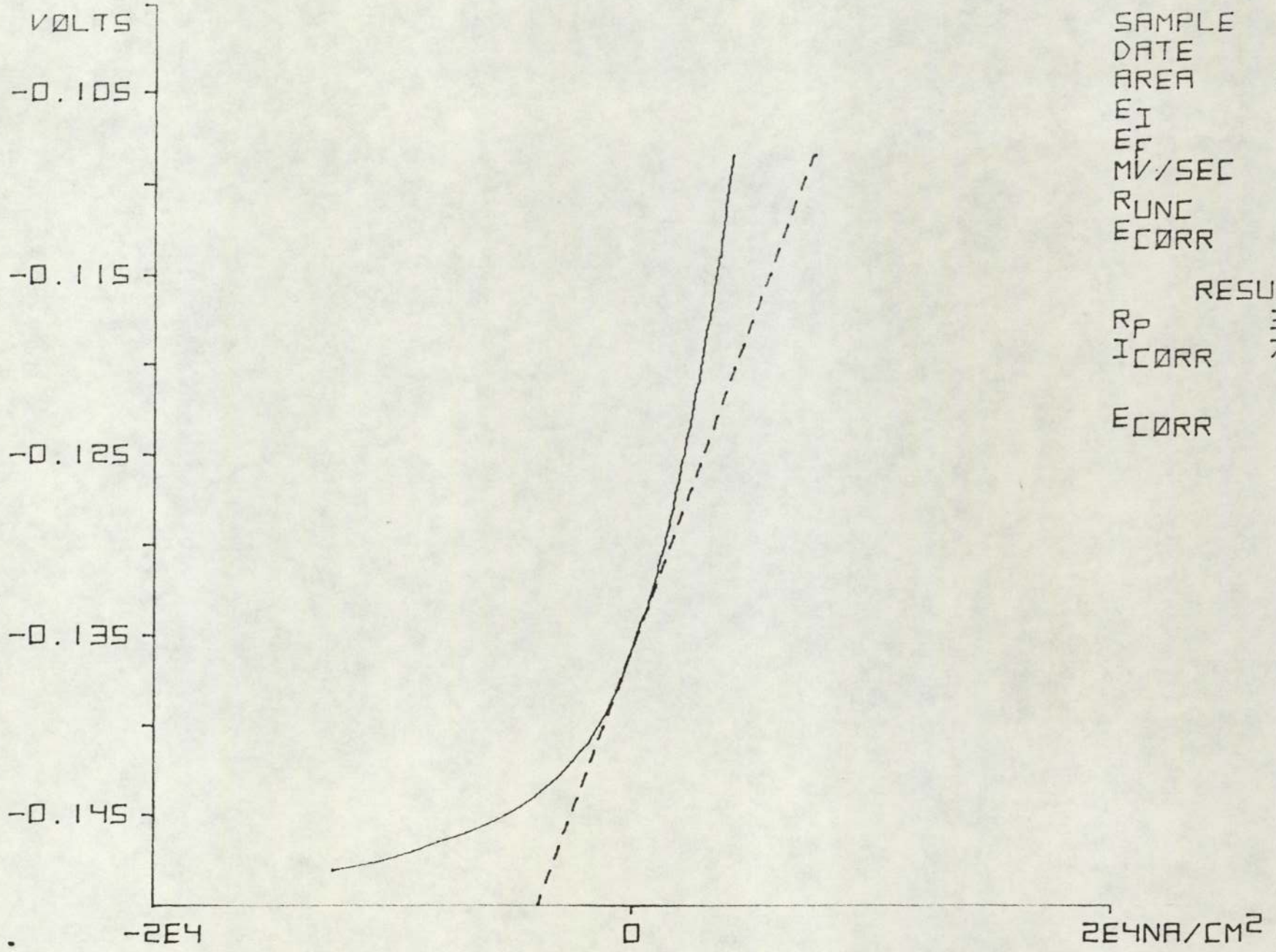

SAMPLE	1001
DATE	30.05
AREA	1.235E1
E_I	-0.148
E_F	-0.108
MV/SEC	0.166
R_{UNC}	1.593
$E_{CØRR}$	-0.128

RESULTS

R_P	3.639E3
$I_{CØRR}$	7.578E3
$E_{CØRR}$	-0.136

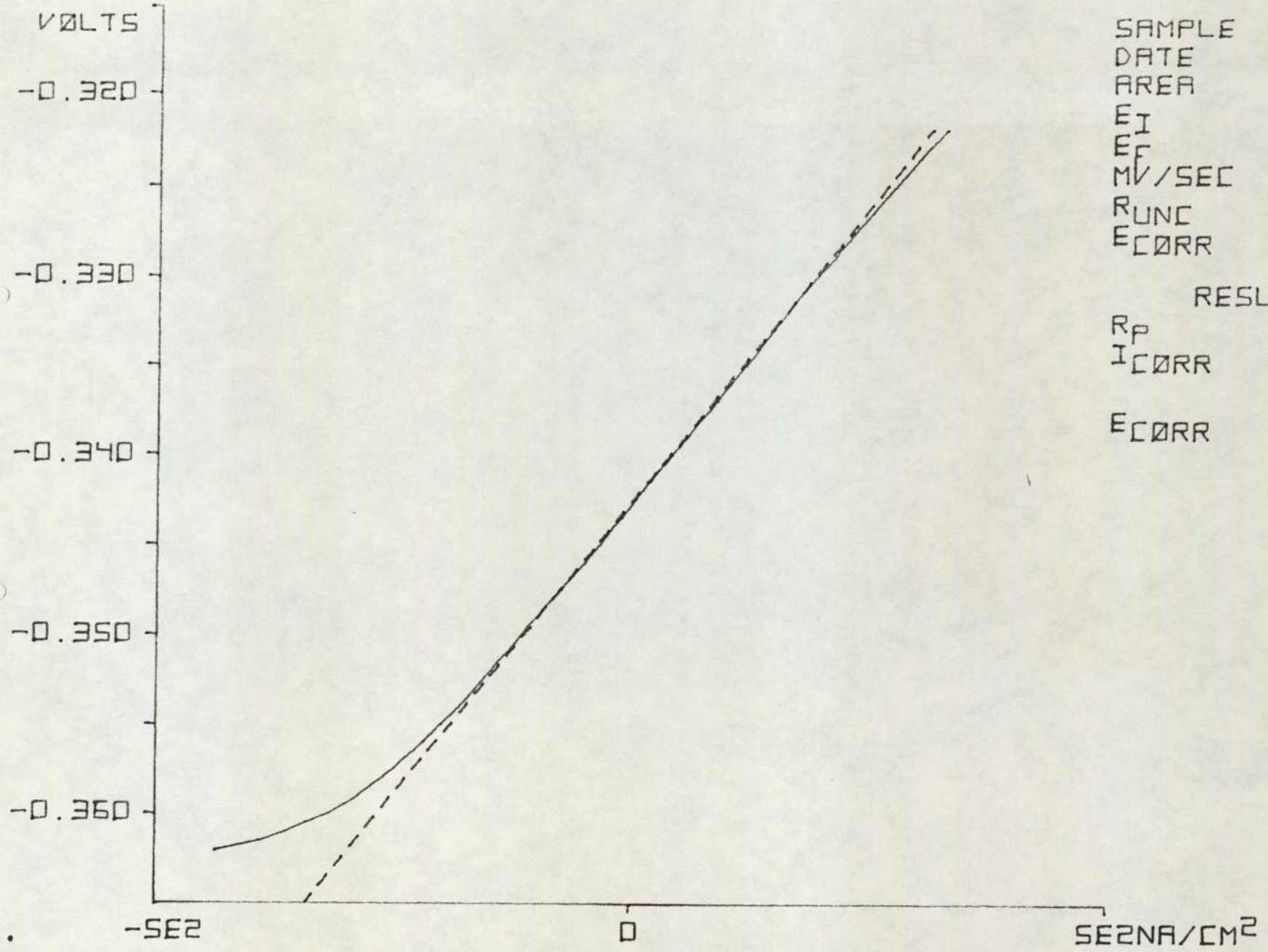

SAMPLE	4002
DATE	06.06
AREA	1.083E1
E_I	-0.362
E_F	-0.322
MV/SEC	0.166
R_{UNC}	2.492
$E_{CØRR}$	-0.342

RESULTS

R_P	6.591E4
$I_{CØRR}$	3.887E2
$E_{CØRR}$	-0.343

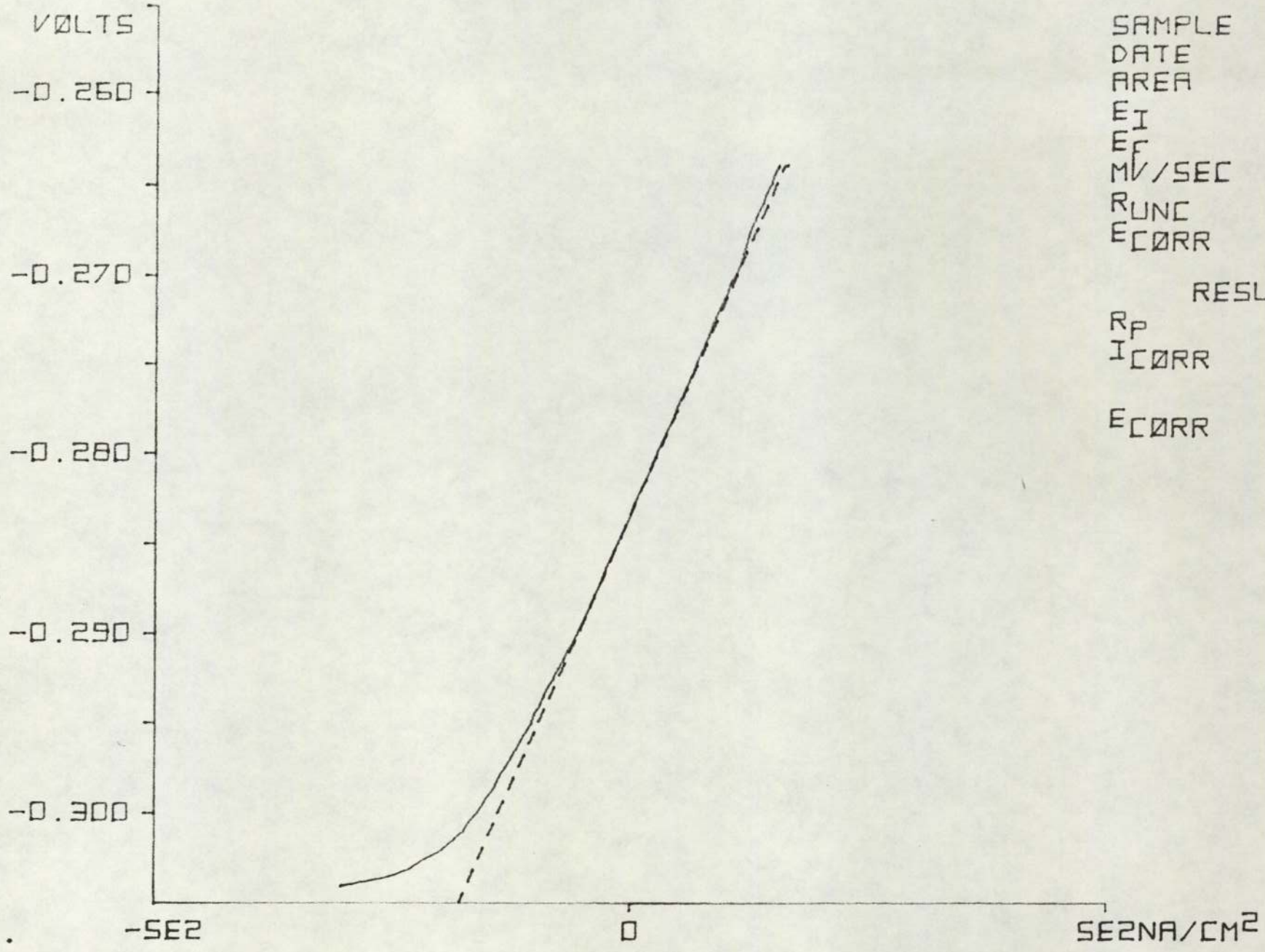

SAMPLE	1002
DATE	06.06
AREA	1.235E1
E_I	-0.304
E_F	-0.264
MV/SEC	0.166
R_{UNC}	2.619
$E_{CØRR}$	-0.284

RESULTS

R_P	1.221E5
$I_{CØRR}$	2.259E2

$E_{CØRR}$ -0.284

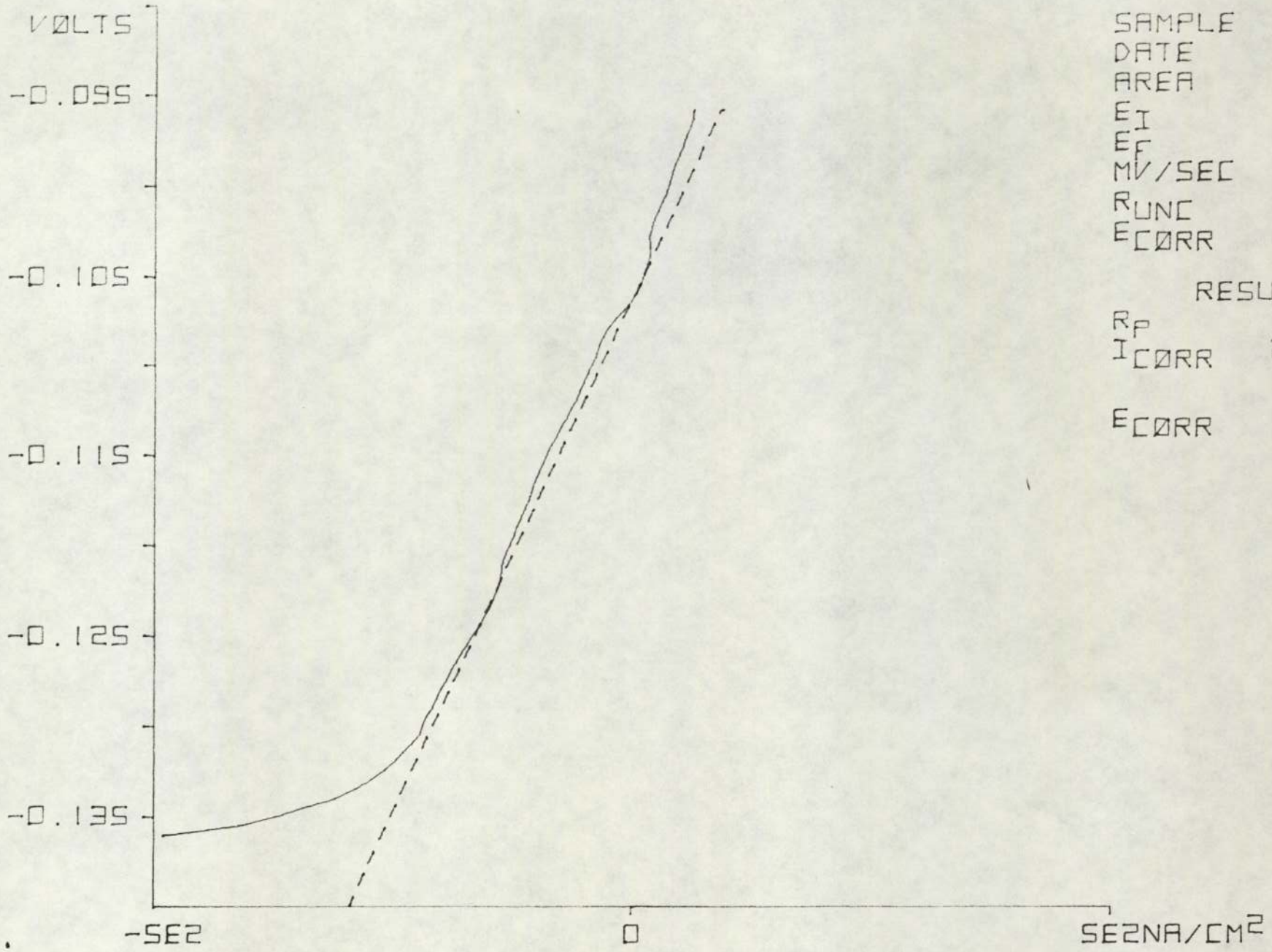

SAMPLE	6002
DATE	06.06
AREA	1.181E1
E_I	-0.136
E_F	-0.096
MV/SEC	0.166
R_{UNC}	3.313
$E_{CØRR}$	-0.116

RESULTS

R_P	1.142E5
$I_{CØRR}$	2.281E2
$E_{CØRR}$	-0.107

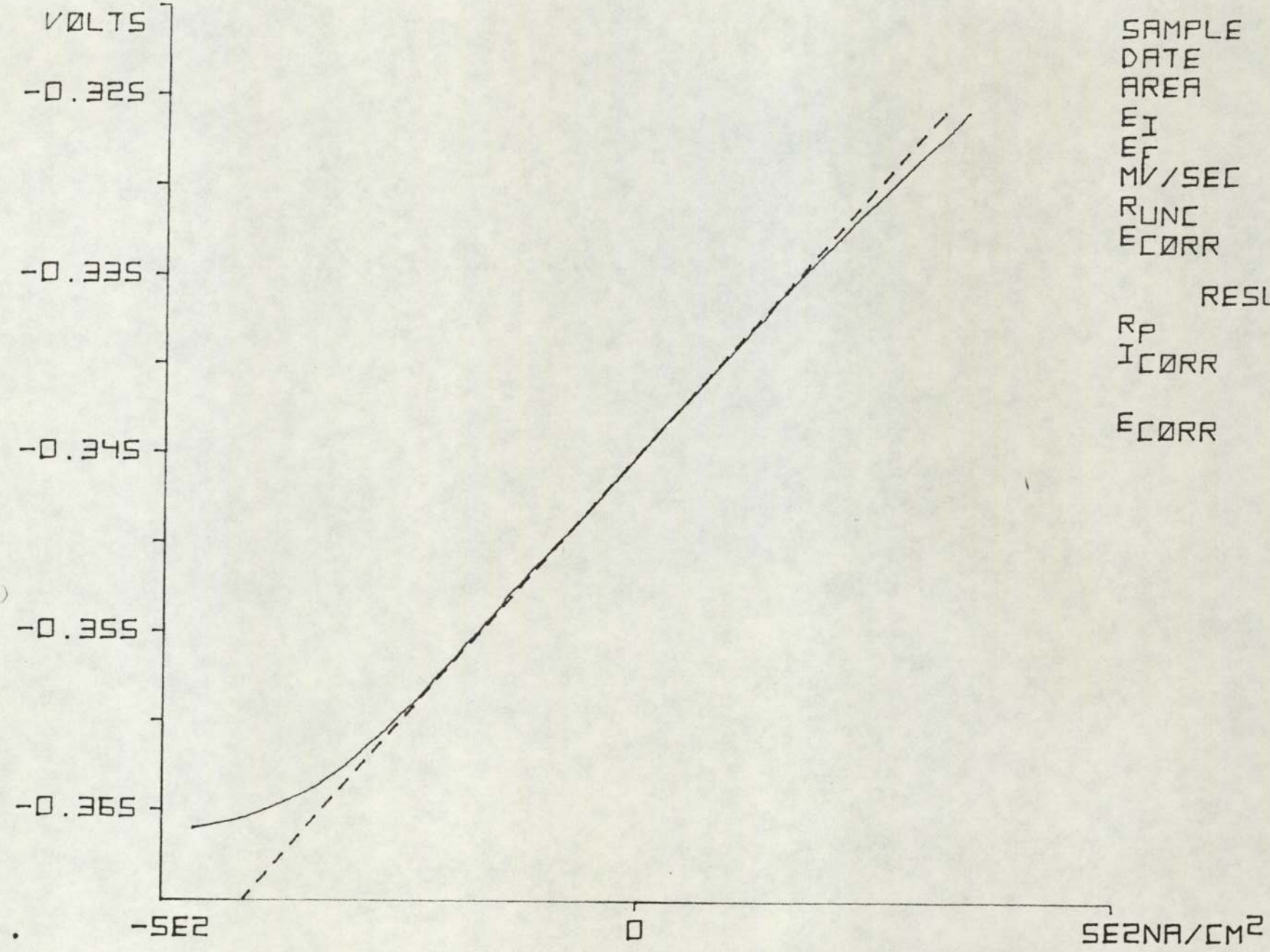

SAMPLE	4003
DATE	13.06
AREA	1.083E1
E_I	-0.366
E_F	-0.326
MV/SEC	0.166
R_{UNC}	1.925
$E_{CØRR}$	-0.346

RESULTS

R_P	6.020E4
$I_{CØRR}$	4.256E2
$E_{CØRR}$	-0.345

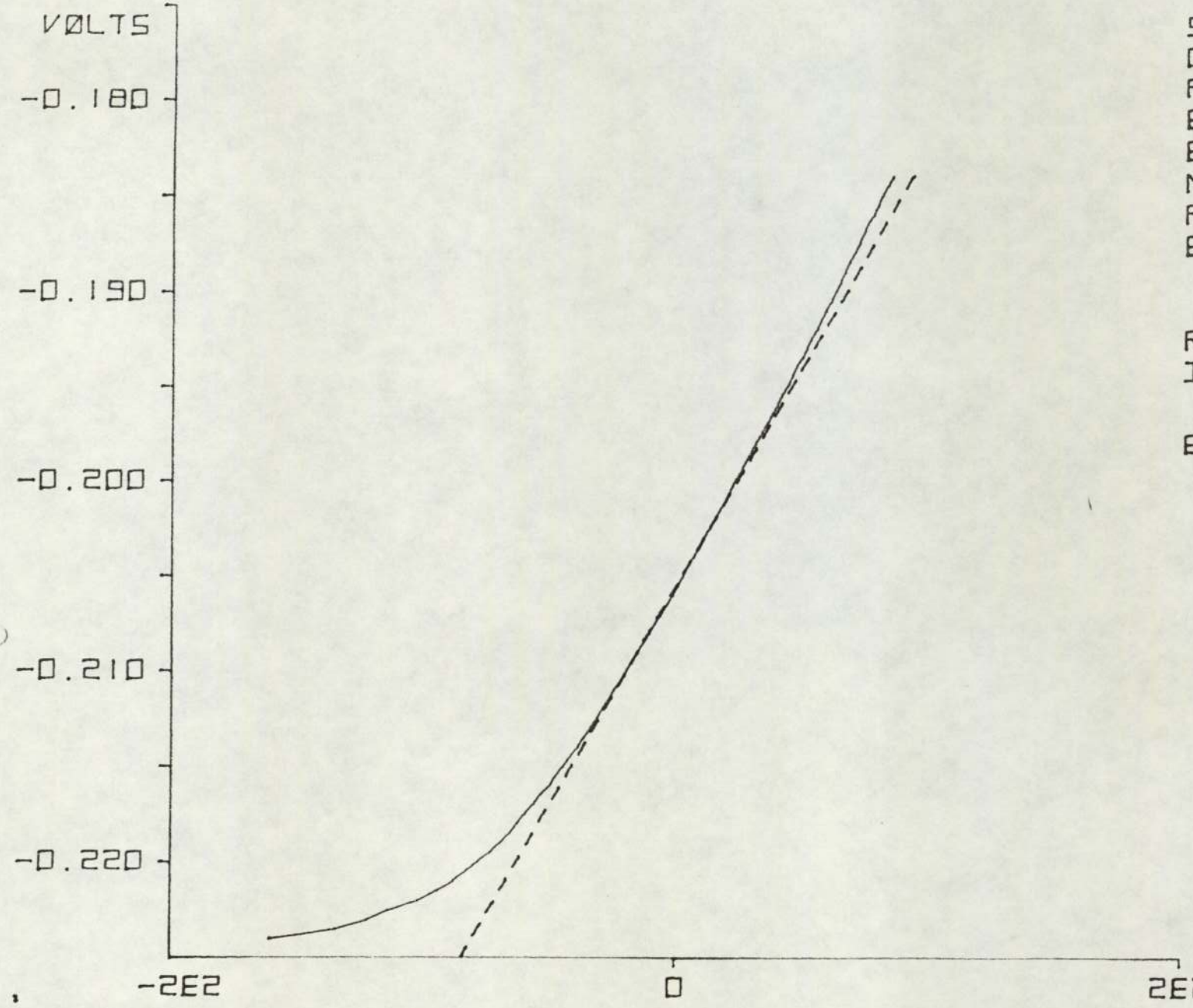

SAMPLE	6003
DATE	13.06
AREA	1.181E1
E_I	-0.224
E_F	-0.184
MV/SEC	0.166
R_{UNC}	2.639
$E_{CØRR}$	-0.204

RESULTS

R_P	2.308E5
$I_{CØRR}$	1.129E2
$E_{CØRR}$	-0.206

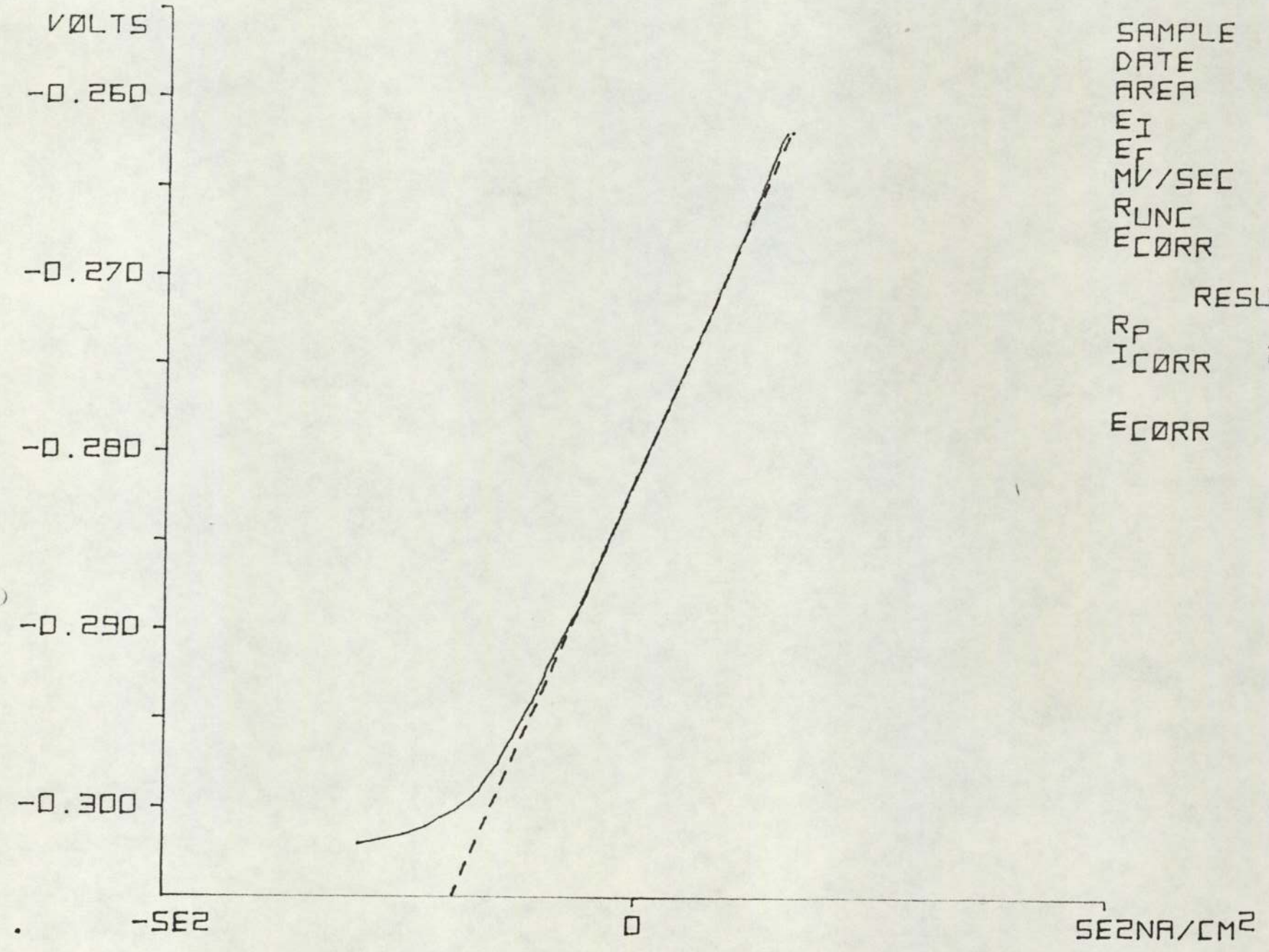

SAMPLE	1003
DATE	13.06
AREA	1.235E1
E_I	-0.302
E_F	-0.262
MV/SEC	0.166
R_{UNC}	1.896
$E_{CØRR}$	-0.282

RESULTS

R_P	1.227E5
$I_{CØRR}$	2.248E2
$E_{CØRR}$	-0.282

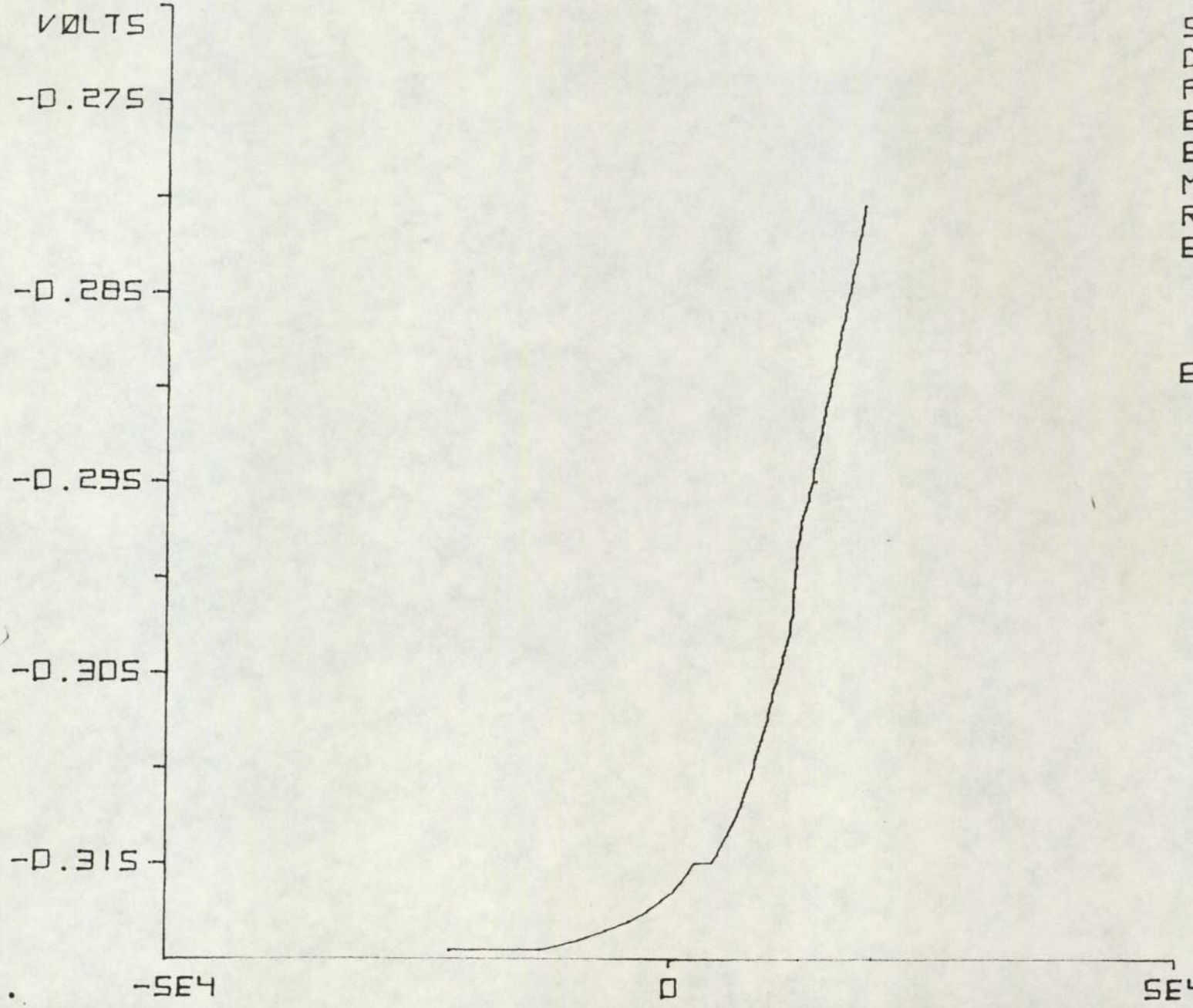

SAMPLE	4110
DATE	09.05
AREA	1.181E1
E_I	-0.320
E_f	-0.280
MV/SEC	0.100
R_{UNC}	1.905
$E_{CØRR}$	-0.300

RESULTS

$E_{CØRR}$ -0.317

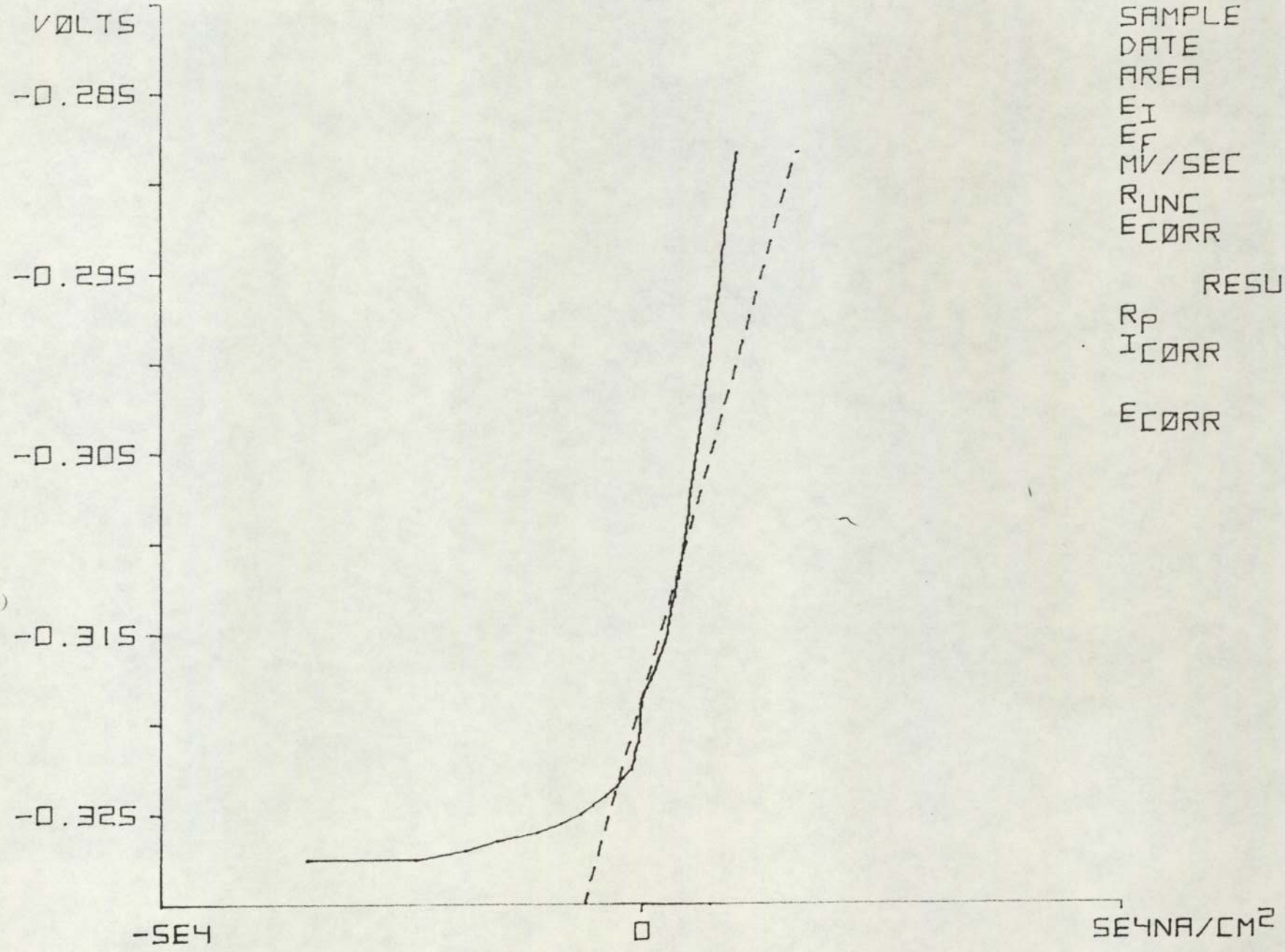

SAMPLE	6110
DATE	09.05
AREA	1.206E1
E_I	-0.328
E_F	-0.288
MV/SEC	0.166
R_{UNC}	1.515
$E_{CØRR}$	-0.308

RESULTS

R_P	1.874E3
$I_{CØRR}$	1.391E4
$E_{CØRR}$	-0.319

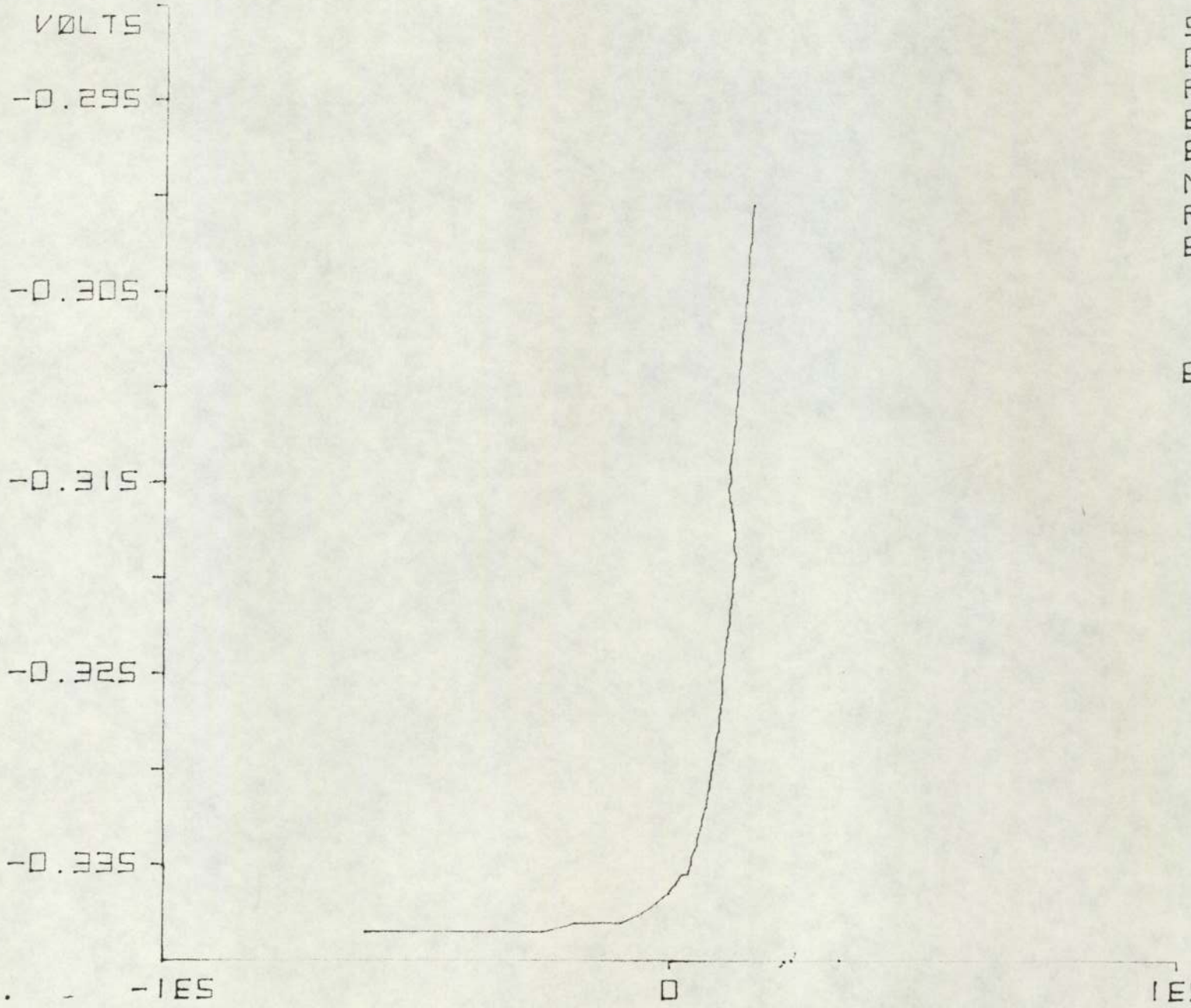

SAMPLE	1110
DATE	09.05
AREA	1.156E1
E_I	-0.340
E_f	-0.300
MV/SEC	0.166
R_{UNC}	2.414
$E_{CØRR}$	-0.320

RESULTS

$E_{CØRR}$ -0.337

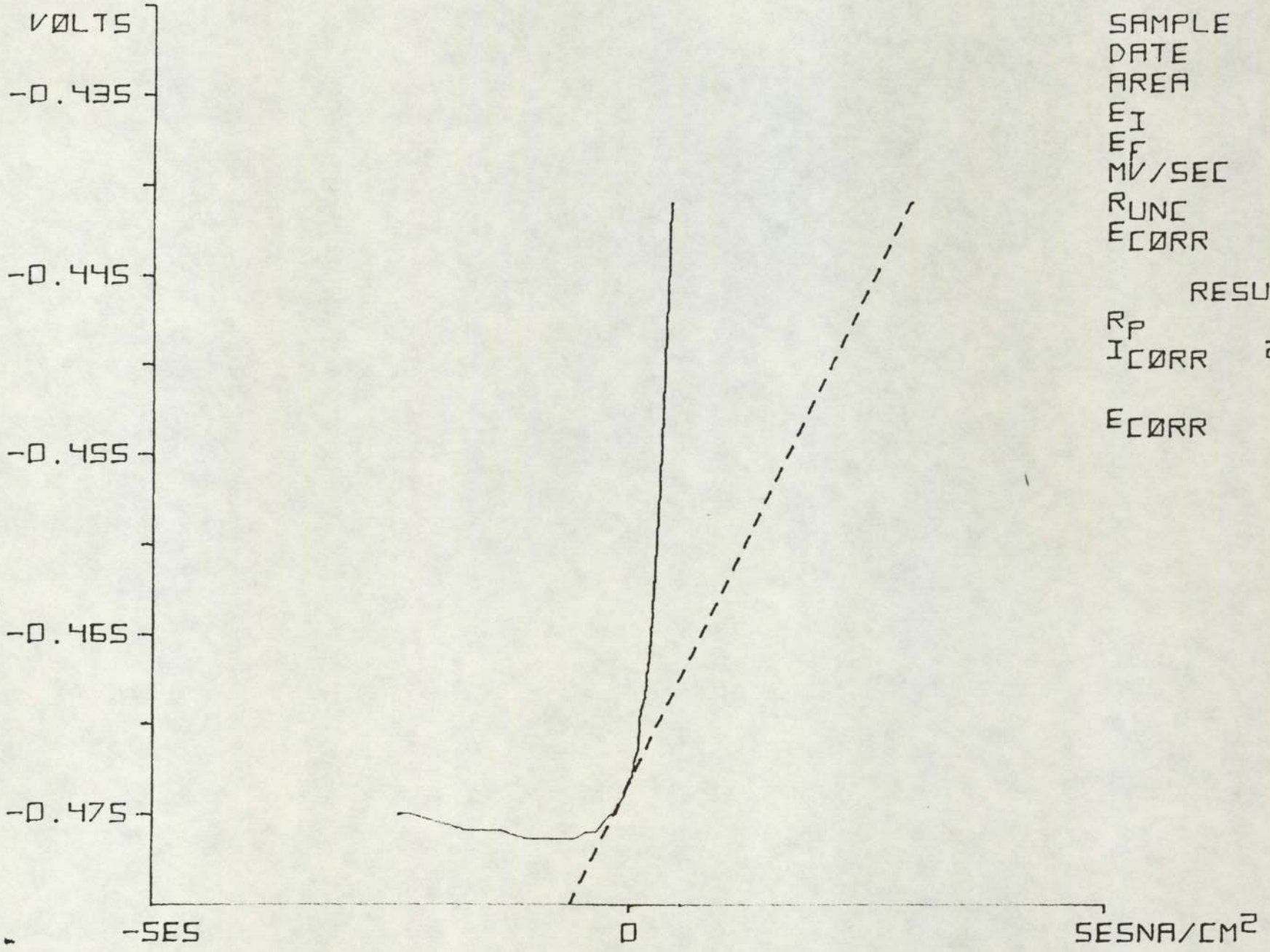

SAMPLE	4111
DATE	16.05
AREA	1.181E1
E_I	-0.480
E_F	-0.440
MV/SEC	0.166
R_{UNC}	1.876
$E_{CØRR}$	-0.460

RESULTS

R_P	1.096E2
$I_{CØRR}$	2.338E5
$E_{CØRR}$	-0.474

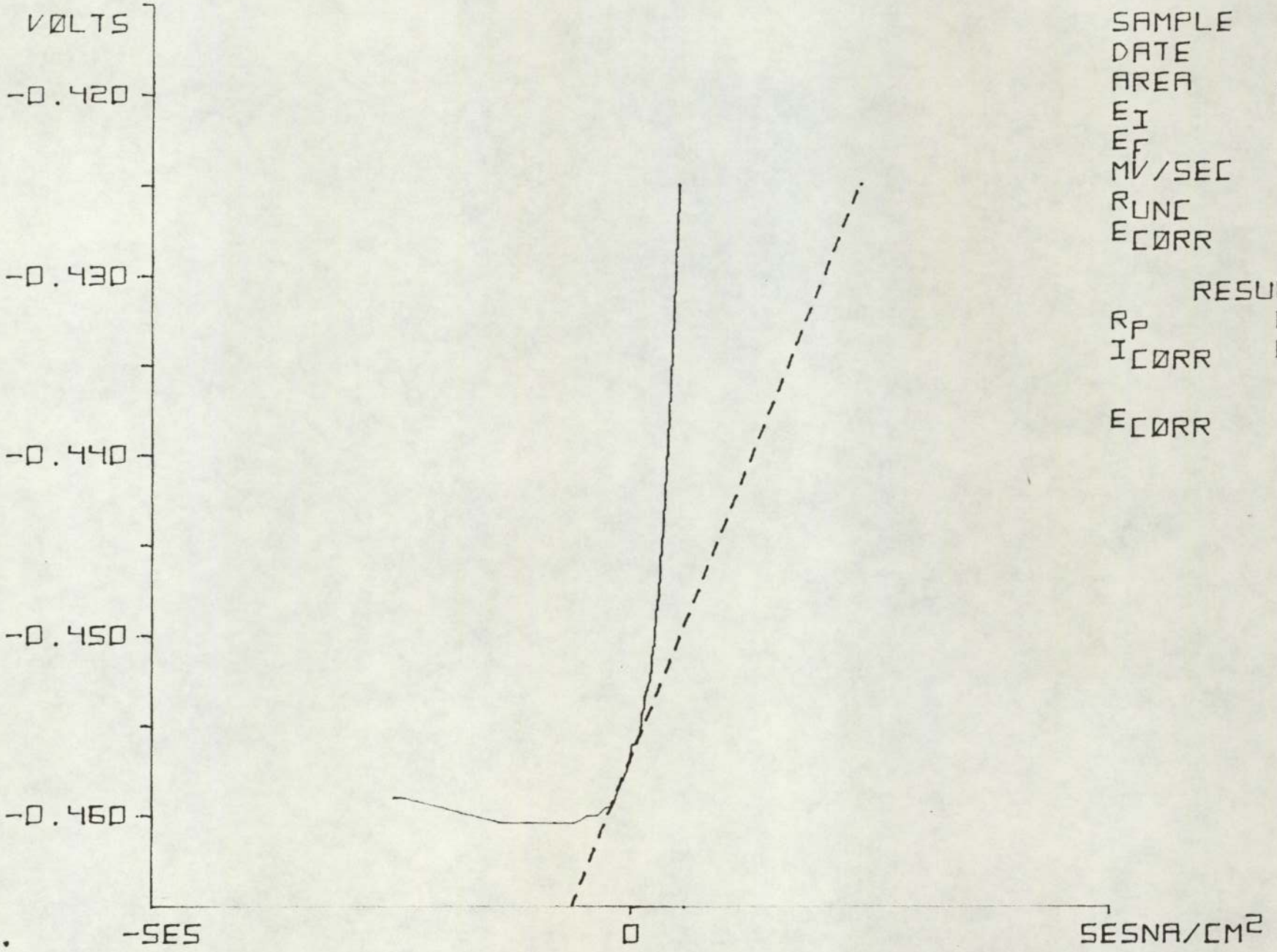

SAMPLE	6111
DATE	16.05
AREA	1.206E1
E_I	-0.464
E_F	-0.424
MV/SEC	0.166
R_{UNC}	1.759
$E_{CØRR}$	-0.444

RESULTS

R_P	1.337E2
$I_{CØRR}$	1.949E5
$E_{CØRR}$	-0.457

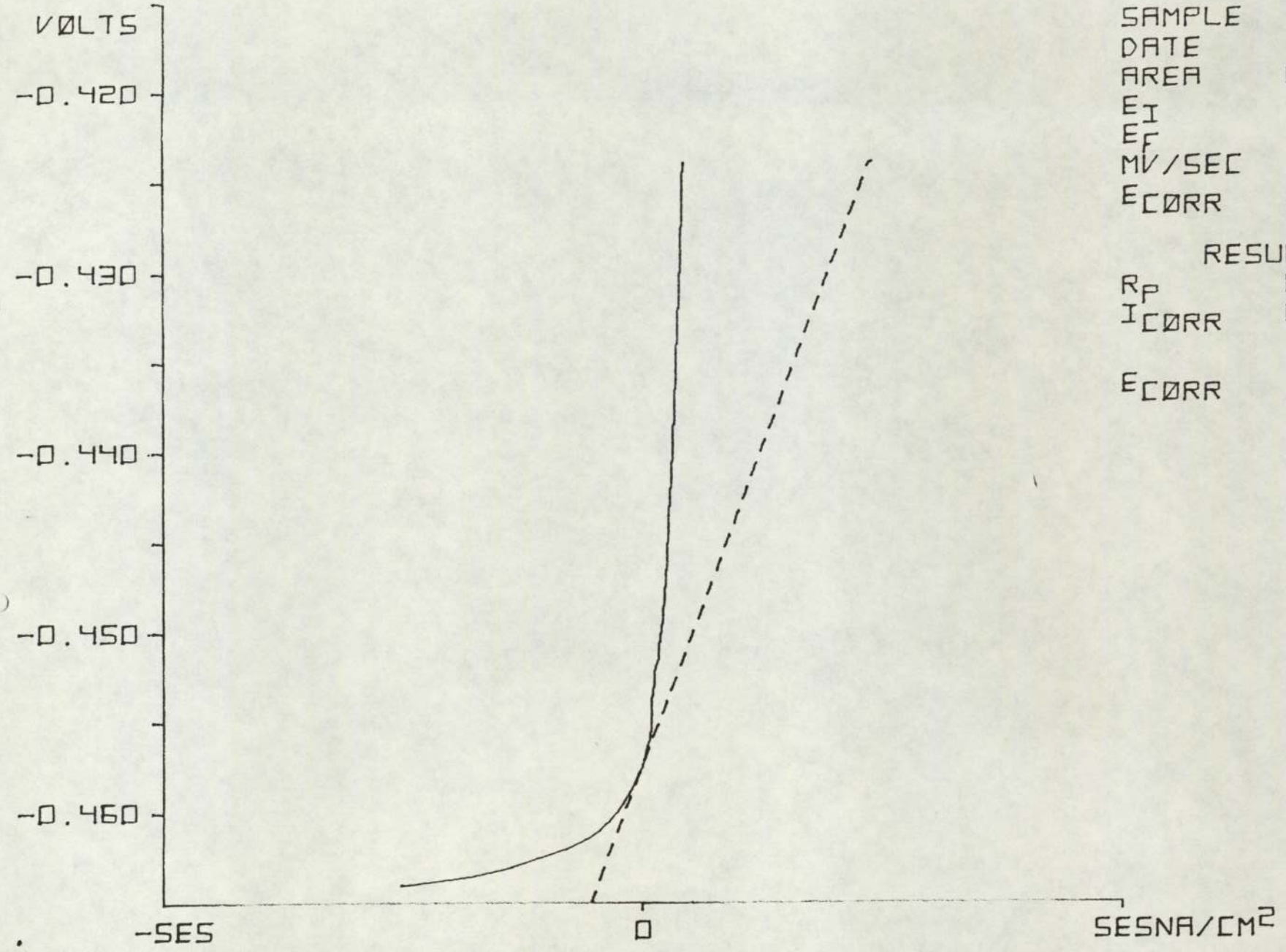

SAMPLE	1111
DATE	16.05
AREA	1.156E1
E_I	-0.464
E_F	-0.424
MV/SEC	0.166
$E_{CØRR}$	-0.444

RESULTS

R_P	1.425E2
$I_{CØRR}$	1.936E5
$E_{CØRR}$	-0.458

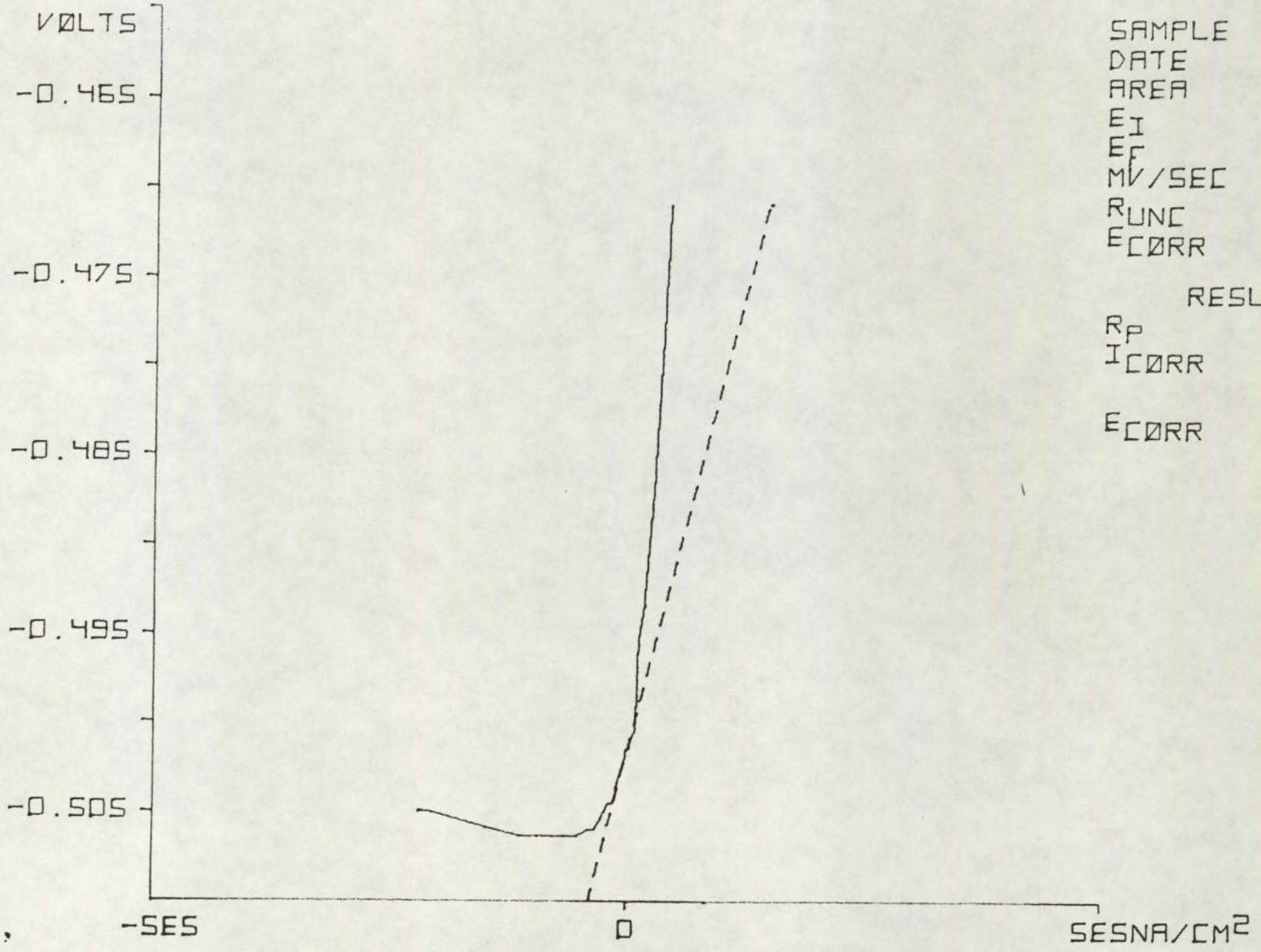

SAMPLE	4112
DATE	23.05
AREA	1.181E1
E_I	-0.510
E_F	-0.470
MV/SEC	0.166
R_{UNC}	2.003
$E_{CØRR}$	-0.490

RESULTS

R_P	2.096E2
$I_{CØRR}$	1.222E5
$E_{CØRR}$	-0.502

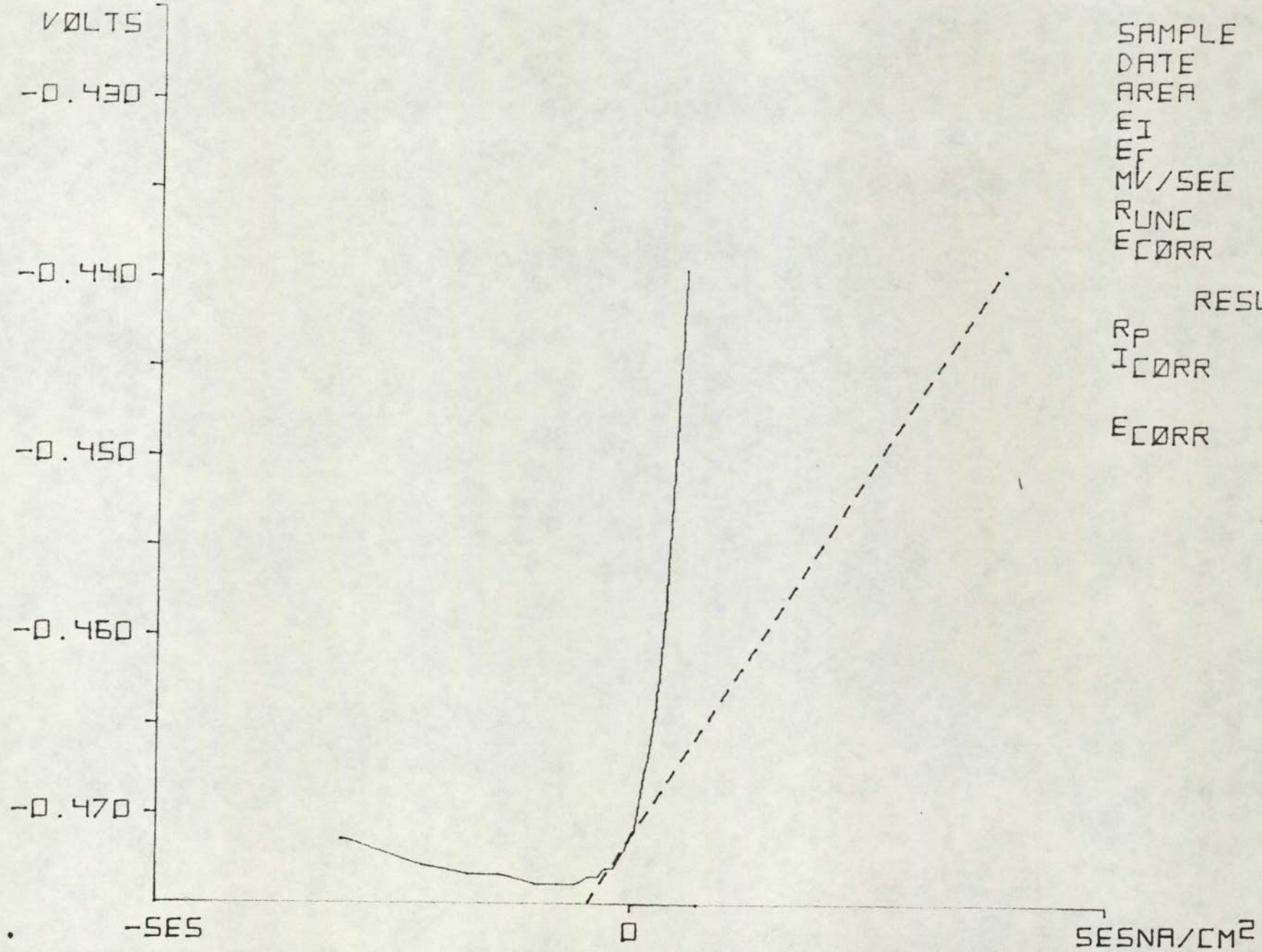

SAMPLE	6112
DATE	23.05
AREA	1.206E1
E_I	-0.478
E_F	-0.438
MV/SEC	0.166
R_{UNC}	1.866
$E_{CØRR}$	-0.458

RESULTS

R_P	8.245E1
$I_{CØRR}$	3.160E5
$E_{CØRR}$	-0.472

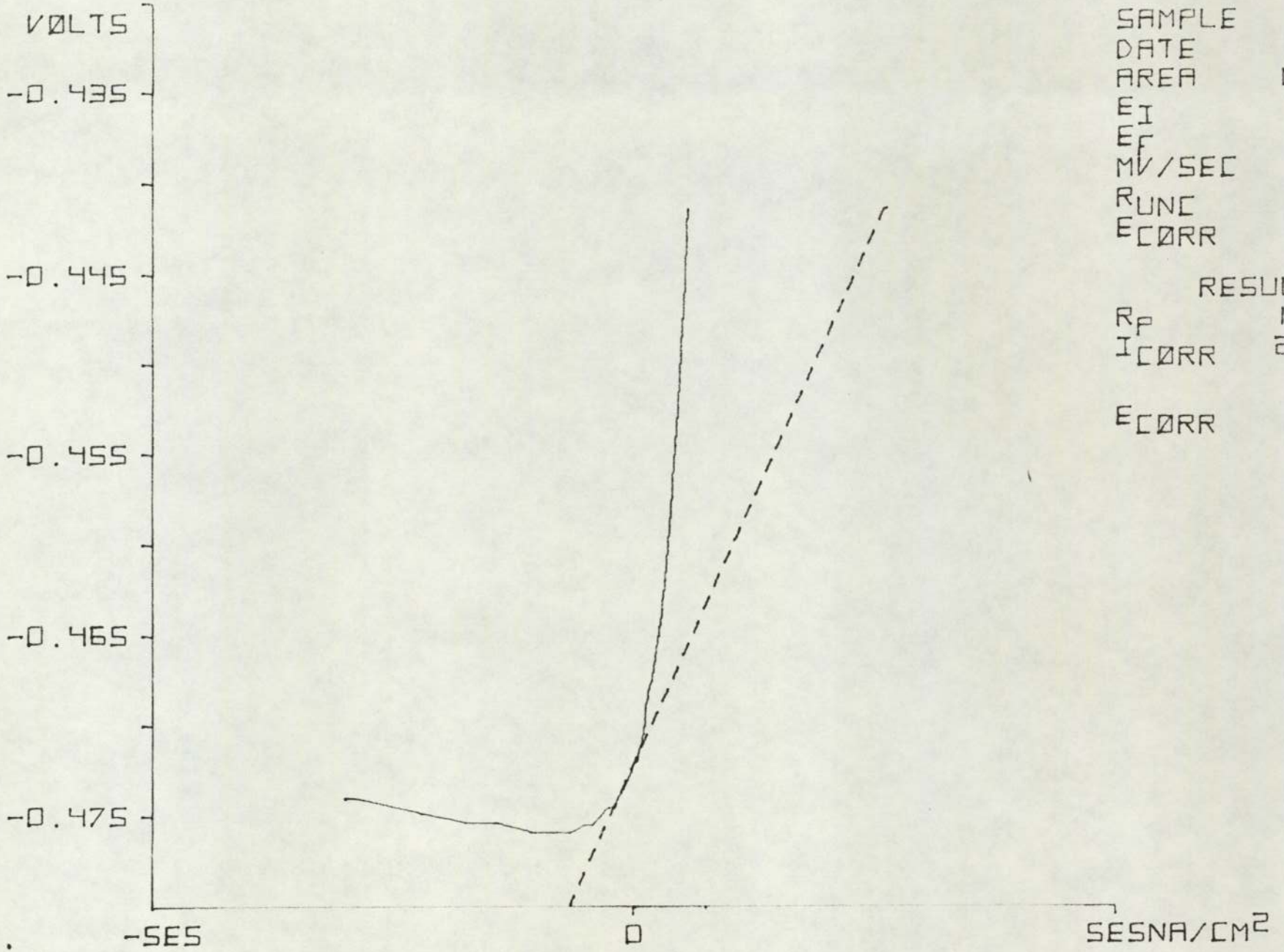

SAMPLE	1112
DATE	23.05
AREA	1.156E1
E_I	-0.480
E_F	-0.440
MV/SEC	0.166
R_{UNC}	1.847
$E_{CØRR}$	-0.460

RESULTS

R_P	1.178E2
$I_{CØRR}$	2.341E5
$E_{CØRR}$	-0.473

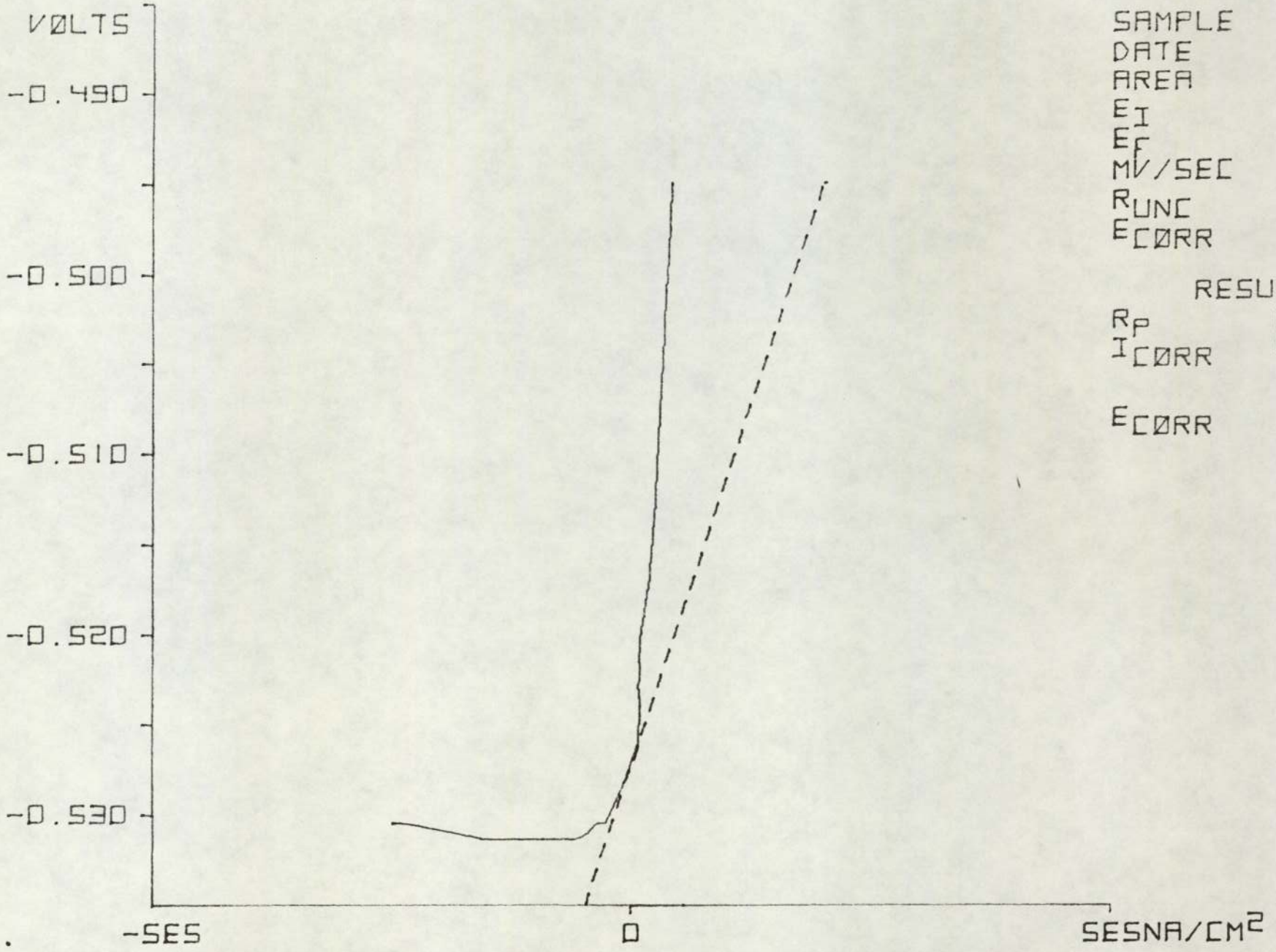

SAMPLE	4113
DATE	30.05
AREA	1.181E1
E_I	-0.534
E_f	-0.494
MV/SEC	0.166
R_{UNC}	1.299
$E_{CØRR}$	-0.514

RESULTS

R_P	1.614E2
$I_{CØRR}$	1.588E5
$E_{CØRR}$	-0.528

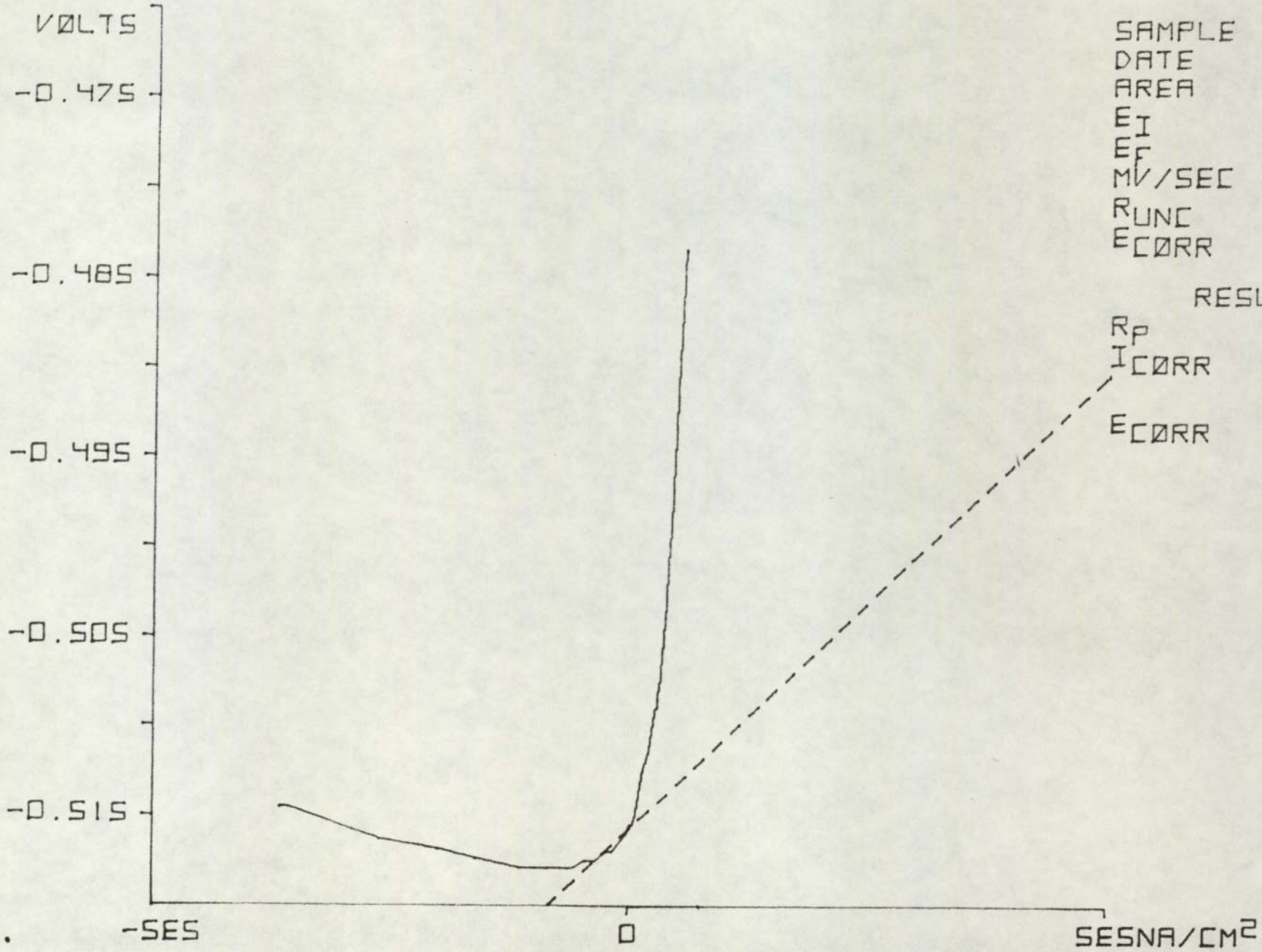

SAMPLE	6113
DATE	30.05
AREA	1.206E1
E_I	-0.522
E_F	-0.482
MV/SEC	0.166
R_{UNC}	1.700
$E_{CØRR}$	-0.502

RESULTS

R_P	5.089E1
$I_{CØRR}$	5.120E5
$E_{CØRR}$	-0.516

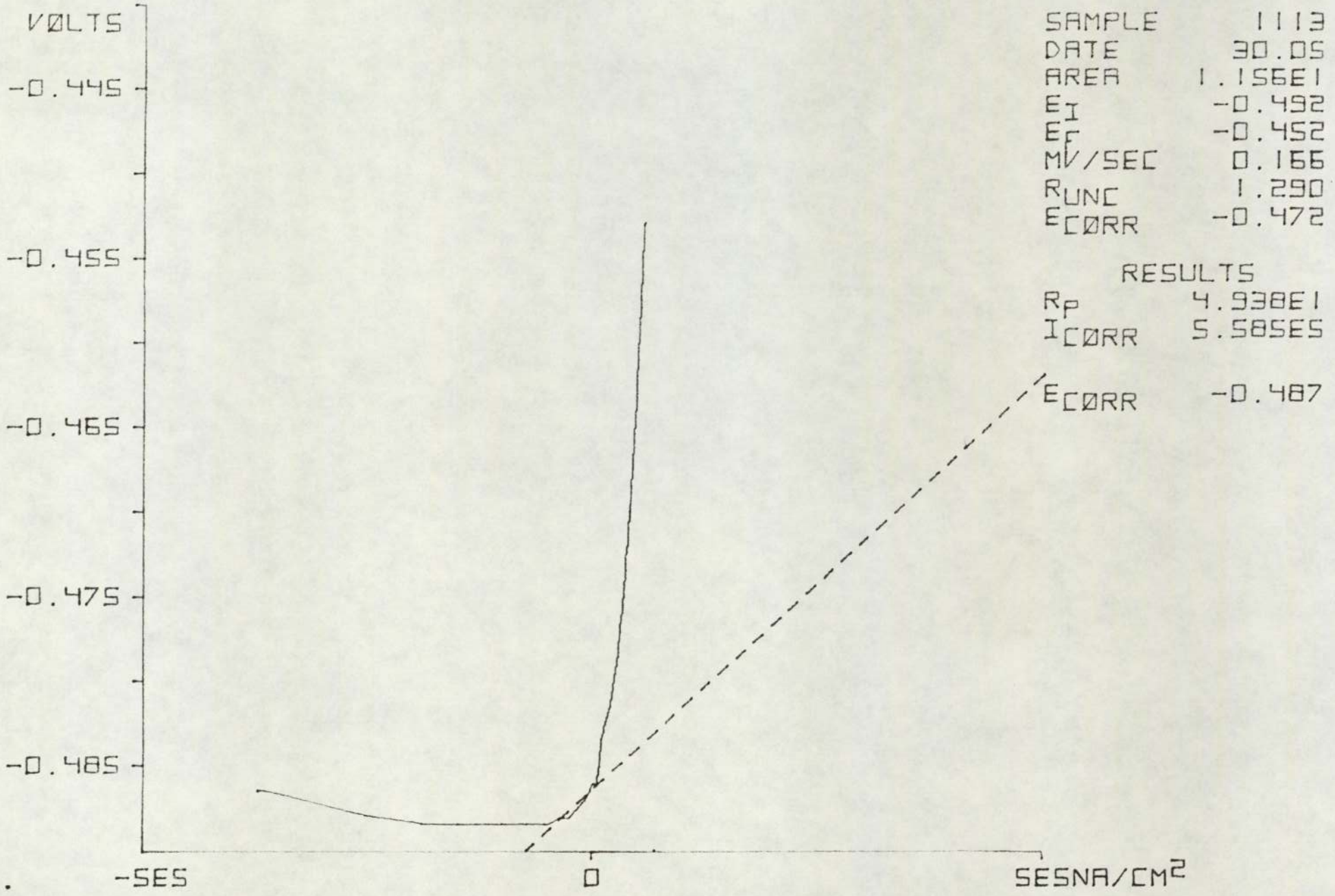

SAMPLE	1113
DATE	30.05
AREA	1.156E1
E_I	-0.492
E_F	-0.452
MV/SEC	0.166
R_{UNC}	1.290
$E_{CØRR}$	-0.472

RESULTS

R_P	4.938E1
$I_{CØRR}$	5.585E5
$E_{CØRR}$	-0.487

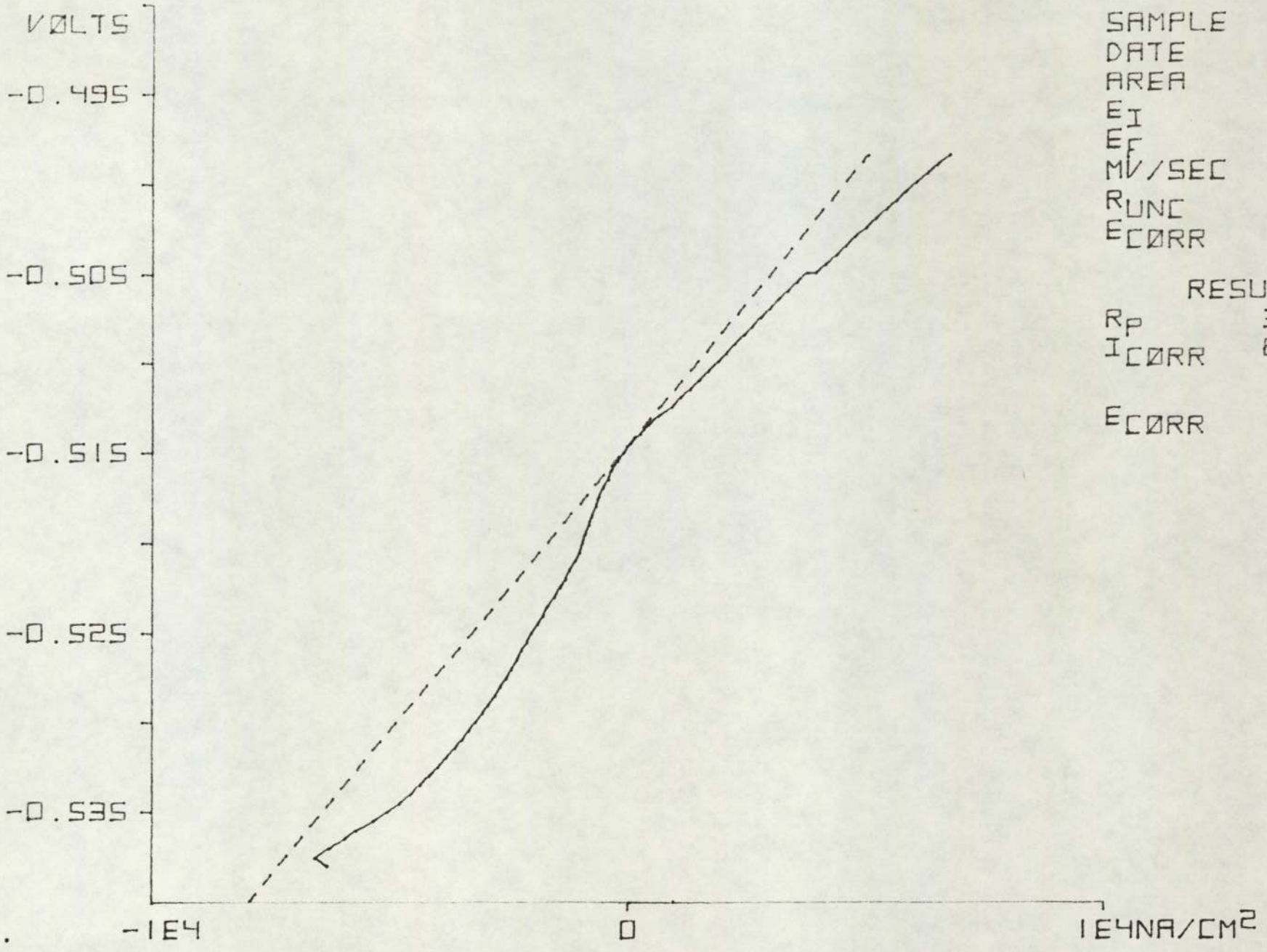

SAMPLE	4210
DATE	09.05
AREA	1.206E1
E_I	-0.538
E_F	-0.498
MV/SEC	0.166
R_{UNC}	1.534
$E_{CØRR}$	-0.518

RESULTS

R_P	3.194E3
$I_{CØRR}$	8.021E3
$E_{CØRR}$	-0.515

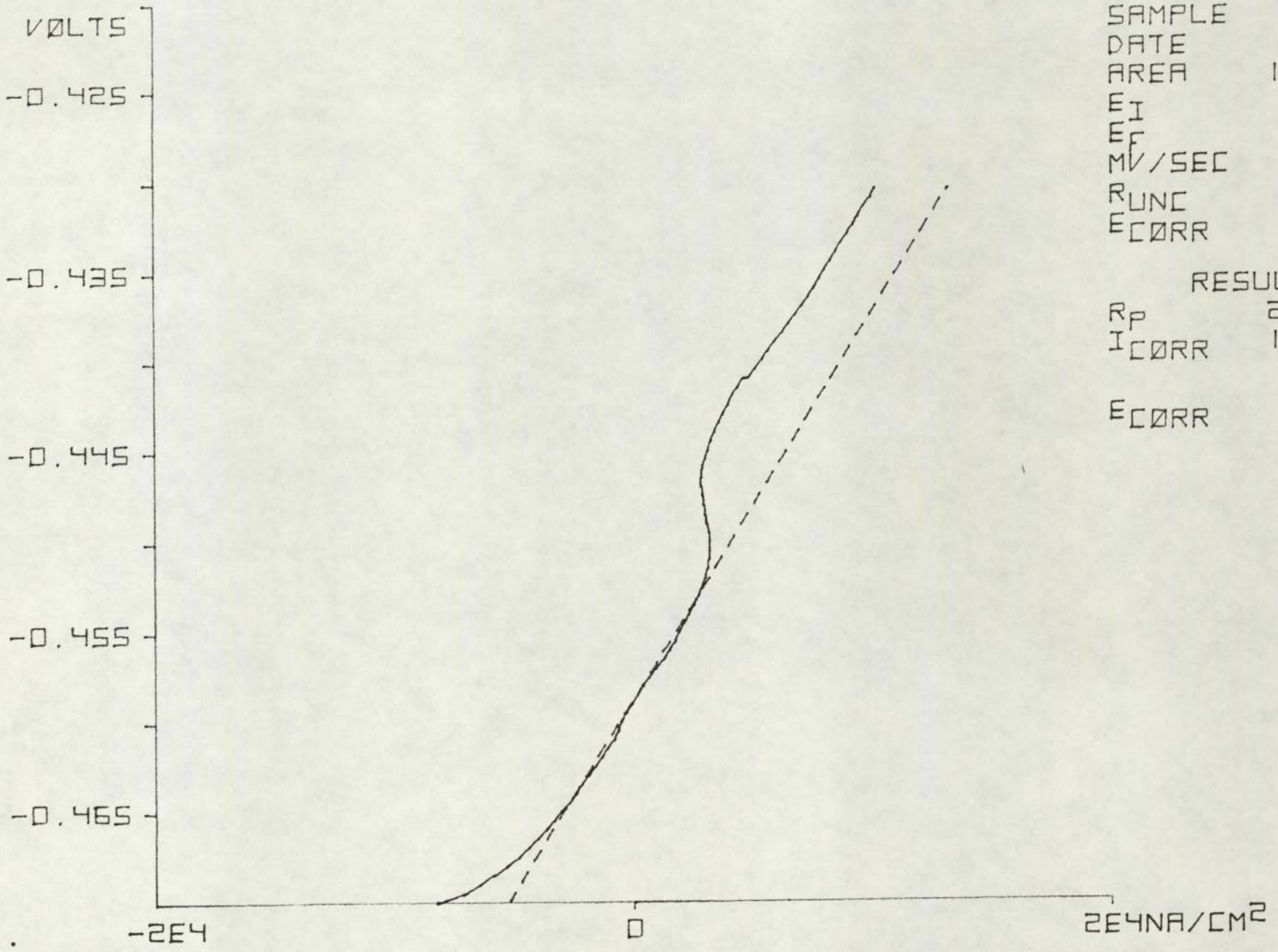

SAMPLE	6210
DATE	09.05
AREA	1.206E1
E_I	-0.470
E_F	-0.430
MV/SEC	0.166
R_{UNC}	1.212
$E_{CØRR}$	-0.450

RESULTS

R_P	2.130E3
$I_{CØRR}$	1.223E4
$E_{CØRR}$	-0.459

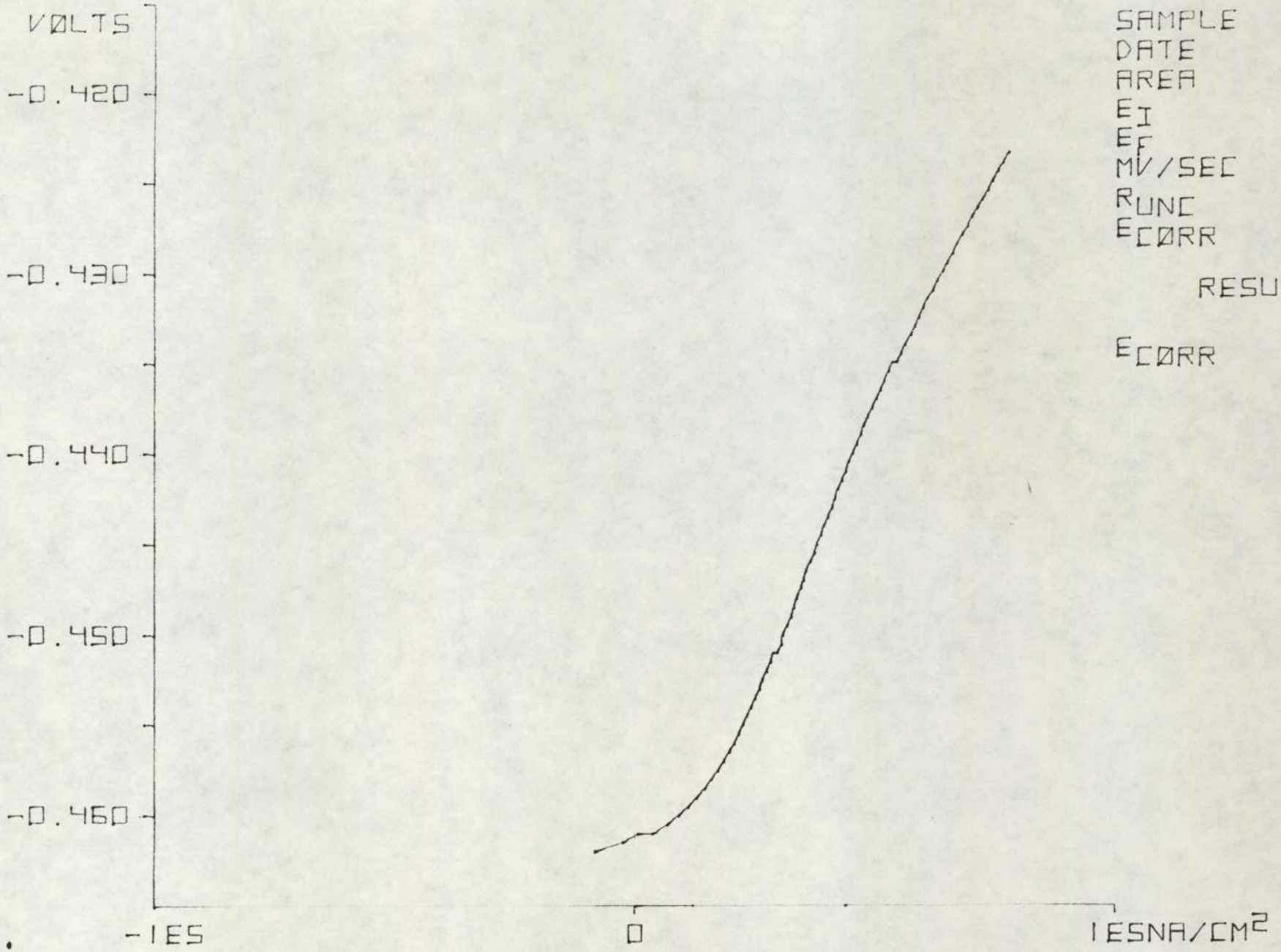

SAMPLE	1210
DATE	09.05
AREA	1.180E1
E_I	-0.462
E_F	-0.422
MV/SEC	0.166
R_{UNC}	1.671
$E_{CØRR}$	-0.442

RESULTS

$E_{CØRR}$ -0.462

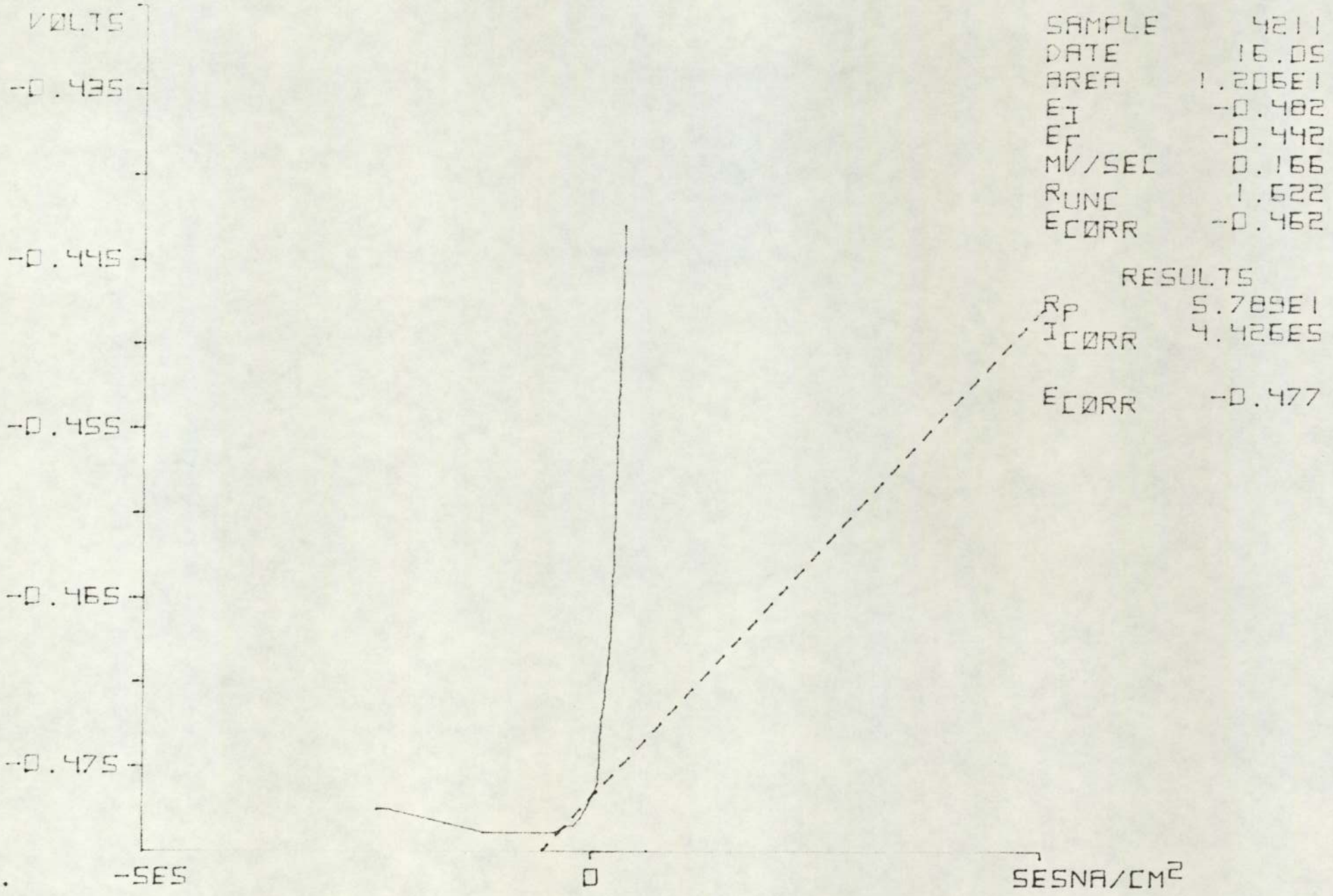

SAMPLE	4211
DATE	16.05
AREA	1.205E1
E_I	-0.482
E_F	-0.442
MV/SEC	0.166
R_{UNC}	1.622
E_{CORR}	-0.462

RESULTS

R_P	5.789E1
I_{CORR}	4.426E5
E_{CORR}	-0.477

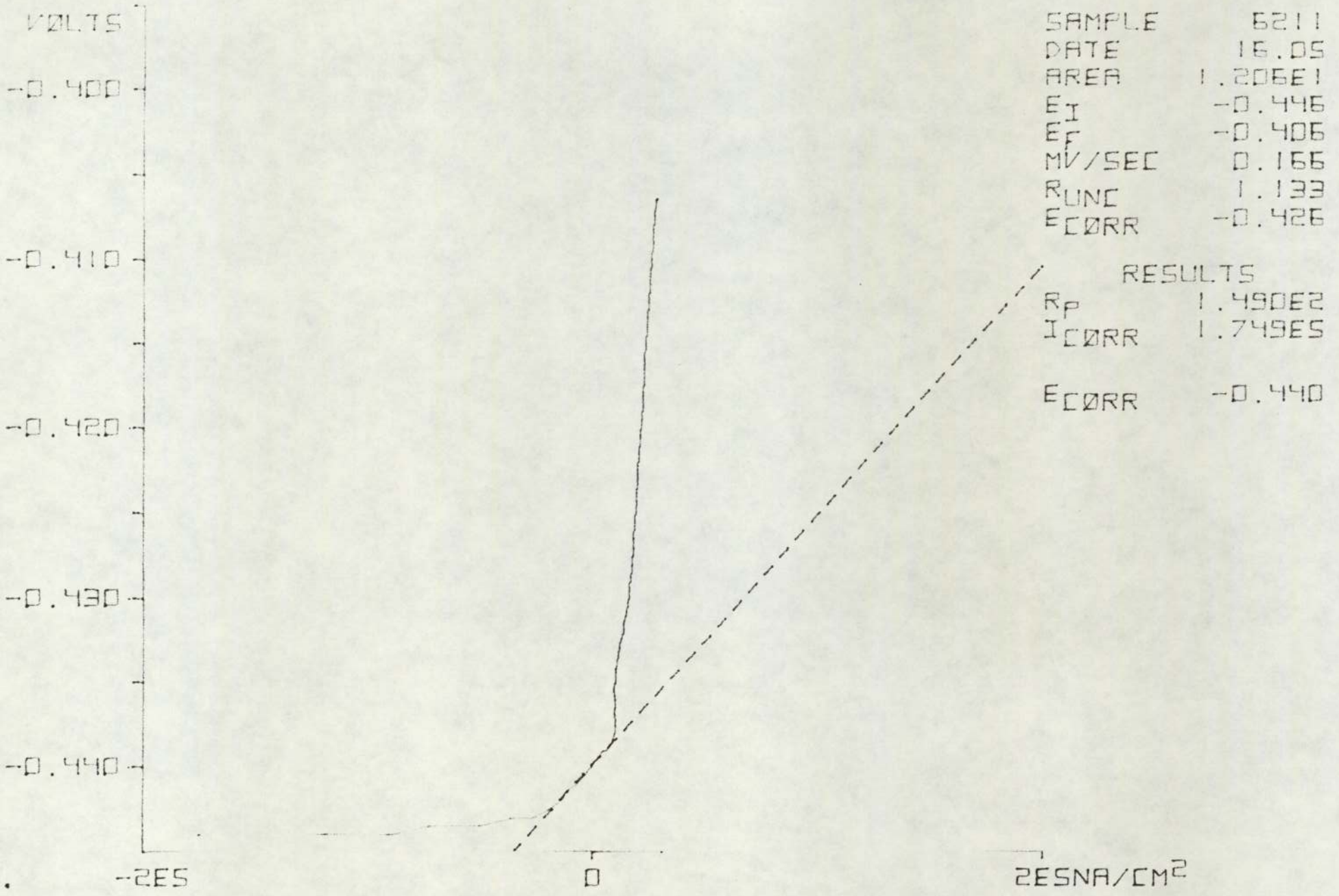

SAMPLE	6211
DATE	16.05
AREA	1.206E1
E_I	-0.446
E_F	-0.406
MV/SEC	0.166
R_{UNC}	1.133
E_{CORR}	-0.426

RESULTS

R_P	1.490E2
I_{CORR}	1.749E5
E_{CORR}	-0.440

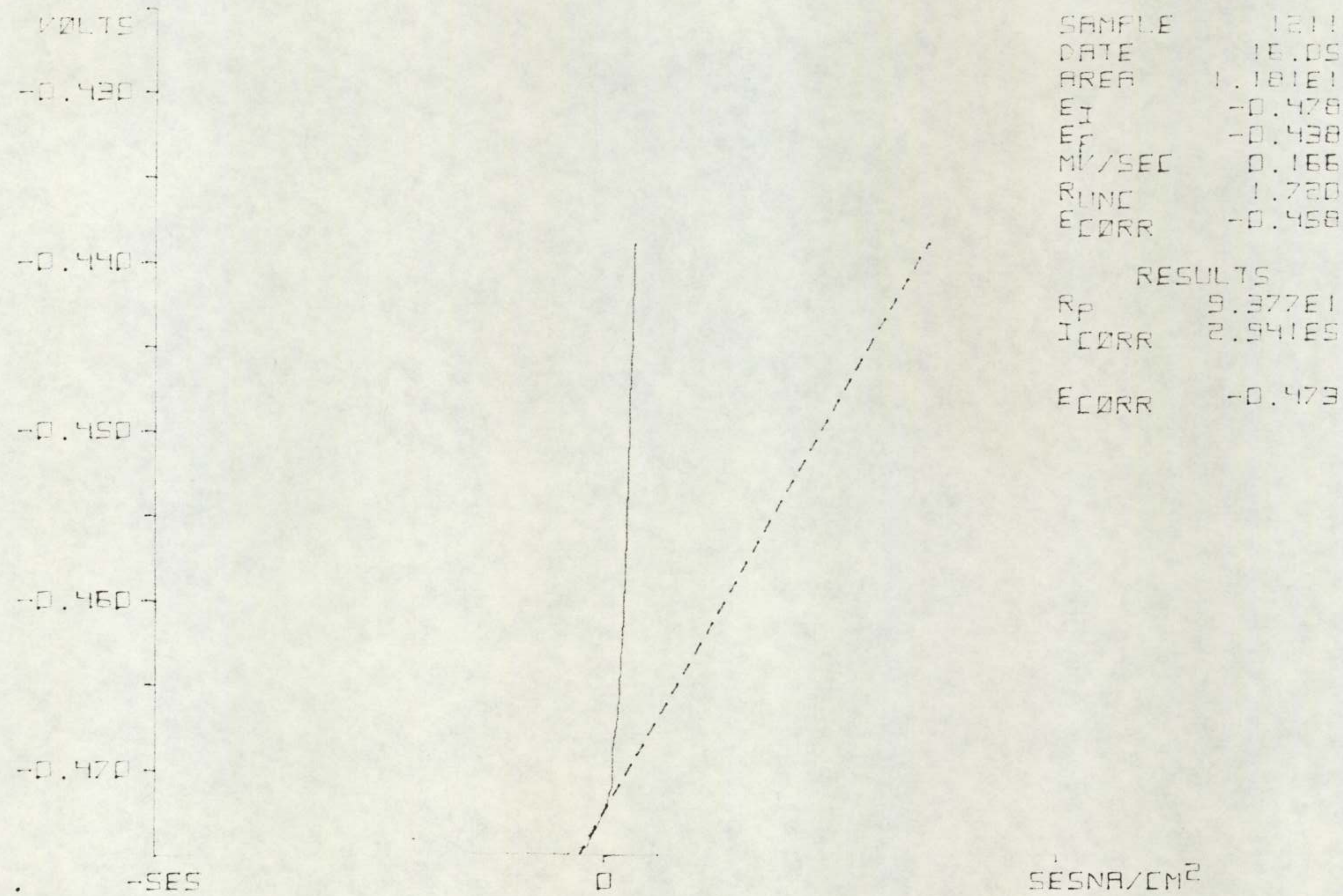

VØLTS
-0.430
-0.440
-0.450
-0.460
-0.470
-SES
0
SESNA/CM2
SAMPLE 1211
DATE 16.05
AREA 1.181E1
EI -0.478
EF -0.438
MV/SEC 0.166
RUNC 1.720
ECØRR -0.458
RESULTS
RP 9.377E1
ICØRR 2.941E5
ECØRR -0.473

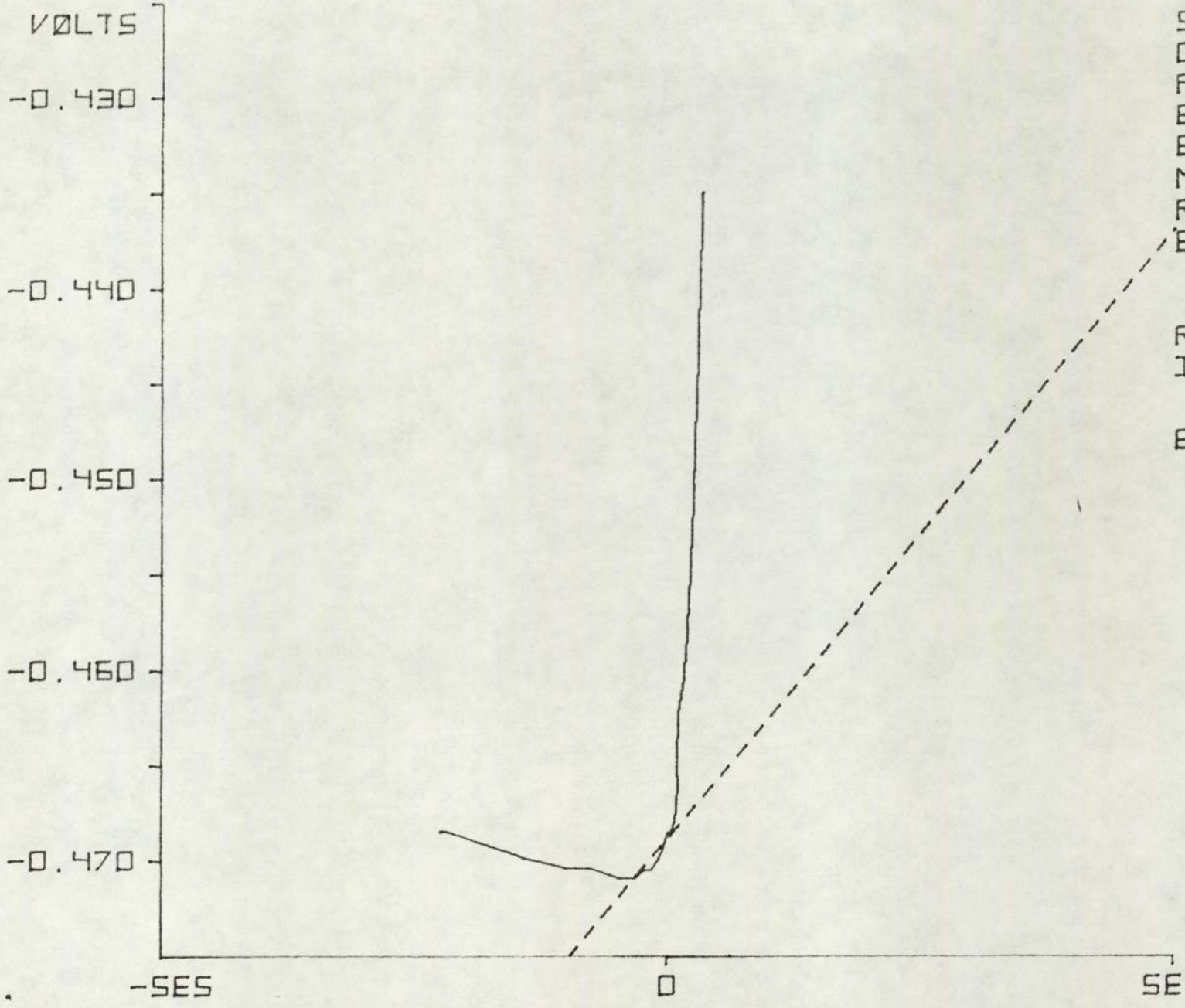

SAMPLE	4212
DATE	23.05
AREA	1.206E1
E_I	-0.474
E_F	-0.434
MV/SEC	0.166
R_{UNC}	2.062
$E_{CØRR}$	-0.454

RESULTS

R_P	6.416E1
$I_{CØRR}$	3.994E5
$E_{CØRR}$	-0.469

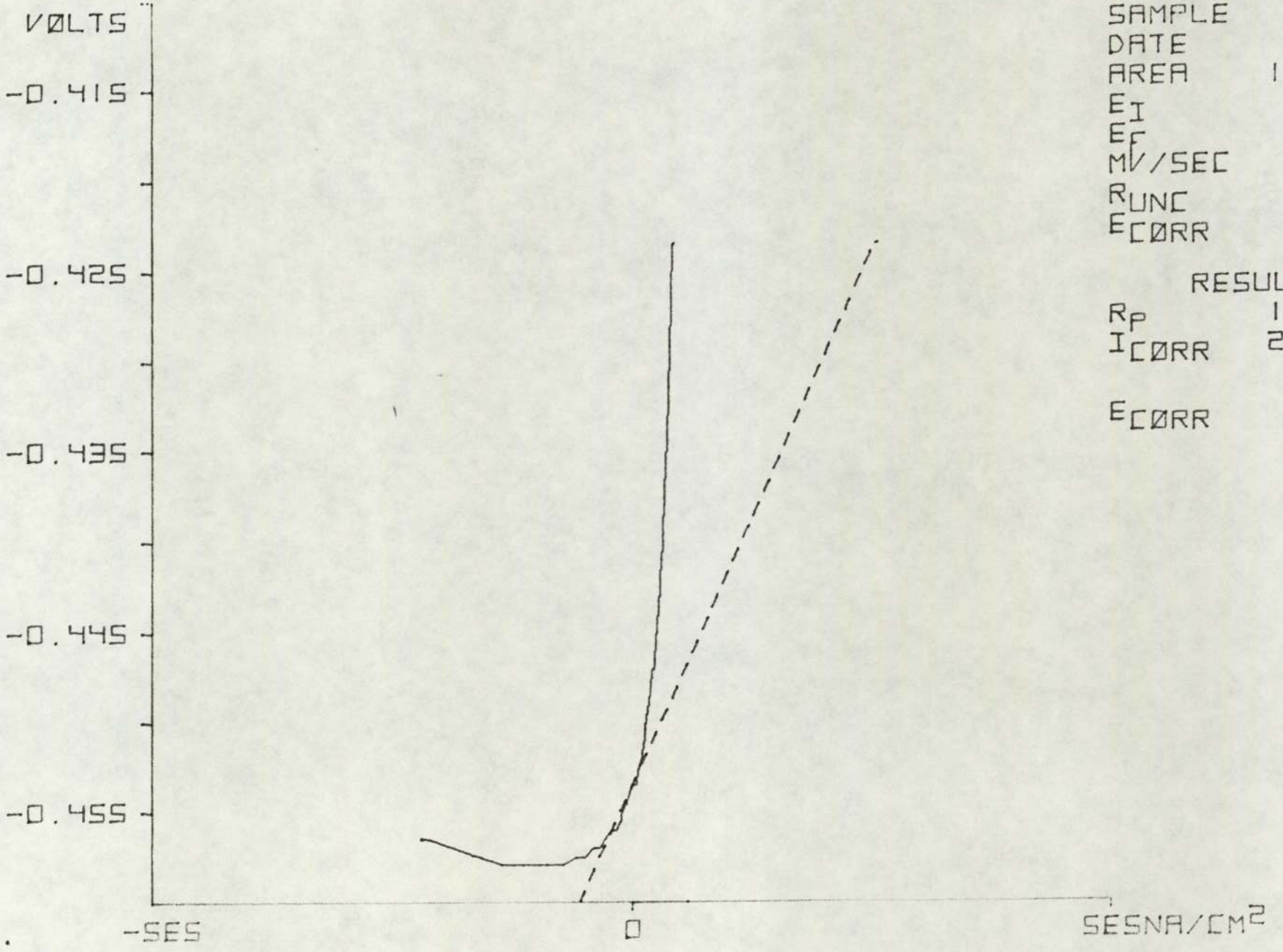

SAMPLE	6212
DATE	23.05
AREA	1.206E1
E_I	-0.462
E_F	-0.422
MV/SEC	0.166
R_{UNC}	2.091
$E_{CØRR}$	-0.442

RESULTS

R_P	1.180E2
$I_{CØRR}$	2.209E5
$E_{CØRR}$	-0.454

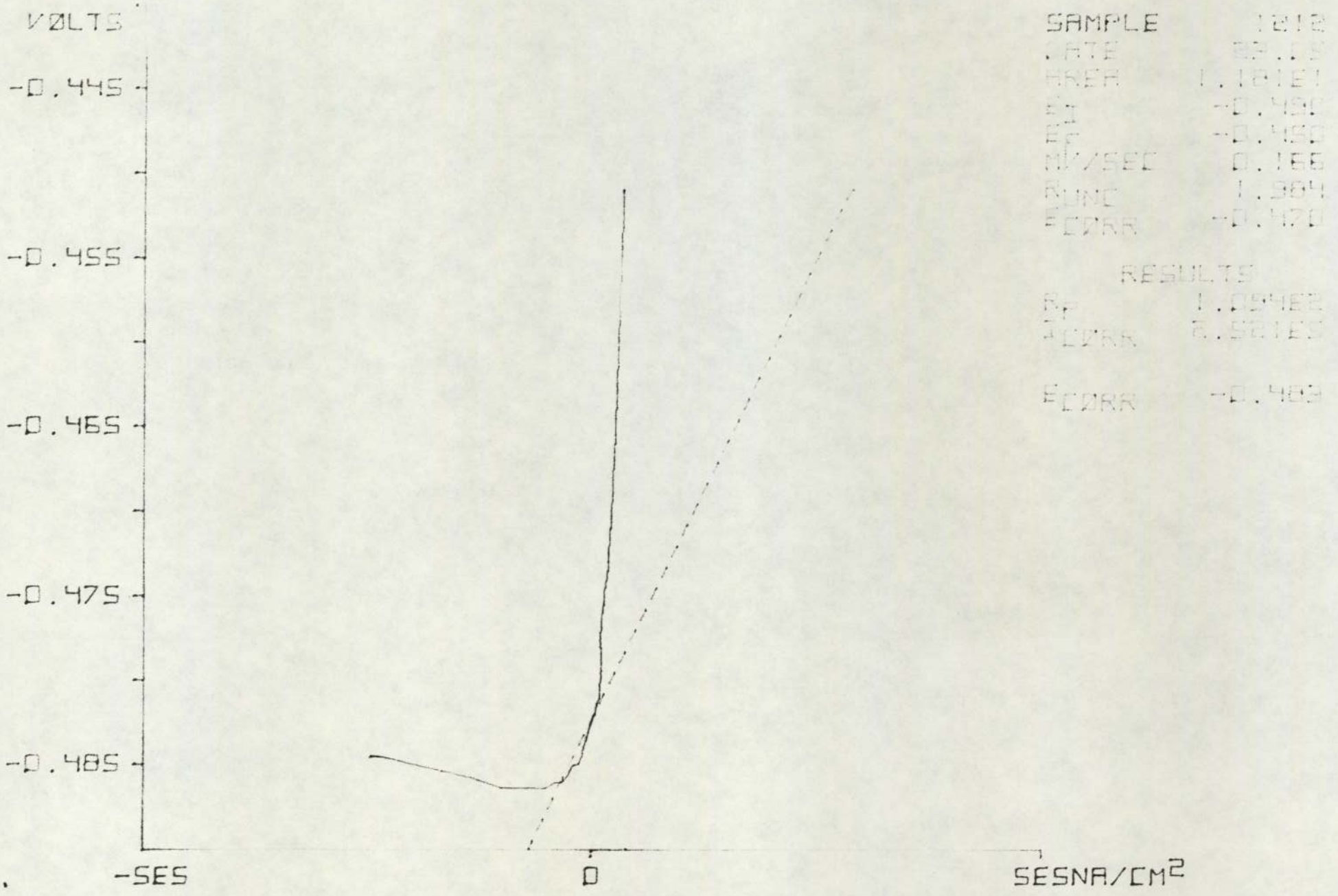
VOLTS
-0.445
-0.455
-0.465
-0.475
-0.485
-SES
0
SESNA/CM2
SAMPLE 1212
RATE
AREA 1.1816E1
EI -0.491
EF -0.455
MV/SEC 0.166
RUNC 1.984
ECORR -0.470
RESULTS
RP 1.0946E2
ICORR 6.5616E3
ECORR -0.469

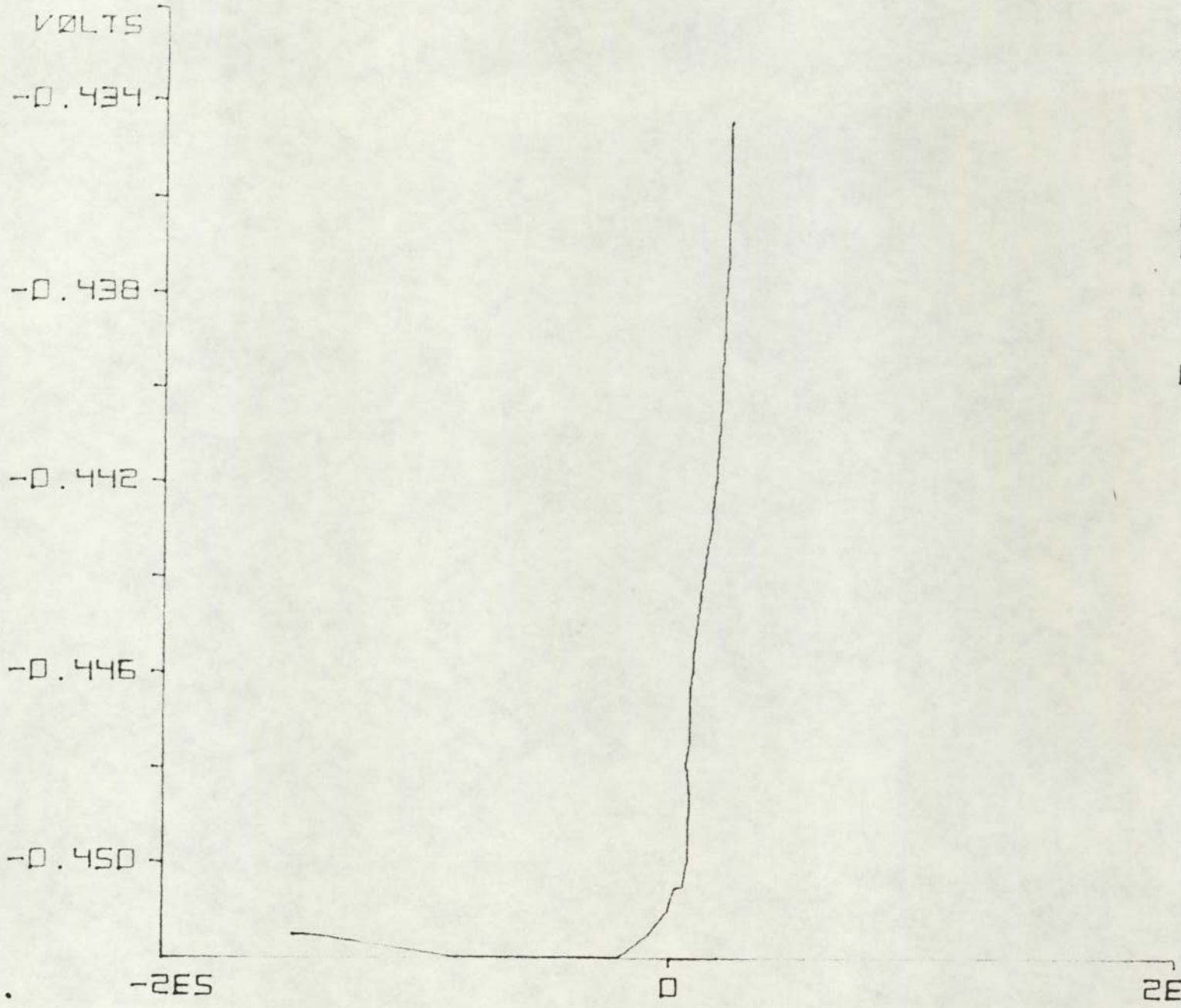

SAMPLE	4213
DATE	30.05
AREA	1.206E1
E_I	-0.454
E_f	-0.434
MV/SEC	0.166
R_{UNC}	1.544
E_{CORR}	-0.444

RESULTS

E_{CORR}	-0.451

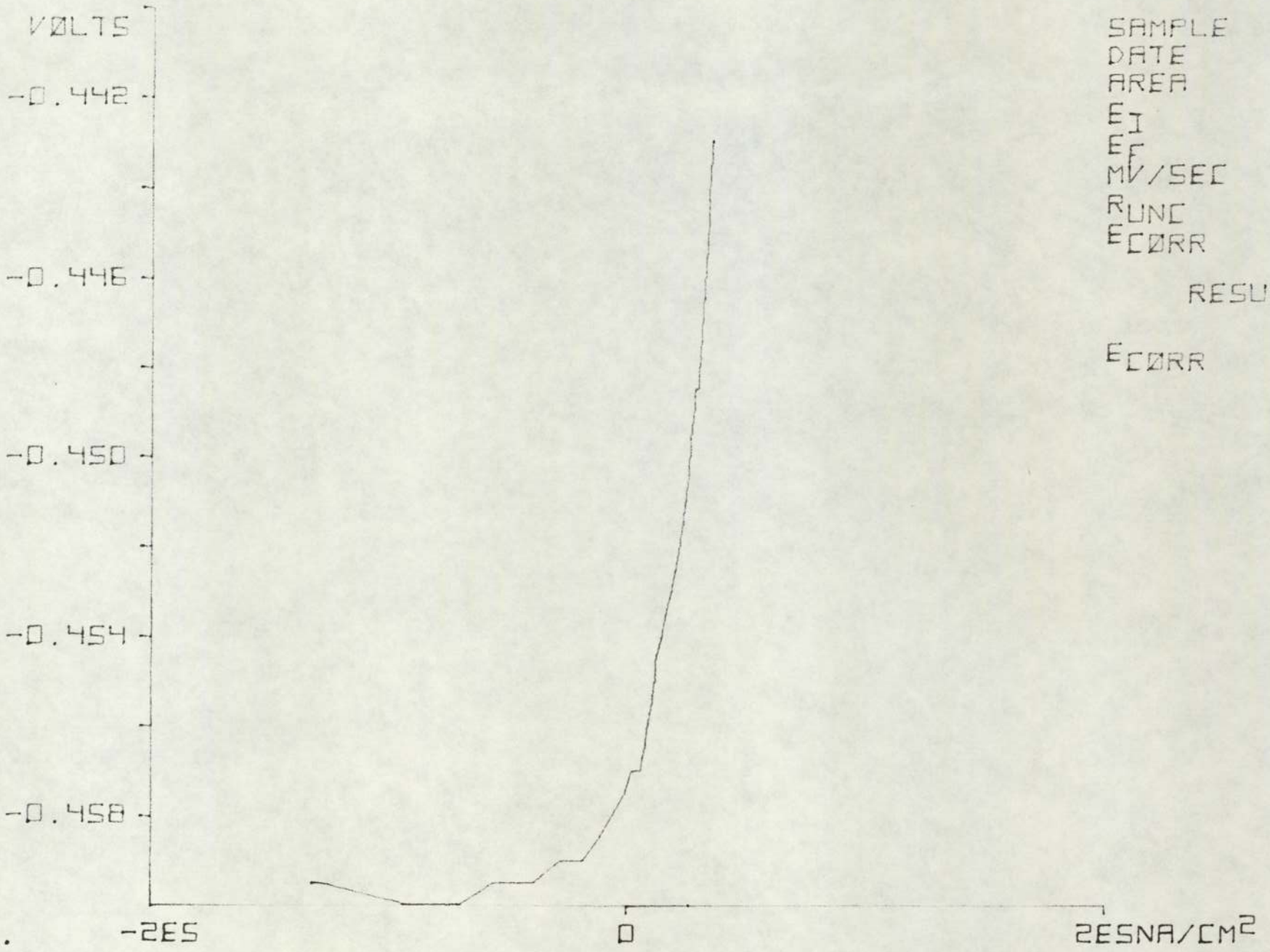

SAMPLE	6213
DATE	30.05
AREA	1.206E1
E_I	-0.462
E_f	-0.442
MV/SEC	0.166
R_{UNC}	1.661
$E_{CØRR}$	-0.452

RESULTS

$E_{CØRR}$ -0.458

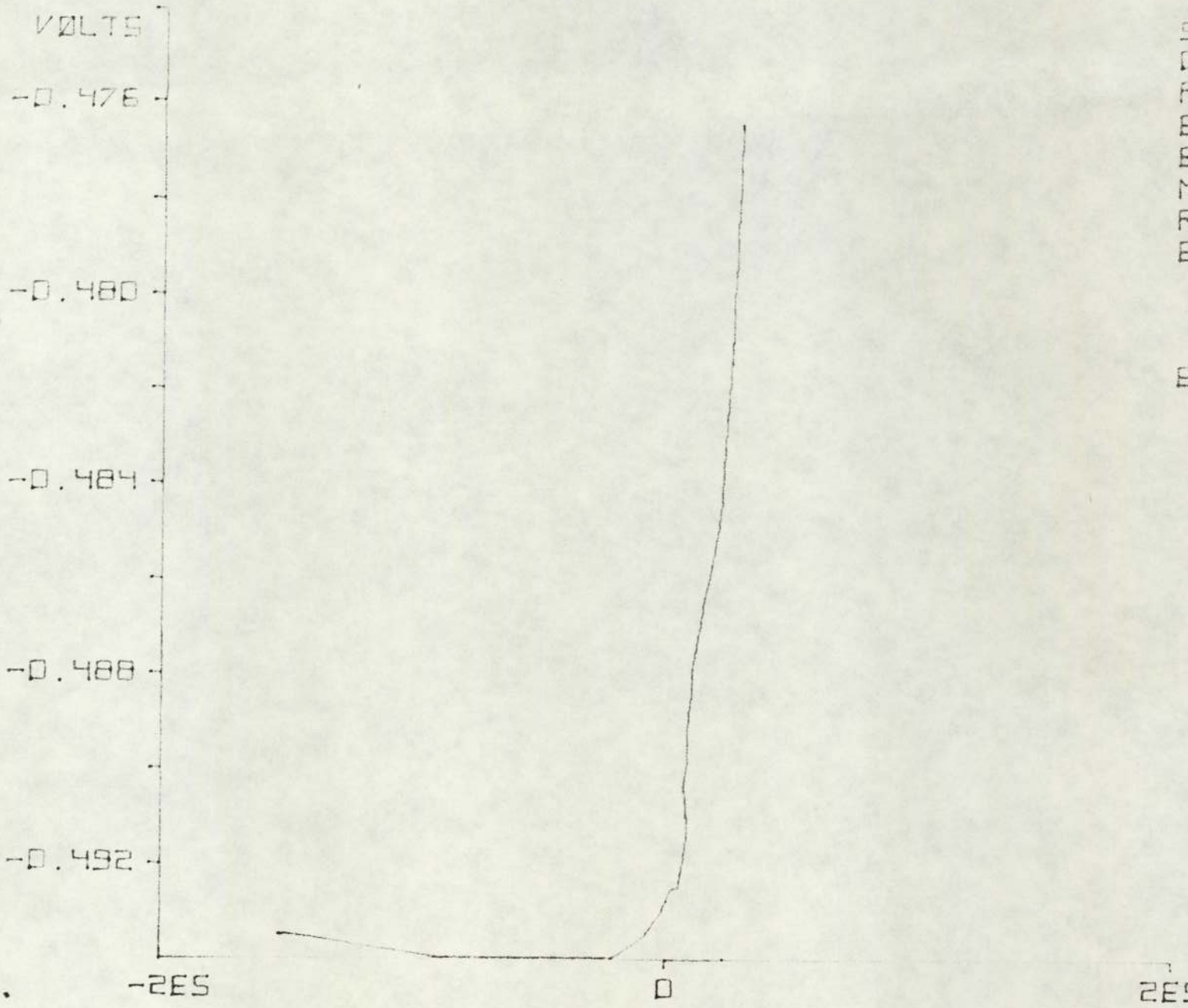

SAMPLE	1213
DATE	30.05
AREA	1.181E1
E_I	-0.496
E_F	-0.476
MV/SEC	0.166
R_{UNC}	1.466
$E_{CØRR}$	-0.486

RESULTS

$E_{CØRR}$ -0.493

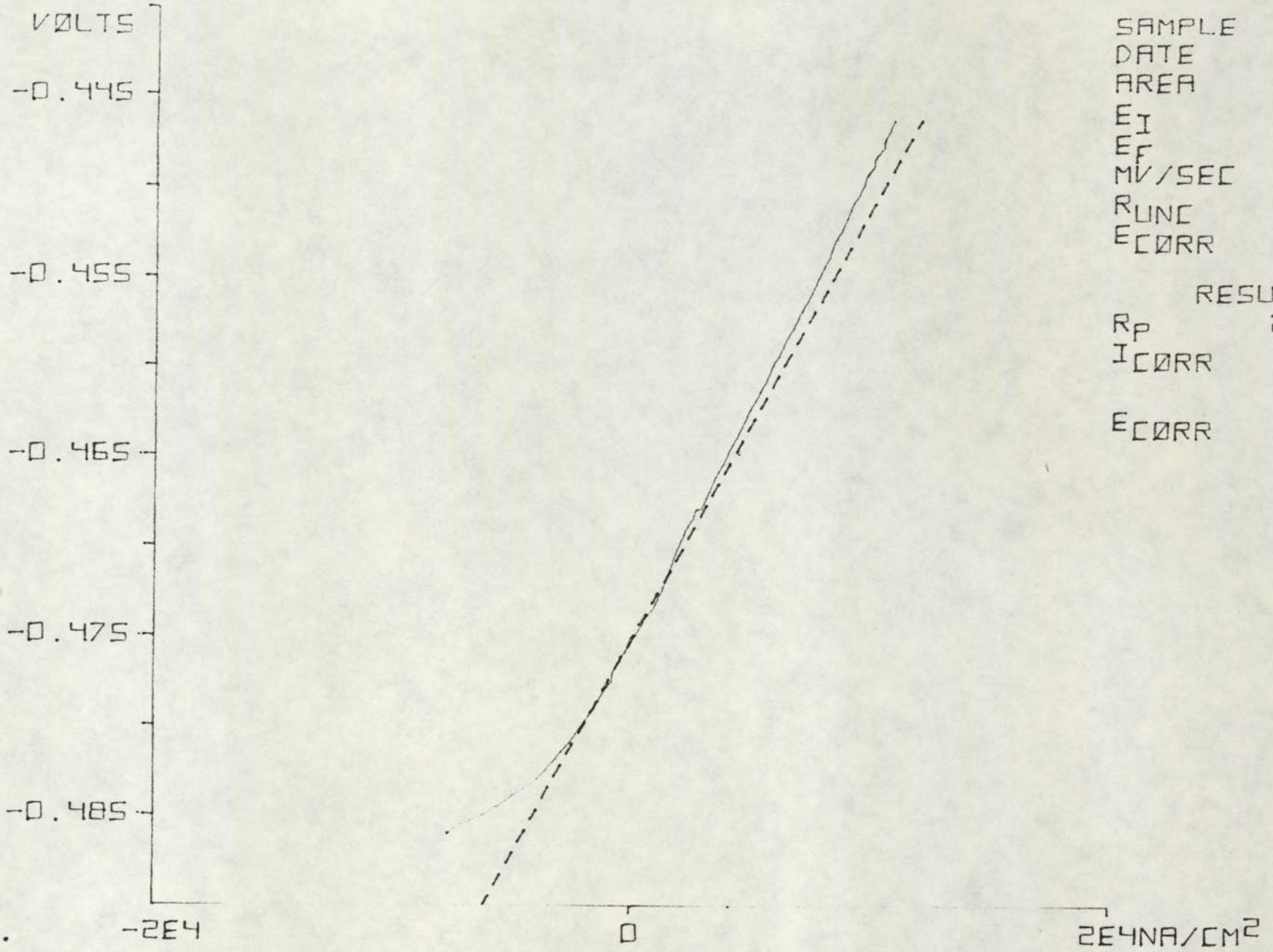

SAMPLE	4310
DATE	16.05
AREA	1.206E1
E_I	-0.486
E_F	-0.446
MV/SEC	0.166
R_{UNC}	2.081
$E_{CØRR}$	-0.466

RESULTS

R_P	2.391E3
$I_{CØRR}$	1.072E4
$E_{CØRR}$	-0.476

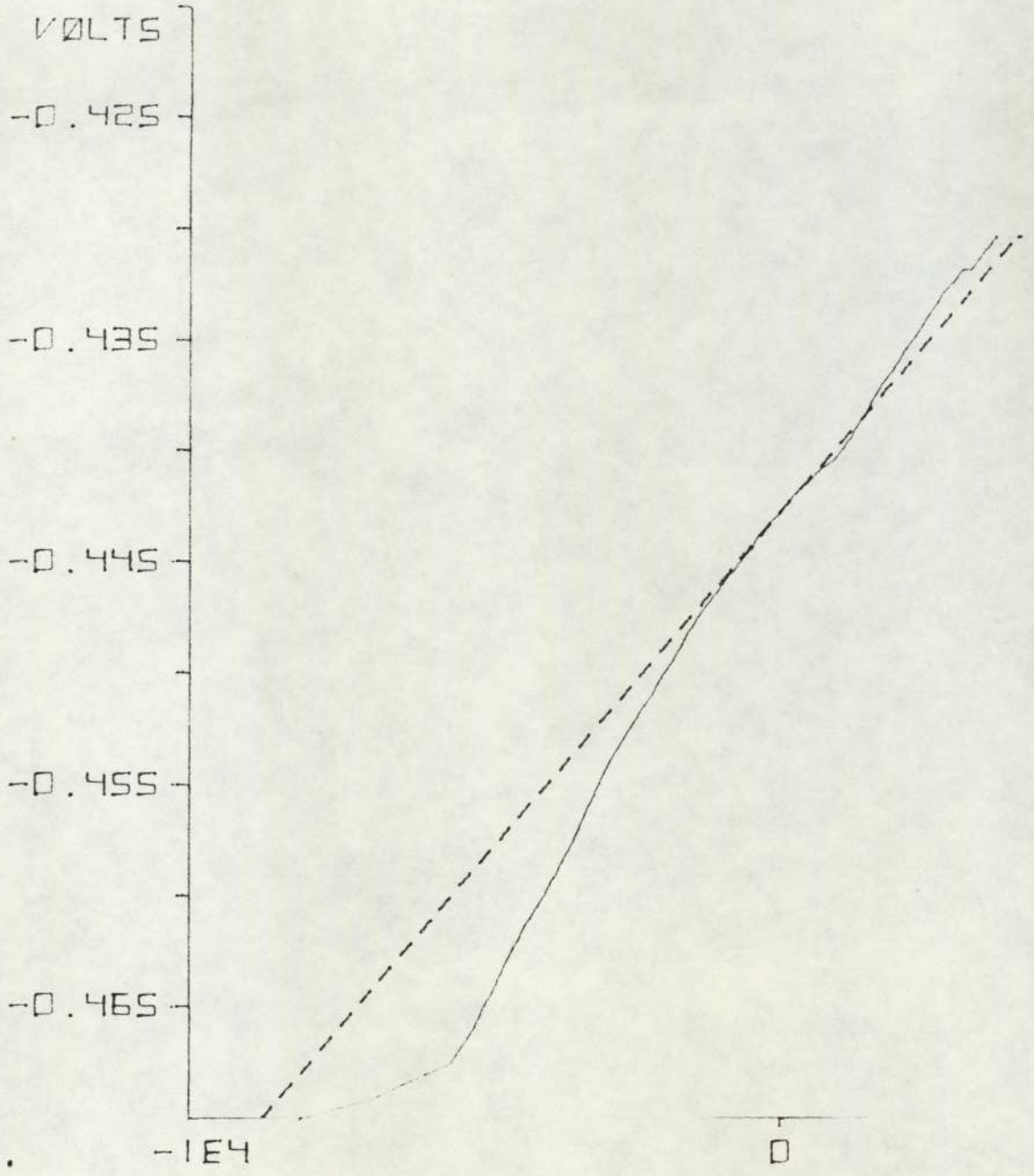

SAMPLE	6310
DATE	16.05
AREA	1.206E1
E_I	-0.470
E_f	-0.430
MV/SEC	0.166
R_{UNC}	1.896
$E_{CØRR}$	-0.450

RESULTS

R_P	3.102E3
$I_{CØRR}$	8.400E3
$E_{CØRR}$	-0.443

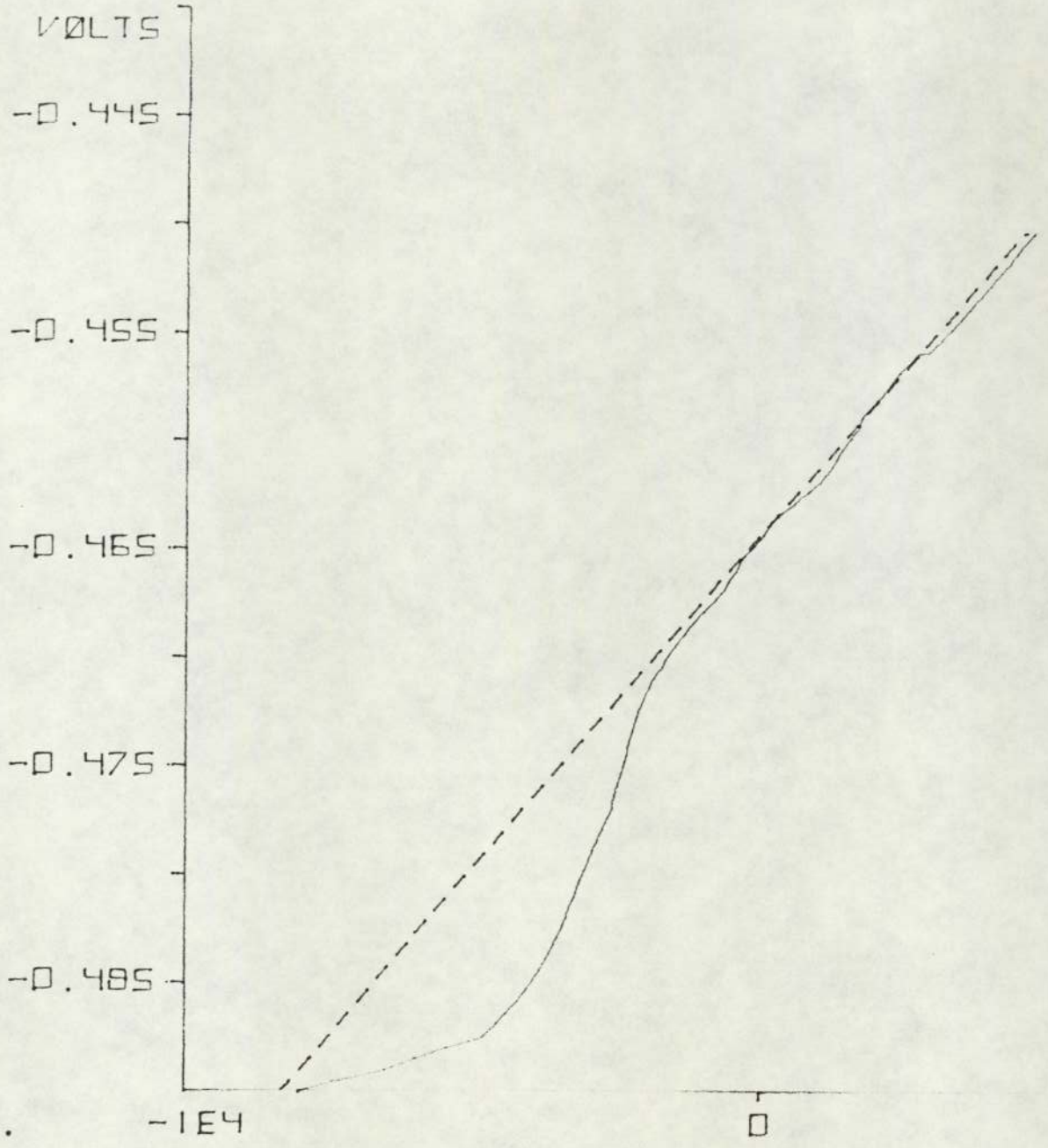

SAMPLE	1310
DATE	16.05
AREA	1.181E1
E_I	-0.490
E_F	-0.450
MV/SEC	0.166
R_{UNC}	2.130
$E_{CØRR}$	-0.470

RESULTS

R_P	3.082E3
$I_{CØRR}$	8.948E3
$E_{CØRR}$	-0.465

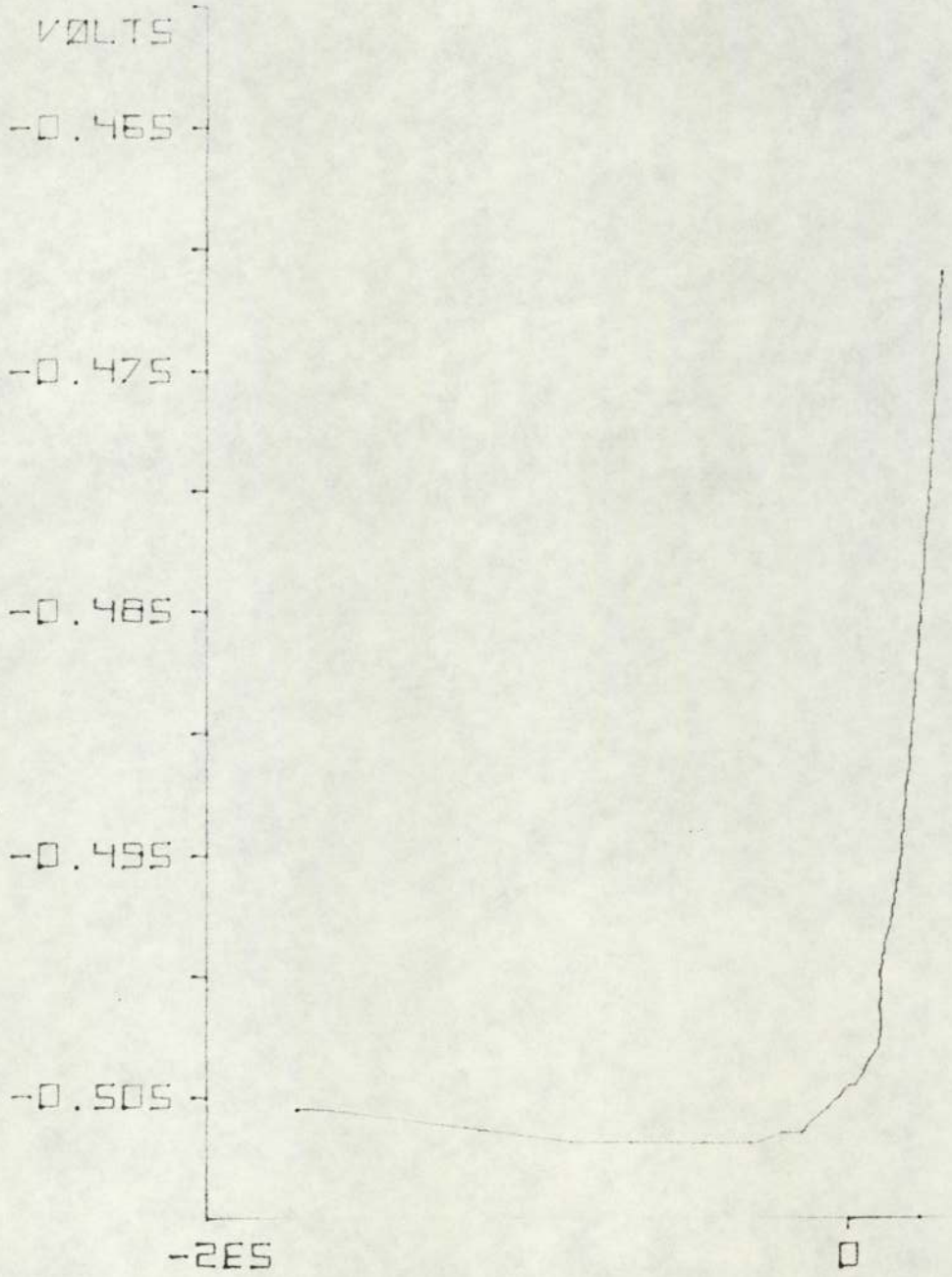

SAMPLE	4311
DATE	23.05
AREA	1.206E1
E_I	-0.510
E_F	-0.470
MV/SEC	0.166
RUNC	2.169
$E_{CØRR}$	-0.490

RESULTS

$E_{CØRR}$ -0.505

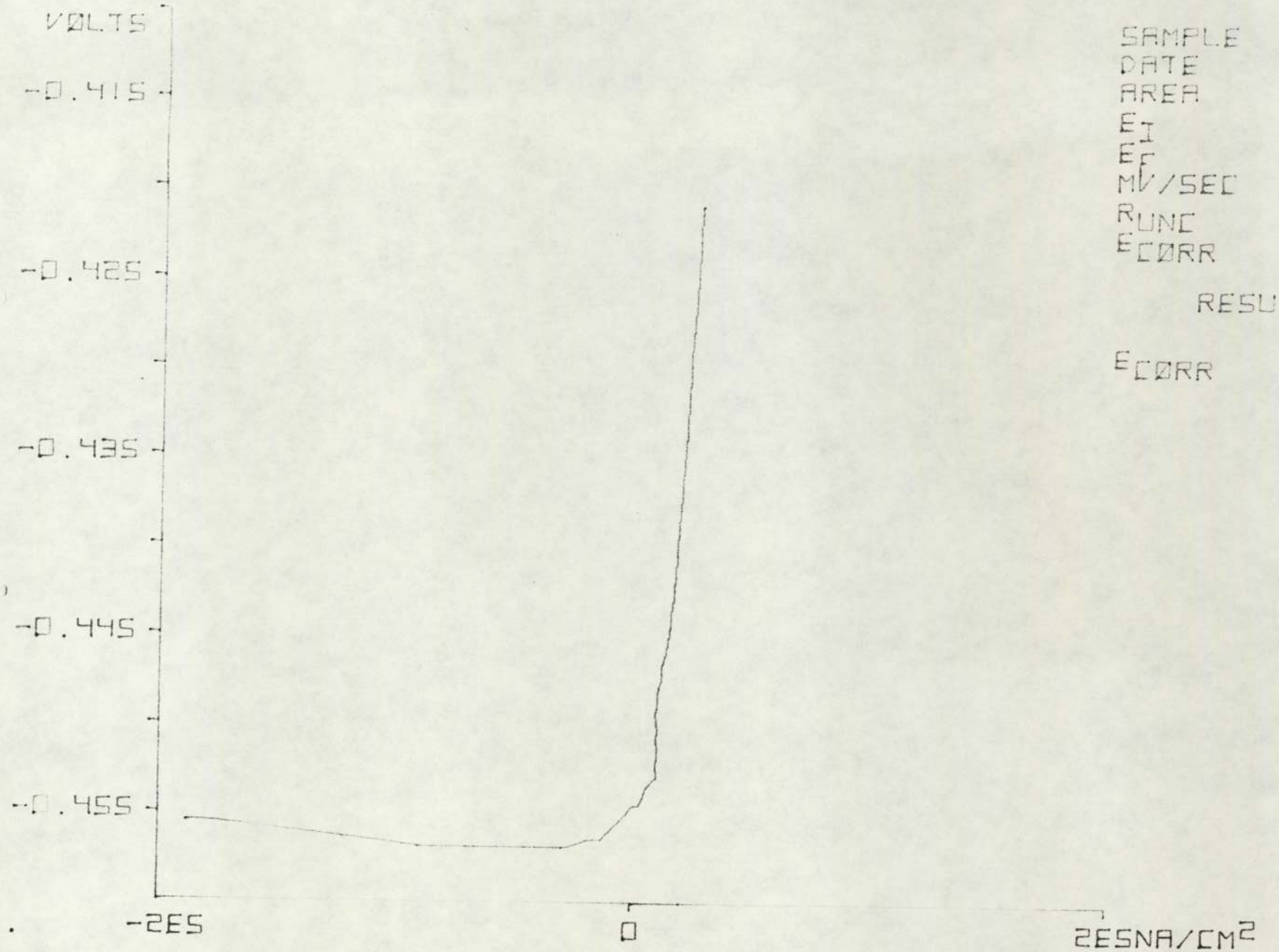

SAMPLE	6311
DATE	23.05
AREA	1.206E1
E_I	-0.460
E_F	-0.420
MV/SEC	0.166
RUNC	2.052
$E_{CØRR}$	-0.440

RESULTS

$E_{CØRR}$	-0.455

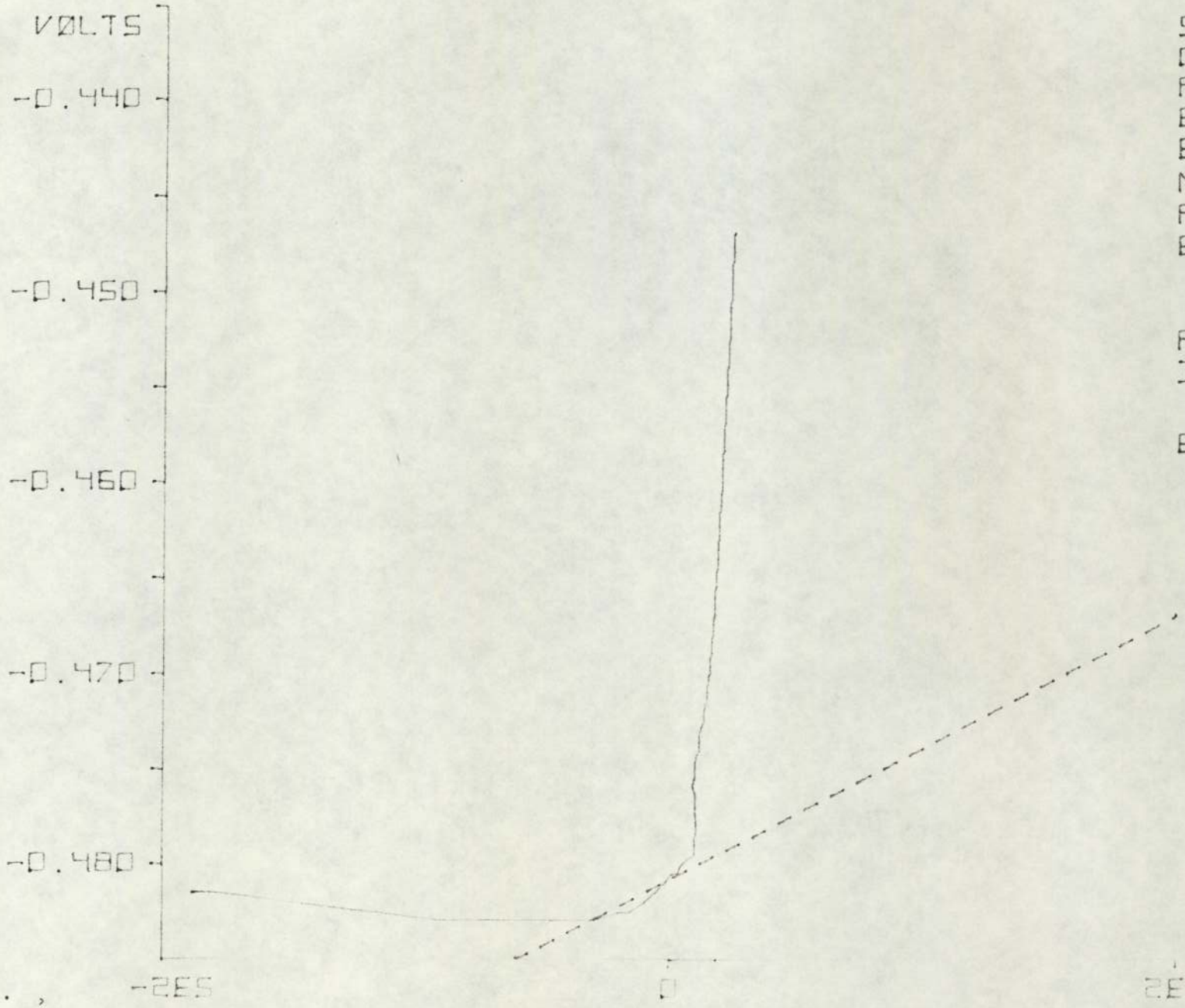

SAMPLE	1311
DATE	23.05
AREA	1.181E1
E_I	-0.486
E_F	-0.446
MV/SEC	0.166
R_{UNC}	2.169
$E_{CØRR}$	-0.466

RESULTS

R_P	7.039E1
$I_{CØRR}$	3.917E5
$E_{CØRR}$	-0.481

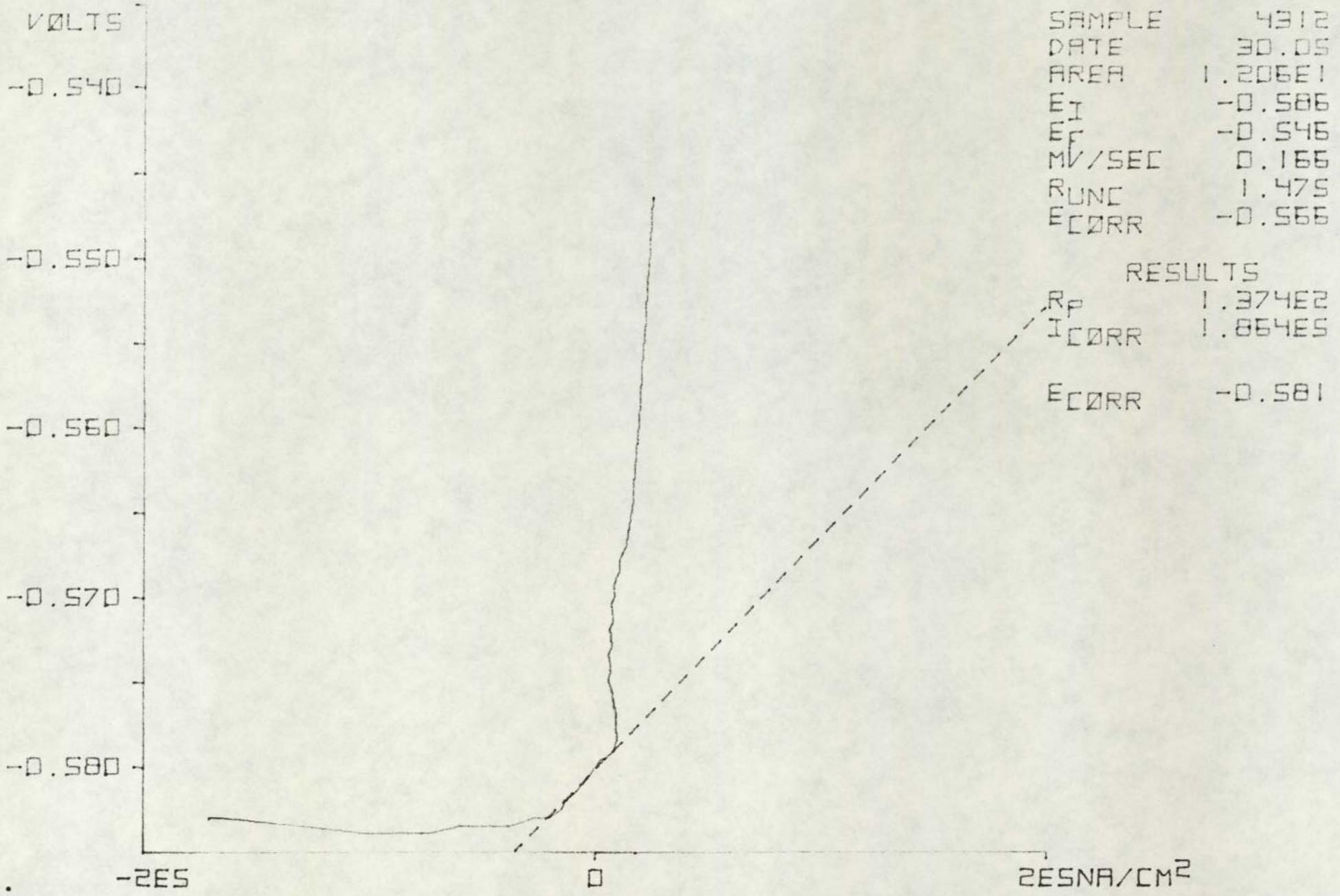

SAMPLE	4312
DATE	30.05
AREA	1.206E1
E_I	-0.586
E_F	-0.546
MV/SEC	0.166
R_{UNC}	1.475
$E_{CØRR}$	-0.566

RESULTS

R_P	1.374E2
$I_{CØRR}$	1.864E5
$E_{CØRR}$	-0.581

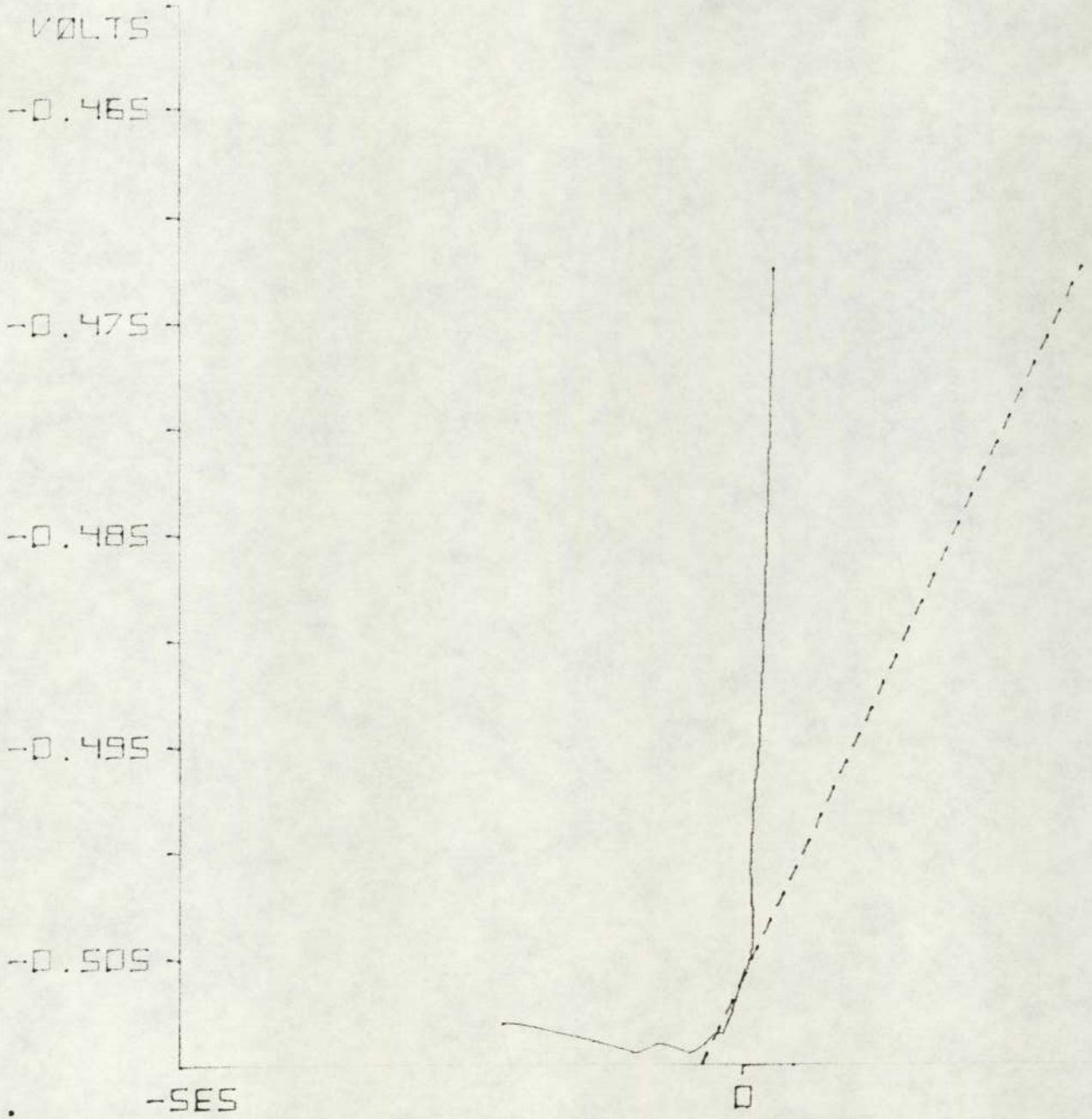

SAMPLE	6312
DATE	30.05
AREA	1.206E1
E_I	-0.512
E_f	-0.472
MV/SEC	0.166
R_{UNC}	1.583
$E_{CØRR}$	-0.492

RESULTS

R_P	1.108E2
$I_{CØRR}$	2.351E5
$E_{CØRR}$	-0.506

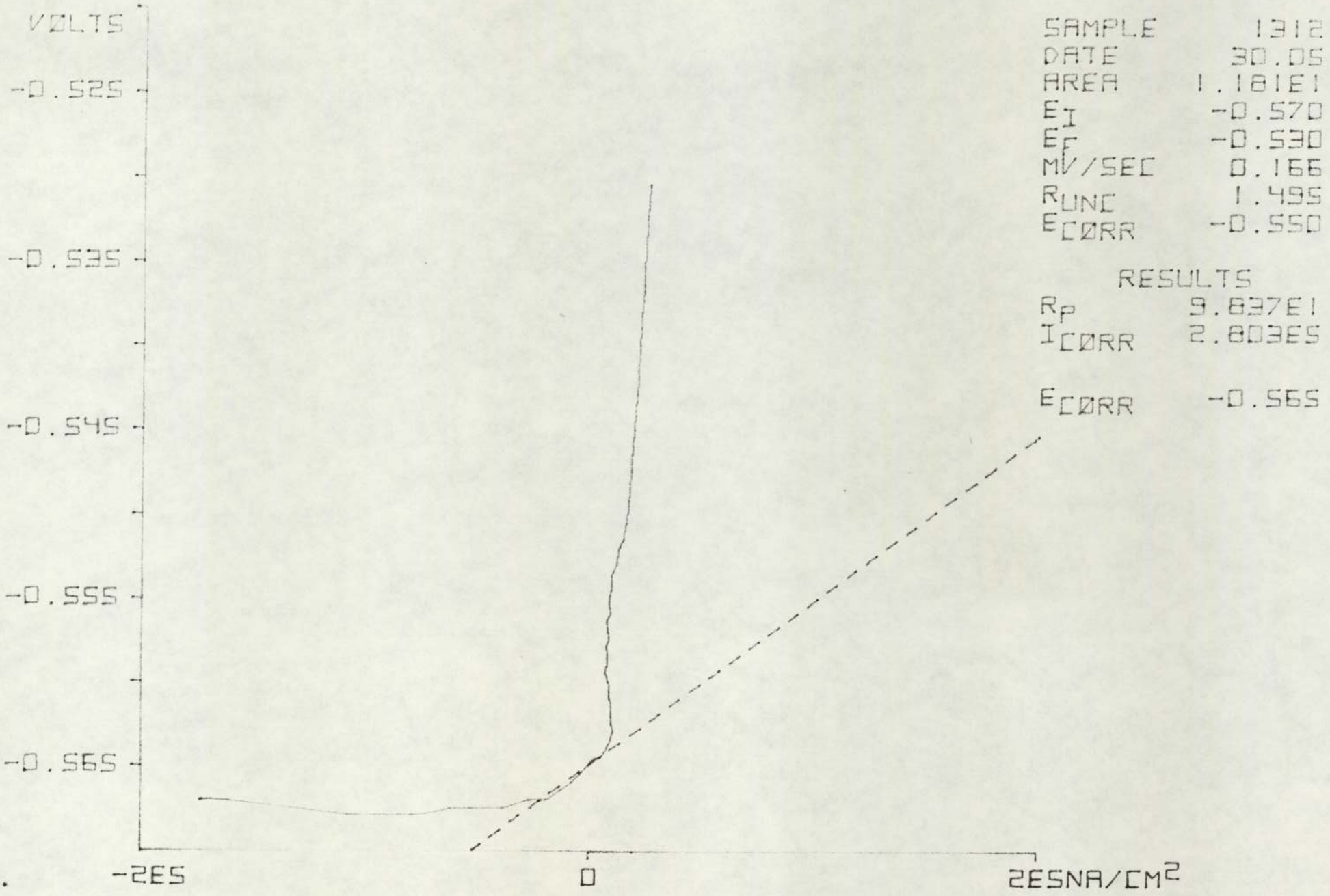

SAMPLE	1312
DATE	30.05
AREA	1.181E1
E_I	-0.570
E_F	-0.530
MV/SEC	0.166
R_{UNC}	1.495
E_{CORR}	-0.550

RESULTS

R_P	9.837E1
I_{CORR}	2.803E5
E_{CORR}	-0.565

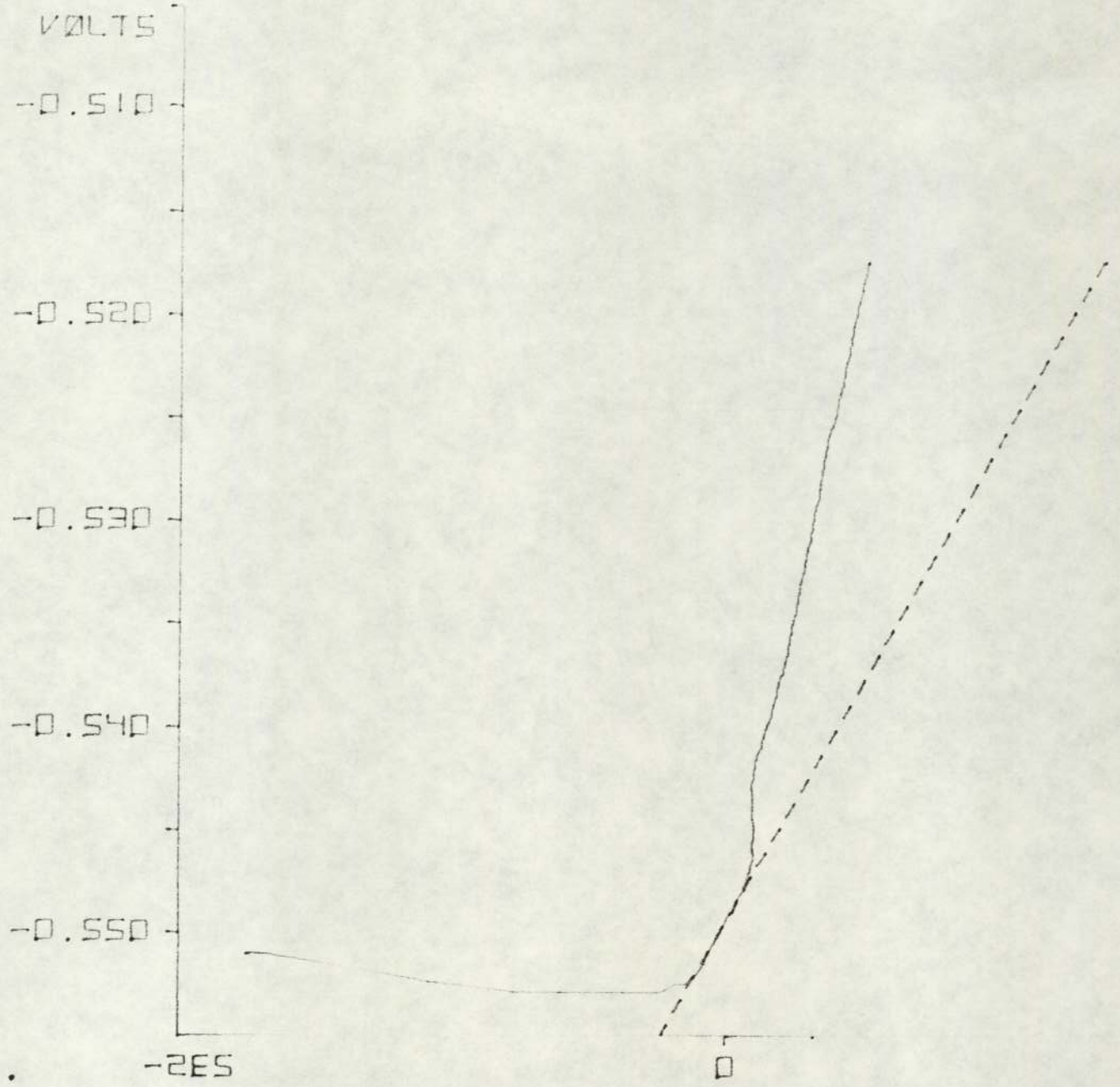

SAMPLE	4313
DATE	05.05
AREA	1.206E1
E_I	-0.556
E_F	-0.516
MV/SEC	0.166
R_{UNC}	2.375
$E_{CØRR}$	-0.536

RESULTS

R_P	2.315E2
$I_{CØRR}$	1.107E5
$E_{CØRR}$	-0.550

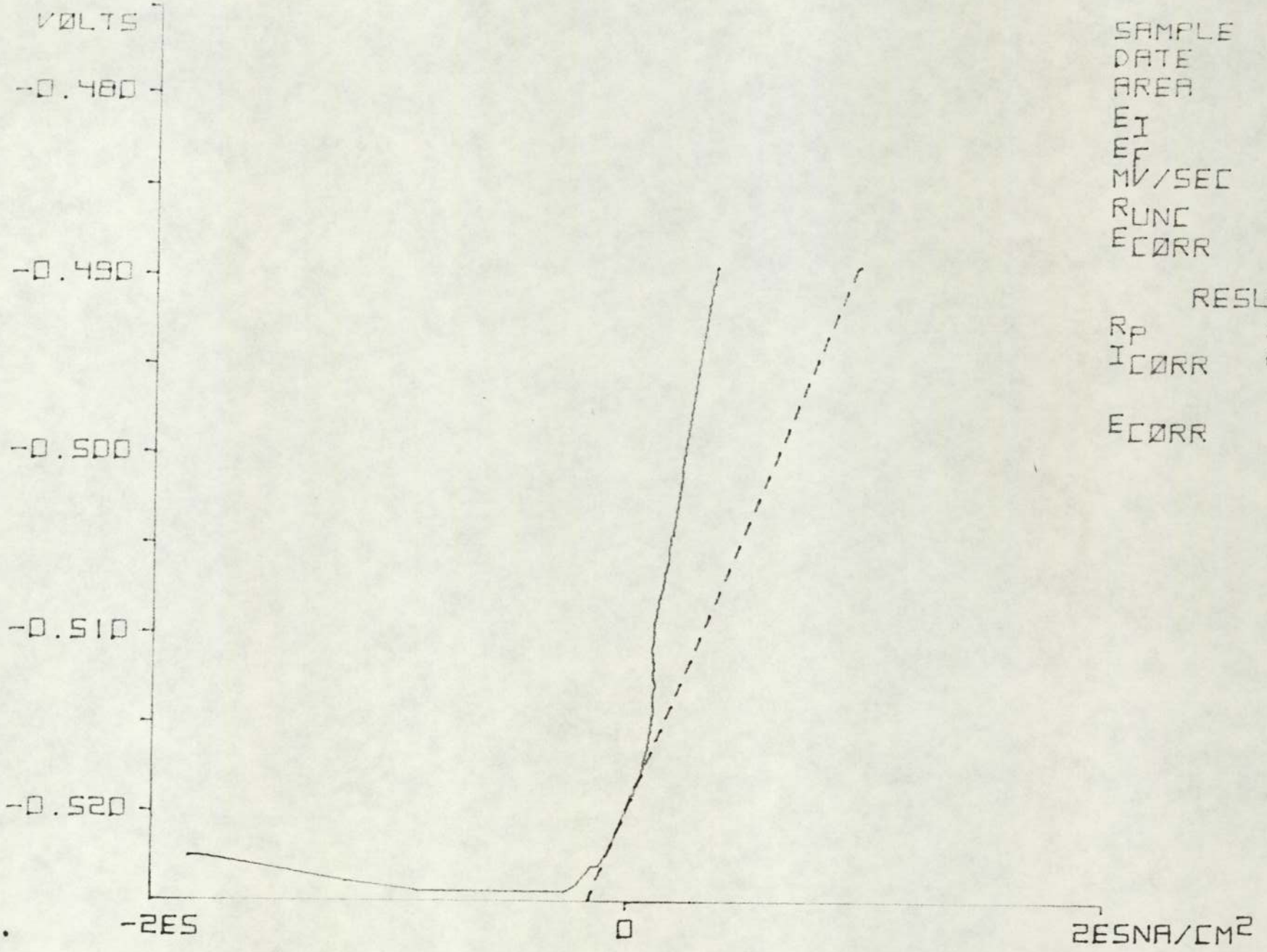

SAMPLE	6313
DATE	06.06
AREA	1.206E1
E_I	-0.528
E_F	-0.488
MV/SEC	0.166
R_{UNC}	2.648
$E_{CØRR}$	-0.508

RESULTS

R_P	3.200E2
$I_{CØRR}$	8.143E4
$E_{CØRR}$	-0.520

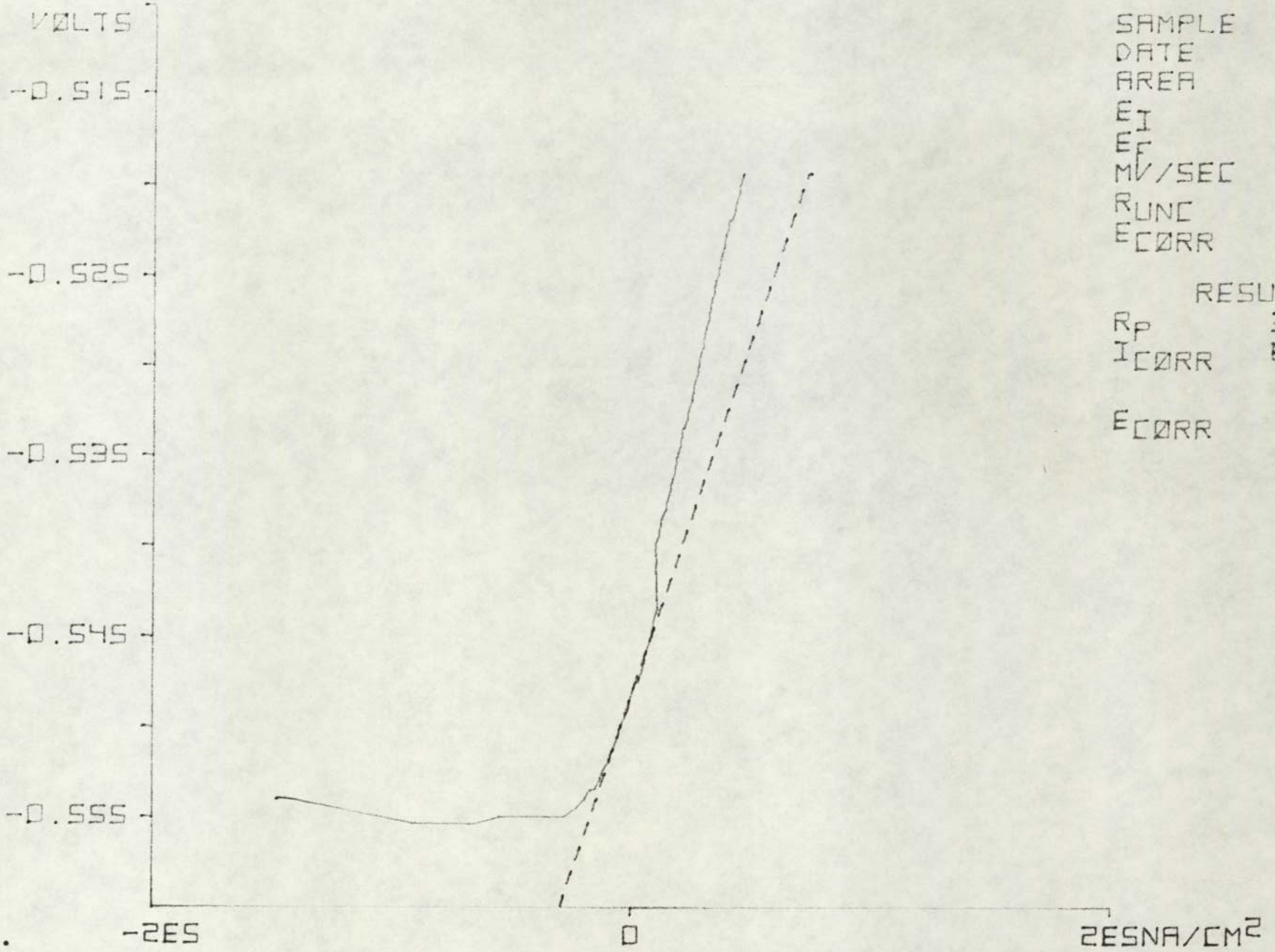

SAMPLE	1313
DATE	06.06
AREA	1.181E1
E_I	-0.558
E_f	-0.518
MV/SEC	0.166
R_{UNC}	2.257
$E_{CØRR}$	-0.538

RESULTS

R_P	3.982E2
$I_{CØRR}$	6.925E4
$E_{CØRR}$	-0.549

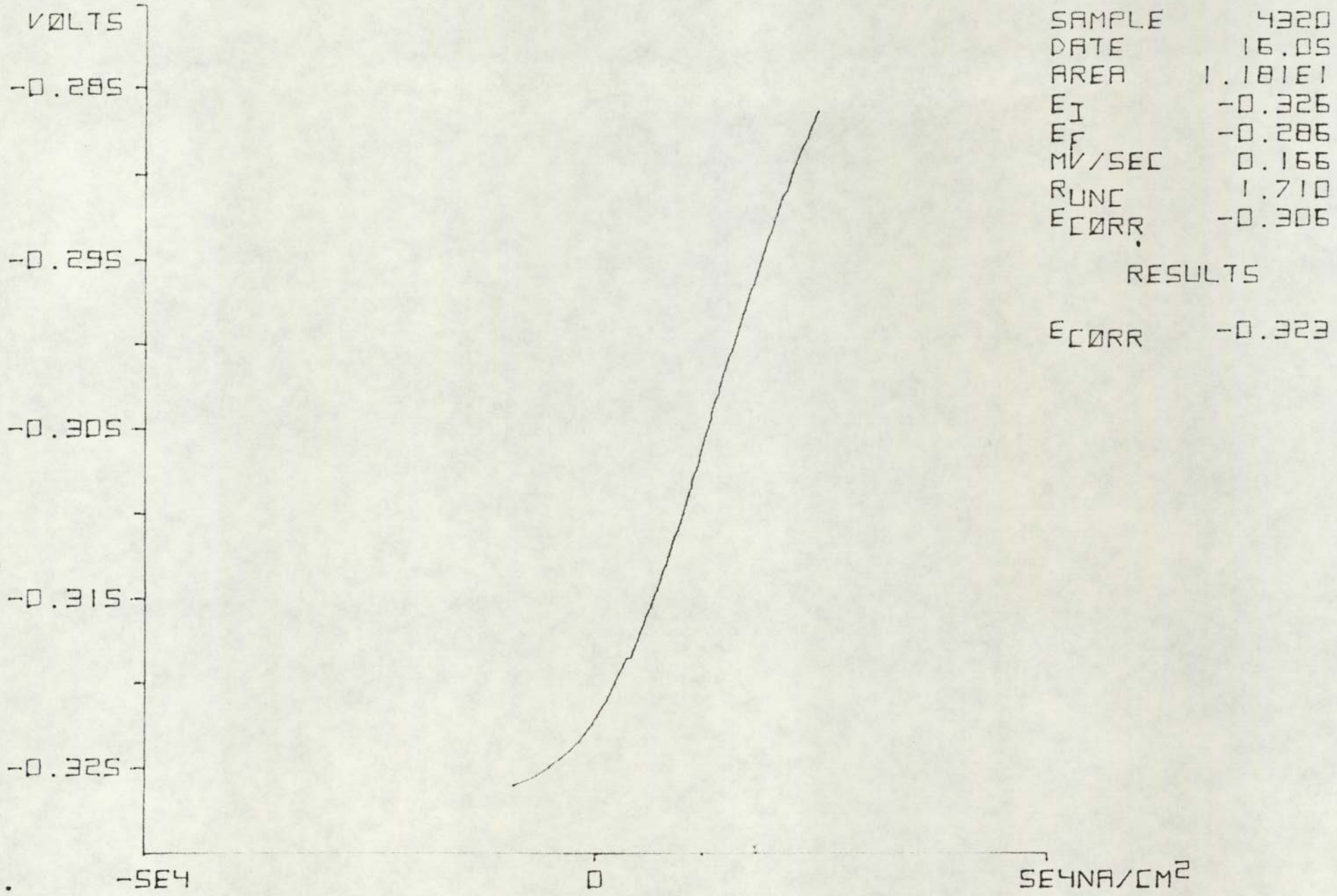

SAMPLE	4320
DATE	16.05
AREA	1.181E1
E_I	-0.326
E_f	-0.286
MV/SEC	0.166
R_{UNC}	1.710
$E_{CØRR}$	-0.306

RESULTS

$E_{CØRR}$	-0.323

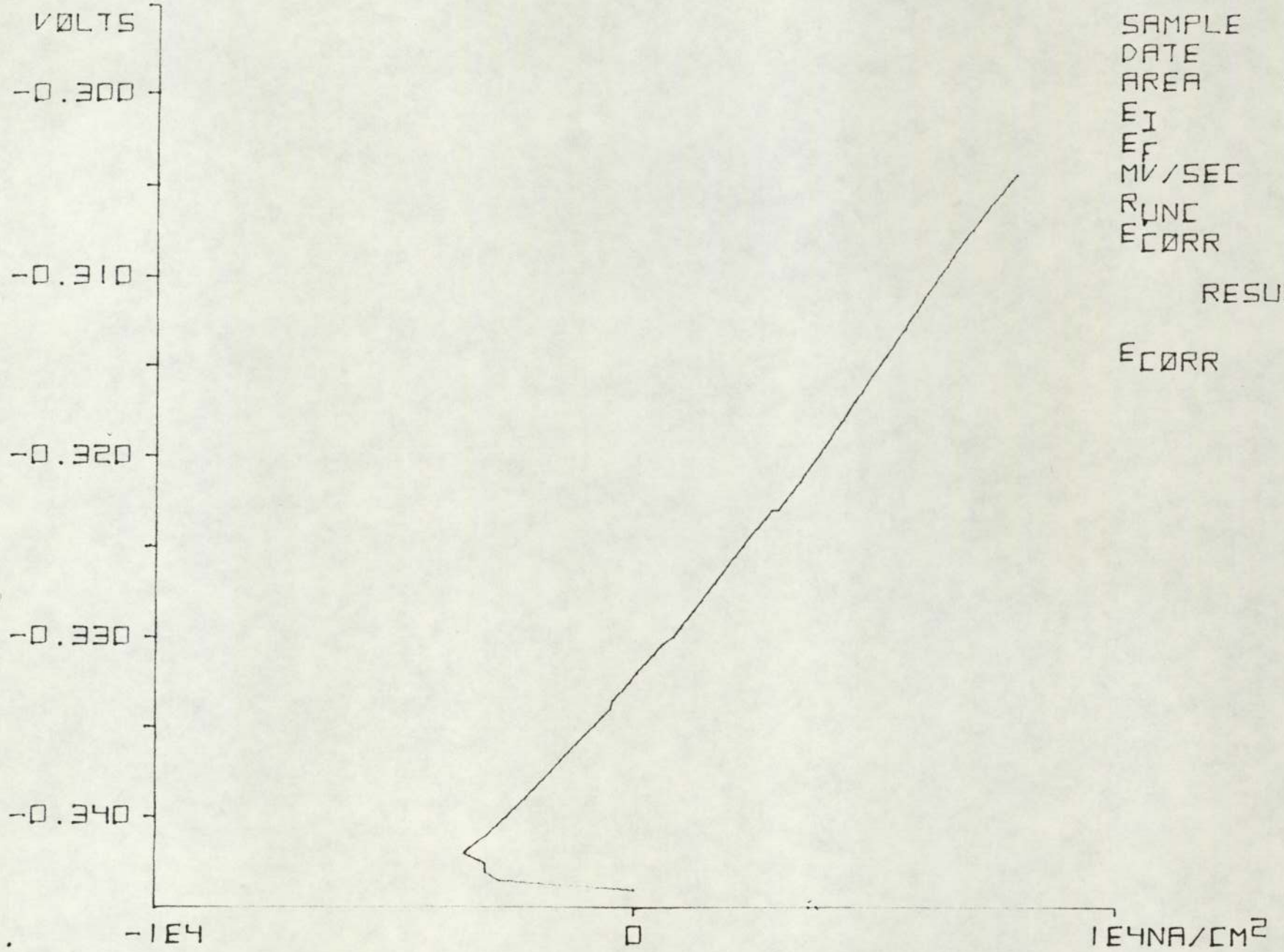

SAMPLE	6320
DATE	16.05
AREA	1.181E1
E_I	-0.344
E_f	-0.304
MV/SEC	0.166
R_{UNC}	2.072
$E_{CØRR}$	-0.324

RESULTS

$E_{CØRR}$	-0.344
	-0.333

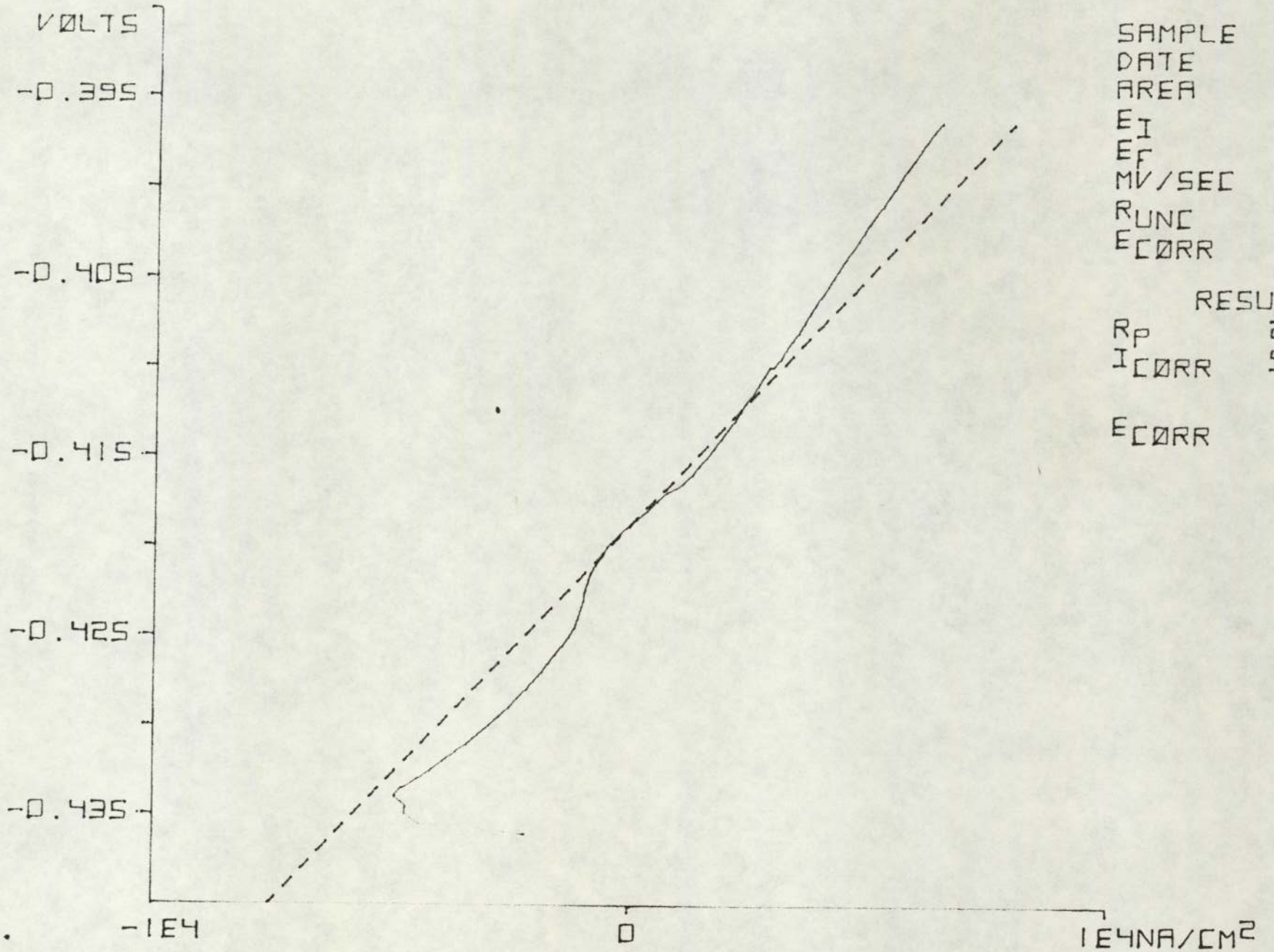

SAMPLE	1320
DATE	16.05
AREA	1.156E1
E_I	-0.436
E_F	-0.396
MV/SEC	0.166
R_{UNC}	2.101
$E_{CØRR}$	-0.416

RESULTS

R_P	2.816E3
$I_{CØRR}$	9.792E3
$E_{CØRR}$	-0.419

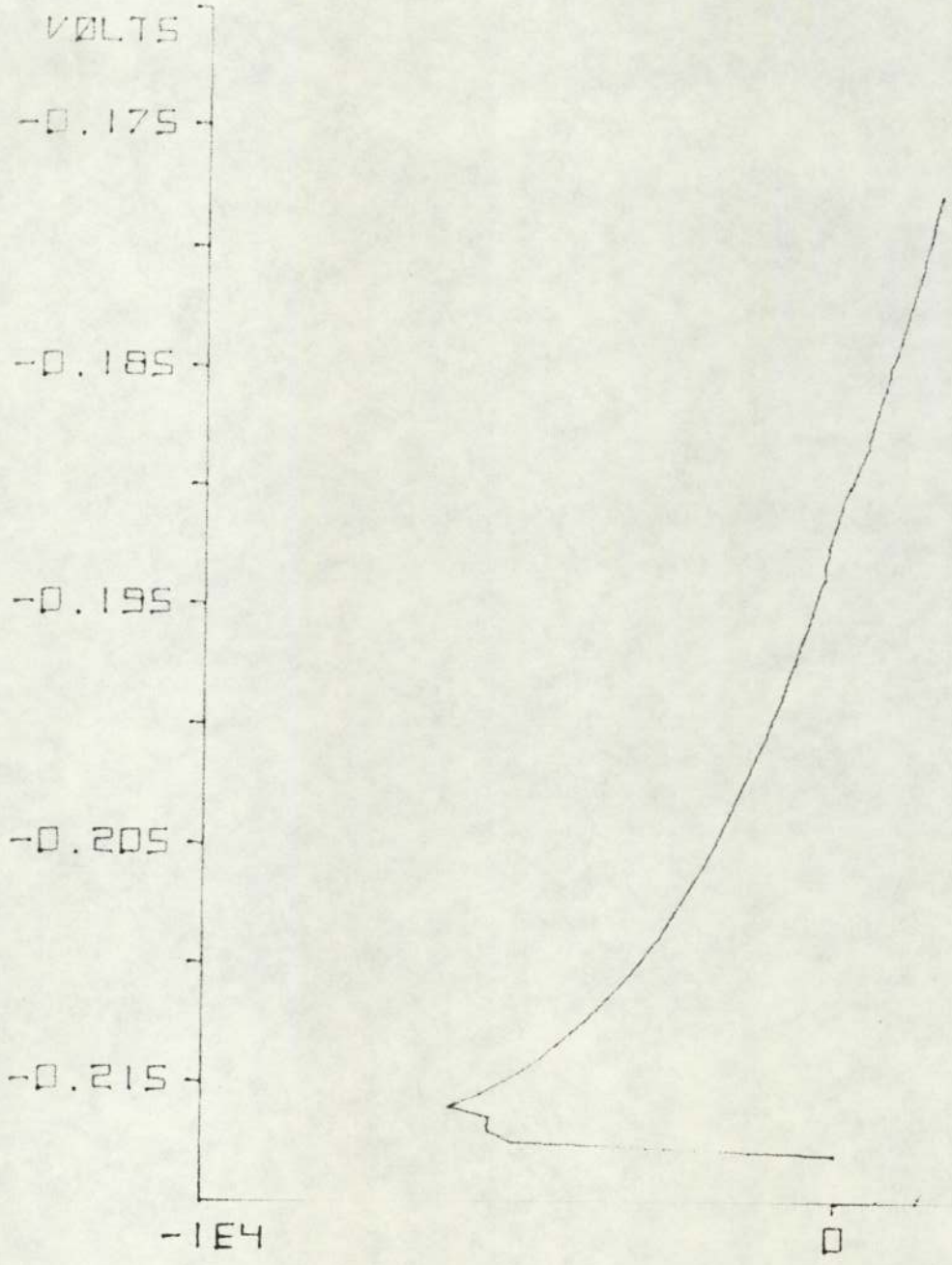

SAMPLE	4321
DATE	23.05
AREA	1.181E1
E_I	-0.218
E_F	-0.178
MV/SEC	0.166
R_{UNC}	2.101
E_{CORR}	-0.198

RESULTS

E_{CORR}	-0.218
	-0.192

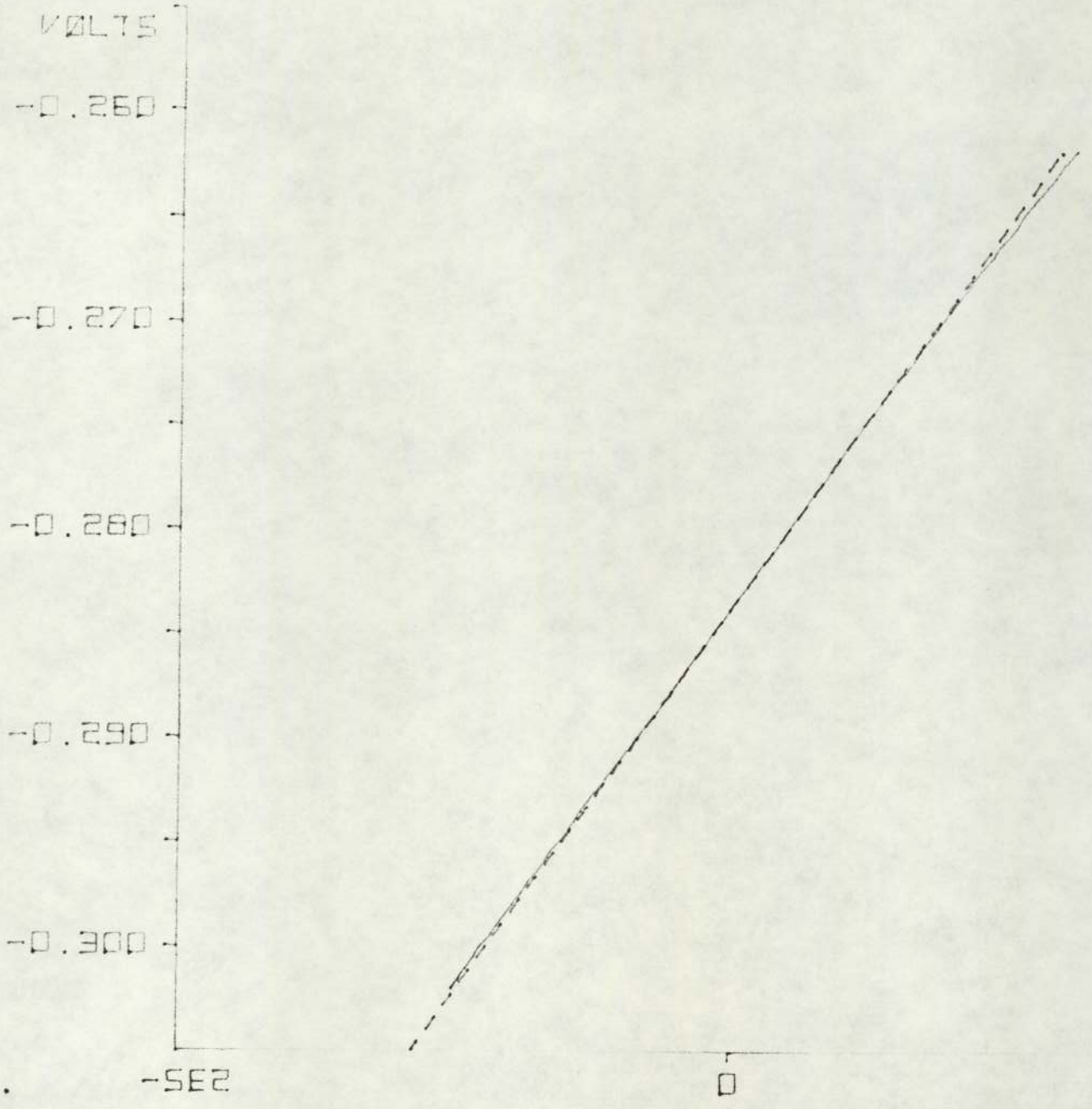

SAMPLE	6321
DATE	23.05
AREA	1.181E1
E_I	-0.302
E_F	-0.262
MV/SEC	0.166
E_{CORR}	-0.282

RESULTS

R_P	7.407E4
I_{CORR}	3.518E2
E_{CORR}	-0.284

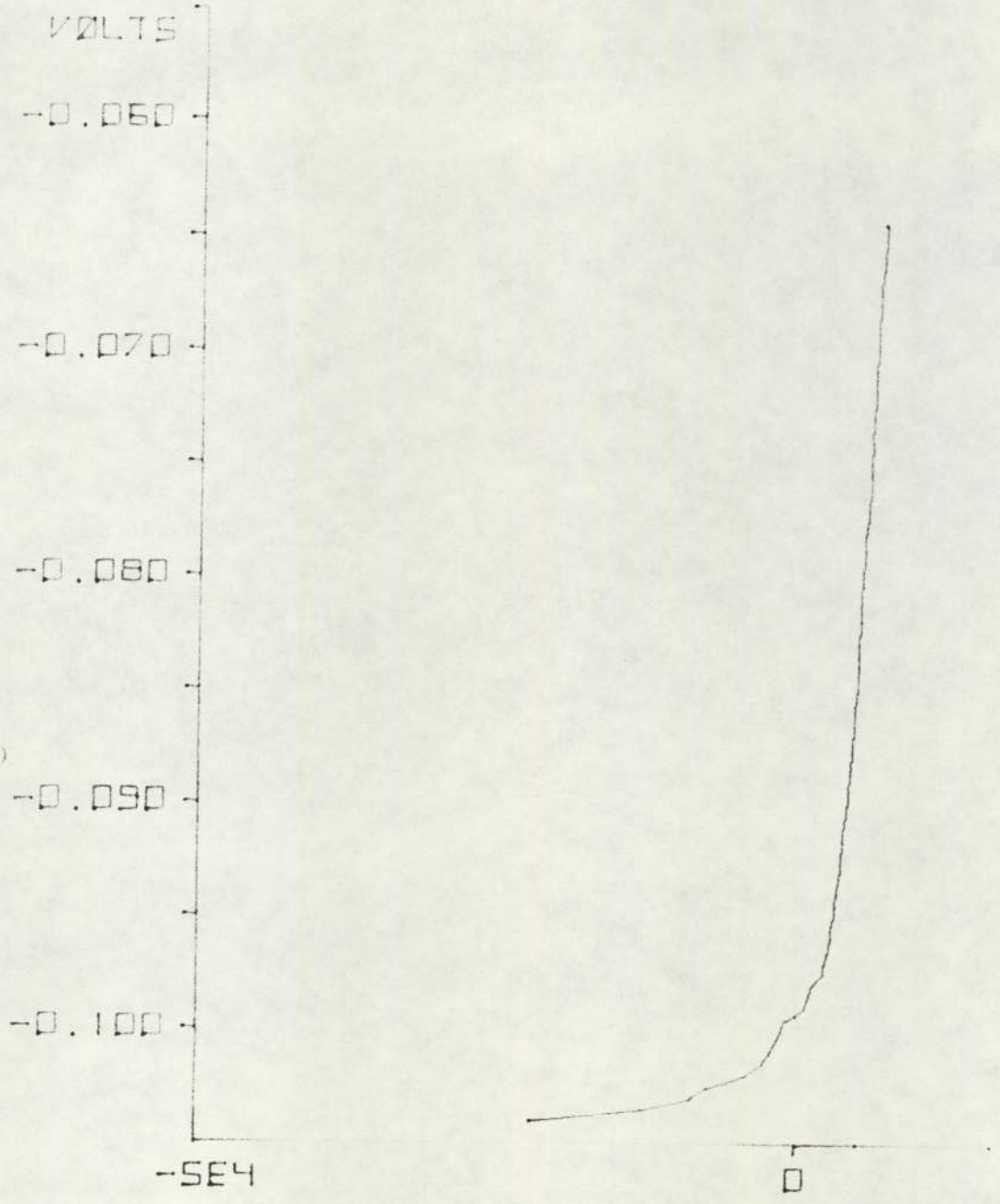

SAMPLE	1321
DATE	23.05
AREA	1.156E1
E_I	-0.104
E_f	-0.064
MV/SEC	0.166
R_{UNC}	1.544
$E_{CØRR}$	-0.084

RESULTS

$E_{CØRR}$ -0.100

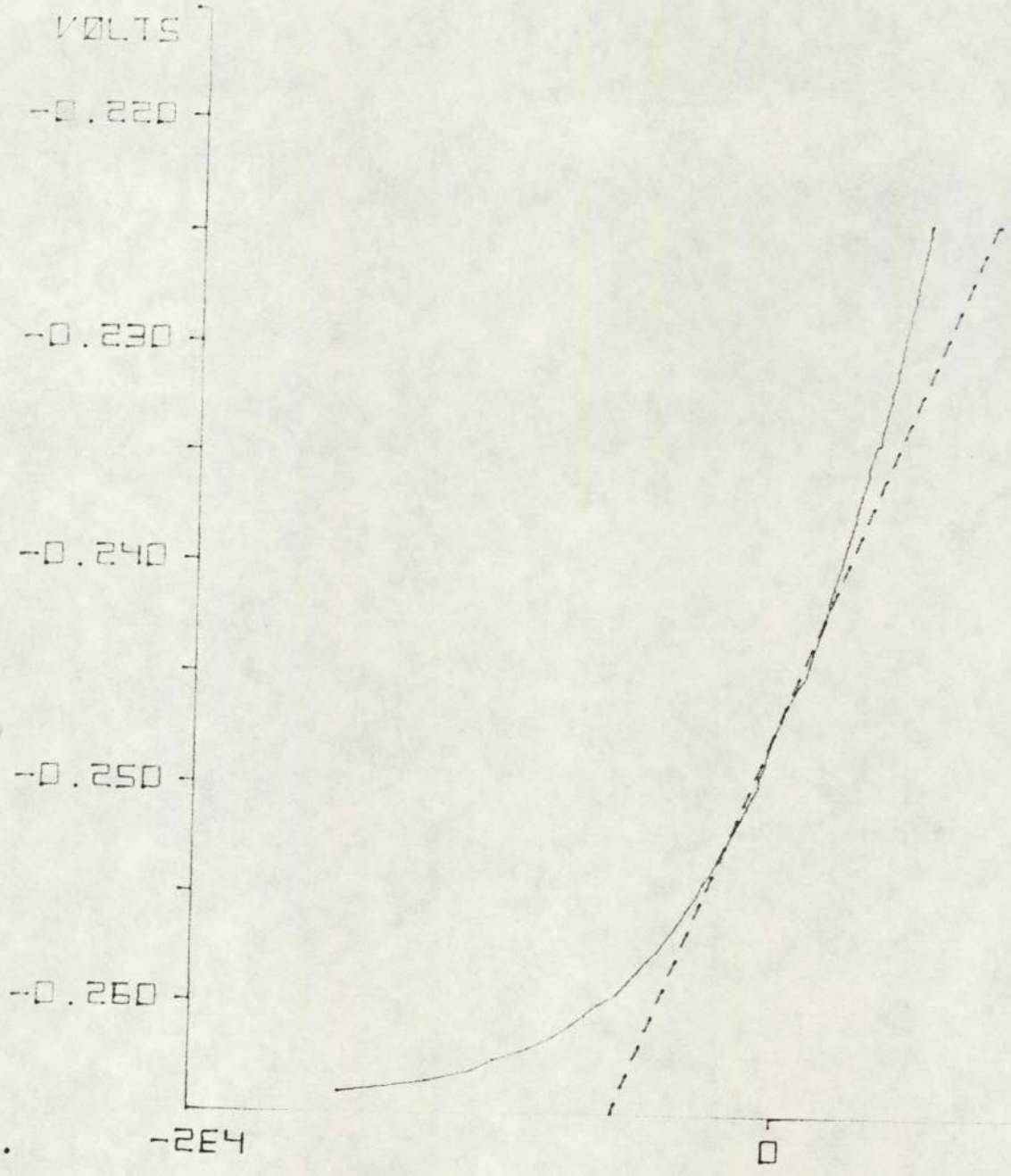

SAMPLE	4322
DATE	30.05
AREA	1.181E1
E_I	-0.264
E_f	-0.224
MV/SEC	0.166
R_{UNC}	1.837
E_{CORR}	-0.244

RESULTS

R_P	3.201E3
I_{CORR}	8.005E3
E_{CORR}	-0.248

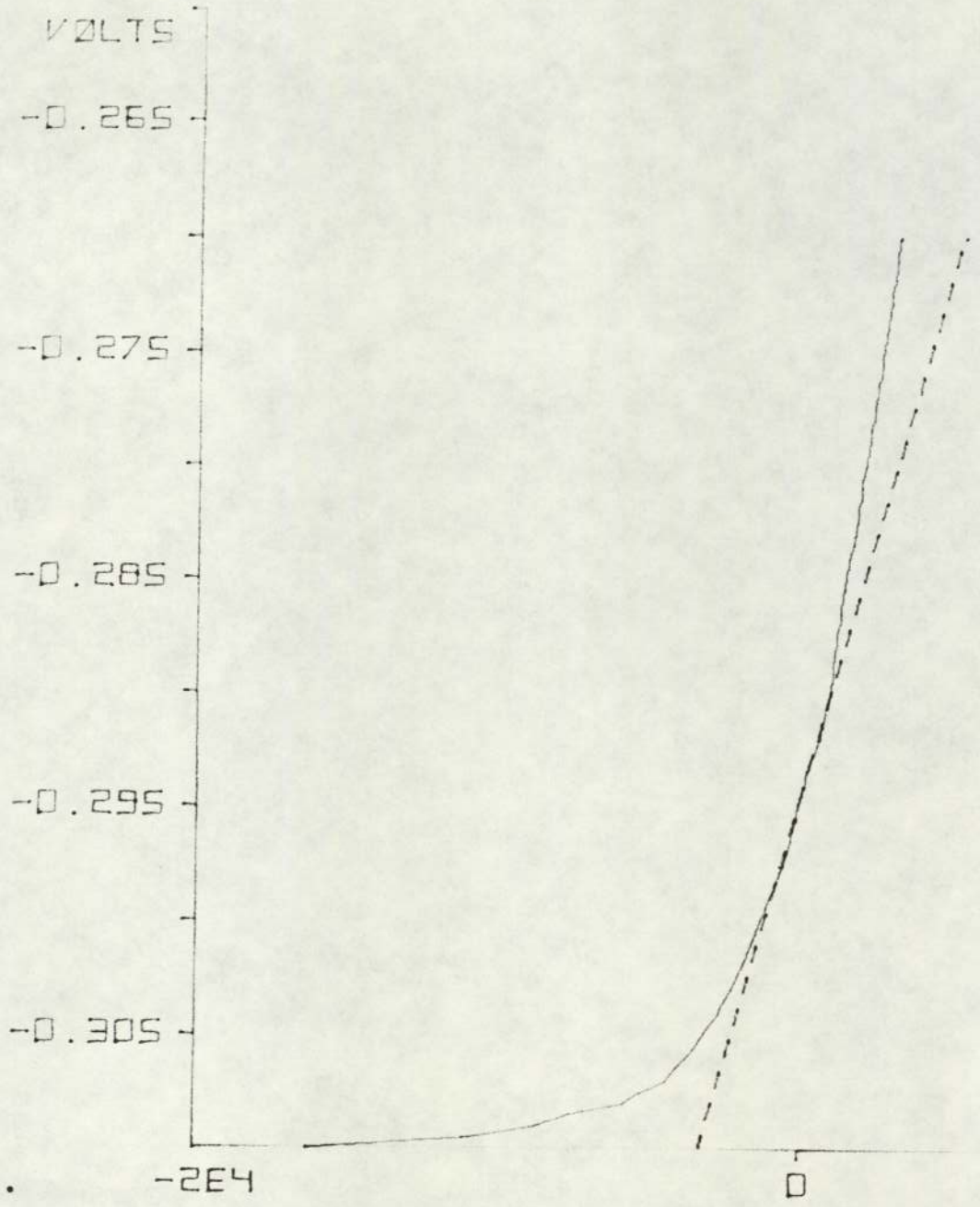

SAMPLE	6322
DATE	30.05
AREA	1.181E1
E_I	-0.310
E_f	-0.270
MV/SEC	0.166
R_{UNC}	1.681
$E_{CØRR}$	-0.290

RESULTS

R_p	4.717E3
$I_{CØRR}$	5.524E3
$E_{CØRR}$	-0.295

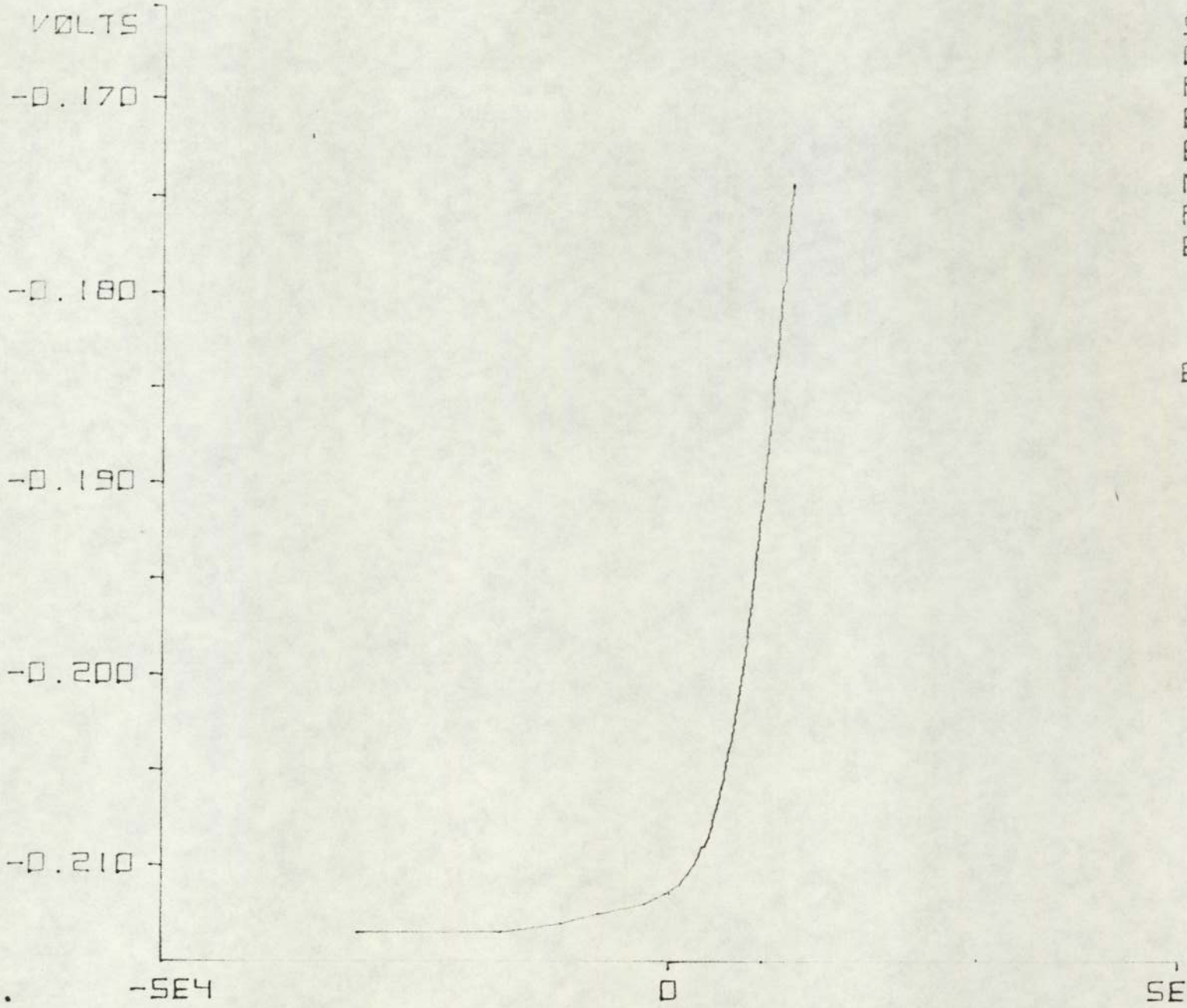

SAMPLE	1322
DATE	30.05
AREA	1.156E1
E_I	-0.214
E_f	-0.174
MV/SEC	0.166
R_{UNC}	1.720
E_{CORR}	-0.194

RESULTS

E_{CORR}	-0.212

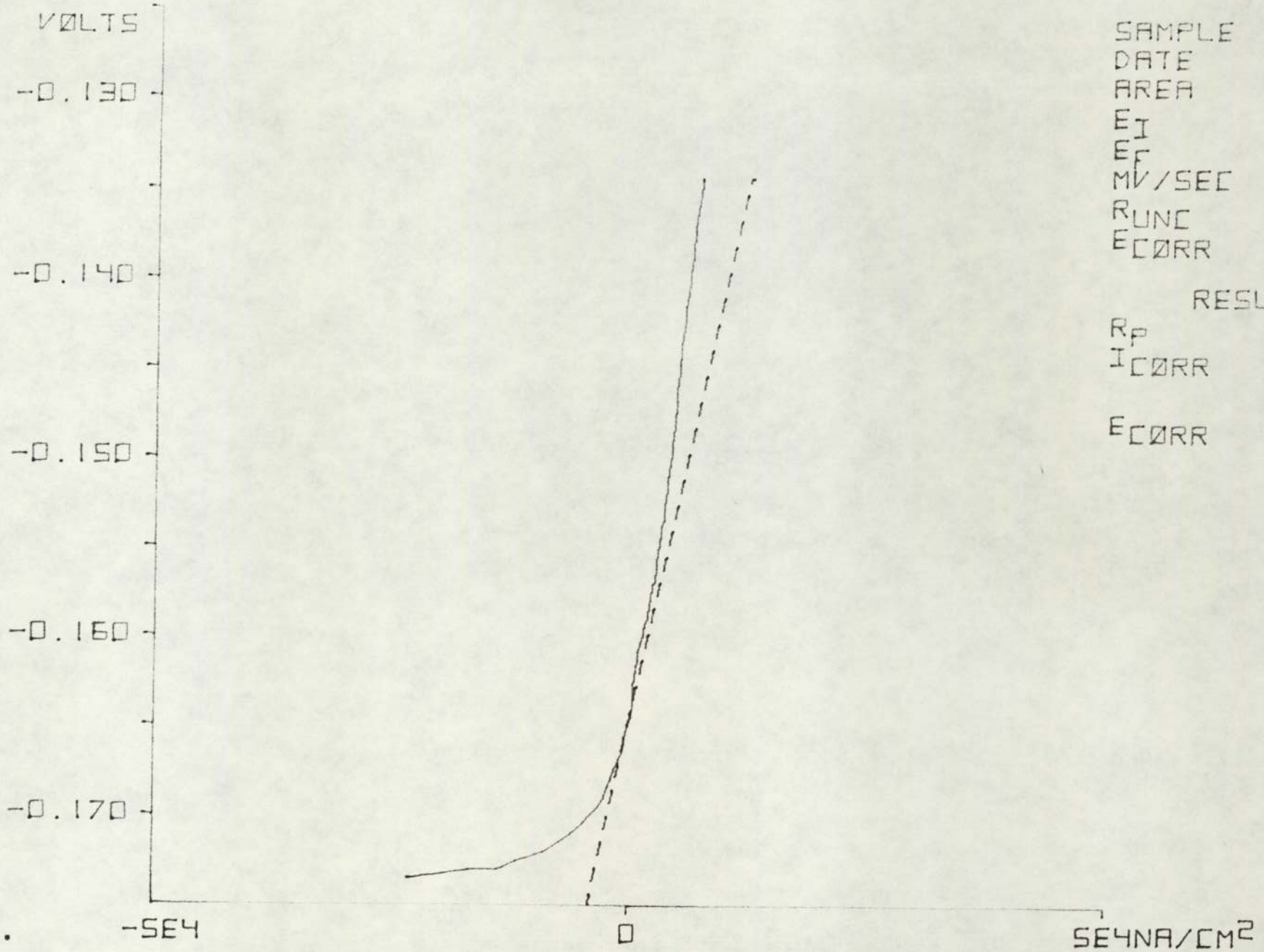

SAMPLE	4323
DATE	06.06
AREA	1.181E1
E_I	-0.174
E_f	-0.134
MV/SEC	0.166
R_{UNC}	2.511
$E_{CØRR}$	-0.154

RESULTS

R_P	2.493E3
$I_{CØRR}$	1.028E4
$E_{CØRR}$	-0.165

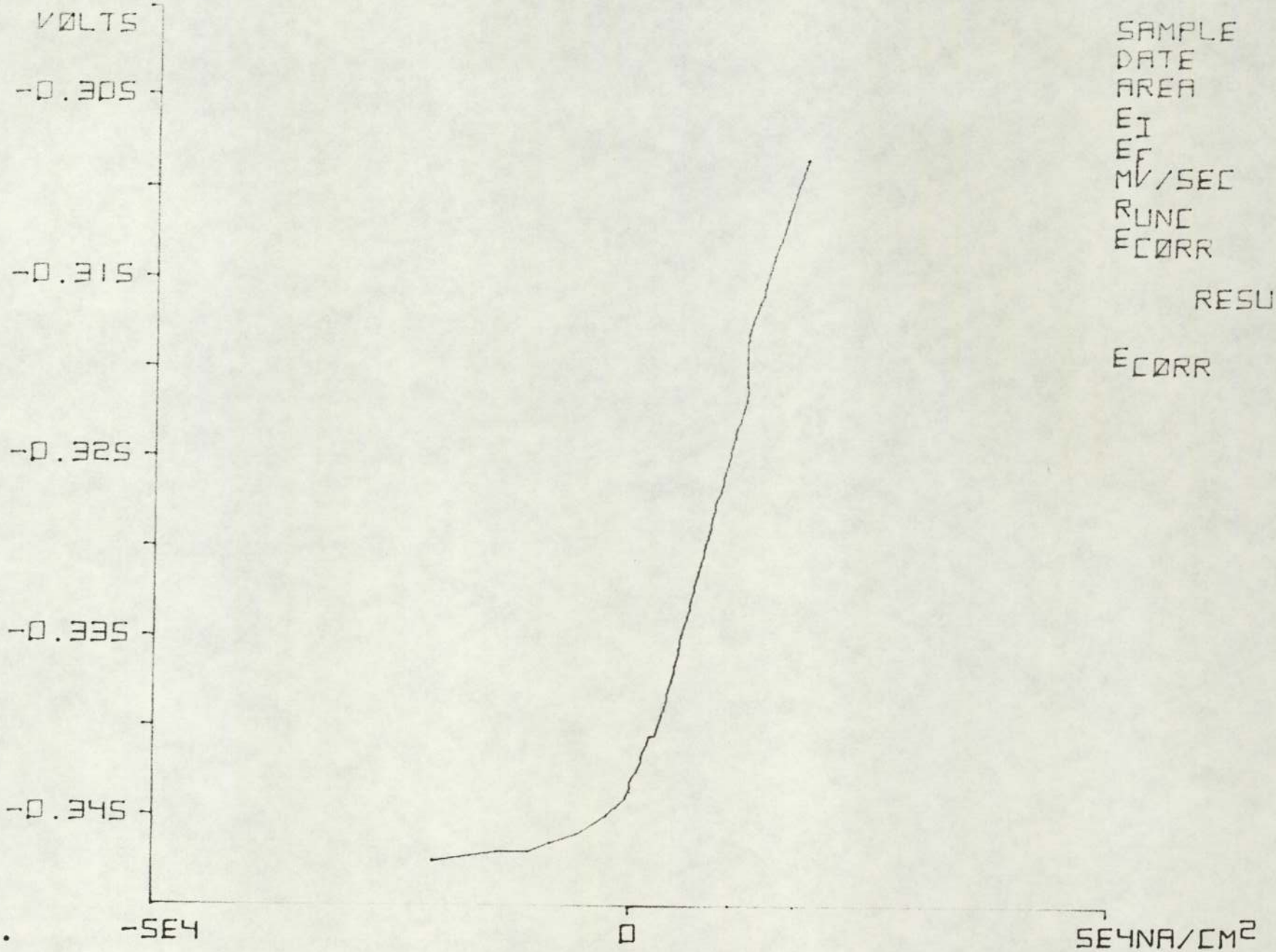

SAMPLE	6323
DATE	06.06
AREA	1.181E1
E_I	-0.348
E_F	-0.308
MV/SEC	0.166
R_{UNC}	2.648
$E_{CØRR}$	-0.328

RESULTS

$E_{CØRR}$ -0.344

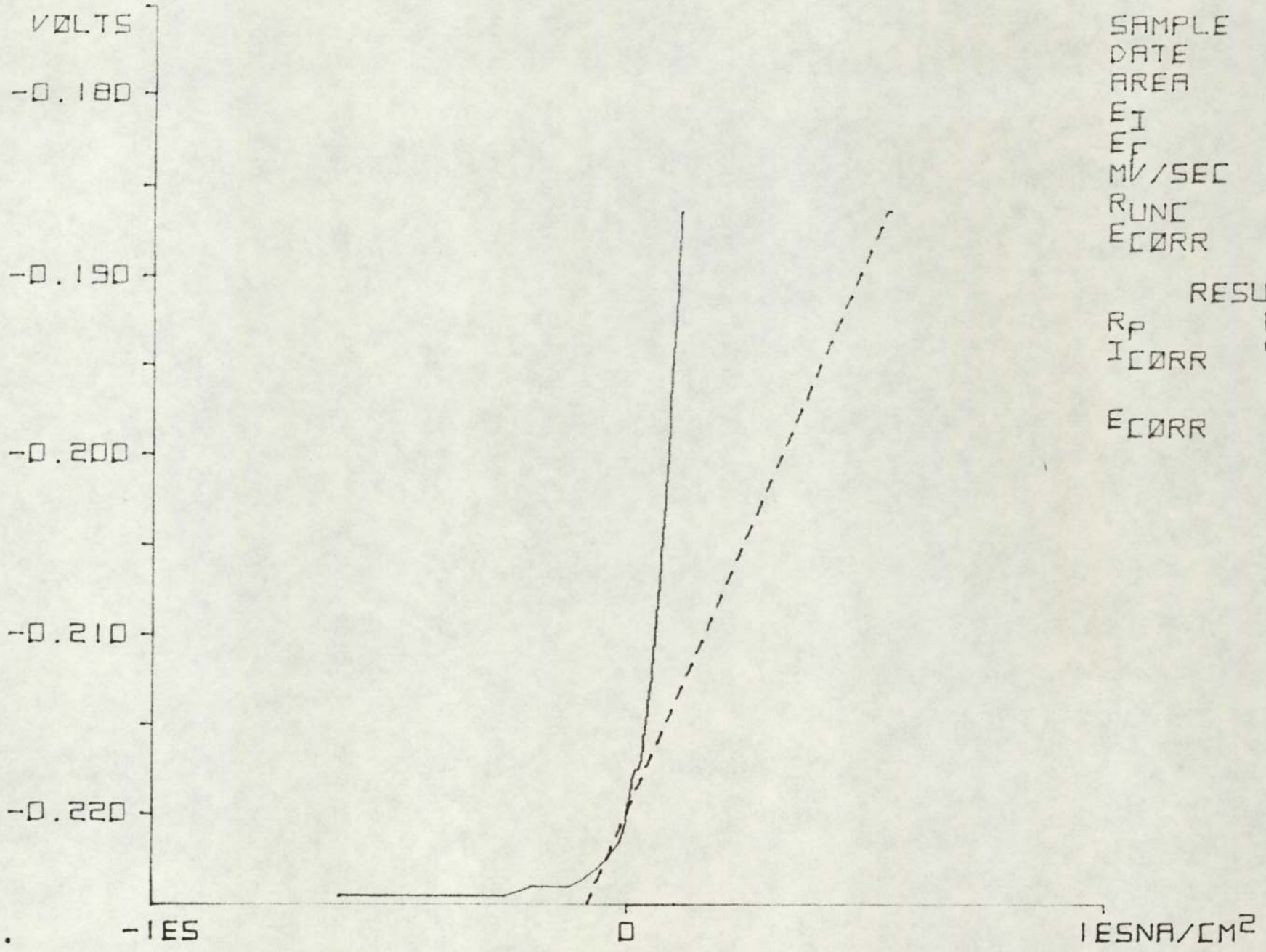

SAMPLE	1323
DATE	06.06
AREA	1.156E1
E_I	-0.226
E_f	-0.186
MV/SEC	0.166
R_{UNC}	2.658
$E_{CØRR}$	-0.206

RESULTS

R_P	6.170E2
$I_{CØRR}$	4.469E4
$E_{CØRR}$	-0.220

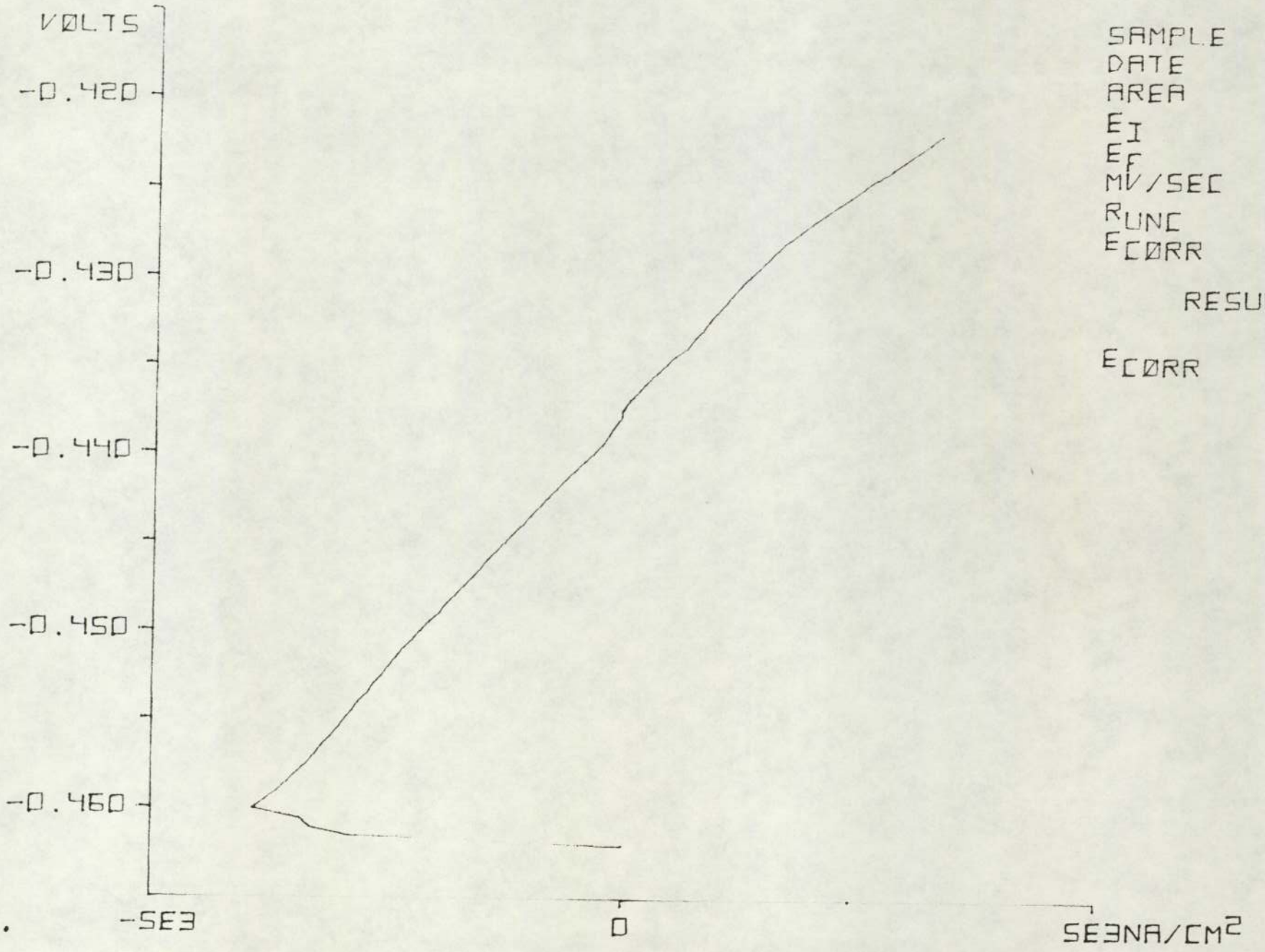

SAMPLE	4330
DATE	16.05
AREA	1.206E1
E_I	-0.462
E_F	-0.422
MV/SEC	0.166
R_{UNC}	1.358
E_{CORR}	-0.442

RESULTS

E_{CORR}	-0.462
	-0.438

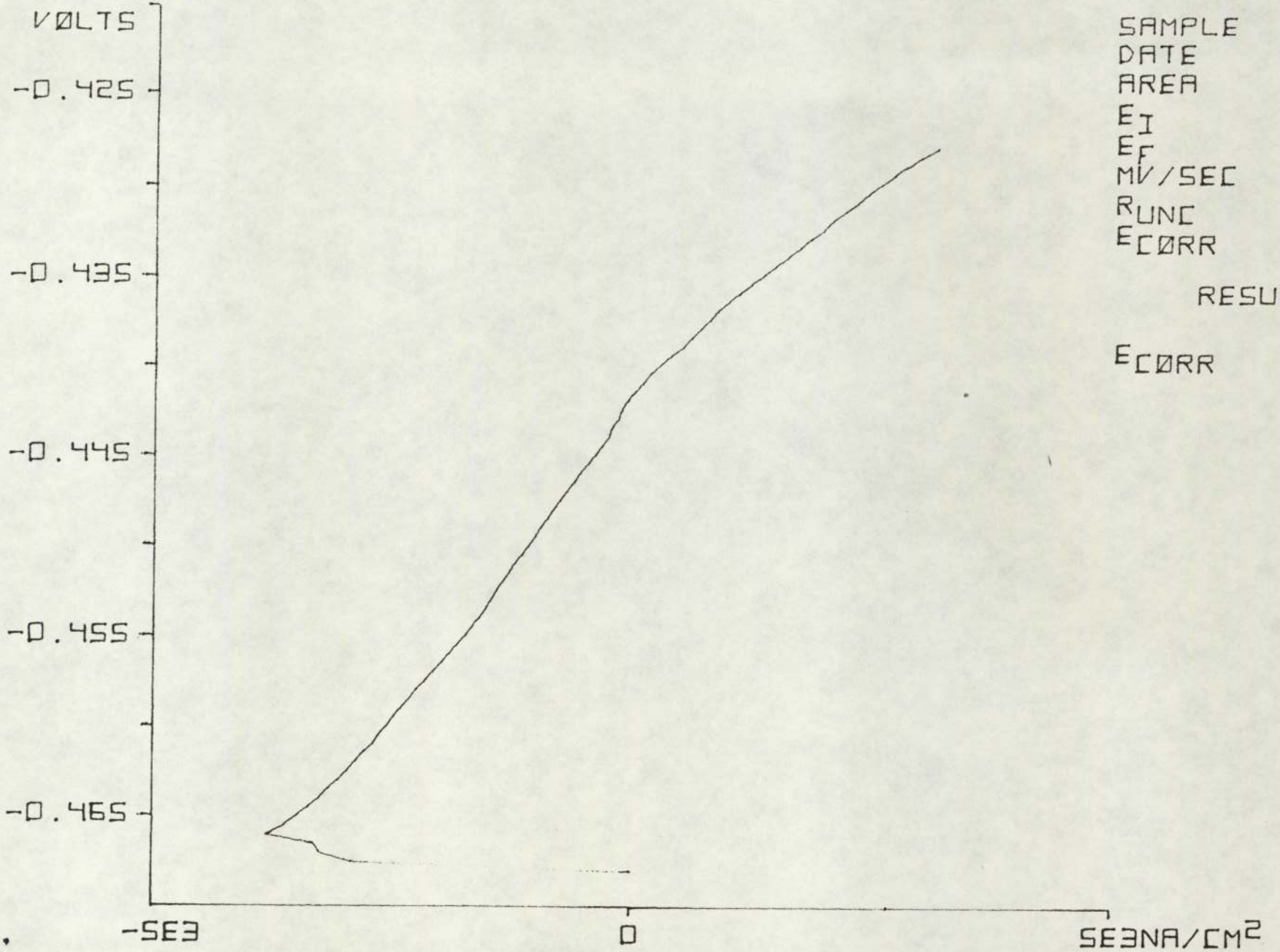

SAMPLE	6330
DATE	16.05
AREA	1.181E1
E_I	-0.468
E_F	-0.428
MV/SEC	0.166
R_{UNC}	1.857
$E_{CØRR}$	-0.448

RESULTS

$E_{CØRR}$	-0.468
	-0.442

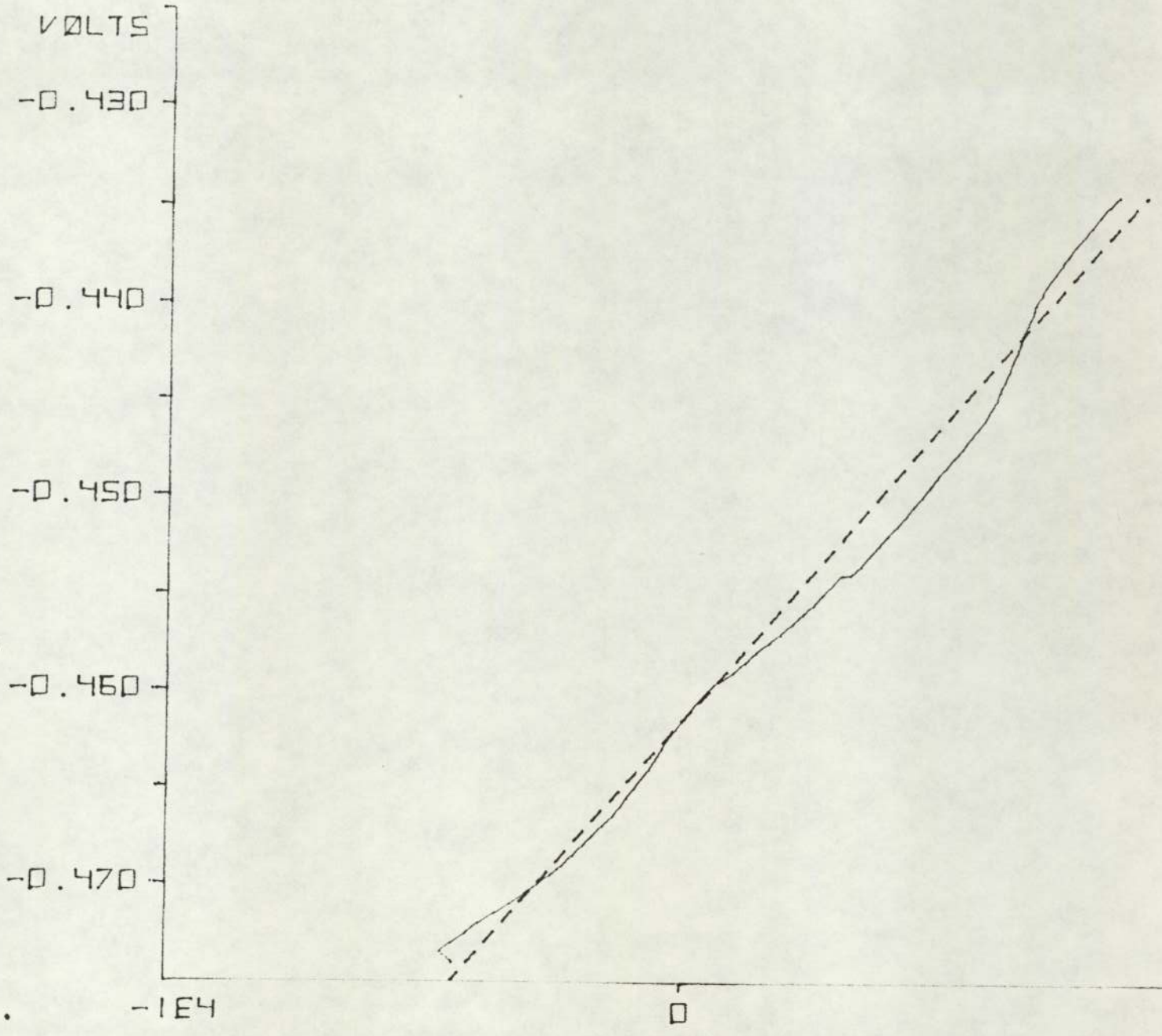

SAMPLE	1330
DATE	16.05
AREA	1.181E1
E_I	-0.474
E_F	-0.434
MV/SEC	0.166
R_{UNC}	1.915
E_{CORR}	-0.454

RESULTS

R_P	3.043E3
I_{CORR}	9.062E3
E_{CORR}	-0.462

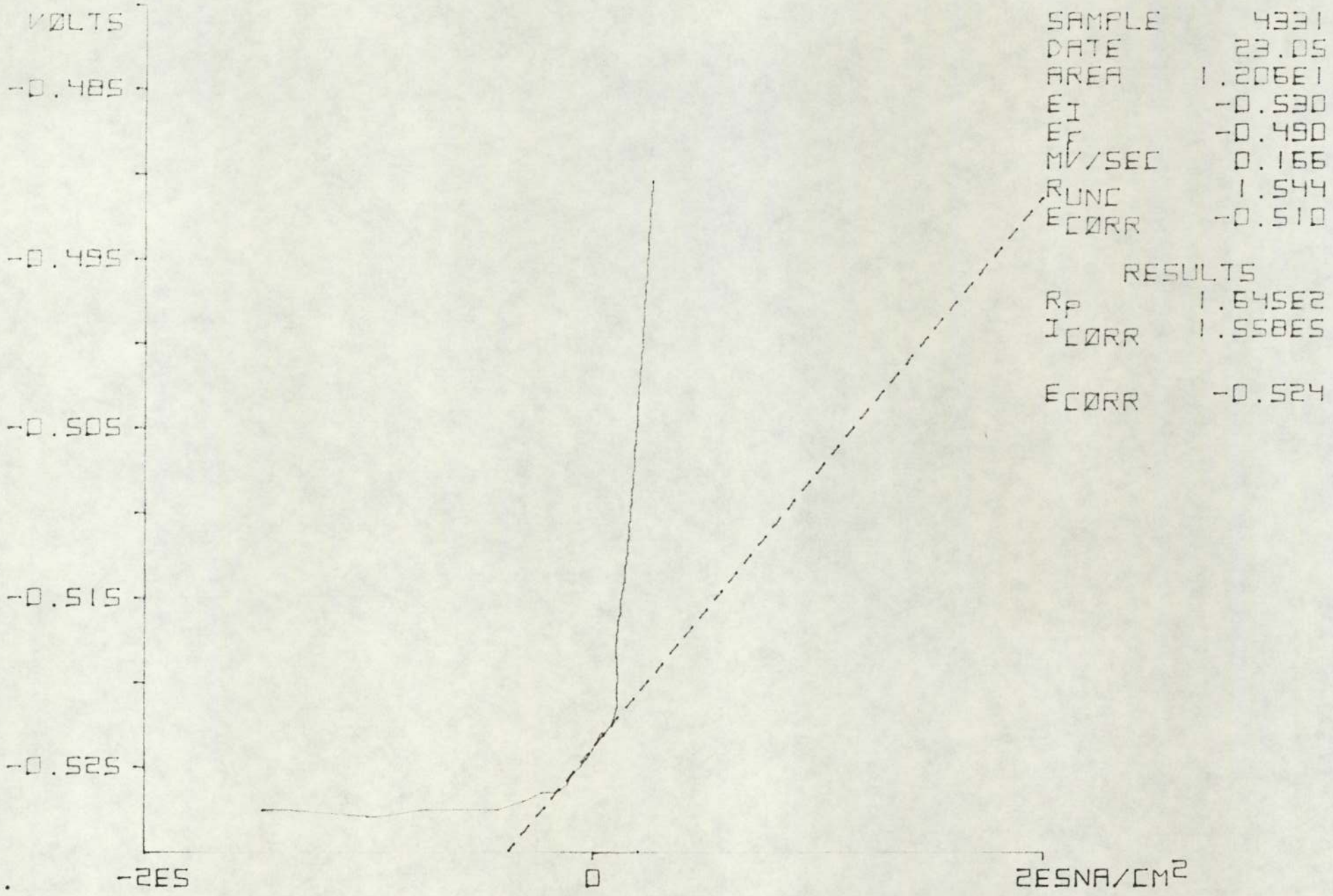

SAMPLE	4331
DATE	23.05
AREA	1.206E1
E_I	-0.530
E_f	-0.490
MV/SEC	0.166
R_{UNC}	1.544
$E_{CØRR}$	-0.510

RESULTS

R_p	1.645E2
$I_{CØRR}$	1.558E5
$E_{CØRR}$	-0.524

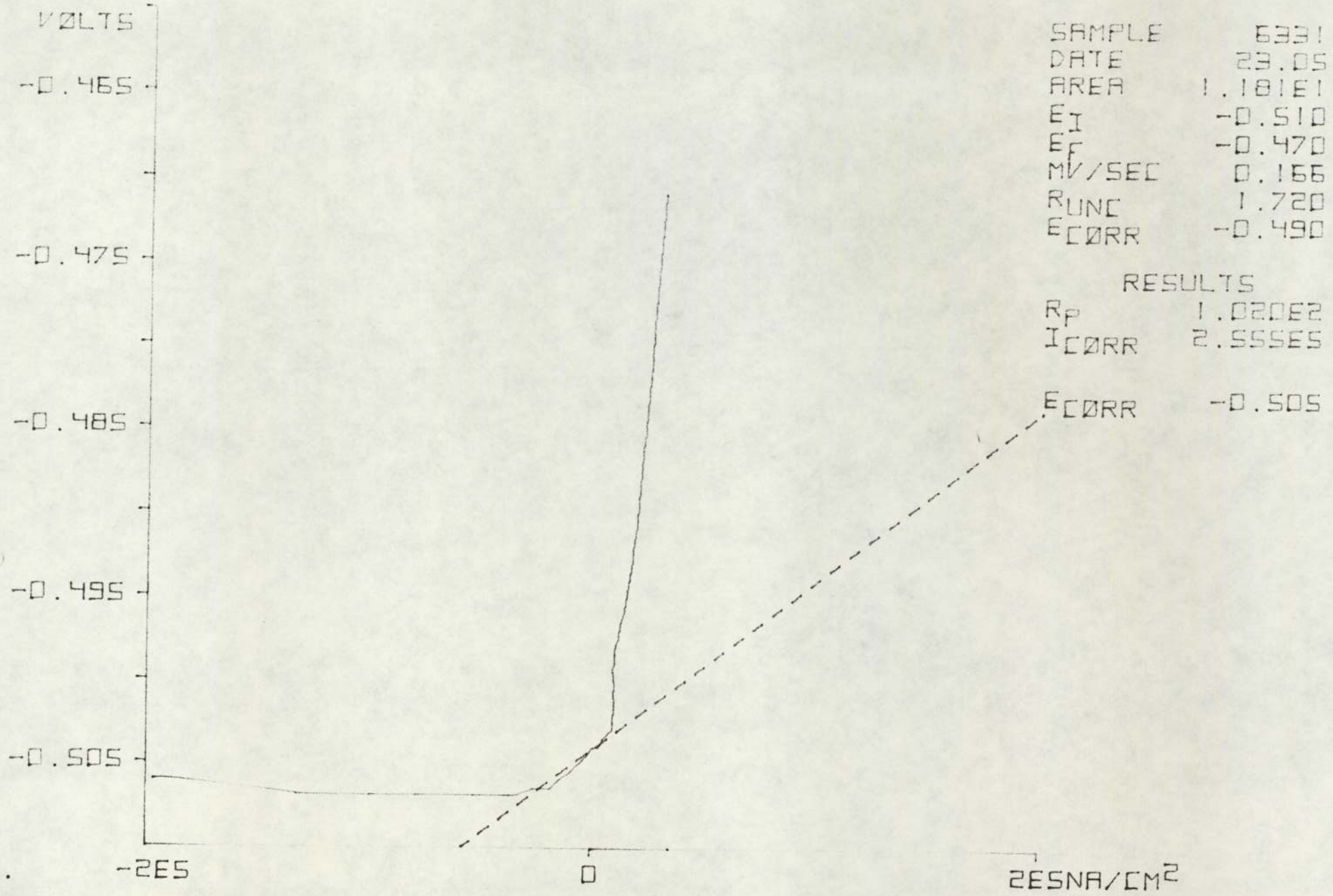

SAMPLE	6331
DATE	23.05
AREA	1.181E1
E_I	-0.510
E_F	-0.470
MV/SEC	0.166
R_{UNC}	1.720
$E_{CØRR}$	-0.490

RESULTS

R_P	1.020E2
$I_{CØRR}$	2.555E5
$E_{CØRR}$	-0.505

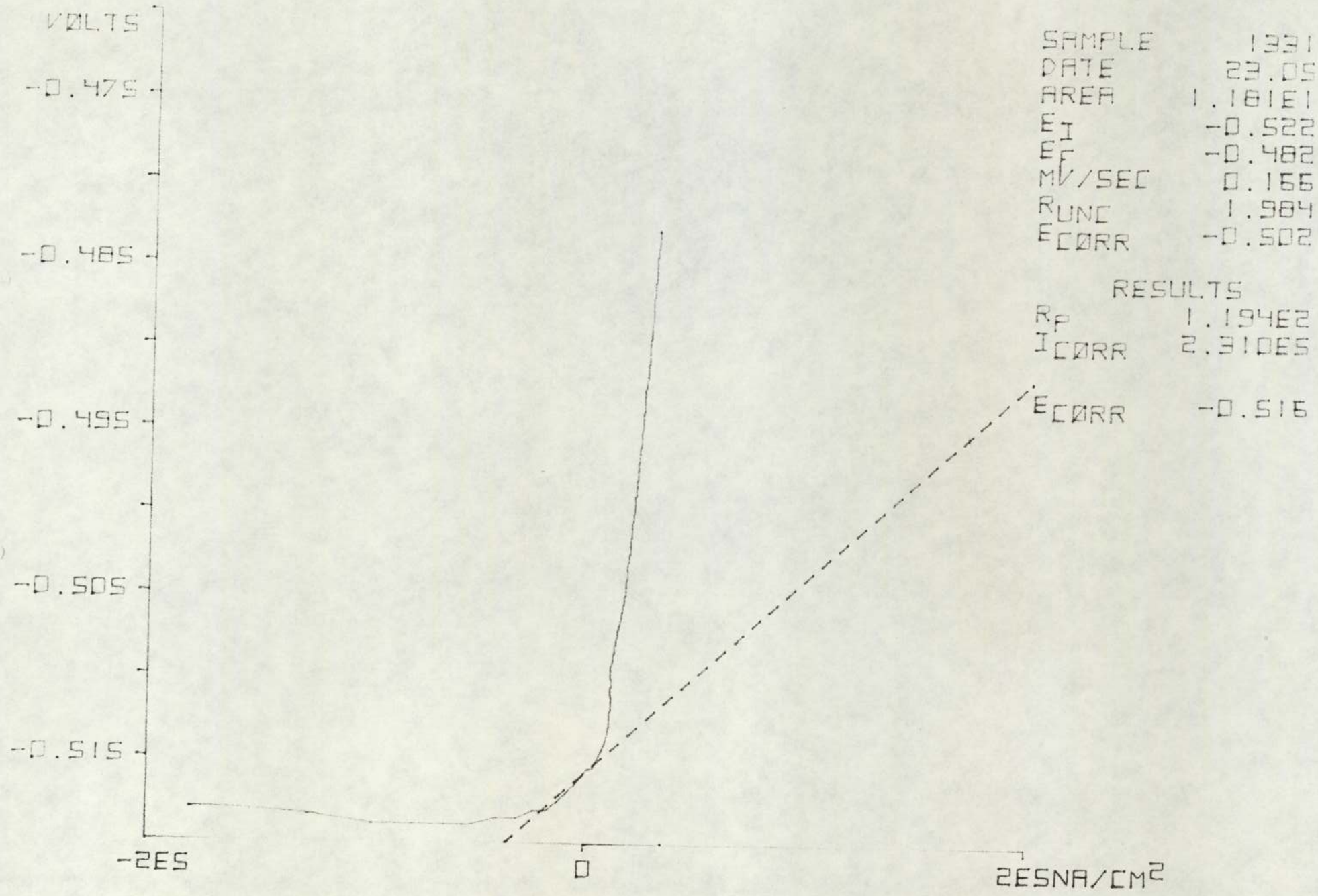

SAMPLE	1331
DATE	23.05
AREA	1.181E1
E_I	-0.522
E_F	-0.482
MV/SEC	0.166
R_{UNC}	1.984
$E_{CØRR}$	-0.502

RESULTS

R_P	1.194E2
$I_{CØRR}$	2.310ES
$E_{CØRR}$	-0.516

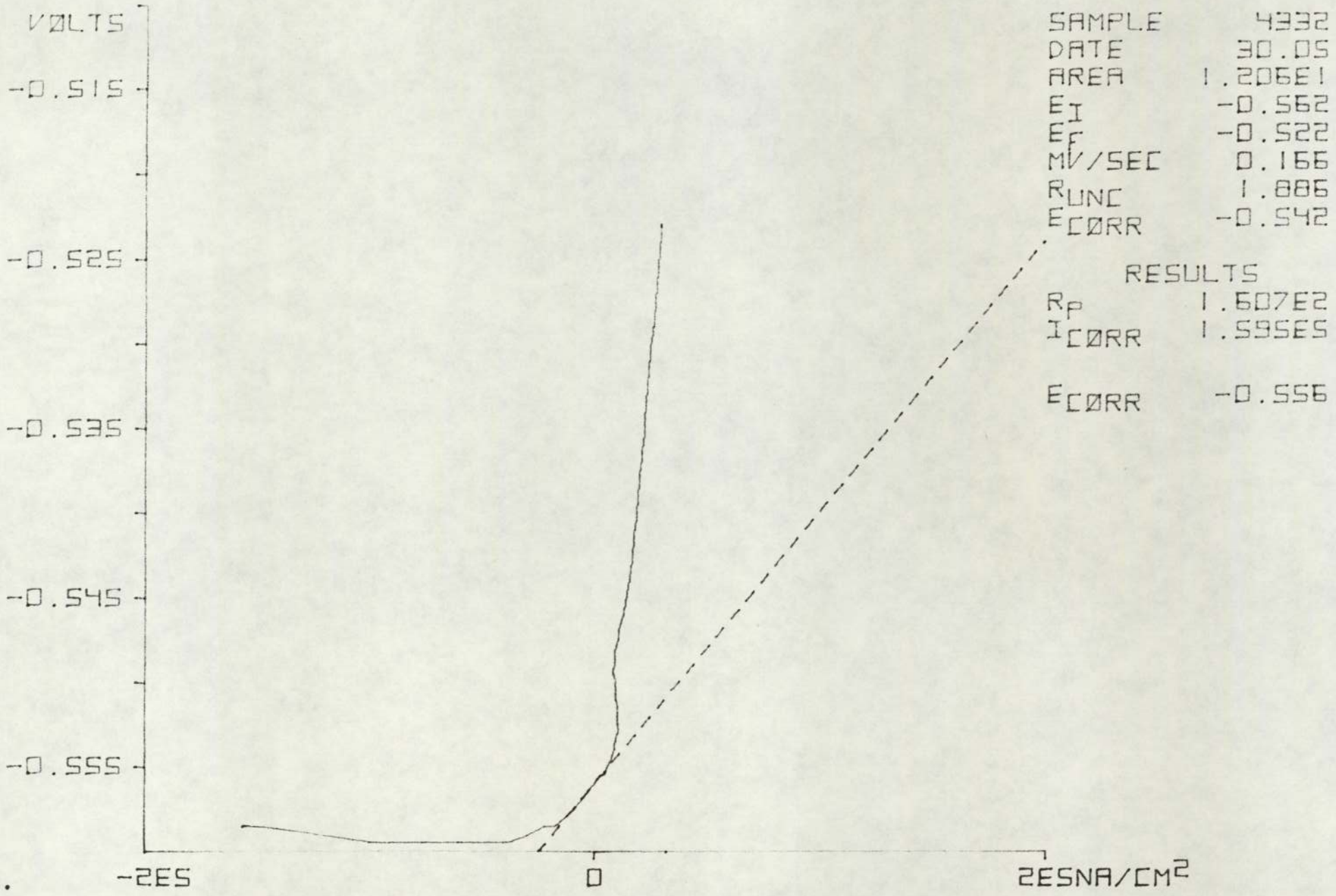
VØLTS
-0.515
-0.525
-0.535
-0.545
-0.555
-2ES
0
2ESNA/CM2
SAMPLE 4332
DATE 30.05
AREA 1.206E1
EI -0.562
Ef -0.522
MV/SEC 0.166
RUNC 1.886
ECØRR -0.542
RESULTS
Rp 1.607E2
ICØRR 1.595ES
ECØRR -0.556

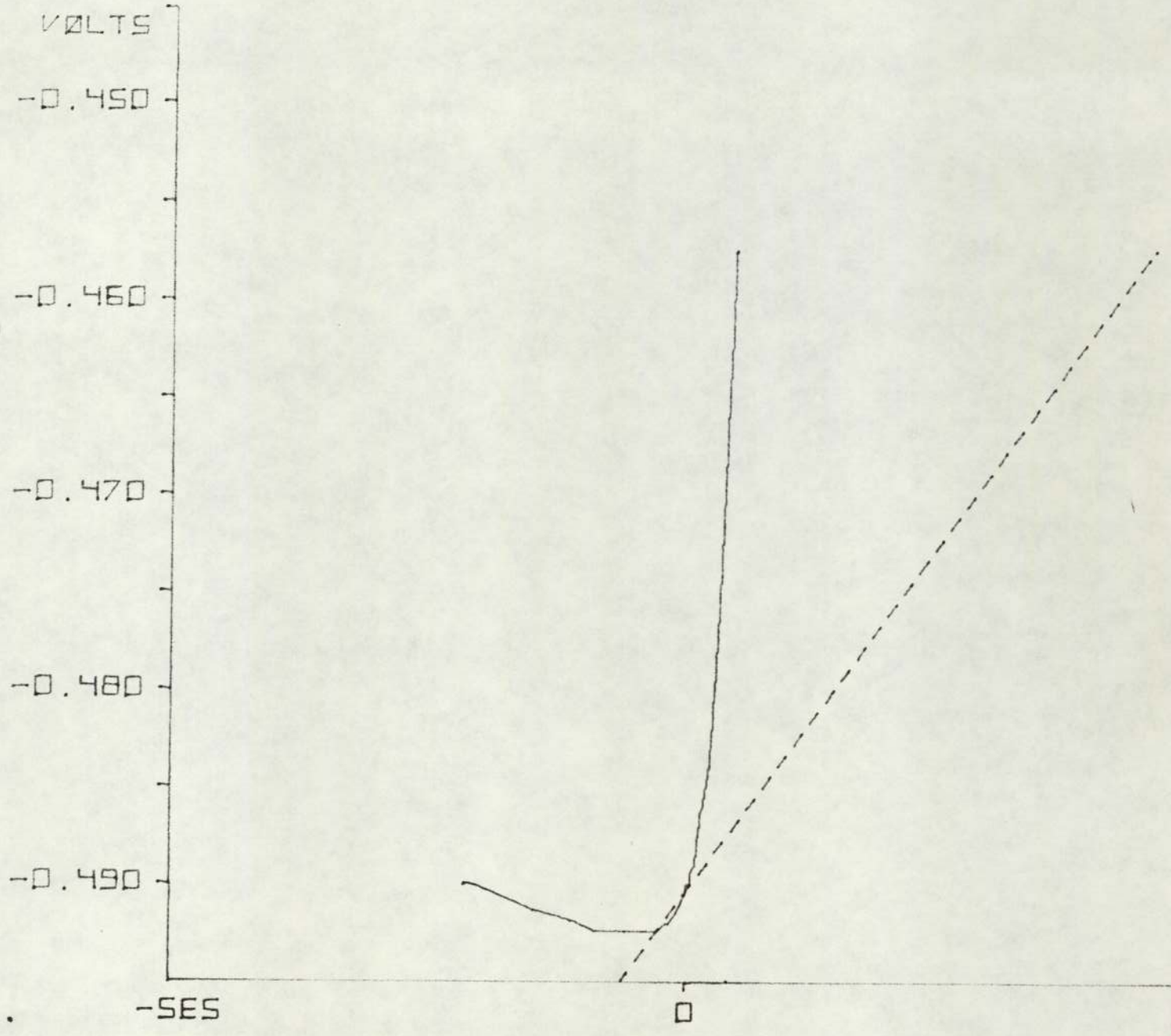

SAMPLE	6332
DATE	30.05
AREA	1.181E1
E_I	-0.496
E_F	-0.456
MV/SEC	0.166
R_{UNC}	2.326
$E_{CØRR}$	-0.476

RESULTS

R_P	7.352E1
$I_{CØRR}$	3.544E5
$E_{CØRR}$	-0.491

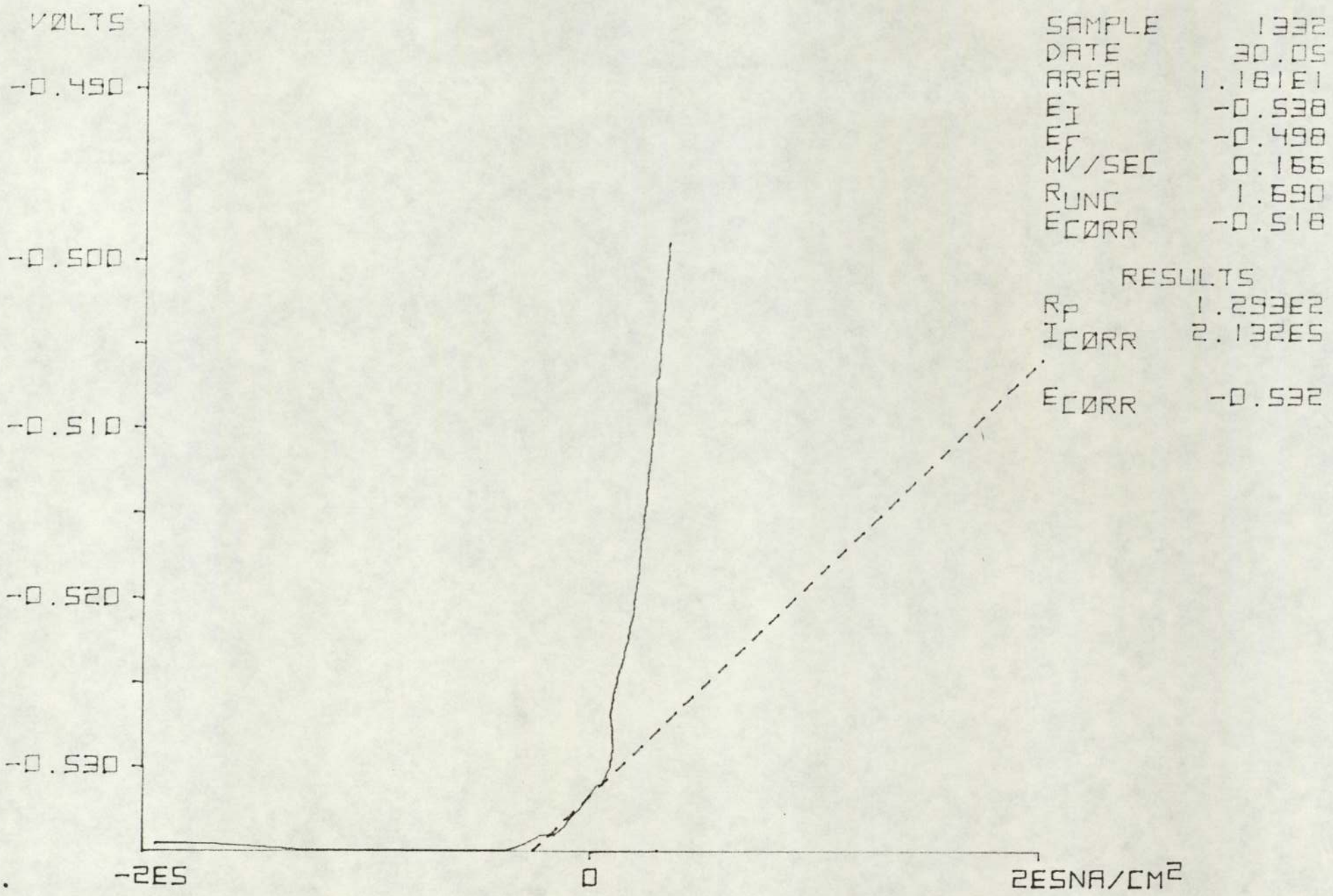

SAMPLE	1332
DATE	30.05
AREA	1.181E1
E_I	-0.538
E_F	-0.498
MV/SEC	0.166
R_{UNC}	1.690
$E_{CØRR}$	-0.518

RESULTS

R_P	1.293E2
$I_{CØRR}$	2.132E5
$E_{CØRR}$	-0.532

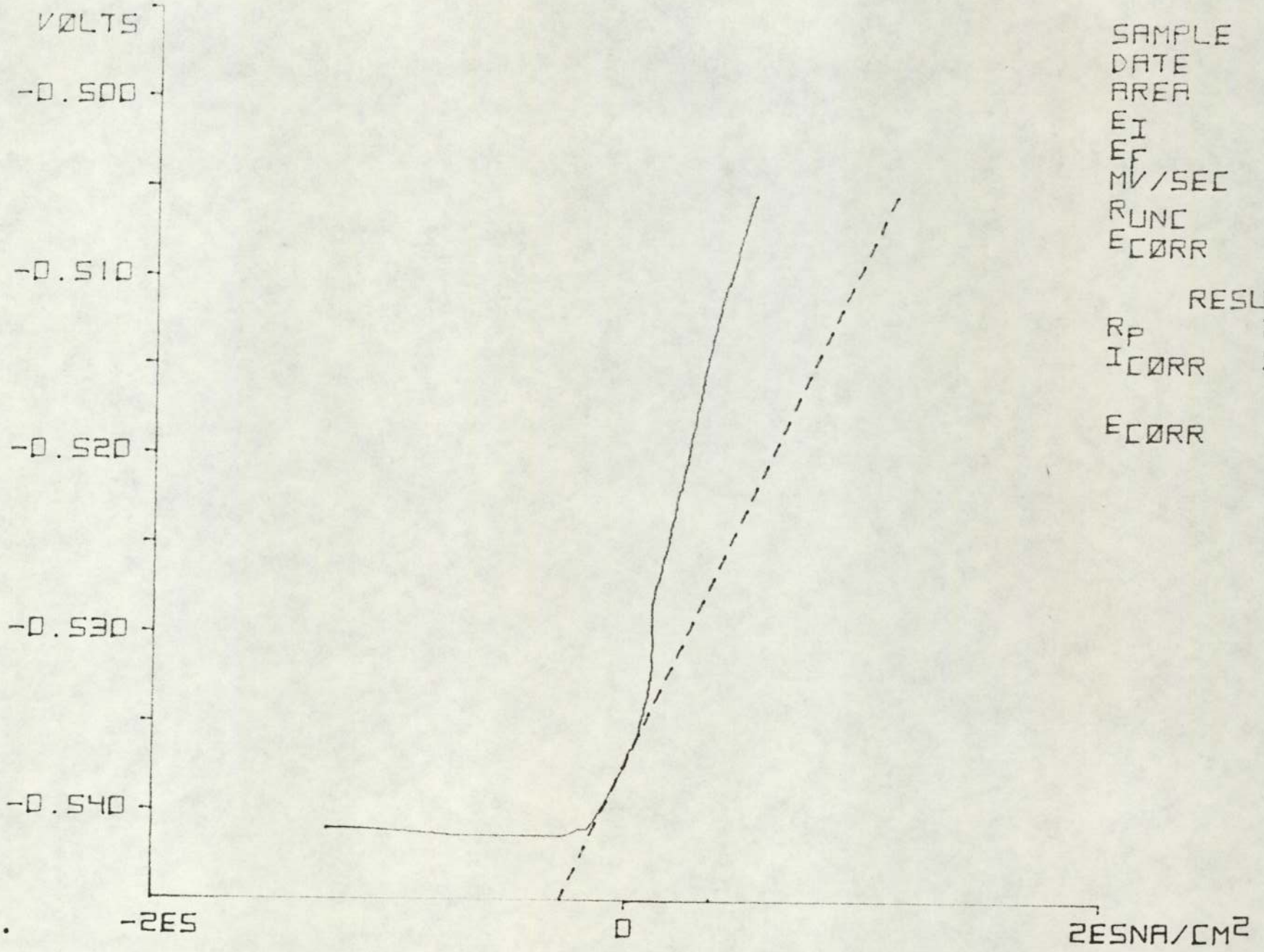

SAMPLE	4333
DATE	06.06
AREA	1.206E1
E_I	-0.544
E_F	-0.504
MV/SEC	0.166
R_{UNC}	2.179
$E_{CØRR}$	-0.524

RESULTS

R_P	2.824E2
$I_{CØRR}$	9.073E4
$E_{CØRR}$	-0.538

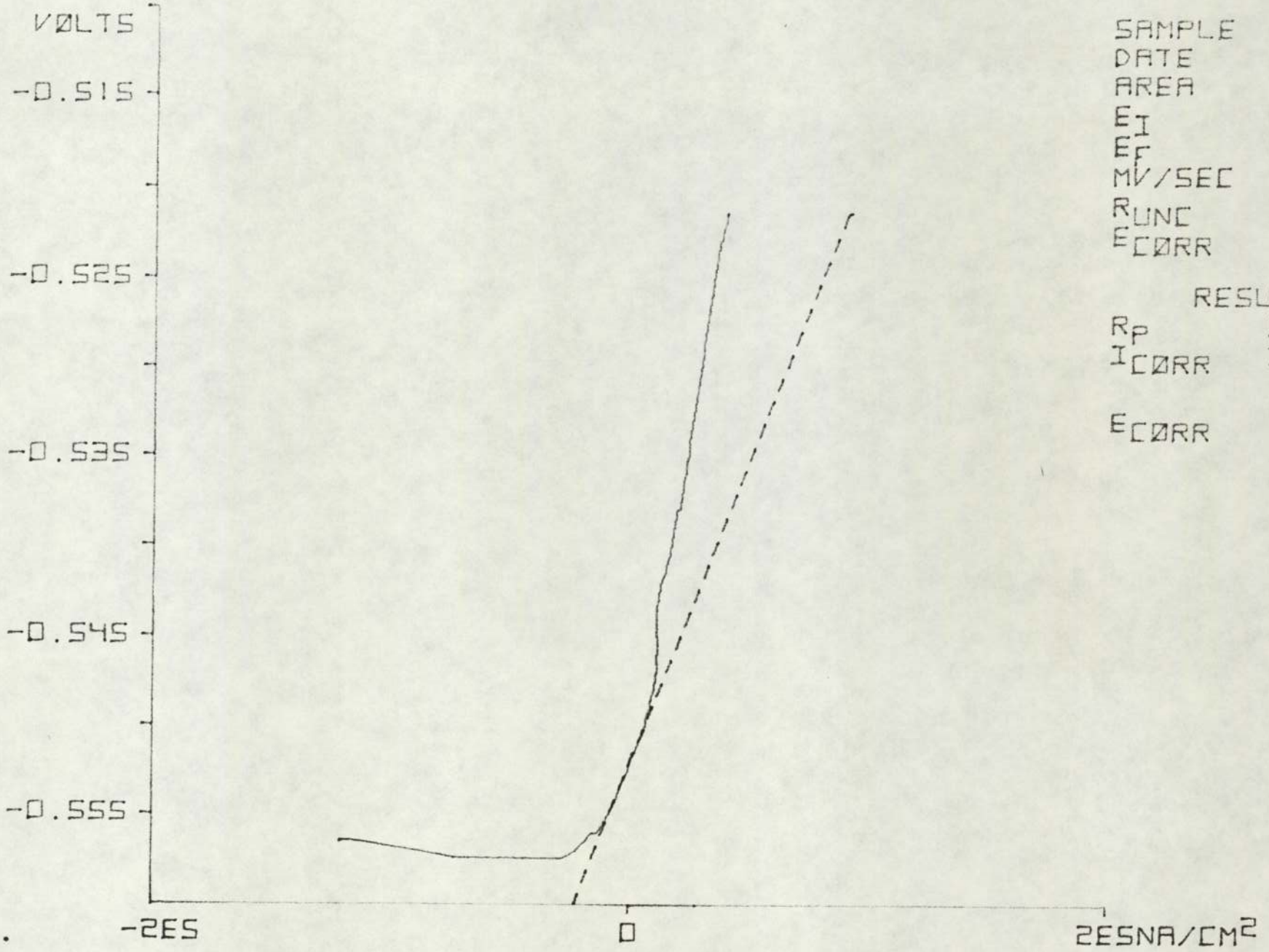

SAMPLE	6333
DATE	06.06
AREA	1.181E1
E_I	-0.560
E_F	-0.520
MV/SEC	0.166
R_{UNC}	2.463
$E_{CØRR}$	-0.540

RESULTS

R_P	3.389E2
$I_{CØRR}$	7.690E4
$E_{CØRR}$	-0.553

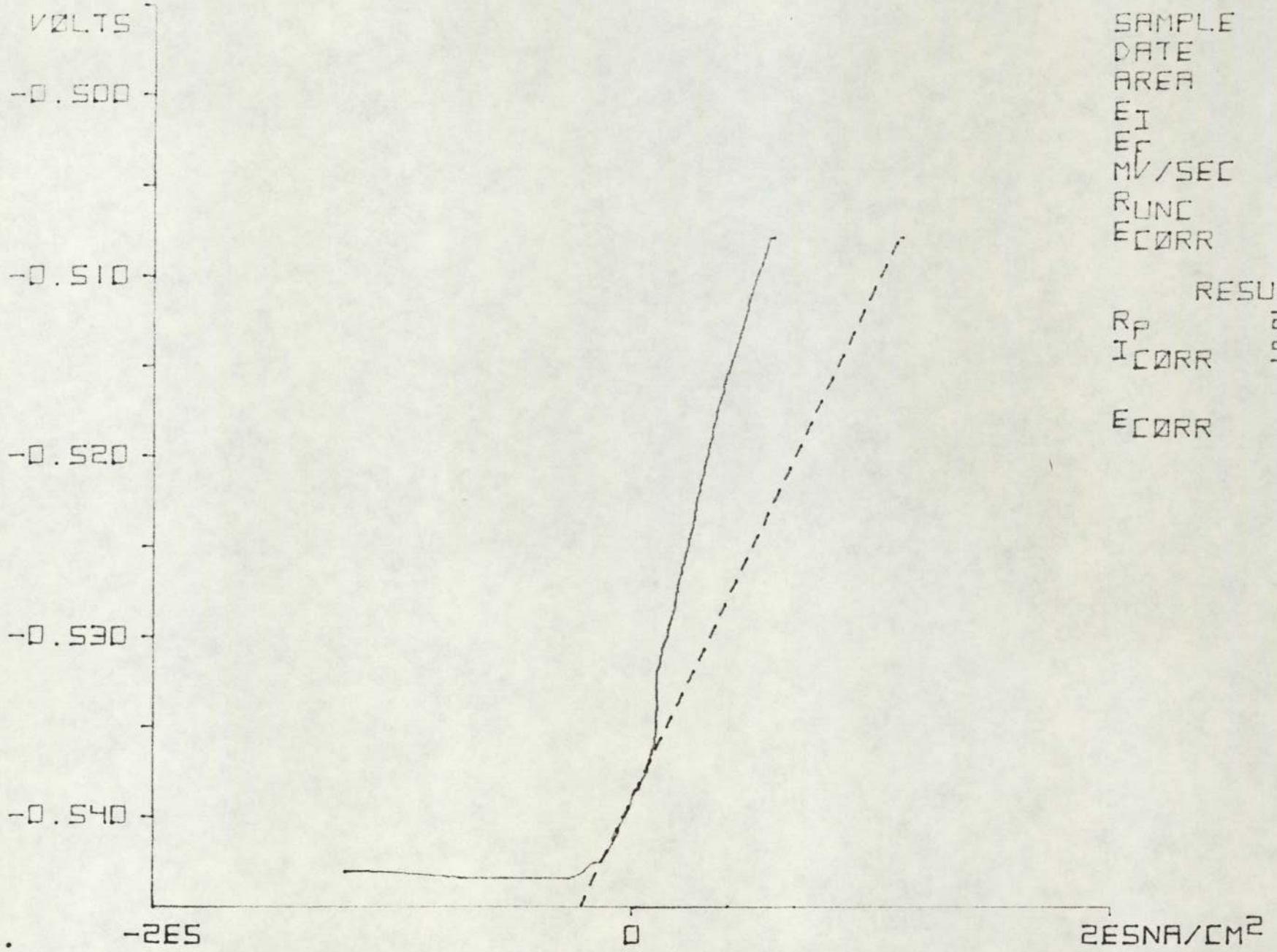

SAMPLE	1333
DATE	06.06
AREA	1.181E1
E_I	-0.546
E_F	-0.506
MV/SEC	0.166
R_{UNC}	2.296
$E_{CØRR}$	-0.526

RESULTS

R_P	2.768E2
$I_{CØRR}$	9.964E4
$E_{CØRR}$	-0.540

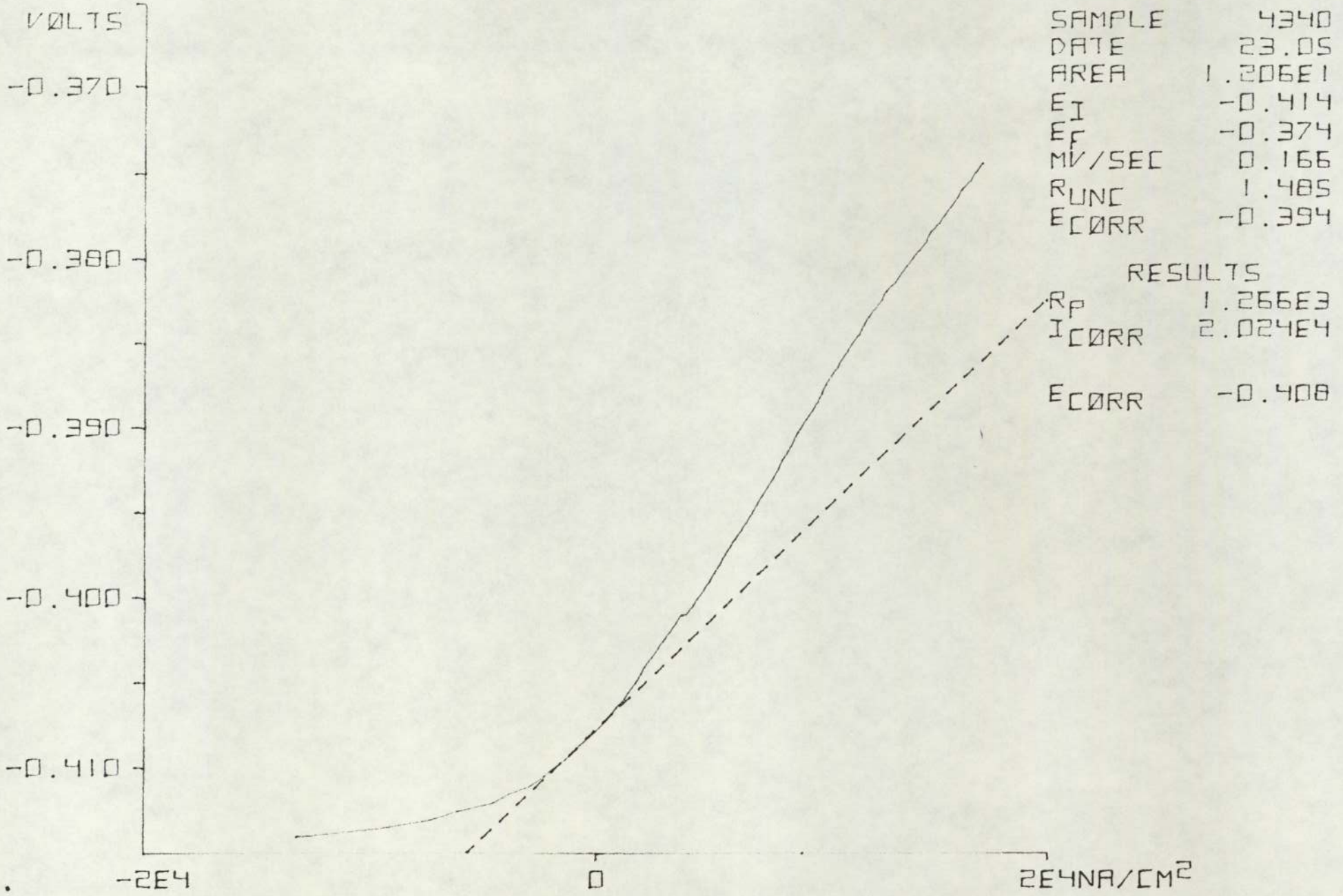

SAMPLE	4340
DATE	23.05
AREA	1.206E1
E_I	-0.414
E_F	-0.374
MV/SEC	0.166
R_{UNC}	1.485
E_{CORR}	-0.394

RESULTS

R_P	1.266E3
I_{CORR}	2.024E4
E_{CORR}	-0.408

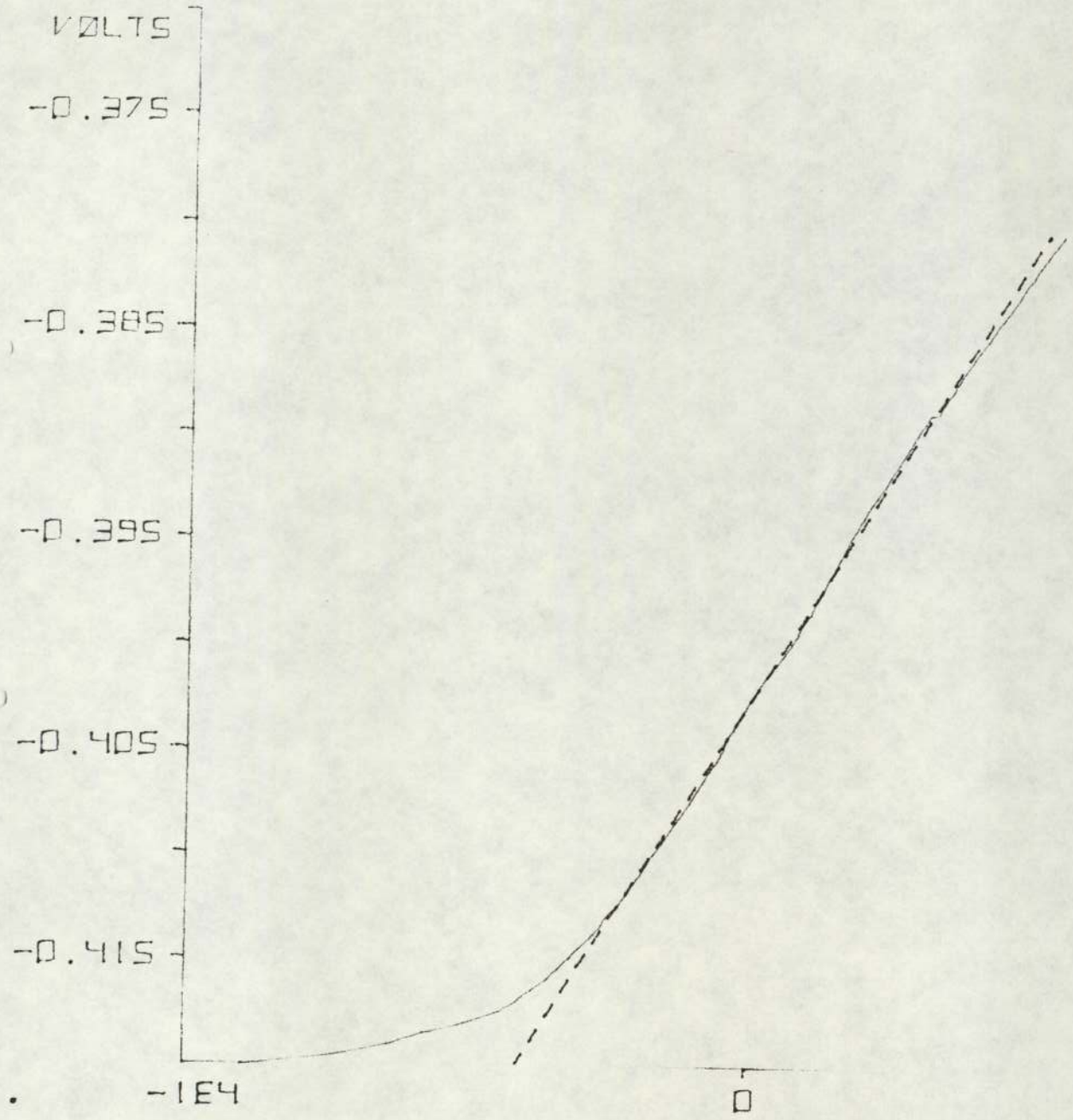

SAMPLE	6340
DATE	23.05
AREA	1.181E1
E_I	-0.420
E_F	-0.380
MV/SEC	0.166
R_{UNC}	1.818
$E_{CØRR}$	-0.400

RESULTS

R_P	4.252E3
$I_{CØRR}$	6.128E3
$E_{CØRR}$	-0.403

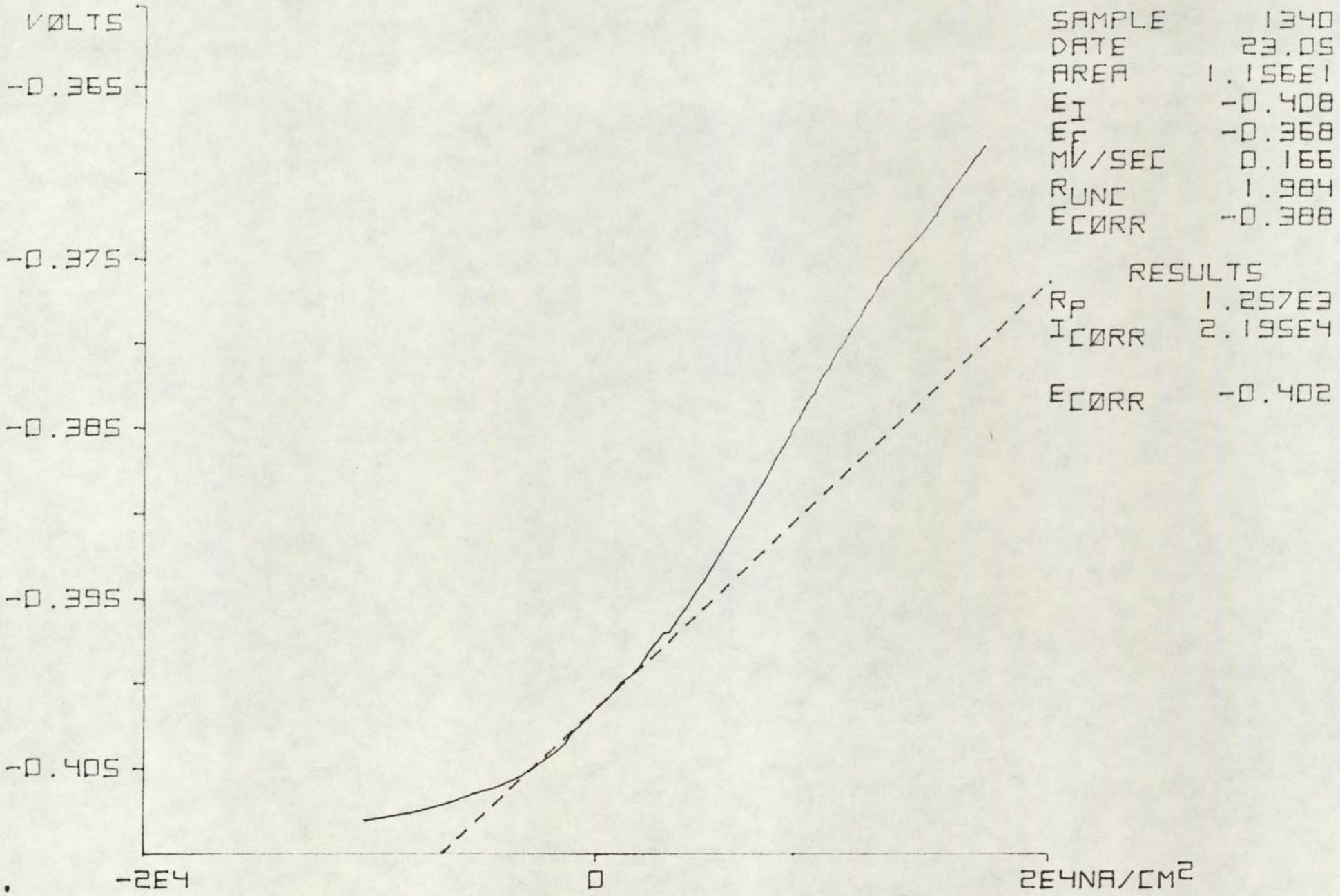
VØLTS
-0.365
-0.375
-0.385
-0.395
-0.405
-2E4
0
2E4NA/CM2
SAMPLE 1340
DATE 23.05
AREA 1.156E1
EI -0.408
EF -0.368
MV/SEC 0.166
RUNC 1.984
ECØRR -0.388
RESULTS
RP 1.257E3
ICØRR 2.195E4
ECØRR -0.402

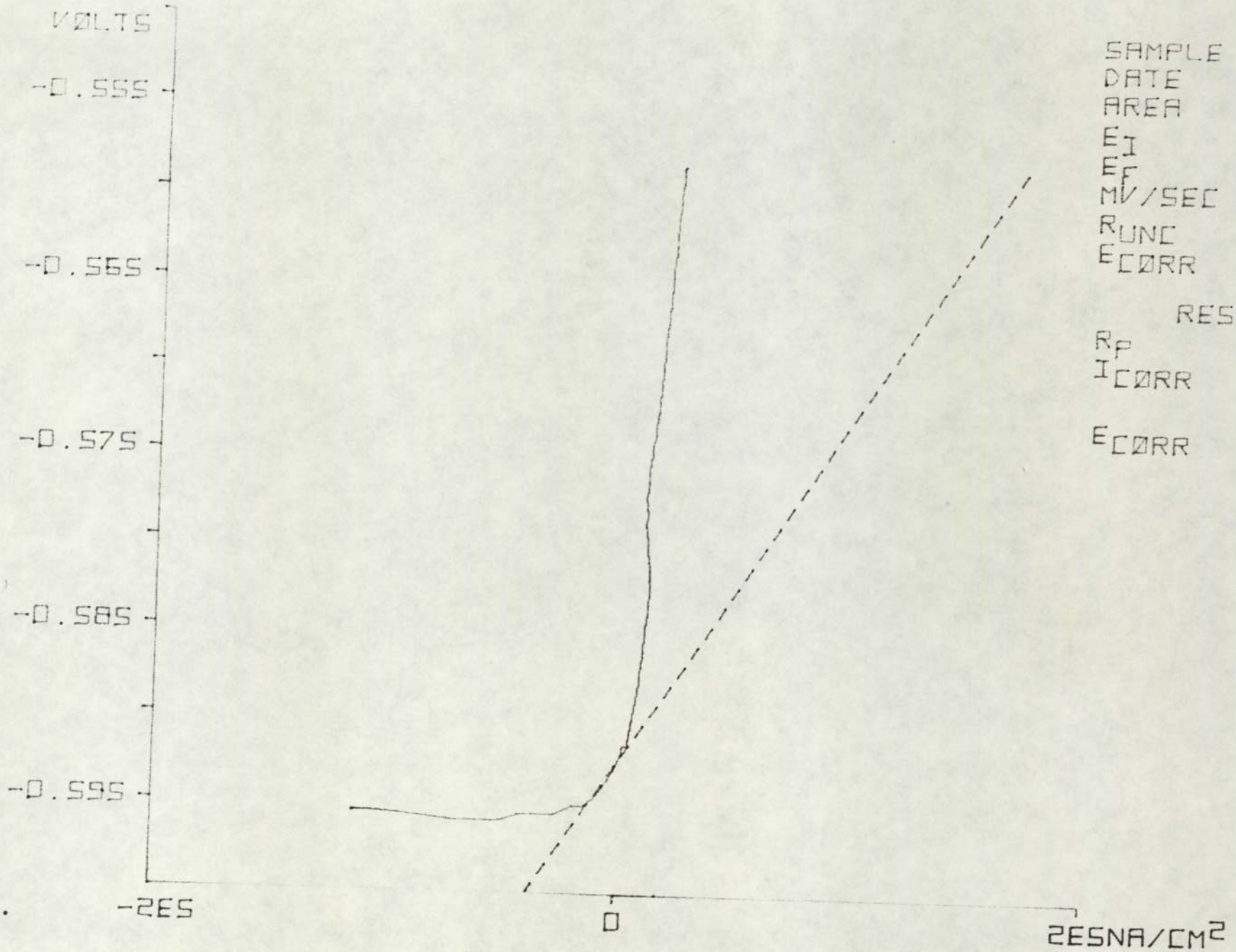

SAMPLE	4341
DATE	30.05
AREA	1.206E1
E_I	-0.598
E_F	-0.558
MV/SEC	0.166
R_{UNC}	1.925
$E_{CØRR}$	-0.578

RESULTS

R_P	1.999E2
$I_{CØRR}$	1.282E5
$E_{CØRR}$	-0.593

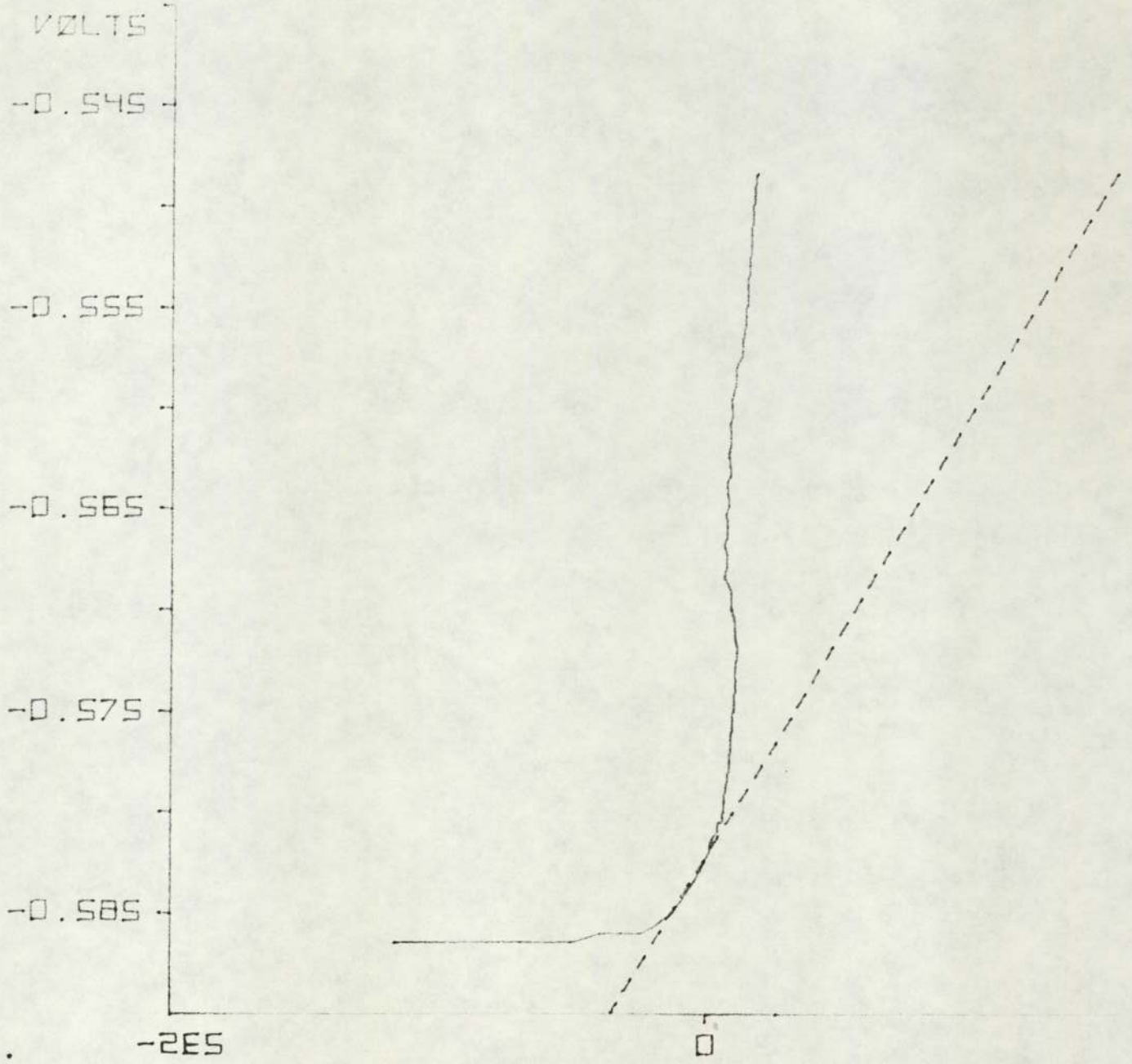

SAMPLE	6341
DATE	30.05
AREA	1.181E1
E_I	-0.588
E_F	-0.548
MV/SEC	0.166
R_{UNC}	1.172
$E_{CØRR}$	-0.568

RESULTS

R_P	2.198E2
$I_{CØRR}$	1.185E5
$E_{CØRR}$	-0.583

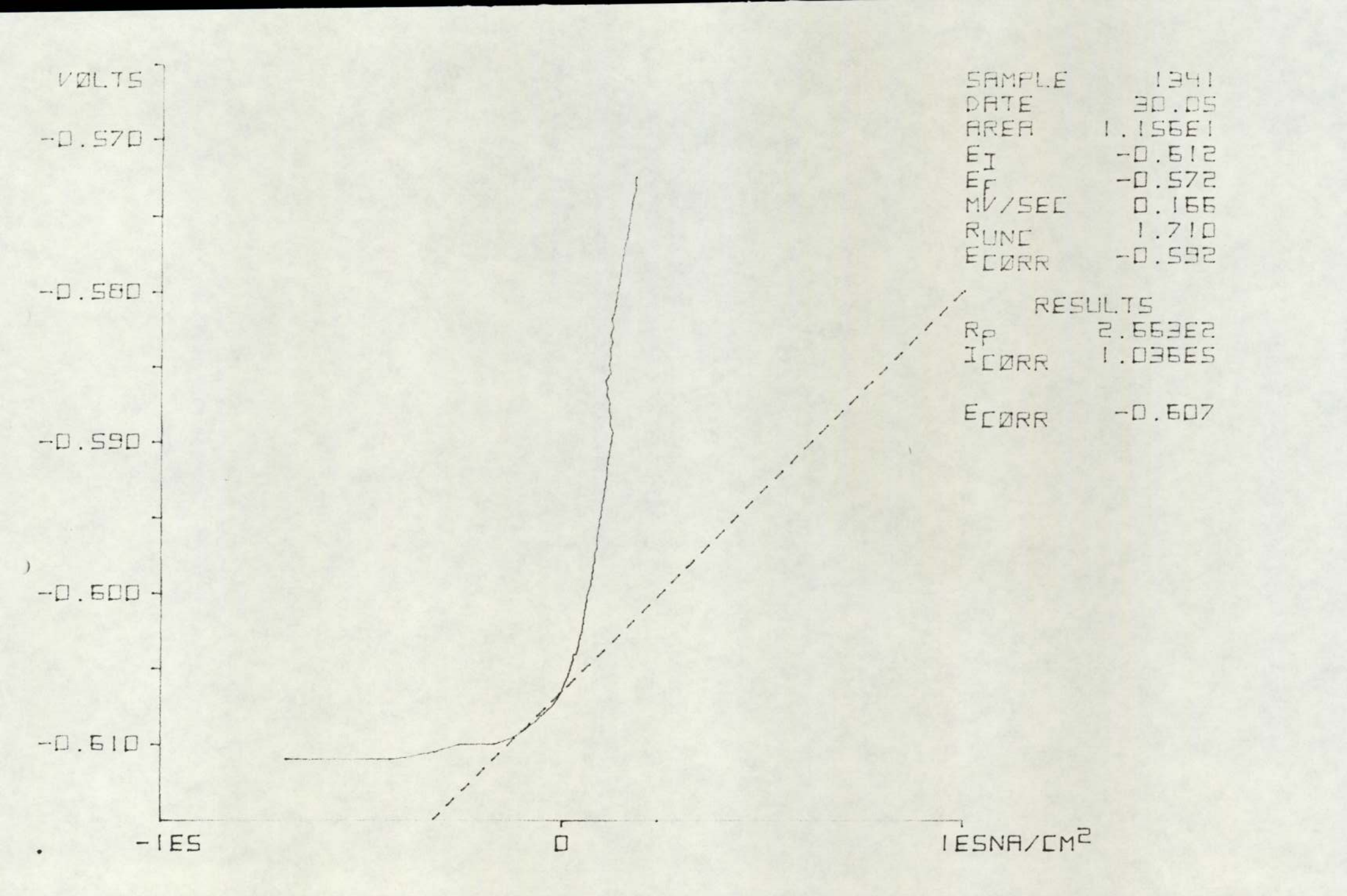
VØLTS
-0.570
-0.580
-0.590
-0.600
-0.610
-1ES
0
1ESNA/CM2
SAMPLE 1341
DATE 30.05
AREA 1.156E1
EI -0.612
EF -0.572
MV/SEC 0.166
RUNC 1.710
ECØRR -0.592
RESULTS
RP 2.663E2
ICØRR 1.036E5
ECØRR -0.607

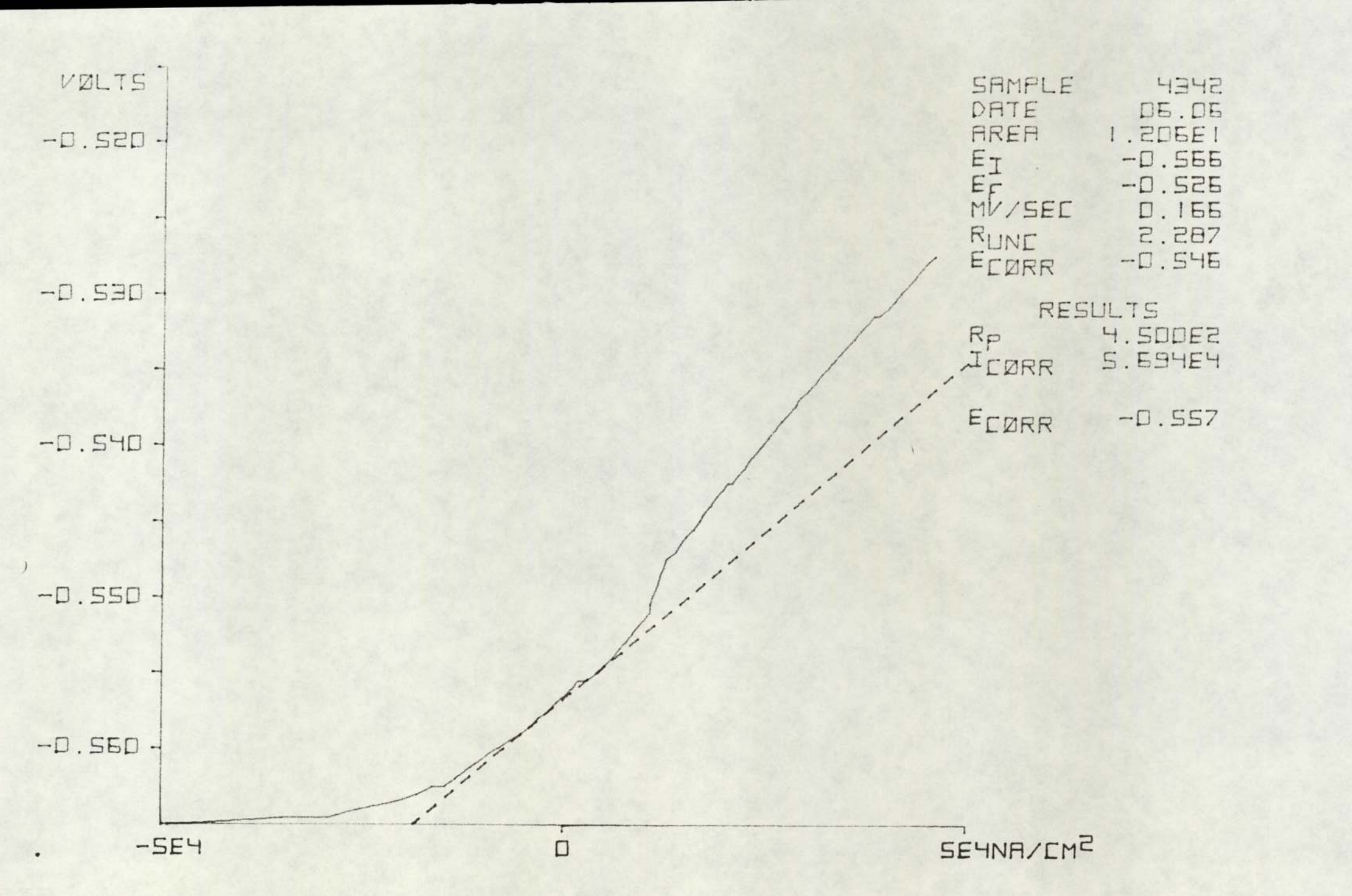
VØLTS
-0.520
-0.530
-0.540
-0.550
-0.560
-5E4
0
5E4NA/CM2
SAMPLE 4342
DATE 06.06
AREA 1.206E1
EI -0.566
EF -0.526
MV/SEC 0.166
RUNC 2.287
ECØRR -0.546
RESULTS
RP 4.500E2
ICØRR 5.694E4
ECØRR -0.557

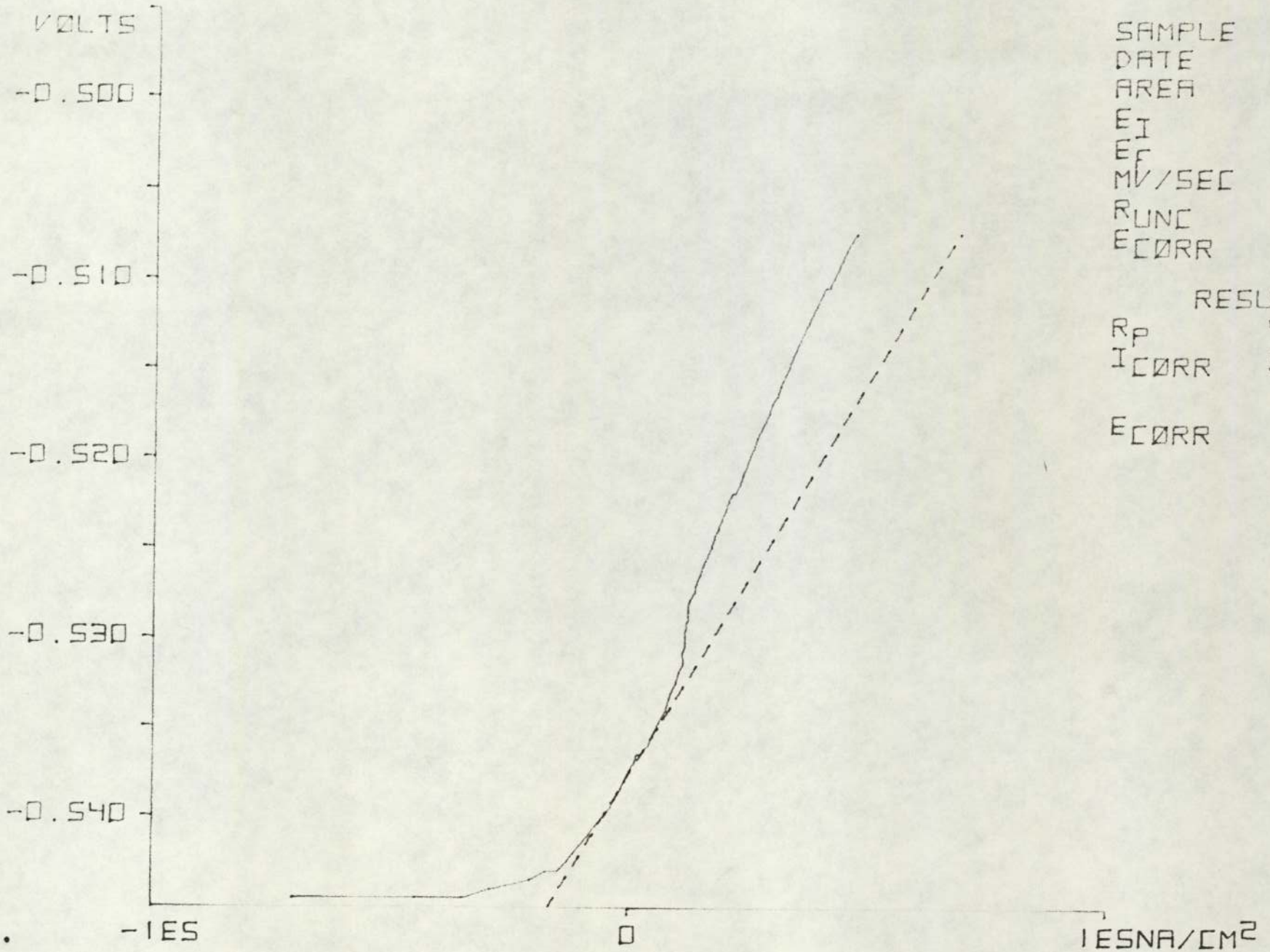

SAMPLE	6342
DATE	06.06
AREA	1.181E1
E_I	-0.546
E_f	-0.506
MV/SEC	0.166
R_{UNC}	2.228
E_{CORR}	-0.526

RESULTS

R_P	4.438E2
I_{CORR}	5.871E4
E_{CORR}	-0.538

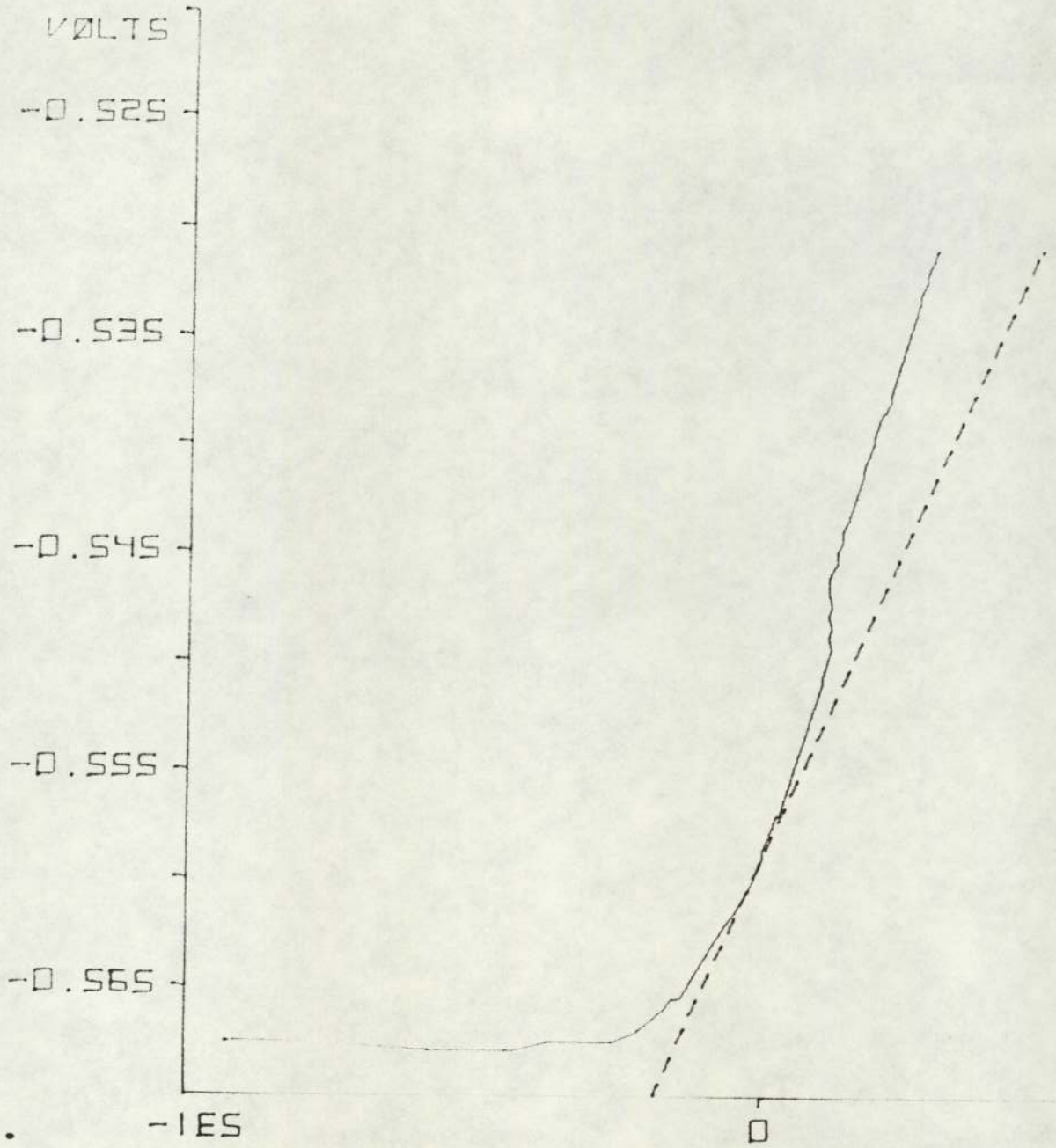

SAMPLE	1342
DATE	06.06
AREA	1.156E1
E_I	-0.570
E_F	-0.530
MV/SEC	0.166
R_{UNC}	2.492
$E_{CØRR}$	-0.550

RESULTS

R_P	5.994E2
$I_{CØRR}$	4.600E4
$E_{CØRR}$	-0.559

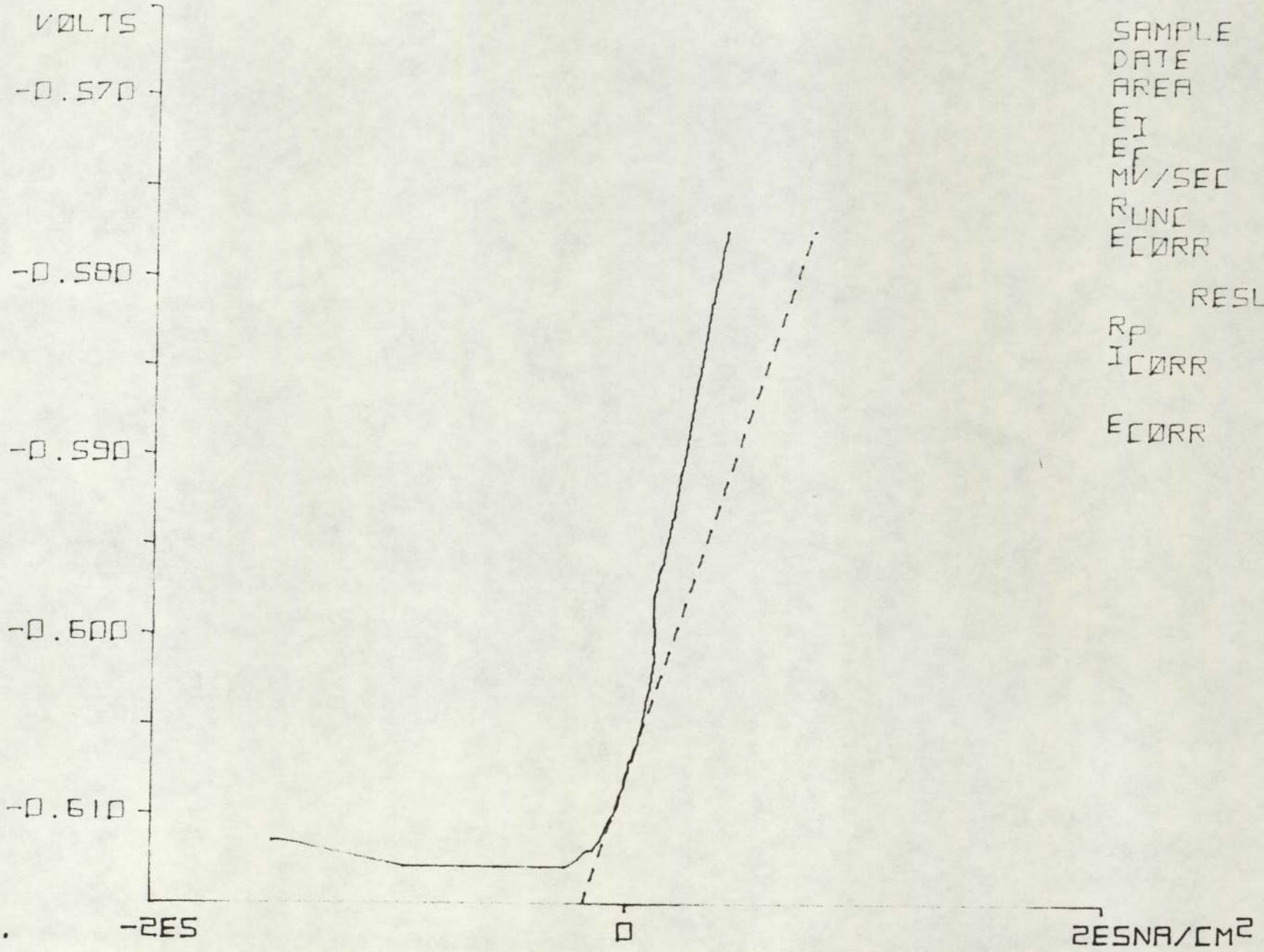

SAMPLE	4343
DATE	13.06
AREA	1.206E1
E_I	-0.616
E_F	-0.576
MV/SEC	0.166
R_{UNC}	2.599
$E_{CØRR}$	-0.596

RESULTS

R_P	3.994E2
$I_{CØRR}$	6.416E4
$E_{CØRR}$	-0.608

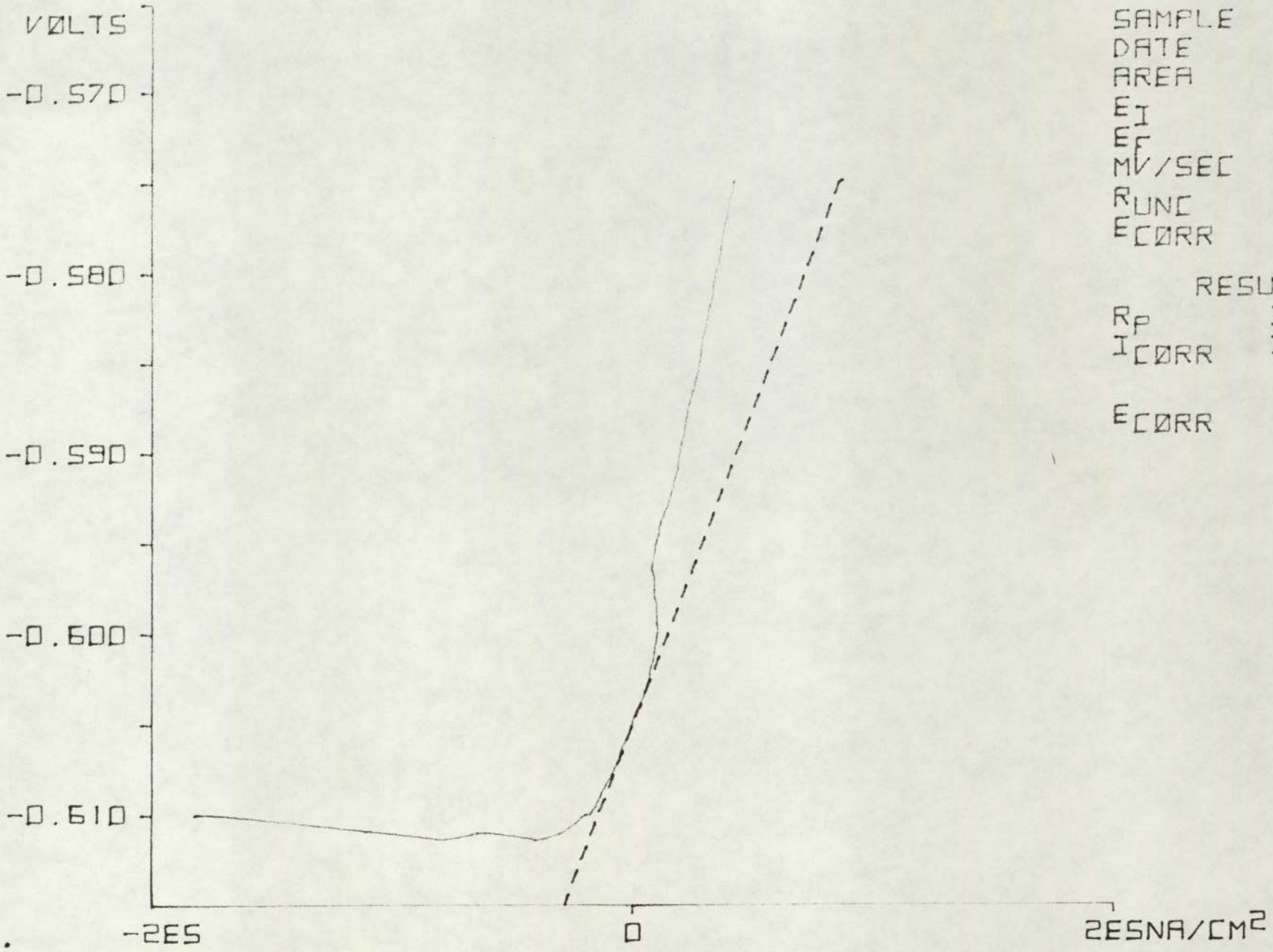

SAMPLE	6343
DATE	13.06
AREA	1.181E1
E_I	-0.614
E_F	-0.574
MV/SEC	0.166
R_{UNC}	1.905
$E_{CØRR}$	-0.594

RESULTS

R_P	3.495E2
$I_{CØRR}$	7.456E4
$E_{CØRR}$	-0.606

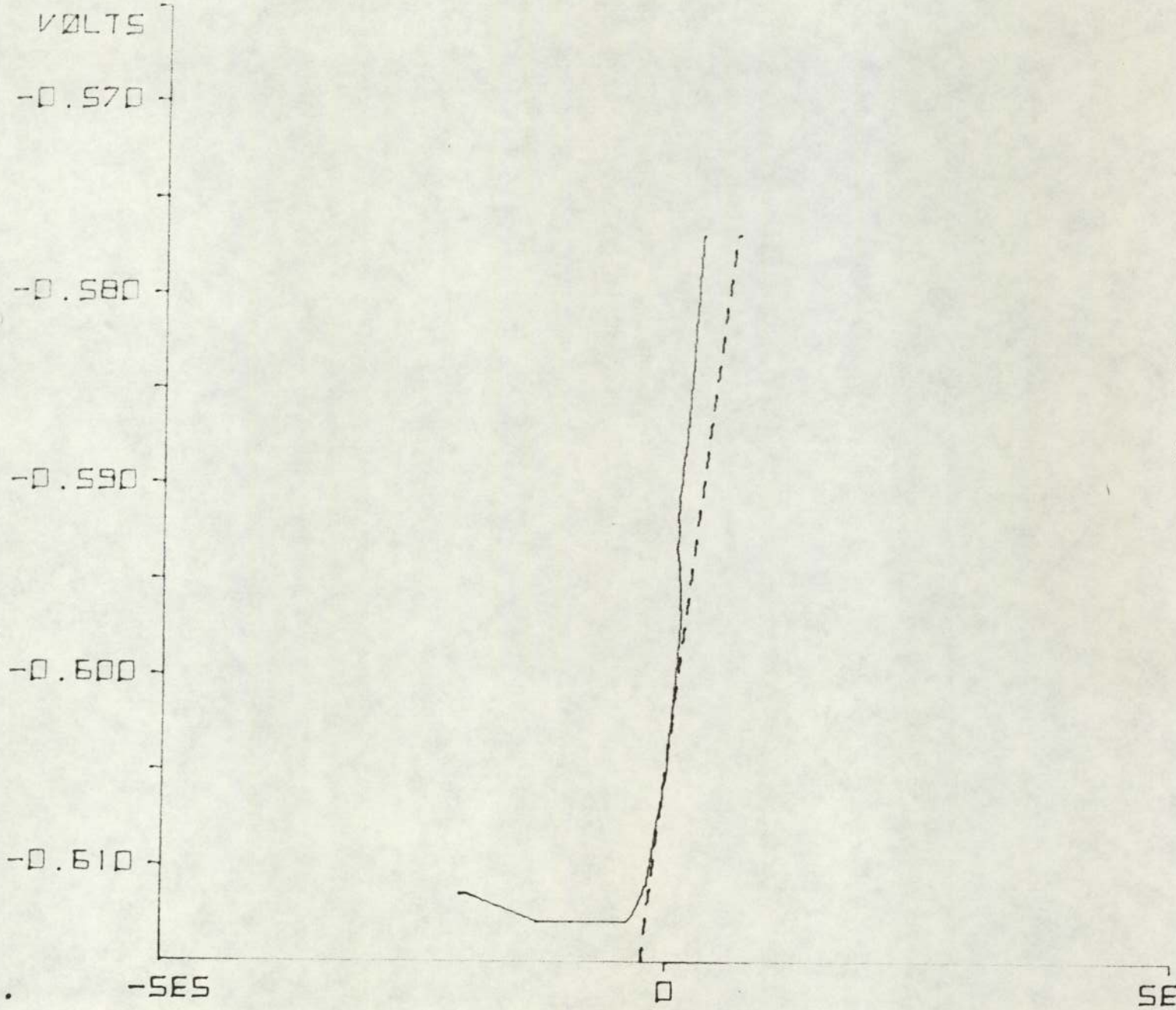

SAMPLE	1343
DATE	13.06
AREA	1.156E1
E_I	-0.616
E_f	-0.576
MV/SEC	0.166
R_{UNC}	1.964
$E_{CØRR}$	-0.596

RESULTS

R_P	4.327E2
$I_{CØRR}$	6.373E4
$E_{CØRR}$	-0.605

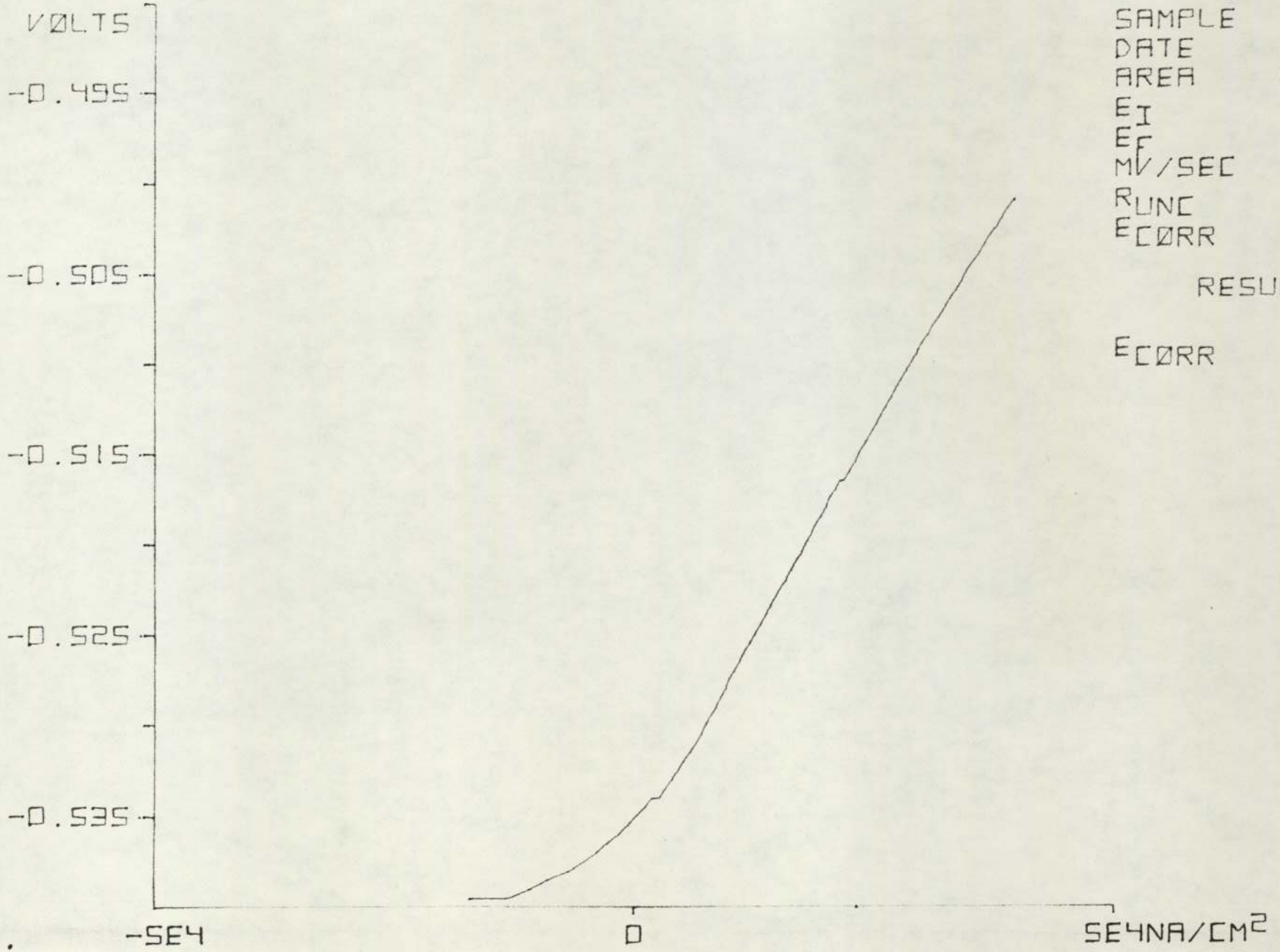

SAMPLE	4350
DATE	05.07
AREA	1.13DE1
E_I	-0.540
E_F	-0.500
MV/SEC	0.166
R_{UNC}	2.326
$E_{CØRR}$	-0.520

RESULTS

$E_{CØRR}$ -0.536

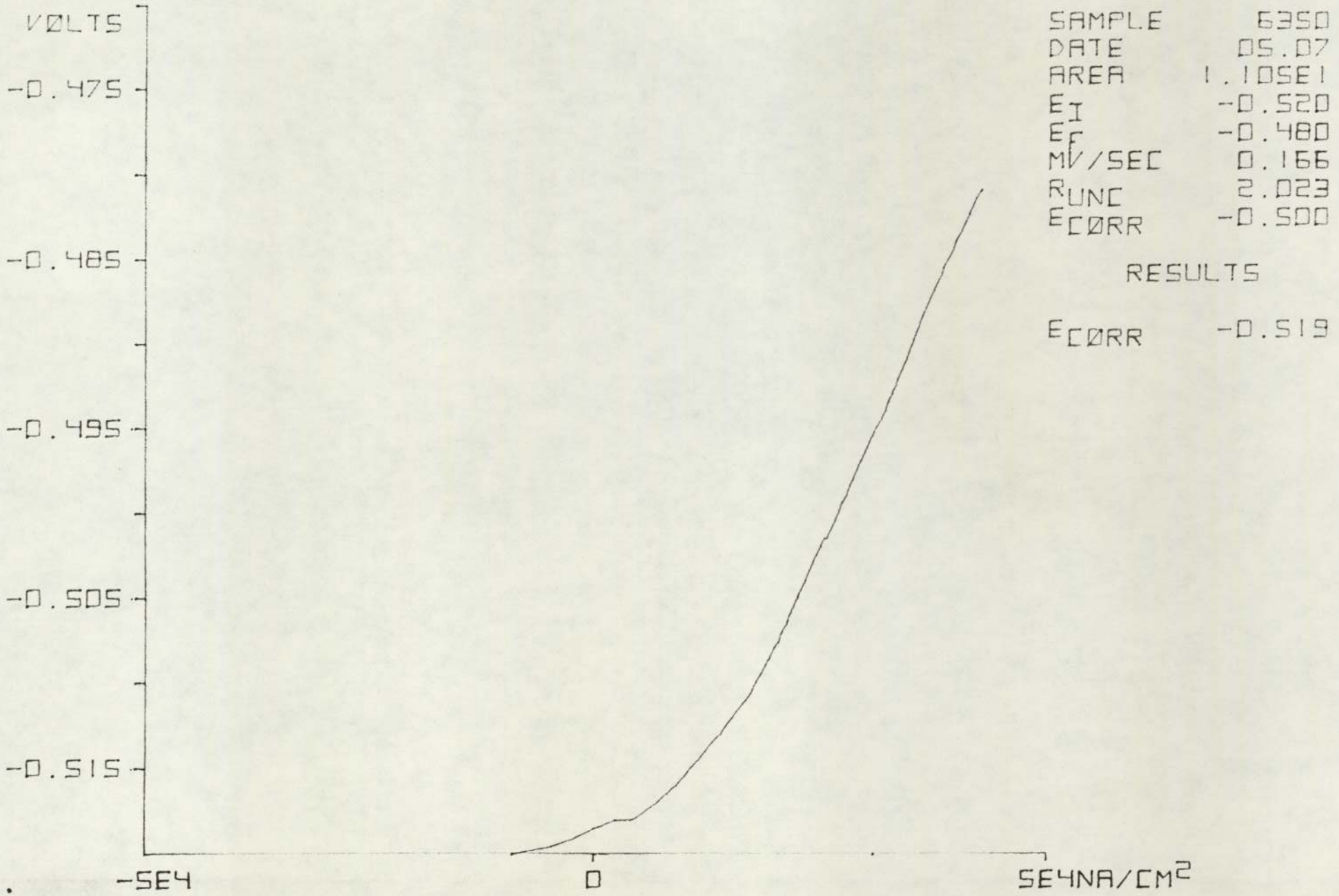

SAMPLE	6350
DATE	05.07
AREA	1.10SE1
E_I	-0.520
E_F	-0.480
MV/SEC	0.166
RUNC	2.023
E_{CORR}	-0.500

RESULTS

E_{CORR} -0.519

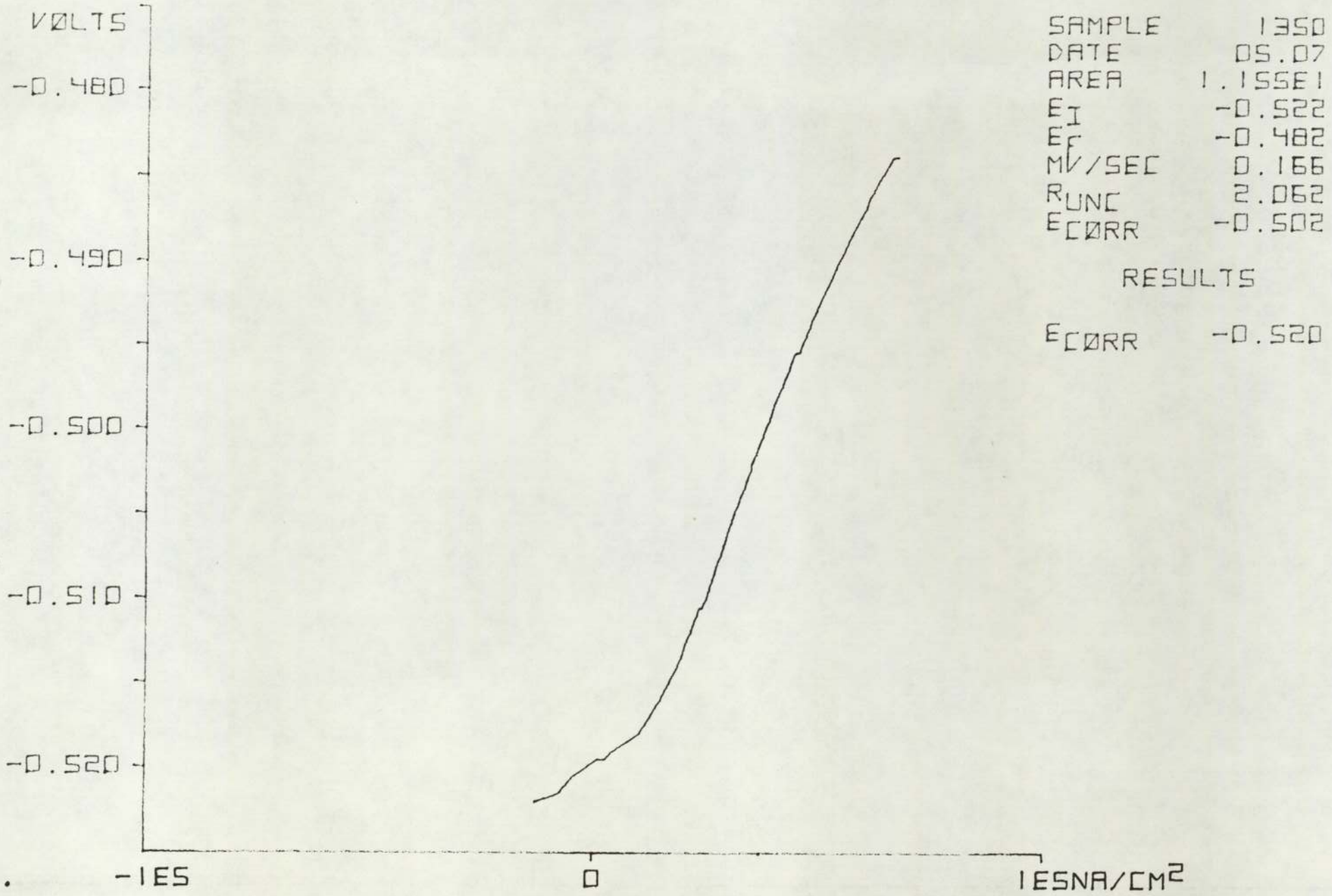

SAMPLE	1350
DATE	05.07
AREA	1.155E1
E_I	-0.522
E_f	-0.482
MV/SEC	0.166
R_{UNC}	2.062
$E_{CØRR}$	-0.502

RESULTS

$E_{CØRR}$ -0.520

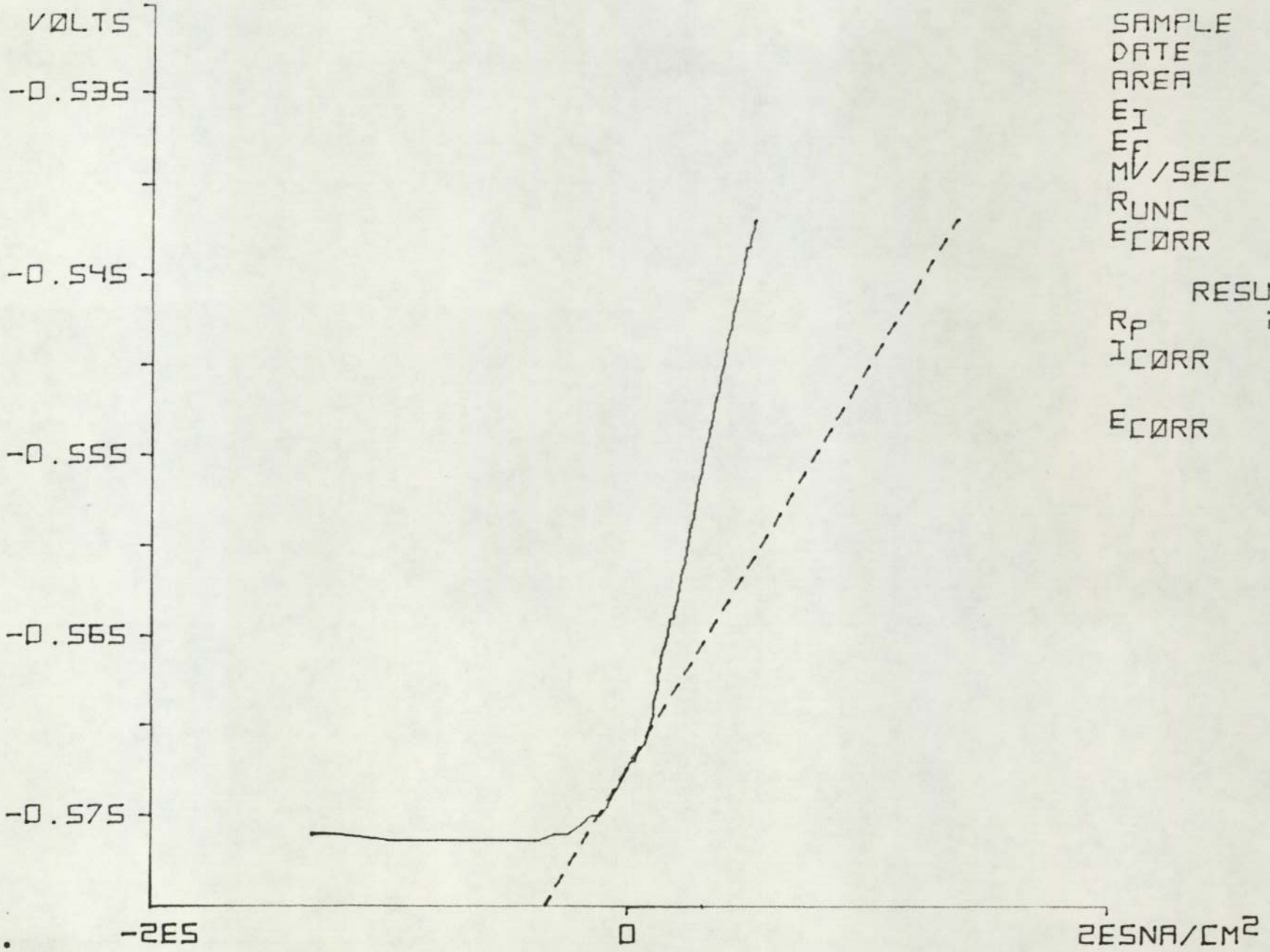

SAMPLE	4351
DATE	12.07
AREA	1.130E1
E_I	-0.580
E_f	-0.540
MV/SEC	0.166
R_{UNC}	2.814
$E_{CØRR}$	-0.560

RESULTS

R_P	2.217E2
$I_{CØRR}$	1.155E5
$E_{CØRR}$	-0.573

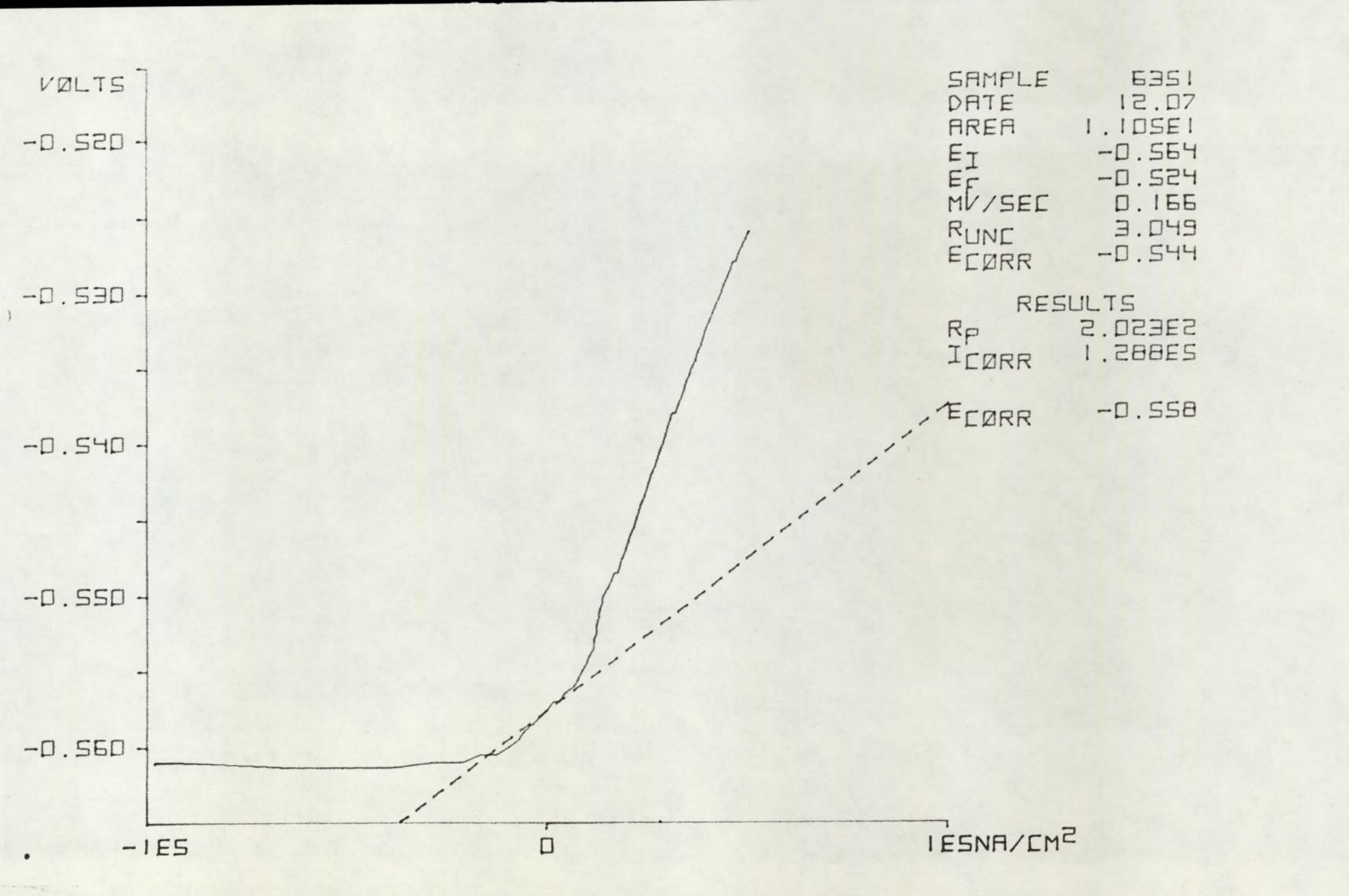
VØLTS
-0.520
-0.530
-0.540
-0.550
-0.560
-1E5
0
1E5NA/CM2
SAMPLE 6351
DATE 12.07
AREA 1.10SE1
EI -0.564
EF -0.524
MV/SEC 0.166
RUNC 3.049
ECØRR -0.544
RESULTS
RP 2.023E2
ICØRR 1.288E5
ECØRR -0.558

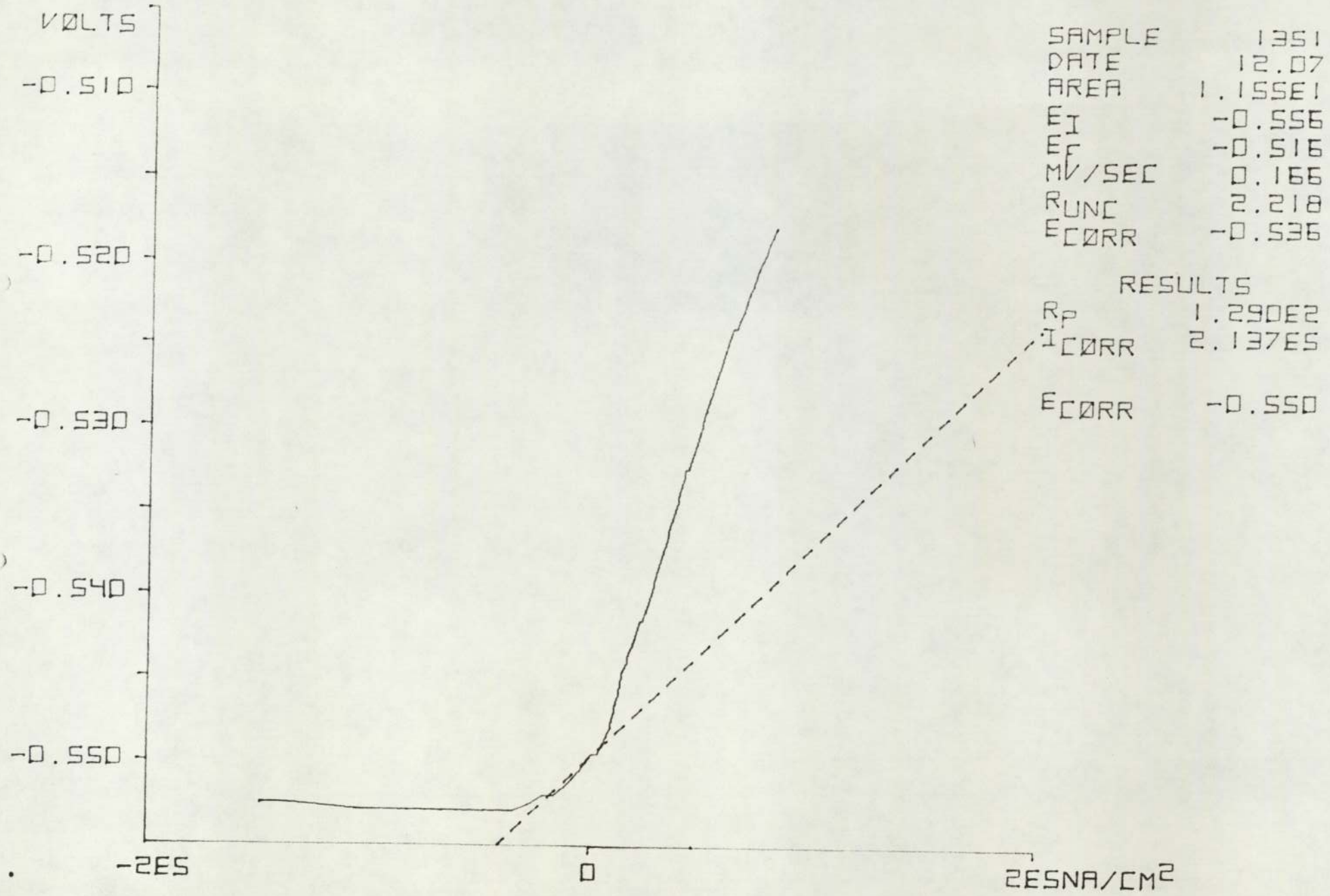

SAMPLE	1351
DATE	12.07
AREA	1.155E1
E_I	-0.556
E_F	-0.516
MV/SEC	0.166
R_{UNC}	2.218
$E_{CØRR}$	-0.536

RESULTS

R_P	1.290E2
$I_{CØRR}$	2.137E5
$E_{CØRR}$	-0.550

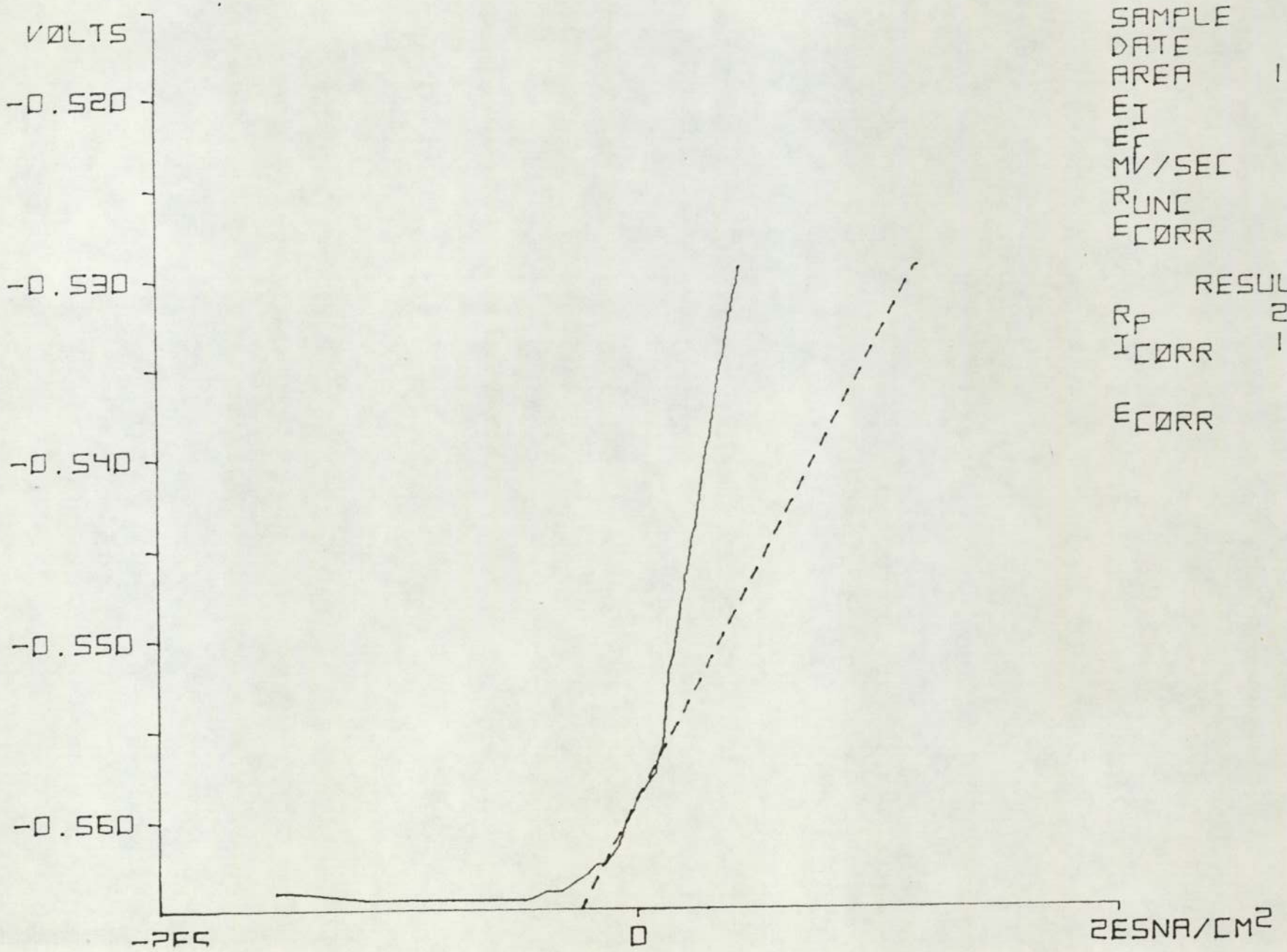

SAMPLE	4352
DATE	19.07
AREA	1.130E1
E_I	-0.568
E_F	-0.528
MV/SEC	0.166
R_{UNC}	2.375
$E_{CØRR}$	-0.548

RESULTS

R_P	2.508E2
$I_{CØRR}$	1.021E5
$E_{CØRR}$	-0.560

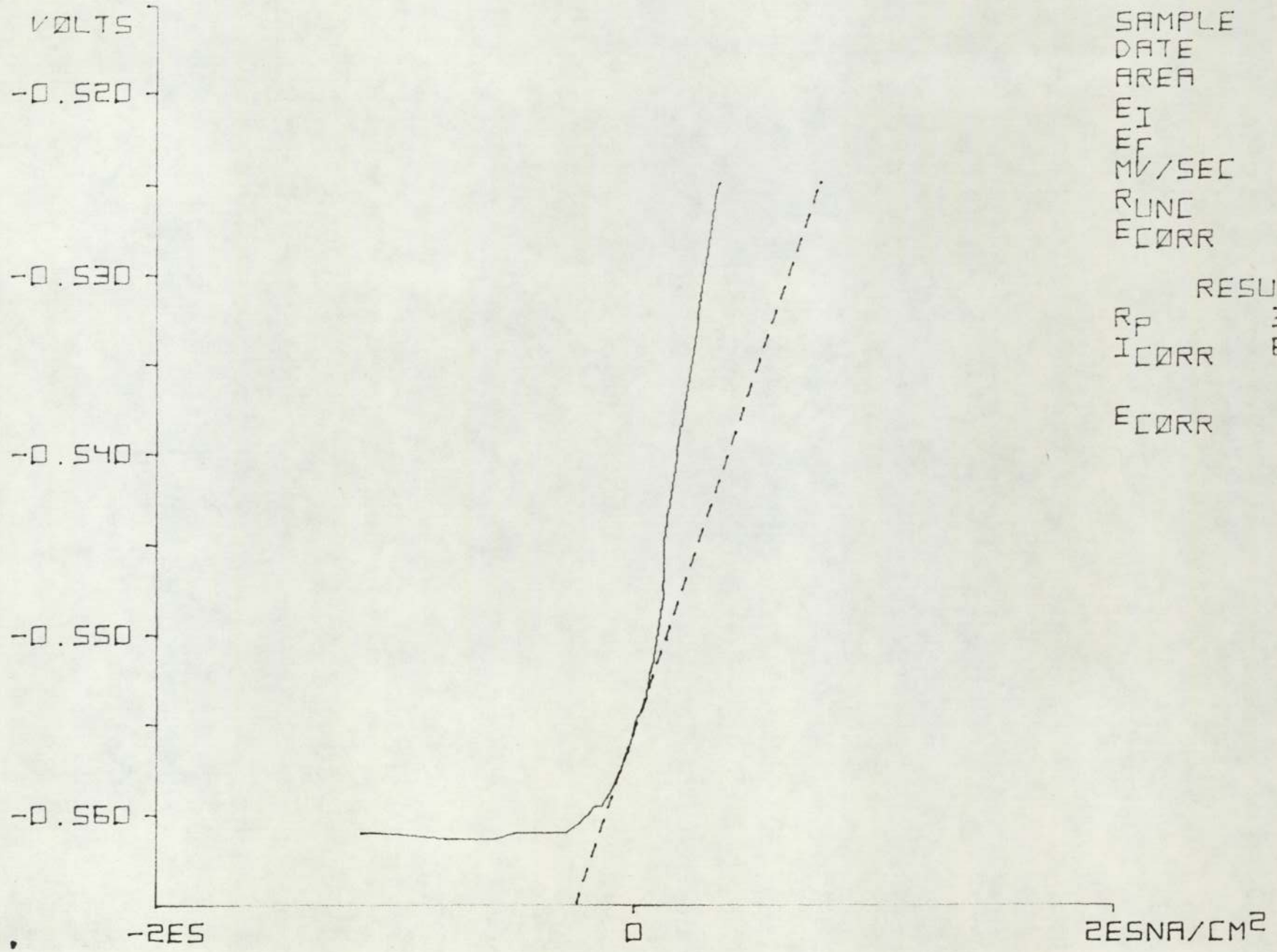

SAMPLE	6352
DATE	19.07
AREA	1.10SE1
E_I	-0.564
E_f	-0.524
MV/SEC	0.166
R_{UNC}	2.668
$E_{CØRR}$	-0.544

RESULTS

R_p	3.948E2
$I_{CØRR}$	6.601E4
$E_{CØRR}$	-0.556

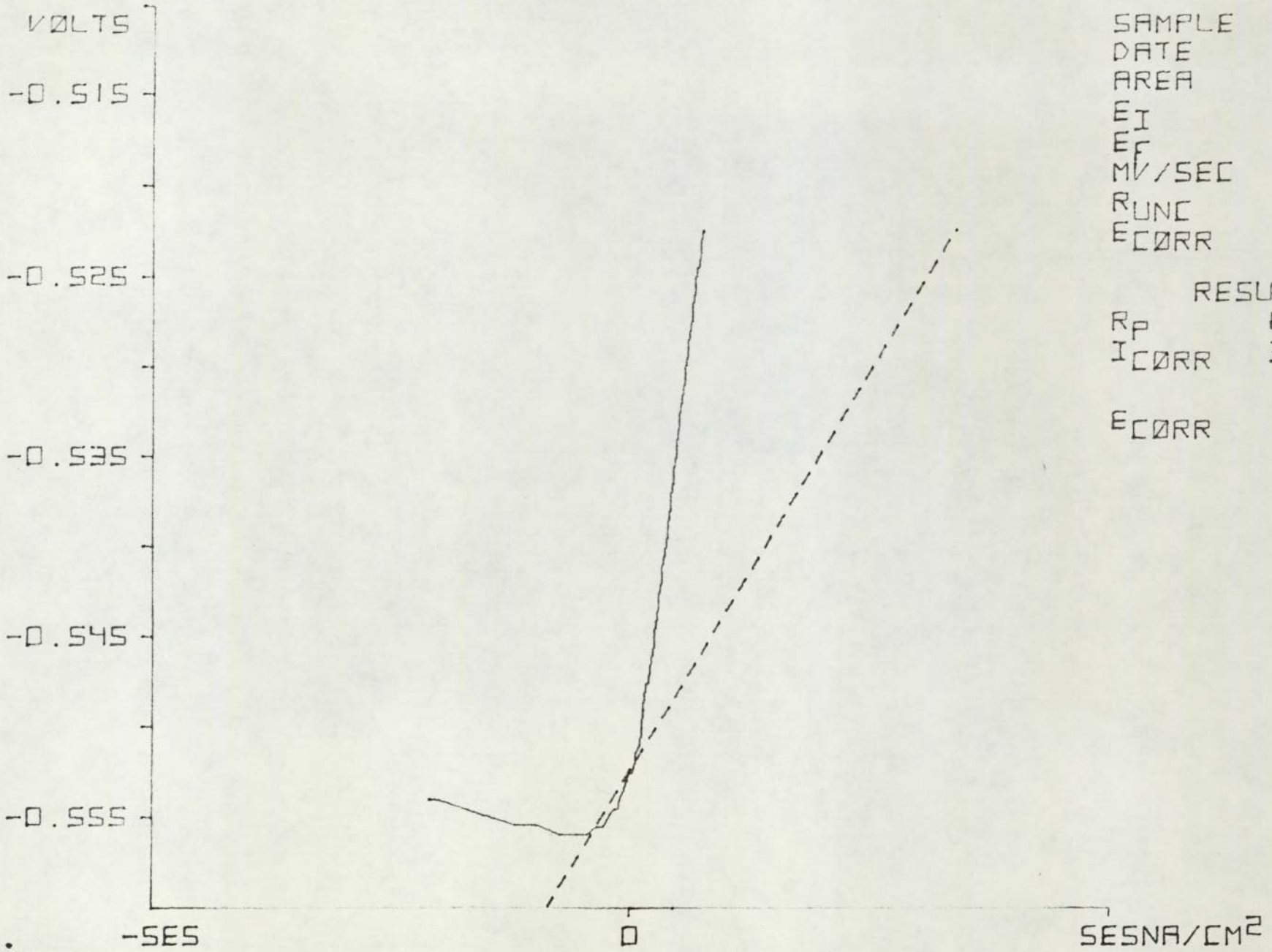

SAMPLE	1352
DATE	19.07
AREA	1.155E1
E_I	-0.560
E_f	-0.520
MV/SEC	0.166
R_{UNC}	2.629
$E_{CØRR}$	-0.540

RESULTS

R_P	8.864E1
$I_{CØRR}$	3.111E5
$E_{CØRR}$	-0.553

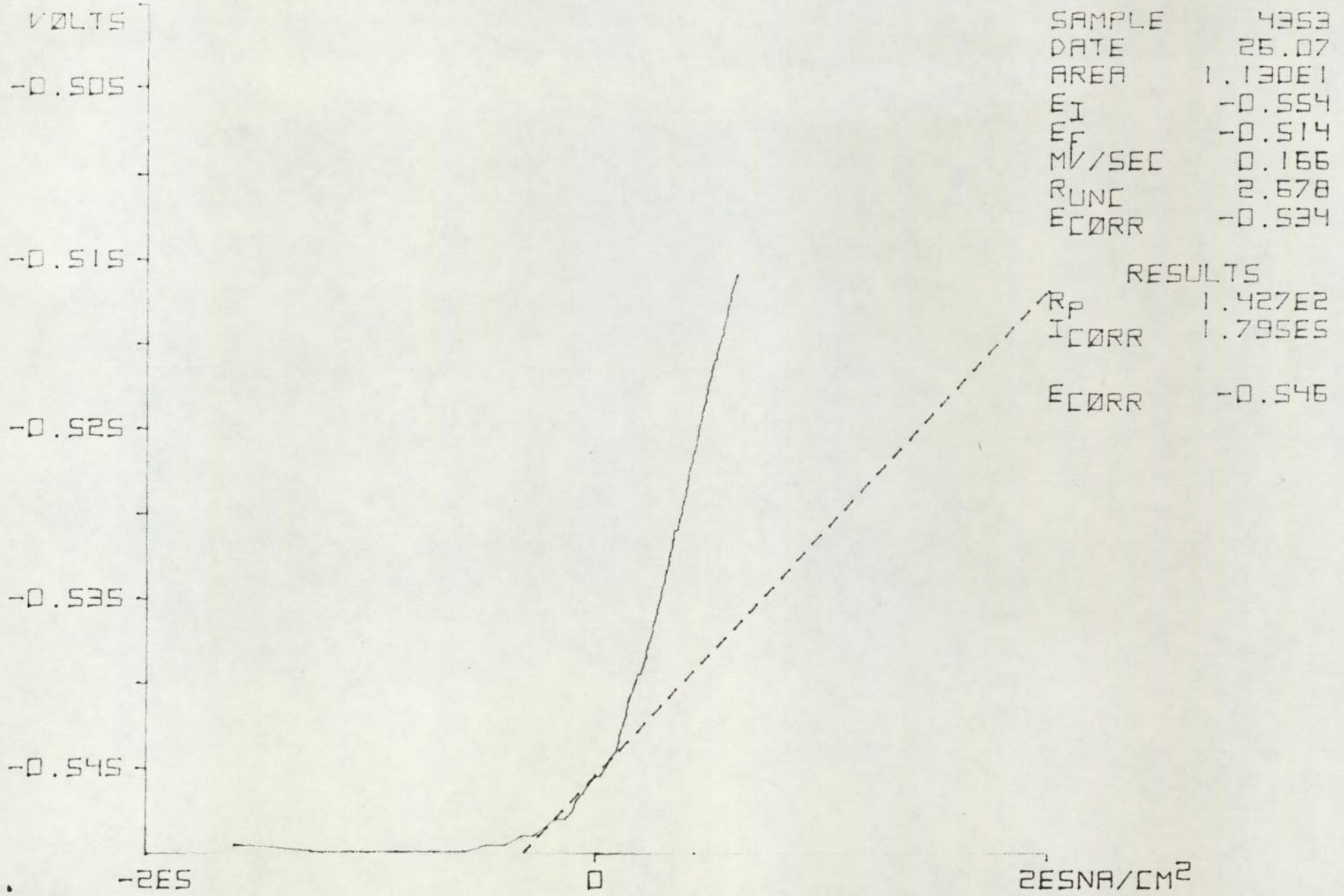

SAMPLE	4353
DATE	25.07
AREA	1.130E1
E_I	-0.554
E_F	-0.514
MV/SEC	0.166
R_{UNC}	2.678
$E_{CØRR}$	-0.534

RESULTS

R_P	1.427E2
$I_{CØRR}$	1.795E5
$E_{CØRR}$	-0.546

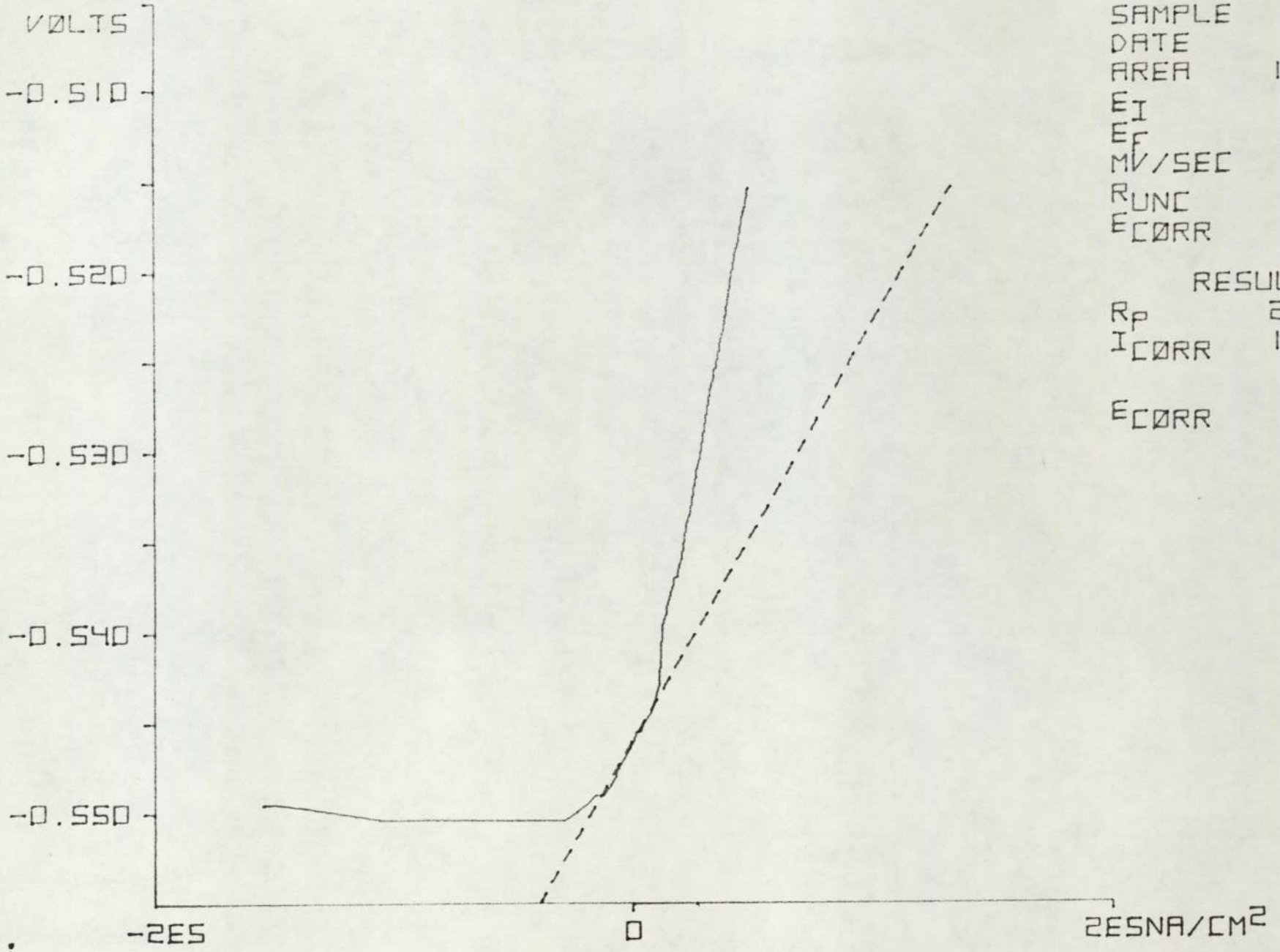

SAMPLE	6353
DATE	26.07
AREA	1.10SE1
E_I	-0.554
E_f	-0.514
MV/SEC	0.166
R_{UNC}	2.805
$E_{CØRR}$	-0.538

RESULTS

R_P	2.29SE2
$I_{CØRR}$	1.13SE5
$E_{CØRR}$	-0.547

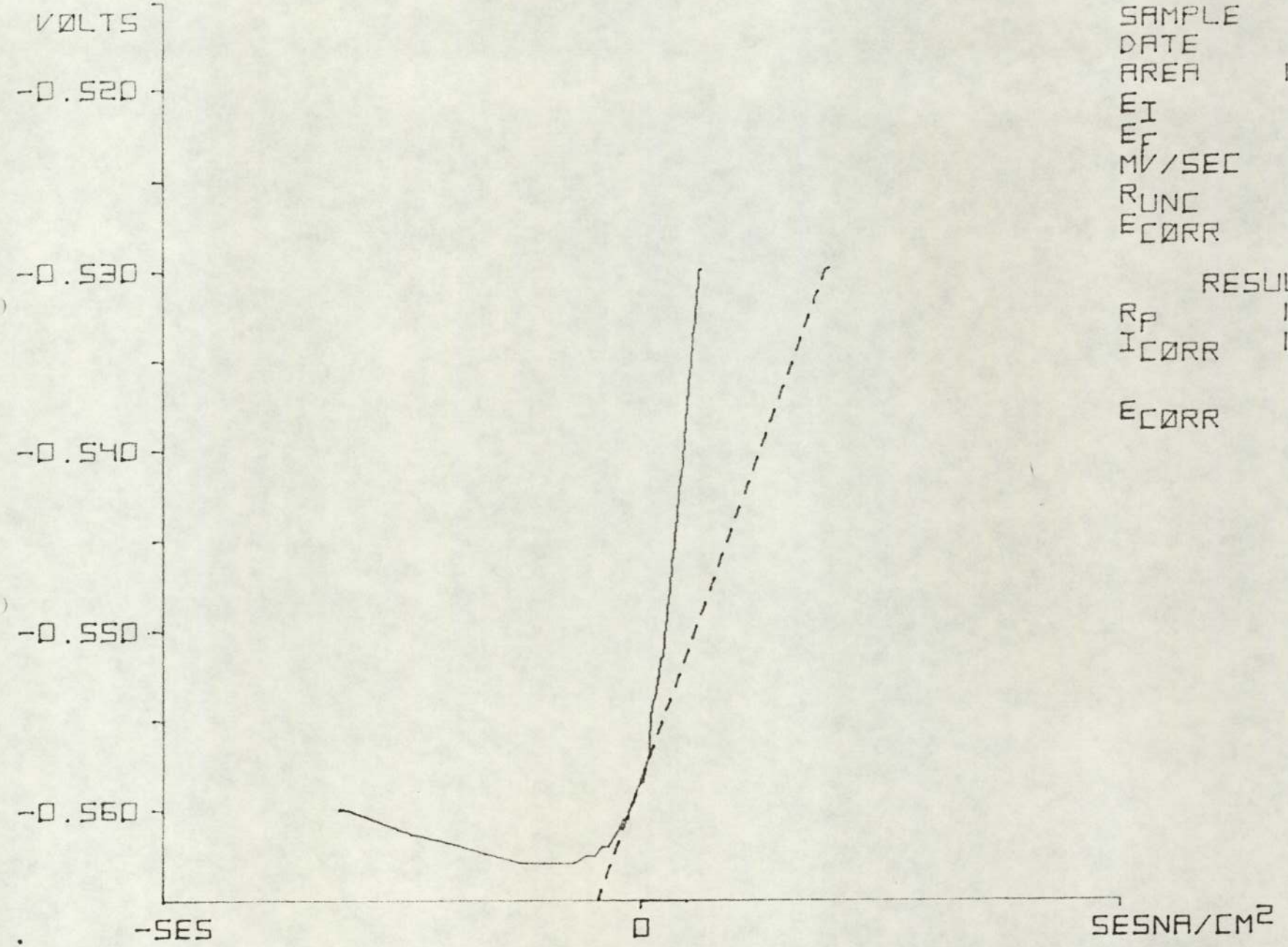

SAMPLE	1353
DATE	26.07
AREA	1.155E1
E_I	-0.568
E_F	-0.528
MV/SEC	0.166
R_{UNC}	2.228
$E_{CØRR}$	-0.548

RESULTS

R_P	1.475E2
$I_{CØRR}$	1.870E5
$E_{CØRR}$	-0.559

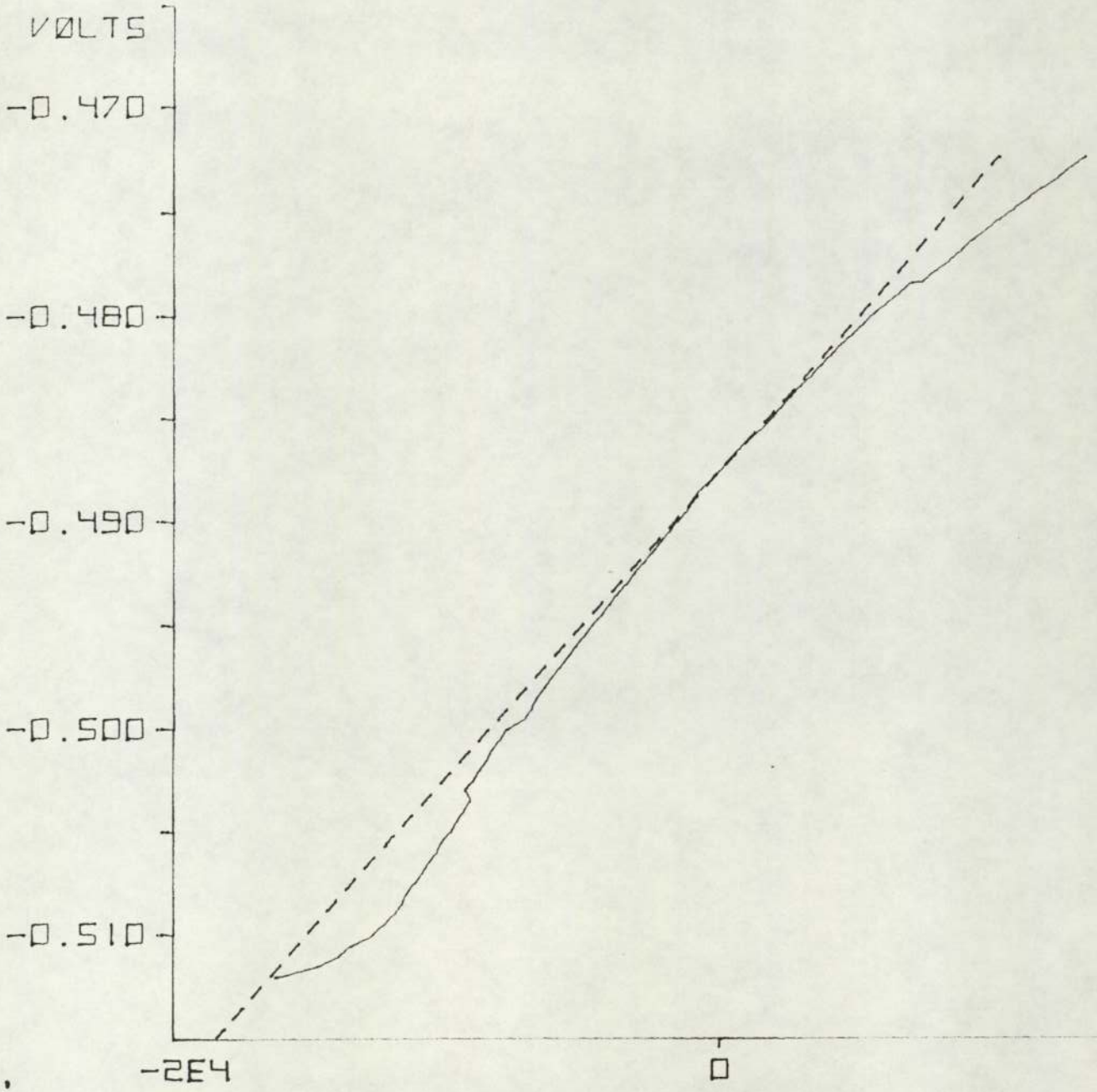

SAMPLE	4360
DATE	05.07
AREA	1.180E1
E_I	-0.512
E_f	-0.472
MV/SEC	0.166
R_{UNC}	0.848
$E_{CØRR}$	-0.492

RESULTS

R_P	1.476E3
$I_{CØRR}$	1.736E4
$E_{CØRR}$	-0.488

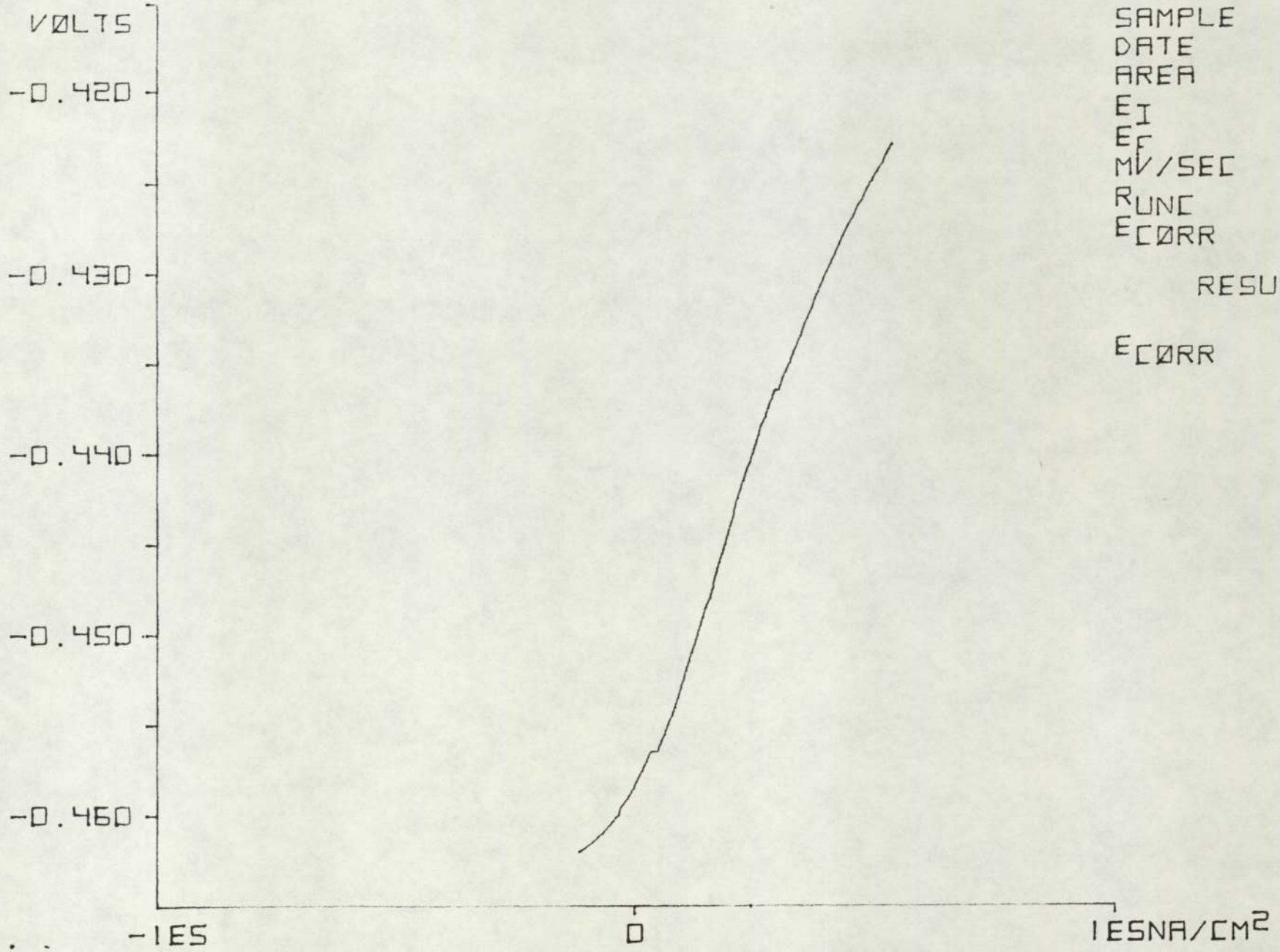

SAMPLE	6360
DATE	05.07
AREA	1.180E1
E_I	-0.462
E_F	-0.422
MV/SEC	0.166
R_{UNC}	1.632
$E_{CØRR}$	-0.442

RESULTS

$E_{CØRR}$	-0.459

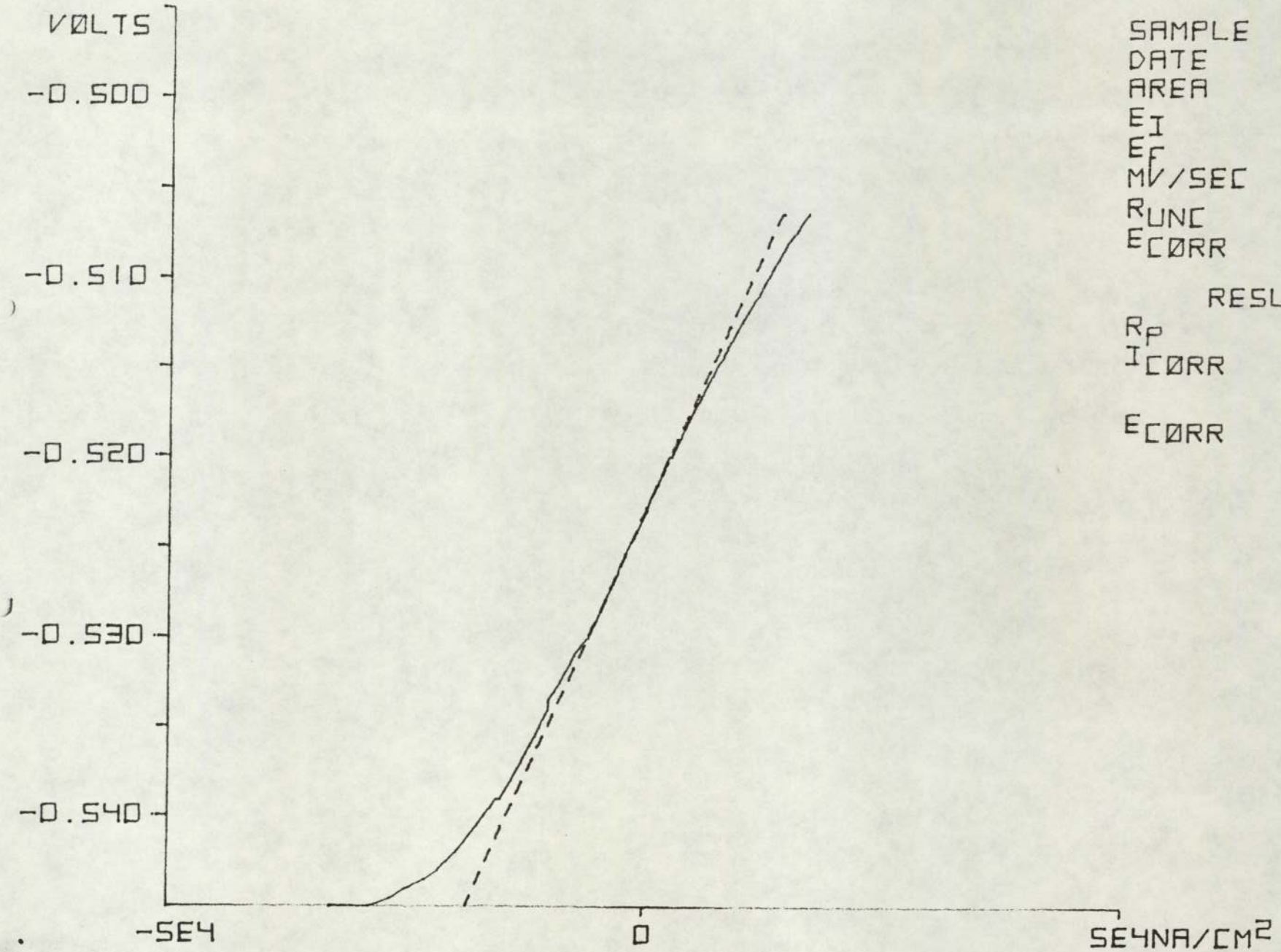

SAMPLE	1360
DATE	05.07
AREA	1.155E1
E_I	-0.546
E_f	-0.506
MV/SEC	0.166
R_{UNC}	2.463
$E_{CØRR}$	-0.526

RESULTS

R_P	1.177E3
$I_{CØRR}$	2.343E4
$E_{CØRR}$	-0.524

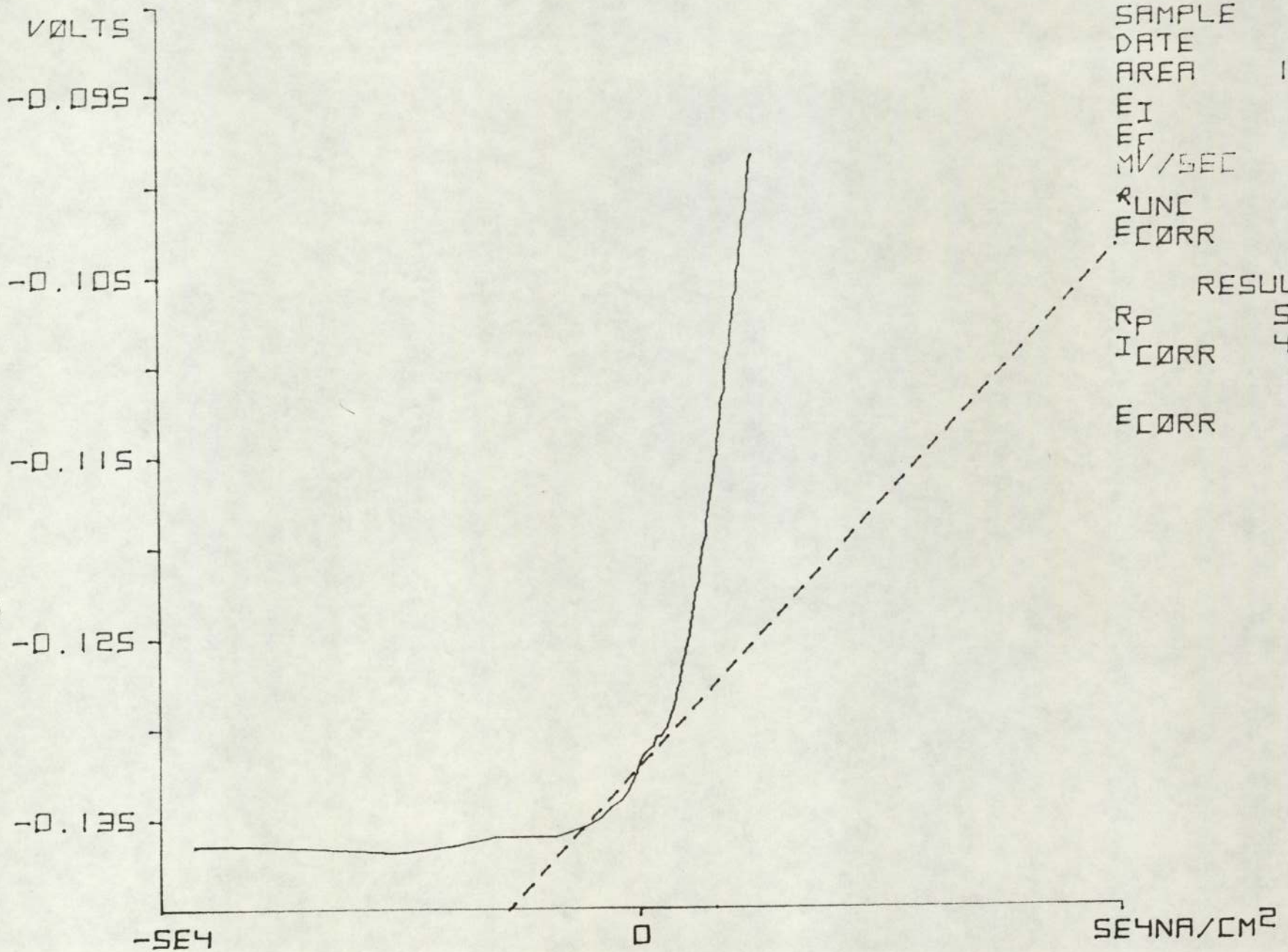
VØLTS
-0.095
-0.105
-0.115
-0.125
-0.135
-5E4
0
5E4NA/CM2
SAMPLE 4361
DATE 12.07
AREA 1.180E1
EI -0.138
EF -0.098
MV/SEC 0.166
*UNC 2.824
ECØRR -0.118
RESULTS
RP 5.779E2
ICØRR 4.434E4
ECØRR -0.133

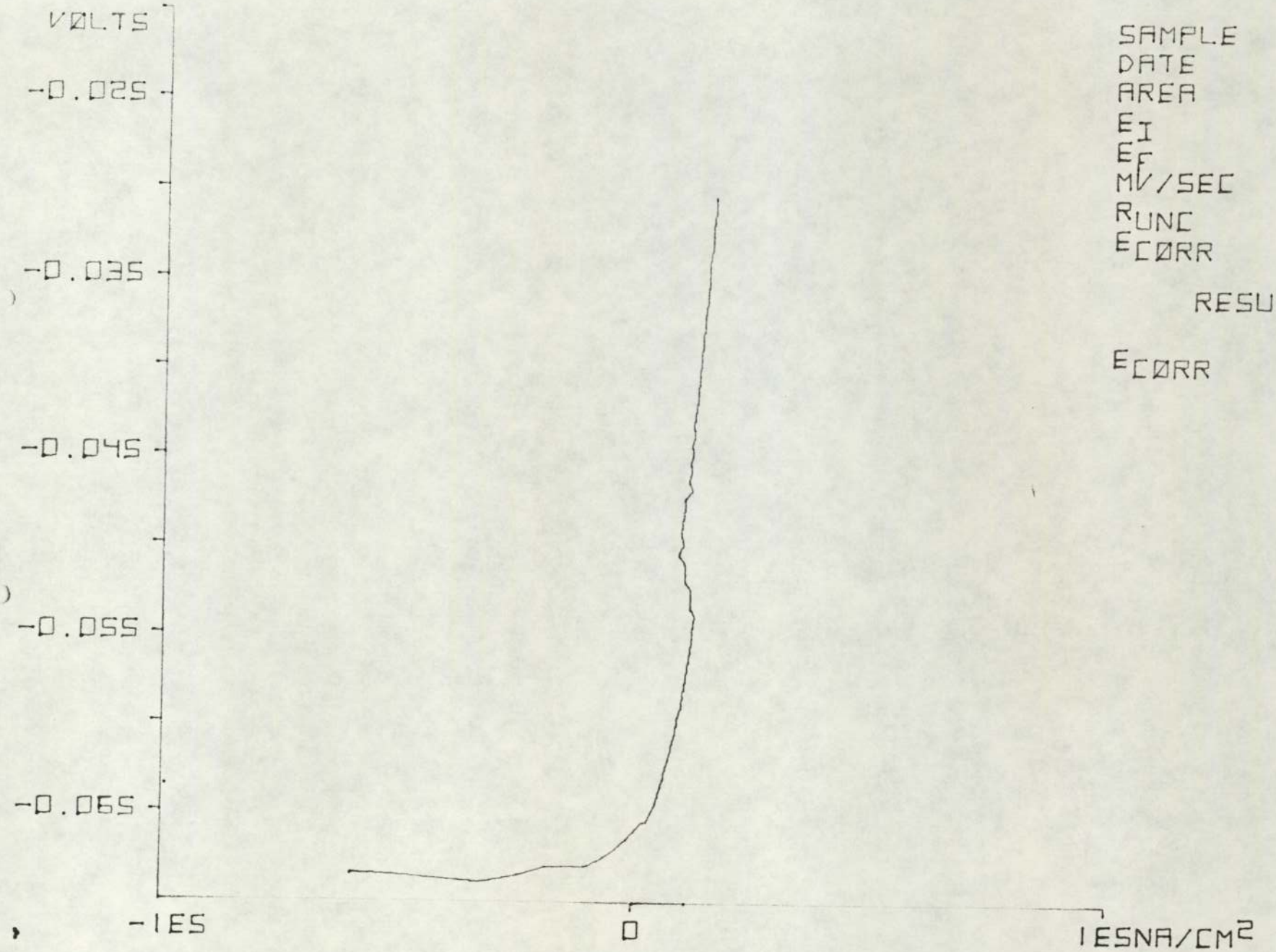

SAMPLE	6361
DATE	12.07
AREA	1.180E1
E_I	-0.070
E_F	-0.030
MV/SEC	0.166
R_{UNC}	2.199
$E_{CØRR}$	-0.050

RESULTS

$E_{CØRR}$ -0.067

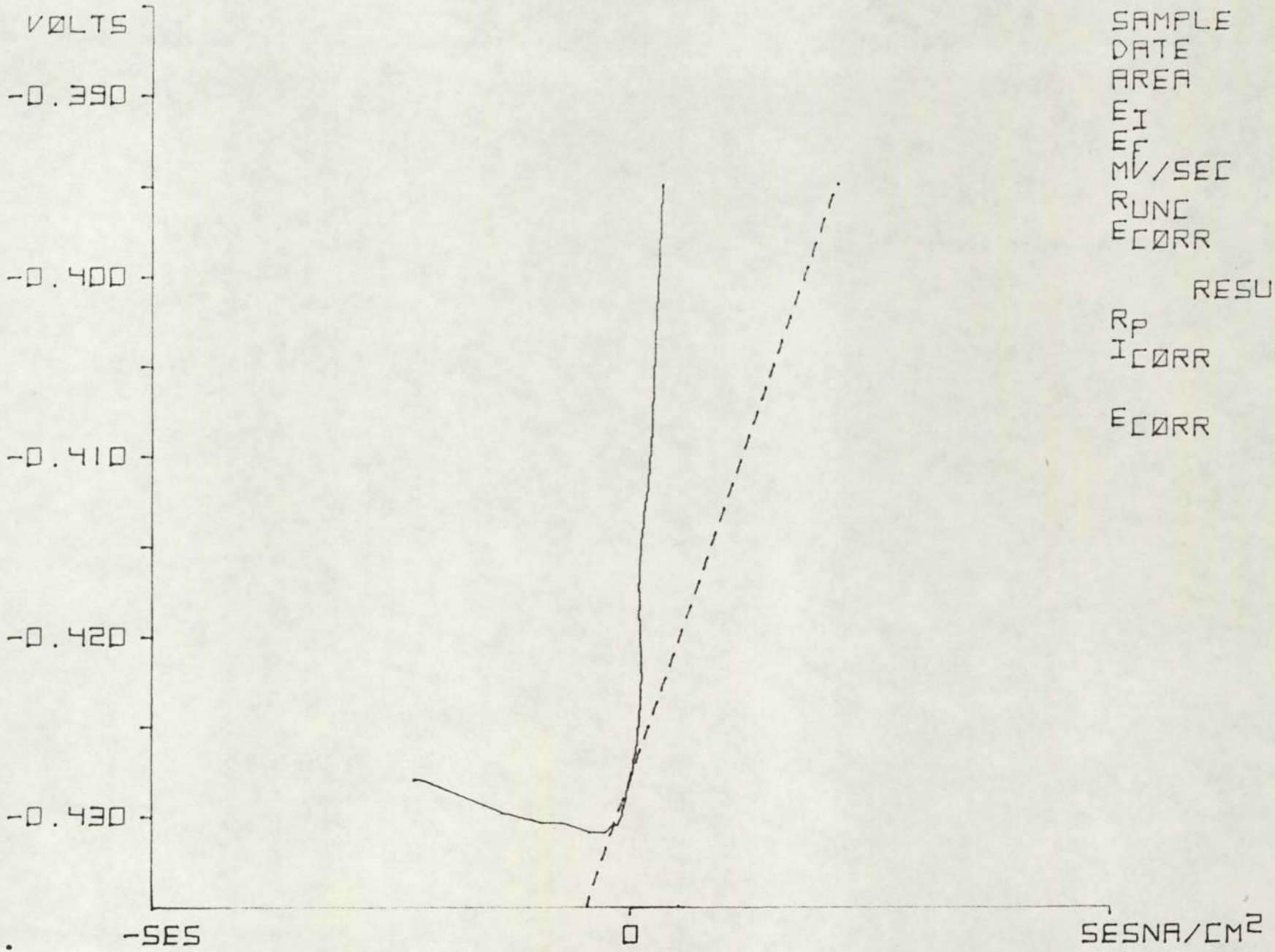

SAMPLE	1361
DATE	12.07
AREA	1.155E1
E_I	-0.434
E_f	-0.394
MV/SEC	0.166
R_{UNC}	2.365
$E_{CØRR}$	-0.414

RESULTS

R_P	1.545E2
$I_{CØRR}$	1.785E5
$E_{CØRR}$	-0.428

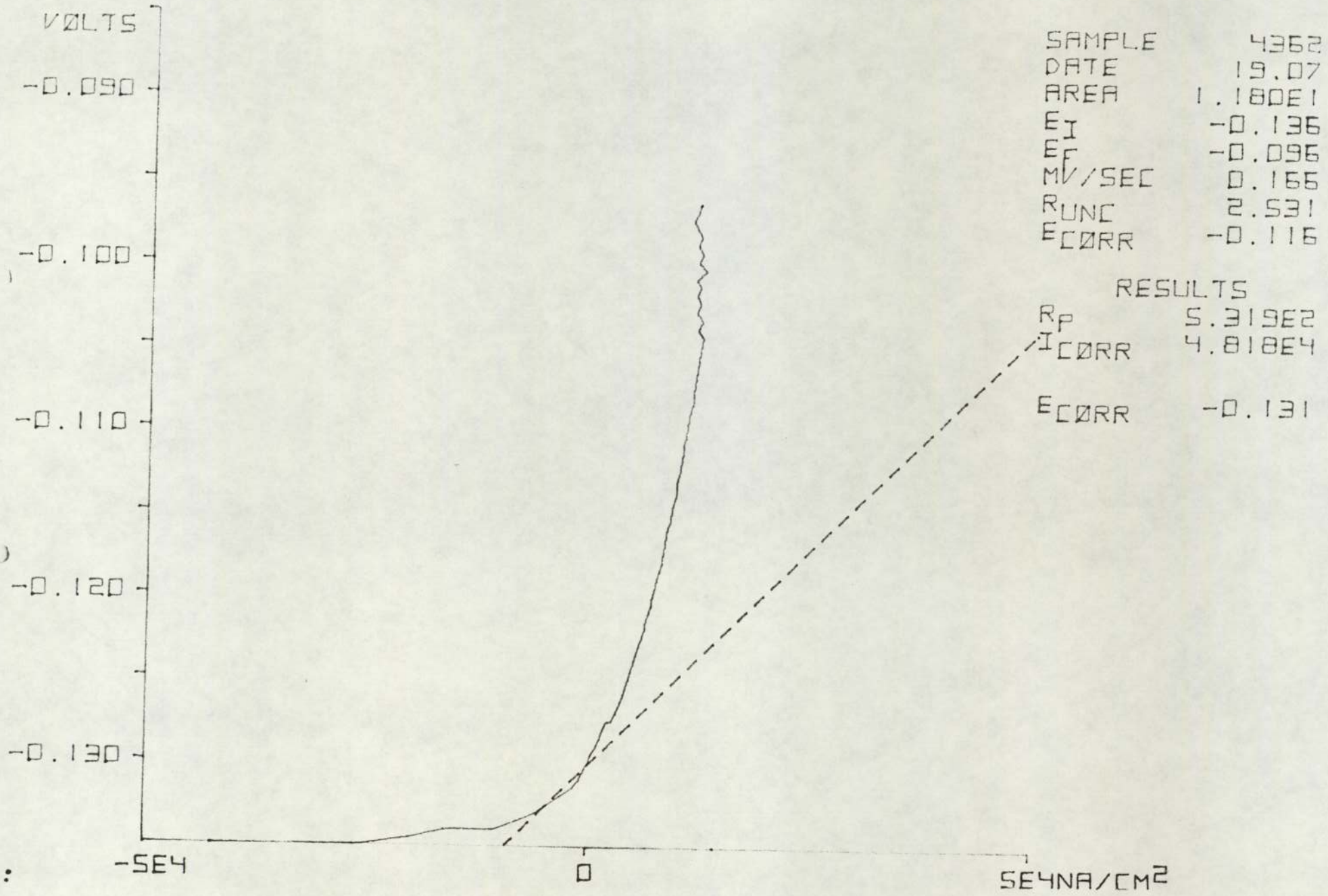
VØLTS
-0.090
-0.100
-0.110
-0.120
-0.130
-5E4
0
5E4NA/CM2
SAMPLE 4362
DATE 19.07
AREA 1.180E1
EI -0.136
EF -0.096
MV/SEC 0.166
RUNC 2.531
ECØRR -0.116
RESULTS
RP 5.319E2
ICØRR 4.818E4
ECØRR -0.131

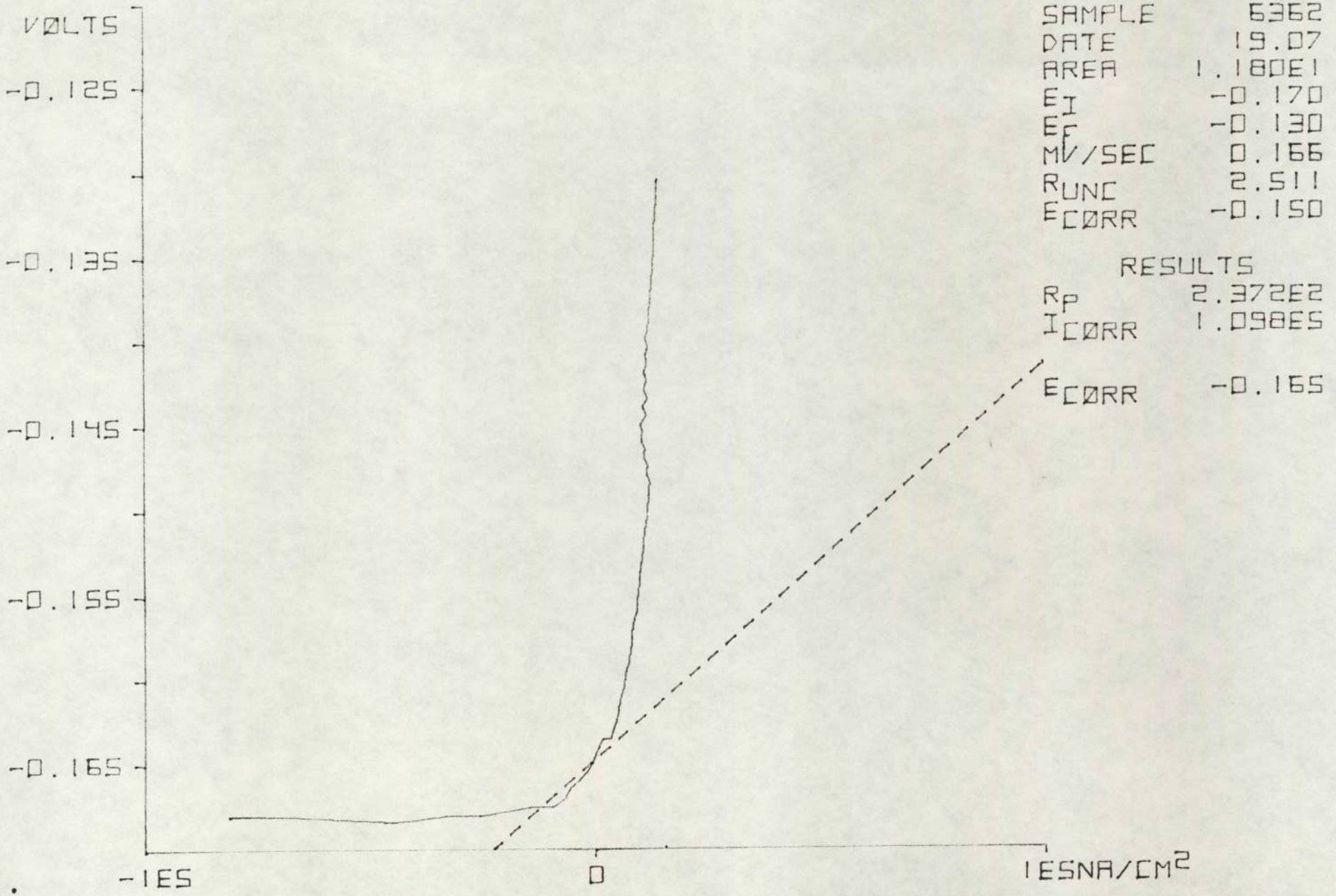

SAMPLE	6362
DATE	19.07
AREA	1.180E1
E_I	-0.170
E_F	-0.130
MV/SEC	0.166
R_{UNC}	2.511
$E_{CØRR}$	-0.150

RESULTS

R_P	2.372E2
$I_{CØRR}$	1.098E5
$E_{CØRR}$	-0.165

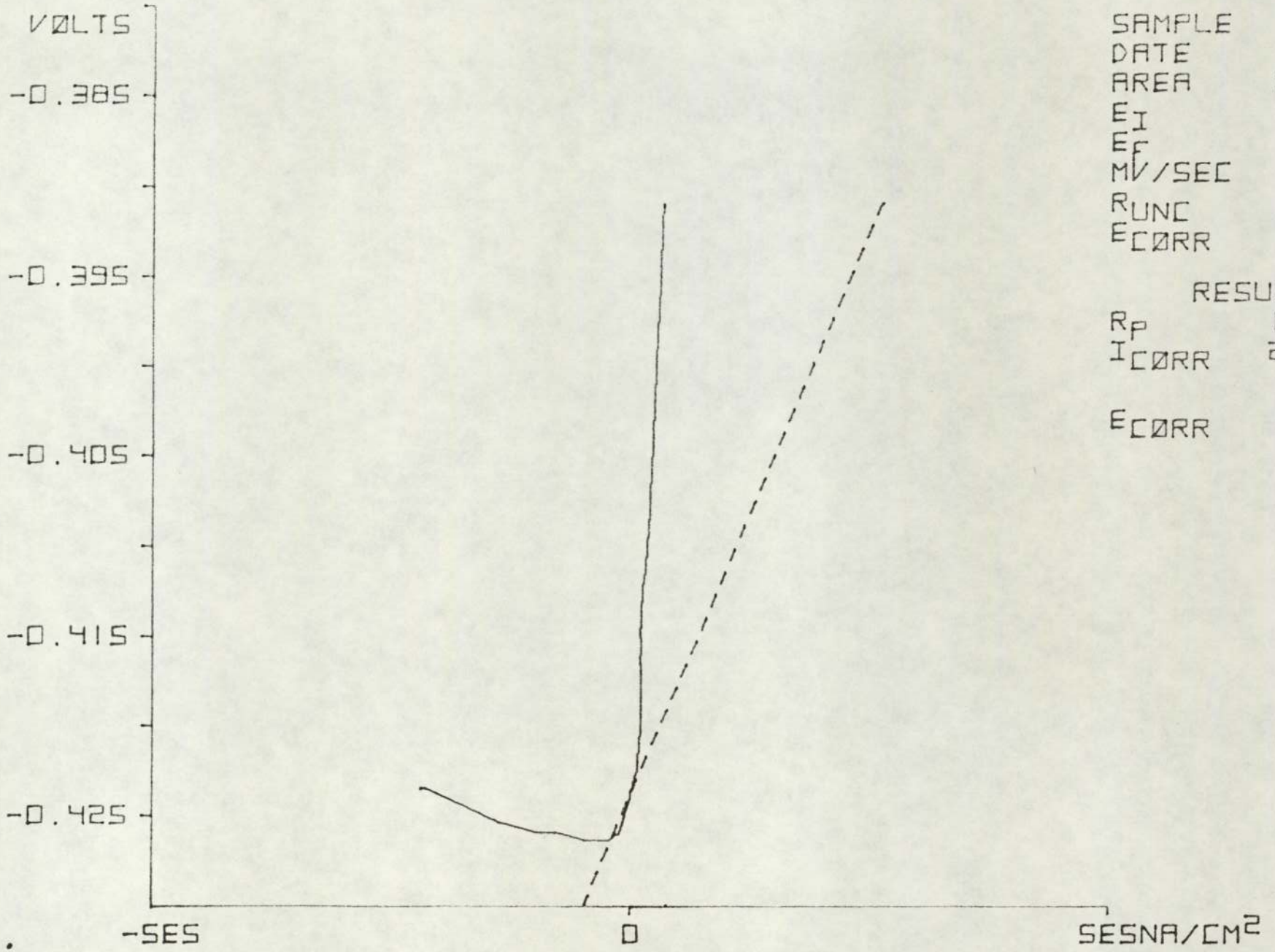

SAMPLE	1362
DATE	19.07
AREA	1.155E1
E_I	-0.430
E_F	-0.390
MV/SEC	0.166
R_{UNC}	2.717
$E_{CØRR}$	-0.410

RESULTS

R_P	1.255E2
$I_{CØRR}$	2.196E5
$E_{CØRR}$	-0.424

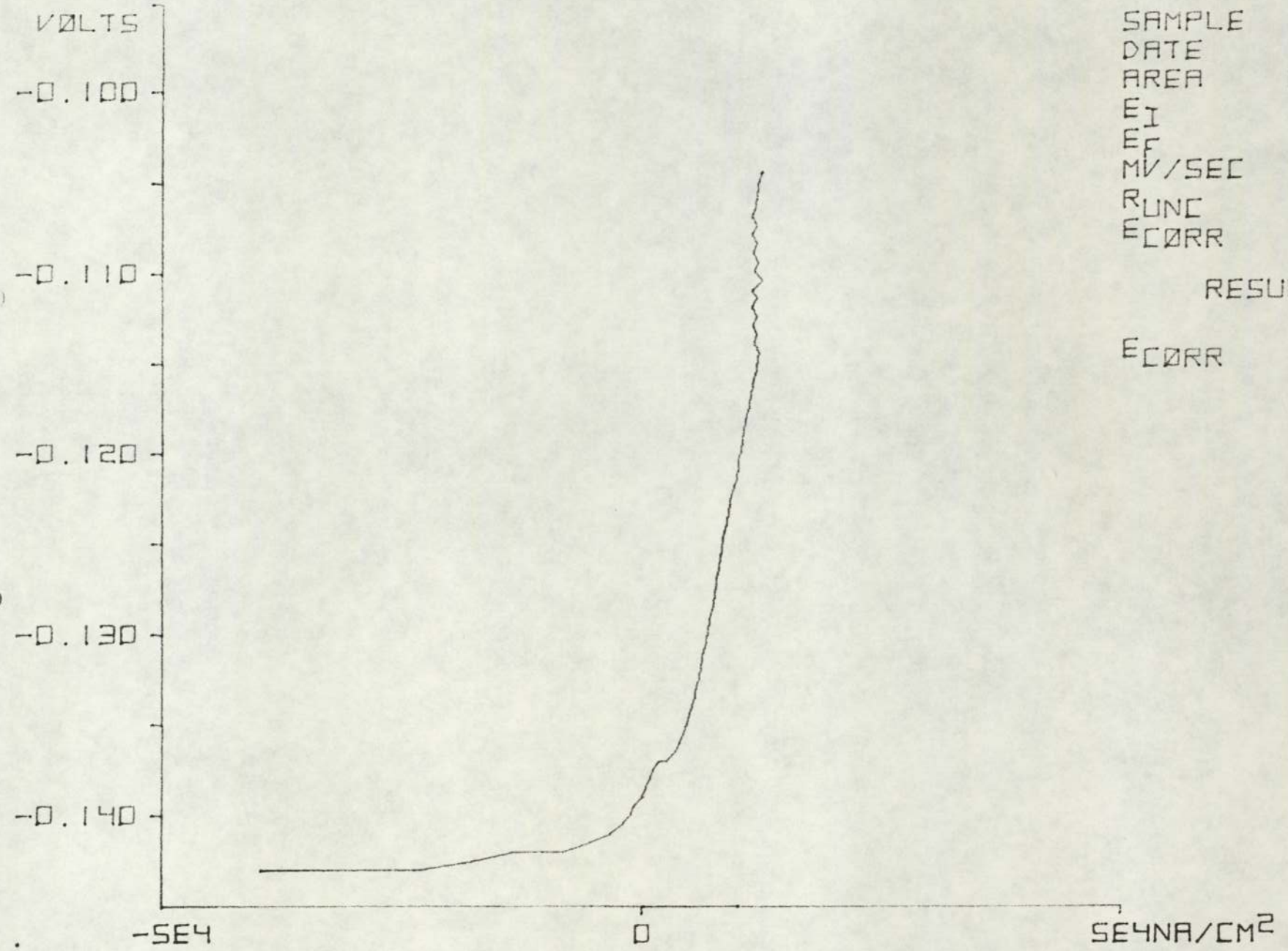

SAMPLE	4363
DATE	26.07
AREA	1.180E1
E_I	-0.144
E_F	-0.104
MV/SEC	0.166
R_{UNC}	2.727
$E_{CØRR}$	-0.124

RESULTS

$E_{CØRR}$ -0.139

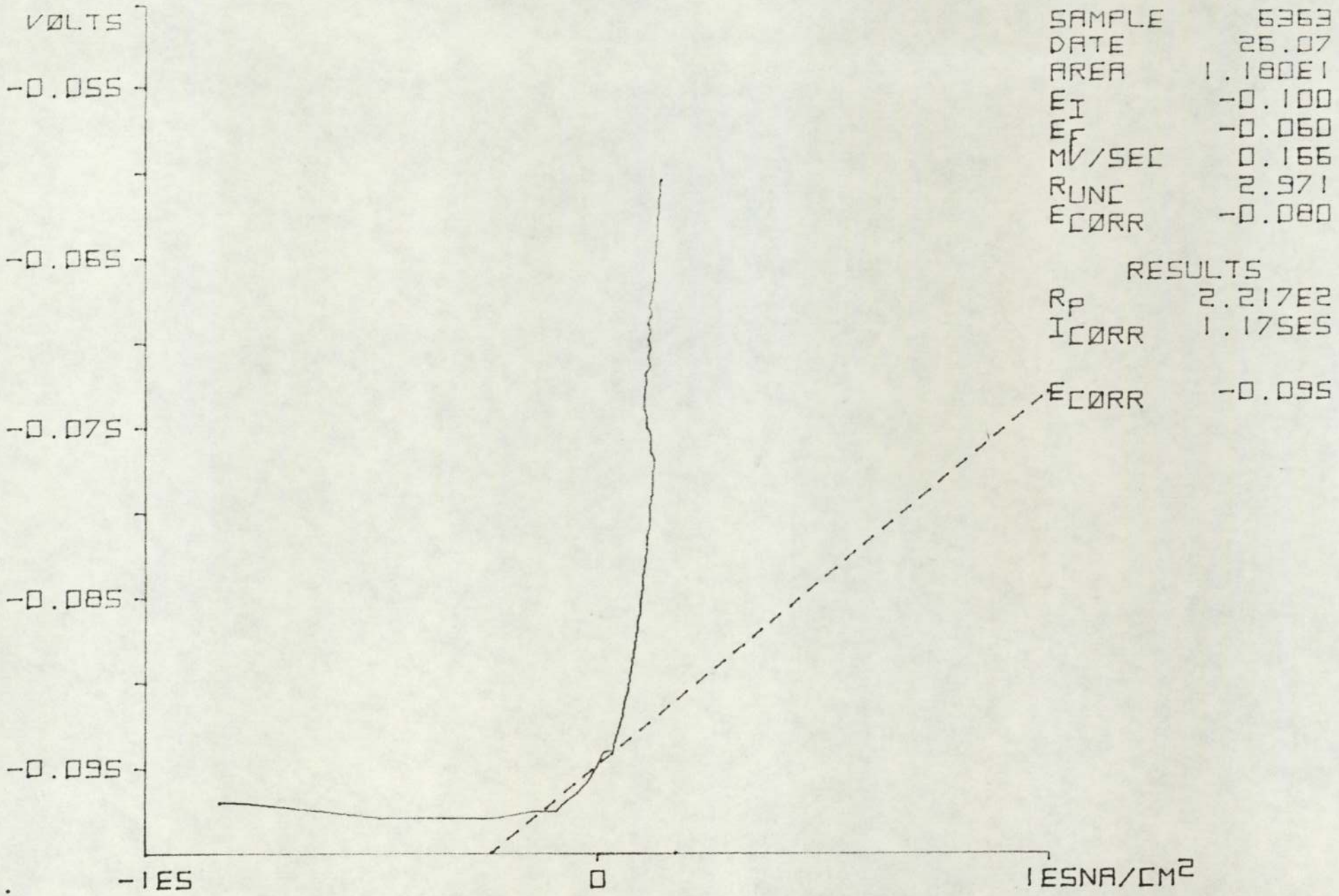

SAMPLE	6363
DATE	26.07
AREA	1.180E1
E_I	-0.100
E_F	-0.060
MV/SEC	0.166
R_{UNC}	2.971
$E_{CØRR}$	-0.080

RESULTS

R_P	2.217E2
$I_{CØRR}$	1.175E5
$E_{CØRR}$	-0.095

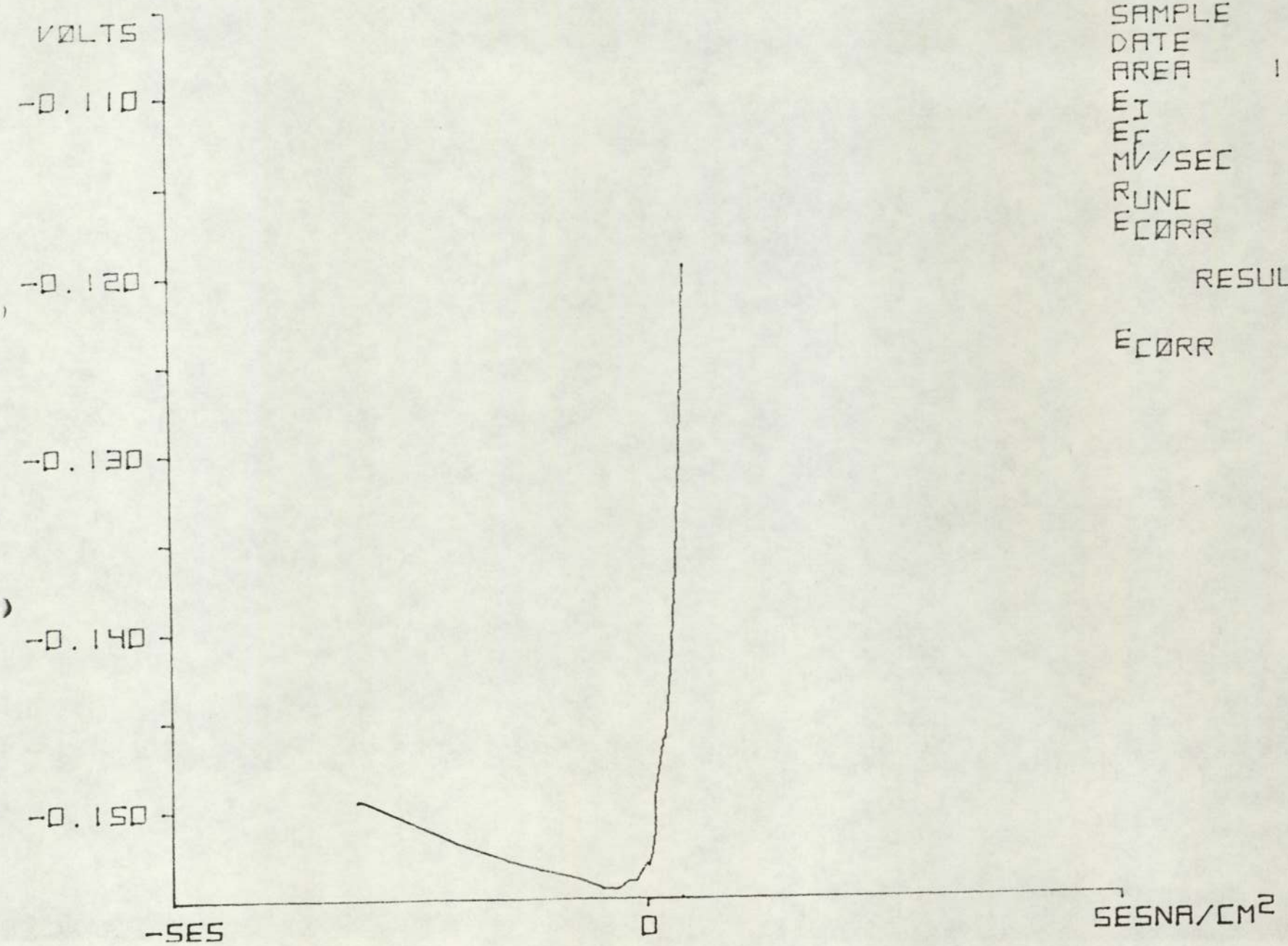

SAMPLE	1363
DATE	26.07
AREA	1.155E1
E_I	-0.158
E_F	-0.118
MV/SEC	0.166
R_{UNC}	2.492
$E_{CØRR}$	-0.138

RESULTS

$E_{CØRR}$ -0.153

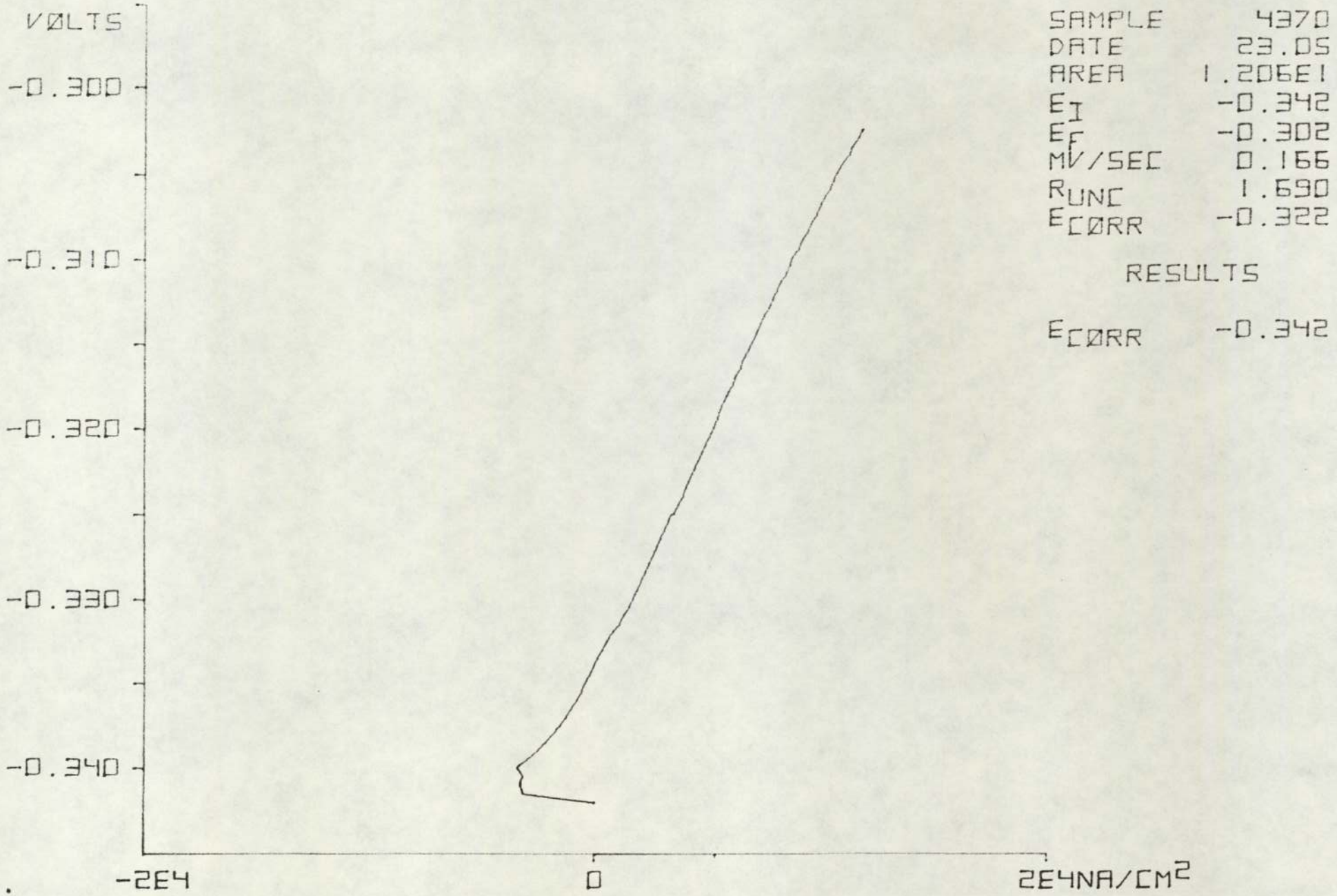

SAMPLE	4370
DATE	23.05
AREA	1.206E1
E_I	-0.342
E_F	-0.302
MV/SEC	0.166
R_{UNC}	1.690
$E_{CØRR}$	-0.322

RESULTS

$E_{CØRR}$	-0.342

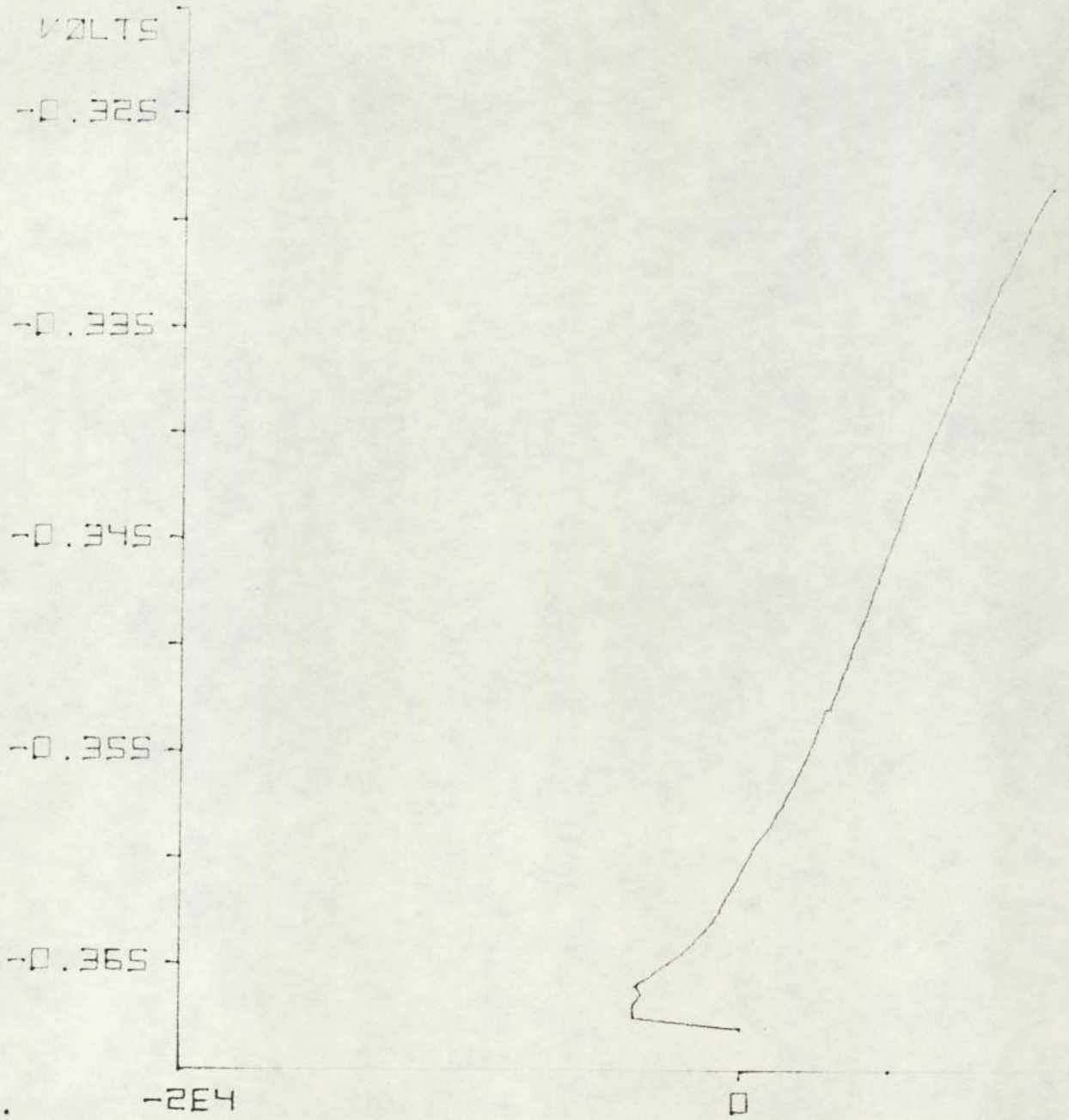

SAMPLE	6370
DATE	23.05
AREA	1.1SEE1
E_I	-0.366
E_f	-0.328
MV/SEC	0.166
RUNC	1.993
E_{CORR}	-0.348

RESULTS

E_{CORR} -0.368

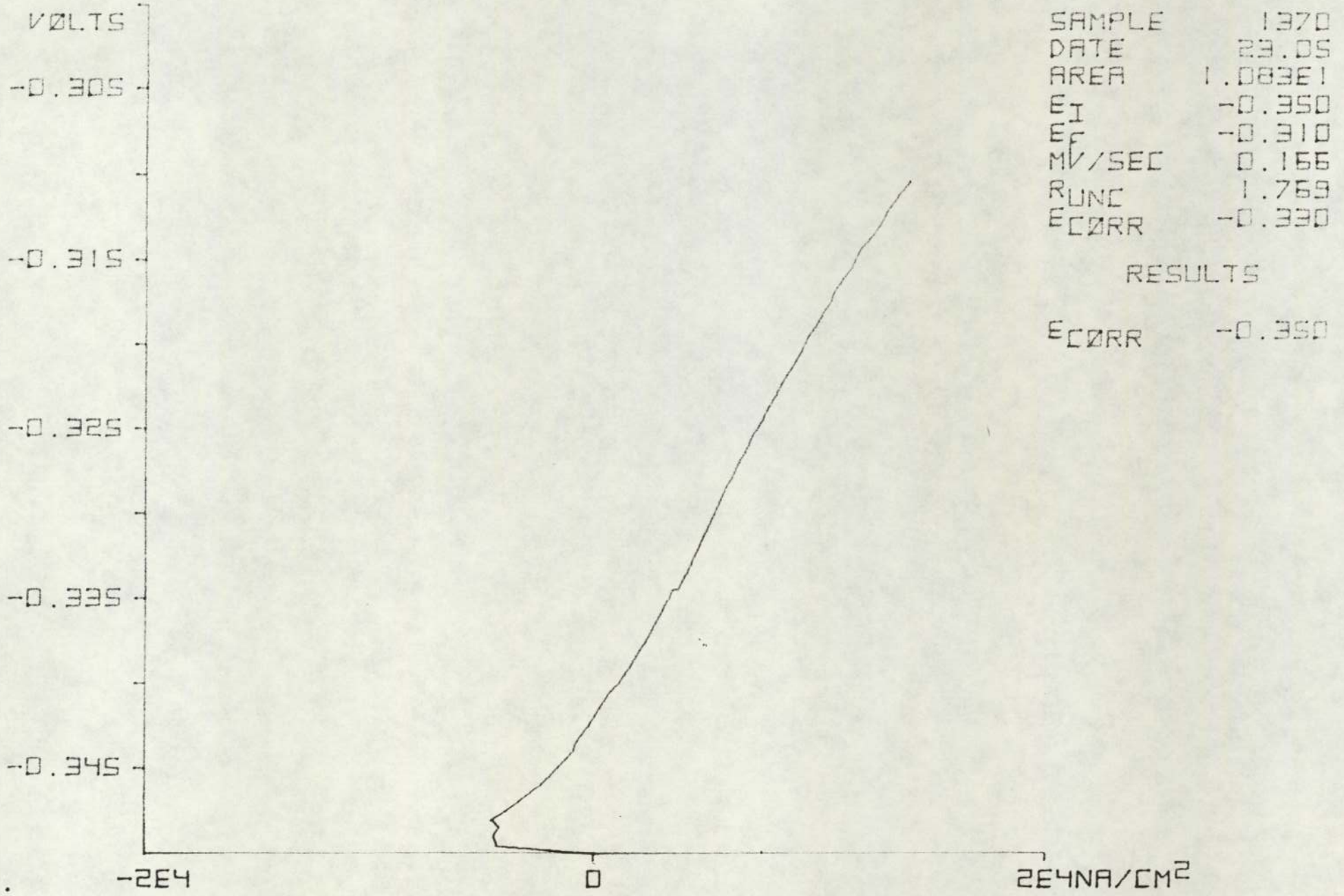

SAMPLE	1370
DATE	23.05
AREA	1.083E1
E_I	-0.350
E_f	-0.310
MV/SEC	0.166
R_{UNC}	1.769
$E_{CØRR}$	-0.330

RESULTS

$E_{CØRR}$	-0.350

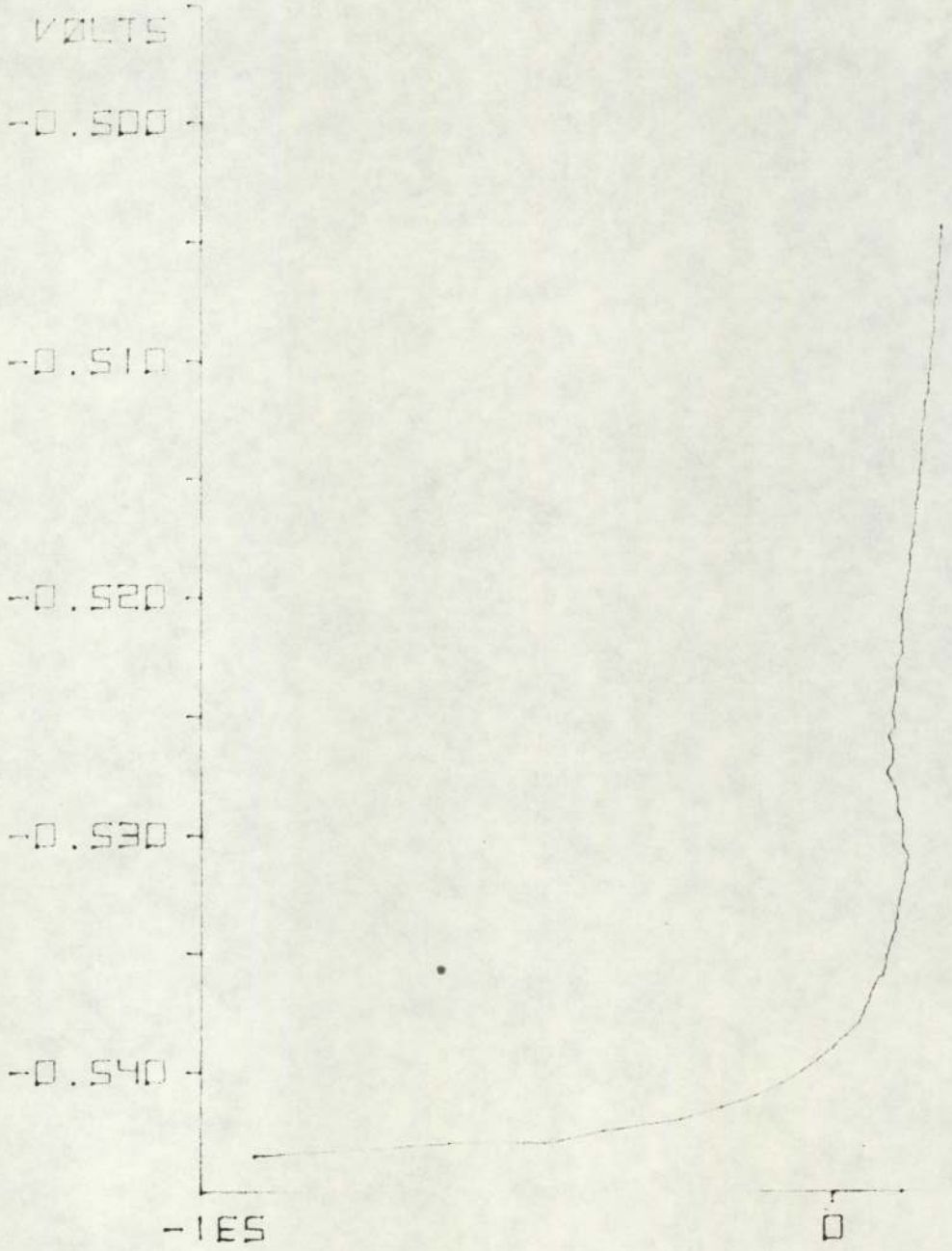

SAMPLE	4371
DATE	30.05
AREA	1.206E1
EI	-0.544
EF	-0.504
MV/SEC	0.166
RUNC	0.780
ECORR	-0.524

RESULTS

ECORR	-0.539

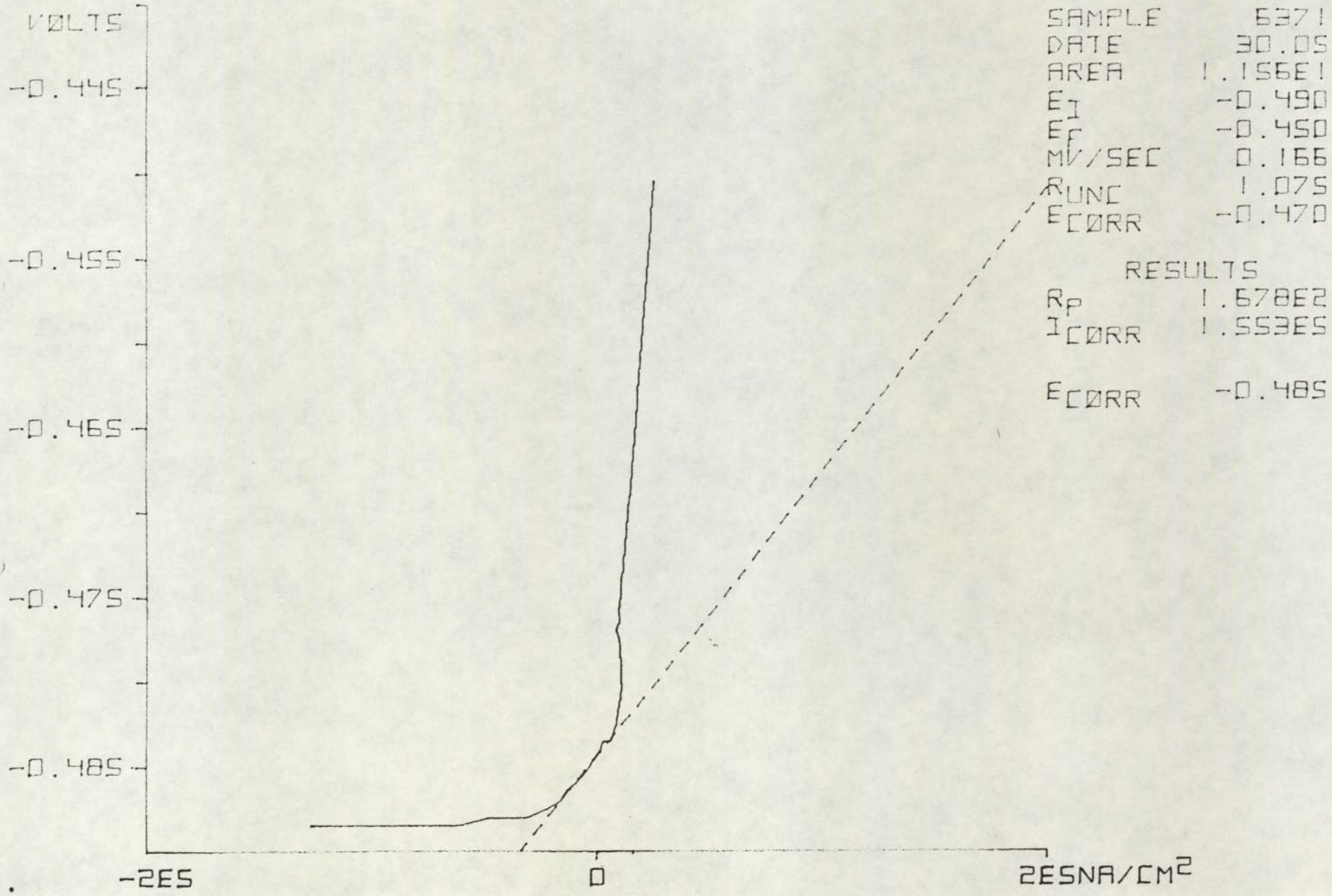

SAMPLE	6371
DATE	30.05
AREA	1.156E1
E_I	-0.490
E_F	-0.450
MV/SEC	0.166
R_{UNC}	1.075
E_{CORR}	-0.470

RESULTS

R_P	1.678E2
I_{CORR}	1.553E5
E_{CORR}	-0.485

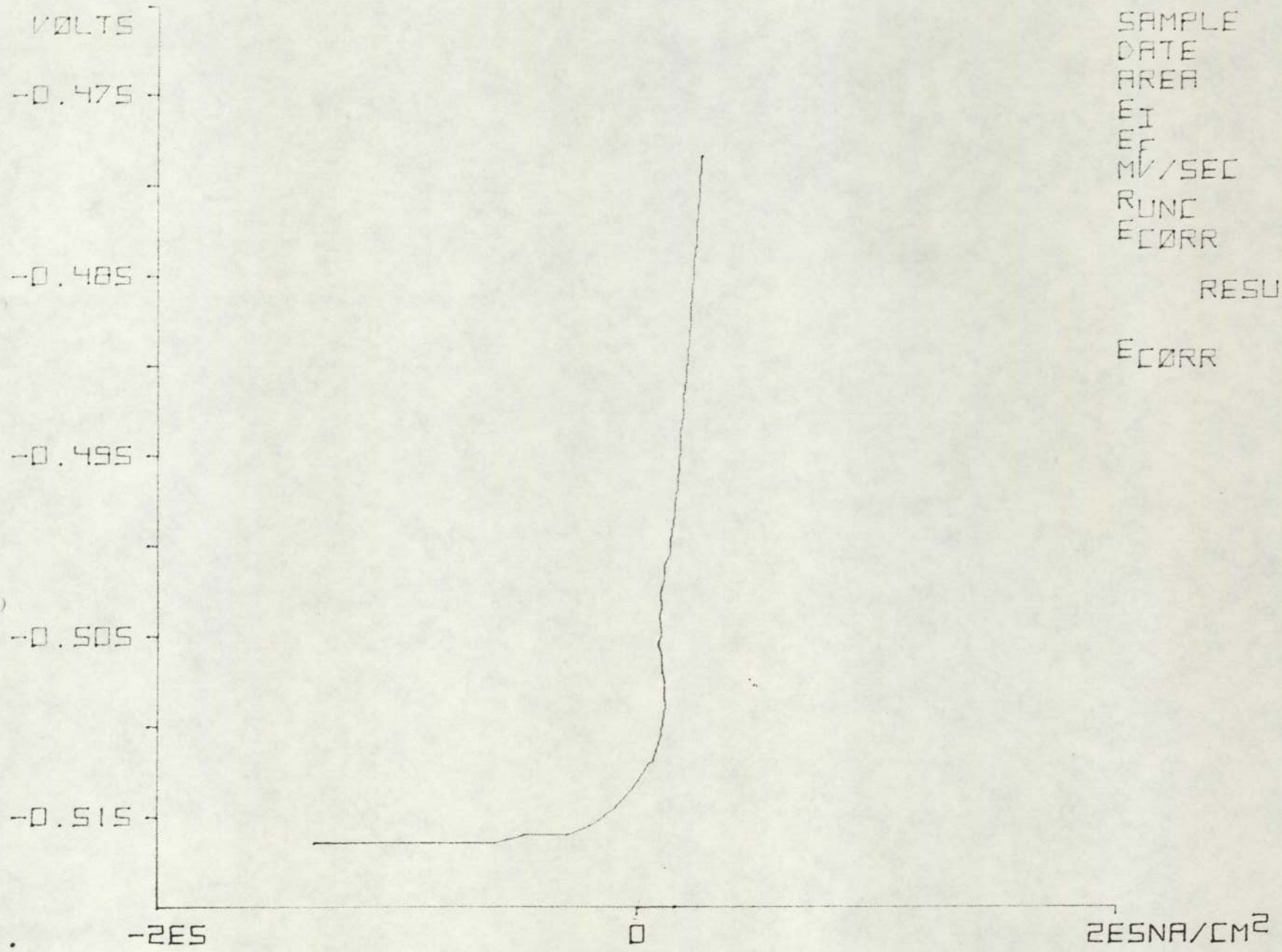

SAMPLE	1371
DATE	30.05
AREA	1.083E1
E_I	-0.518
E_f	-0.478
MV/SEC	0.166
R_{UNC}	1.192
$E_{CØRR}$	-0.498

RESULTS

$E_{CØRR}$ -0.514

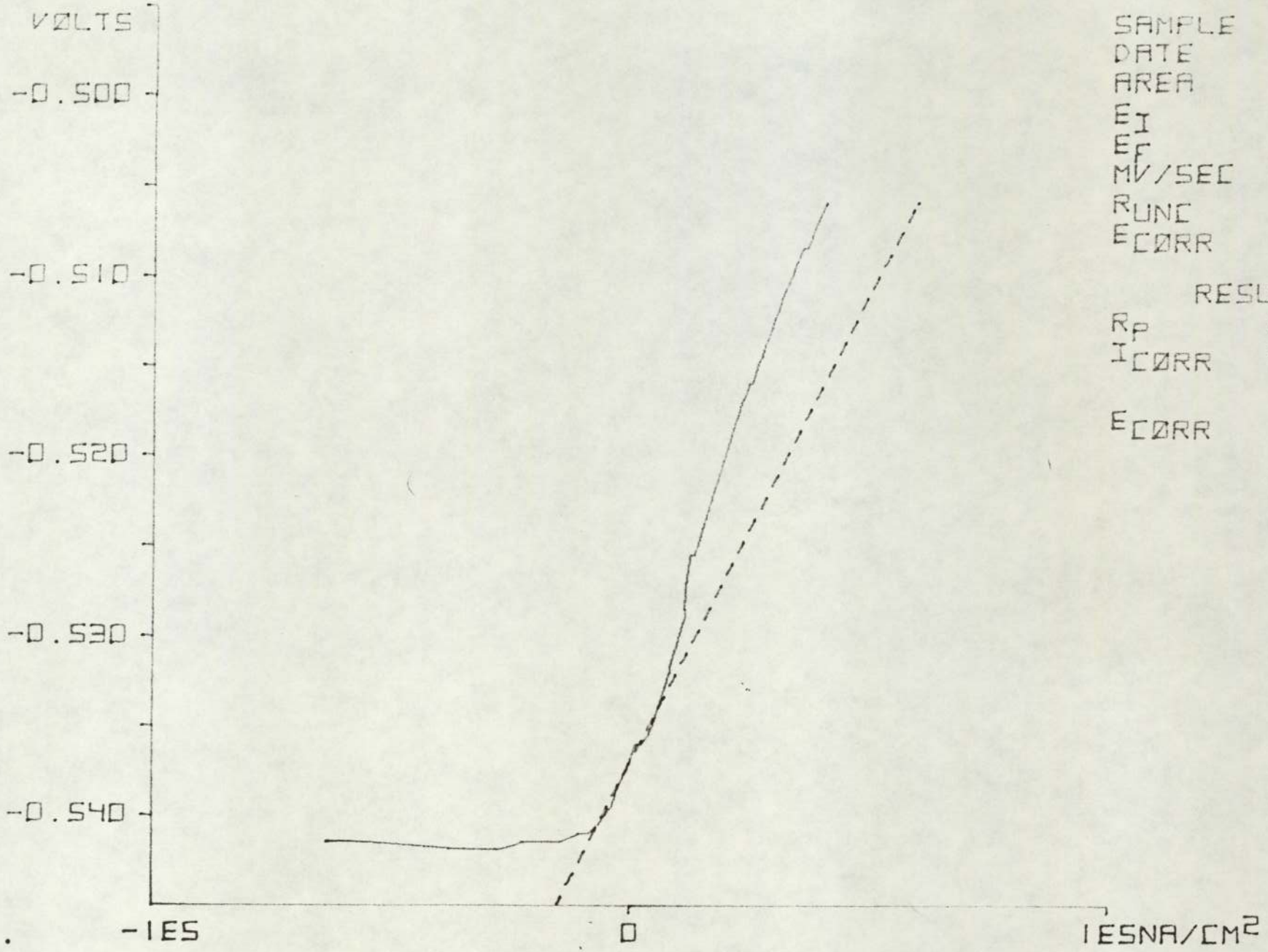

SAMPLE	4372
DATE	06.06
AREA	1.206E1
E_I	-0.544
E_f	-0.504
MV/SEC	0.166
R_{UNC}	3.606
E_{CORR}	-0.524

RESULTS

R_P	5.208E2
I_{CORR}	4.920E4
E_{CORR}	-0.537

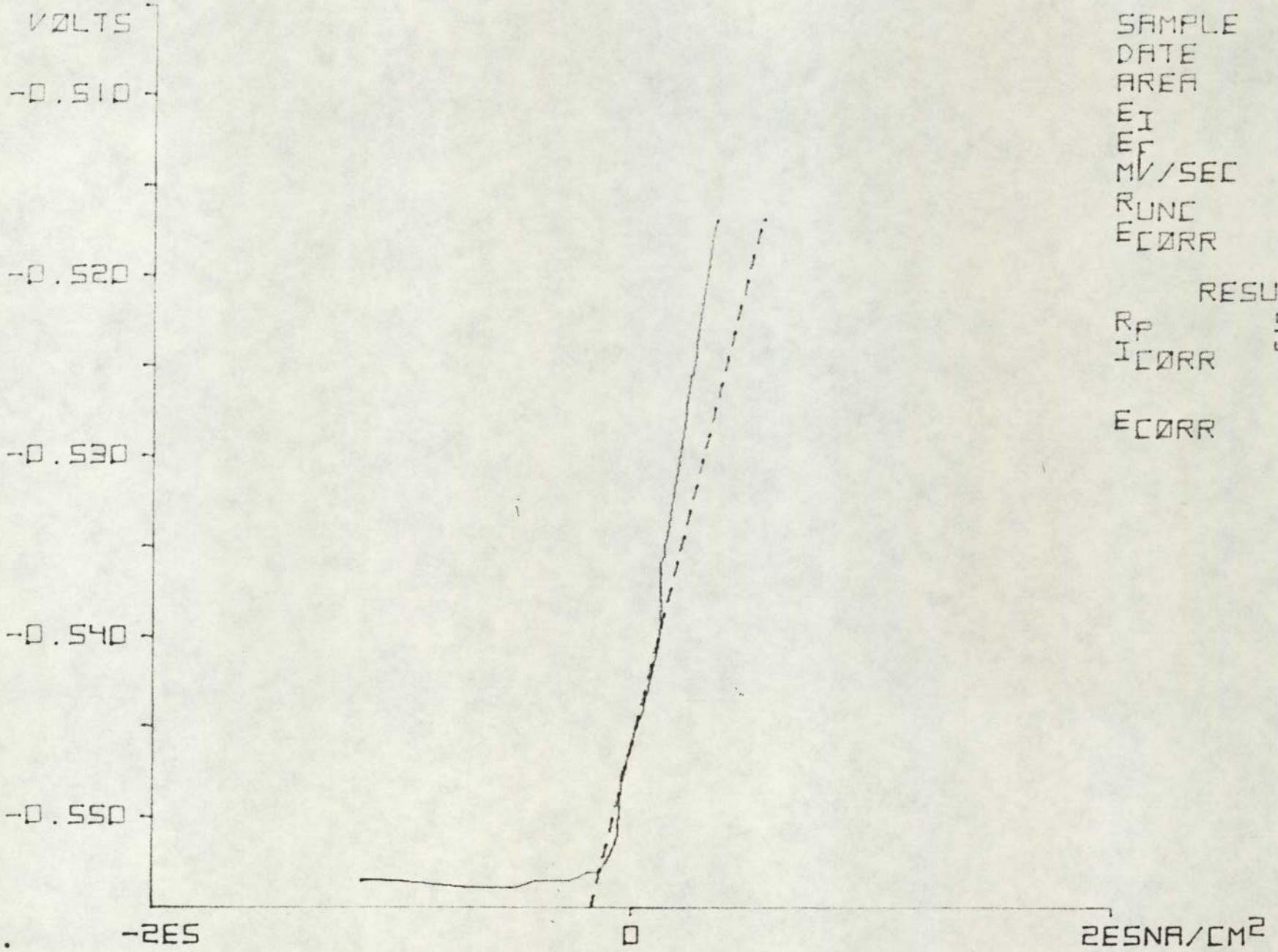

SAMPLE	6372
DATE	06.06
AREA	1.156E1
E_I	-0.556
E_F	-0.516
MV/SEC	0.166
R_{UNC}	2.081
$E_{CØRR}$	-0.536

RESULTS

R_P	5.436E2
$I_{CØRR}$	4.793E4
$E_{CØRR}$	-0.546

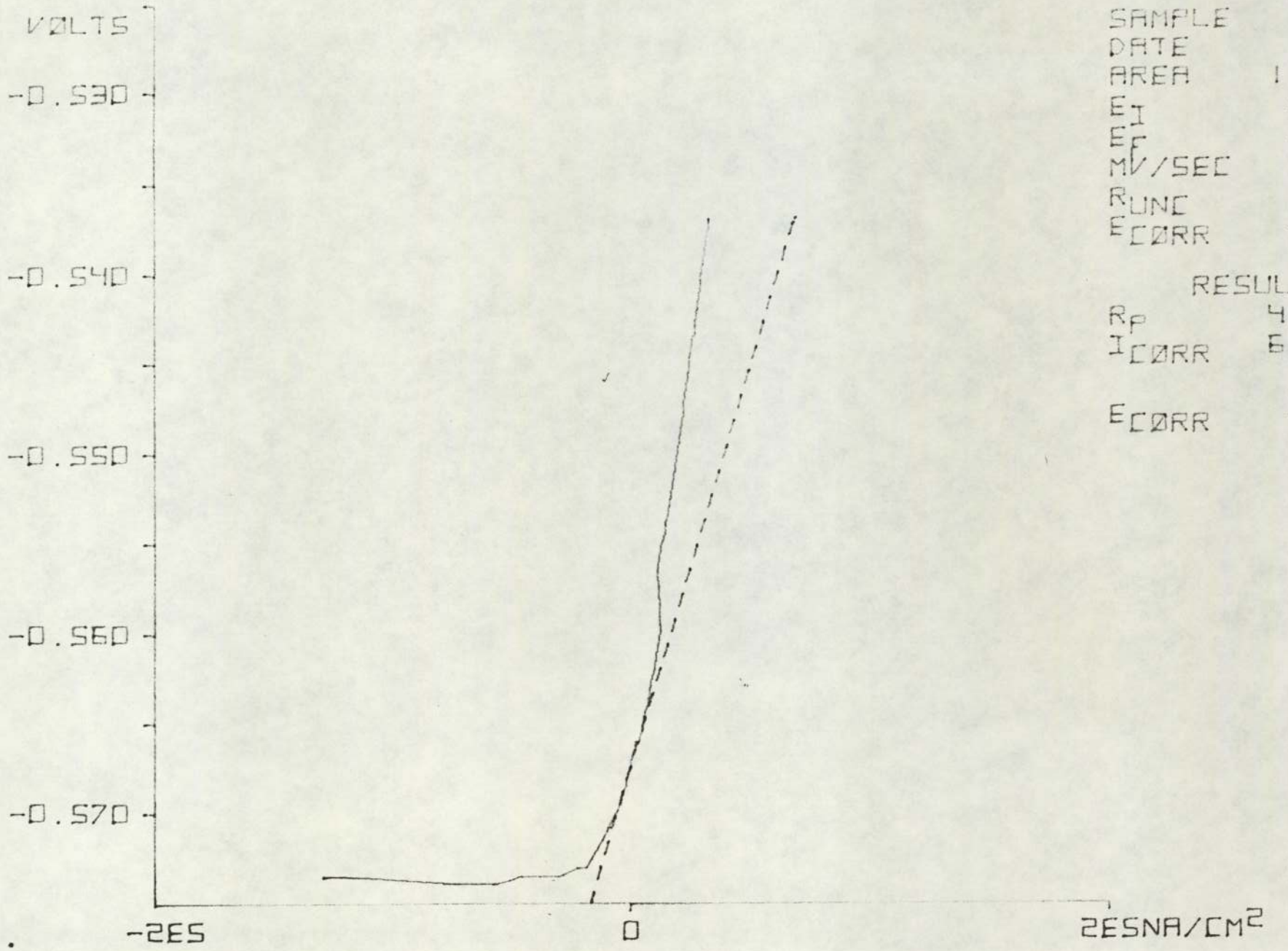

SAMPLE	1372
DATE	06.06
AREA	1.083E1
E_I	-0.576
E_f	-0.536
MV/SEC	0.166
RUNC	2.052
E_{CORR}	-0.556

RESULTS

R_P	4.480E2
I_{CORR}	6.155E4
E_{CORR}	-0.568

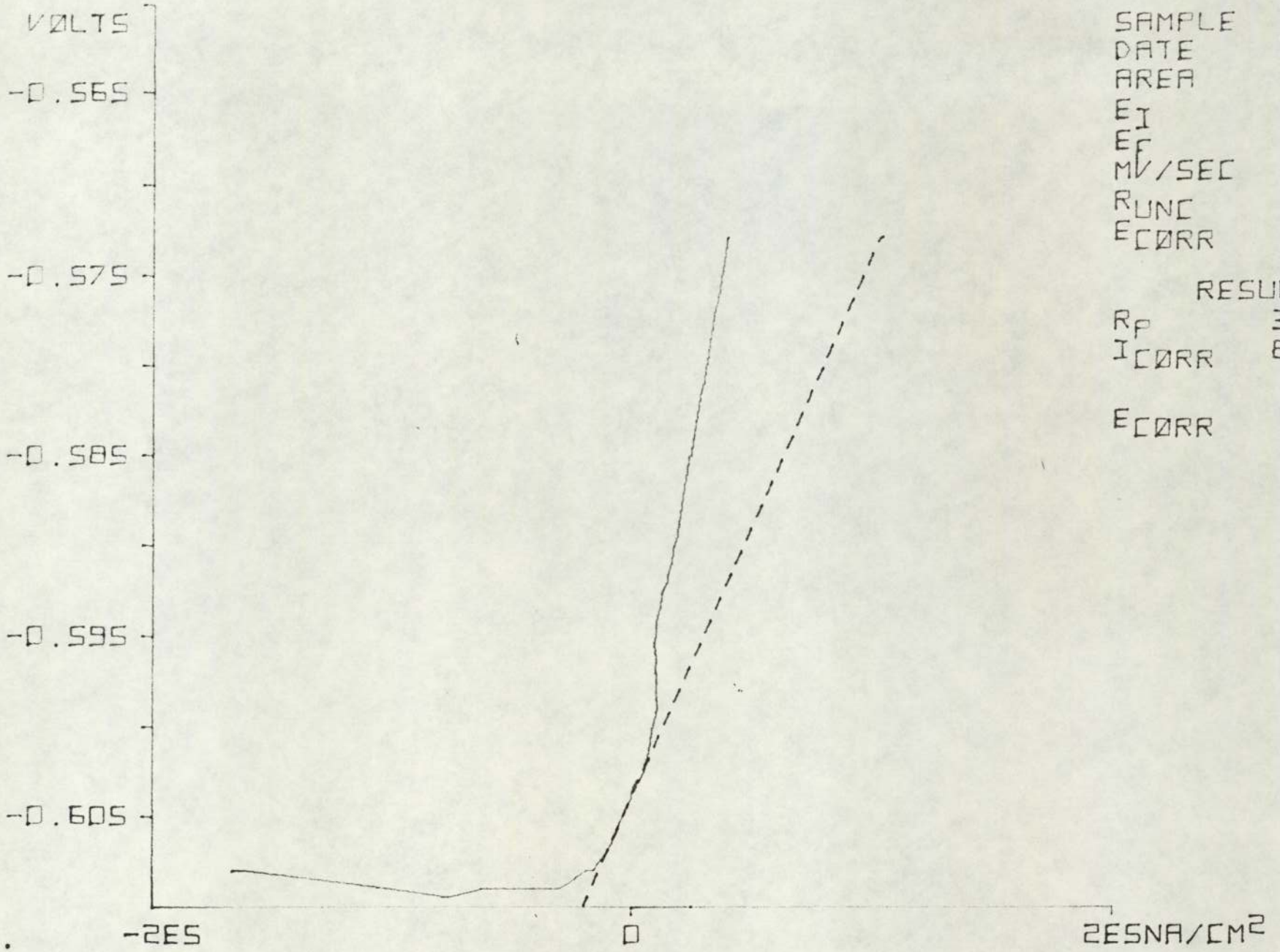

SAMPLE	4373
DATE	13.06
AREA	1.206E1
E_I	-0.612
E_f	-0.572
MV/SEC	0.166
R_{UNC}	1.984
$E_{CØRR}$	-0.592

RESULTS

R_P	3.007E2
$I_{CØRR}$	8.522E4
$E_{CØRR}$	-0.604

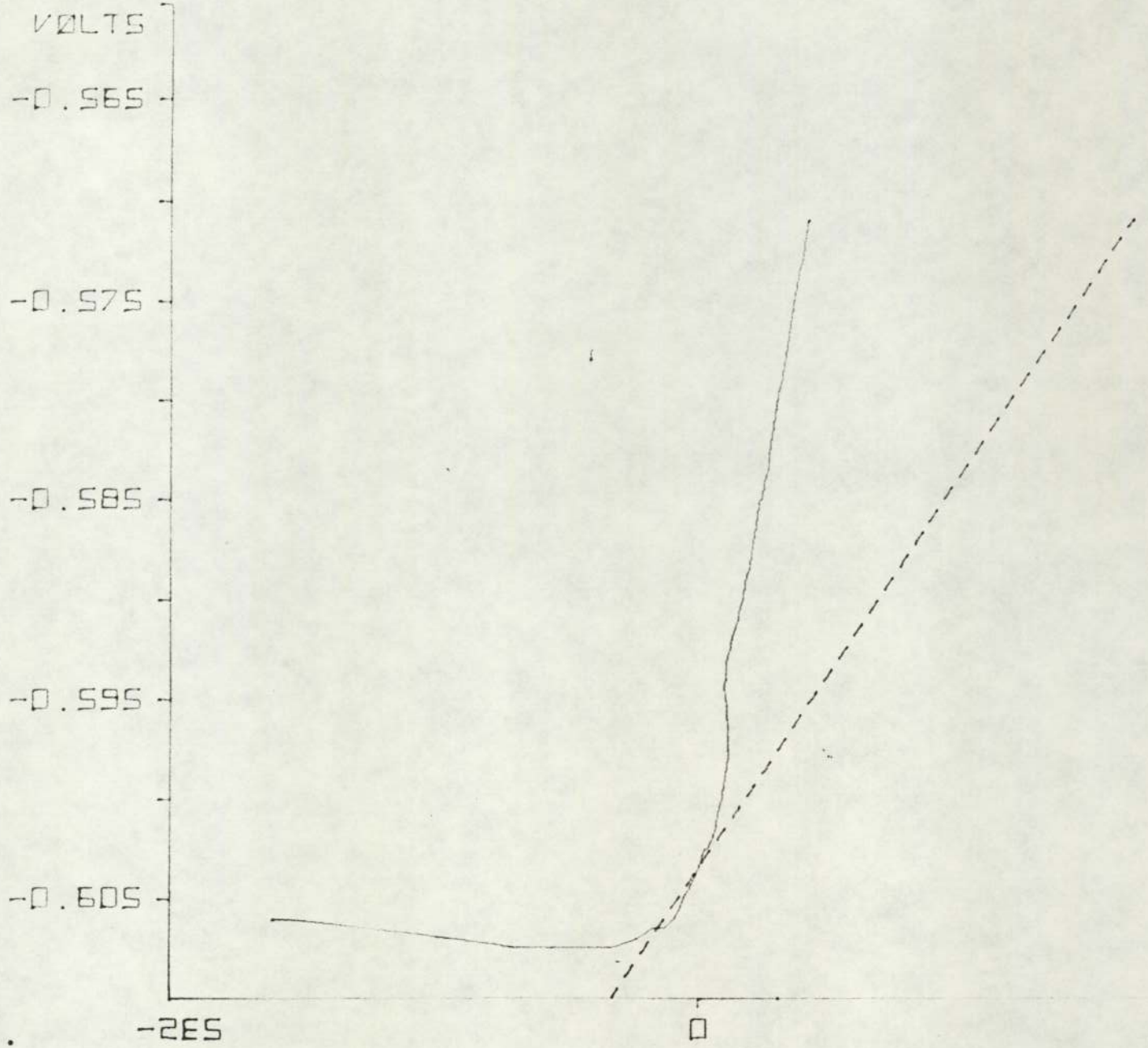

SAMPLE	6373
DATE	13.06
AREA	1.156E1
E_I	-0.610
E_f	-0.570
MV/SEC	0.166
R_{UNC}	2.169
$E_{CØRR}$	-0.590

RESULTS

R_P	1.994E2
$I_{CØRR}$	1.307E5
$E_{CØRR}$	-0.604

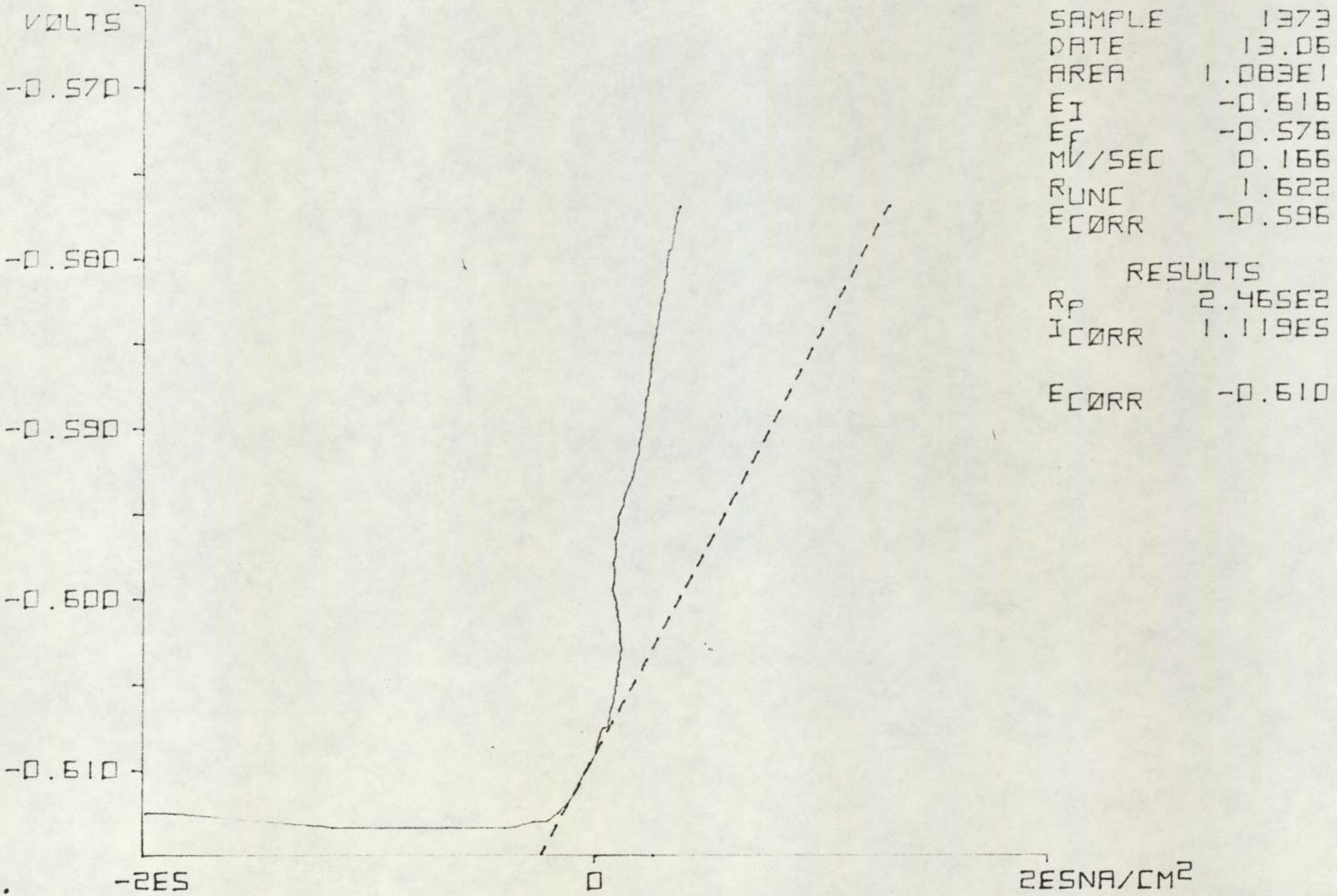

SAMPLE	1373
DATE	13.06
AREA	1.083E1
E_I	-0.616
E_f	-0.576
MV/SEC	0.166
R_{UNC}	1.622
$E_{CØRR}$	-0.596

RESULTS

R_p	2.465E2
$I_{CØRR}$	1.119E5
$E_{CØRR}$	-0.610

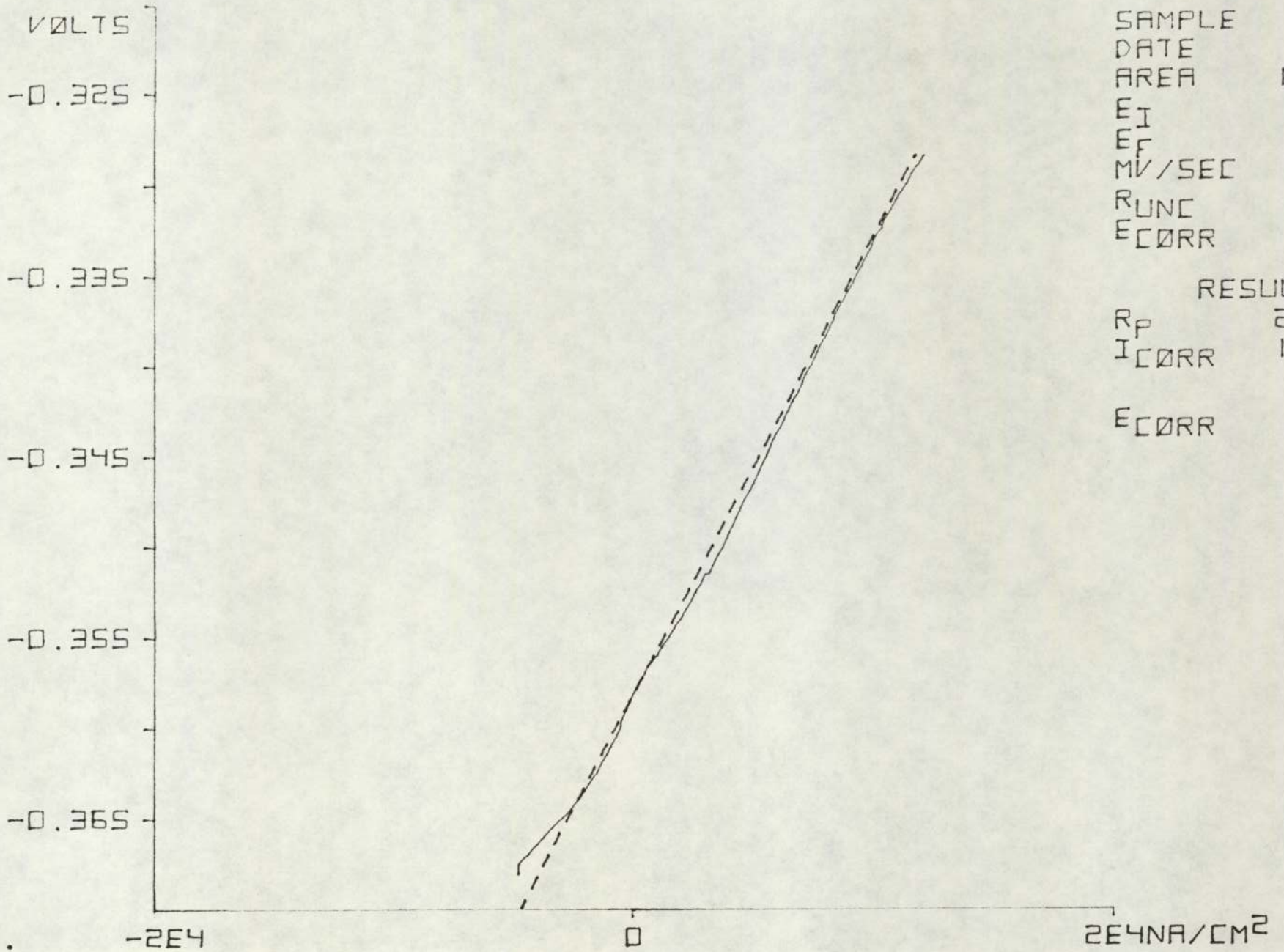

SAMPLE	4380
DATE	23.05
AREA	1.206E1
E_I	-0.368
E_F	-0.328
MV/SEC	0.166
R_{UNC}	1.945
$E_{CØRR}$	-0.348

RESULTS

R_P	2.532E3
$I_{CØRR}$	1.012E4
$E_{CØRR}$	-0.359

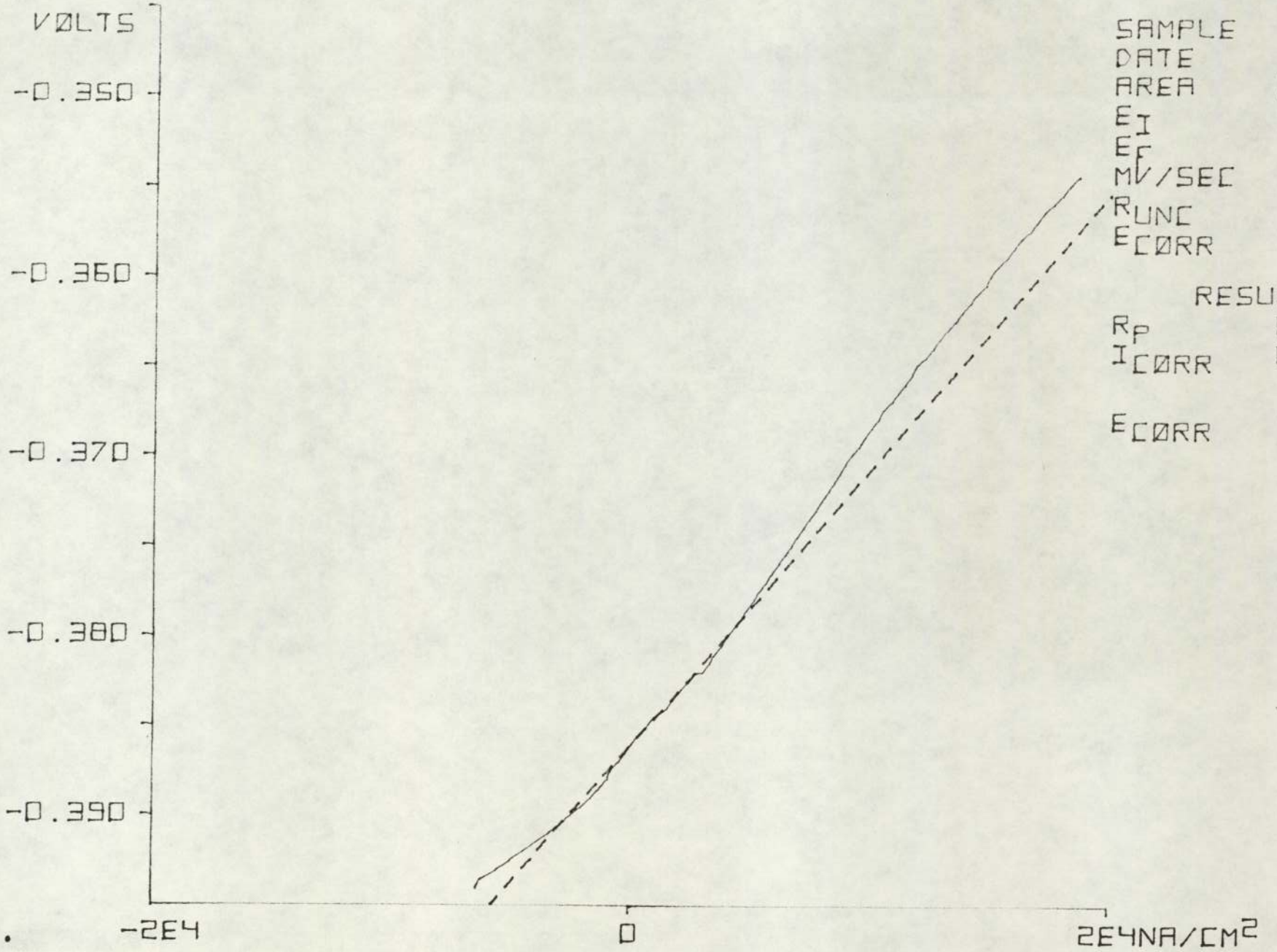

SAMPLE	6380
DATE	23.05
AREA	1.206E1
E_I	-0.394
E_F	-0.354
MV/SEC	0.166
R_{UNC}	1.945
$E_{CØRR}$	-0.374

RESULTS

R_P	1.544E3
$I_{CØRR}$	1.688E4
$E_{CØRR}$	-0.387

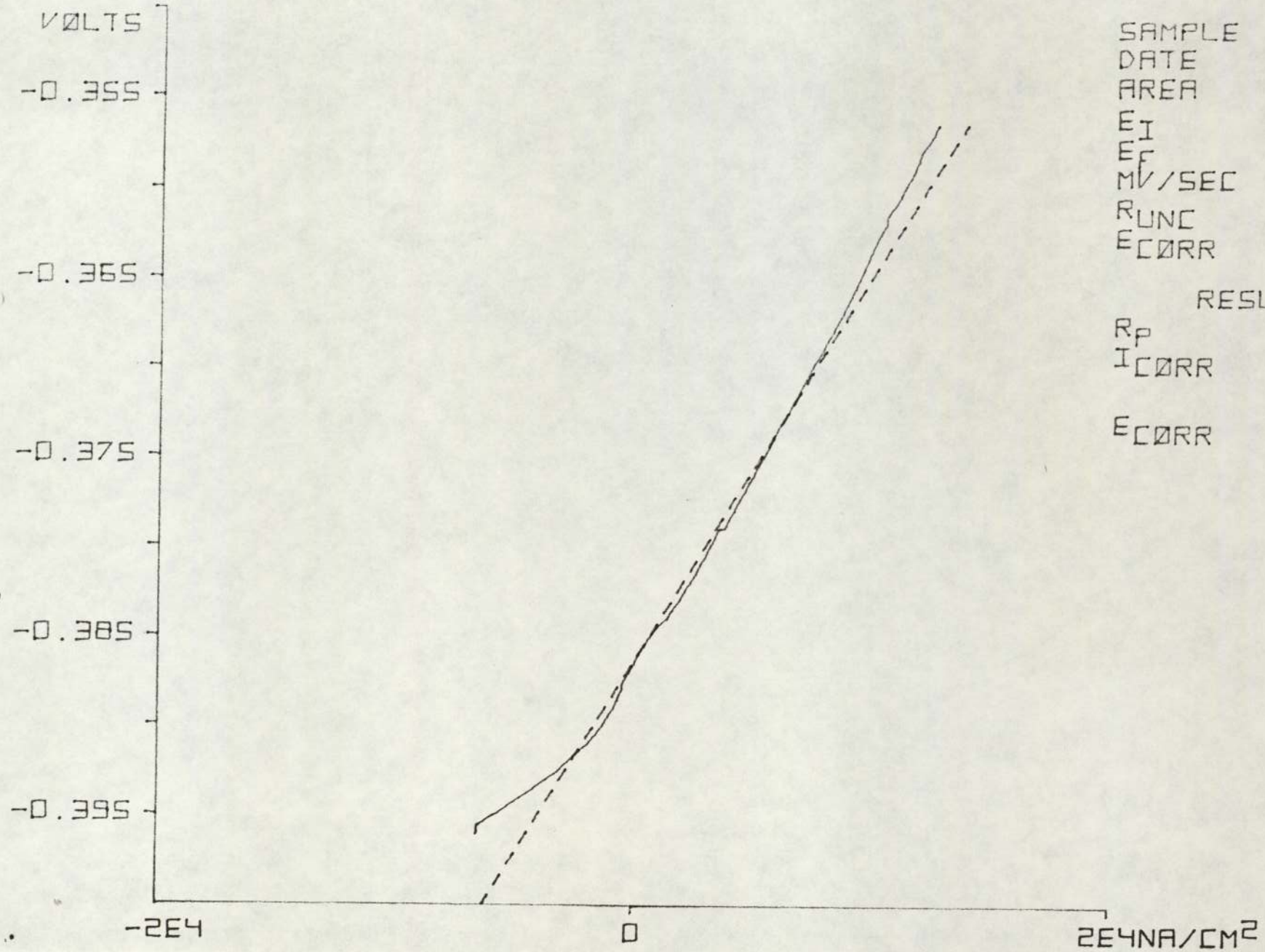

SAMPLE	1380
DATE	23.05
AREA	1.083E1
E_I	-0.396
E_f	-0.356
MV/SEC	0.166
R_{UNC}	1.837
$E_{CØRR}$	-0.376

RESULTS

R_P	2.177E3
$I_{CØRR}$	1.267E4
$E_{CØRR}$	-0.387

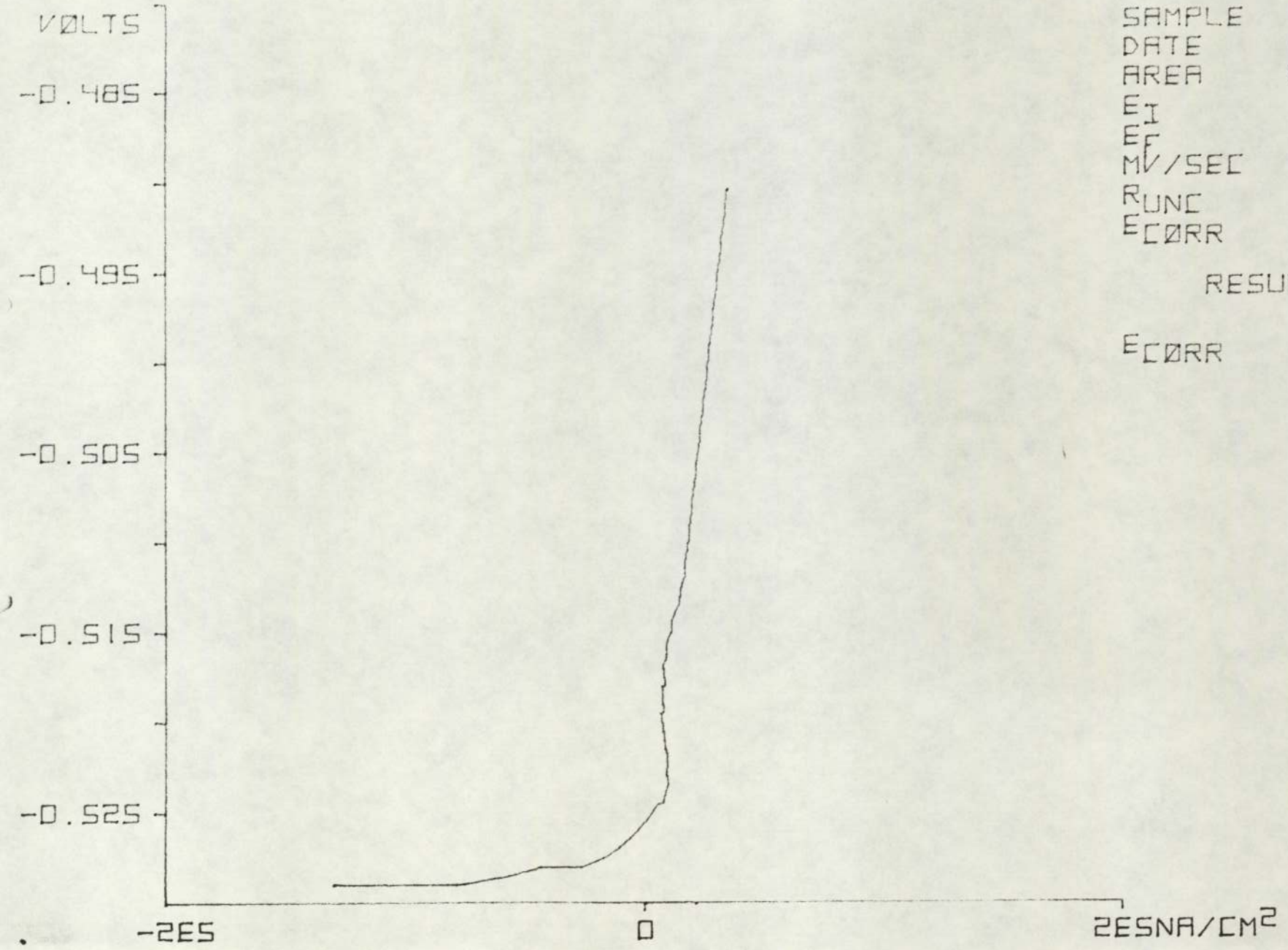

SAMPLE	4381
DATE	30.05
AREA	1.206E1
E_I	-0.530
E_F	-0.490
MV/SEC	0.166
R_{UNC}	0.886
$E_{CØRR}$	-0.510

RESULTS

$E_{CØRR}$ -0.526

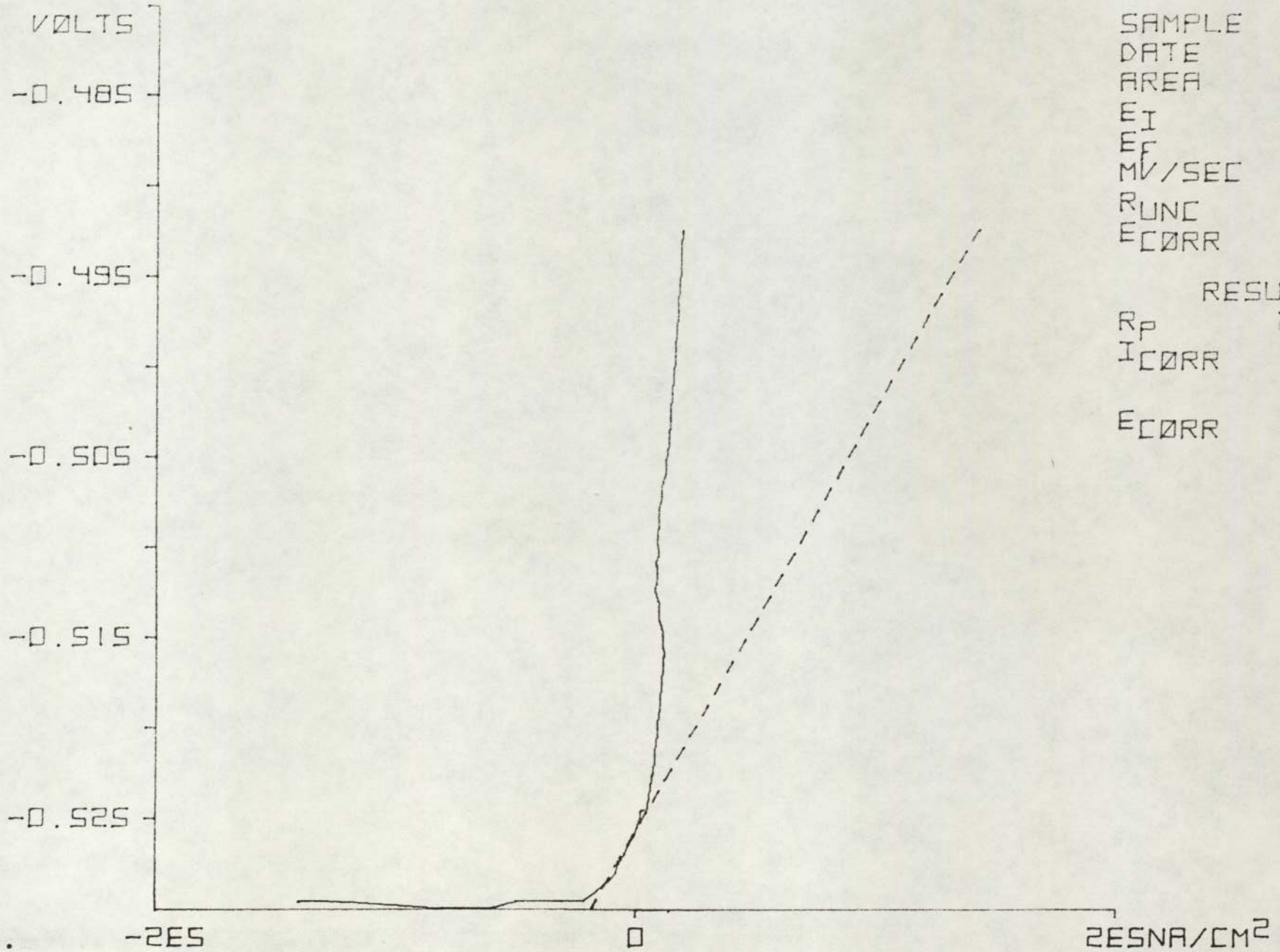

SAMPLE	6381
DATE	30.05
AREA	1.206E1
E_I	-0.532
E_f	-0.492
MV/SEC	0.166
R_{UNC}	1.642
$E_{CØRR}$	-0.512

RESULTS

R_P	2.327E2
$I_{CØRR}$	1.101E5
$E_{CØRR}$	-0.526

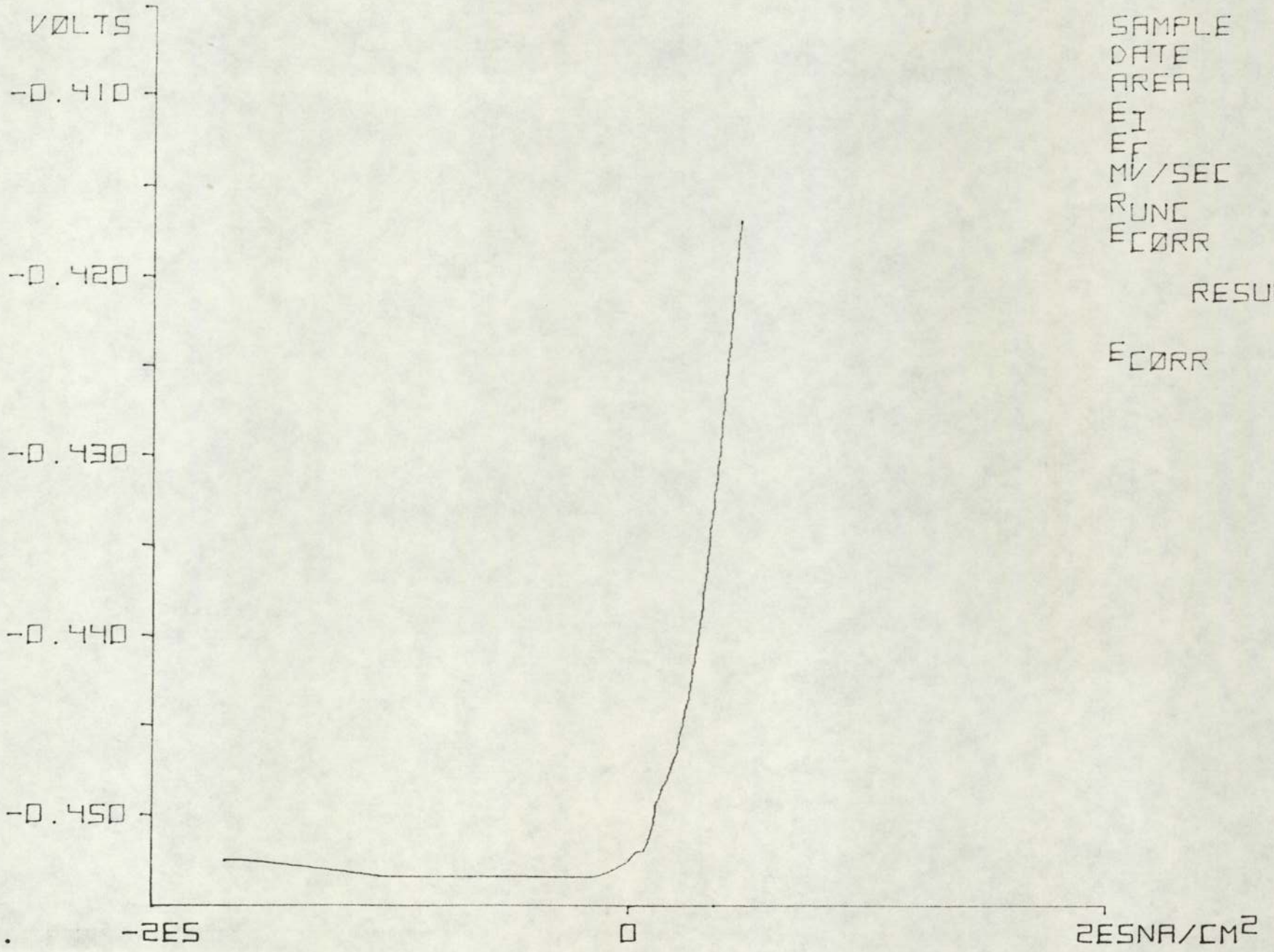

SAMPLE	1381
DATE	30.05
AREA	1.083E1
E_I	-0.456
E_f	-0.416
MV/SEC	0.166
R_{UNC}	1.905
$E_{CØRR}$	-0.436

RESULTS

$E_{CØRR}$ -0.453

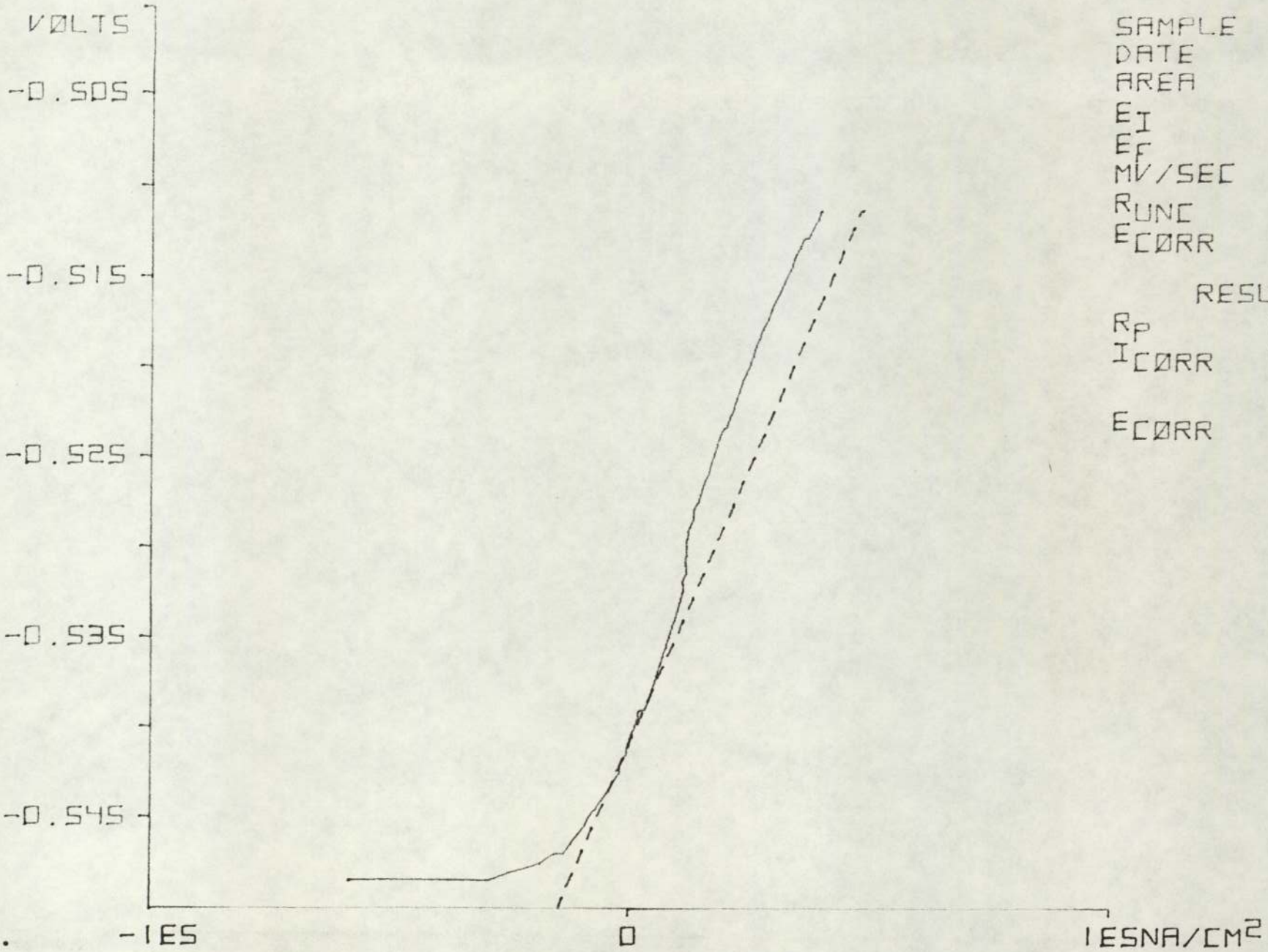

SAMPLE	4382
DATE	05.06
AREA	1.206E1
E_I	-0.550
E_f	-0.510
MV/SEC	0.166
R_{UNC}	2.414
$E_{CØRR}$	-0.530

RESULTS

R_P	6.172E2
$I_{CØRR}$	4.152E4
$E_{CØRR}$	-0.541

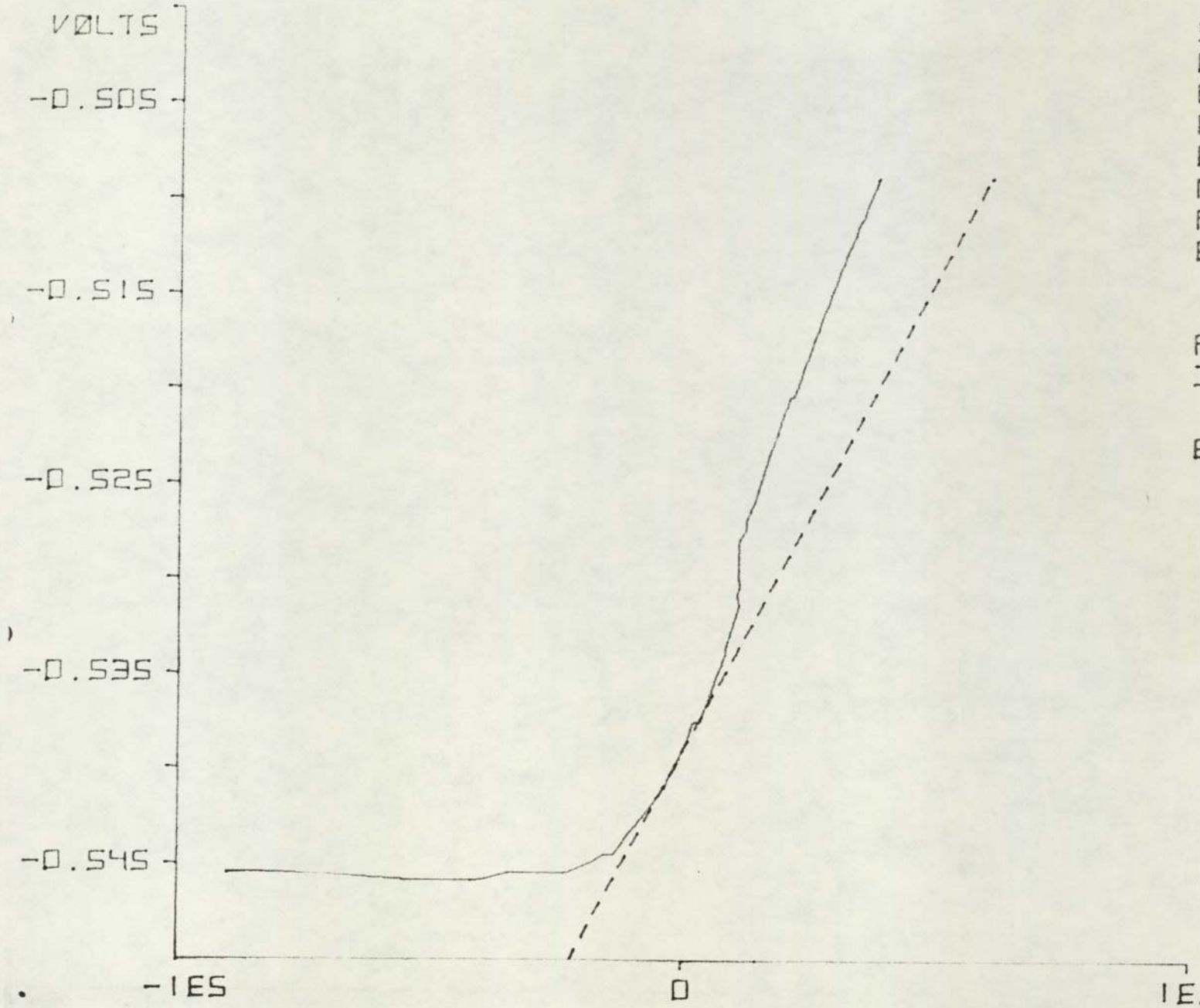

SAMPLE	6382
DATE	06.06
AREA	1.206E1
E_I	-0.548
E_F	-0.508
MV/SEC	0.166
R_{UNC}	2.267
$E_{CØRR}$	-0.528

RESULTS

R_P	5.006E2
$I_{CØRR}$	5.205E4
$E_{CØRR}$	-0.539

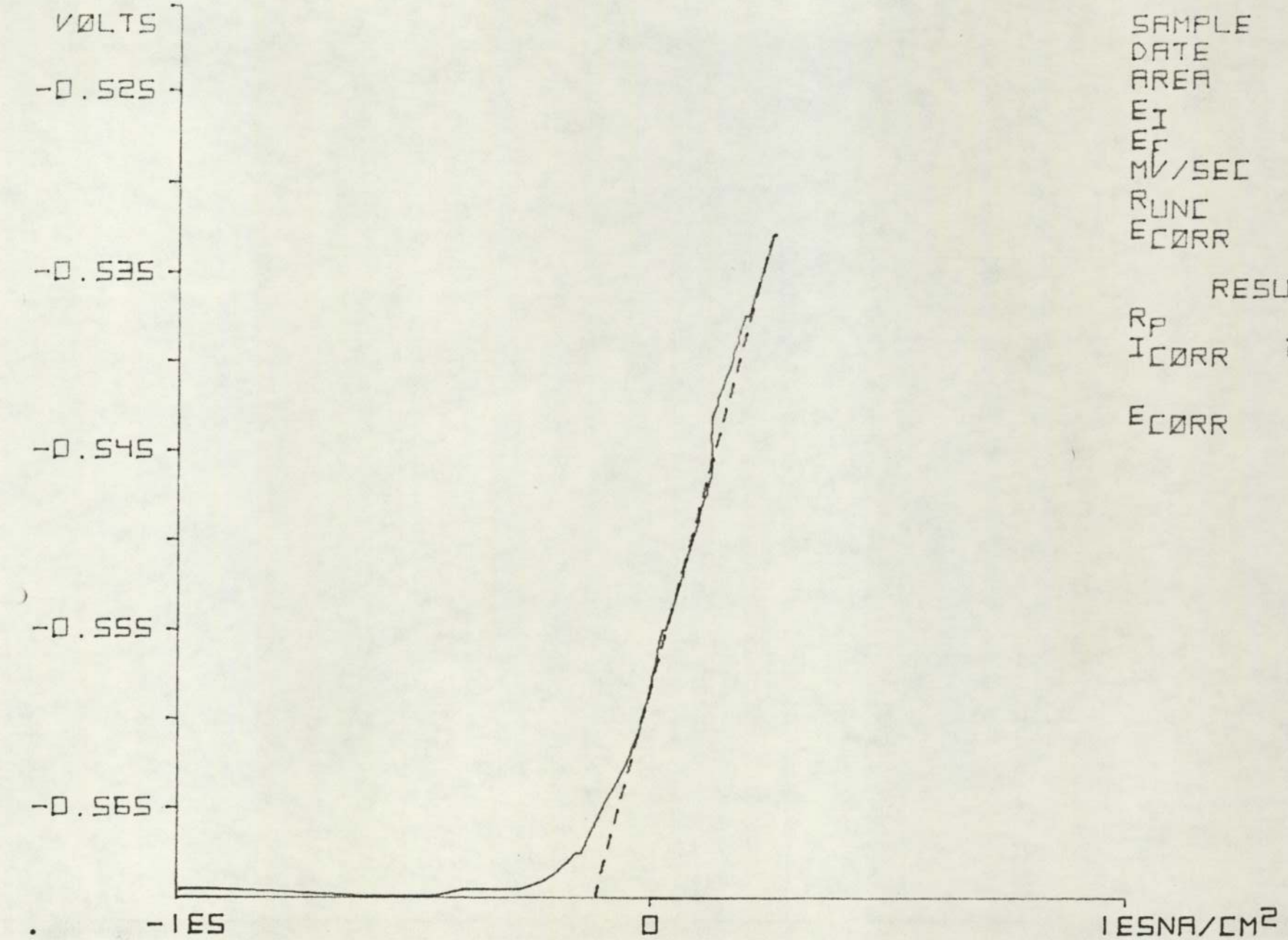

SAMPLE	1382
DATE	06.06
AREA	1.083E1
E_I	-0.572
E_F	-0.532
MV/SEC	0.166
R_{UNC}	2.687
$E_{CØRR}$	-0.552

RESULTS

R_P	1.016E3
$I_{CØRR}$	2.715E4
$E_{CØRR}$	-0.559

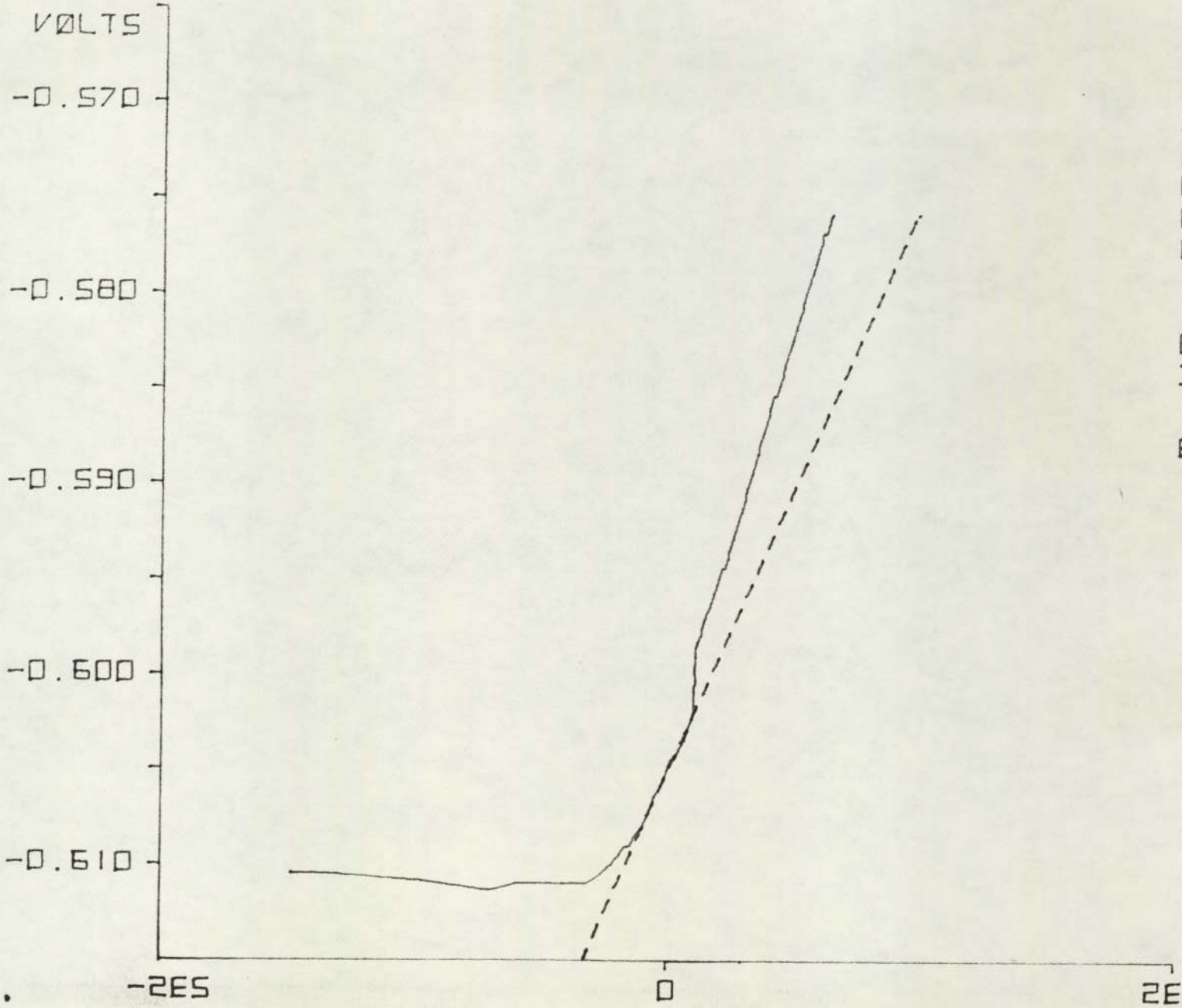

SAMPLE	4383
DATE	13.06
AREA	1.206E1
E_I	-0.614
E_F	-0.574
MV/SEC	0.166
R_{UNC}	2.160
$E_{CØRR}$	-0.594

RESULTS

R_P	3.017E2
$I_{CØRR}$	8.492E4
$E_{CØRR}$	-0.606

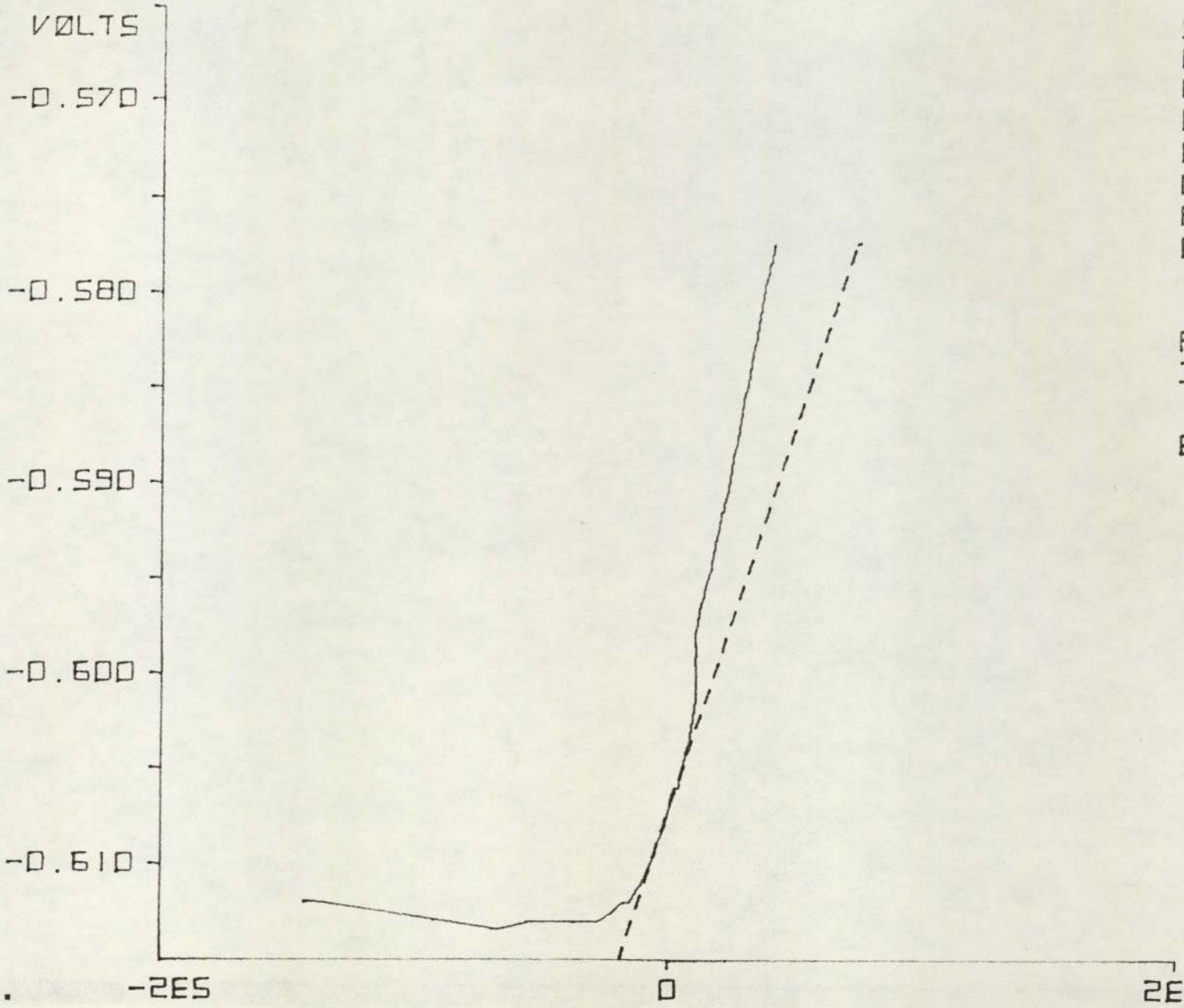

SAMPLE	6383
DATE	13.06
AREA	1.206E1
E_I	-0.616
E_F	-0.576
MV/SEC	0.166
R_{UNC}	2.296
$E_{CØRR}$	-0.596

RESULTS

R_P	4.076E2
$I_{CØRR}$	6.393E4
$E_{CØRR}$	-0.608

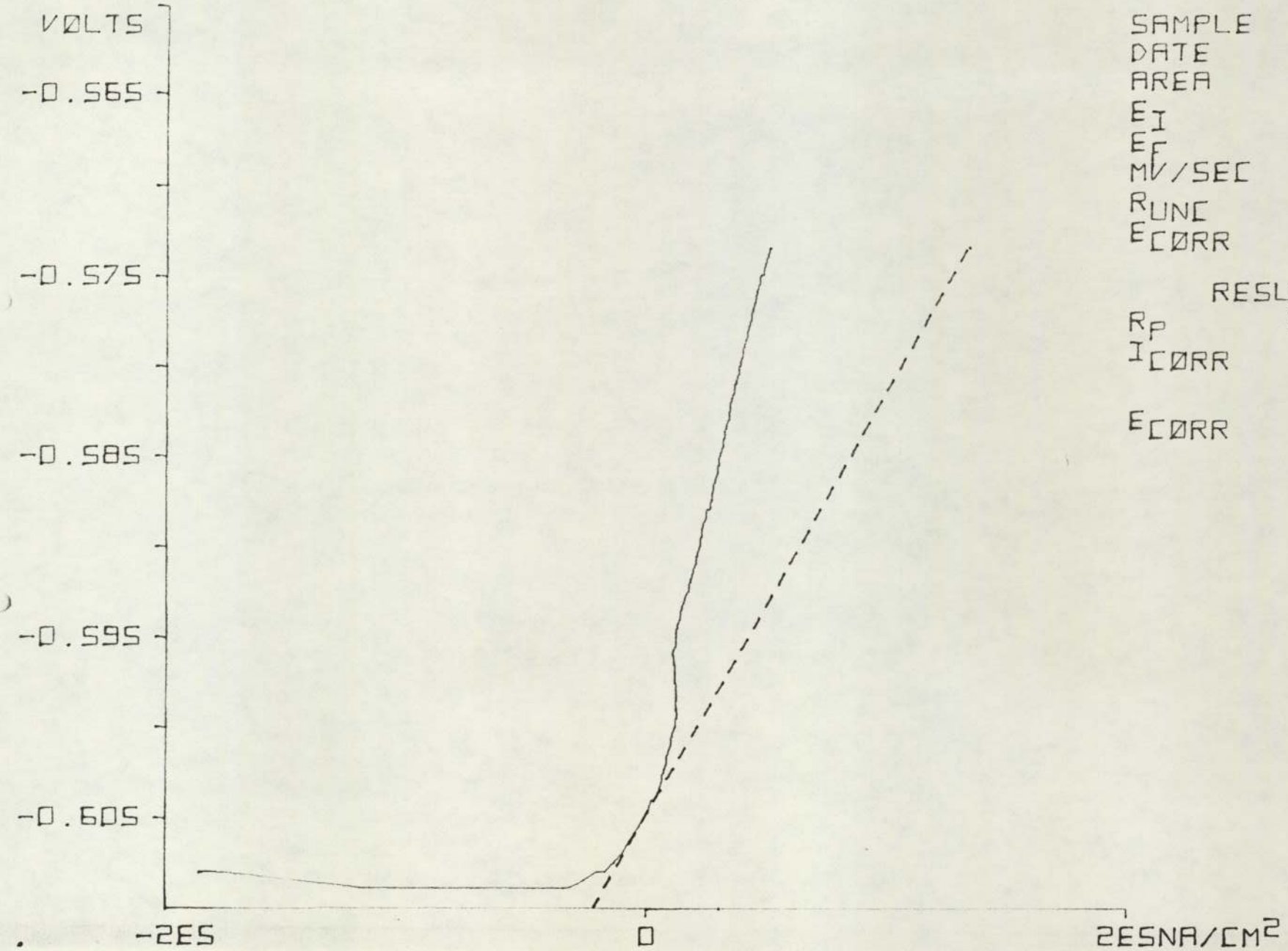

SAMPLE	1383
DATE	13.06
AREA	1.083E1
E_I	-0.612
E_F	-0.572
MV/SEC	0.166
R_{UNC}	2.111
$E_{CØRR}$	-0.592

RESULTS

R_P	2.343E2
$I_{CØRR}$	1.177E5
$E_{CØRR}$	-0.605

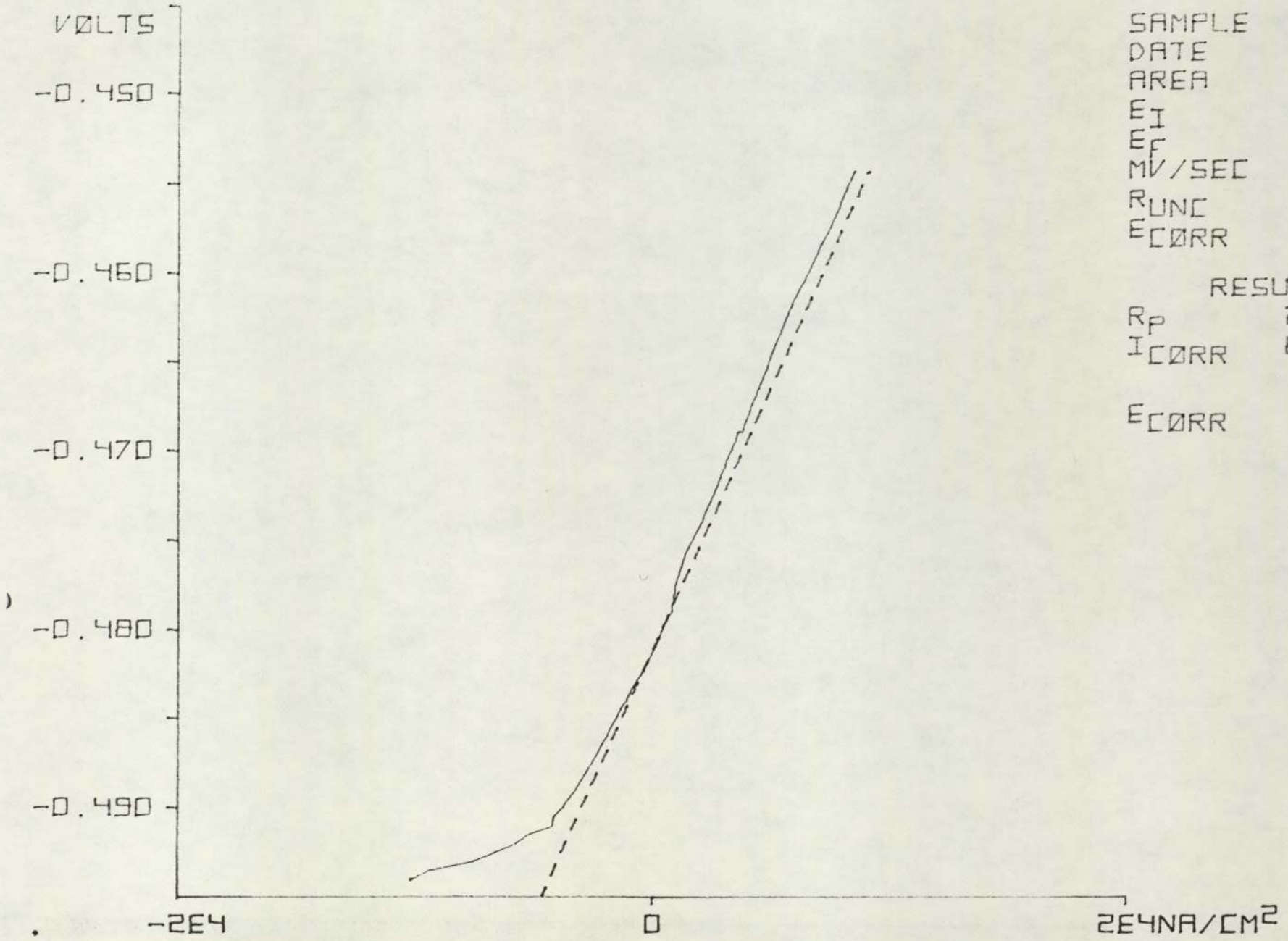

SAMPLE	4390
DATE	23.05
AREA	1.181E1
E_I	-0.494
E_F	-0.454
MV/SEC	0.166
R_{UNC}	1.622
$E_{CØRR}$	-0.474

RESULTS

R_P	2.957E3
$I_{CØRR}$	8.666E3
$E_{CØRR}$	-0.482

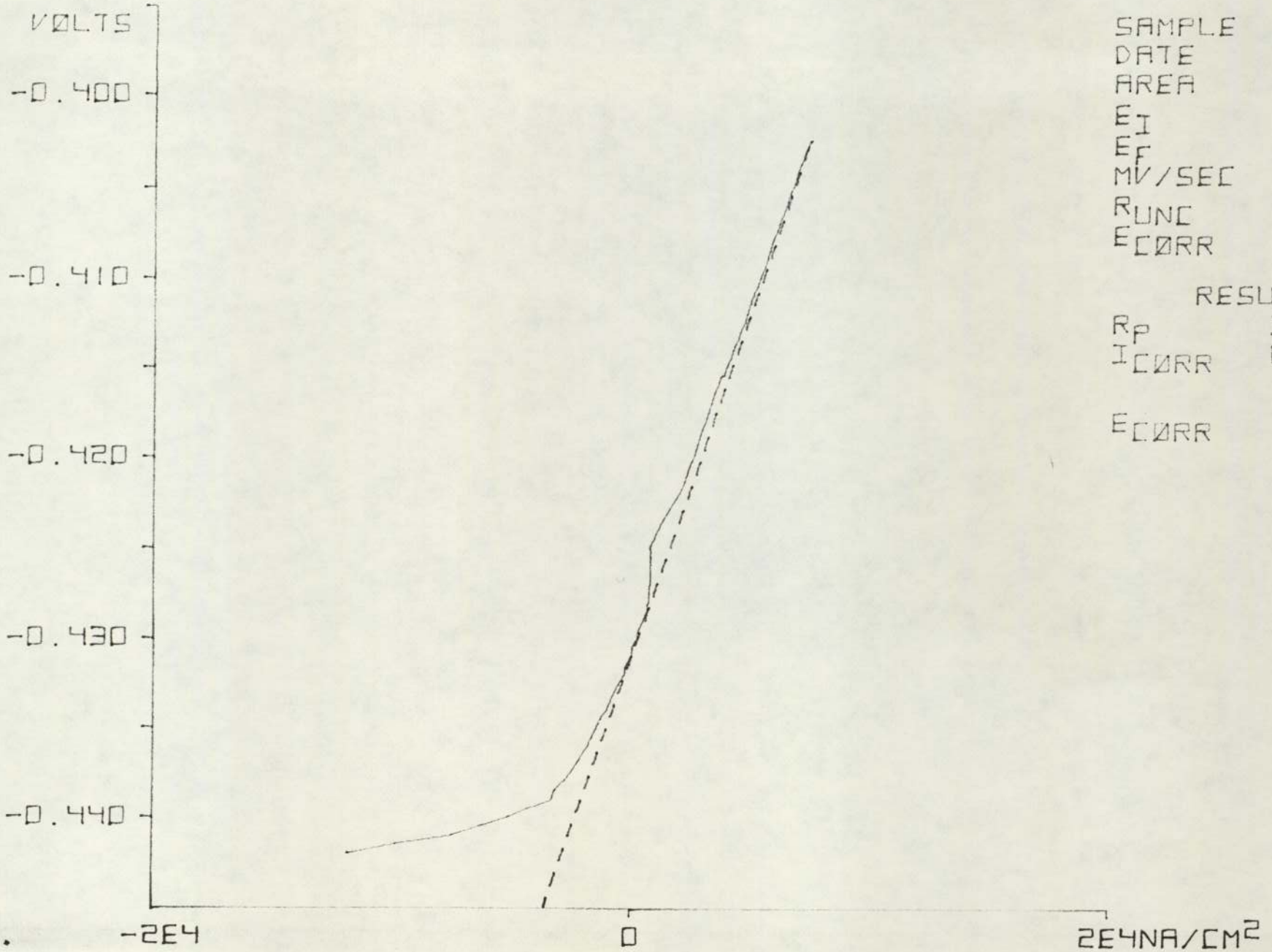

SAMPLE	6390
DATE	23.05
AREA	1.156E1
E_I	-0.442
E_F	-0.402
MV/SEC	0.166
R_{UNC}	1.593
$E_{CØRR}$	-0.422

RESULTS

R_P	3.879E3
$I_{CØRR}$	6.718E3
$E_{CØRR}$	-0.431

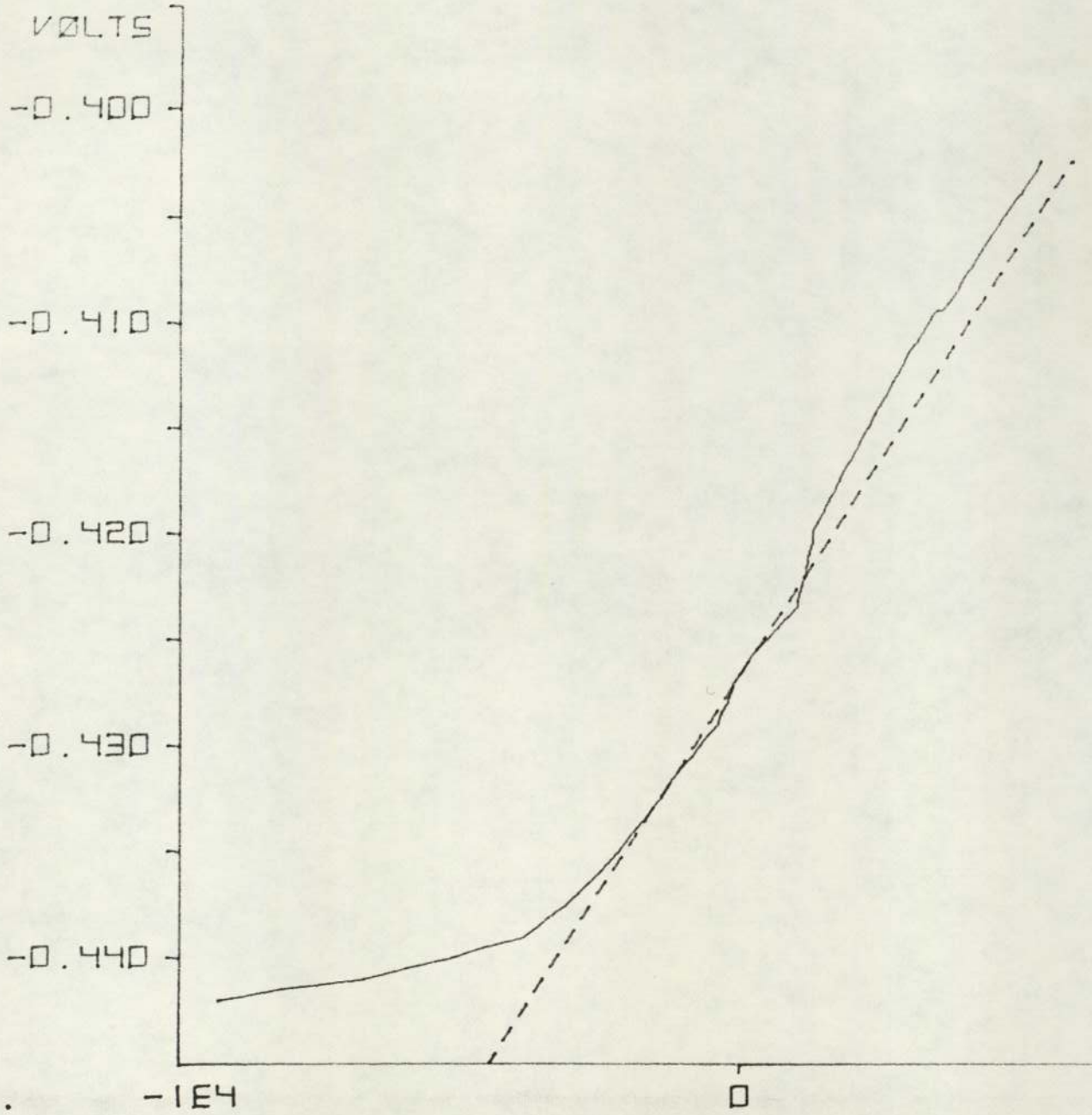

SAMPLE	1390
DATE	23.05
AREA	1.156E1
E_I	-0.442
E_F	-0.402
MV/SEC	0.166
R_{UNC}	1.710
$E_{CØRR}$	-0.422

RESULTS

R_P	4.114E3
$I_{CØRR}$	6.702E3
$E_{CØRR}$	-0.427

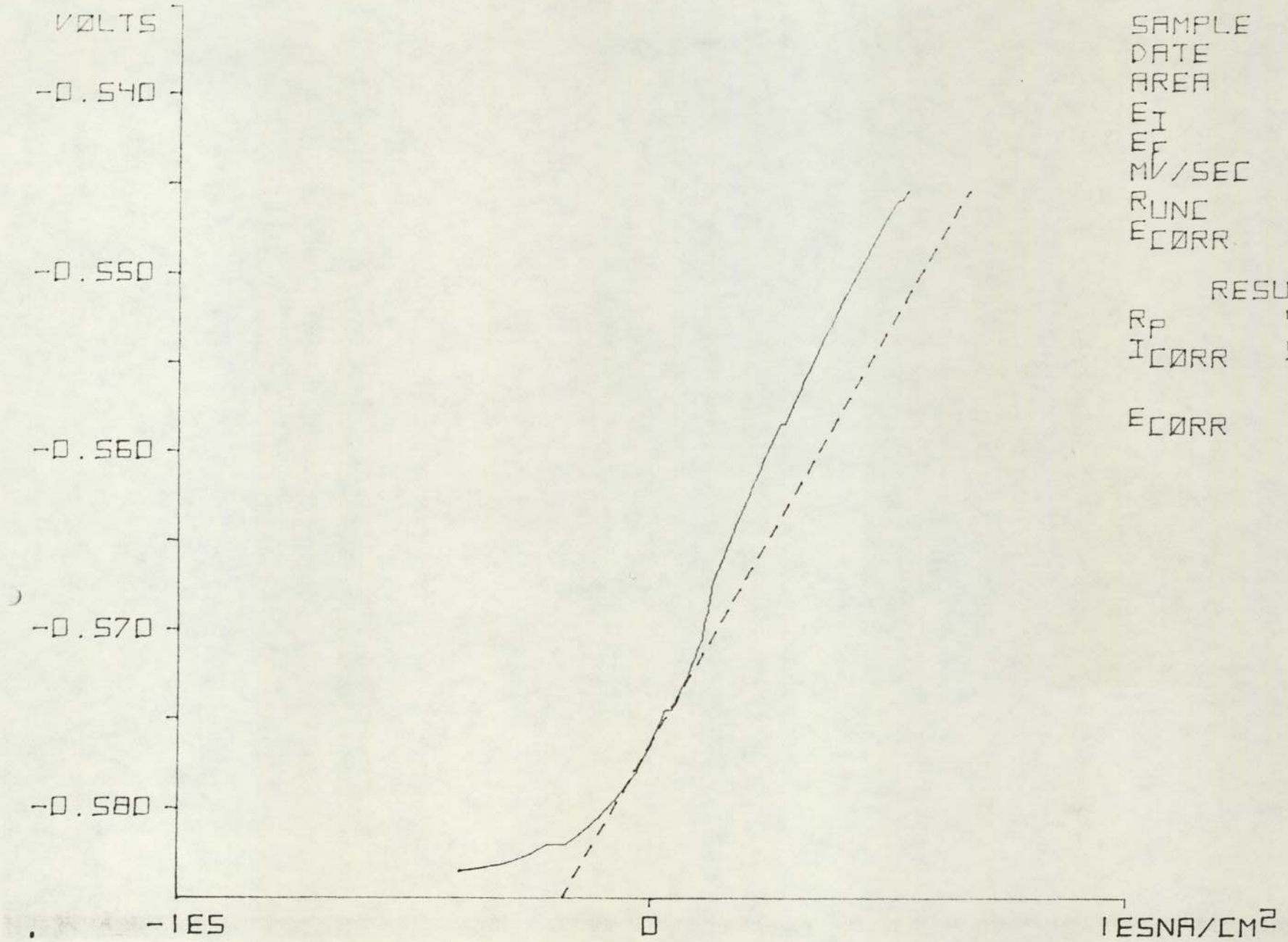

SAMPLE	4391
DATE	30.05
AREA	1.181E1
E_I	-0.584
E_F	-0.544
MV/SEC	0.166
R_{UNC}	1.769
$E_{CØRR}$	-0.564

RESULTS

R_P	4.668E2
$I_{CØRR}$	5.581E4
$E_{CØRR}$	-0.577

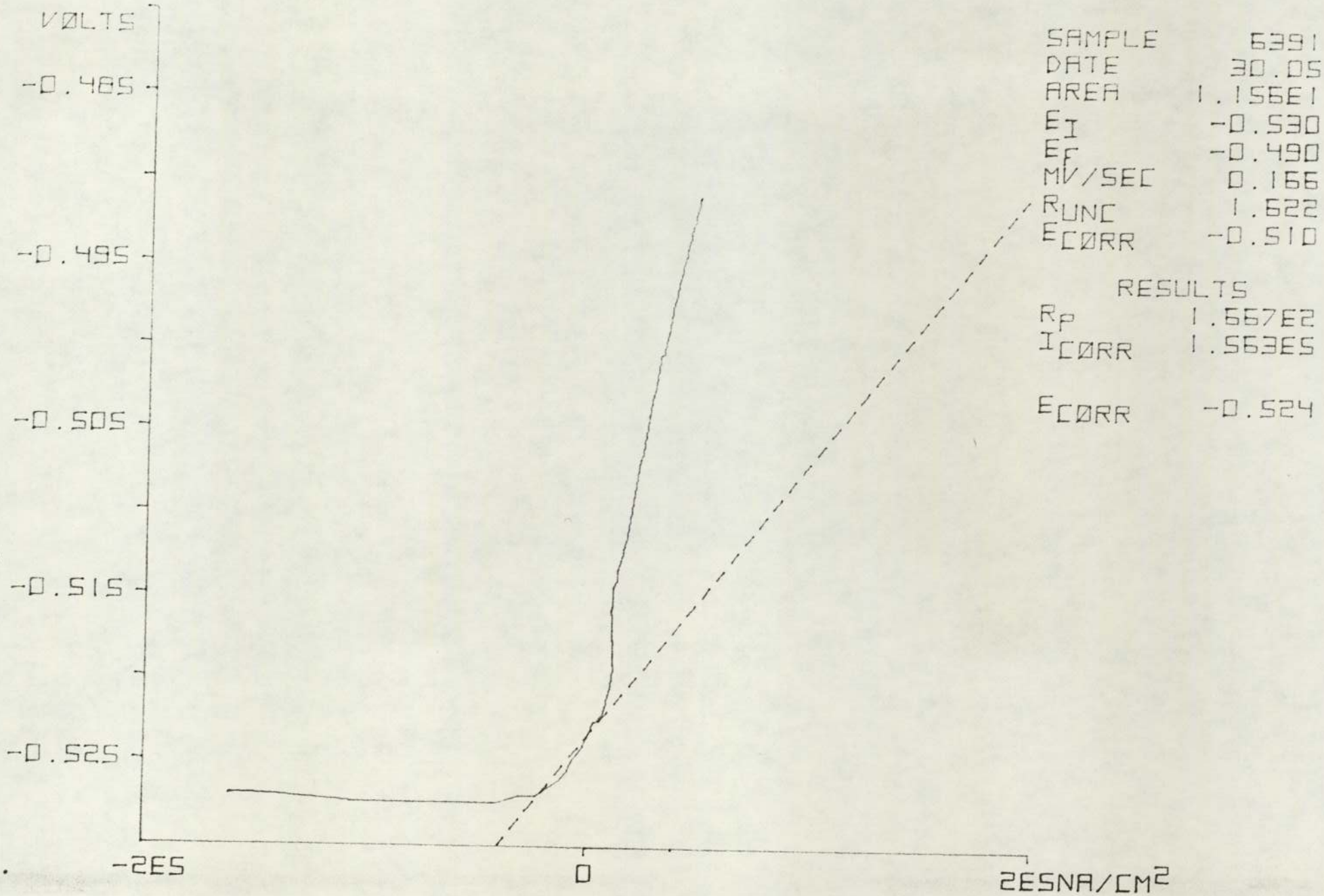

SAMPLE	6391
DATE	30.05
AREA	1.156E1
E_I	-0.530
E_f	-0.490
MV/SEC	0.166
R_{UNC}	1.622
$E_{CØRR}$	-0.510

RESULTS

R_p	1.667E2
$I_{CØRR}$	1.563E5
$E_{CØRR}$	-0.524

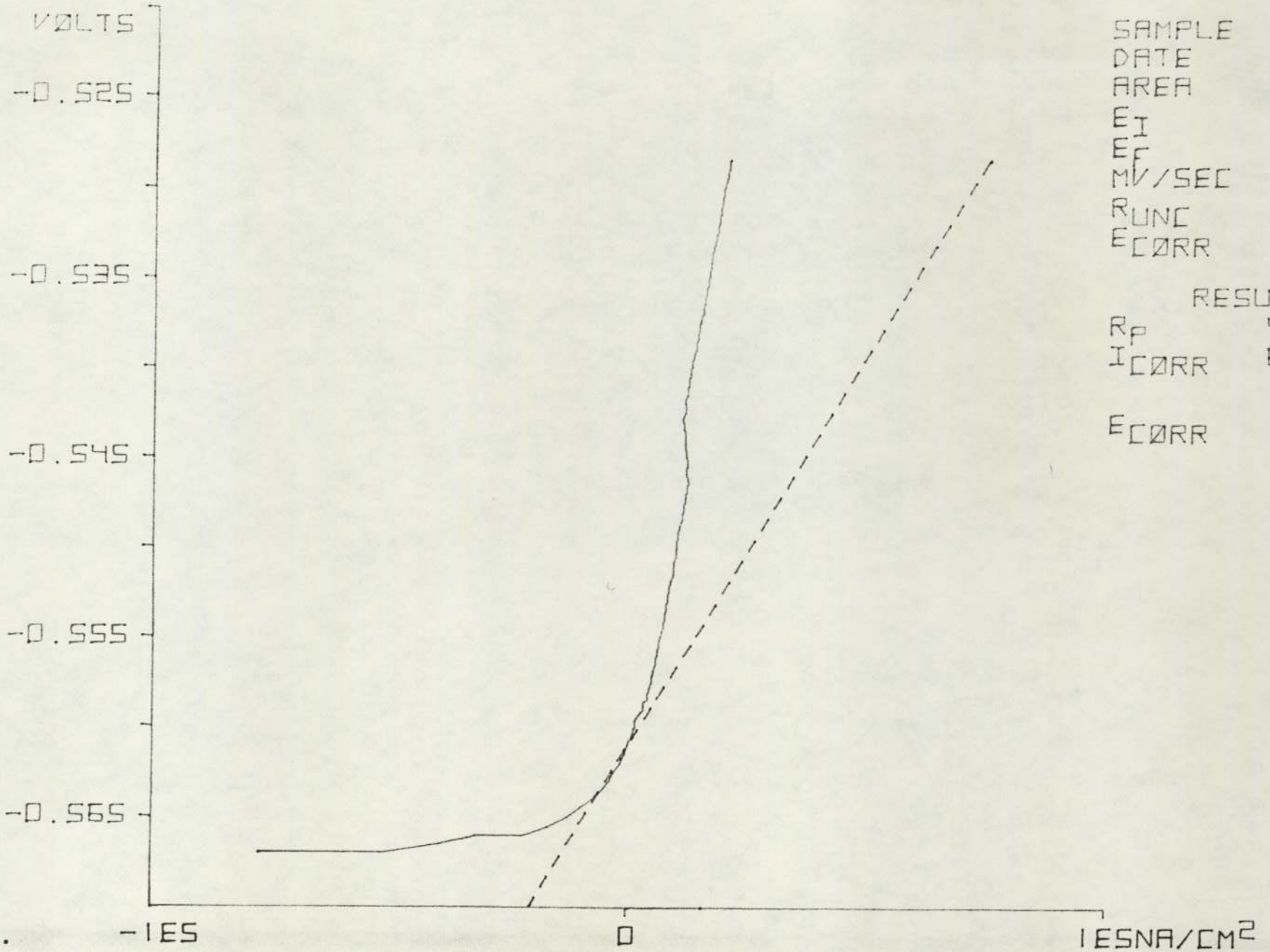

SAMPLE	1391
DATE	30.05
AREA	1.156E1
E_I	-0.568
E_F	-0.528
MV/SEC	0.166
R_{UNC}	1.524
$E_{CØRR}$	-0.548

RESULTS

R_P	4.370E2
$I_{CØRR}$	6.310E4
$E_{CØRR}$	-0.562

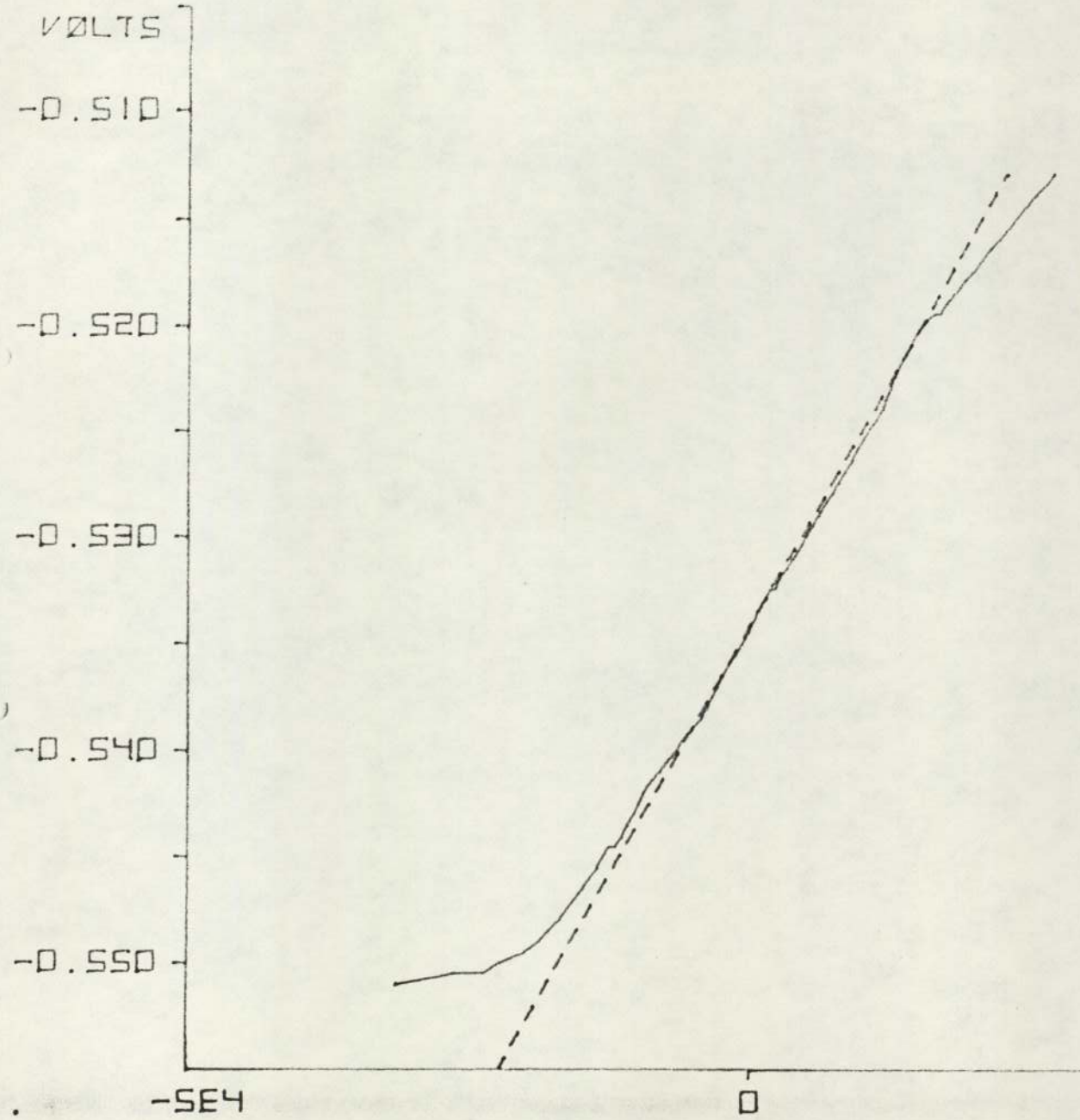

SAMPLE	4392
DATE	06.06
AREA	1.181E1
E_I	-0.552
E_F	-0.512
MV/SEC	0.166
R_{UNC}	3.020
$E_{CØRR}$	-0.532

RESULTS

R_P	9.435E2
$I_{CØRR}$	2.716E4
$E_{CØRR}$	-0.535

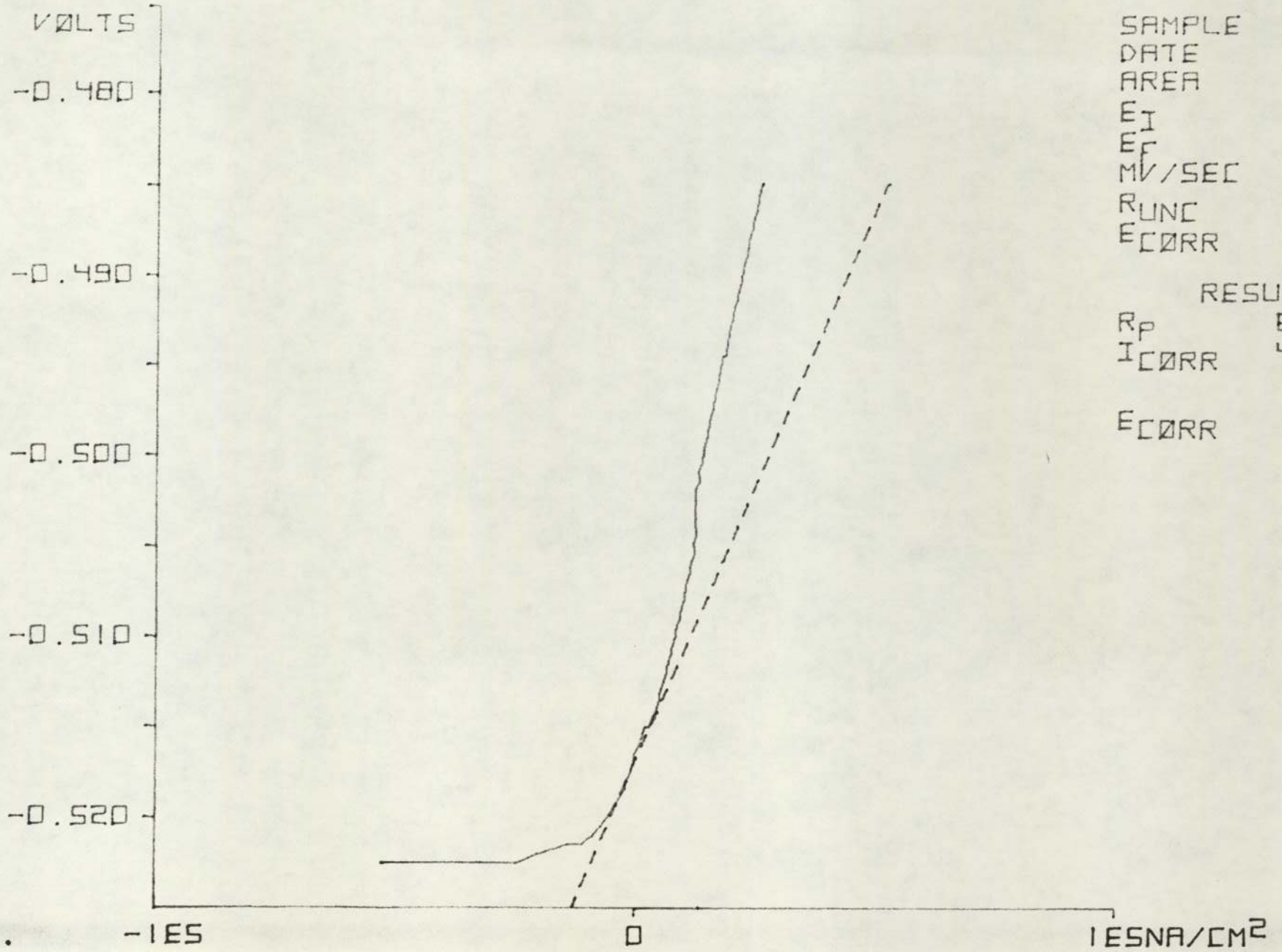

SAMPLE	6392
DATE	06.06
AREA	1.156E1
E_I	-0.524
E_F	-0.484
MV/SEC	0.166
R_{UNC}	2.775
$E_{CØRR}$	-0.504

RESULTS

R_P	6.154E2
$I_{CØRR}$	4.234E4
$E_{CØRR}$	-0.517

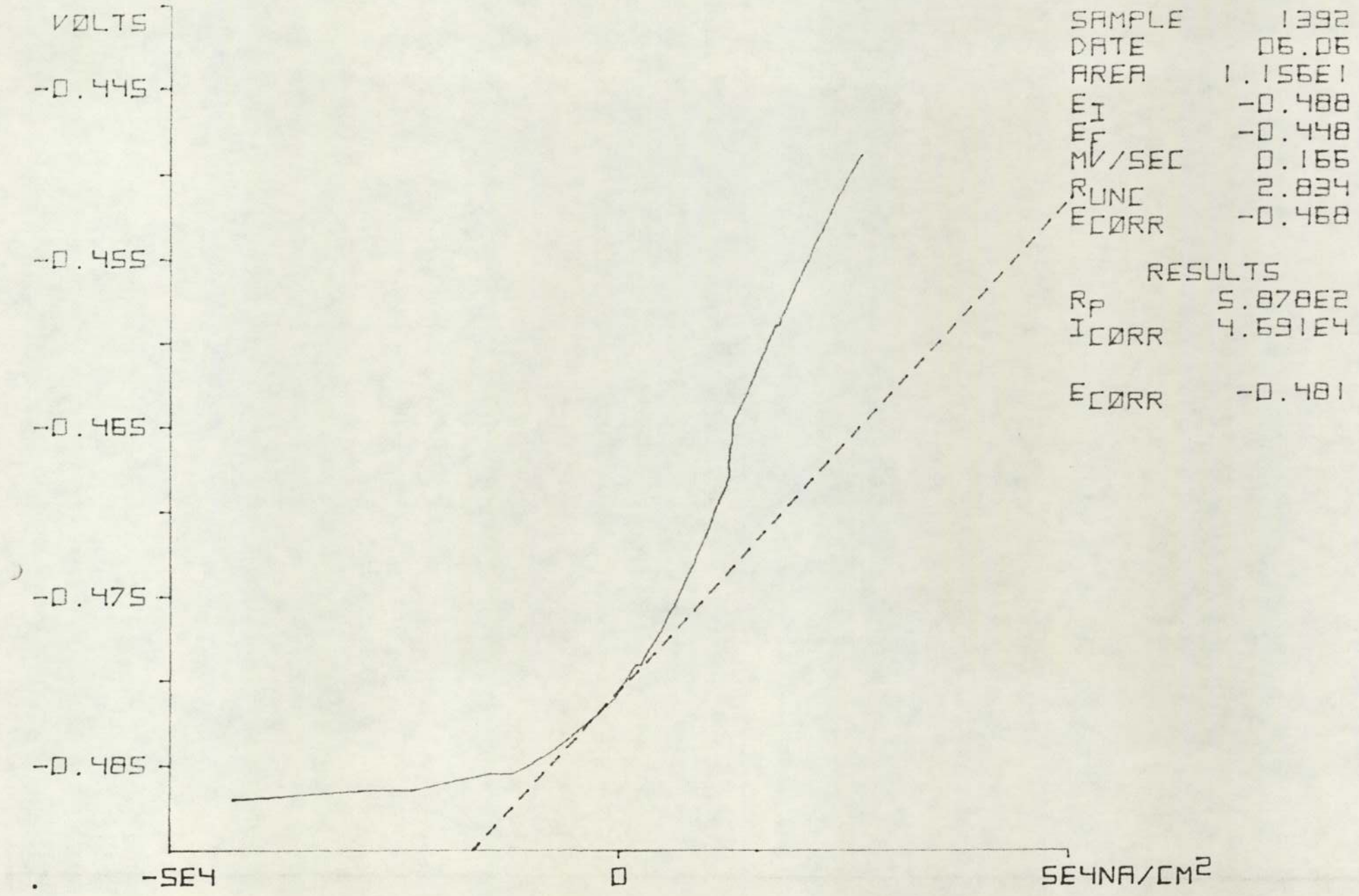

SAMPLE	1392
DATE	06.06
AREA	1.156E1
E_I	-0.488
E_F	-0.448
MV/SEC	0.166
R_{UNC}	2.834
E_{CORR}	-0.468

RESULTS

R_P	5.878E2
I_{CORR}	4.691E4
E_{CORR}	-0.481

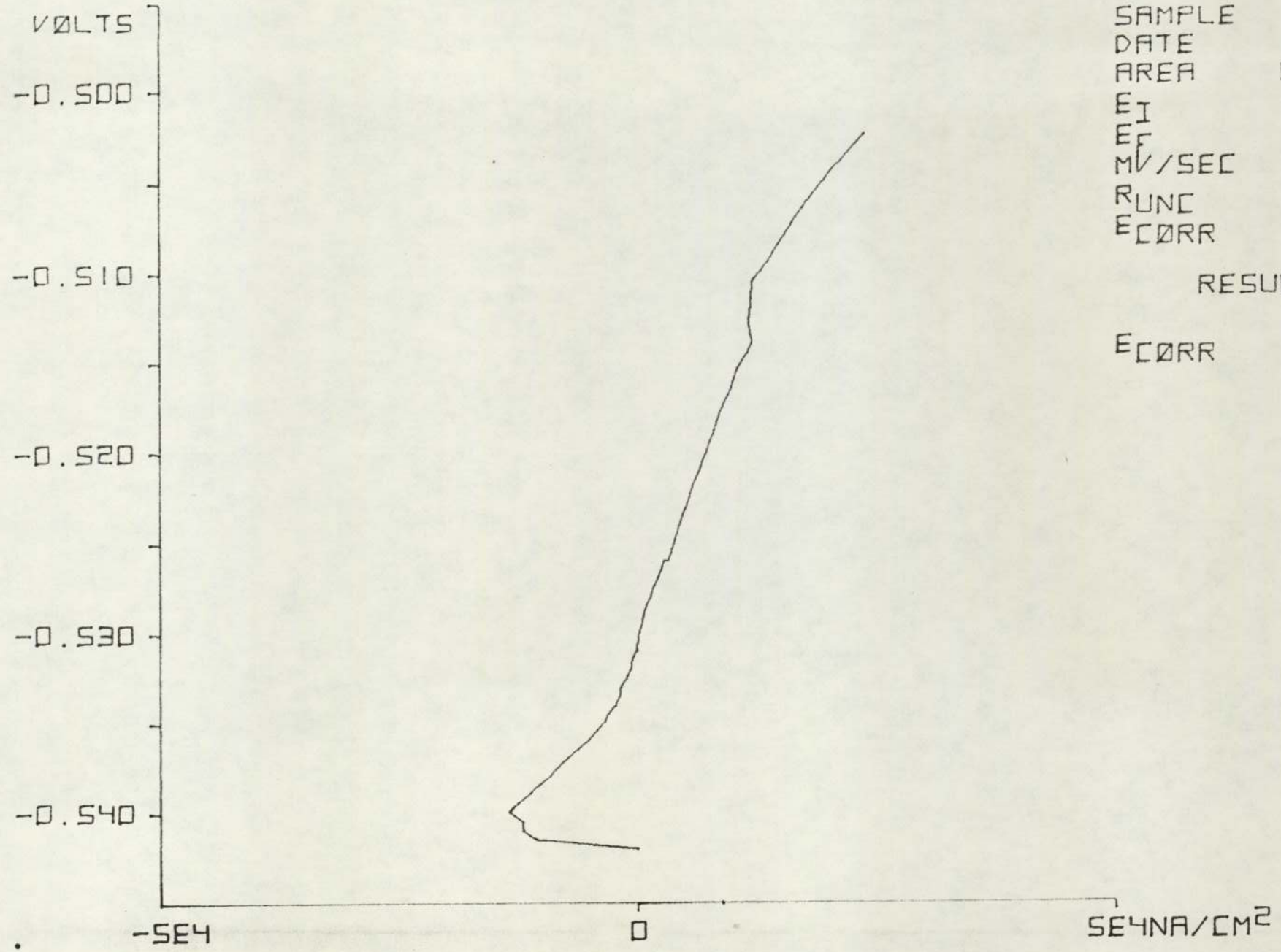

SAMPLE	4393
DATE	13.06
AREA	1.181E1
E_I	-0.542
E_F	-0.502
MV/SEC	0.166
R_{UNC}	2.023
$E_{CØRR}$	-0.522

RESULTS

$E_{CØRR}$	-0.542
	-0.531

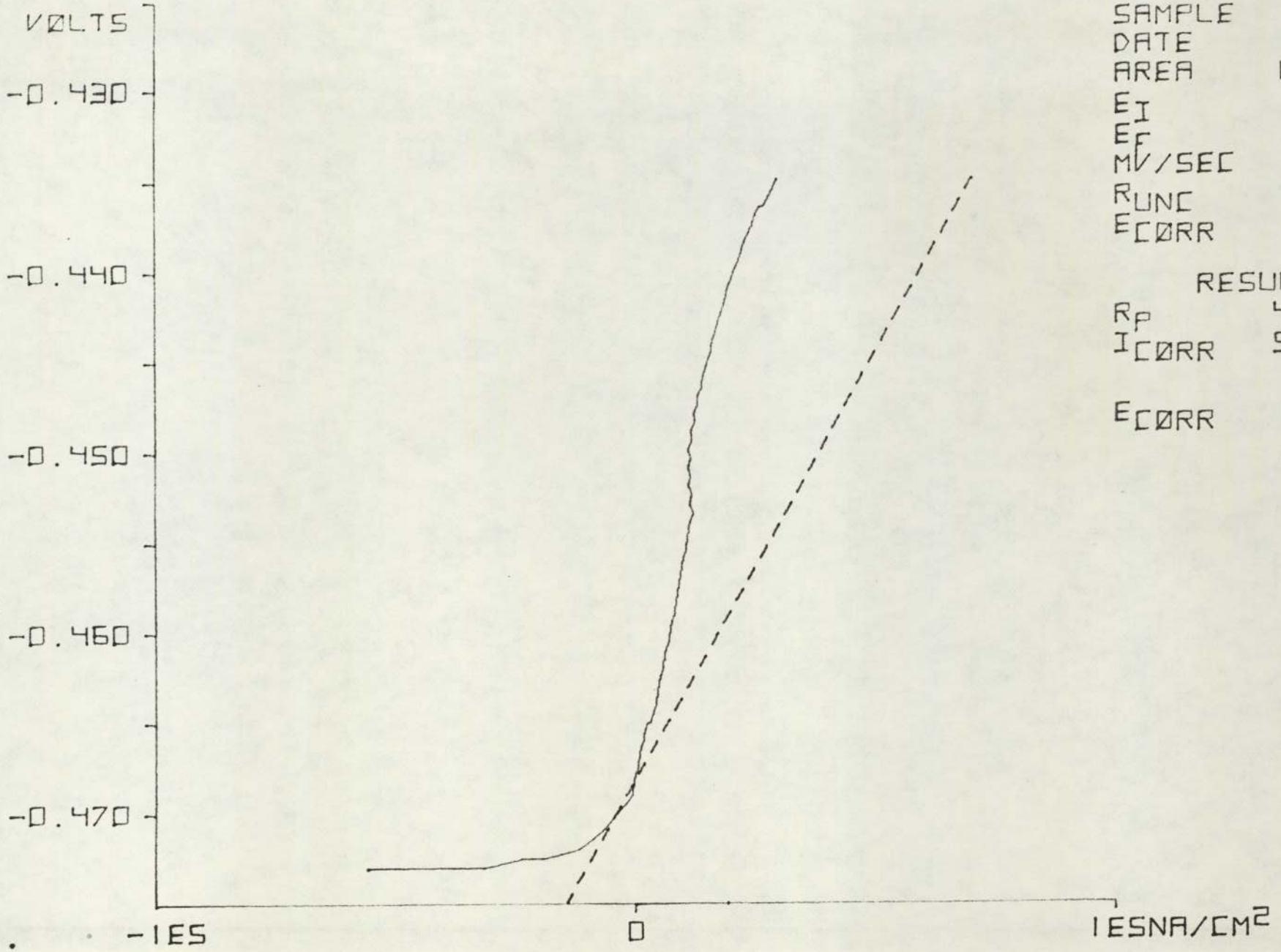

SAMPLE	6393
DATE	13.06
AREA	1.156E1
E_I	-0.474
E_F	-0.434
MV/SEC	0.166
R_{UNC}	1.876
E_{CORR}	-0.454

RESULTS

R_P	4.723E2
I_{CORR}	5.517E4
E_{CORR}	-0.469

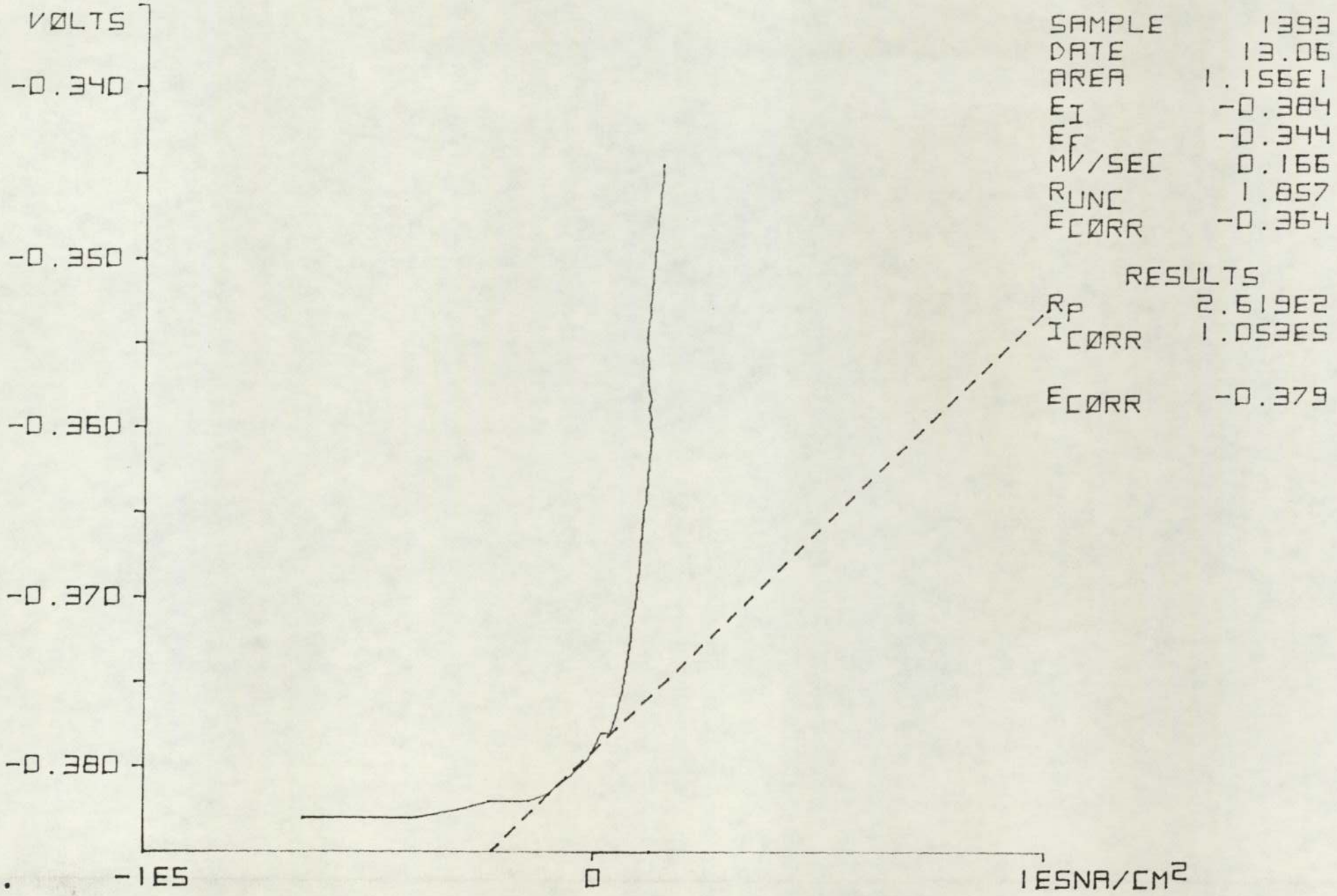

SAMPLE	1393
DATE	13.06
AREA	1.156E1
E_I	-0.384
E_F	-0.344
MV/SEC	0.166
R_{UNC}	1.857
$E_{CØRR}$	-0.364

RESULTS

R_P	2.619E2
$I_{CØRR}$	1.053E5
$E_{CØRR}$	-0.379

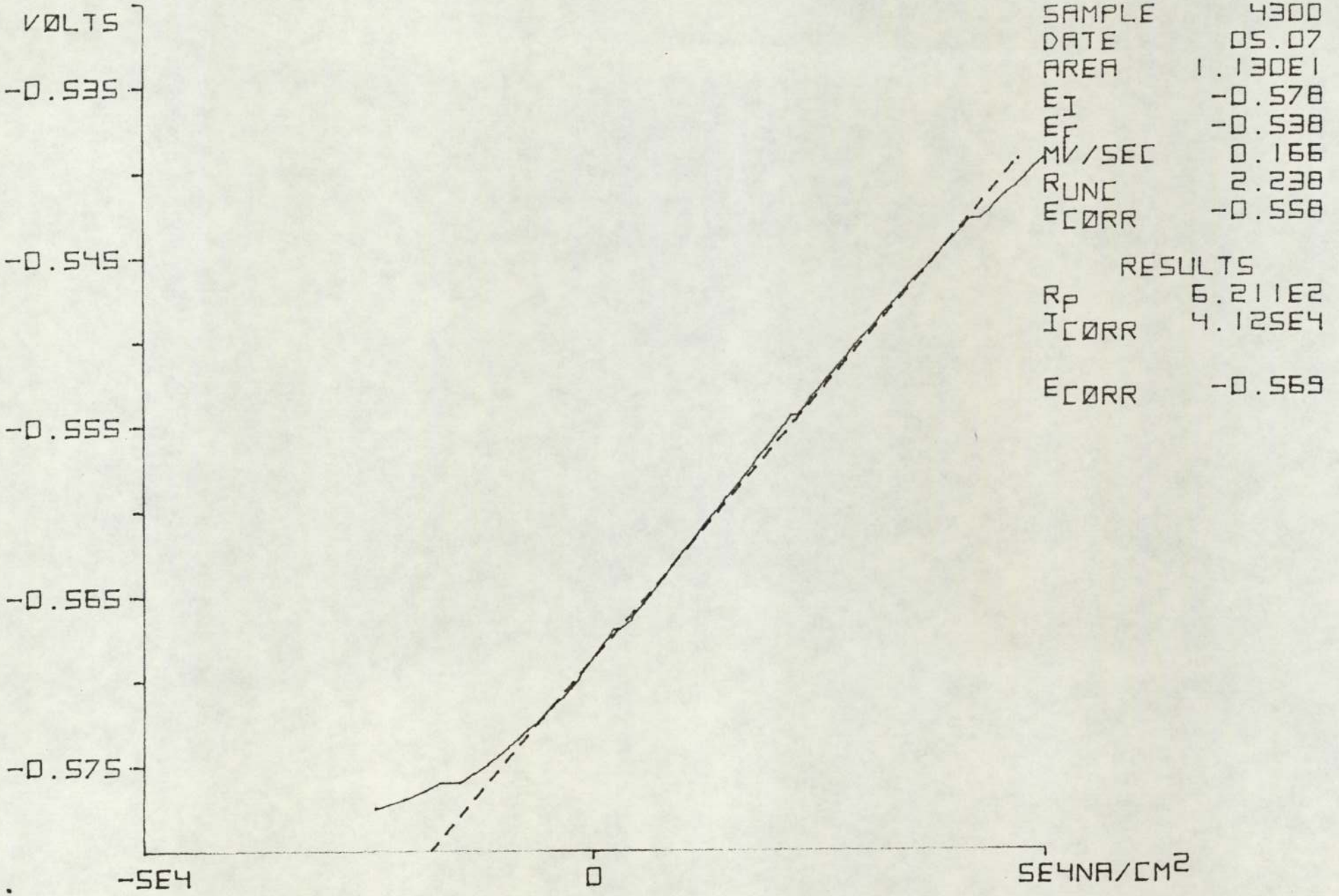
VØLTS
-0.535
-0.545
-0.555
-0.565
-0.575
-5E4
0
5E4NA/CM2
SAMPLE 4300
DATE 05.07
AREA 1.130E1
EI -0.578
EF -0.538
MV/SEC 0.166
RUNC 2.238
ECØRR -0.558
RESULTS
RP 6.211E2
ICØRR 4.125E4
ECØRR -0.569

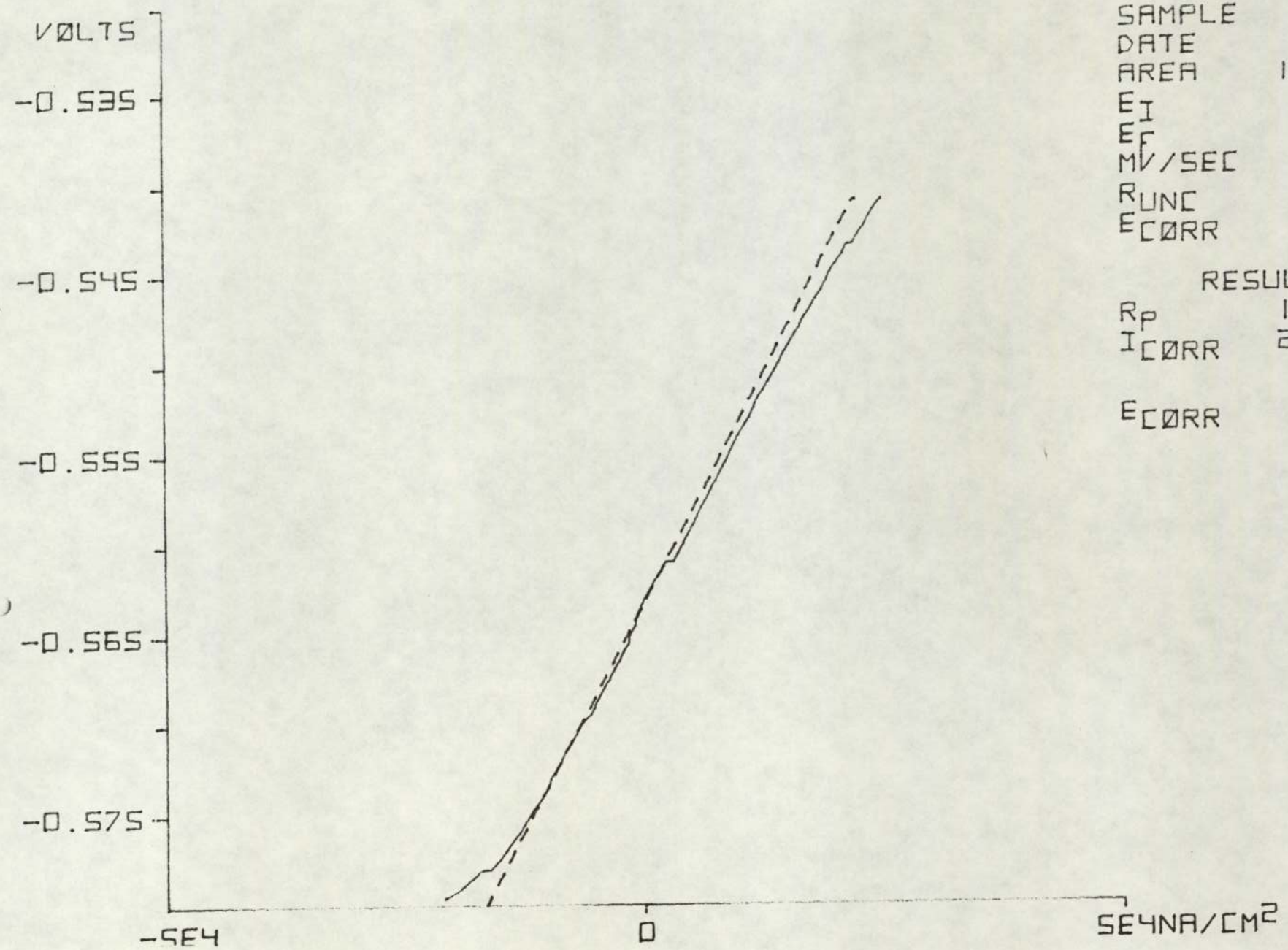

SAMPLE	6300
DATE	05.07
AREA	1.155E1
E_I	-0.580
E_F	-0.540
MV/SEC	0.166
R_{UNC}	2.248
$E_{CØRR}$	-0.560

RESULTS

R_P	1.005E3
$I_{CØRR}$	2.592E4
$E_{CØRR}$	-0.564

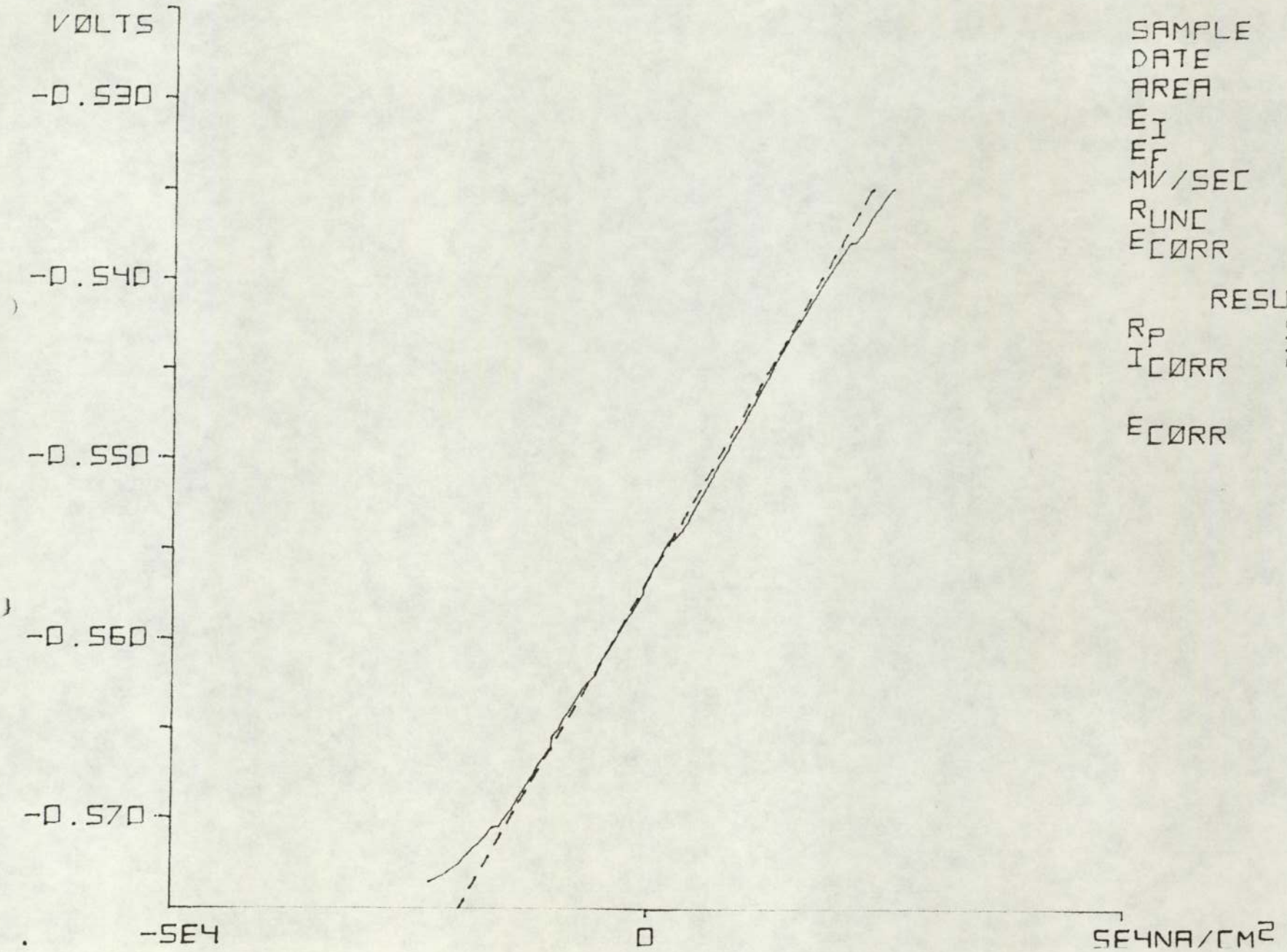

SAMPLE	1300
DATE	05.07
AREA	1.155E1
E_I	-0.574
E_F	-0.534
MV/SEC	0.166
R_{UNC}	2.336
$E_{CØRR}$	-0.554

RESULTS

R_P	9.328E2
$I_{CØRR}$	2.956E4
$E_{CØRR}$	-0.557

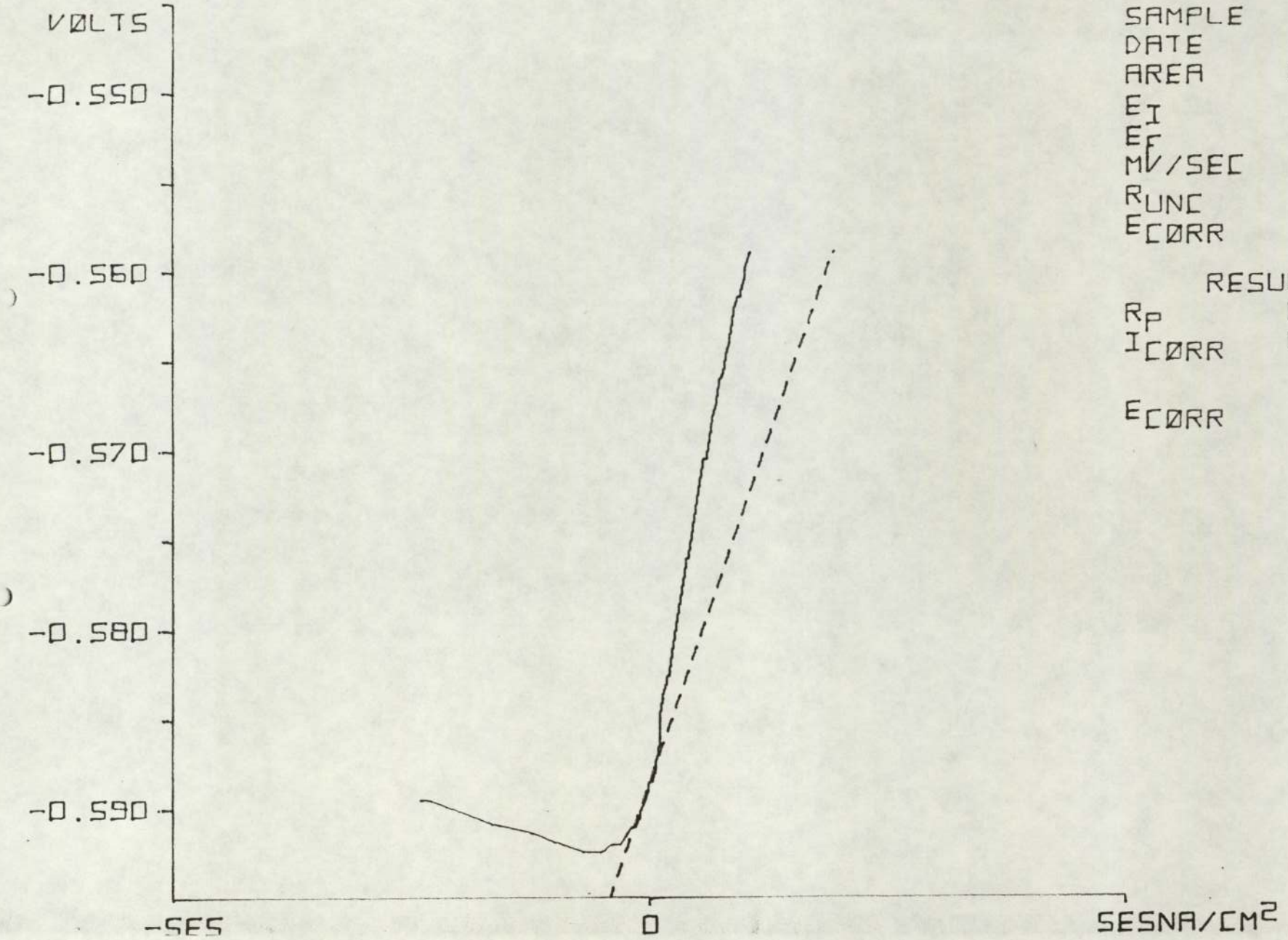

SAMPLE	4301
DATE	12.07
AREA	1.130E1
E_I	-0.596
E_F	-0.556
MV/SEC	0.166
R_{UNC}	2.424
$E_{CØRR}$	-0.576

RESULTS

R_P	1.538E2
$I_{CØRR}$	1.666E5
$E_{CØRR}$	-0.589

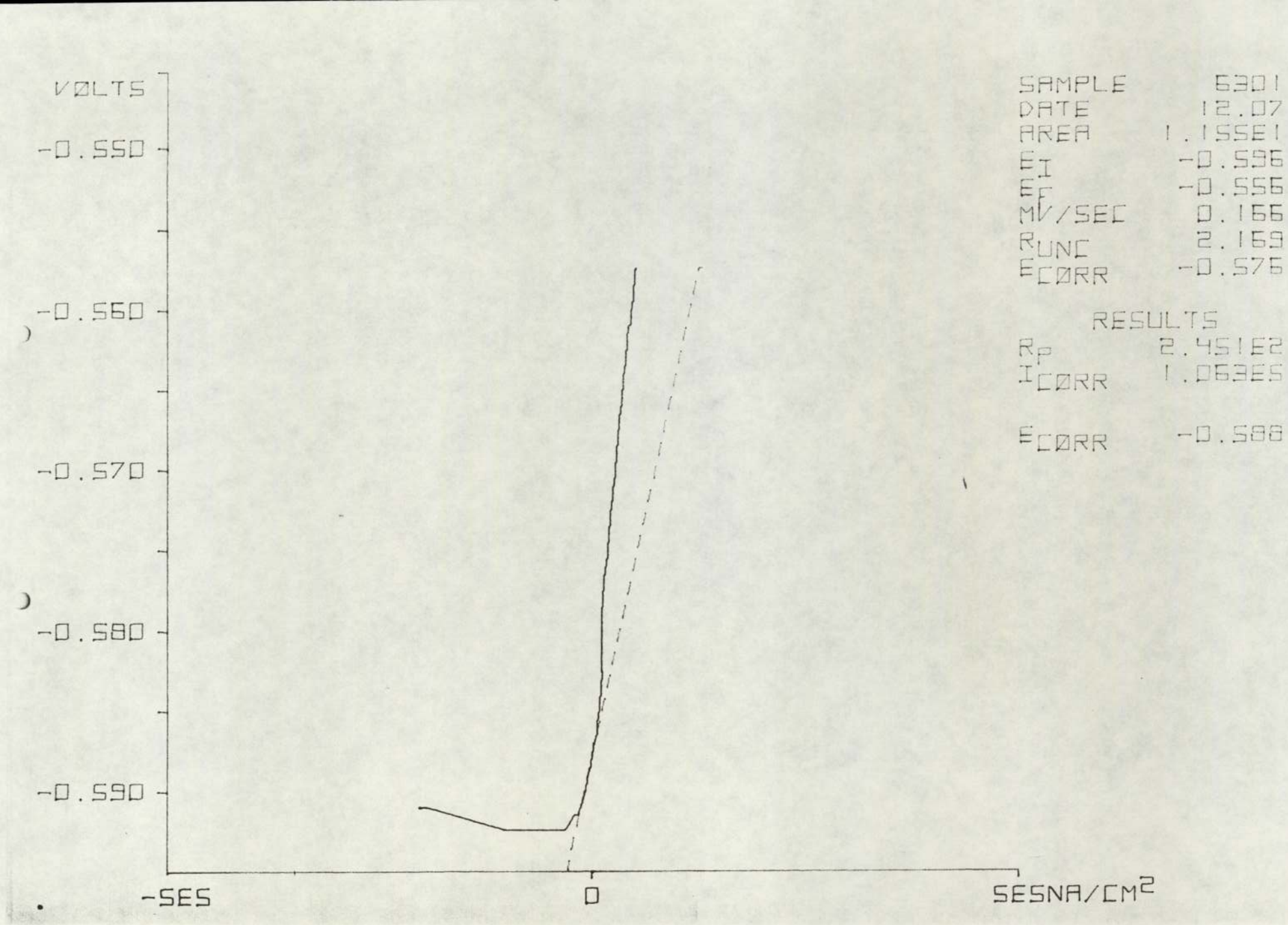
VØLTS
-0.550
-0.560
-0.570
-0.580
-0.590
-SES
0
SESNA/CM2
SAMPLE 6301
DATE 12.07
AREA 1.155E1
EI -0.596
EF -0.556
MV/SEC 0.166
RUNC 2.169
ECØRR -0.576
RESULTS
RP 2.451E2
ICØRR 1.063E5
ECØRR -0.588

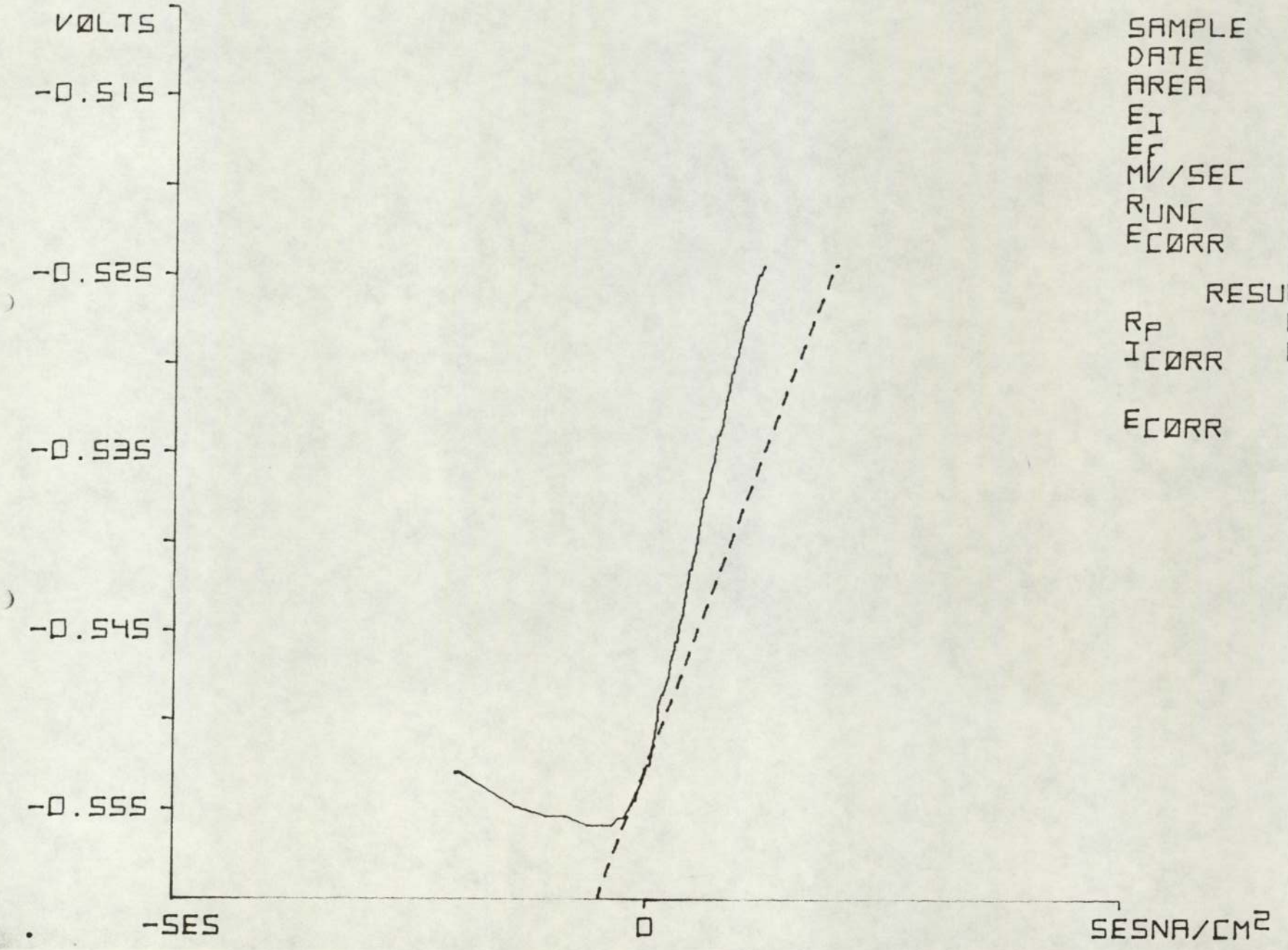

SAMPLE	1301
DATE	12.07
AREA	1.155E1
E_I	-0.560
E_f	-0.520
MV/SEC	0.166
R_{UNC}	2.981
$E_{CØRR}$	-0.540

RESULTS

R_P	1.437E2
$I_{CØRR}$	1.919E5
$E_{CØRR}$	-0.553

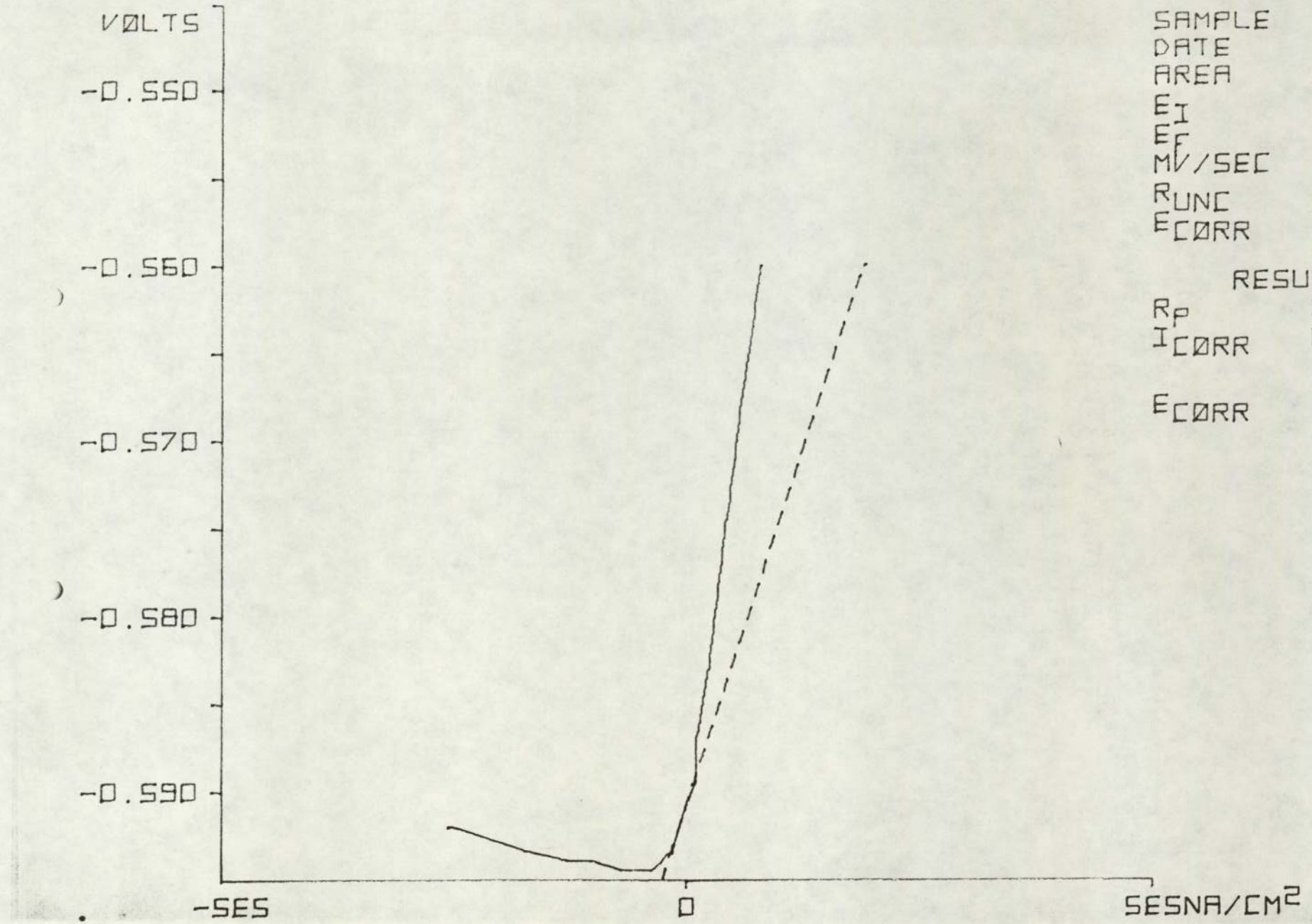

SAMPLE	4302
DATE	19.07
AREA	1.130E1
E_I	-0.598
E_F	-0.558
MV/SEC	0.166
R_{UNC}	2.189
$E_{CØRR}$	-0.578

RESULTS

R_P	1.618E2
$I_{CØRR}$	1.583E5
$E_{CØRR}$	-0.591

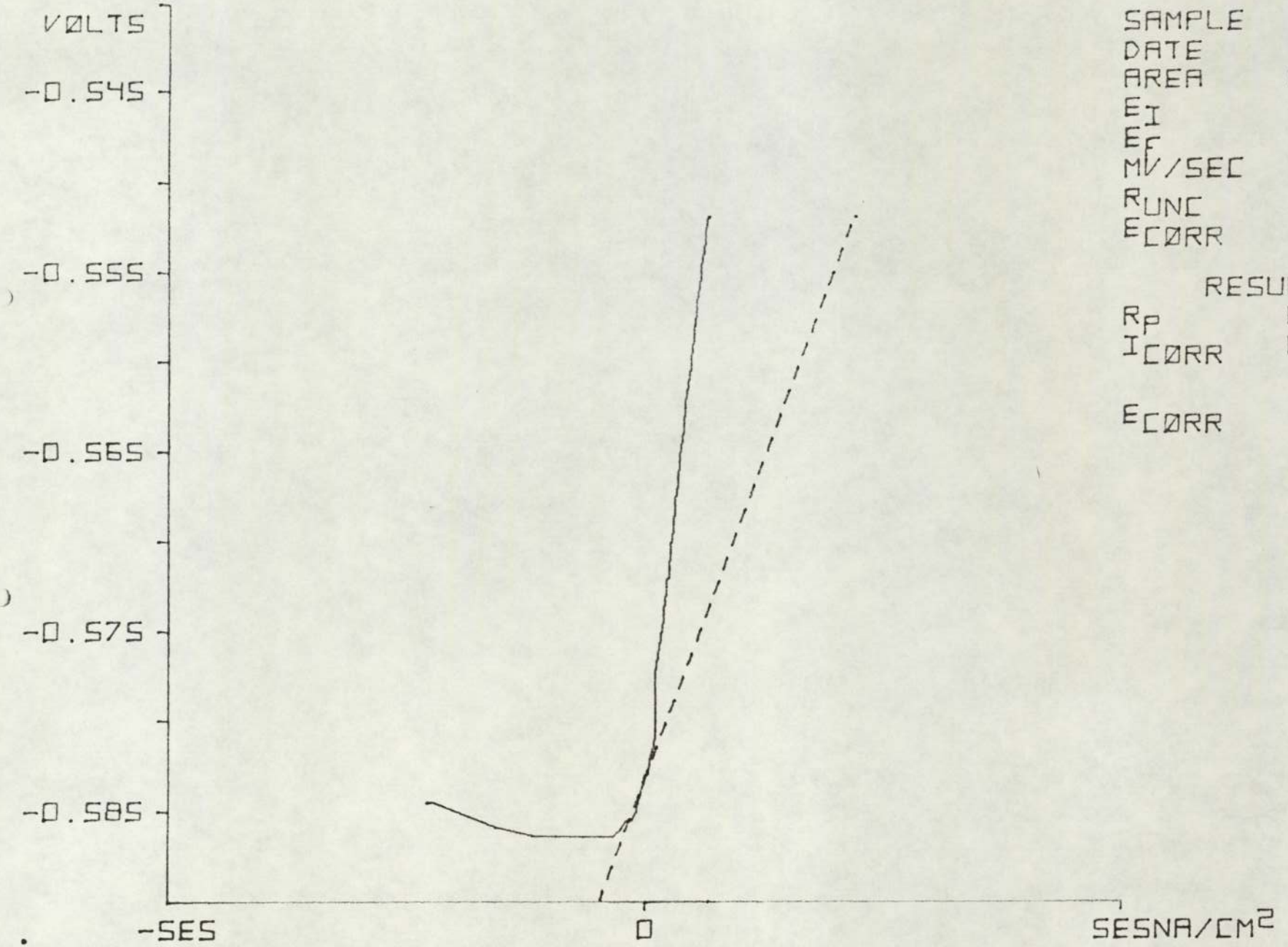

SAMPLE	6302
DATE	19.07
AREA	1.155E1
E_I	-0.590
E_f	-0.550
MV/SEC	0.166
R_{UNC}	2.111
$E_{CØRR}$	-0.570

RESULTS

R_P	1.434E2
$I_{CØRR}$	1.817E5
$E_{CØRR}$	-0.584

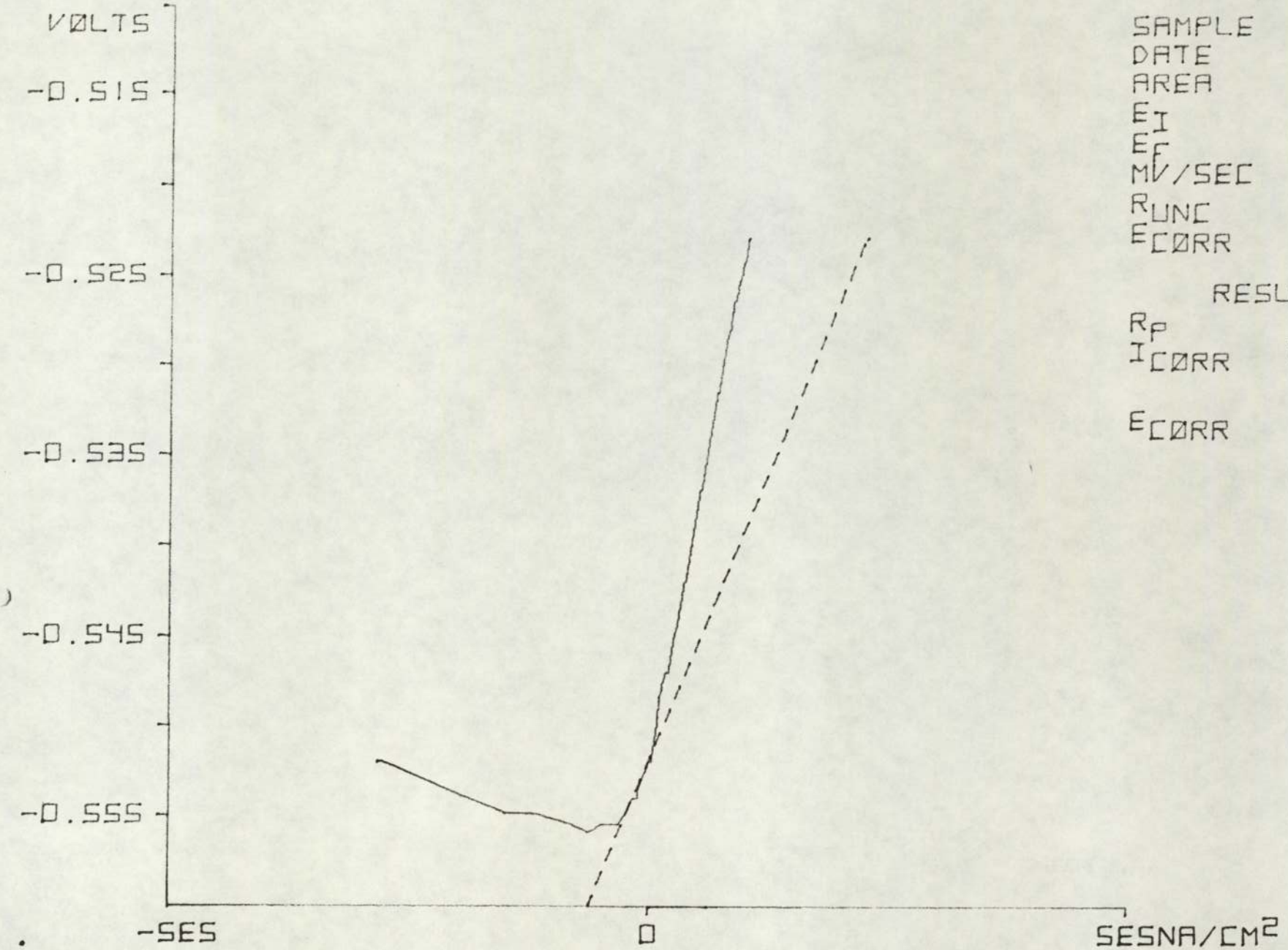

SAMPLE	1302
DATE	19.07
AREA	1.155E1
E_I	-0.560
E_F	-0.520
MV/SEC	0.166
R_{UNC}	2.560
$E_{CØRR}$	-0.540

RESULTS

R_P	1.289E2
$I_{CØRR}$	2.139E5
$E_{CØRR}$	-0.552

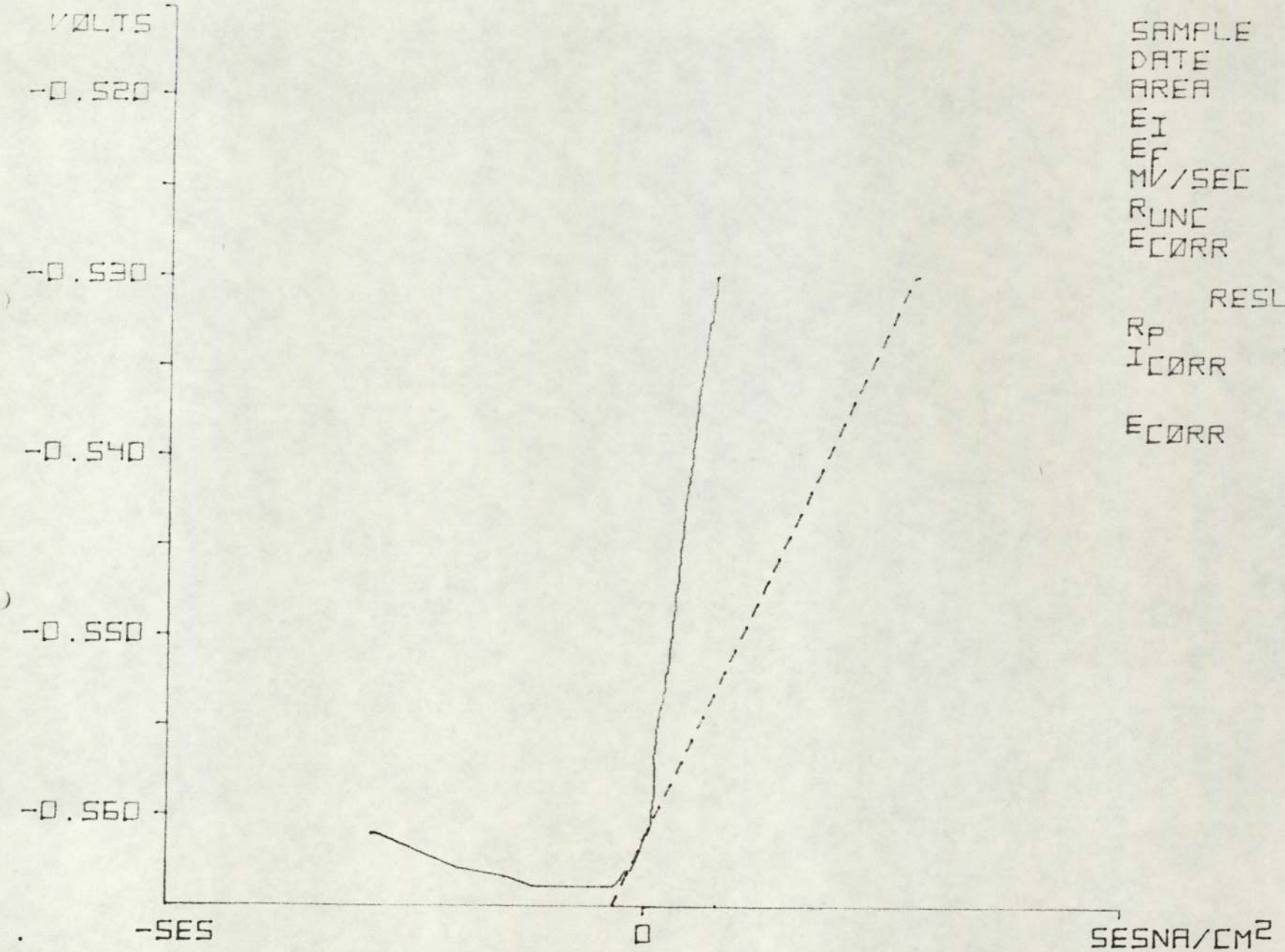

SAMPLE	4303
DATE	26.07
AREA	1.13DE1
E_I	-0.568
E_f	-0.528
MV/SEC	0.166
R_{UNC}	2.179
$E_{CØRR}$	-0.548

RESULTS

R_P	1.125E2
$I_{CØRR}$	2.278E5
$E_{CØRR}$	-0.562

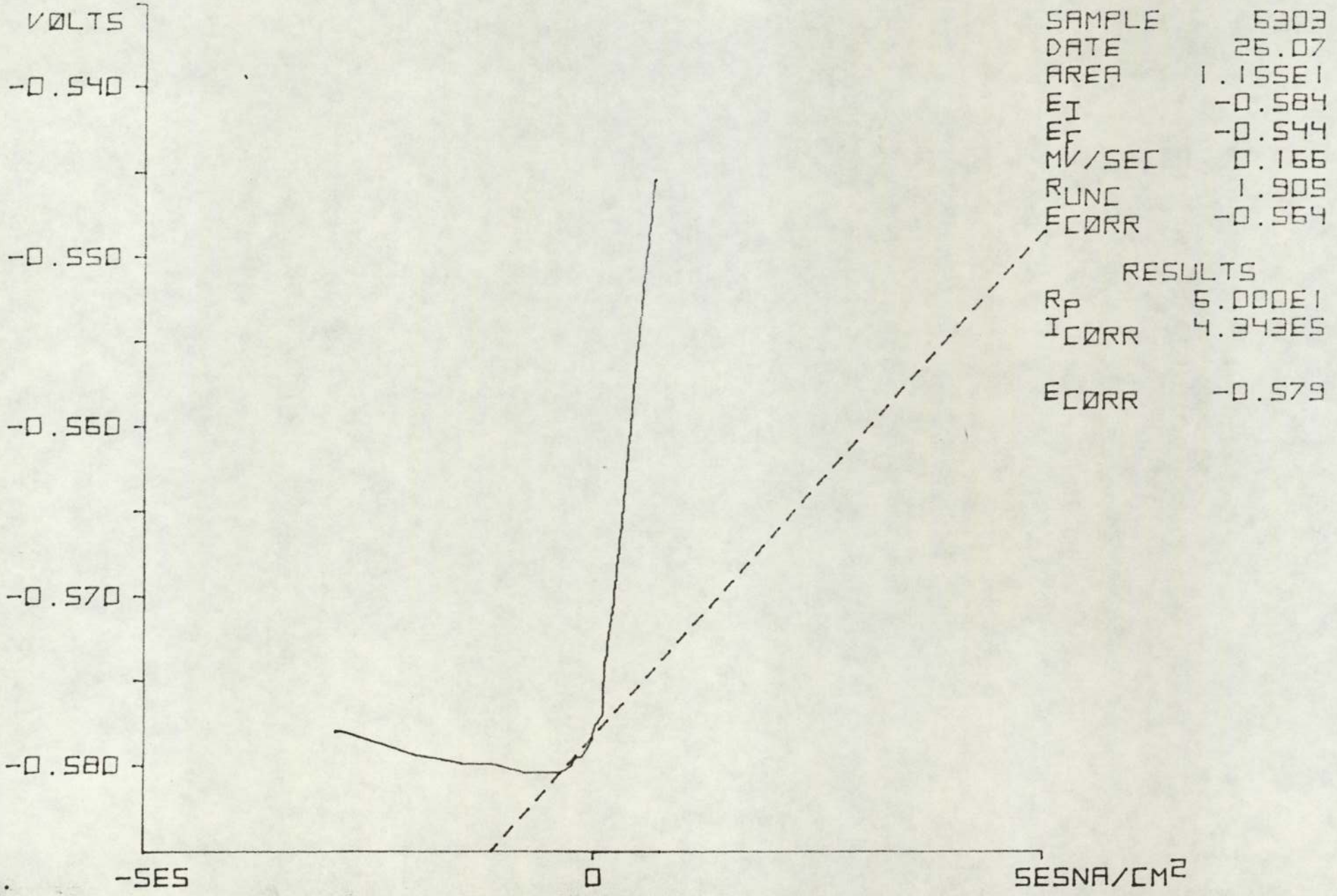

SAMPLE	6303
DATE	26.07
AREA	1.155E1
E_I	-0.584
E_F	-0.544
MV/SEC	0.166
R_{UNC}	1.905
$E_{CØRR}$	-0.564

RESULTS

R_P	6.000E1
$I_{CØRR}$	4.343E5
$E_{CØRR}$	-0.579

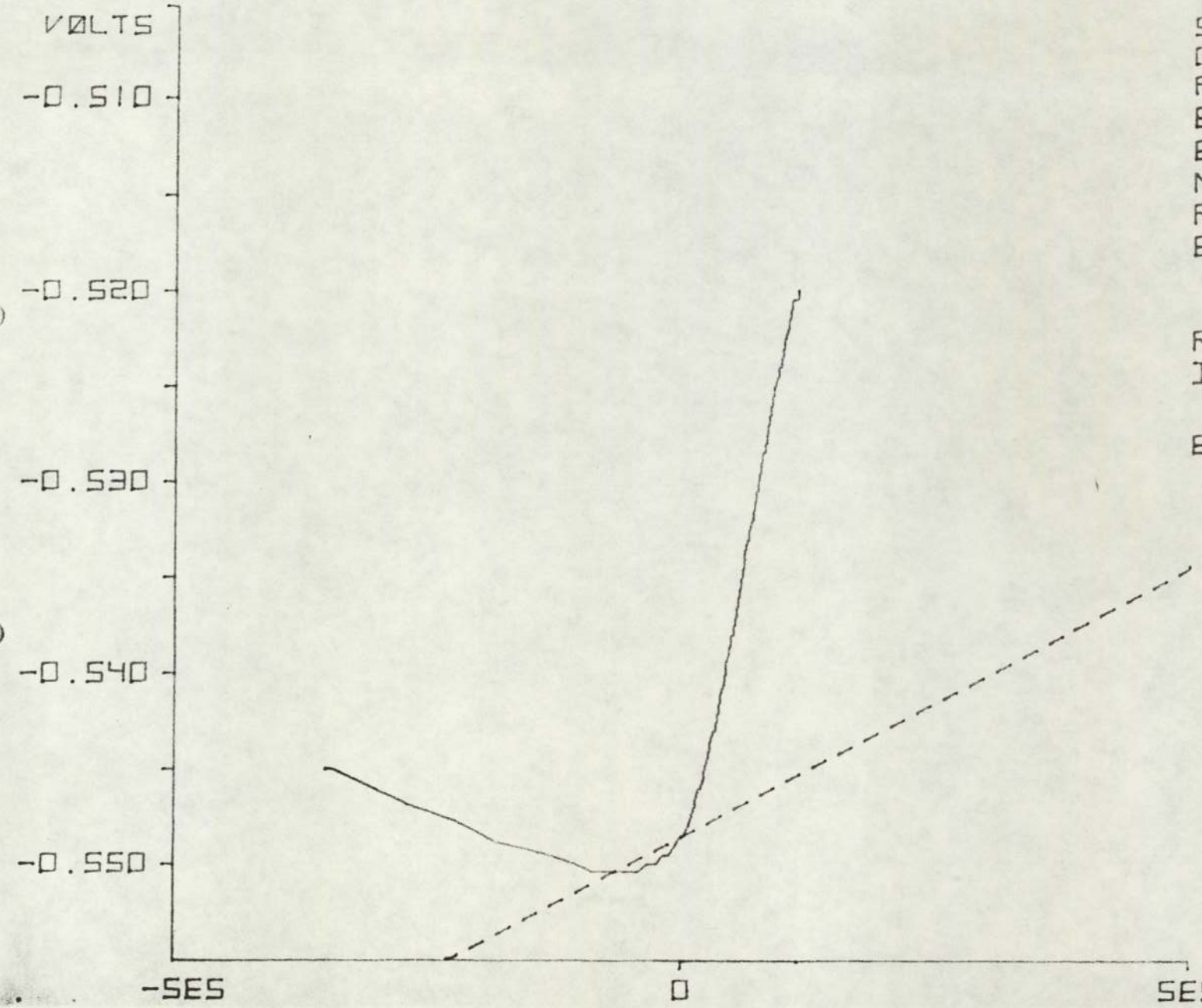

SAMPLE	1303
DATE	26.07
AREA	1.155E1
E_I	-0.556
E_F	-0.516
MV/SEC	0.166
R_{UNC}	2.775
$E_{CØRR}$	-0.536

RESULTS

R_P	2.809E1
$I_{CØRR}$	9.818E5
$E_{CØRR}$	-0.549

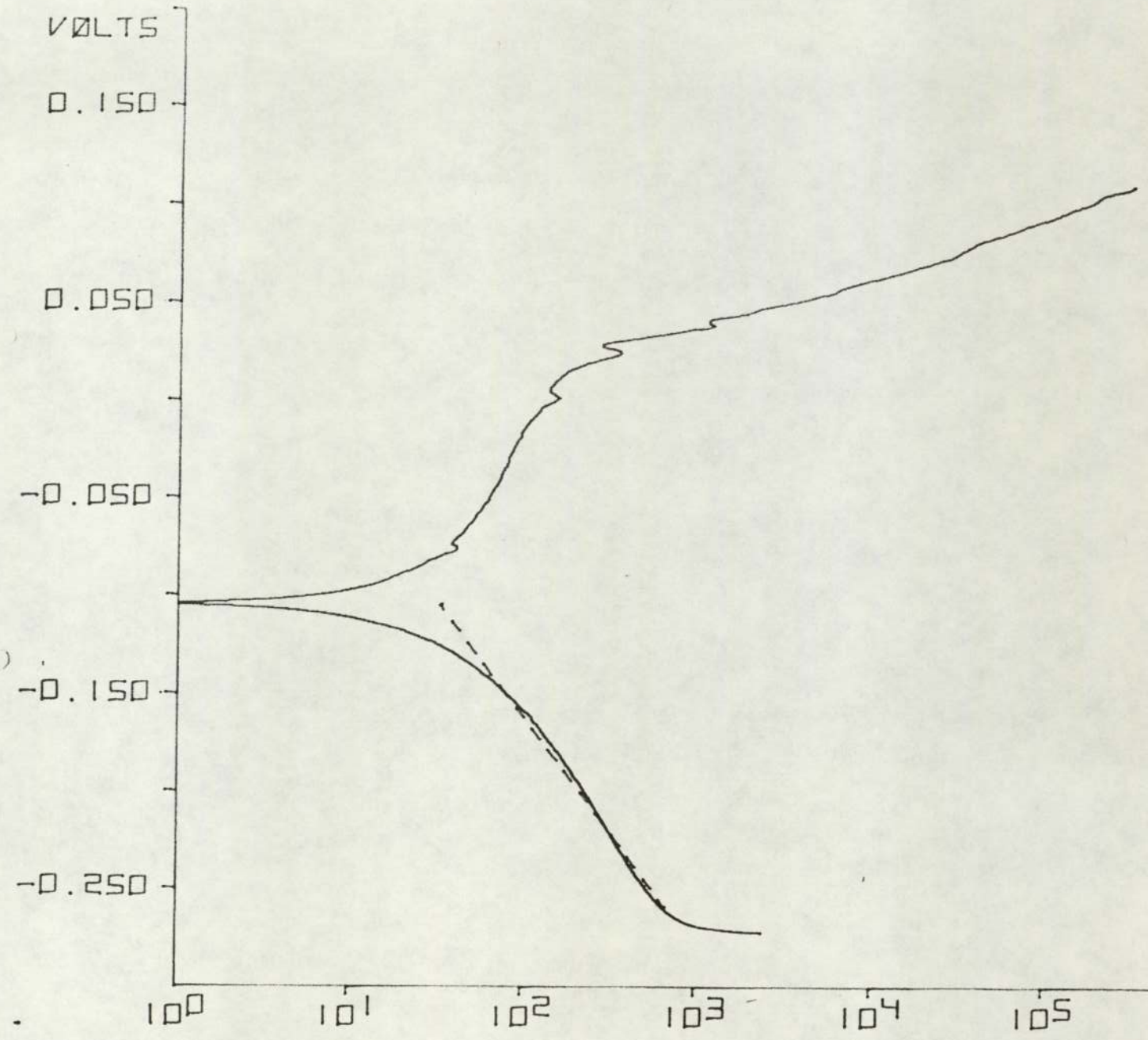

SAMPLE	4000
DATE	25.04
AREA	1.206E1
E_I	-0.272
E_F	0.128
MV/SEC	0.100
R_{UNC}	4.789
$E_{CØRR}$	-0.072

RESULTS

CTC	0.118
ATC	NØT FØUND
R_P	7.163E5
$E_{CØRR}$	-0.105

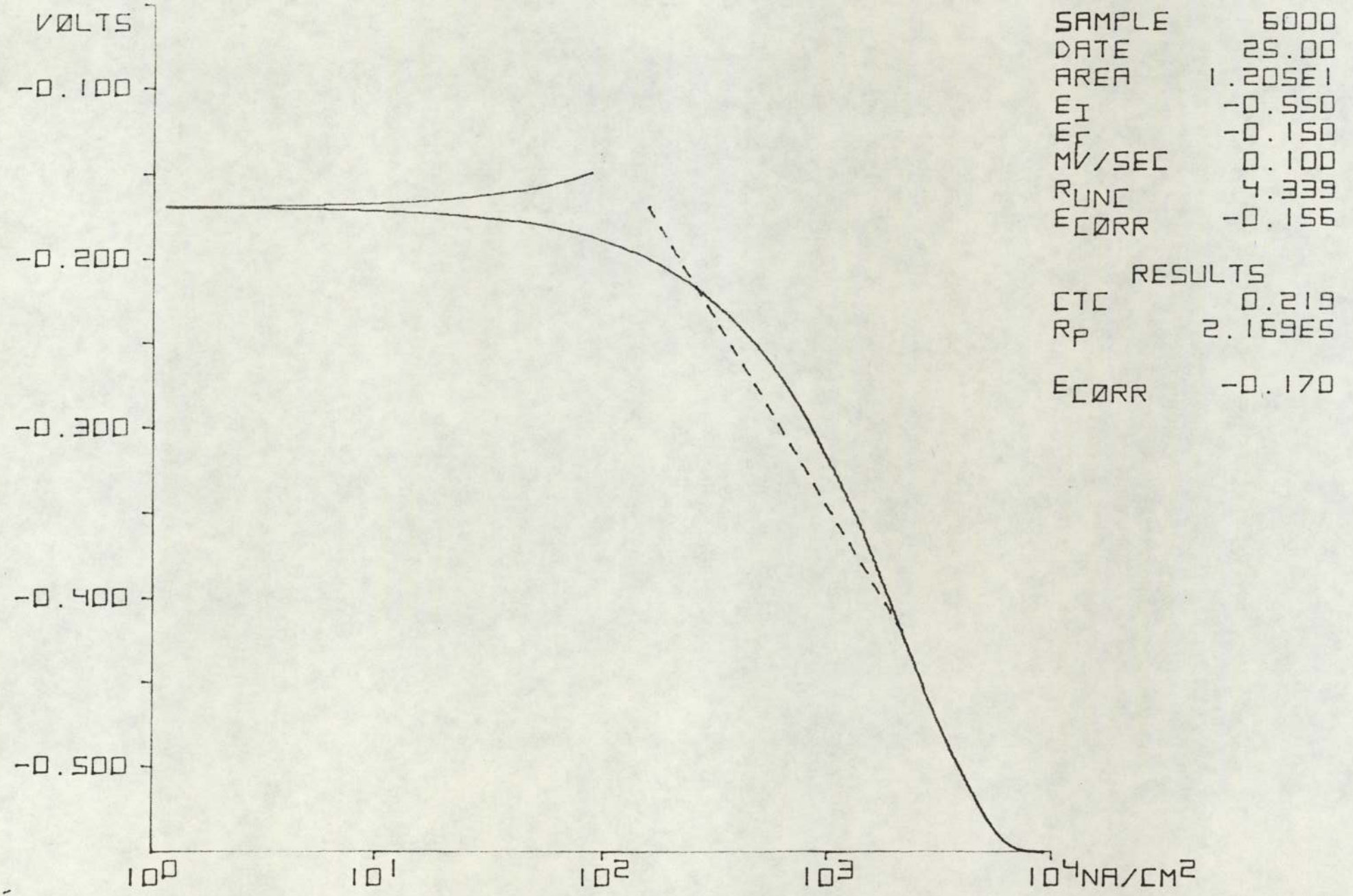

SAMPLE	6000
DATE	25.00
AREA	1.205E1
E_I	-0.550
E_F	-0.150
MV/SEC	0.100
R_{UNC}	4.339
$E_{CØRR}$	-0.156

RESULTS

CTC	0.219
R_P	2.169E5
$E_{CØRR}$	-0.170

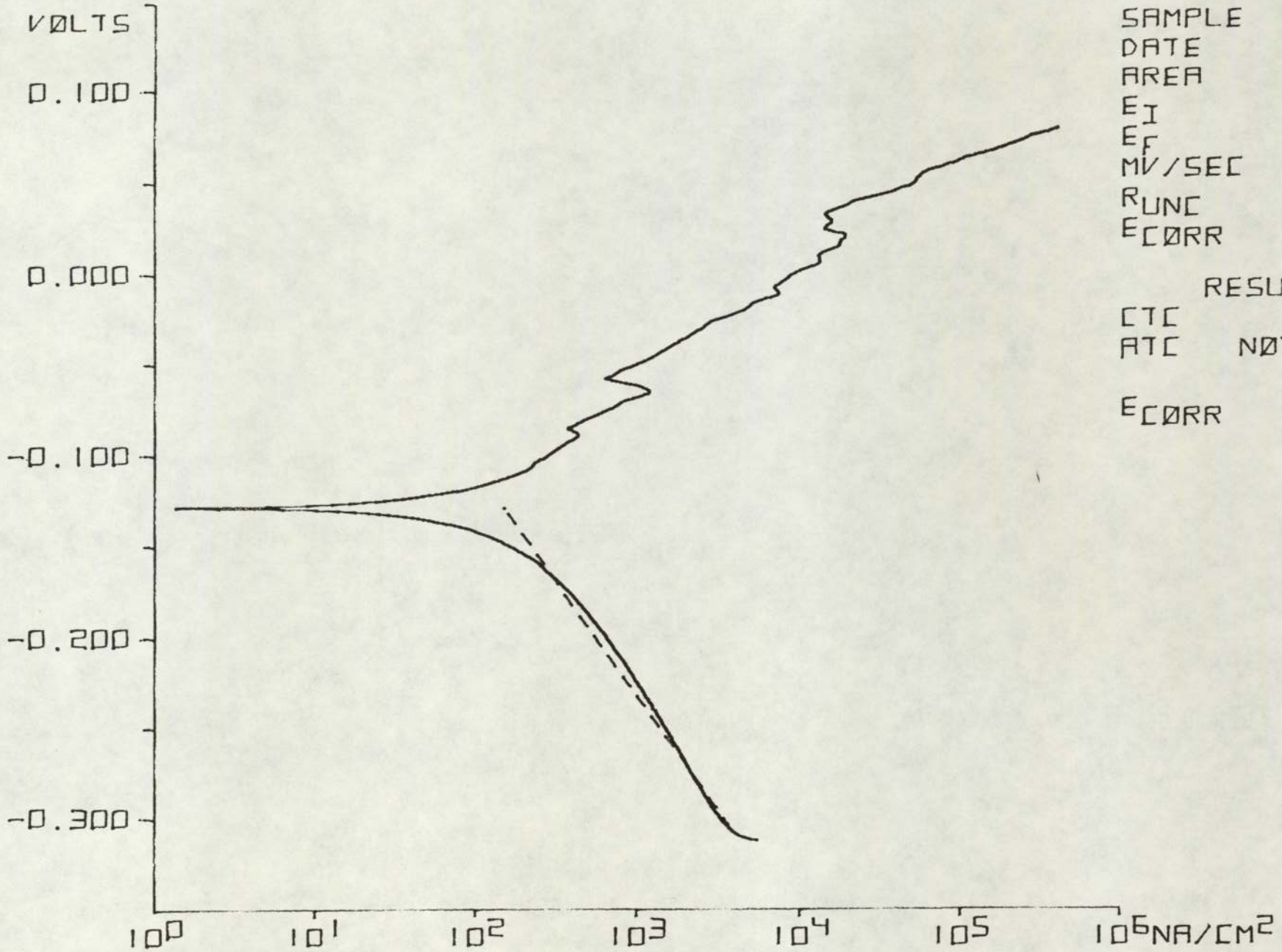

SAMPLE	1000
DATE	25.04
AREA	1.0SSE1
E_I	-0.312
E_F	0.088
MV/SEC	0.100
R_{UNC}	2.208
$E_{CØRR}$	-0.112

RESULTS

CTC	0.127
ATC	NØT FØUND
$E_{CØRR}$	-0.129

12.0 APPENDIX-2.

Falex Test

Graph of Slightly Scuffed Specimen

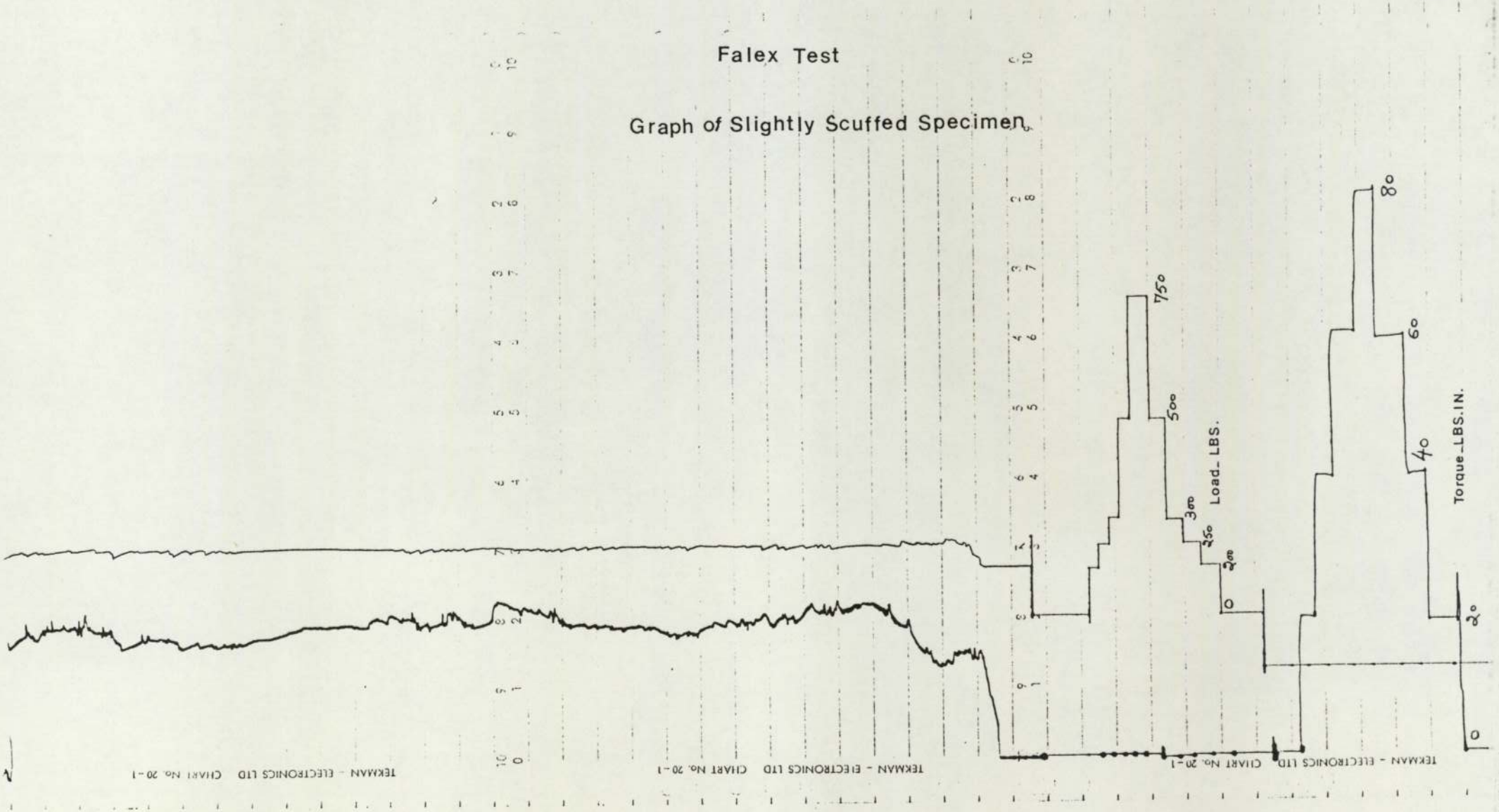

Falex Test

Graph of Scuffed Specimen

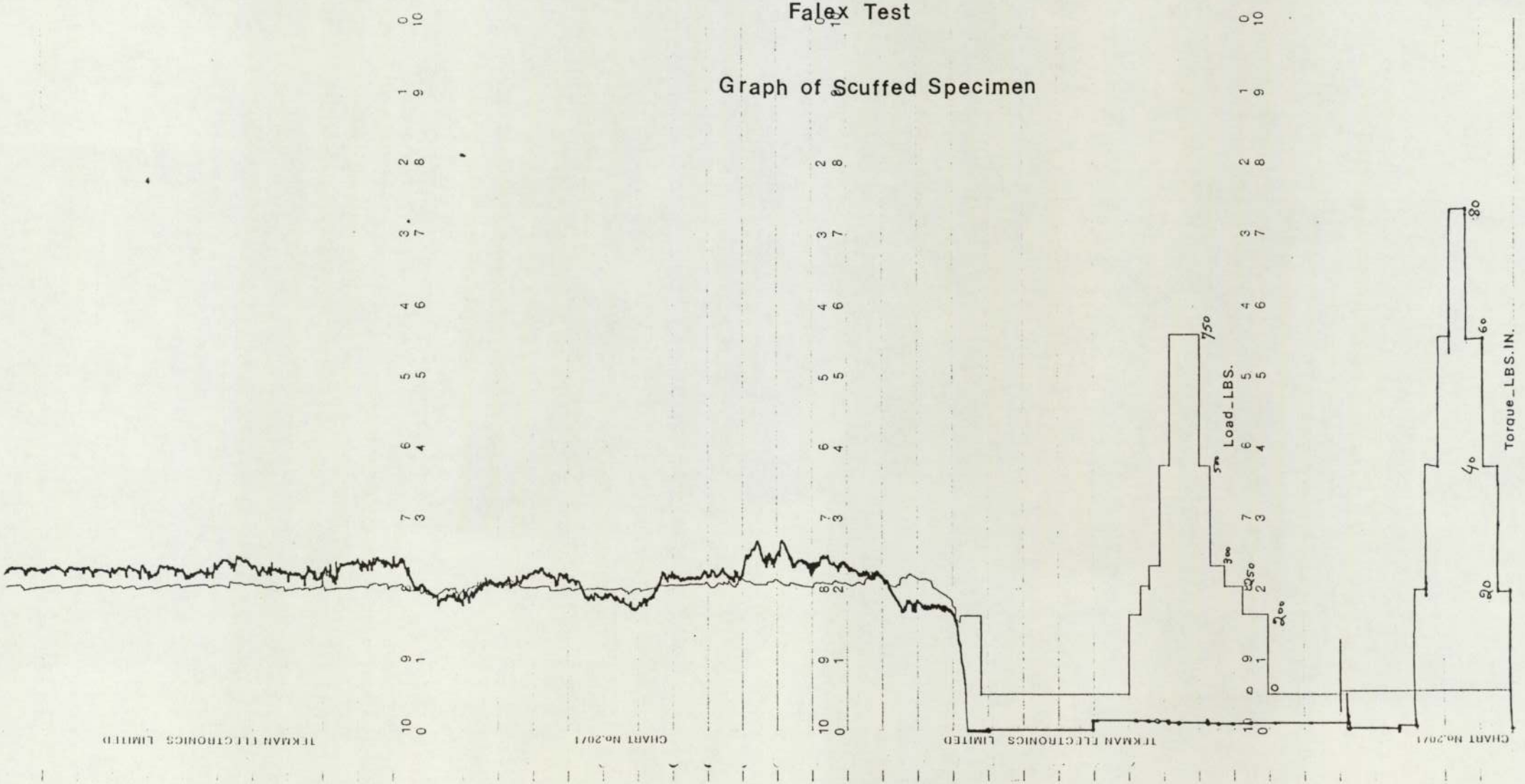

Falex Test

Graph of Badly Scuffed Specimen

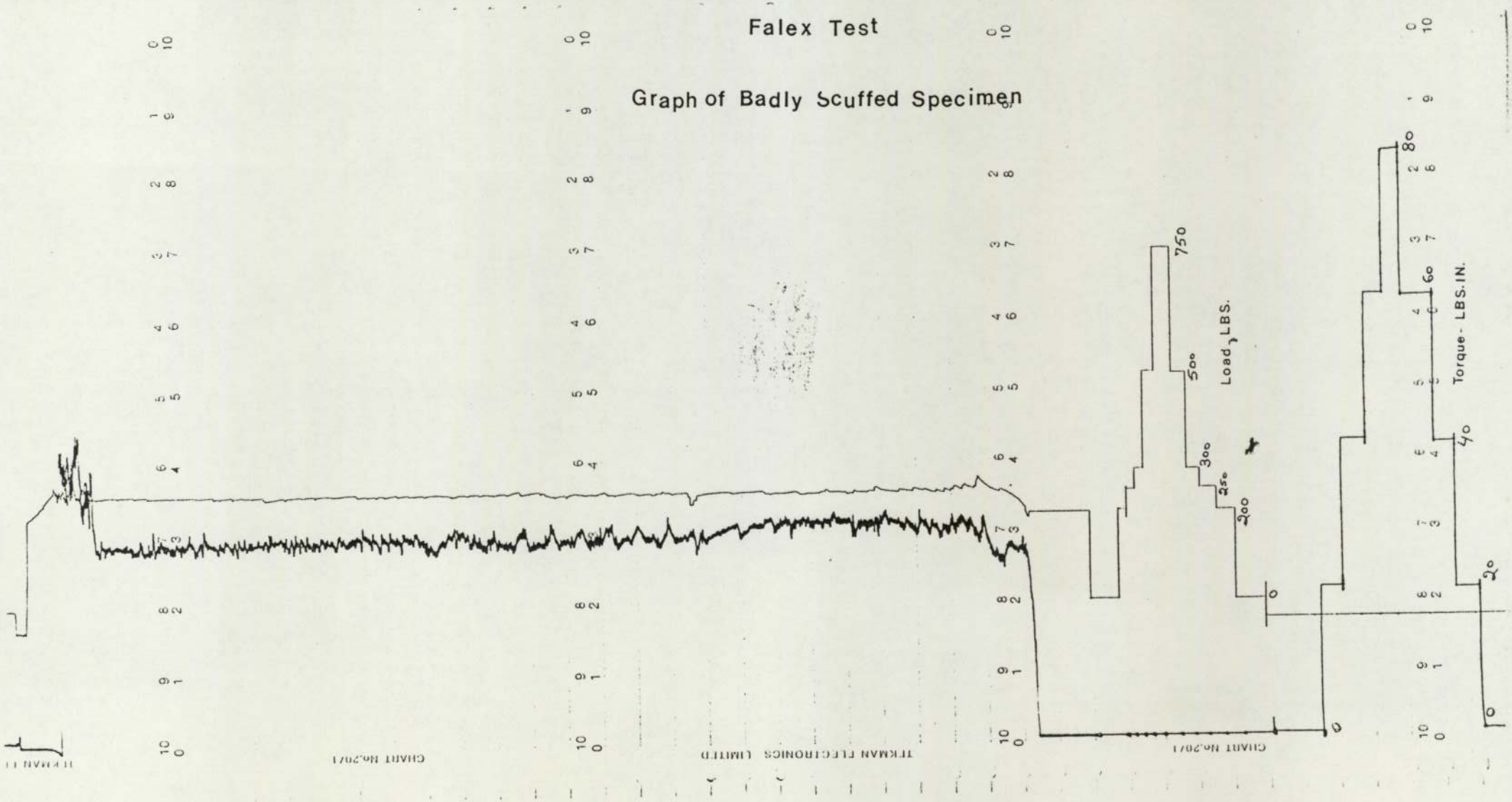

Falex Test

Graph of Totally Seized and Sheared Specimen

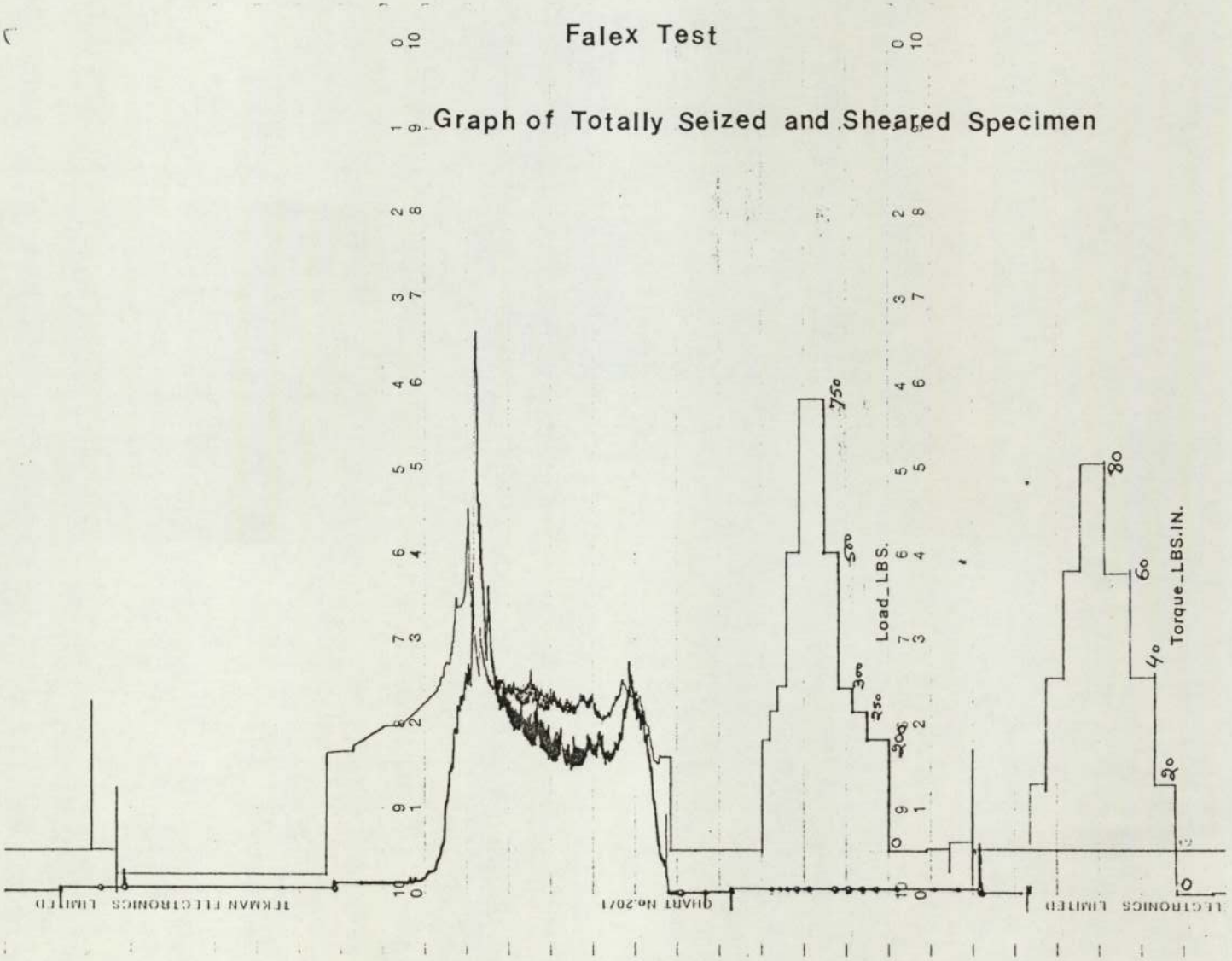

LIST OF REFERENCES.

1. B.Berghans, Process for the Surface Treatment of Metal Pieces (German), German patent DRP 668.639 (1932).

2. Abar Company's Literature, December 1984.

3. Kolbel J., The Nitride Layer Formation in Glow Discharge Nitriding (German) Forschungsberichte des Landes Nordhein-Westfalen, No.1555, West deutscher Verlag, Koln. 1965.

4. P.C.Jindal, Ionitriding of Steels, J.Vac.SCI.Technology, Vol.15, No.2, 313-317, March/April 1978.

5. A.M.Taylor and K.M.Tookey, Ionitriding a Proceess with Future, Metallurgia, Vol.48, 64-66, February 1981.

6. B.Edenhofer, Physical and Metallurgical Aspects of Plasma Nitriding, Heat-Treatment of Metals, Vol.1, 23-28, 1974.

7. W.Kovacs, J.Conybear, B.Edenhofer, F.Hombeck, R.Chaney, J.Barber, J.Houvion and C.France, Ionitriding, a Particularly Versatile Case Hardening Procees, Industrial Heating,Vol.XLVIII,No.9, 24-29, 1981.

8. A.M.Staines and T.Bell, Plasma Nitriding of High Alloy Steels, Heat treatment-media and methods, 58-69, 1979, Instit. of Metallurgist.

9. Dawes C. and Tranter D.F., Recent Developments in Surface Hardening Techniques, Metals Technology, Vol.5, 278-285, August 1978.

10. Guthershultze A., Physik, Vol.49, 358 & 473, 1928.

11. Kiessling E., Physik, Vol.96, 365, 1953.

12. Little P.F. and Von Engel A., The Hollow Cathode Effect and the Theory of Glow Discharge, Proc. Royal Soc. London, Series A, Vol.224, 209, 1954.

13. G.J.Dixon, S.A.Plumb, H.C.Child, Processing Aspects of Plasma Nitriding, Heat-Treatment 81, 137-146, 1981.

14. G.J.Dixon, Geomertrical Aspects of Ionitriding, B.Sc. Degree Project, The Aston University, January 1979.

15. Hanau R., Physical Review, Vol.76, 153-154, 1949.

16. T.Bell, B.J.Birch, V.Korotchemko and S.P.Evans, Controlled Nitriding in Ammonia-Hydrogen Mixtures, Heat-Treatment 73, 51-57, Dec. 1973.

17. B.J.Lightfoot and D.H.Jack, Kinetics of Nitriding With or Without White Layer Formation, Heat-Treatment 73, 59-65, 1973.

18. E.C.Rollason, Metallurgy for Engineers,4th edition,Edward Arnold,1973.

19. Metals Hand Book., Heat-Treating, Vol.4, 9th edition, American Society for Metals, 1981.

20. Source Book on Nitriding, ASM Publication, August 1977.

21. Bogdanov V.V., Lakhtin Y.M., Neustroev G.N., Ryazanora A.L., Metal

Science and Heat-Treatment, No.4, 257-260, April 1968.

22. Mitchel E. and Dawes C., Molten Salt Bath Nitriding, Metal Treatment and Drop Forging, Vol.31, 3-16 (Jannuary), 49-58 (February), 88-96 (March), 195-200 (May), 226-234 (June), 265-276 (July), 1964.

23. Metals Hand Book, Vol.2, 8th edition, 1964, American Soceity For Metals, 1964.

24. T.Bell, Ferritic Nitrocarburising, Heat-Treatment of Metals, 1975.2, 39-49, 1975.

25. C.P.Alekseeva, G.S.Krivonogov and Yu.Yu.Cherkis, Characterstics of Alloying and Phase Composition of Nitrided Austinitic Stainless Steel, Translated from Metallovedenie,Termicheskaya Obrabotka Metallov, No.1, 19-23, Jannuary 1979.

26. Taylor E., Tufftride only Skin Deep, Metal Engineering Quarterly, Vol.11, No.2, 12-16, May 1971.

27. Degussa Company Literature, September 1980.

28. Hudis M., Journal of Applied Physics, Vol. 44, 1489-1496, 1973.

29. B.Edenhofer, Production and Structure of Highly Ductile Plasma Nitrided Layers Without a White Layer, Heat-Treatment 79, 22-24, May 1979.

30. Tibbetts G.G., Journal of Applied Physics, Vol. 45, 5072-5073, 1974.

31. B.Edenhofer and T.J.Bewley, Low Temperature Nitriding, Heat-Treatment 76, 7-13, May 1976.

32. Stahl and Eisen, The Structure of Nitrided Quenched and Tempered Steels, (German), Vol.78, 1881-1889, December 1958 (BISI Translation No. 1241).

33. K.H. Jack, Nitriding, Heat-Treatment 73, 39-50, 1973.

34. Fast J.D. and Verrij M.B., Diffusion of Nitrogen in Iron, Journal of Iron and Steel Institute, Vol.76, 24-27, January 1954.

35. Jack K.H., Binary and Ternary Interstitial Alloys(Part 1. The Iron Nitrogen System:The Structure of Fe_4N and Fe_2N), Proceeding of Royal Soceity of London, Series A, Vol.195, 34-40, Nov.-Feb. 1948-49.

36. Naman F.K. and Langenscheid G.A., Contribution to Iron-Nitrogen-Carbon System, Archiv Fur das Eisenhutten-Wasen, Vol.36, 677-682, Sept. 1965 (Available as translation BISI 4583).

37. Neustroev G.N. and Bogdanov V.V., Low Temperature Cyaniding of Structural Steels, Metal Science and Heat-Treatment, No.10, 856-859, 1970.

38. Prenosil B., Structure of Layers Produced by Bath Nitriding and Nitriding in Ammonia Atmospheres with Hydrocarbon Additions, Harterei-Technische Mitteilungen, Vol.20, 41-49, April 1965 (Available as translation BISI 4720).

39. P.Astley, Liquid Nitriding:Development and Present Applications,

Heat Treatment 73, 93-97, 1973.

40. T.C.Askwith, The Basic Mechanism of Wear, Surfacing Journal, Vol. 11, No. 4, 2-6, 1980.

41. Z.Lisowski, A Modified Theory of Adhesive Wear in Lubricated Contacts, Wear, Vol.68, 333-345, 1981.

42. T.S.Eyre, The Mechanism of Wear, Tribology International, Vol.11, 91-96, April 1978.

43. Charles Lipson, Adhesive and Abrasive wear, Machine Design, Vol.25, 74-77, Dec. 1969.

44. Nam P.Suh, The Delamination Theory of Wear, Wear,Vol.25,111-124,1973.

45. Marshal B.Peterson, Major-Britt K.Gabel, Martin J.Devine, Understanding Wear, ASTM Standardisation News, September 1974.

46. A.W.J.deGee, Friction and Wear as Related to the Composition, Structure and Properties of Metals, International Metals Reviews, Vol.24, No.2, 57-67, 1979.

47. Faville-Levally, Falex Machine Operating manual, 1982.

48. "CASSEL", Manual of Heat-Treatment and Case Hardening, ICI Ltd.,1964.

49. Princeton Applied Research, Model-350, Corrosion Measurement System, Operating Manual, 1979.

50. Acetic Acid -Salt Spray (Fog) Testing: ASTM Publication, Designation: B287-74 (Reapproved 1980).

51. M.Stern and A.L.Geary, Electrochemical Polarisation, J.Electro-Chemical Society, Vol.104, 56-63, 1958.

52. C.Wagner and W.Traud, Z.Elektrochemie, Vol.44, 391-462, 1938.

53. A.Stern and R.M.Roth, J.Electrochemical Soc., Vol.104, 390-392, 1957.

54. S.Gerchakov, L.R.Voey, F.Mansfeld, An Improved Method for Analysis of Polarisation Resistance Data, Corrosion, Vol.37, 696-700, Dec. 1981.

55. S.Barnarrt, Linear Corrosion Kinetics, Corrosion Science, Vol.9, 145-149, 1971.

56. F.Mansfeld, Some errors in Linear Polarisation and their Corrections, Corrosion, Vol.30, 92-97, 1974.

57. H.E.Townsend, H.J.Cleary, L. Allegra, Break Down of Oxide Films on Steel Exposed to Chloride Solution, Corrosion, Vol.37, No.7, 384-387,1981.

58. J.P.Chilton, Principles of Metallic Corrosion, 2nd Edition, The Chemical Society, 1968.

59. U.R.Evans, Corrosion and Oxidation of metals, 1st Supplementary Volume, Edward Arnold, 1968.

60. Donald Peckner and I.M.Berustein, Hand Book of Stainless Steel,

McGraw Hill Publication, 1977.

61. C.Dawes and D.F. Tranter, Nitrotec Surface Treatment, its Development and Application in the Design and Manufacture of Automobile Components, Heat-Treatment of Metals, Vol.4, 85-90, 1982.

62. S.E.Vanes, The Nitrotec Surface Treatment Process, Metals and Materials, J. Institute of Metals, Vol.1, No.4, 238-243, April 1985.

63. Rozendaal, HCG, Colijn, PF and Mittemeijer, E.J, Heat-Treatment 84, Book No. 312, The Metal Society, 1984.

64. C.Dawes, D.F.Tanter, C.J.Smith, Reappraisal of Nitrocarburising and Nitrogen When Applied to Design and Manufacture of Non-alloy Steel Automobile Components, Met. Tech., Vol.6, 345-353, Sept. 1979.

65. C.Dawes, D.F.Tranter, C.G.Smith, Nitriding of Non-alloy Steels, Heat-Treatment of Metals, Vol.1, 1-4, 1980.

66. Noren T.M. and Kindbrom L. , The Structure of Nitrided Quenched and Tempered Steels (German), Stahl Und Eisen, Vol.78, 1881-1891, Dec. 1958 (Available as translation BISI 1241).

67. Z.1.Zhang and T.Bell, Structure and Corrosion Resistance of Plasma Nitrided Stainless Steel, Surface Engineering, Vol.1, 131-136, 1985.

68. Edward B.Hale,Chun-Ping Meng and R.A.Kosher, Measurement of the Wear Properties of Metallic Solids with a Falex Lubricant Testing Machine, Rev. Sci. Instrum., Vol.53, No.8, 1255-1260, August 1982.